The Chemistry of Three-coordinate Bis(trimethylsilyl)amido Complexes of the First-Row Transition Metals

And

Designing a Solution-Stable Distannene: The Decisive Role of London Dispersion Effects

By

CARY R. STENNETT

DISSERTATION

Submitted in partial satisfaction of the requirements for the degree of

DOCTOR OF PHILOSOPHY

in

CHEMISTRY

in the

OFFICE OF GRADUATE STUDIES

of the

UNIVERSITY OF CALIFORNIA

DAVIS

Approved:

Philip P. Power, Chair

Alan L. Balch

William H. Casey

Committee in Charge

2021

Abstract.

A series of studies of the chemistry of first-row transition metal $M\{N(SiMe_3)_2\}_3$ complexes is described herein. Both divalent $M\{N(SiMe_3)_2\}_2$ and trivalent $M\{N(SiMe_3)_2\}_3$ transition metal complexes have been described in the literature since the early 1960s. However, while the divalent complexes have been the subject of a great deal of study, comparatively little attention has been paid to the trivalent complexes since their initial discovery. The reason for this disparity appears to be the notion that the steric crowding in these molecules results in their low reactivity. Although work in this laboratory has periodically examined these complexes, our most recent interest stemmed from the observation that the detailed molecular structure of the vanadium complex $V\{N(SiMe_3)_2\}_3$ had been absent from the literature as recently as 2019, despite the complex having been reported in 1971. By isolating this complex as violet-colored crystals, Wagner and coworkers determined that the original report of 'brown' $V\{N(SiMe_3)_2\}_3$ had probably mischaracterized this material. This observation encouraged us to reexamine the chemistry of these classic metal amido complexes, which revealed a vibrant chemistry that had not been described until now.

Chapter 2 describes the synthesis and characterization of a series of $M\{N(SiMe_3)_2\}_3L_2$ complexes (L = nitrile or isocyanide ligand) of titanium and vanadium. Although it had been initially thought that the considerable steric crowding in $M\{N(SiMe_3)_2\}_3$ complexes precluded the formation of Lewis base complexes, it is shown that the formation of such donor complexes is possible by judicious selection of the donor molecule (isocyanide or nitrile bases). A spectroscopic study of these complexes revealed that the donors are only weakly bound in solution, with stronger binding in the case of the vanadium complexes. Furthermore, we observed no complex formation for M = Cr, Mn, Fe, or Co, a property that we attribute to the absence of empty, low-energy orbitals available in the later metals to accept electrons from donor molecules.

In Chapter 3, we exploit the observations made in Chapter 2 to show that $V\{N(SiMe_3)_2\}_3$ can be oxidized by reagents similar in shape to the Lewis bases used to form $M\{N(SiMe_3)_2\}_3L_2$ complexes. Thus, the reaction of $V\{N(SiMe_3)_2\}_3$ with iodosylbenzene (PhIO) or trimethylsilylazide (Me_3SiN_3) afforded the

vanadium(V) complexes $V(=O)\{N(SiMe_3)_2\}_3$ or $V(=NSiMe_3)\{N(SiMe_3)_2\}_3$, respectively, which were studied structurally and spectroscopically. Despite several reports of its attempted synthesis, $V(=O)\{N(SiMe_3)_2\}_3$ had not been isolated until now. It had been suggested that the V=O moiety reacts with a ligand trimethylsilyl group to give the $V(OSiMe_3)(=NSiMe_3)\{N(SiMe_3)_2\}_2$ isomer. Indeed, we show this to be the case, and provide a kinetic study of this transformation in solution.

Chapter 4 describes the reduction of $M\{N(SiMe_3)_2\}_3$ (M = V, Cr, Fe) complexes with the metal hydride reagents $LiAlH_4$ or $AlH_3(NMe_3)$. Thus, the reaction of $V\{N(SiMe_3)_2\}_3$ with $LiAlH_4$ afforded the highly unstable polyhydride $[V(\mu_2\text{-}H)_6[Al\{N(SiMe_3)_2\}_2]_3][Li(OEt_2)_3]$. In contrast, the reaction of $V\{N(SiMe_3)_2\}_3$ with $LiAlH_4$ in the presence of 12-crown-4 gave the rare terminal hydride $[VH\{N(SiMe_3)_2\}_3][Li(12\text{-crown-}4)_2]$. The presence of this hydride was verified by the preparation and spectroscopic study of the corresponding deuteride complex $[VD\{N(SiMe_3)_2\}_3][Li(12\text{-crown-}4)_2]$ by the reaction of $V\{N(SiMe_3)_2\}_3$ with $LiAlD_4$ in the presence of 12-crown-4. The reaction of $LiAlH_4$ with $M\{N(SiMe_3)_2\}_3$ (M = Cr, Fe) in the presence of 12-crown-4 afforded the ionic metal(II) complexes $[M\{N(SiMe_3)_2\}_3][Li(12\text{-crown-}4)_2]$, rather than any hydride complexes. In the absence of 12-crown-4, the reaction of $Fe\{N(SiMe_3)_2\}_3$ with $LiAlH_4$ gave the so-called "hydrido inverse crown" complex $[Fe(\mu_2\text{-}H)\{N(SiMe_3)_2\}_2(\mu_2\text{-}Li)]_2$, while treatment of the same trisamide with $AlH_3{\cdot}NMe_3$ afforded the mixed-metal polyhydride $Fe(\mu_2\text{-}H)_6[Al\{N(SiMe_3)_2\}_2]_2[Al\{N(SiMe_3)_2\}(NMe_3)]$.

Chapter 5 describes attempts to prepare divalent $M\{N(SiMe_3)_2\}_2$ complexes of titanium and vanadium by reduction of the corresponding $M(Cl)\{N(SiMe_3)_2\}_2$ complexes. Additionally, efforts to determine the fate and role of the bromine atom in the synthesis of $M\{N(SiMe_3)_2\}_3$ (M = Mn, Co) complexes by oxidation of the divalent $M\{N(SiMe_3)_2\}_2$ with $BrN(SiMe_3)_2$ are detailed. Reduction of $Ti(Cl)\{N(SiMe_3)_2\}_2$ with 5 %(wt) sodium on sodium chloride afforded the unusual mixed-metal, mixed-valent Ti(III/IV) hydride complex $Ti_2(\mu\text{-}H)_2\{N(SiMe_3)_2\}_3\{N(SiMe_3)(SiMe_2CH)\}(Na)$ rather than "$Ti\{N(SiMe_3)_2\}_2$," while the analogous reaction using $V(Cl)\{N(SiMe_3)_2\}_2$ gave only a mixture of intractable products. After isolation of $Co\{N(SiMe_3)_2\}_3$ formed by the reaction of $BrN(SiMe_3)_2$ with

$Co\{N(SiMe_3)_2\}_2$, storage of the mother liquor afforded a small amount of crystalline, polymeric $[(\mu\text{-}Br)Co\{\mu\text{-}N(SiMe_3)(SiMe_2CH_2CH_2Me_2Si)(Me_3Si)\mu\text{-}N\}Co(\mu\text{-}Br)]_\infty$, indicating that the three products of this reaction are $Co\{N(SiMe_3)_2\}_3$, $HN(SiMe_3)_2$, and the aforementioned polymer. In order to better understand the role of bromine in these oxidations, we also treated $M\{N(SiMe_3)_2\}_2$ (M = Mn or Co) with elemental bromine. Surprisingly, treatment of $Mn\{N(SiMe_3)_2\}_2$ with bromine gave the trisamide $Mn\{N(SiMe_3)_2\}_3$ as the only isolated product. In contrast, the reaction of $Co\{N(SiMe_3)_2\}_2$ with elemental bromine gave the heteroleptic $[Co(Br)\{\mu\text{-}N(SiMe_3)_2\}]_2$.

Chapters 6 and 7 differ from the preceding chapters in that the focus is no longer the chemistry of transition metal amide complexes. In Chapter 6, the synthesis and characterization of several homoleptic, dimeric aryloxide and thiolate complexes of iron are described. Thus, treatment of $[Fe\{N(SiMe_3)_2]_2$ with the appropriate phenol or thiol affords the dimers $\{Fe(OC_6H_2\text{-}2,6\text{-}Bu^t_2\text{-}4\text{-}Me)_2\}_2$ and $\{Fe(OC_6H_3\text{-}2,6\text{-}Bu^t_2)_2\}_2$, or the monomeric $Fe\{SC_6H_3\text{-}2,6\text{-}(C_6H_3\text{-}2,6\text{-}Pr^i_2)_2\}_2$. Recrystallization of $\{Fe(OC_6H_2\text{-}2,6\text{-}Bu^t_2\text{-}4\text{-}Me)_2\}_2$ or $\{Fe(OC_6H_3\text{-}2,6\text{-}Bu^t_2)_2\}_2$ from diethyl ether gives the corresponding three-coordinate ether complexes $Fe(OC_6H_3\text{-}2,6\text{-}Bu^t_2\text{-}4\text{-}Me)_2(OEt_2)$ and $Fe(OC_6H_3\text{-}2,6\text{-}Bu^t_2)_2(OEt_2)$. However, recrystallization of the thiolate $Fe\{SC_6H_3\text{-}2,6\text{-}(C_6H_3\text{-}2,6\text{-}Pr^i_2)_2\}_2$ from diethyl ether afforded no new products. $Fe(OC_6H_3\text{-}2,6\text{-}Bu^t_2\text{-}4\text{-}Me)_2(OEt_2)$ and $Fe(OC_6H_3\text{-}2,6\text{-}Bu^t_2)_2(OEt_2)$ were found to weakly coordinate ether in solution, a property which allowed the complete assignment of the ^1H NMR spectra of the parent dimers and the monomeric diethyl ether complexes. In contrast to the weak coordination of diethyl ether, the iron aryloxides were shown to strongly complex ammonia as exemplified by the four-coordinate $Fe(OC_6H_2\text{-}2,6\text{-}Bu^t_2\text{-}4\text{-}Me)_2(NH_3)_2$, which does not lose diethyl ether in solution or under heating and low pressure. Alternatively, $Fe\{SC_6H_3\text{-}2,6\text{-}(C_6H_3\text{-}2,6\text{-}Pr^i_2)_2\}_2$ was shown to reversibly bind either one or two ammonia molecules, giving the products $Fe\{SC_6H_3\text{-}2,6\text{-}(2,6\text{-}Pr^i_2\text{-}C_6H_3)_2\}_2(NH_3)$ and $Fe\{SC_6H_3\text{-}2,6\text{-}(2,6\text{-}Pr^i_2\text{-}C_6H_3)_2\}_2(NH_3)_2$.

In Chapter 7, work on the design of a 'dispersion effect donor' ligand which is capable of stabilizing a dimeric R_2SnSnR_2 species in solution is described. The vast majority of distannene (R_2SnSnR_2) molecules

possess only weak Sn-Sn interactions and thus dissociate into monomeric stannylene (SnR_2) fragments in solution. However, we show that the reaction of 2 eq. of LiC_6H_2-2,4,6-$Cy_3 \cdot OEt_2$ (Cy = cyclohexyl) with $SnCl_2$ afforded the distannene $\{Sn(C_6H_2\text{-}2,4,6\text{-}Cy_3)_2\}_2$, which remains a dimer in solution even at elevated temperatures. A computational study revealed that the origin of its stability is the London dispersion attraction between multiple close contacts of ligand C-H moieties across the Sn-Sn bond. Whereas the only previous example of a distannene to remain a dimer in solution at ambient temperature was shown to be stabilized by strong covalent interactions between tin atoms, we show here that Sn-Sn interactions in $\{Sn(C_6H_2\text{-}2,4,6\text{-}Cy_3)_2\}_2$ are comparatively weak, and that its stability is mainly due to London dispersion effects.

“I don’t really care very much about the theory.”

-Sir Geoffrey Wilkinson

Acknowledgements

This work is the result of collaboration, and I would thus like to thank the scientists that worked with me to make it possible. I first thank Professor Philip Power. It is an exceptionally rare honor to have worked alongside a scholar of such quality. Although I often had misgivings about my own ability to carry out this work, these concerns were never shared by Professor Power. Moreover, it would not have been possible without the daily (almost without exception!) conversations we have had about chemistry over the last several years. I thank Dr. Jim Fettinger for crystallographic assistance throughout this work. I'm quite certain that I'll never reach his level of mastery, but the quality of hands-on training in practical crystallography that Jim has provided has added a very useful and enjoyable skill to my set. I thank Thien Nguyen for carrying out the work that resulted in the initial isolation of the vanadium oxo complex described in Chapter 3, and for ongoing friendly and scientific exchanges. I thank Dr. Petra Vasko for providing the calculations in Chapter 4, and I thank Dr. Markus Bursch and Professor Stephan Grimme for providing the calculations in Chapter 7. I also extend a special thanks to Dr. Clifton Wagner. His determination of the structure of the anionic vanadium polyhydride in Chapter 4 was the impetus for carrying out the work described therein. Moreover, the field of transition metal chemistry can be something of a lonely and frustrating place in this laboratory, but the frequent conversations we shared about chemistry helped to make the work more exciting and the frustration bearable. I only hope that I have been able to return the favor. Although not mentioned in the text, I deeply thank Tyler and Jim Smithers. This chemistry is exceptionally sensitive to its surrounding environment, and none of the work described herein would have been possible without the bespoke glassware and on-demand repair provided by Tyler and Jim, a fact that has been sadly forgotten by many in this department and elsewhere. It is my sincerest hope that there is an eventual resurgence in the interest in teaching crafts such as these, lest they be entirely lost.

I thank the members of this laboratory generally, and especially (in no particular order), Joshua Queen, who is not only full of good ideas, but is a friend of top-quality to boot; Dr. Chun-Yi Lin, who kept the office lively and the morale high on those otherwise lonely weekends; Dr. David Liptrot, whose "Friday

Arguments" with me proved to be surprisingly good for my health; Alice Phung for sharing her frequent experiments in the kitchen with us; Dr. Kristian Mears, whose kindness and experience have been a very welcome addition to this laboratory; Qihao Zhu, for his friendly demeanor and the very frequent assistance he willingly provided to help me maintain the laboratory; and Wenxing Zou, whose sense of humor never failed to get a laugh out of me. I also thank some of the scholars that visited this laboratory that have left lasting impressions on me: Prof. Sirous Jamali, Dr. Beate Steller, Dr. Hannah Sullivan, and Jan Kulenkampff. The importance of the diversity of thought brought to the laboratory by these people with whom I have formed lasting friendships cannot be overestimated.

I also thank the undergraduate students with whom I have worked over the last several years: Skylar Osler (to whom I owe a special debt of gratitude: the first two years that I spent in graduate school would have been insufferable without your support, encouragement, and friendship), Thien Nguyen, Kelly Gullet, Ella Schwirzke, Nicole Hila Davila, and Sam Cao. Each of you are students of exceptional quality who have provided me with innumerable opportunities to both teach and learn. Seeing your growth as people and scientists has been an immensely enjoyable experience. I hope and believe that we can maintain fruitful relationships as time passes, and I am excited to see how each of your lives unfold.

Lastly, I would like to thank my family for their patience with me during this trying time. I thank my mother and father for their and constantly understanding and positive attitudes while I sought to make this work happen while so far away from home. Above all others, I thank Adrienna Olmos, who has openly urged me never to settle for less at every stage of this entire endeavor, well before even attending university. It was your encouragement that pushed me to make chemistry a serious pursuit, it was your encouragement that convinced me that I could work with a world class scholar, and it is the same that continues to move me forward all these years later. It is no overstatement to say that I would not have been able to do this without your help.

Table of Contents

Chapter 1. General Introduction.

The study of the transition metal bis(trimethylsilyl)amide complexes $M\{N(SiMe_3)_2\}_n$ (M = transition element, n = 1, 2, or 3) began in the early 1960s with the isolation of trivalent $Fe\{N(SiMe_3)_2\}_3$ and divalent $Co\{N(SiMe_3)_2\}_2$ by Bürger and Wannagat.[1] The synthesis of these complexes by metathesis of metal(II) or metal(III) halides with the alkali metal bis(trimethylsilyl)amide salt remains the standard route by which these complexes are prepared.[2,3] These early studies were milestones not only in the development of metal amide chemistry, but of the chemistry of low-coordinate transition metal complexes in general. While the low-coordinate nature of these complexes was initially assumed on the basis of their volatility, it was later confirmed by structural studies of the molecules in the vapor and crystalline phases. Since their initial report, at least one transition metal $M\{N(SiMe_3)_2\}_n$ complex (n = 1, 2, or 3) has been reported for all of the first-row transition elements. This general introduction is a survey of the known, structurally characterized first-row transition metal $M\{N(SiMe_3)_2\}_n$ complexes, their complexes with typical Lewis bases $M\{N(SiMe_3)_2\}_nL_m$ (L = a typical Lewis base, i.e. tetrahydrofuran, pyridine, or trimethylphosphine; m = 1 or 2), and of their reduced salts. Additional mention is made of some heavier transition metal complexes in the rare cases where such complexes have been characterized. Although transition metal amide complexes have been the subject of a 2009 book,[4] substantial progress in this area has been made since that time (in publications included in this dissertation and elsewhere) as described here.

{MN(SiMe$_3$)$_2$}$_4$ Complexes. Neutral, donor-free bis(trimethylsilyl)amide complexes of transition metals in the +1 oxidation state are currently the rarest (and the latest) class of M{N(SiMe$_3$)$_2$}$_n$ complexes to be structurally characterized, with only three examples known (i.e., where M = Co, Ni, Cu). The earliest reported example of these complexes is the copper tetramer [CuN(SiMe$_3$)$_2$]$_4$, which was reported Burger and Wannagat in 1964,[5] and structurally characterized by Cot and coworkers in 1992 (although the connectivity in the structure had been communicated privately by Hursthouse in 1980).[6,7] In this report, the Cu(I) complex was prepared by reaction of LiN(SiMe$_3$)$_2$ with the Cu(II) halide CuCl$_2$. Its synthesis from the reaction of copper(I) chloride and NaN(SiMe$_3$)$_2$ was later reported by Maverick and coworkers in 1998.[8] Similar to the initially reported preparation of the copper tetramer, a 2015 report by this group has shown that [NiN(SiMe$_3$)$_2$]$_4$ was formed by thermal decomposition of the unstable Ni(II) complex Ni{N(SiMe$_3$)$_2$}$_2$, which was prepared by reaction of NiI$_2$ with NaN(SiMe$_3$)$_2$.[5,9] In contrast to the copper and nickel tetramers, the cobalt congener was prepared by Ohki and coworkers in 2016 by reduction of the Co(II) amide Co{N(SiMe$_3$)$_2$}$_2$ with pinacolborane. Here, the tetramer was formed in low (9 %) yield, due to the concomitant formation of a high nuclearity cluster, Co$_7$H$_6${N(SiMe$_3$)$_2$}$_6$, during this synthesis. Each of these complexes adopts the tetrameric structure shown in Figure 1.1 with metals bridged by the amide ligands. The structural parameters are given in Table 1.1 Due to their similar structures, the heavier silver and gold analogues are also included in the table.[10,11] Their structures consist of coplanar M$_4$N$_4$ arrays. Although this array approaches a perfect square, the N-M-N angle deviates slightly from linearity in all cases. In each complex, the torsion angle between the M$_4$ and Si-N-Si planes approaches 90°.

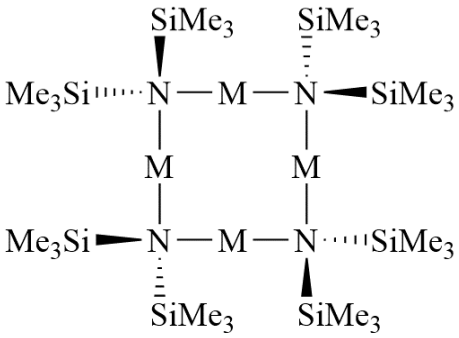

Figure 1.1. General structure of transition metal {MN(SiMe$_3$)$_2$}$_4$ complexes.

Table 1.1. Selected average distances (Å) in $\{MN(SiMe_3)_2\}_4$ complexes.

	M-N	M-M (trans)	M-M (cis)
$\{CoN(SiMe_3)_2\}_4$ [12]	1.952(3)	3.368(2)	2.573(1)
$\{NiN(SiMe_3)_2\}_4$ [9]	1.9158(5)	3.4413(6)	2.4333(3)
$\{CuN(SiMe_3)_2\}_4$ [6]	1.917(5)	3.796(1)	2.685(7)
$\{AgN(SiMe_3)_2\}_4$ [10]	2.155(5)	4.244(1)	3.000(9)
$\{AuN(SiMe_3)_2\}_4$ [11]	2.084(2)	4.2749(3)	3.0228(2)

Table 1.2. Selected average angles (°) in $\{MN(SiMe_3)_2\}_4$ complexes.

	M-M-M	Σ∠ M-M-M	M-N-M	N-M-N	N-N-N	Σ∠ N-N-N	∠M_4-NSi_2
$\{CoN(SiMe_3)_2\}_4$ [12]	90.00(4)	360.0(1)	82.6(1)	172.5(2)	90.2(1)	360.0(5)	94.38(4)
$\{NiN(SiMe_3)_2\}_4$ [9]	90.0(1)	360.00(2)	78.85(3)	168.85(3)	90.00(2)	360.00(7)	93.97(3)
$\{CuN(SiMe_3)_2\}_4$ [6]	90	360	88.9(3)	178.8(4)	90.00(1)	360.00(3)	91.13(1)
$\{AgN(SiMe_3)_2\}_4$ [10]	90.00(3)	360.00(6)	88.5(2)	177.5(2)	90.00(1)	360.00(4)	90.48(1)
$\{AuN(SiMe_3)_2\}_4$ [11]	90	360	93.01(1)	176.99(1)	90.00(1)	360.00(2)	89.36(2)

$M\{N(SiMe_3)_2\}_2$ Complexes. The general properties of $M\{N(SiMe_3)_2\}_2$ complexes (M = Mn, Fe, Co) reflect the behavior of $Mn\{N(SiMe_3)_2\}_2$, which was described exhaustively in a 1979 study by Horvath.[13] The preparation and properties of divalent $M\{N(SiMe_3)_2$ complexes have since been reviewed.[3] As previously mentioned, $Co\{N(SiMe_3)_2\}_2$ was the first reported divalent transition metal complex of the bis(trimethylsilyl)amide ligand.[1] It was later determined that the authors had likely isolated the THF complex $Co\{N(SiMe_3)_2\}_2$·(THF) (vide infra), owing to its synthesis in strongly-coordinating THF solvent.[1,3] Since that report, donor-free $M\{N(SiMe_3)_2\}_2$ complexes have been structurally characterized for manganese,[14] iron,[15] and cobalt.[16] The nickel complex has been reported, but due to its thermal instability it has not been structurally characterized (vide supra).[9] These complexes are

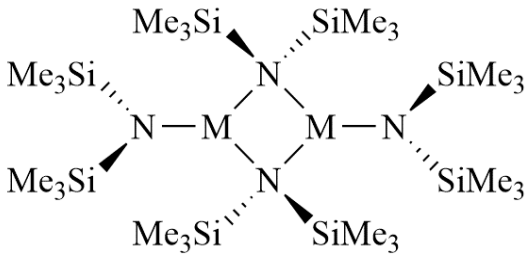

Figure 1.2. General structure of transition metal $[M\{N(SiMe_3)_2\}_2]_2$ complexes.

accessible either by metathesis of a metal(II) halide and an alkali metal bis(trimethylsilyl)amide in a weakly-coordinating solvent (i.e. diethyl ether) or by repeated distillation of the THF complexes.[3] In the original report of the cobalt complex, the authors took the high volatility of the complex as evidence that it was monomeric. However, it has since been shown that these complexes are amide-bridged dimers of the form $[M\{N(SiMe_3)_2\}_2]_2$ in the crystalline phase (although the structure of the nickel congener has yet to be reported).[14–16] The iron complex has been shown to be mostly monomeric in solution,[15] and the manganese, iron, and cobalt complexes were determined by gas electron diffraction to have linear, monomeric structures in the gas phase.[17]

The general structure of the $[M\{N(SiMe_3)_2\}_2]_2$ dimers is shown in Figure 1.2 and selected structural parameters are given in Tables 1.3 and 1.4. The structures consist of planar, amide bridged M_2N_2 cores. In contrast to the nearly orthogonal torsion angles between the M_4 and ligand NSi_2 planes of the $\{MN(SiMe_3)_2\}_4$ tetramers, the bridging and the terminal NSi_2 planes in the $[M\{N(SiMe_3)_2\}_2]_2$ dimers are twisted with respect to the M_2N_2 plane, with torsion angles approaching 60° in all cases. Although the M-M separations of the dimers are somewhat short, they are longer than the M-M(cis) separations in the tetramers. These distances are greater than the sum of the covalent radii of the respective metals (by ca. 0.3-0.5 Å), precluding covalent interaction between the metals. However, the magnetic moments of the complexes were measured to be μ_{eff} = 6.52 μ_B (Mn), 7.04 μ_B (Fe), and 10.16 μ_B (Co).[17] Each of these values are significantly lower than the respective spin-only values, indicating that the high-spin metal ions of the dimers are anti-ferromagnetically coupled.

Table 1.3. Selected average bond distances (Å) in $[M\{N(SiMe_3)_2\}_2]_2$ complexes.

	M-N_t	M-N_b	M-M
$[Mn\{N(SiMe_3)_2\}_2]_2$ [16]	1.952(3)	1.998(2)	2.811(2)
$[Fe\{N(SiMe_3)_2\}_2]_2$ [15]	1.925(2)	2.085(1)	2.663(2)
$[Co\{N(SiMe_3)_2\}_2]_2$ [16]	1.916(4)	2.062(4)	2.583(2)

Table 1.4. Selected average angles (°) in $[M\{N(SiMe_3)_2\}_2]_2$ complexes.

	$M\text{-}N_b\text{-}M$	$N_b\text{-}M\text{-}N_b$	$N_b\text{-}M\text{-}N_t$	$M\text{-}M\text{-}N_t$	$\angle M_2N_2\text{-}N_tSi_2$	$\angle M_2N_2\text{-}N_bSi_2$
$[Mn\{N(SiMe_3)_2\}_2]_2$ [16]	80.62(9)	99.38(1)	130.31(4)	180	69.06(4)	62.96(4)
$[Fe\{N(SiMe_3)_2\}_2]_2$ [15]	79.41(9)	100.68(1)	129.70(1)	180	70.41(9)	64.31(4)
$[Co\{N(SiMe_3)_2\}_2]_2$ [16]	77.59(16)	102.4(2)	128.79(10)	180	71.76(9)	63.50(4)

$M\{N(SiMe_3)_2\}_3$ Complexes. Along with divalent $Co\{N(SiMe_3)_2\}_3$, the trivalent $Fe\{N(SiMe_3)_2\}_3$ was the first reported example of a transition metal complex of the bis(trimethylsilyl)amide ligand.[1] Since this early report, homoleptic three-coordinate $M\{N(SiMe_3)_2\}_3$ complexes have been prepared[1,5,18,19] and structurally characterized[19–24] for the first-row transition metals from scandium to cobalt. These complexes are typically prepared by reaction of the appropriate metal(III) halide with an alkali metal bis(trimethylsilyl)amide salt.[2] However, there are no commercially available or synthetically useful metal(III) halide salts of manganese or cobalt. Thus, the manganese and cobalt complexes of this series were not reported until 1989.[19] These were prepared by the oxidation of the corresponding $M\{N(SiMe_3)_2\}_2$ species by $BrN(SiMe_3)_2$.

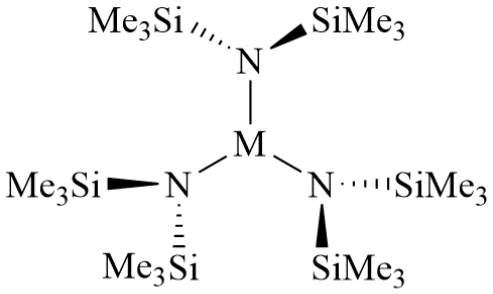

Figure 1.3. General structure of transition metal $M\{N(SiMe_3)_2\}_3$ complexes.

The general structure of the $M\{N(SiMe_3)_2\}_3$ complexes is shown in Figure 1.3. With the exception of the scandium analogue (which has pyramidal geometry at the metal), the transition metal $M\{N(SiMe_3)_2\}_3$ complexes feature trigonal planar MN_3 cores. The NSi_2 planes are twisted with respect to the MN_3 plane (or the N_3 plane, in the case of the scandium analogue) at an angle of ca. 50 °, making these molecules chiral. Thus, $M\{N(SiMe_3)_2\}_3$ complexes crystallize as racemates of their Δ and Λ isomers.

Table 1.5. Selected average distances (Å) angles (°) in M{N(SiMe$_3$)$_2$}$_3$ complexes.

	M-N	N-M-N	Σ∠N-M-N	∠MN$_3$-NSi$_2$
Sc{N(SiMe$_3$)$_2$}$_3$ [25]	2.0522(11)	114.56(4)	343.68(4)	49.43(2)
Ti{N(SiMe$_3$)$_2$}$_3$ [21]	1.937(3)	120	360	49.65(4)
V{N(SiMe$_3$)$_2$}$_3$ [22]	1.9173(11)	120	360	50.30(1)
Cr{N(SiMe$_3$)$_2$}$_3$ [23]	1.890(3)	120	360	51.35(3)
Mn{N(SiMe$_3$)$_2$}$_3$ [19]	1.889(4)	120	360	50.01(4)
Fe{N(SiMe$_3$)$_2$}$_3$ [24]	1.9182(10)	120	360	49.20(3)
Co{N(SiMe)$_2$}$_3$ [19]	1.872(4)	120	360	49.01(6)

M{N(SiMe$_3$)$_2$}$_2$L Complexes. Three-coordinate M{N(SiMe$_3$)$_2$}$_2$L complexes incorporating a single neutral Lewis basic ligand have been reported for the first-row transition metals manganese, iron, cobalt, and nickel. In fact, the original reports of the divalent compounds probably concerned the THF complexes of these metals, given their synthesis in THF solvent.[1,5] Their general structure is shown in Figure 1.4, and selected structural parameters are listed in Table 1.6. The complexes feature MN$_2$L cores with essentially planar coordination geometries around the metal. Because of the structural variability of n-heterocyclic carbene (and similar) ligands, the majority of M{N(SiMe$_3$)$_2$}$_2$L complexes now feature ligands of this type. As the general structures of these complexes do not differ significantly from their counterparts binding more typical Lewis bases (and for the sake of brevity), this survey includes only M{N(SiMe$_3$)$_2$}$_2$L complexes where L = tetrahydrofuran, pyridine, or trimethylphosphine (for manganese, tricyclopentylphosphine). Despite having been characterized in detail the mono(THF) complex Mn{N(SiMe$_3$)$_2$}$_2$(THF),[13] its structure has to date not been reported.

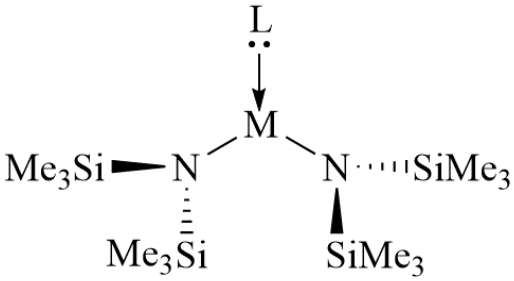

Figure 1.4. General structure of transition metal M{N(SiMe$_3$)$_2$}$_2$L complexes.

Table 1.6. Selected average distances (Å) angles (°) in $M\{N(SiMe_3)_2\}_3L$ complexes.

	M-N	M-L	N-M-N	N-M-L	Σ∠N-M-(N/L)	$\angle MN_2L\text{-}NSi_2$
M = Mn, L = PR_3 (R = cyclopentyl)	2.0167(8)	2.6658(4)	128.10(5)	112.04(4)* 119.73(4)*	359.87(8)	51.41(2)* 81.02(2)*
M = Fe, L = THF [15]	1.915(5)	2.071(6)	144.0(3)	107.9(1)	359.9(4)	67.02(8)
M = Co, L = THF [26]	1.900(1)	2.036(2)	141.86(10)	109.07(5)	360.0(1)	68.55(3)
M = Ni, L = THF	1.861(3)	2.015(4)	140.68(19)	109.59(12)	359.9(3)	69.09(18)* 60.76(17)*
M = Fe, L = py [27]	1.923(3)	2.108(3)	142.9(2)	108.53(7)	360.0(4)	88.87(7)* 77.99(11)* 65.15(11)*
M = Co, L = py [28]	1.904(3)	2.055(5)	140.7(2)	109.7(1)	360.0(2)	67.93(6)
M = Fe, L = PMe_3 [27]	1.935(4)	2.475(2)	139.02(19)	110.49(9)	359.9(3)	55.5(2)
M = Co, L = PMe_3 [26]	1.916(2)	2.9377(7)	138.15(8)	110.91(4)	359.9(1)	85.74(3)

Note: in cases where the range of angles is over 5°, all angles are reported and marked with an asterisk(*)

$M\{N(SiMe_3)_2\}_2L_2$ Complexes. Four-coordinate $M\{N(SiMe_3)_2\}_2L_2$ complexes (L = a neutral Lewis basic ligand) have been reported for the first-row transition metals chromium, manganese, iron, and cobalt. It is noteworthy that divalent $Cr\{N(SiMe_3)_2\}_2$ has been reported only as the donor stabilized complexes $Cr\{N(SiMe_3)_2\}L_2$ (i.e. L = pyridine, tetrahydrofuran), or $Cr\{N(SiMe_3)_2\}L$ (L = the bidentate ligands ethylenediamine or 2,2'-bipyridine). Also of note is that the bis(THF) complex $Mn\{N(SiMe_3)_2\}_2(THF)_2$ is the only structurally characterized THF complex of this type for manganese, while only the mono(THF) complexes are structurally characterized for iron, cobalt, and nickel. The general structure of the complexes featuring unidentate ligands is shown in Figure 1.5, and selected structural

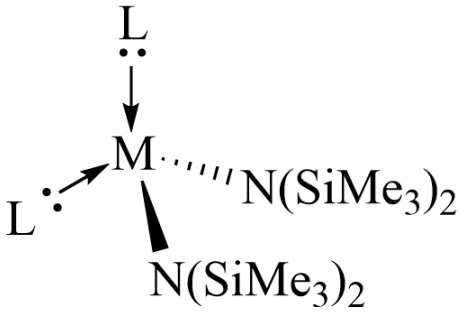

Figure 1.5. General structure of $M\{N(SiMe_3)_2\}_2L_2$ complexes (M = Mn, Fe, Co, Ni; L = THF, pyridine).

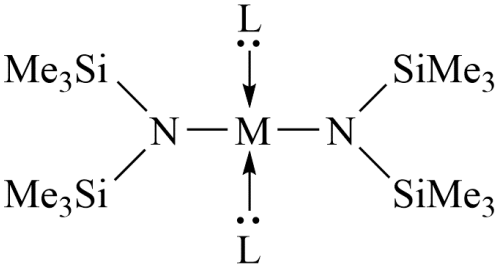

Figure 1.6. Structure of square planar $Cr\{N(SiMe_3)_2\}_2L_2$ complexes (L = THF, pyridine) and $Ni\{N(SiMe_3)_2\}_2L_2$ (L = pyridine)

parameters are listed in Table 1.7. The complexes generally have distorted tetrahedral geometry at the metal except for the complexes of chromium and nickel, which have the square planar geometry at the metal that is typical of four-coordinate transition metal complexes having d^4 or d^8 electron counts.[29,30]

Table 1.7. Selected average distances (Å) angles (°) in square planar $Cr\{N(SiMe_3)_2\}_3L_2$ complexes.

	M-N	M-L	N-M-N	L-M-L	N-M-L
M = Mn, L = THF [31,32]	2.0383(10)	2.2174(9)	131.68(6)	86.42(5)	98.52(5)* 99.29(5)* 117.22(6)* 115.19(6)*
M = Mn, L = py [28]	2.0605(5)	2.269(3)	127.18(3)	86.77(4)	99.47(3)* 100.11(3)* 118.27(3)* 118.64(3)*
M = Fe, L = py [28]	1.9953(6)	2.1921(6)	127.07(4)	86.34(4)	99.97(4)* 11.42(4)* 118.17(4)* 118.31(4)*
M = Co, L = py [28]	1.9833(7)	2.1521(7)	123.17(4)	90.01(4)	101.91(4)* 102.36(4)* 117.40(4)* 117.72(4)*

Note: in cases where the range of angles is over 5°, all angles are reported and marked with an asterisk(*)

Table 1.8. Selected average distances (Å) angles (°) in square planar $Cr\{N(SiMe_3)_2\}_3L_2$ complexes.

	M-N	M-L	N-M-L	Σ∠N-M-(N/L)	$\angle MN_2L_2$-NSi_2
M = Cr, L = THF [29]	2.089(10)	2.090(12)	90	360	73* 56*
M = Cr, L = py [30]	2.042(2)	2.099(3)	90.0(1)	360.0(3)	68.08(5)
M = Ni, L = py [9]	1.942(6)	1.9309(9)	90.00(3)	360.0(1)	66.72(2)

Note: in cases where the range of angles is over 5°, all angles are reported and marked with an asterisk(*)

Anionic [M{N(SiMe$_3$)$_2$}$_2$]$^-$ Complexes. Reduced [M{N(SiMe$_3$)$_2$}$_2$]$^-$ salts have been reported for manganese, chromium, iron, and cobalt.[33,34] These were prepared by reduction of the corresponding neutral M{N(SiMe$_3$)$_2$}$_2$ complex with potassium metal in the presence of either 18-crown-6 or 2.2.2-cryptand. Their general structure is given in Figure 1.7, and selected structural parameters are given in Table 1.9. The structures of these complexes are noteworthy for the strictly linear coordination environment around the transition metal, a characteristic which was shown to result in their single molecule magnet behavior.[33,34] In contrast to these results, the reduction of divalent Mn{N(SiMe$_3$)$_2$}$_2$ with potassium in the presence of 18-crown-6 afforded the dianionic, metal-metal bonded dimer [Mn{N(SiMe$_3$)$_2$}$_2$]$_2^{2-}$.[34] The structure of this complex is shown in Figure 1.8, and selected structural parameters are shown in Table 1.10.

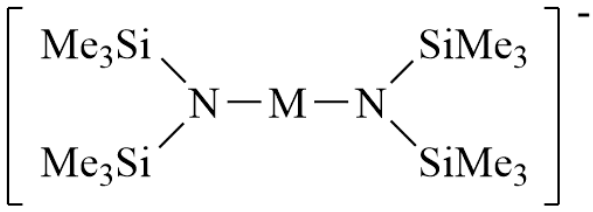

Figure 1.7. General structure of anionic transition metal [M{N(SiMe$_3$)$_2$}$_2$]$^-$ complexes.

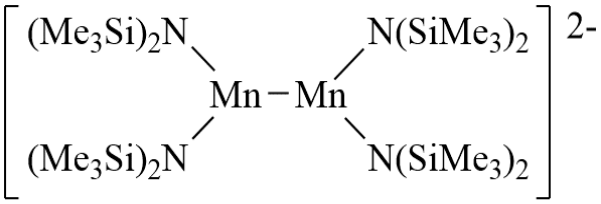

Figure 1.7. Structure of [Mn{N(SiMe$_3$)$_2$}$_2$]$_2^{2-}$

Table 1.9. Selected average distances (Å) angles (°) in [M{N(SiMe$_3$)$_2$}$_2$]$^-$ complexes.

	M-N	N-M-N	∠NSi$_2$-NSi$_2$
M = Cr	2.0649(17)	180	0
M = Fe	1.9213(6)	180	0
M = Co	1.8978(11)	180	0

Table 1.10. Selected average distances (Å) angles (°) in [Mn{N(SiMe$_3$)$_2$}$_2$]$_2^{2-}$.

Mn-Mn	Mn-N	N-Mn-N	∠MnN$_2$-MnN$_2$
2.802(2)	2.144(4)	110.8(2)	20.1(3)

Anionic [M{N(SiMe$_3$)$_2$}$_3$]$^-$ Complexes. [M{N(SiMe$_3$)$_2$}$_3$]$^-$ anions are typically prepared either by treatment of divalent M{N(SiMe$_3$)$_2$}$_2$ with an alkali metal bis(trimethylsilyl)amide in the presence of a crown ether (M = Mn, Fe, Co)[35] or by reduction of trivalent M{N(SiMe$_3$)$_2$}$_3$ with an alkali metal in the presence of a crown ether or cryptand (M = Sc, V, Cr, Fe).[22,25,36] No such complex is known for titanium, despite its attempted preparation using both of these methods.[21,22] The most recently reported example, [Ni{N(SiMe$_3$)$_2$}$_3$]$^-$, was prepared by reaction of NiBr$_2$ with 3 eq. of NaN(SiMe$_3$)$_2$ in the presence of the chelating base PMDETA (*N*,*N*,*N*′,*N*″,*N*″-pentamethyldiethylenetriamine).[37] The general structure of these molecules is shown in Figure 1.8 and selected structural parameters of the anions are given in Table 1.11. Where multiple structures are reported (due to use of a different alkali metal or chelating base), the earliest reported example is used in the table.

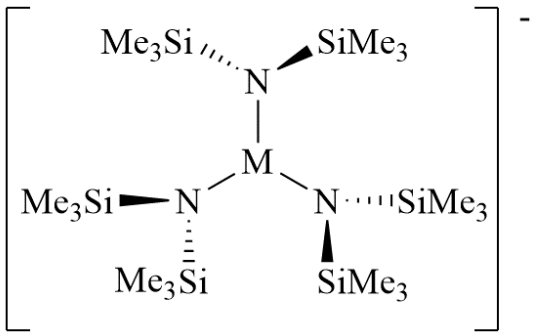

Figure 1.8. General structure of transition metal M{N(SiMe$_3$)$_2$}$_3$]$^-$ complexes.

Table 1.11. Selected average distances (Å) angles (°) in [M{N(SiMe$_3$)$_2$}$_3$]$^-$ complexes.

	M-N	N-M-N	Σ∠N-M-N	Σ∠MN$_3$-NSi$_2$
M = Sc [25]	2.129(8)	119.99(3)	359.9(1)	71.94(3)* 51.38(3)* 46.78(3)*
M = V [21]	2.0254(6)	120.00(3)	360.01(9)	65.11(3)* 50.28(3)* 54.60(3)*
M = Cr [21]	2.0267(7)	123.90(5)* 120.29(5)* 115.81(5)*	360.00(8)	63.49(3)* 49.59(3)* 53.80(3)*
M = Mn [35]	2.070(3)	120.0(1)	360.0(4)	53.56(15)* 54.40(15)* 43.86(14)*
M = Fe [35]	1.984(2)	119.9(1)	360.0(4)	46.19(5)
M = Co [35]	1.976(2)	120.00(6)	360.0(2)	49.40(3)
M = Ni [37]	1.928(2)	120.00(8)	360.0(3)	48.01(5)

Note: in cases where the range of angles is over 5°, all angles are reported and marked with an asterisk(*)

Discussion. The observations made from this survey prompted the reexamination of first-row transition metal bis(trimethylsilyl)amide complexes described in this dissertation. Among these observations, perhaps the most immediately apparent is that, until the publication of the work in this dissertation, no $M\{N(SiMe_3)_2\}_3L_n$ complexes had been reported for the first-row transition elements. This dearth of reported compounds is almost certainly due to the perception of very high steric bulk surrounding the metal atom in $M\{N(SiMe_3)_2\}_3$ complexes. Indeed, the work of Bradley and coworkers in the 1970s indicated that these molecules "are highly reactive but cannot form complexes with donor molecules such as THF due to steric hindrance."[38] However, in Chapter 2 it is shown that through judicious selection of the donor molecule, this is not strictly the case. $Ti\{N(SiMe_3)_2\}_3$ and $V\{N(SiMe_3)_2\}_3$ were shown to form five-coordinate $M\{N(SiMe_3)_2\}_3L_2$ complexes when treated with isocyanide or nitrile bases.[39] This finding suggested to us that other complexes with a coordination number higher than 3 may be accessible despite the considerable steric bulk of $M\{N(SiMe_3)_2\}_3$ complexes. Thus, in Chapter 3, the reactivity of $V\{N(SiMe_3)_2\}_3$ with iodosylbenzene (PhIO) or trimethylsilyl azide (Me_3SiN_3), which are structurally 'slim' reagents similar to the isocyanide and nitrile bases used in Chapter 2, is described. These reactions afforded the oxo complex $V(=O)\{N(SiMe_3)_2\}_3$, the attempted synthesis of which had been reported previously on at least two occasions,[40,41] and the imido complex $V(=NSiMe_3)\{N(SiMe_3)_2\}_3$.[42]

We further noted from this survey that the reduction chemistry of the divalent and trivalent $M\{N(SiMe_3)_2\}_2$ and $M\{N(SiMe_3)_2\}_3$ complexes is quite well explored. However, save for a few reports of the synthesis of iron and cobalt hydrides from the reaction of main group hydrides with $M\{N(SiMe_3)_2\}_2$, little is known about the reduction of these complexes using reagents other than alkali metals.[12,43,44] Work to expand the understanding of this chemistry is described in Chapter 4. It was also noted that while divalent $M\{N(SiMe_3)_2\}_2$ complexes are known for the first-row transition metals from chromium to nickel, no such complexes are reported for titanium or vanadium. Additionally, an established route to trivalent $M\{N(SiMe_3)_2\}_3$ complexes of manganese and cobalt by oxidation of the corresponding divalent $M\{N(SiMe_3)_2\}_3$ by $BrN(SiMe_3)_2$ was reported in 1989.[19] The fate of the bromine in this reaction, however,

was not known. Chapter 5 describes work to resolve these two lingering problems in the early and late first-row transition metal bis(trimethylsilyl)amides.

References.

(1) Bürger, H.; Wannagat, U. Silylamido-Derivate von Eisen Und Kobalt. *Monatsh. Chem.* **1963**, *94*, 1007–1012.

(2) Bradley, D. C.; Copperthwaite, R. G.; Extine, M. W.; Reichert, W. W.; Chisholm, M. H. Transition Metal Complexes of Bis(Trimethyl-Silyl)Amine (1,1,1,3,3,3-Hexamethyldisilazane). In *Inorganic Syntheses*; Inorganic Syntheses; 1978; Vol. 18, pp 112–120.

(3) Andersen, R. A.; Bryan, A. M.; Faust, M.; Power, P. P. Divalent Manganese, Iron, and Cobalt Bis(Trimethylsilyl)Amido Derivatives and Their Tetrahydrofuran Complexes. *Inorg. Synth.* **2018**, *37*, 1–14.

(4) Lappert, M. F.; Power, P. P.; Protchenko, A.; Seeber, A. *Metal Amide Chemistry*; Chichester, U.K. : Wiley: Chichester, U.K., 2009.

(5) Bürger, H.; Wannagat, U. Silylamido-Verbindungen von Chrom, Mangan, Nickel Und Kupfer. *Monatsh. Chem.* **1964**, *95*, 1099–1102.

(6) Miele, P.; Foulon, J. D.; Hovnanian, N.; Durand, J.; Cot, L. Synthesis and Crystal Structure of a Volatile Molecular Precursor of Copper: Copper(I) Bis(Trimethylsilyl)Amide Tetramer. *Eur. J. Solid State Inorg. Chem.* **1992**, *29*, 573–583.

(7) Lappert, M. F.; Power, P. P.; Sanger, A. R.; Srivastava, R. C. *Metal and Metalloid Amides*; Ellis Horwood Ltd.: Chichester, U.K., 1980.

(8) James, A. M.; Laxman, R. K.; Fronczek, F. R.; Maverick, A. W. Phosphorescence and Structure of a Tetrameric Copper(I)−Amide Cluster. *Inorg. Chem.* **1998**, *37*, 3785–3791.

(9) Faust, M.; Bryan, A. M.; Mansikkamäki, A.; Vasko, P.; Olmstead, M. M.; Tuononen, H. M.; Grandjean, F.; Long, G. J.; Power, P. P. The Instability of Ni{$N(SiMe_3)_2$}$_2$: A Fifty Year Old Transition Metal Silylamide Mystery. *Angew. Chem. Int. Ed.* **2015**, *54*, 12914–12917.

(10) Hitchcock, P. B.; Lappert, M. F.; Pierssens, L. J.-M. Synthesis and X-Ray Molecular Structures of the Silver(I) Amides [{Ag[μ-$N(SiMe_3)_2$]}$_4$] and [{Ag[μ-$NCMe_2(CH_2)_3CMe_2$]}$_4$]. *Chem. Commun.* **1996**, No. 10, 1189–1190.

(11) Bunge, S. D.; Just, O.; Rees William S., Jr. [{Au[μ-$N(SiMe_3)_2$]}$_4$]: The First Base-Free Gold Amide. *Angew. Chem. Int. Ed.* **2000**, *39*, 3082–3084.

(12) Ohki, Y.; Shimizu, Y.; Araake, R.; Tada, M.; Sameera, W. M. C.; Ito, J.-I.; Nishiyama, H. $Co_6H_8(P^iPr_3)_6$: A Cobalt Octahedron with Face-Capping Hydrides. *Angew. Chem. Int. Ed.* **2016**, *55*, 15821–15825.

(13) Horvath, B.; Möseler, R.; Horvath, E. G. Manganese(II) Silylamides. *Zeitschrift für Anorg. und Allg. Chemie* **1979**, *450*, 165–177.

(14) Bradley, D. C.; Hursthouse, M. B.; Abdul Malik, K. M.; Möseler, R. The Crystal Molecular Structure of "Bis(Hexamethyldisilylamido) Manganese." *Transit. Met. Chem.* **1978**, *3*, 253–254.

(15) Olmstead, M. M.; Power, P. P.; Shoner, S. C. Three-Coordinate Iron Complexes: X-Ray Structural Characterization of the Iron Amide-Bridged Dimers $[Fe(NR_2)_2]_2$ (R = $SiMe_3$, C_6H_5) and the Adduct $Fe[N(SiMe_3)_2]_2$(THF) and Determination of the Association Energy of the Monomer Fe{$N(SiMe_3)_2$}$_2$ in Solution. *Inorg. Chem.* **1991**, *30*, 2547–2551.

(16) Murray, B. D.; Power, P. P. Three-Coordinate Metal Amides of Manganese(II) and Cobalt(II): Synthesis and X-Ray Structure of the First Tris(Silylamide) of Manganese and the X-Ray Crystal Structures of $[M_2(N(SiMe_3)_2)_4]$ (M = Mn, Co). *Inorg. Chem.* **1984**, *23*, 4584–4588.

(17) Andersen, R. A.; Faegri, K.; Green, J. C.; Haaland, A.; Lappert, M. F.; Leung, W. P.; Rypdal, K.

Synthesis of Bis[Bis(Trimethylsilyl)Amido]Iron(II). Structure and Bonding in $M[N(SiMe_3)_2]_2$ (M = Manganese, Iron, Cobalt): Two-Coordinate Transition-Metal Amides. *Inorg. Chem.* **1988**, *27*, 1782–1786.

(18) Alyea, E. C.; Bradley, D. C.; Copperthwaite, R. G. Three-Co-Ordinated Transition Metal Compounds. Part I. The Preparation and Characterization of Tris(Bistrimethylsilylamido)-Derivatives of Scandium, Titanium, Vanadium, Chromium, and Iron. *J. Chem. Soc. Dalton Trans.* **1972**, No. 14, 1580–1584.

(19) Ellison, J. J.; Power, P. P.; Shoner, S. C. First Examples of Three-Coordinate Manganese(III) and Cobalt(III): Synthesis and Characterization of the Complexes $M[N(SiMe_3)_2]_3$ (M = Mn or Co). *J. Am. Chem. Soc.* **1989**, *111*, 8044–8046.

(20) Ghotra, J. S.; Hursthouse, M. B.; Welch, A. J. Three-Co-Ordinate Scandium(III) and Europium(III); Crystal and Molecular Structures of Their Trishexamethyldisilylamides. *J. Chem. Soc., Chem. Commun.* **1973**, 669–670.

(21) Putzer, M. A.; Magull, J.; Goesmann, H.; Neumüller, B.; Dehnicke, K. Synthese, Eigenschaften Und Kristallstrukturen Der Titan(III)-Amido-Komplexe $Ti[N(SiMe_3)_2]_3$, $[TiCl_2\{N(SiMe_3)_2\}(THF)_2]$ Und $[Na(12\text{-Krone-}4)_2][TiCl_2\{N(SiMe_3)_2\}_2]$. *Chem. Ber.* **1996**, *129*, 1401–1405.

(22) Wagner, C. L.; Phan, N. A.; Fettinger, J. C.; Berben, L. A.; Power, P. P. New Characterization of V{N(SiMe3)2}3: Reductions of Tris[Bis(Trimethylsilyl)Amido]Vanadium(III) and -Chromium(III) To Afford the Reduced Metal(II) Anions $[M\{N(SiMe_3)_2\}_3]^-$ (M = V and Cr). *Inorg. Chem.* **2019**, *58*, 6095–6101.

(23) Köhn, R. D.; Kociok-Köhn, G.; Haufe, M. The Chemistry of 1,3,5-Triazacyclohexane Complexes, 3. High Yield Synthesis of $[Cr\{N(SiMe_3)_2\}_3]$ and Accurate Structure Determination by Cocrystallization with Me_6Si_2. *Chem. Ber.* **1996**, *129*, 25–27.

(24) Hursthouse, M. B.; Rodesiler, P. F. Crystal and Molecular Structure of Tris(Hexamethyldisilylamido)Iron(III). *J. Chem. Soc. Dalton Trans.* **1972**, 2100–2102.

(25) Woen, D. H.; Chen, G. P.; Ziller, J. W.; Boyle, T. J.; Furche, F.; Evans, W. J. Solution Synthesis, Structure, and CO_2 Reduction Reactivity of a Scandium(II) Complex, $\{Sc[N(SiMe_3)_2]_3\}^-$. *Angew. Chem. Int. Ed.* **2017**, *56*, 2050–2053.

(26) Bryan, A. M.; Long, G. J.; Grandjean, F.; Power, P. P. Synthesis, Spectroscopic Characterization, and Determination of the Solution Association Energy of the Dimer $[Co\{N(SiMe_3)_2\}_2]_2$: Magnetic Studies of Low-Coordinate Co(II) Silylamides $[Co\{N(SiMe_3)_2\}_2L]$ (L = PMe_3, Pyridine, and THF) and Related Species That . *Inorg. Chem.* **2013**, *52*, 12152–12160.

(27) Bodenstein, T.; Eichhöfer, A. Magnetic Anisotropy in Trigonal Planar Fe(II) Bis(Trimethylsilyl)Amido Complexes of the Type $[Fe\{N(SiMe_3)_2\}_2L]$—Experiment and Theory. *Dalton Trans.* **2019**, *48*, 15699–15712.

(28) Panda, A.; Stender, M.; Olmstead, M. M.; Klavins, P.; Power, P. P. Reactions of $M\{N(SiMe_3)_2\}_2$ (M=Mn, Fe or Co) with Pyridine and 4,4′-Bipyridyl: Structural and Magnetic Studies. *Polyhedron* **2003**, *22*, 67–73.

(29) Bradley, D. C.; Hursthouse, M. B.; Newing, C. W.; Welch, A. J. Square Planar and Tetrahedral Chromium(II) Complexes; Crystal Structure Determinations. *J. Chem. Soc., Chem. Commun.* **1972**, No. 9, 567–568.

(30) Deng, Y.-F.; Han, T.; Wang, Z.; Ouyang, Z.; Yin, B.; Zheng, Z.; Krzystek, J.; Zheng, Y.-Z. Uniaxial Magnetic Anisotropy of Square-Planar Chromium(II) Complexes Revealed by Magnetic and HF-EPR Studies. *Chem. Commun.* **2015**, *51*, 17688–17691.

(31) Bradley, D. C.; Hursthouse, M. B.; Ibrahim, A. A.; Malik, K. M. A.; Motevalli, M.; Möseler, R.; Powell, H.; Runnacles, J. D.; Sullivan, A. C. Synthesis and Chemistry of the

Bis(Trimethylsilyl)Amido Bis-Tetrahydrofuranates of the Group 2 Metals Magnesium, Calcium, Strontium and Barium. X-Ray Crystal Structures of $Mg[N(SiMe_3)_2]_2{\cdot}2THF$ and Related $Mn[N(SiMe_3)_2]_2{\cdot}2THF$. *Polyhedron* **1990**, *9*, 2959–2964.

(32) Hamilton, C. R.; Baglia, R. A.; Gordon, A. D.; Zdilla, M. J. Synthesis of Tetranuclear, Four-Coordinate Manganese Clusters with "Pinned Butterfly" Geometry Formed by Metal-Mediated N−N Bond Cleavage in Diphenylhydrazine. *J. Am. Chem. Soc.* **2011**, *133*, 4208–4211.

(33) Werncke, C. G.; Bunting, P. C.; Duhayon, C.; Long, J. R.; Bontemps, S.; Sabo-Etienne, S. Two-Coordinate Iron(I) Complex $[Fe\{N(SiMe_3)_2\}_2]^-$: Synthesis, Properties, and Redox Activity. *Angew. Chem. Int. Ed.* **2015**, *54*, 245–248.

(34) Werncke, C. G.; Suturina, E.; Bunting, P. C.; Vendier, L.; Long, J. R.; Atanasov, M.; Neese, F.; Sabo-Etienne, S.; Bontemps, S. Homoleptic Two-Coordinate Silylamido Complexes of Chromium(I), Manganese(I), and Cobalt(I). *Chem. – A Eur. J.* **2016**, *22*, 1668–1674.

(35) Putzer, M. A.; Neumüller, B.; Dehnicke, K.; Magull, J. Synthese Und Kristallstrukturen Der Amido-Komplexe $[Na(12\text{-Krone-}4)_2][M\{N(SiMe_3)_2\}_3]$ Mit M = Mn, Fe Und Co. *Chem. Ber.* **1996**, *129*, 715–719.

(36) Werncke, C. G.; Müller, I. The Ambiguous Behaviour of Diphosphines towards the Quasilinear Iron(I) Complex [Fe(N(SiMe3)2)2]− – between Inertness, P–C Bond Cleavage and C–C Double Bond Isomerisation. *Chem. Commun.* **2020**, *56*, 2268–2271.

(37) Borys, A. M.; Hevia, E. Beyond $Ni\{N(SiMe_3)_2\}_2$: Synthesis of a Stable Solvated Sodium Tris-Amido Nickelate. *Organometallics* **2021**, *40*, 442–447.

(38) Bradley, D. C. Steric Control of Metal Coordination. *Chem. Br.* **1975**, *11*, 393–397.

(39) Stennett, C. R.; Fettinger, J. C.; Power, P. P. Unexpected Coordination Complexes of the Metal Tris-Silylamides $M\{N(SiMe_3)_2\}_3$ (M = Ti, V). *Inorg. Chem.* **2020**, *59*, 1871–1882.

(40) Bürger, H.; Smrekar, O.; Wannagat, U. Silylamido-Verbindungen Des Vanadiums. *Monatshefte für Chemie und verwandte Teile anderer Wissenschaften* **1964**, *95*, 292–302.

(41) Duan, Z.; Schmidt, M.; Young, V. G.; Xie, X.; McCarley, R. E.; Verkade, J. G. The Novel Bis(Oxo-Bridged) Dinuclear Vanadium(IV) Complex $\{(\mu\text{-}O)_2V_2[N(SiMe_3)_2]_4\}$: An Unexpected Reaction Product. *J. Am. Chem. Soc.* **1996**, *118*, 5302–5303.

(42) Stennett, C. R.; Nguyen, T. H.; Power, P. P. Characterization of the "Absent" Vanadium Oxo $V(=O)\{N(SiMe_3)_2\}_3$, Imido $V(=NSiMe_3)\{N(SiMe_3)_2\}_3$, and Imido-Siloxy $V(=NSiMe_3)(OSiMe_3)\{N(SiMe_3)_2\}_2$ Complexes Derived from $V\{N(SiMe_3)_2\}_3$ and Kinetic Study of the Spontaneous Conversion of the Oxo Complex into Its Imido-Siloxy Isomer. *Inorg. Chem.* **2020**, *59*, 11079–11088.

(43) Araake, R.; Sakadani, K.; Tada, M.; Sakai, Y.; Ohki, Y. $[Fe_4]$ and $[Fe_6]$ Hydride Clusters Supported by Phosphines: Synthesis, Characterization, and Application in N_2 Reduction. *J. Am. Chem. Soc.* **2017**, *139*, 5596–5606.

(44) Gieshoff, T. N.; Chakraborty, U.; Villa, M.; Jacobi von Wangelin, A. Alkene Hydrogenations by Soluble Iron Nanocluster Catalysts. *Angew. Chem. Int. Ed.* **2017**, *56*, 3585–3589.

Chapter 2. Unexpected Coordination Complexes of the Metal Tris-silylamides $M\{N(SiMe_3)_2\}_3$ (M = Ti, V)

Cary R. Stennett, James C. Fettinger, and Philip P. Power*

Department of Chemistry, University of California, Davis, One Shields Avenue, Davis, California 95616, United States

This work is dedicated to the memory of Professor Donald C. Bradley.

Reprinted with permission from *Inorg. Chem.* 2020, 59, 3, 1871–1882.

Abstract

The synthesis, molecular structures, and spectroscopic details of a series of isocyanide and nitrile complexes of the early first-row transition metal tris(silyl)amides $M\{N(SiMe_3)_2\}_3$ (M = Ti, V) are reported. Previously, first-row transition metal tris(silyl)amides were thought to be incapable of forming complexes with Lewis bases due to their excessive steric crowding. However, it is now shown that simple treatment of the base-free trisamides with two equivalents of the appropriate base at room temperature result in the formation of the trigonal bipyramidal complexes $Ti\{N(SiMe_3)_2\}_3(1\text{-}AdNC)_2$ (**1**), $Ti\{N(SiMe_3)_2\}_3(CyNC)_2$ (**2**), $Ti\{N(SiMe_3)_2\}_3(Bu^tNC)_2$ (**3**), $Ti\{N(SiMe_3)_2\}_3(PhCN)_2$ (**4**), $V\{N(SiMe_3)_2(1\text{-}AdNC)_2$ (**5**), $V\{N(SiMe_3)_2\}_3(CyNC)_2$ (**6**), $V\{N(SiMe_3)_2\}_3(Bu^tNC)_2$ (**7**), and $V\{N(SiMe_3)_2\}_3(PhCN)_2$ (**8**) which incorporate two donor ligands (1-AdNC = 1-adamantyl isocyanide, CyNC = cyclohexyl isocyanide, Bu^tNC = *tert*-butyl isocyanide, PhCN = benzonitrile). All complexes display a characteristic increase in the frequency of the multiple bonded C-N stretching mode which is observed to be in the range of 2170-2190 cm^{-1} for the isocyanide complexes **1**-**3** and **5**-**7**, and at 2250 cm^{-1} for nitrile complex **8**. This effect was not observed for the titanium nitrile complex **4**, suggesting weak binding of the donor to titanium. Paramagnetic ^{1}H-NMR studies showed these complexes to have detectable, though extremely broadened signals attributable to the trimethylsilyl groups of the amide ligands (δ = ca. 2.8 ppm for titanium isocyanide complexes, ca. 4.5-4.7

ppm for vanadium isocyanide complexes). A variable-temperature ^{1}H-NMR study showed that in solution these complexes exist as mixtures of the five-coordinate species and a putative four-coordinate species coordinating a single Lewis basic ligand. Electronic spectroscopy indicated that the vanadium complexes **5-8** bind the Lewis bases more strongly than the corresponding titanium complexes, where the spectra of complexes **1-4** are essentially identical to the base-free $Ti\{N(SiMe_3)_2\}_3$ at the temperatures and concentrations studied. In contrast to these results, no corresponding complexes were detected for the metal silylamides $M\{N(SiMe_3)_2\}_3$ (M = Cr, Mn, Fe, or Co) when treated with the isocyanide or nitrile bases.

Introduction

Beginning with the pioneering work of Bürger and Wannagat, who described the synthesis of $Fe\{N(SiMe_3)_2\}_3$[1] and $Cr\{N(SiMe_3)_2\}_3$[2] in the early 1960s, three coordinate, homoleptic complexes of the bis(trimethylsilyl)amide ligand have been isolated and structurally characterized for the first-row transition metals from scandium to cobalt,[3–8] as well as for most lanthanides[3,9–15], and the actinides uranium[16] and plutonium.[17] The reactivity of the three-coordinate transition metal complexes of 'hard' ligands including the amides was reviewed by Cummins in the 1990s. This showed that little was known about their reactivity with small molecules,[18] and a more recent book also indicates that their chemistry is not extensively investigated.[19] Early work by Bradley and coworkers on the transition metal amides $M\{N(SiMe_3)_2\}_3$ led to the conclusion that they were unlikely to form complexes with Lewis bases, due to the fact that they "are highly reactive but cannot form complexes with donor molecules such as THF due to steric hindrance,"[20] and the view that "there is little room for additional ligands" in $M\{N(SiMe_3)_2\}_3$ complexes.[21] In contrast, numerous Lewis base complexes of the related divalent bis(trimethylsilyl) amide complexes of the first-row transition metals from chromium to nickel have been isolated and characterized.[22–26]

A few higher coordinate complexes having three $-N(SiMe_3)_2$ ligands have been reported, however. For example, in the case of scandium, the bimetallic dianions containing bridging N_2^{2-}, $\{K(crypt)\}_2([\{(Me_3Si)_2N\}_3Sc]_2\{\mu\text{-}\eta^1\text{:}\eta^1\text{-}N_2\})$,[27] bridging oxalate, $\{K_2(18\text{-c-}6)_3\}\{[\{(Me_3Si)_2N\}_3Sc]_2[\mu\text{-}C_2O_4\text{-}\kappa^1O\text{:}\kappa^1O'']\}$,[28] and the radical CO_2^- complex $[\{(Me_3Si)_2N\}_3Sc(\mu\text{-OCO-}\kappa^1O\text{:}\kappa^1O')K(18\text{-c-}6)]_n$[28] are

known. For titanium, the complex $Ti\{N(SiMe_3)_2\}_3X$, where X = chloro-,[29] fluoro-,[30] or methyl-[31], and for chromium, the four-coordinate nitrosyl complex $Cr\{N(SiMe_3)_2\}_3(NO)$[22] have been prepared. It is worth noting, however, that these species are either charge-separated, or have a different oxidation state from the parent complexes (+4 in the case of titanium, and +2 in the case of chromium). While the three bis(trimethylsilyl)amide ligands obviously generate a very crowded environment at the metal, the above reports indicate that coordination numbers higher than three are possible. Nonetheless, there are no examples of the formation of simple complexes with neutral Lewis base donors, save for an apparently lone report of the coordination of THF, PPh_3, $AsPh_3$, and pyridine by $V\{N(SiMe_3)_2\}_3$ as determined by UV-Vis reflection spectroscopy.[32] However, this disclosure has not been supported by other data.

Scheme 2.1: Synthesis of five-coordinate donor complexes of $M\{N(SiMe_3)_2\}_3$ (M = Ti, V)

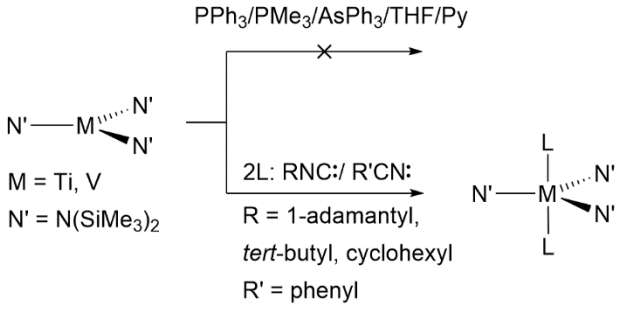

The absence of isolated examples of such complexes seems to corroborate Bradley's early observations. Further, examination of these structures reveals the presence of many close interligand hydrogen-hydrogen contacts, a feature that has been recently shown both experimentally and computationally to indicate the presence of London dispersion force stabilization.[33,34] It is possible that this stabilization contributes to the low reactivity and the absence of a coordination chemistry for these molecules. With these considerations in mind, we sought to examine the ability of these complexes to coordinate simple two-electron donor species. Herein we report the synthesis of a series of five-coordinate isocyanide and nitrile complexes of the early transition metal trisamides $Ti\{N(SiMe_3)_2\}_3$ and $V\{N(SiMe_3)_2\}_3$. They were obtained by direct reaction of the tris amides with the appropriate isocyanide or nitrile (Scheme 2.1). They include $Ti\{N(SiMe_3)_2\}_3(1\text{-}AdNC)_2$ (**1**) (1-Ad = 1-adamantanyl), $Ti\{N(SiMe_3)_2\}_3(CyNC)_2$ (**2**) (Cy = cyclohexyl), $Ti\{N(SiMe_3)_2\}_3(Bu^tNC)_2$ (**3**), $Ti\{N(SiMe_3)_2\}_3(PhCN)_2$ (**4**), $V\{N(SiMe_3)_2\}_3(1\text{-}AdNC)_2$ (**5**), $V\{N(SiMe_3)_2\}_3(CyNC)_2$ (**6**), $V\{N(SiMe_3)_2\}_3(Bu^tNC)_2$ (**7**), and

$V\{N(SiMe_3)_2\}_3(PhCN)_2$ (**8**), which were characterized by X-ray crystallography, as well as by ^{1}H-NMR, infrared, and electronic spectroscopies. In sharp contrast to the formation of the titanium and vanadium complexes **1**-**8**, none of the species $M\{N(SiMe_3)_2\}_3$ (M = Cr, Mn, Fe, or Co), forms a complex with these isocyanide or nitrile Lewis bases.

Experimental Details

General Considerations. All manipulations were performed by using modified Schlenk techniques or in a Vacuum Atmospheres drybox under nitrogen or argon. Solvents were dried and collected using an S2 Grubbs-type[35] solvent purification system (Glass Contour) and degassed using the freeze, pump, thaw method. All physical measurements were obtained under strictly anaerobic and anhydrous conditions. The reported yields are of single-crystalline material, and further workup of the mother liquor was not attempted. IR spectra were recorded as Nujol mulls between CsI windows on a Perkin-Elmer 1430 spectrophotometer. UV-visible spectra were recorded as dilute hexane solutions in 3.5 mL quartz cuvettes using an OLIS modernized Cary 14 UV/VIS/NIR spectrophotometer. Melting points were determined on a Meltemp II apparatus using flame-sealed glass capillaries and are uncorrected. Magnetic susceptibilities were measured by Evans' method in deuterated benzene (**1**-**3**, **4**-**7**) or deuterated toluene (**4**, **8**) and were corrected using the appropriate diamagnetic constants.[36,37] Elemental analyses were not attempted due to the high air and moisture sensitivity of these complexes. Furthermore, high silicon content has been shown elsewhere to result in erroneous values for carbon and nitrogen, making accurate combustion analysis of these complexes difficult or impossible to obtain.[6,15,23] $Ti\{N(SiMe_3)_2\}_3$ and $V\{N(SiMe_3)_2\}_3$ were prepared according to literature procedures.[38] Cyclohexyl isocyanide and benzonitrile were purchased commercially and dried by overnight storage over 4 Å molecular sieves before use. Adamantyl isocyanide and *tert*-butyl isocyanide were prepared by the method of Hofmann[39] and dried by overnight storage as a hexane solution (adamantyl isocyanide) or neat (*tert*-butyl isocyanide) over 4 Å molecular sieves before use.

$Ti\{N(SiMe_3)_2\}_3(1\text{-}AdNC)_2$ (1). $Ti\{N(SiMe_3)_2\}_3$ (0.5 g, 0.95 mmol) and 1-adamantyl isocyanide (0.32 g, 2.0 mmol) were combined in a 50 mL flask. Hexane (ca. 40 mL) was then added to afford a blue-

green colored mixture which was gently heated (50 °C) with stirring until the solids were completely dissolved. The stirring was stopped, and the resulting pale blue solution was stored overnight at room temperature to give 0.38 g (47 %) of complex **1** as blue-green crystals. m.p.: 155 °C (dec.). UV/Vis: λ/nm (ε/M^{-1}): 577 (500), 1206 (200). IR (Nujol) $\tilde{\nu}$ [cm^{-1}] = 2170 (ν_sCN), 400 (shoulder, $\nu_s MN_3$), 380 ($\nu_{as} MN_3$). ^{1}H-NMR (400 MHz, [D_6] benzene, 25 °C): δ = 2.85 (br, $SiMe_3$), 1.18 (m, 1-Ad). μ_{eff}: 2.05 μ_B.

Ti{N(SiMe$_3$)$_2$}$_3$(CyNC)$_2$ (2). Cyclohexyl isocyanide (0.25 mL, 2.0 mmol) was added in one portion by syringe to a stirred solution of Ti{N($SiMe_3$)$_2$}$_3$ (0.5 g, 0.95 mmol) in ca. 15 mL hexanes, resulting in the formation of a green precipitate. The blue-green mixture was gently warmed (50 °C) until the green precipitate was completely dissolved. The stirring was then stopped, and the solution was stored overnight at room temperature to give 0.46 g (65 %) of complex **3** as blue-green crystals. m.p. 137-138 °C (dec.). UV/Vis: λ/nm (ε/M^{-1}): 573 (500), 1211 (200). IR (Nujol) $\tilde{\nu}$ [cm^{-1}] = 2180 (ν_sCN), 400 (shoulder, $\nu_s MN_3$), 380 ($\nu_{as} MN_3$). ^{1}H-NMR (400 MHz, [D_6] benzene, 25 °C): δ = 2.93 (br), 2.37 (br), 1.00 (br, Cy), 0.76 (br, Cy). μ_{eff}: 2.13 μ_B.

Ti{N(SiMe$_3$)$_2$}$_3$(Bu^{t}NC)$_2$ (3). *tert*-Butyl isocyanide (0.25 mL, 2.0 mmol) was added in one portion by syringe to a stirred solution of Ti{N($SiMe_3$)$_2$}$_3$ (0.5 g, 0.95 mmol) in ca. 15 mL hexanes. The resulting blue-green mixture was gently warmed (50 °C) until the green precipitate was completely dissolved. The solution was then filtered to remove a small amount of colorless precipitate. The solution was stored overnight at room temperature to give 0.29 g (44 %) of complex **4** as green crystals. m.p.: 112-113 (dec.). UV/Vis: λ/nm (ε/M^{-1}): 575 (700), 1208 (400). IR (Nujol) $\tilde{\nu}$ [cm^{-1}] = 2170 (ν_sCN), 400 (shoulder, $\nu_s MN_3$), 380 ($\nu_{as} MN_3$). ^{1}H-NMR (400 MHz, [D_6] benzene, 25 °C): δ = 2.76 (br, $SiMe_3$), 1.71 (br, Bu^t). μ_{eff}: 2.14 μ_B.

Ti{N(SiMe$_3$)$_2$}$_3$(PhCN)$_2$ (4). Excess benzonitrile (ca. 20 mL) and blue, crystalline Ti{N($SiMe_3$)$_2$}$_3$ (0.5 g, 0.95 mmol) were reacted neat with stirring, resulting in the formation of a blue-green precipitate. The mixture was gently warmed (ca. 50 °C) to dissolve the formed precipitate. The pale blue solution was then allowed to stand overnight at room temperature to give 0.42 g (60 %) of **4** as blue-green crystals. m.p. 119-121 °C (dec). UV/Vis: λ/nm (ε/M^{-1}): 576 (500), 1200 (200). IR (Nujol) $\tilde{\nu}$ [cm^{-1}] = 2220 (ν_sCN), 410

($\nu_s MN_3$), 370 ($\nu_{as} MN_3$). ^{1}H-NMR (400 MHz, [D_6] benzene, 25 °C): δ = 7.35 (s), 6.91 (s), 6.75 (s) 6.64 (m). μ_{eff}: 2.07 μ_B

V{N(SiMe$_3$)$_2$}$_3$(1-AdNC)$_2$ (5). V{N(SiMe$_3$)$_2$}$_3$ (0.5 g, 0.94 mmol) and 1-adamantyl isocyanide (0.32 g, 2.0 mmol) were combined in a 50 mL flask. Hexane (ca. 40 mL) was then added to afford a blue mixture with a red precipitate. The mixture was gently heated (50 °C) with stirring until the solids were completely dissolved. Stirring was stopped, and the resulting dark blue solution was stored overnight at room temperature to give 0.39 g (49 %) of complex **5** as dark red crystals. m.p. 144 °C (dec.). UV/Vis: λ/nm (ε/M^{-1}) 624 (800), 871 (500 M), 1274 (600 M). IR (Nujol) $\tilde{\nu}$ [cm^{-1}] = 2180 (ν_sCN), 415 ($\nu_s MN_3$), 390 ($\nu_{as} MN_3$). ^{1}H-NMR (400 MHz, [D_6] benzene, 25 °C): δ = 4.68 (br, SiMe$_3$), 1.13 (br, 1-Ad), 0.89 (br, 1-Ad). μ_{eff}: 2.97 μ_B.

V{N(SiMe$_3$)$_2$}$_3$(CyNC)$_2$ (6). Cyclohexyl isocyanide (0.16 mL, 1.3 mmol) was added in one portion by syringe to a stirred, purple-colored solution of V{N(SiMe$_3$)$_2$}$_3$ (0.35 g, 0.66 mmol) in ca. 15 mL hexanes. The solution immediately became blue with concomitant formation of a red precipitate. The mixture was gently warmed (50 °C) until the precipitate completely dissolved. Stirring was then stopped, and the solution was stored at room temperature overnight to give 0.29 g (59 %) of complex **6** as dark red crystals. m.p. 132-134 °C (dec.). UV/Vis: λ/nm (ε/M^{-1}): 621 (700), 865 (500), 1269 (600). IR (Nujol) $\tilde{\nu}$ [cm^{-1}] = 2180 (ν_sCN), 400 ($\nu_s MN_3$), 380 ($\nu_{as} MN_3$). ^{1}H-NMR (300 MHz, [D_6] benzene, 25 °C): δ = 4.61(br, SiMe$_3$), 1.36 (br, Cy), 0.89 (br, Cy). μ_{eff}: 2.99 μ_B.

V{N(SiMe$_3$)$_2$}$_3$(Bu^{t}NC)$_2$ (7). *tert*-Butyl isocyanide (0.25 mL, 2.0 mmol) was added in one portion by syringe to a stirred solution of V{N(SiMe$_3$)$_2$}$_3$ (0.5 g, 0.95 mmol) in ca. 15 mL hexanes. The solution immediately became blue with concomitant formation of a red precipitate. The mixture was gently warmed (50 °C) until the precipitate completely dissolved. The solution was stored overnight at room temperature to give 0.29 g (44 %) of complex **7** as dark red crystals. m.p. 114-116 °C (dec.). UV/Vis: λ/nm (ε/M^{-1}): 626 (700), 871 (400), 1274 (600). IR (Nujol) $\tilde{\nu}$ [cm^{-1}] = 2150 (ν_sCN), 410 ($\nu_s MN_3$), 380 ($\nu_{as} MN_3$).^{1}H-NMR (400 MHz, [D_6] benzene, 25 °C): δ = 4.75 (br, SiMe$_3$), 3.22 (br, Bu^t). μ_{eff}: 3.16 μ_B.

$V\{N(SiMe_3)_2\}_3(PhCN)_2$ (8). Excess benzonitrile (ca. 20 mL) and purple, crystalline $V\{N(SiMe_3)_2\}_3$ (0.5 g, 0.94 mmol) were reacted at room temperature to afford an orange/brown solution with concomitant formation of a red solid. The mixture was gently warmed (50 °C) with stirring to completely dissolve the solid. The orange brown solution was then allowed to stand overnight at room temperature to give 0.39 g (56 %) of **8** as red crystalline rods. m.p. 95-97 °C (dec.). UV/Vis: λ/nm (ε/M^{-1}): 514 (1300), 622 (700), 1275 (700). IR (Nujol) $\tilde{\nu}$ [cm^{-1}] = 2250 (ν_sCN), 410 ($\nu_s MN_3$), 380 ($\nu_{as} MN_3$). ^{1}H-NMR (300 MHz, [D_6] benzene, 25 °C): δ = 3.65 (br, $SiMe_3$). μ_{eff}: 2.76 μ_B.

X-Ray Crystallography. Crystals of **1**-**8** were removed from the reaction flask under a flow of argon and covered in Paratone® oil. Suitable crystals were selected, mounted on a MiTeGen MicroLoop™, and then placed in the cold nitrogen stream of the diffractometer. Data collection was performed at 90 K using Mo Kα radiation (λ = 0.71073 Å) on a Bruker Apex II diffractometer. Absorption corrections were applied using SADABS (or TWINABS in the case of complex **6**).[40,41] The structures were solved by intrinsic phasing using SHELXT[42] and refined by least squares methods using SHELXL.[43] All non-hydrogen atoms were refined anisotropically. Structures of **1**, **2**, and **5** were refined further by determination of the appropriate twin law and subsequent BASF/TWIN refinement.

Results and Discussion

Synthesis. Efforts in this laboratory to isolate and characterize the reported THF, PPh_3, and pyridine complexes[32] of $V\{N(SiMe_3)_2\}_3$ by treatment of the trisamide with an excess of the relevant base yielded the starting amide as the sole vanadium species. Reasoning that the slightly larger covalent radius of titanium[44] might permit the coordination of a donor molecule, the same bases were reacted with $Ti\{N(SiMe_3)_2\}_3$ but no complexation was detected. Further attempts to form complexes were made with the less sterically demanding trimethylphosphine, which also did not yield any new complexes. Bradley and coworkers' $Cr\{N(SiMe_3)_2\}_3(NO)$ complex[22] showed that a small ligand like NO could be accommodated by these trisamides. However, it should be borne in mind that in this complex the chromium was deemed to be in the oxidation state of +2, thereby increasing the effective radius and decreasing the steric crowding at the

metal. In 1995, Westerhausen and coworkers reported the isolation of the second-row metal nitrile complex $Y\{N(SiMe_3)_2\}_3(PhCN)_2$,[45] and the lanthanide isocyanide complex, $Nd\{N(SiMe_3)_2\}_3(CyNC)_2$, was isolated by Edelstein and coworkers in 2002.[46] Although the environment at these metals is far less sterically crowded (Y-N distance: 2.224(6) Å,[45] Nd-N distance: 2.29(2) Å[10]) than that of the corresponding titanium (Ti-N = 1.938(3) Å)[4] or vanadium (V-N = 1.9173(11) Å)[5] complexes, we reasoned that the donor ability and low steric demand of isocyanide or nitrile ligands might permit the isolation of higher coordinate complexes of these trisamides.

The bis-ligand complexes **1**-**8** were obtained in moderate yields by the simple addition of two equivalents (or an excess) of the appropriate isocyanide or nitrile to hexane solutions of either $Ti\{N(SiMe_3)_2\}_3$ or $V\{N(SiMe_3)_2\}_3$. In all cases, upon addition of the base an immediate color change of the solution occurred, followed by precipitation of the product. Gentle heating to ca. 50 °C with stirring dissolved the precipitates that were formed, and overnight storage of the resulting solution at ambient temperature gave the crystalline product in moderate yield. All of the complexes are very air sensitive. It was further observed that the complexes of *tert*-butyl isocyanide are unstable with respect to the loss of base during extended exposure to a glove box atmosphere as evidenced by the slow change in color to that of the donor-free trisamides. Such instability was not observed for the remainder of the complexes. Attempts to isolate the analogous donor complexes of the trisamides of chromium, manganese, iron, and cobalt under the same synthetic conditions were unsuccessful.

Structures. Representative molecular drawings of titanium complexes **1**-**4** are shown in Figure 2.1, and selected bond distances and angles of complexes **1**-**8** are given in Table 1. Like the donor-free silylamide complexes, **1**-**6** and **8** crystallize as racemates, with Λ and Δ enantiomers appearing as pairs in the unit cell. The crystal examined for vanadium complex **7**, however, crystallized in the chiral space group $C222_1$, with the crystal containing only the Λ enantiomer. Though the molecular structures of **1**-**8** share similar geometry, the crystal structures of the Bu^tNC (**3**, **7**) and 1-AdNC (**1**, **5**) derivatives contain crystallographically required symmetry such that only one half of the molecule is required to generate the

whole complex. The remaining molecular structures have no crystallographically required symmetry. Each of the structures has near-ideal trigonal bipyramidal geometry, however, with the sum of the equatorial N-M-N angles between the -$N(SiMe_3)_2$ ligands approaching 360 ° and an average axial E-M-N angle between the axial donor atom and the N of the -$N(SiMe_3)_2$ ligands of approximately 90 °. The three metal-nitrogen amide bonds are lengthened in comparison to those of the donor free complexes by ca. 0.1 Å for the Ti and ca. 0.08 Å for the V complexes, cf. Ti-N = 1.938(3) Å, V-N = 1.9173(11) Å in $M\{N(SiMe_3)_2\}_3$, M = Ti or V. Comparison of the metal amide bond length in the titanium complexes with relevant Ti(III) species is hindered by the scarcity of structurally characterized five-coordinate titanium(III) amide complexes. However, the Ti-N_{amide} bonds of **1**-**4** fall within the range of reported values in the known complexes, cf. the dinitrogen complexes $[\{(Tren^{TMS})Ti^{III}\}_2(\mu\text{-}\eta^1\text{:}\eta^1\text{-}N_2)]$ (1.964 Å, $Tren^{TMS}$ = $N(CH_2CH_2NSiMe_3)_3$), and $[Ti\{PhC(NSiMe_3)_2\}]_2((\mu\text{-}\eta^1\text{:}\eta^1\text{-}N_2)$ (2.164 Å).[47,48] In comparison, structurally characterized five-coordinate vanadium(III) amide complexes are more common, and the V-N_{amide} distances of complexes **5**-**8** fall within the expected range. A slight reduction of the torsion angle between the MN_3 and NSi_2 planes of **1**-**8** (cf. Table 2.1) is observed in comparison to the analogous angles of the donor-free complexes (48.76(4) °, Ti; 49.415(5) °, V).[4,5]

Formation of the trigonal bipyramidal complexes results in the rotation of the -$SiMe_3$ from their positions in the donor-free complexes. However, the D_3 symmetry of the $M\{N(SiMe_3)_2\}_3$ moiety is retained in all cases (Figure 2.2). Retention of D_3 symmetry by the trisamido moiety upon coordination of a donor was previously suggested on the basis of UV-Vis reflection spectroscopy in the case of $V\{N(SiMe_3)_2\}_3$ and its purported complexes with several donors.[32] Though we were unable to independently duplicate these results, the molecular structures of complexes **1**-**8** show that this symmetry is indeed retained upon coordination of Lewis bases by the metal atom in these complexes.

As previously mentioned, the donor-free trisamides contain several close (< 2.4 Å) interligand H-H contacts, which have been shown to be indicative of dispersion force stabilization.[33,34] Though the geometry at the metal is distorted in complexes **1**-**8** from that of the donor-free complexes, several such

contacts remain present in these molecules. The close contacts found in complex **3** are illustrated in Figure 2.3, and similarly positioned contacts are present in each of the complexes **1**-**8**.

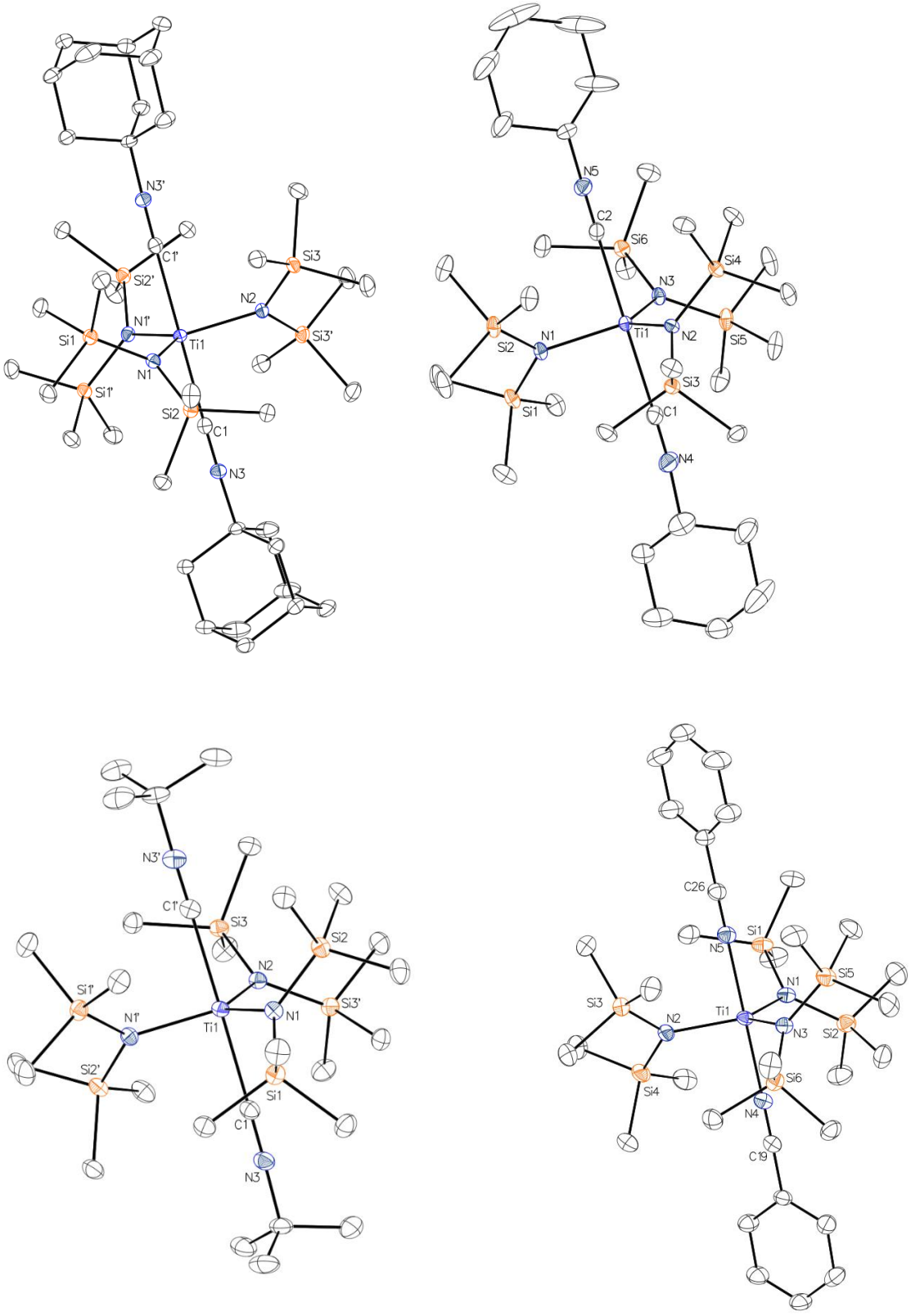

Figure 2.1: Molecular structures of the titanium complexes **1**-**4**, with thermal ellipsoids shown at 30% probability. Hydrogen atoms have been removed for clarity. The corresponding vanadium complexes **5**-**8** are isostructural.

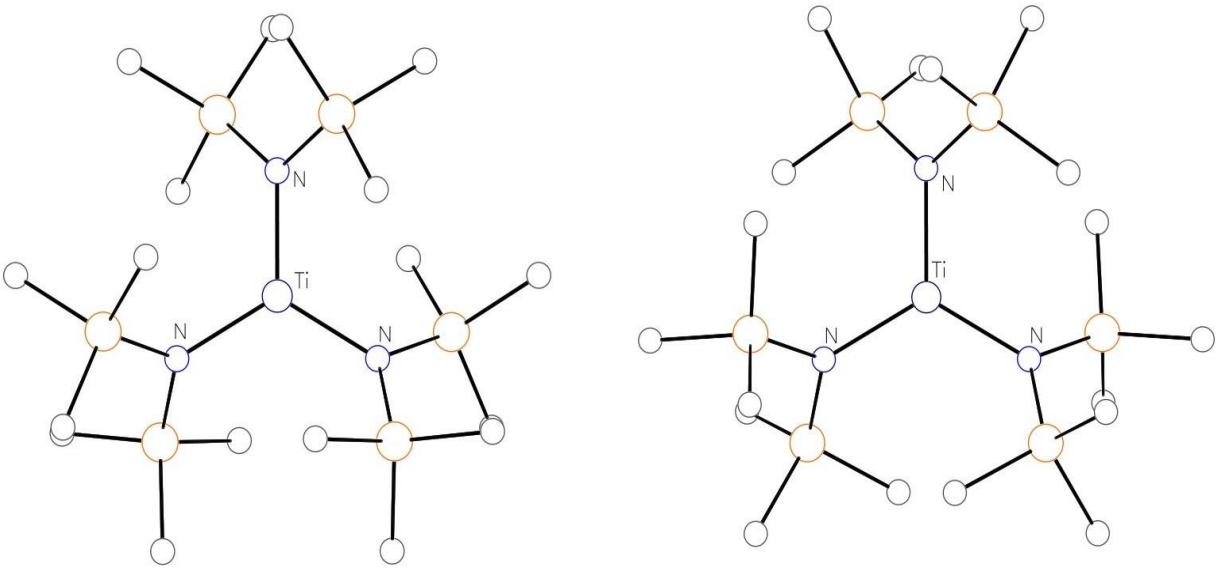

Figure 2.2: View down the 3-fold axis of donor-free Ti{N(SiMe$_3$)$_2$}$_3$ (left) and the (1-Ad)NC complexed Ti{N(SiMe$_3$)$_2$}$_3$ moiety of complex **1** (right, 1-AdNC ligands not shown) showing the change of geometry upon coordination of the two axial ligands. Though the 3-fold rotational symmetry is retained upon complex formation, rotation of the trimethylsilyl groups of the amide results in decreased crowding of the metal by the amide ligands. Similar changes in geometry are found in complexes **2**-**8**. Hydrogen atoms and axial ligands have been removed for clarity.

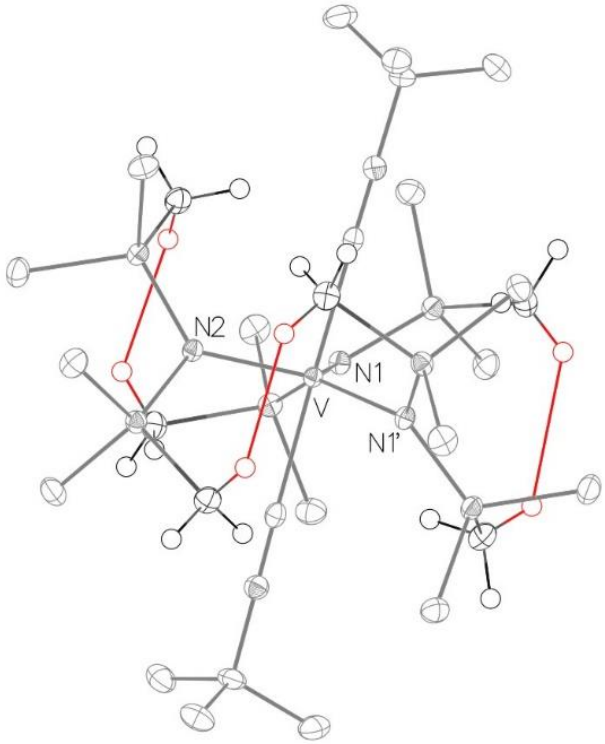

Figure 2.3: Close (< 2.4 A) interligand H-H contacts in complex **3** highlighted in red. Similar contacts are found in complexes **1**, **2**, and **4**-**8**.

Spectroscopy. Important infrared absorbances in complexes **1**-**8** are given in Table 2.2. All complexes possess a characteristic multiple bonded C-N stretching band that is readily identified in the infrared spectrum. For the isocyanide complexes **1**-**3** and **5**-**7**, this band appears in the range 2170-2190 cm^{-1}, which is markedly higher in energy than that of the corresponding stretching band of the free isocyanides (2120-2140 cm^{-1}).[49,50] A similar increase in the energy of this stretching band is seen in the nitrile complex **8** (2250 cm^{-1}) compared with that of the free nitrile (ca. 2220 cm^{-1}).[51] This increase in stretching frequency has been observed previously for positively charged metal ion complexes of isocyanides, and it has been posited to be due to the poor backdonation of electron density from the metal into the molecular orbitals of the isocyanide and the inductive effect of the metal ion.[52] This effect is not observed, however, for the nitrile complex **4**. Here, the characteristic stretching band appears at the same energy as that of the free nitrile, suggesting that the donor is very weakly bound in **4**. As the D_3 symmetry of the $M(NSi_2)_3$ moiety in complexes **1**-**8** is retained upon coordination of the two donors, we anticipated that the M-N_3 stretching bands reported previously for the base-free $M\{N(SiMe_3)_2\}_3$ complexes would be retained in the infrared spectra of these complexes.[5,53] The frequency of the degenerate asymmetric equatorial M-N_3 stretching band in base-free $Ti\{N(SiMe_3)_2\}_3$ (380 cm^{-1}, E) was found to remain unchanged in the titanium isocyanide complexes **1**-**3**. The symmetric M-N_3 stretching band in these complexes appeared at a lower frequency than that found in the base-free complex (420 cm^{-1}, A_1), appearing as a shoulder at ca. 390 cm^{-1}. These bands are unchanged in the titanium nitrile complex **4**, again highlighting the weak coordination of the benzonitrile ligand in this complex. Strangely, equatorial M-N_3 stretching frequencies appear essentially unchanged in the vanadium complexes, except in the cyclohexyl isocyanide complex **6**, where the asymmetric M-N_3 stretching band appears at lower frequency than the base-free complex as a weak shoulder at 400 cm^{-1}.

Proton NMR studies of paramagnetic complexes **1**-**8** (Table 2.3) were undertaken in order to compare the spectra of these complexes with those of the donor-free species. Furthermore, the striking difference in color between the crystalline (dark red) and solution (intense blue) phases of vanadium

complexes **5-7** suggests variable coordination of the isocyanide that should be apparent in the NMR spectra. The spectra of titanium isocyanide complexes **1**-**3** in deuterated benzene show a characteristic broadened signal appearing in the range 2.79 to 2.93 ppm attributable to the trimethylsilyl protons. A broadened multiplet centered at 1.18 ppm was assigned to the protons of the adamantyl moiety in titanium complex **1**, with the trimethylsilyl signal appearing at 2.86 ppm. The spectrum of the titanium complex **2** is somewhat more complicated, with several broadened signals attributable to the cyclohexyl groups appearing at 2.37 (overlapping with the signal of the trimethylsilyl protons at 2.93 ppm), 0.99, 0.76, and 0.14 ppm. We anticipated that the spectrum of the *tert*-butyl isocyanide titanium complex **3** would be much simpler, given that the *tert*-butyl isocyanide group should only provide one signal in the proton NMR spectrum. Indeed, the *tert*-butyl groups of titanium complex **3** do provide the simplest spectrum, showing only a single broadened signal at 1.72 ppm overlapping with the trimethylsilyl signal at 2.79 ppm. Although accurate integration of these signals is not possible due to both the broadening and the overlap of the signals, the signals integrate to a 5:1 ratio, allowing the signal at 2.79 to be assigned to the trimethylsilyl protons. In no case, however, was free isocyanide observed in the spectra of titanium complexes **1**-**3**, indicating complete coordination of the isocyanide in these complexes. The spectra of titanium benzonitrile complex **4** is quite different from that of the isocyanide complexes **1**-**3**. No obvious signal in the range of -150 to 150 ppm could be assigned to the trimethylsilyl groups of the complex. Integration of the broadened signals found at 6.69 and 6.87 ppm (which are very near the chemical shifts of free benzonitrile) suggests that these signals are due to the benzonitrile protons. A large excess (70 equivalents) of benzonitrile was added to a sample of **4** in an attempt to observe this complex in solution, but no new signals attributable to the trimethylsilyl protons were observed. In no case was the presence of base-free $Ti\{N(SiMe_3)_2\}_3$ detected in the proton NMR spectra of complexes **1**-**4**. However, it is noteworthy, that the spectrum of the base-free titanium complex is unusually complicated when compared to that of the corresponding vanadium species, and no signal could clearly be attributed to the trimethylsilyl groups of the free $Ti\{N(SiMe_3)_2\}_3$ species. (see SI).

Overall, the vanadium isocyanide complexes **5-7** have proton NMR spectra that are similar to the spectra of titanium isocyanide complexes **1-3,** with extremely broad signals centered at ca. 4.5-4.7 ppm attributable to the trimethylsilyl protons, and less broadened signals attributable to the isocyanide ligands. The recently reported proton NMR spectrum of donor-free $V\{N(SiMe_3)_2\}_3$ displays a broad singlet at 19.49 ppm in deuterated toluene,[5] and we found the corresponding signal appears at 19.90 ppm in deuterated benzene (see SI). The spectra of isocyanide complexes **5-7** reveal an absence of this signal and the appearance of the characteristic broadened signal at 4.5-4.7 ppm. These data suggest that there is no free $V\{N(SiMe_3)_2\}_3$ in solution, though it is unclear from these experiments the extent to which the metal coordinates the isocyanide ligand, as no signals are present at room temperature that would suggest multiple distinct metal amide complexes in solution. In the case of cyclohexyl isocyanide complex **6**, signals at 0.89 and 1.36 ppm seem to indicate the presence of free isocyanide, though the integration of these multiplets does not corroborate this notion (the intensities of these signals are essentially opposite to those in the corresponding signals of the free isocyanide). A somewhat clearer picture is shown by the benzonitrile complex **8**. Here the signal for the donor-free $V\{N(SiMe_3)_2\}_3$ complex is observed, along with a very broad signal centered at ca. 3.7 ppm. These data suggest the presence of at least one and probably two metal amide complexes in solution, though the equilibrium constants for this reaction are currently unclear. Strangely, no signals corresponding to free benzonitrile were observed, further complicating the unusual solution behavior of these complexes. However, addition of an excess (70 equivalents) of benzonitrile to a sample of **8** results in the expected disappearance of the signal for donor-free $V\{N(SiMe_3)_2\}_3$, leaving only the trimethylsilyl proton signals of complex **8** visible in the spectrum.

To rationalize the solution behavior of these complexes, variable-temperature proton NMR spectroscopy was performed on vanadium complex **5** (Figure 2.4). The room temperature spectrum of **5** in deuterated toluene shows a heavily broadened signal centered at ca. 4.6 ppm (see SI). This signal sharpens

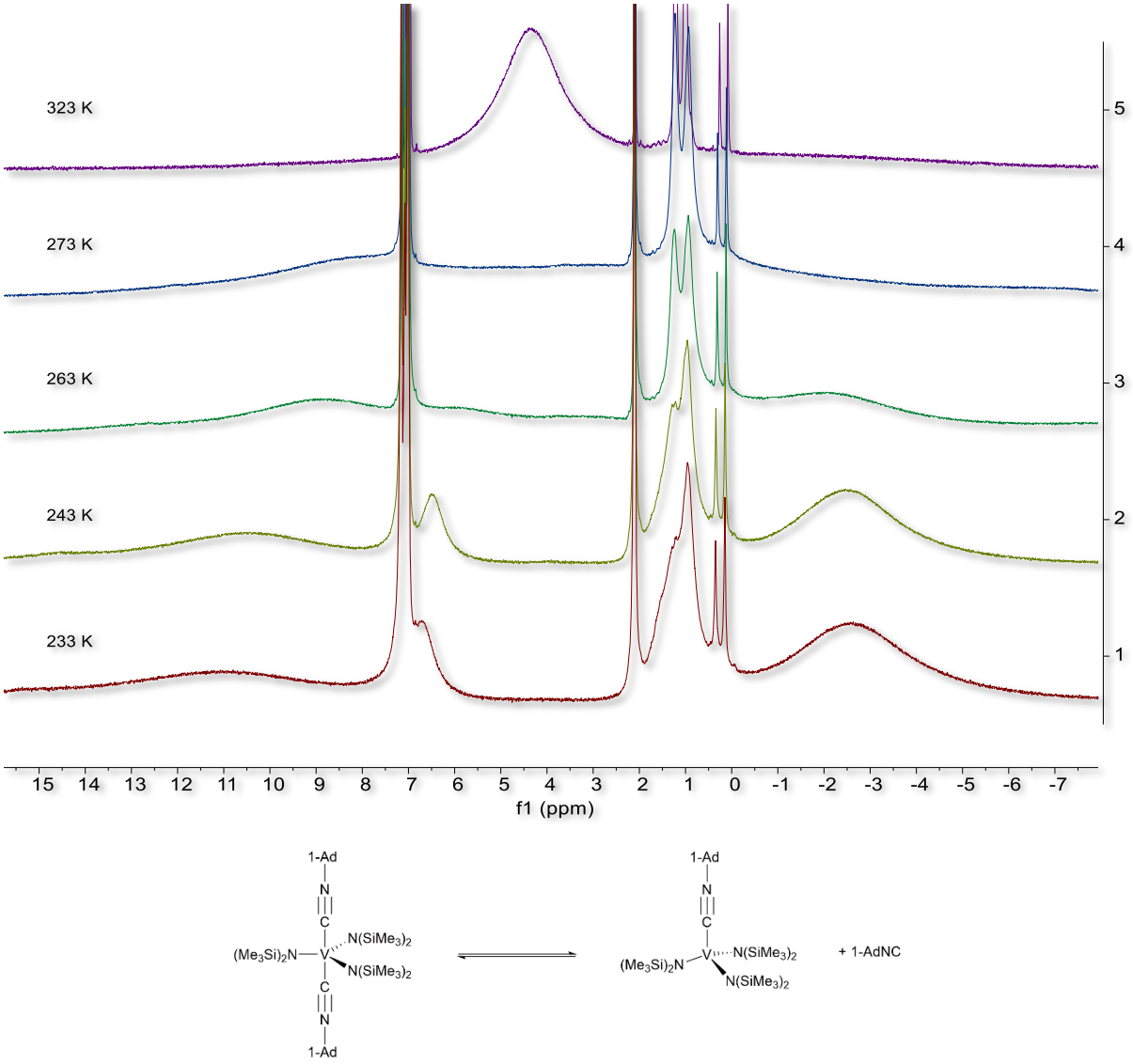

Figure 2.4: Variable-temperature proton NMR spectra of complex **5**. At 323 K, fast exchange between five-coordinate **5** and the proposed species formed upon loss of an isocyanide ligand gives a single signal for the trimethylsilyl protons at ca. 4.6 ppm. Cooling to 243 K resolves this signal into three new signals at 10.5, 6.5, and -2.5 ppm.

significantly upon warming the sample to 323 K. Cooling to 273 K results in broadening of the signal, but continued cooling shows the appearance of several new spectral features. At 243 K, three distinct signals become apparent at -2.5, 6.5, and 10.5 ppm. These spectra do not show the presence of any donor-free tris(silyl)amide, which has a characteristic signal at 28.5 ppm in deuterated toluene at 233 K (see SI). From these data, it appears that complex **5** exists in solution as a mixture of five-coordinate complex **5**, which should have a single absorption in the proton NMR, and a four-coordinate complex binding only one

isocyanide ligand, which should have distinct signals for protons that are distal and proximal to the isocyanide ligand. Broadening and overlap of these signals precludes their integration, making their assignment difficult. In an attempt circumvent this difficulty, ten equivalents of 1-adamantyl isocyanide were added to a sample of **5**. No obvious change in the spectrum was observed at room temperature. Upon cooling to 243 K, the same three broad signals are found in the spectrum that were seen in the spectrum of untreated **5** (see SI). These signals appear in the same 1:2:2 intensity ratio as shown in the 243 K spectrum in Figure 4, indicating no appreciable change in the concentration of either species present in solution upon addition of excess isocyanide. Of note, however, is the fact that a large amount of crystalline **5** formed during the process of cooling the sample complicates any quantitative information that can be gathered by these methods. Despite this, these data offer some insight into the unusually high magnetic moments that were measured for complexes **1**-**3** (> 2.0 μ_B) and **5**-**7** (ca. 3.0 μ_B). In all cases, the diamagnetic corrections used in calculating the magnetic moment were determined assuming the formula of the five-coordinate structures. The magnetic moments determined are therefore artificially high, as both the molar mass and the diamagnetic constants of the species in solution must be significantly lower than what is implied by the structure found in the solid state.

The room temperature electronic spectra of complexes **1**-**8** versus that of the base-free trisamides are shown in Figure 2.5. The spectra of the titanium complexes **1**-**4** show only the presence of the base-free trisamide, indicating that $Ti\{N(SiMe_3)_2\}_3$ does not complex these bases at room temperature at the low concentrations studied (ca. 0.4 mM). For the vanadium isocyanide complexes **5**-**7**, however, the electronic spectra show strong coordination in solution at these concentrations. No base-free $V\{N(SiMe_3)_2\}_3$ is apparent in the room temperature spectra of vanadium isocyanide complexes **5-7,** and each spectrum displays new absorbances at ca. 620 and 870 nm. While the absence of any absorbances attributable to base-free $V\{N(SiMe_3)_2\}_3$ in the spectra indicate that any vanadium species in solution is coordinated by the corresponding isocyanide, these spectra do not conclusively establish whether the vanadium coordinates one or two isocyanide ligands in solution. The spectrum of the vanadium benzonitrile complex **8** is unique,

in that it contains absorbances that are attributable to both the base-free vanadium complex, as well as that of benzonitrile complex **8**, indicating partial dissociation of the nitrile ligands. However, the room temperature spectrum of **8** contains overlapping absorbances, making assignment of these absorbances

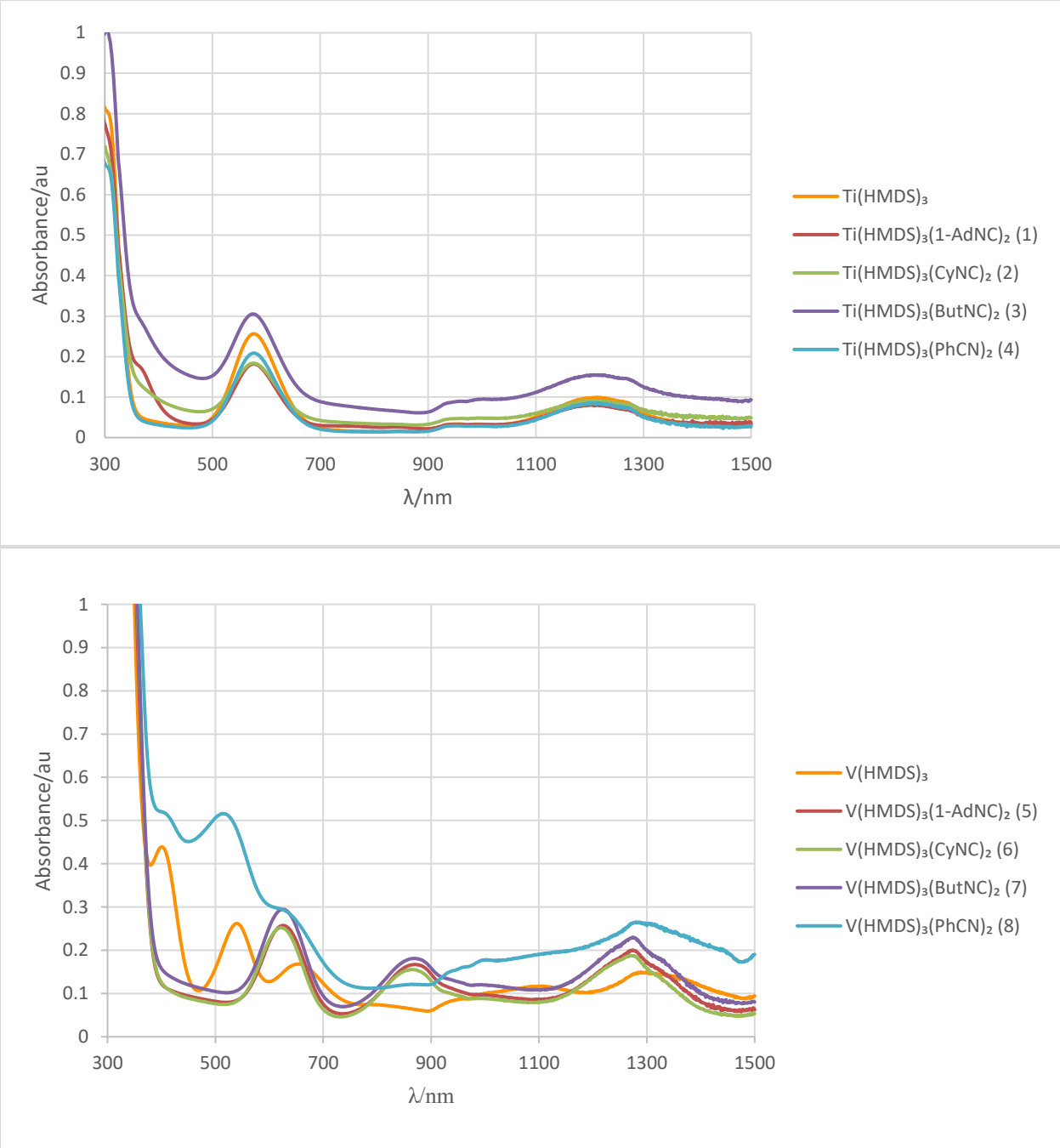

Figure 2.5: Top: room temperature electronic spectra of titanium complexes **1-4** and Ti{N(SiMe$_3$)$_2$}$_3$ in hexane indicating that the isocyanide or nitrile ligands are essentially fully dissociated in solution. Bottom: room temperature electronic spectra of complexes **5-8** and V{N(SiMe$_3$)$_2$}$_3$ in hexane indicating ligand complexation in all cases. (HMDS = -N(SiMe$_3$)$_2$).

difficult. The number and energy of the absorbances found in both the titanium and vanadium complexes are consistent with the d-d transitions expected for a ^2D (d^1, Ti^{3+}) or ^3F (d^2, V^{3+}) ground state term in a ligand field of D_3 symmetry. In this ligand environment, the ^2D ground state term of the titanium complexes splits into $^2A_1$, ^2E, and ^2E, and the ^3F ground state term of the vanadium complexes splits into ^3E, $^3A_2$, ^3E, and ($^3A_1$, $^3A_2$), in order of increasing energy.[54,55] These data indicate that, at least for the vanadium complexes, the spectra of the solution species are consistent with the trigonal bipyramidal structure found in the solid state.

Studies with later M{N(SiMe$_3$)$_2$}$_3$ complexes. Although the isolation of Lewis base complexes **1**-**8** illustrates that while the environment in M{N(SiMe$_3$)$_2$}$_3$ complexes is quite crowded, the absence of a coordination chemistry describing M{N(SiMe$_3$)$_2$}$_3$ complexes of early first-row transition metals cannot be rationalized on the basis of steric considerations alone. Given the trend of decreasing covalent radii with increasing atomic number of the first-row transition elements, it is expected that this steric crowding should increase in the later transition elements. However, the experimental data suggest that the difference in steric crowding at these metals is quite small, with Ti-N, V-N, Cr-N, and Fe-N distances in the donor free M{N(SiMe$_3$)$_2$}$_3$ complexes of 1.938(3), 1.9173(11), 1.889(2), and 1.907(3) Å, respectively.[5] Despite this, the same experimental conditions that yielded complexes **1**-**8** failed to yield any new corresponding complexes of the remaining first-row M{N(SiMe$_3$)$_2$}$_3$ complexes (M = Cr, Mn, Fe, and Co). Examination of the electronic structures of these complexes suggests that formation of donor complexes of these later molecules may be prevented by ligand field effects. In the trigonal planar field of M{N(SiMe$_3$)$_2$}$_3$ complexes, the d-orbital splittings are a_1 (d_z^2), e (d_{xz}, d_{yz}), and e ($d_{x^2-y^2}$, d_{xy}) in order of increasing energy.[20] For Ti(III), the a_1 orbital is singly occupied, and for V(III), there is one electron each in the a_1 and e orbitals. Thus, in both cases, low-lying unoccupied e orbitals are available to accept the incoming electron pairs of the ligands. Beginning with Cr(III) however, the e orbital becomes doubly occupied, leaving no low-lying vacant orbital available to accept the ligand lone pairs (the remaining set of e orbitals are relatively high in

energy)[20] for chromium(III) or in the subsequent M(III) ions. Consequently, it is expected that these later metals will have greater difficulty in forming donor complexes similar to those of complexes **1**-**8.**

Conclusion.

The synthesis of complexes titanium complexes **1**-**4** and vanadium complexes **5**-**8** conclusively shows that metal trisamides of the form $M\{N(SiMe_3)_2\}_3$ can form isolable Lewis base complexes, despite conflicting early reports. Efforts to prepare the earlier reported complexes of vanadium with PPh_3, $AsPh_3$, or THF were unsuccessful, but the high steric crowding found in $M\{N(SiMe_3)_2\}_3$ (M = Ti or V) does not preclude complex formation with isocyanide or nitrile ligands. Further, examination of the structures of these molecules reveals many close contacts between C-H moieties in both the base-free molecules and in the Lewis base complexes. The extent to which these contacts stabilize these molecules is currently under investigation. The spectroscopic studies reported herein do not conclusively show the extent to which these bases coordinate the metal amides in solution, although low temperature ^{1}H-NMR shows that these complexes are in equilibrium between the isolated five-coordinate species and a four-coordinate species formed upon loss of one Lewis base. The electronic spectra clearly show that the vanadium trisamide more strongly binds in solution the isocyanide and nitrile bases than the corresponding titanium trisamide, a difference for which we currently have no cogent explanation. Nonetheless, the complexes isolated here show that the coordination chemistry and reactivity of these classic metal amides remains poorly understood, and further studies are warranted.

Associated Content.

Supporting information

The Supporting Information, including spectra (NMR, infrared, UVVis), crystallographic data, and photographs of bulk material is available free of charge on the ACS Publications website at https://doi.org/10.1021/acs.inorgchem.9b03084. CCDC 1958662−1958669 contain the supplementary crystallographic data for this work. These data can be obtained free of charge via

www.ccdc.cam.ac.uk/data_request/cif, or by emailing data_request@ccdc.cam.ac.uk, or by contacting The Cambridge Crystallographic Data Centre, 12 Union Road, Cambridge CB2 1EZ, UK; fax: + 44 1223 336033.

Author Information.

Corresponding authors

*pppower@ucdavis.edu

ORCID

Cary R. Stennett: 0000-0002-2727-5747

James C. Fettinger: 0000-0002-6428-4909

Philip P. Power: 0000-0002-6262-3209

Notes

The authors declare no competing financial interest.

Acknowledgements

We wish to acknowledge the US National Science Foundation (CHE-1565501) for support of this work and for the purchase of a dual-source X-ray diffractometer (CHE-0840444).

Table 2.1: Selected bond distances (Å) and angles (°) for complexes 1-8. (E = carbon or nitrogen from an isocyanide (**1**-**3** and **5**-**7**) or nitrile ligand (**4** and **8**).

	$Ti\{N(SiMe_3)_2\}_3(1\text{-}AdNC)_2$ (1)	**$Ti\{N(SiMe_3)_2\}_3(CyNC)_2$ (2)**	**$Ti\{N(SiMe_3)_2\}_3(Bu^tNC)_2$ (3)**	**$Ti\{N(SiMe_3)_2\}_3(PhCN)_2$ (4)**	**$V\{N(SiMe_3)_2\}_3(1\text{-}AdNC)_2$ (5)**	**$V\{N(SiMe_3)_2\}_3(CyNC)_2$ (6)**	**$V\{N(SiMe_3)_2\}_3(Bu^tNC)_2$ (7)**	**$V\{N(SiMe_3)_2\}_3(PhCN)_2$ (8)**
M-N (avg)	2.042(1)	2.040(1)	2.0425(8)	2.0328(7)	2.005(1)	2.005(2)	2.004(1)	1.9946(8)
$M\text{-}E_{ax}$ (avg)	2.2864(13)	2.293(2)	2.2944(16)	2.2044(8)	2.2059(18)	2.198(2)	2.2076(17)	2.1361(9)
N-M-N (avg)	119.67(4)	119.99(5)	120.00(3)	120.00(3)	120.00(3)	119.99(7)	120.00(4)	120.00(3)
∑ N-M-N	360.00(7)	359.99(16)	360.01(8)	359.99(8)	360.09(13)	359.99(20)	360.00(11)	360.00(10)
E_{ax}-M-N (avg)	90.00(3)	89.99(4)	89.99(7)	89.99(2)	90.00(4)	90.00(5)	90.00(2)	90.01(2)
$E_{ax}\text{-}M\text{-}E_{ax}$	179.98(7)	177.71(12)	178.46(7)	179.00(4)	179.94(10)	179.23(13)	178.94(10)	179.01(5)
$\angle MN_3\text{-}NSi_2$ (avg)	47.31(2)	46.55(3)	46.64(2)	47.97(2)	47.92(2)	47.48(4)	47.52(2)	48.77(2)

Table 2.2: Selected infrared stretching energies (cm^{-1}) of complexes 1-8

	Ti{N(SiMe$_3$)$_2$}$_3$ (1-AdNC)$_2$ (1)	**Ti{N(SiMe$_3$)$_2$}$_3$ (CyNC)$_2$ (2)**	**Ti{N(SiMe$_3$)$_2$}$_3$ (Bu^{t}NC)$_2$ (3)**	**Ti{N(SiMe$_3$)$_2$}$_3$(PhCN)$_2$ (4)**	**V{N(SiMe$_3$)$_2$}$_3$ (1-AdNC)$_2$ (5)**	**V{N(SiMe$_3$)$_2$}$_3$ (CyNC)$_2$ (6)**	**V{N(SiMe$_3$)$_2$}$_3$ (Bu^{t}NC)$_2$ (7)**	**V{N(SiMe$_3$)$_2$}$_3$ (PhCN)$_2$ (8)**
ν_sCN	2170	2180	2170	2220	2180	2180	2150	2250
ν_sMN$_3$	400	400	400	410	415	400	410	410
ν_{as}MN$_3$	380	380	380	370	390	380	380	380

Table 2.3. ^{1}H-NMR absorbances (ppm) of the trimethylsilyl protons of complexes 1-8

	Ti{N(SiMe$_3$)$_2$}$_3$ (1-AdNC)$_2$ (1)	**Ti{N(SiMe$_3$)$_2$}$_3$ (CyNC)$_2$ (2)**	**Ti{N(SiMe$_3$)$_2$}$_3$ (Bu^{t}NC)$_2$ (3)**	**Ti{N(SiMe$_3$)$_2$}$_3$(PhCN)$_2$ (4)**	**V{N(SiMe$_3$)$_2$}$_3$ (1-AdNC)$_2$ (5)**	**V{N(SiMe$_3$)$_2$}$_3$ (CyNC)$_2$ (6)**	**V{N(SiMe$_3$)$_2$}$_3$ (Bu^{t}NC)$_2$ (7)**	**V{N(SiMe$_3$)$_2$}$_3$ (PhCN)$_2$ (8)**
δSiMe$_3$	2.85	2.93	2.76	-	4.68	4.61	4.75	3.65

References.

(1) Bürger, H.; Wannagat, U. Silylamido-Derivate von Eisen Und Kobalt. *Monatsh. Chem.* **1963**, *94*, 1007–1012.

(2) Bürger, H.; Wannagat, U. Silylamido-Verbindungen von Chrom, Mangan, Nickel Und Kupfer. *Monatsh. Chem.* **1964**, *95*, 1099–1102.

(3) Ghotra, J. S.; Hursthouse, M. B.; Welch, A. J. Three-Co-Ordinate Scandium(III) and Europium(III); Crystal and Molecular Structures of Their Trishexamethyldisilylamides. *J. Chem. Soc., Chem. Commun.* **1973**, No. 18, 669–670.

(4) Putzer, M. A.; Magull, J.; Goesmann, H.; Neumüller, B.; Dehnicke, K. Synthese, Eigenschaften Und Kristallstrukturen Der Titan(III)-Amido-Komplexe $Ti[N(SiMe_3)_2]_3$, $[TiCl_2\{N(SiMe_3)_2\}(THF)_2]$ Und $[Na(12\text{-Krone-}_4)_2][TiCl_2\{N(SiMe_3)_2\}_2]$. *Chem. Ber.* **1996**, *129*, 1401–1405.

(5) Wagner, C. L.; Phan, N. A.; Fettinger, J. C.; Berben, L. A.; Power, P. P. New Characterization of $V\{N(SiMe_3)_2\}_3$: Reductions of Tris[Bis(Trimethylsilyl)Amido]Vanadium(III) and -Chromium(III) To Afford the Reduced Metal(II) Anions $[M\{N(SiMe_3)_2\}_3]^-$ (M = V and Cr). *Inorg. Chem.* **2019**, *58*, 6095–6101.

(6) Köhn, R. D.; Kociok-Köhn, G.; Haufe, M. The Chemistry of 1,3,5-Triazacyclohexane Complexes, 3. High Yield Synthesis of $[Cr\{N(SiMe_3)_2\}_3]$ and Accurate Structure Determination by Cocrystallization with Me_6Si_2. *Chem. Ber.* **1996**, *129*, 25–27.

(7) Ellison, J. J.; Power, P. P.; Shoner, S. C. First Examples of Three-Coordinate Manganese(III) and Cobalt(III): Synthesis and Characterization of the Complexes $M[N(SiMe_3)_2]_3$ (M = Mn or Co). *J. Am. Chem. Soc.* **1989**, *111*, 8044–8046.

(8) Hursthouse, M. B.; Rodesiler, P. F. Crystal and Molecular Structure of Tris(Hexamethyldisilylamido)Iron(III). *J. Chem. Soc. Dalton Trans.* **1972**, No. 19, 2100–2102.

(9) S. Rees William, J.; Just, O.; S. Van Derveer, D. Molecular Design of Dopant Precursors for Atomic Layer Epitaxy of SrS:Ce. *J. Mater. Chem.* **1999**, *9*, 249–252.

(10) Andersen, R. A.; Templeton, D. H.; Zalkin, A. Structure of Tris(Bis(Trimethylsilyl)Amido)Neodymium(III), $Nd[N(Si(CH_3)_3)_2]_3$. *Inorg. Chem.* **1978**, *17*, 2317–2319.

(11) Brady, E. D.; Clark, D. L.; Gordon, J. C.; Hay, P. J.; Keogh, D. W.; Poli, R.; Scott, B. L.; Watkin, J. G. Tris(Bis(Trimethylsilyl)Amido)Samarium: X-Ray Structure and DFT Study. *Inorg. Chem.* **2003**, *42*, 6682–6690.

(12) Hitchcock, P. B.; Hulkes, A. G.; Lappert, M. F.; Li, Z. Cerium(III) Dialkyl Dithiocarbamates from $[Ce\{N(SiMe_3)_2\}_3]$ and Tetraalkylthiuram Disulfides, and $[Ce(K_2\text{-}S_2CNEt_2)_4]$ from the Ce^{III} Precursor; Tb^{III} and Nd^{III} Analogues. *Dalton Trans.* **2004**, No. 1, 129–136.

(13) Herrmann, W. A.; Anwander, R.; Munck, F. C.; Scherer, W.; Dufaud, V.; Huber, N. W.; Artus, G. R. J. Lanthanoiden-Komplexe, IX [1]. Reaktivitätsbestimmender Einfluß Der Ligandenkonstitution Bei Seltenerdamiden: Herstellung Und Struktur Sterisch Überladener Alkoxid-Komplexe / Lanthanoid Complexes, IX [1]. Reactivity Control of Lanthanoid Amides through Li. *Z. Naturforsch., B: Chem. Sci.* **1994**, *49*, 1789.

(14) Bienfait, A. M.; Wolf, B. M.; Törnroos, K. W.; Anwander, R. Trivalent Rare-Earth-Metal Bis(Trimethylsilyl)Amide Halide Complexes by Targeted Oxidations. *Inorg. Chem.* **2018**, *57*, 5204–5212.

(15) Niemeyer, M. Synthesis and Structural Characterization of Several Ytterbium Bis(Trimethylsilyl)Amides Including Base-Free $[Yb\{N(SiMe_3)_2\}_2(\mu\text{-}Cl)]_2$ — A Coordinatively Unsaturated Complex with Additional Agostic $Yb\cdots(H_3C—Si)$ Interactions. *Z. Anorg. Allg. Chem.* **2002**, *628*, 647–657.

(16) Stewart, J. L.; Andersen, R. A. Trivalent Uranium Chemistry: Molecular Structure of $[(Me_3Si)_2N]_3U$. *Polyhedron* **1998**, *17*, 953–958.

(17) Gaunt, A. J.; Enriquez, A. E.; Reilly, S. D.; Scott, B. L.; Neu, M. P. Structural Characterization of $Pu[N(SiMe_3)_2]_3$, a Synthetically Useful Nonaqueous Plutonium(III) Precursor. *Inorg. Chem.* **2008**, *47*, 26–28.

(18) Cummins, C. C. Three-Coordinate Complexes of "Hard" Ligands: Advances in Synthesis, Structure and Reactivity. *Progress in Inorganic Chemistry*. January 1, 1997, pp 685–836.

(19) Lappert, M. F.; Power, P. P.; Protchenko, A.; Seeber, A. *Metal Amide Chemistry*; Chichester, U.K. : Wiley: Chichester, U.K., 2009.

(20) Bradley, D. C. Steric Control of Metal Coordination. *Chem. Br.* **1975**, *11*, 393–397.

(21) Bradley, D. C.; Newing, C. W. Low Spin Four-Co-Ordinated Chromium Nitrosyl Dialkylamides and Alkoxides. *J. Chem. Soc. D Chem. Commun.* **1970**, No. 4, 219–220.

(22) Bradley, D. C.; Hursthouse, M. B.; Newing, C. W.; Welch, A. J. Square Planar and Tetrahedral Chromium(II) Complexes; Crystal Structure Determinations. *J. Chem. Soc., Chem. Commun.* **1972**, No. 9, 567–568.

(23) Bradley, D. C.; Hursthouse, M. B.; Ibrahim, A. A.; Malik, K. M. A.; Motevalli, M.; Möseler, R.; Powell, H.; Runnacles, J. D.; Sullivan, A. C. Synthesis and Chemistry of the Bis(Trimethylsilyl)Amido Bis-Tetrahydrofuranates of the Group 2 Metals Magnesium, Calcium, Strontium and Barium. X-Ray Crystal Structures of $Mg[N(SiMe_3)_2]_2{\cdot}2THF$ and Related $Mn[N(SiMe_3)_2]_2{\cdot}2THF$. *Polyhedron* **1990**, *9*, 2959–2964.

(24) Olmstead, M. M.; Power, P. P.; Shoner, S. C. Three-Coordinate Iron Complexes: X-Ray Structural Characterization of the Iron Amide-Bridged Dimers $[Fe(NR_2)_2]_2$ (R = $SiMe_3$, C_6H_5) and the Adduct $Fe[N(SiMe_3)_2]_2(THF)$ and Determination of the Association Energy of the Monomer $Fe\{N(SiMe_3)_2\}_2$ in Solution. *Inorg. Chem.* **1991**, *30*, 2547–2551.

(25) Bryan, A. M.; Long, G. J.; Grandjean, F.; Power, P. P. Synthesis, Spectroscopic Characterization, and Determination of the Solution Association Energy of the Dimer $[Co\{N(SiMe_3)_2\}_2]_2$: Magnetic Studies of Low-Coordinate Co(II) Silylamides $[Co\{N(SiMe_3)_2\}_2L]$ (L = PMe_3, Pyridine, and THF) and Related Species That Reveal Very Large Zero-Field Splittings . *Inorg. Chem.* **2013**, *52*, 12152–12160.

(26) Faust, M.; Bryan, A. M.; Mansikkamäki, A.; Vasko, P.; Olmstead, M. M.; Tuononen, H. M.; Grandjean, F.; Long, G. J.; Power, P. P. The Instability of $Ni\{N(SiMe_3)_2\}_2$: A Fifty Year Old Transition Metal Silylamide Mystery. *Angew. Chem. Int. Ed.* **2015**, *54*, 12914–12917.

(27) Woen, D. H.; Chen, G. P.; Ziller, J. W.; Boyle, T. J.; Furche, F.; Evans, W. J. End-On Bridging Dinitrogen Complex of Scandium. *J. Am. Chem. Soc.* **2017**, *139*, 14861–14864.

(28) Woen, D. H.; Chen, G. P.; Ziller, J. W.; Boyle, T. J.; Furche, F.; Evans, W. J. Solution Synthesis, Structure, and CO2 Reduction Reactivity of a Scandium(II) Complex, $\{Sc[N(SiMe_3)_2]_3\}^-$. *Angew. Chem. Int. Ed.* **2017**, *56*, 2050–2053.

(29) Airoldi, C.; Bradley, D. C.; Chudzynska, H.; Hursthouse, M. B.; Malik, K. M. A.; Raithby, P. R. Preparation, Properties, and Crystal Structures of the Monochlorotris[Bis(Trimethylsilyl)Amido]-Compounds of Titanium, Zirconium, and Hafnium. *J. Chem. Soc. Dalton Trans.* **1980**, No. 10, 2010–2015.

(30) Laurent, F.; Cyr-Athis, O.; Legros, J. P.; Choukroun, R.; Valade, L. $FTi[N(SiMe_3)_2]_3$: Synthesis, Crystal Structure and Evaluation of This New Molecule as a Precursor to Titanium Nitride. *New J. Chem.* **1994**, *18*, 575–580.

(31) Bradley, D. C.; Chudzynska, H.; Backer-Dirks, J. D. J.; Hursthouse, M. B.; Ibrahim, A. A.; Motevalli, M.; Sullivan, A. C. Synthesis, Photochemistry and X-Ray Crystal Structures of the Methyltris[Bis(Trimethylsilyl)Amido] Compounds $MeTi[N(SiMe_3)_2]_3$ and $MeZr[N(SiMe_3)_2]_3$. *Polyhedron* **1990**, *9*, 1423–1427.

(32) Geyer-Lippmann, J. Silylamide, Alkoxide Und Oberflächen-Verbindungen von Vanadin Auf Silicagel: Darstellung, Struktur Und Reactivität, Ph.D. Dissertation, der Freien Universität Berlin, 1981.

(33) Liptrot, D. J.; Guo, J.-D.; Nagase, S.; Power, P. P. Dispersion Forces, Disproportionation, and Stable High-Valent Late Transition Metal Alkyls. *Angew. Chem. Int. Ed.* **2016**, *55*, 14766–14769.

(34) Casitas, A.; Rees, J. A.; Goddard, R.; Bill, E.; DeBeer, S.; Fürstner, A. Two Exceptional Homoleptic Iron(IV) Tetraalkyl Complexes. *Angew. Chem. Int. Ed.* **2017**, *56*, 10108–10113.

(35) Pangborn, A. B.; Giardello, M. A.; Grubbs, R. H.; Rosen, R. K.; Timmers, F. J. Safe and Convenient Procedure for Solvent Purification. *Organometallics* **1996**, *15*, 1518–1520.

(36) Evans, D. F. 400. The Determination of the Paramagnetic Susceptibility of Substances in Solution by Nuclear Magnetic Resonance. *J. Chem. Soc.* **1959**, No. 0, 2003–2005.

(37) Bain, G. A.; Berry, J. F. Diamagnetic Corrections and Pascal's Constants. *J. Chem. Educ.* **2008**, *85*, 532.

(38) Bradley, D. C.; Copperthwaite, R. G.; Extine, M. W.; Reichert, W. W.; Chisholm, M. H. Transition Metal Complexes of Bis(Trimethyl-Silyl)Amine (1,1,1,3,3,3-Hexamethyldisilazane). *Inorganic Syntheses*. January 1, 1978, pp 112–120.

(39) Gokel, G. W.; Widera, R. P.; Weber, W. P. Phase-Transfer Hofmann Carbylamine Reaction: Tert-Butyl Isocyanide. *Org. Synth.* **1976**, *55*, 76.

(40) Sheldrick, G. M. *SADABS*; University of Göttingen, Germany, 1996.

(41) Sheldrick, G. M. *TWINABS*; University of Göttingen, Germany, 2012.

(42) Sheldrick, G. M. SHELXT - Integrated Space-Group and Crystal-Structure Determination. *Acta Crystallogr. Sect. A Found. Crystallogr.* **2015**, *A71*, 3–8.

(43) Sheldrick, G. M. Crystal Structure Refinement with SHELXL. *Acta Crystallogr. Sect. C, Struct. Chem.* **2015**, *C71*, 3–8.

(44) Pyykkö, P.; Atsumi, M. Molecular Single-Bond Covalent Radii for Elements 1–118. *Chem. – A Eur. J.* **2009**, *15*, 186–197.

(45) Westerhausen, M.; Hartmann, M.; Pfitzner, A.; Schwarz, W. Bis(Trimethylsilyl)Amide Und -Methanide Des Yttriums — Molekülstrukturen von Tris(Diethylether-O)Lithium-(μ-Chloro)-Tris[Bis(Trimethylsilyl) Methyl]Yttriat, Solvensfreiem Yttrium-Tris[Bis(Trimethylsilyl)amid] Sowie Dem Bis(Benzonitril)-Komplex. *Z. Anorg. Allg. Chem.* **1995**, *621*, 837–850.

(46) Jank, S.; Hanss, J.; Reddmann, H.; Amberger, H.-D.; Edelstein, N. M. Electronic Structures of Highly Symmetrical Compounds of f Elements. 34 [1] Synthesis and Spectroscopic Characterization of Biscyclohexylisocyanide Adducts Derived from the Tris(Bis(Trimethylsilyl)Amido)Lanthanide(III) Moiety as Well as Crystal, Molecular. *Z. Anorg. Allg. Chem.* **2002**, *628*, 1355–1365.

(47) Doyle, L. R.; Wooles, A. J.; Jenkins, L. C.; Tuna, F.; McInnes, E. J. L.; Liddle, S. T. Catalytic Dinitrogen Reduction to Ammonia at a Triamidoamine–Titanium Complex. *Angew. Chem. Int. Ed.* **2018**, *57*, 6314–6318.

(48) Hagadorn, J. R.; Arnold, J. Low-Valent Chemistry of Titanium Benzamidinates Leading to New Ti μ-N_2, μ-O, Alkyl Derivatives, and the Cyclometalation of TMEDA. *J. Am. Chem. Soc.* **1996**, *118*, 893–894.

(49) Zakrzewski, J.; Huras, B.; Kiełczewska, A. Synthesis of Isoselenocyanates. *Synthesis* **2016**, *48*, 85–96.

(50) Baldwin, J. E.; Derome, A. E.; Riordan, P. D. Deoxygenation of Isocyanates to Isonitriles: A Mechanistic Study by Nuclear Magnetic Resonance. *Tetrahedron* **1983**, *39*, 2989–2994.

(51) Zhu, C.; Ji, L.; Wei, Y. A Facile and Efficient One-Pot Synthesis of Nitriles from Aldehydes Using Hypervalent Iodine(III) Reagents in Aqueous Ammonium Acetate. *Synthesis* **2010**, *2010*, 3121–3125.

(52) Nakamoto, K. *Infrared and Raman Spectra of Inorganic and Coordination Compounds : Applications in Coordination, Organometallic, and Bioinorganic Chemistry*; John Wiley & Sons: New York, UNITED STATES, 2009.

(53) Alyea, E. C.; Bradley, D. C.; Copperthwaite, R. G. Three-Co-Ordinated Transition Metal Compounds. Part I. The Preparation and Characterization of Tris(Bistrimethylsilylamido)-Derivatives of Scandium, Titanium, Vanadium, Chromium, and Iron. *J. Chem. Soc. Dalton Trans.* **1972**, No. 14, 1580–1584.

(54) Alyea, E. C.; Bradley, D. C.; Copperthwaite, R. G.; Sales, K. D. Three-Co-Ordinated Transition-Metal Compounds. Part II. Electronic Spectra and Magnetism of Tris(Bistrimethylsilylamido)Derivatives of Scandium, Titanium, Vanadium, Chromium, and Iron. *J. Chem. Soc. Dalton Trans.* **1973**, No. 2, 185–191.

(55) Bersuker, I. B. Crystal Field Theory. In *Electronic Structure and Properties of Transition Metal Compounds*; John Wiley & Sons, Ltd, 2010; pp 84–131.

Supporting information

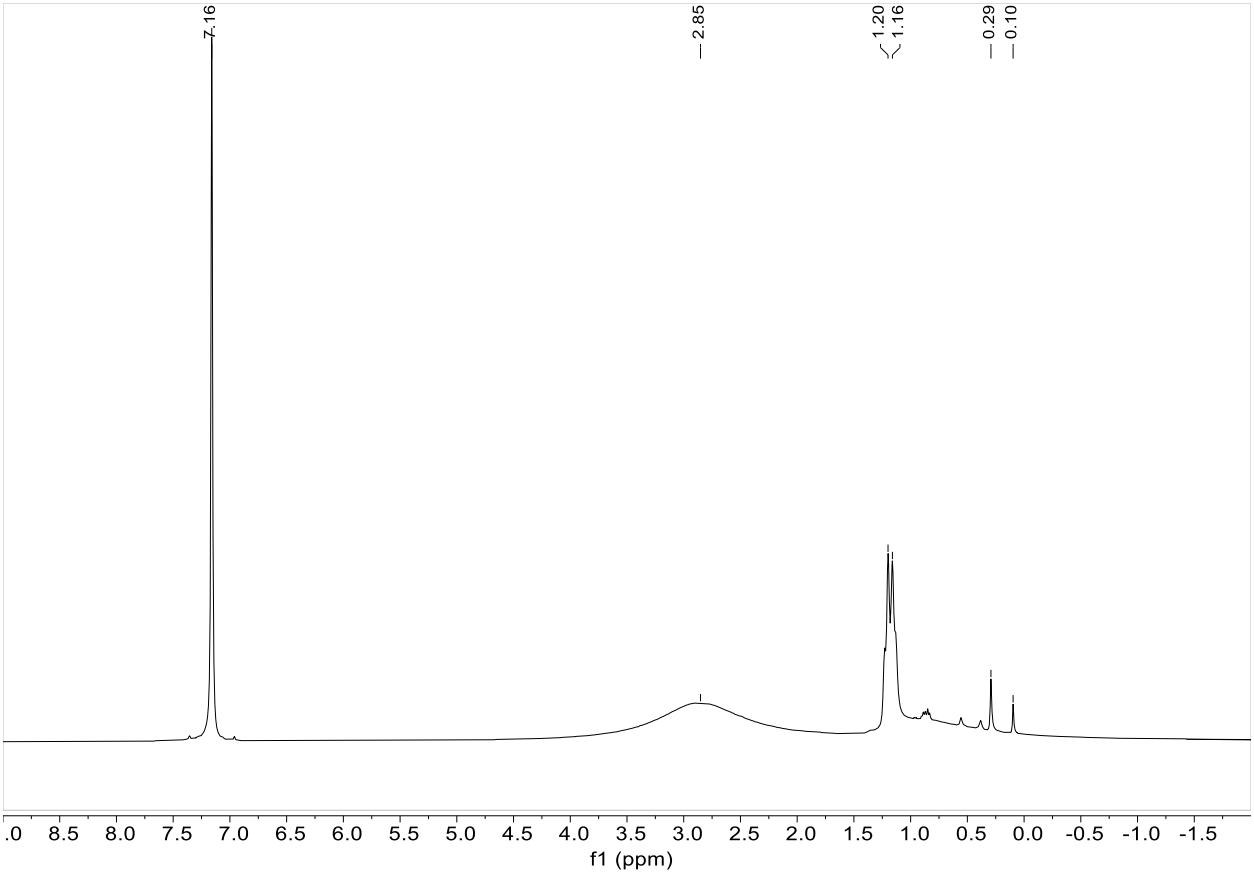

Figure 2.S1. ^{1}H-NMR Spectrum of Ti{N(SiMe$_3$)$_2$}$_3$ (1-AdNC)$_2$ in benzene-d$_6$ at 25 °C

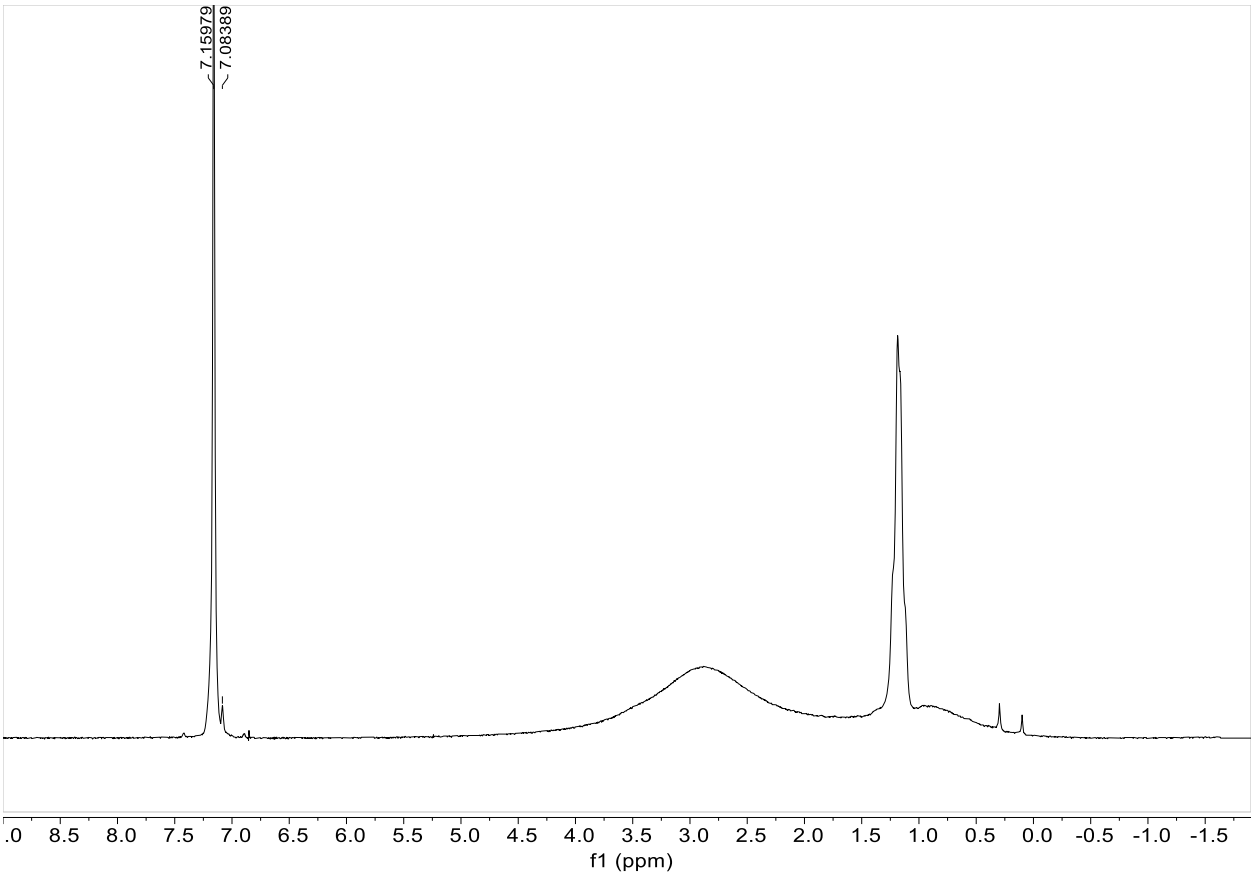

Figure 2.S2. Evans' Method ^{1}H-NMR Spectrum of $Ti\{N(SiMe_3)_2\}_3$ $(1\text{-AdNC})_2$ in benzene-d_6 (16 mM) at 25 °C

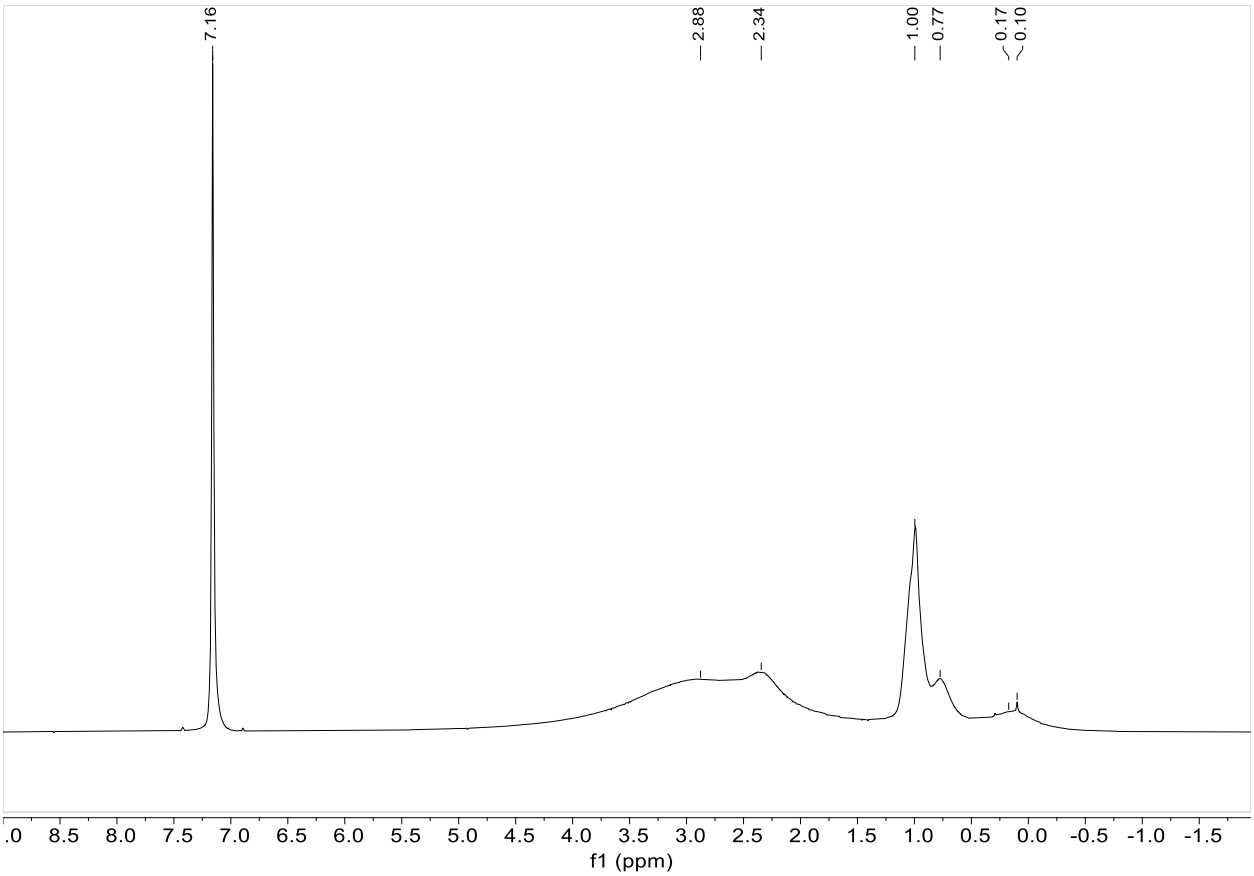

Figure 2.S3. ^{1}H-NMR Spectrum of Ti{N(SiMe$_3$)$_2$}$_3$ (CyNC)$_2$ in benzene-d$_6$ at 25 °C

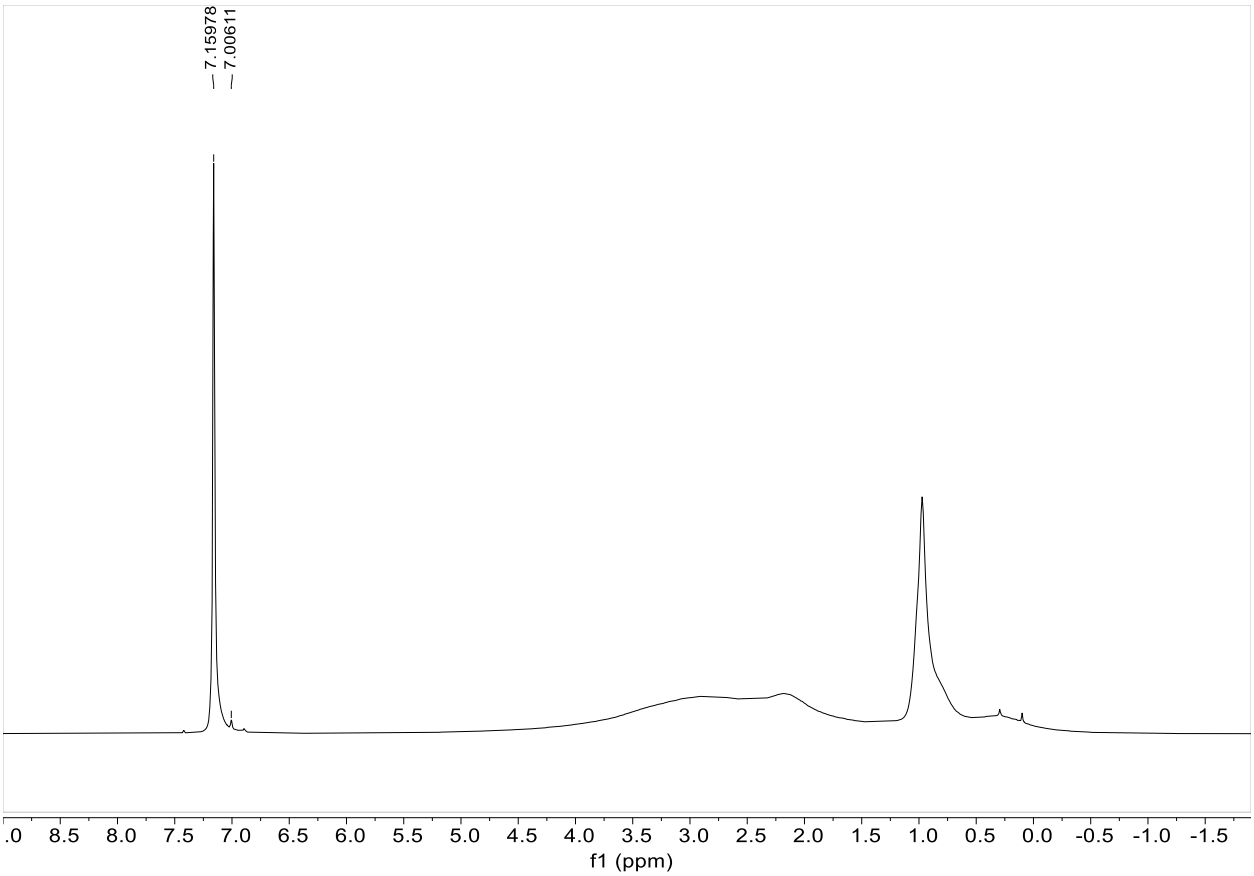

Figure 2.S4. Evans' Method ^{1}H-NMR Spectrum of $Ti\{N(SiMe_3)_2\}_3$ $(CyNC)_2$ in benzene-d_6 (27 mM) at 25 °C

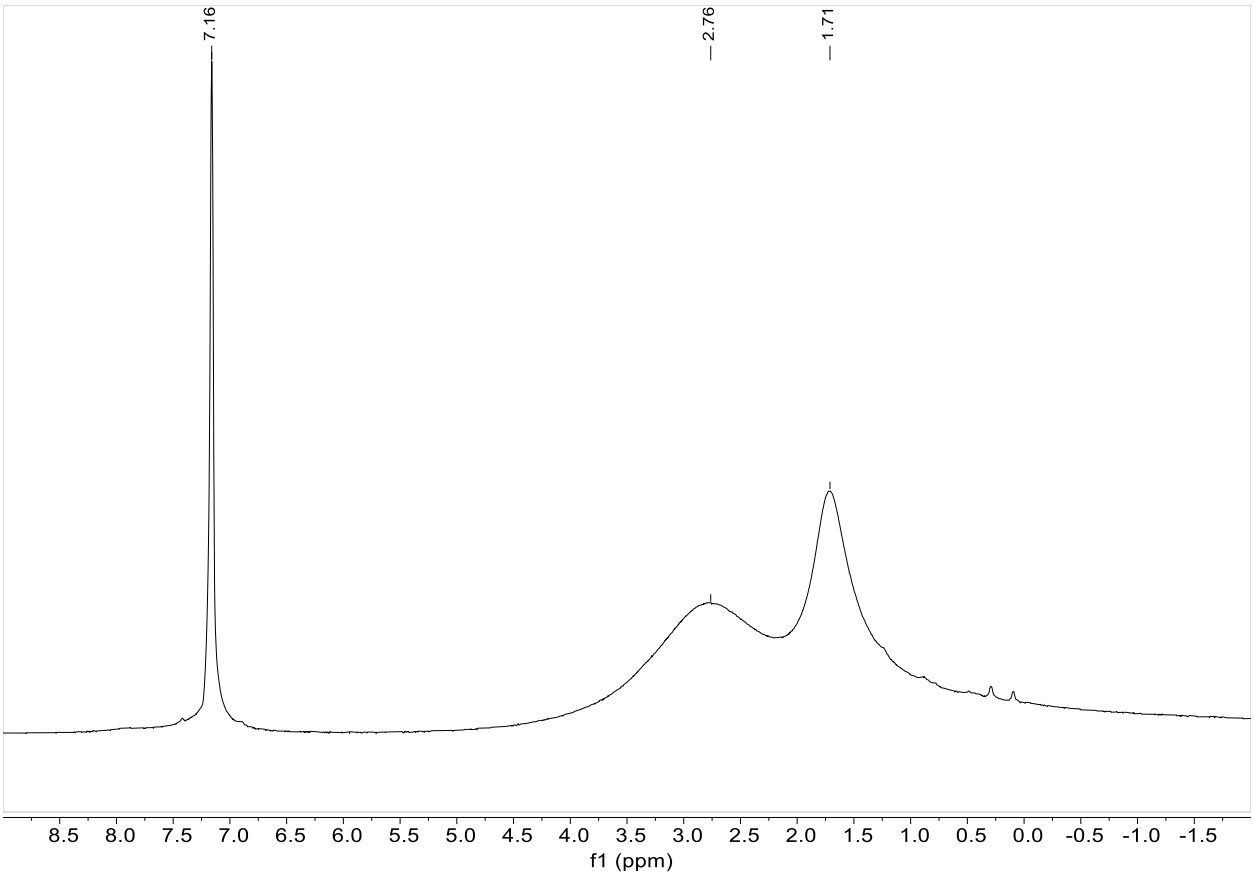

Figure 2.S5. ^{1}H-NMR Spectrum of $Ti\{N(SiMe_3)_2\}_3(Bu^tNC)_2$ in benzene-d_6 at 25 °C

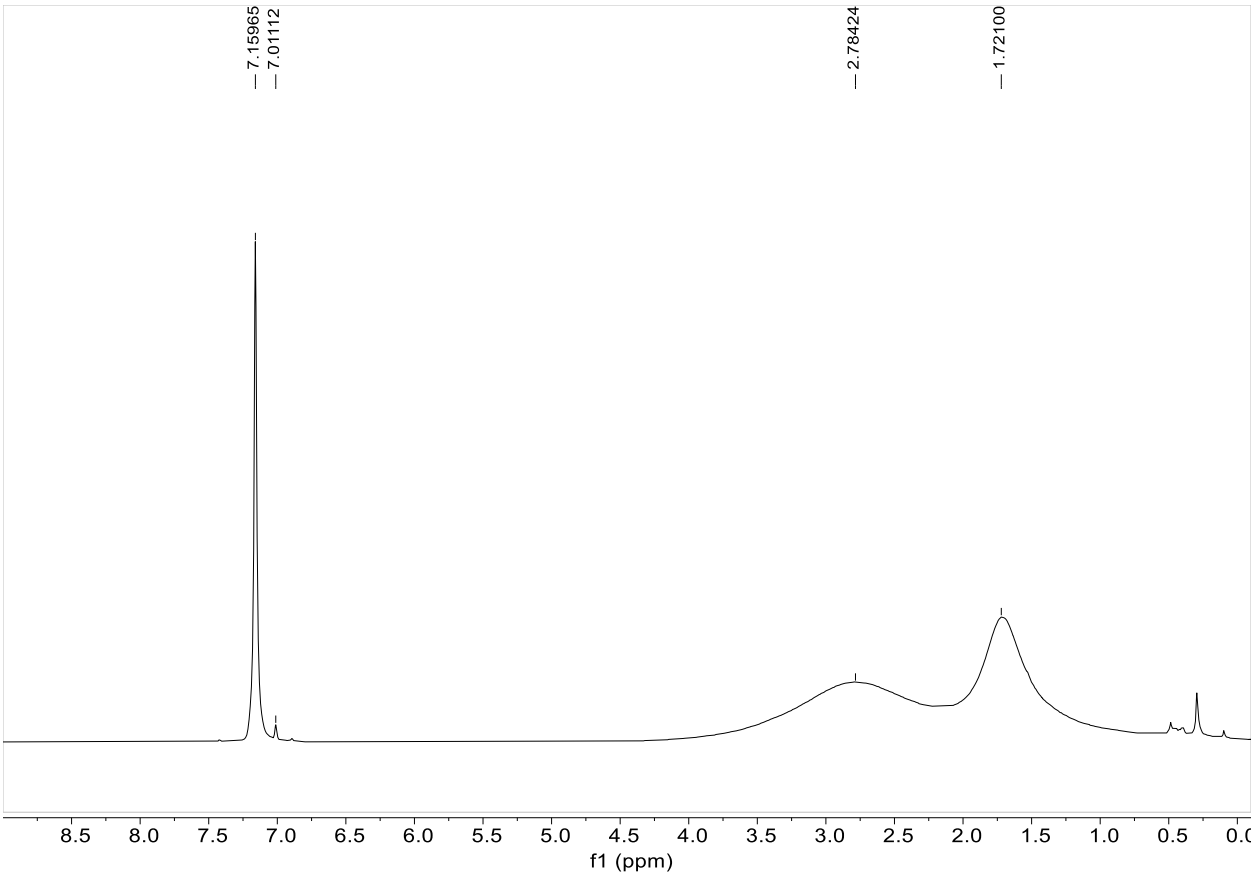

Figure 2.S6. Evans' Method ^{1}H-NMR Spectrum of $Ti\{N(SiMe_3)_2\}_3(Bu^tNC)_2$ in benzene-d_6 (25 mM) at 25 °C

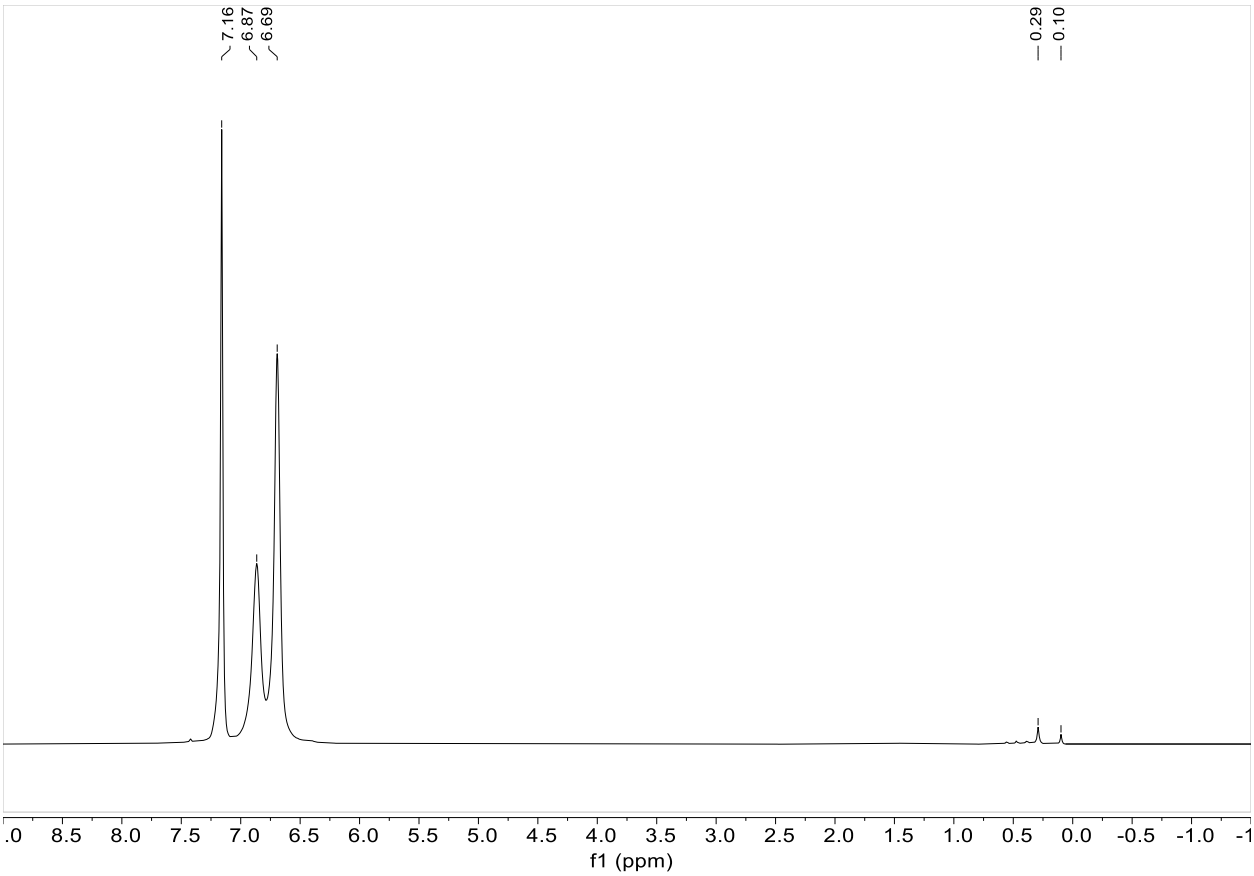

Figure 2.S7. ^{1}H-NMR Spectrum of $Ti\{N(SiMe_3)_2\}_3(PhCN)_2$ in benzene-d_6 at 25 °C

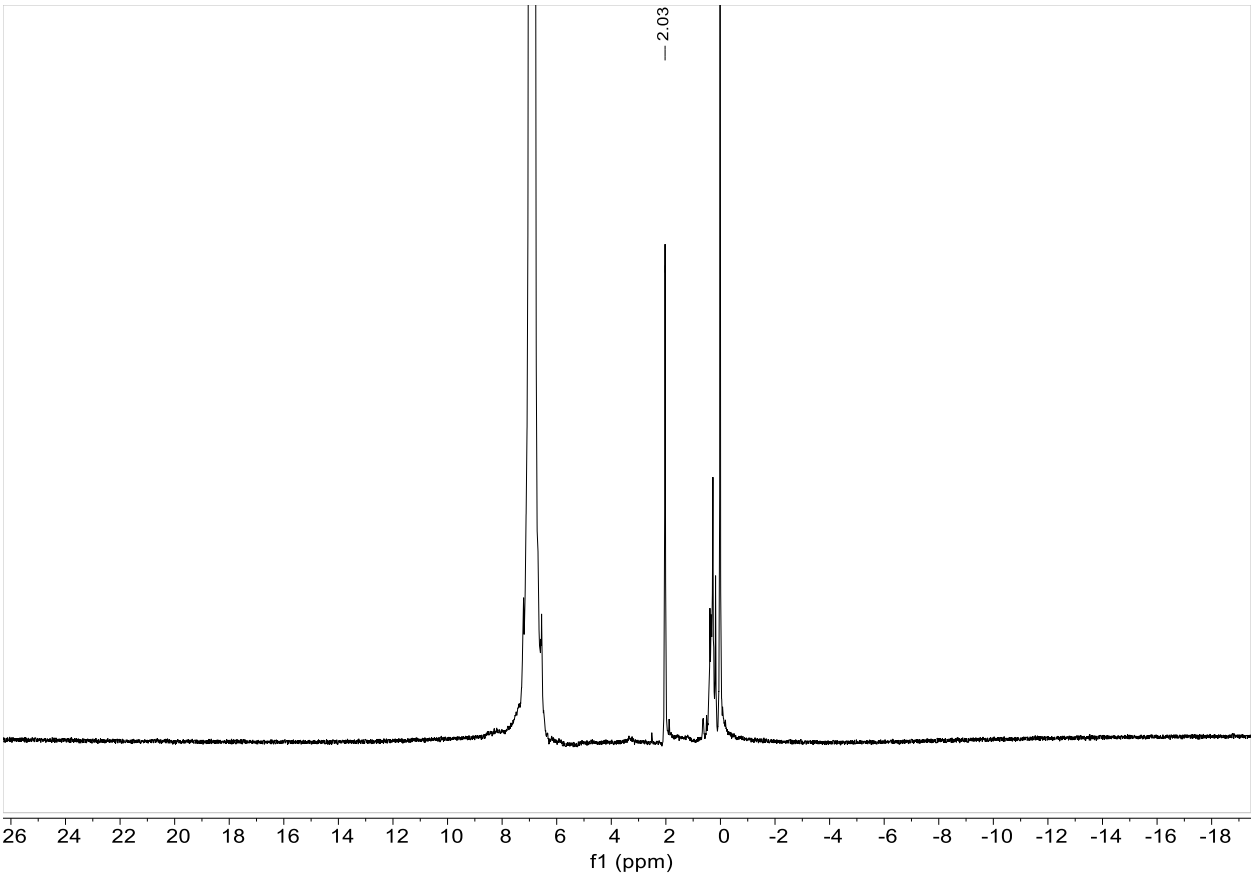

Figure 2.S8. ^{1}H-NMR Spectrum of $Ti\{N(SiMe_3)_2\}_3(PhCN)_2$ in toluene-d_8 at 25 °C, 70 equivalents of PhCN added

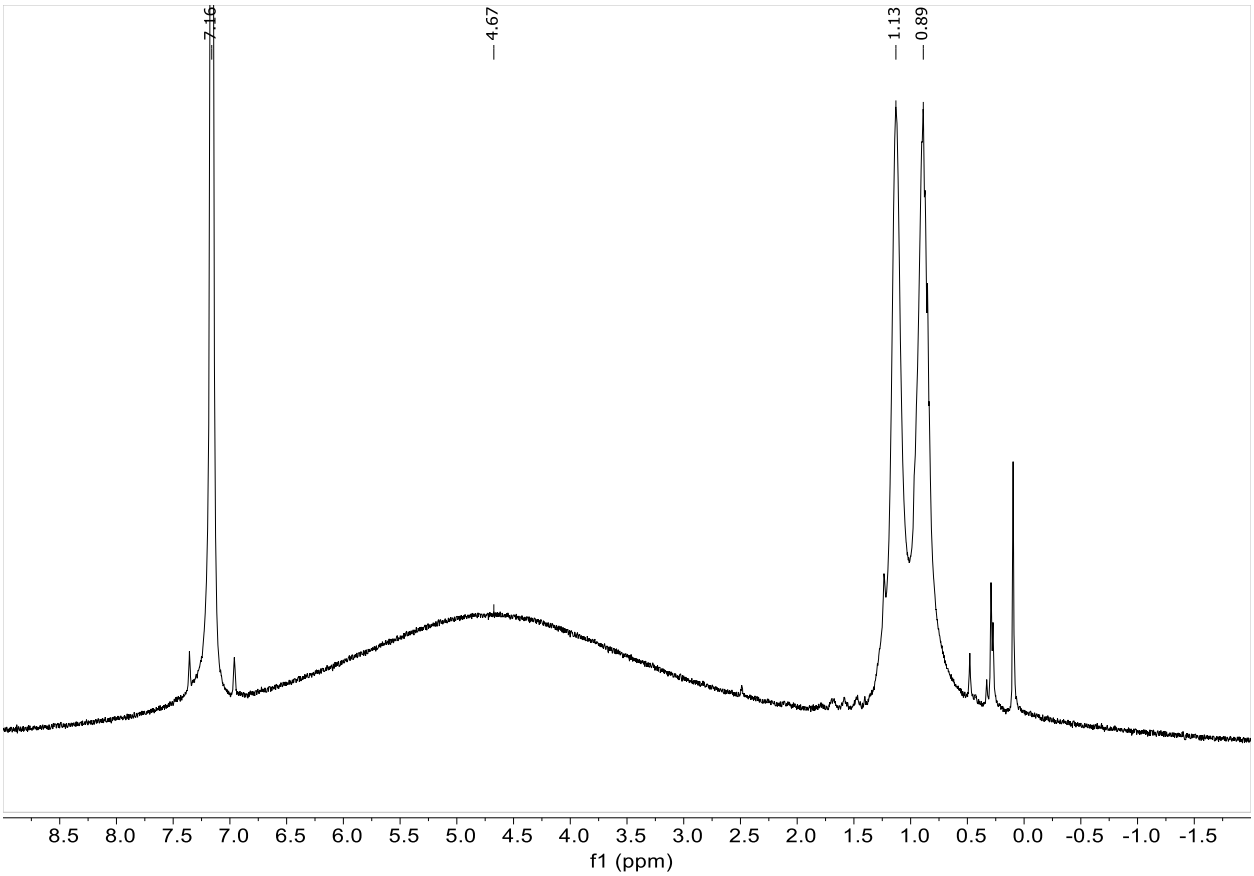

Figure 2.S9. ^{1}H-NMR Spectrum of $V\{N(SiMe_3)_2\}_3$ $(1\text{-AdNC})_2$ in benzene-d_6 at 25 °C

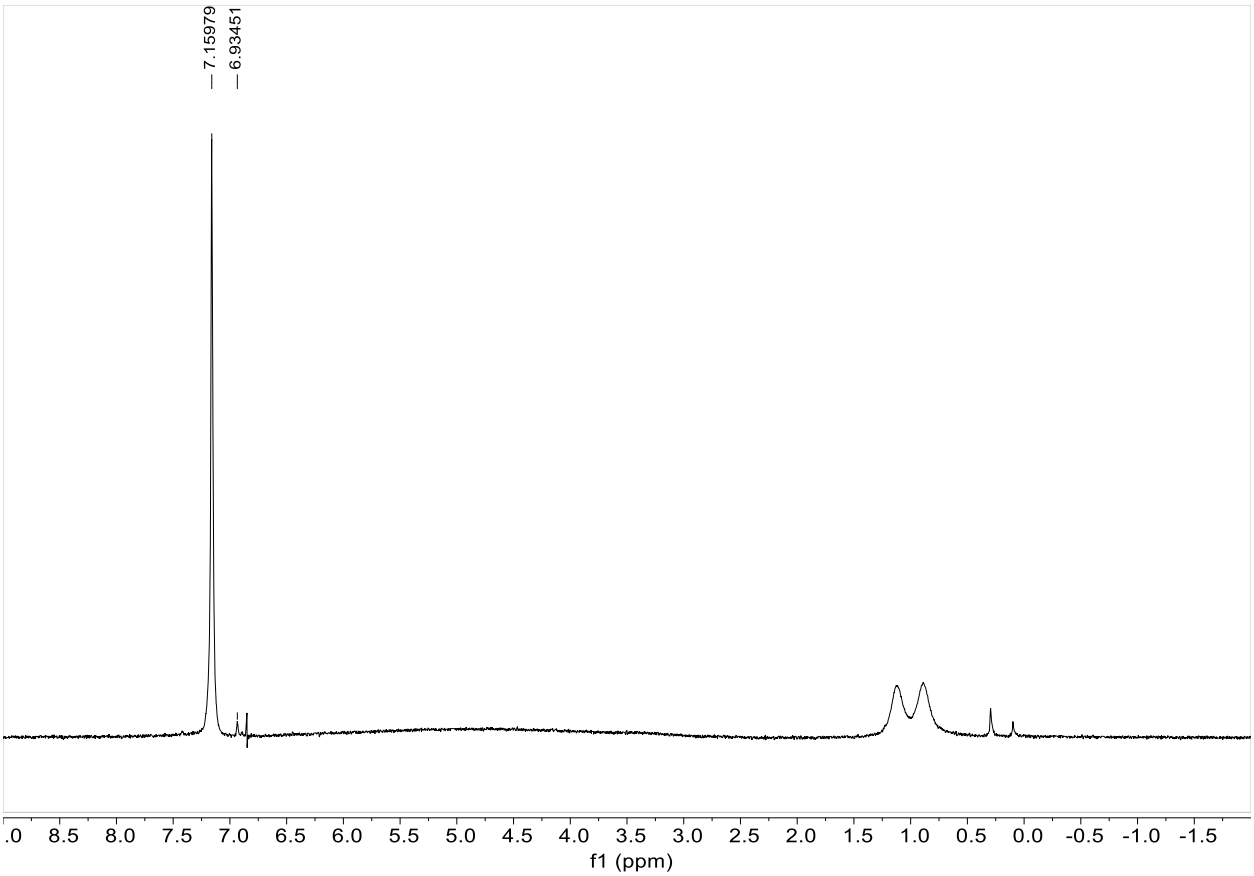

Figure 2.S10. Evans' Method ^{1}H-NMR Spectrum of V{N(SiMe$_3$)$_2$}$_3$ (1-AdNC)$_2$ in benzene-d$_6$ (16 mM) at 25 °C

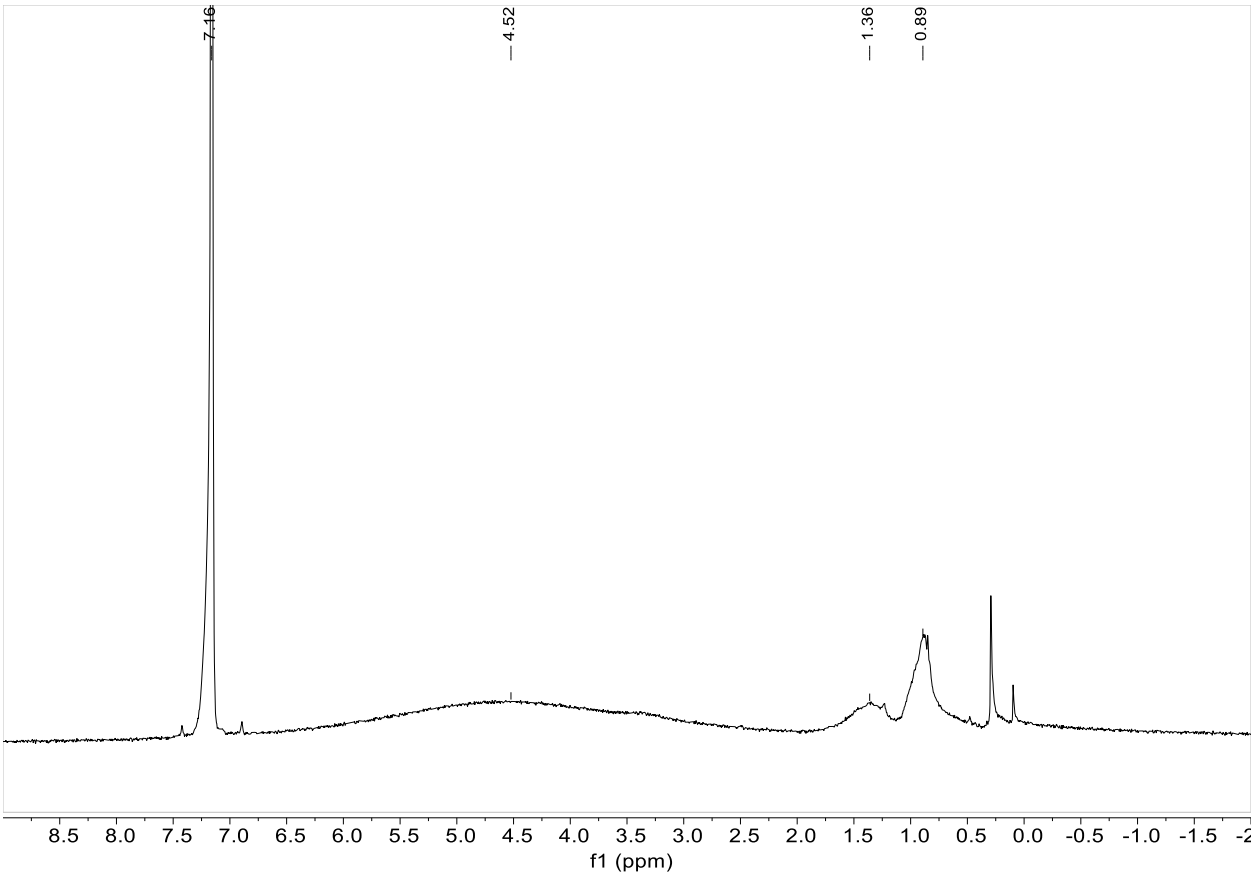

Figure 2.S11. ^{1}H-NMR Spectrum of $V\{N(SiMe_3)_2\}_3$ $(CyNC)_2$ in benzene-d_6 at 25 °C

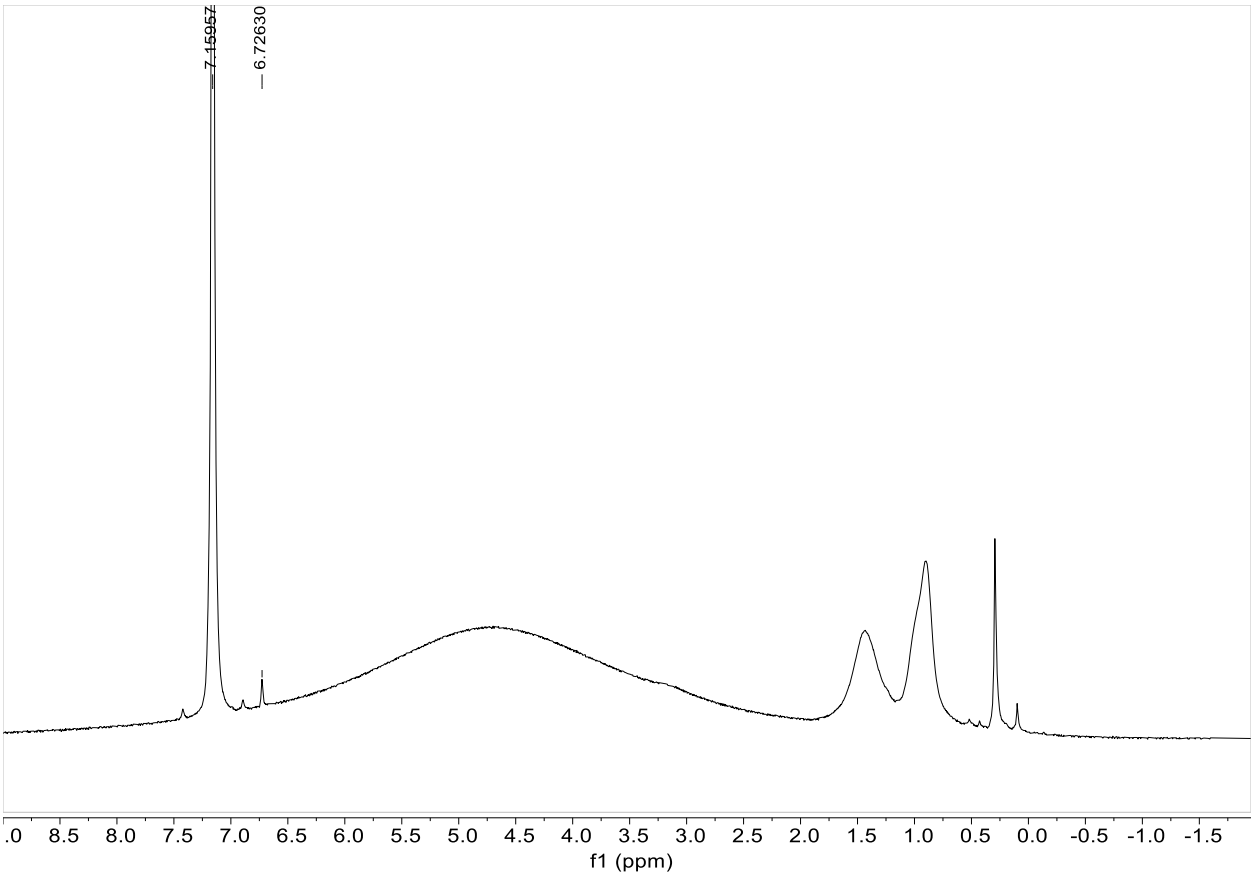

Figure 2.S12. Evans' Method ^{1}H-NMR Spectrum of $V\{N(SiMe_3)_2\}_3$ $(CyNC)_2$ in benzene-d_6 (32 mM) at 25 °C

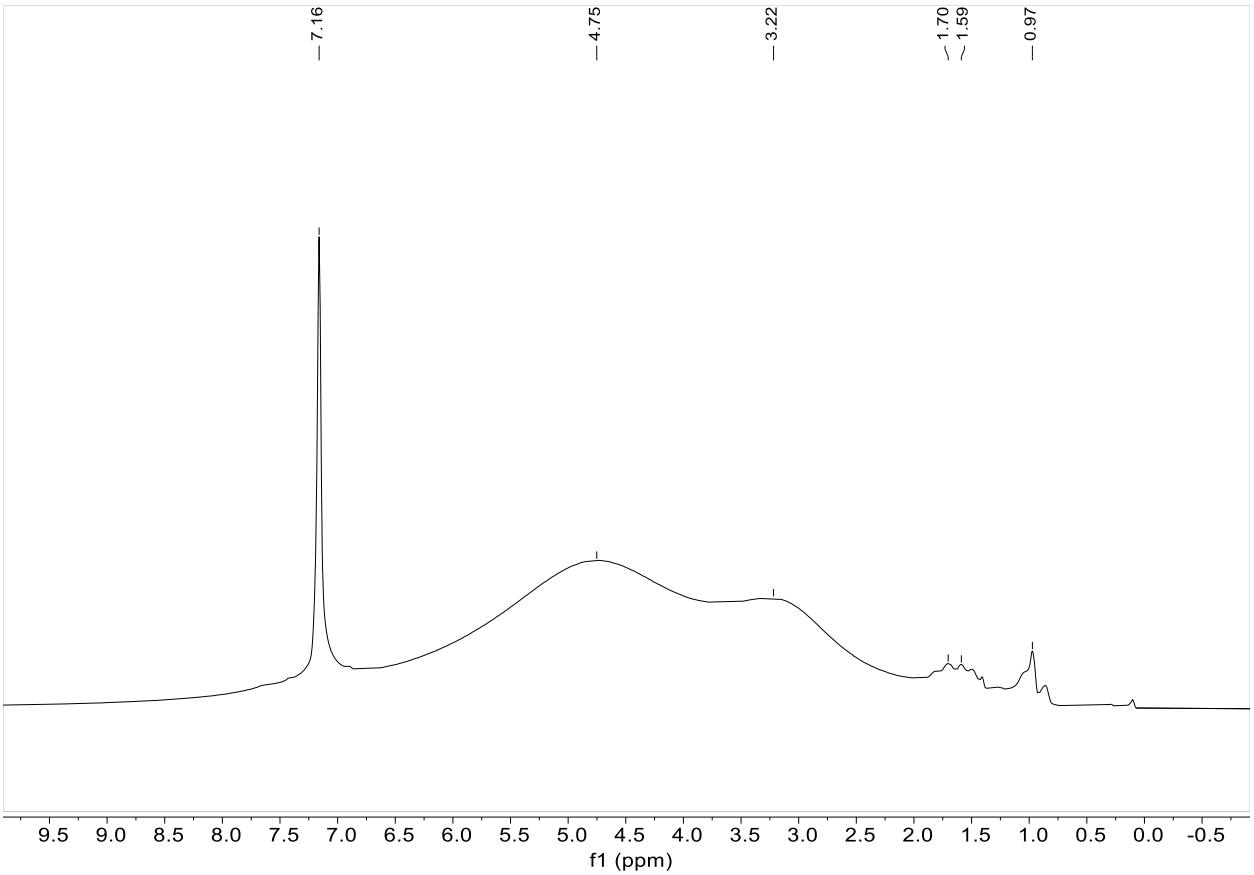

Figure 2.S13. ^{1}H-NMR Spectrum of $V\{N(SiMe_3)_2\}_3$ $(Bu^tNC)_2$ in benzene-d_6 at 25 °C

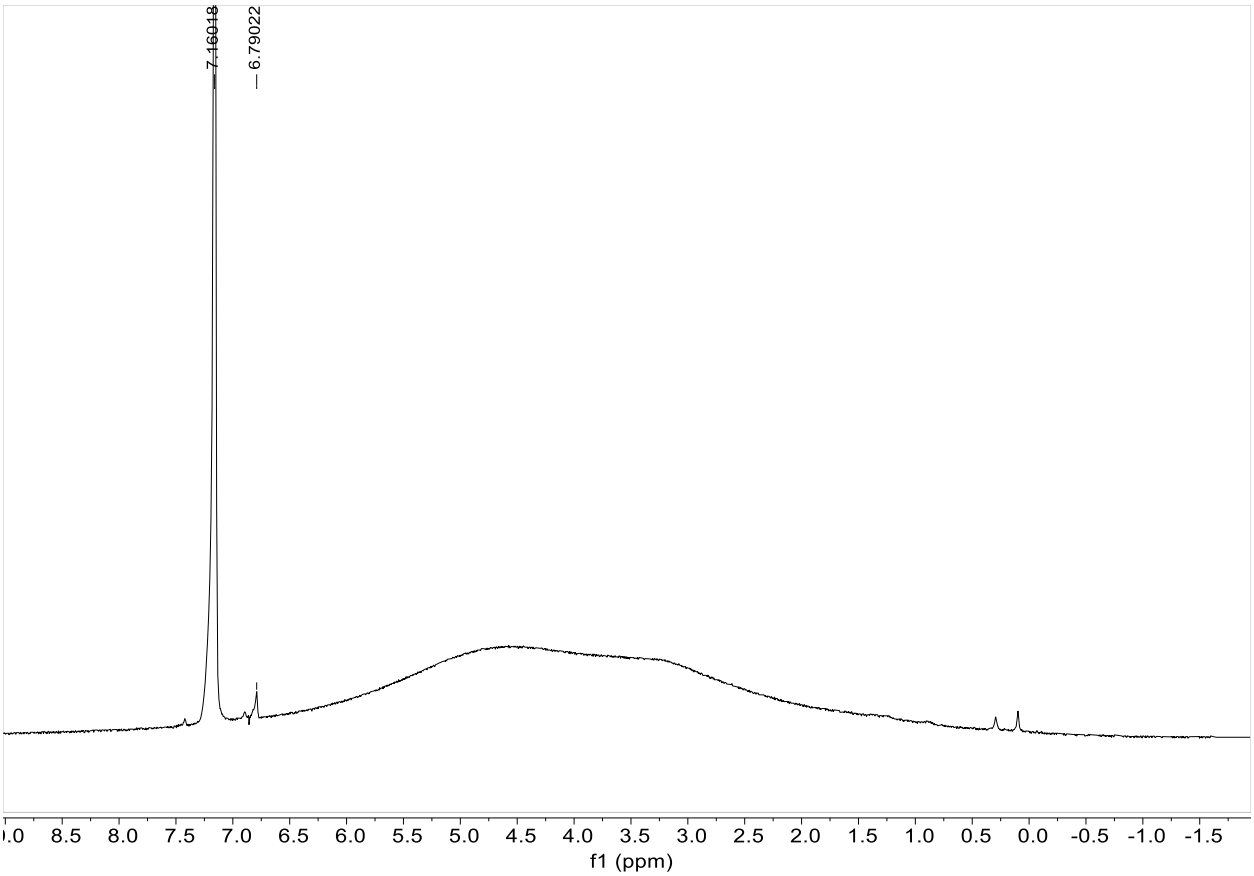

Figure 2.S14. Evans' Method ^{1}H-NMR Spectrum of $V\{N(SiMe_3)_2\}_3$ $(Bu^tNC)_2$ in benzene-d_6 (24 mM) at 25 °C

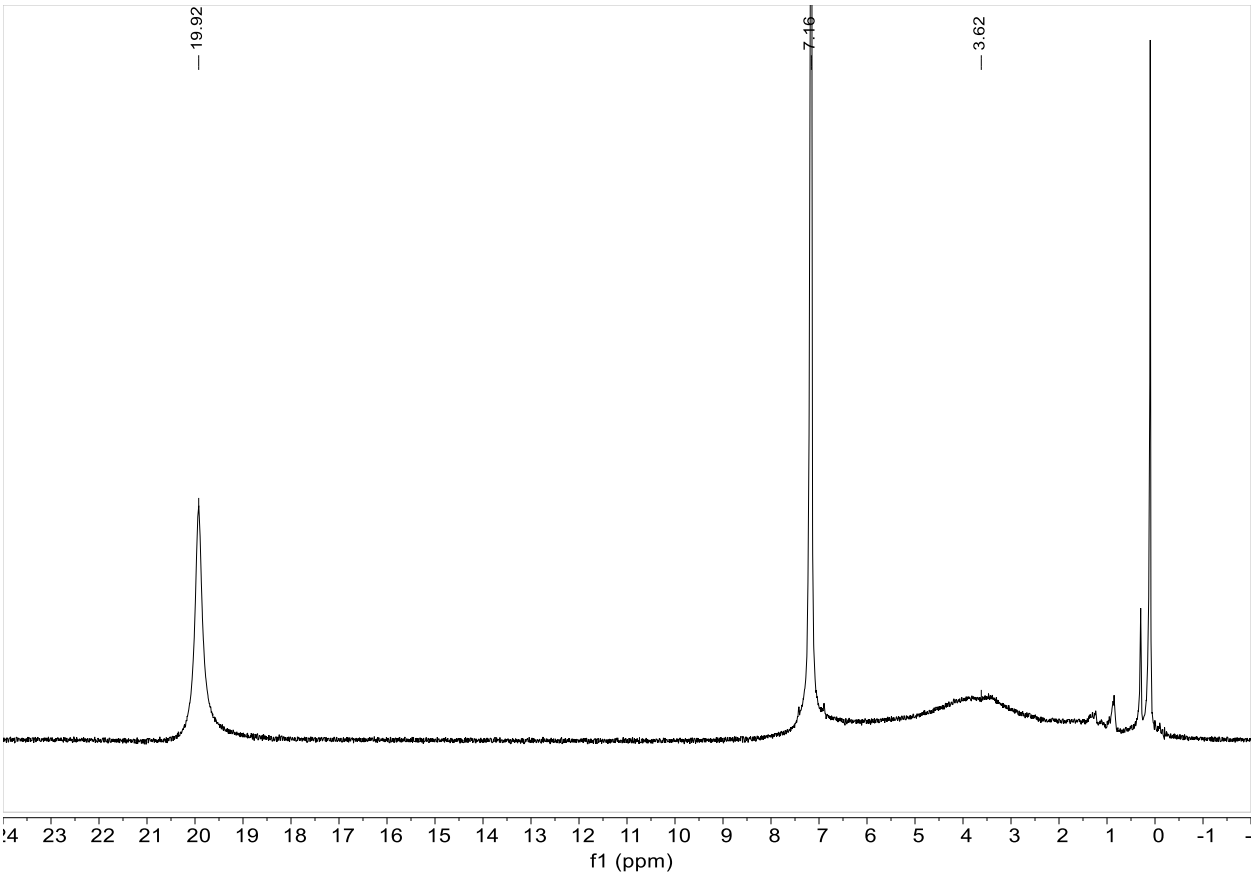

Figure 2.S15. ^{1}H-NMR Spectrum of $V\{N(SiMe_3)_2\}_3(PhCN)_2$ in benzene-d_6 at 25 °C

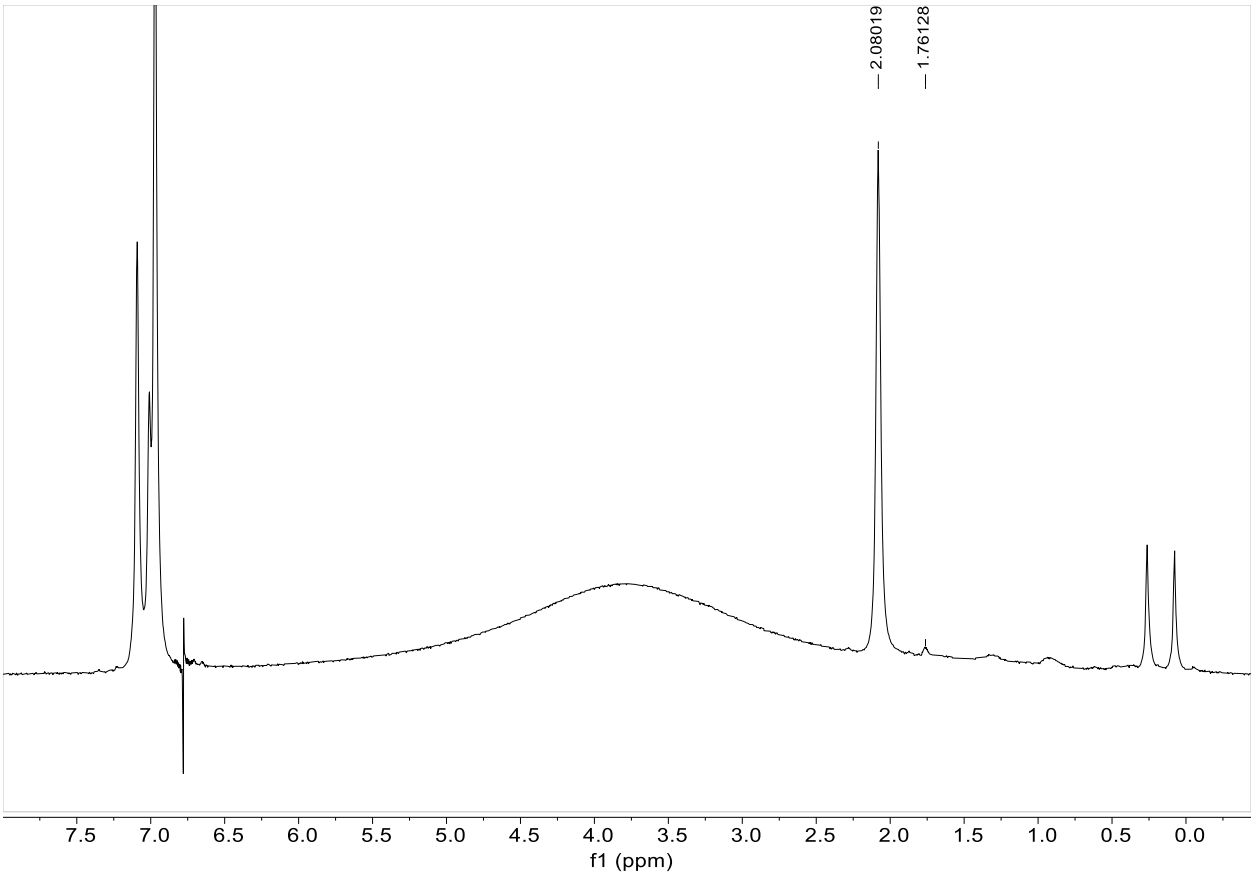

Figure 2.S16. Evans' Method 1H-NMR Spectrum of V{N(SiMe3)2}3 (PhCN)2 in toluene-d8 (27 mM) at 25 °C. The unusual signal at ca. 6.25 ppm was found to be a radio frequency artifact but does not affect determination of μ_{eff} by the absorbances indicated in the spectrum.

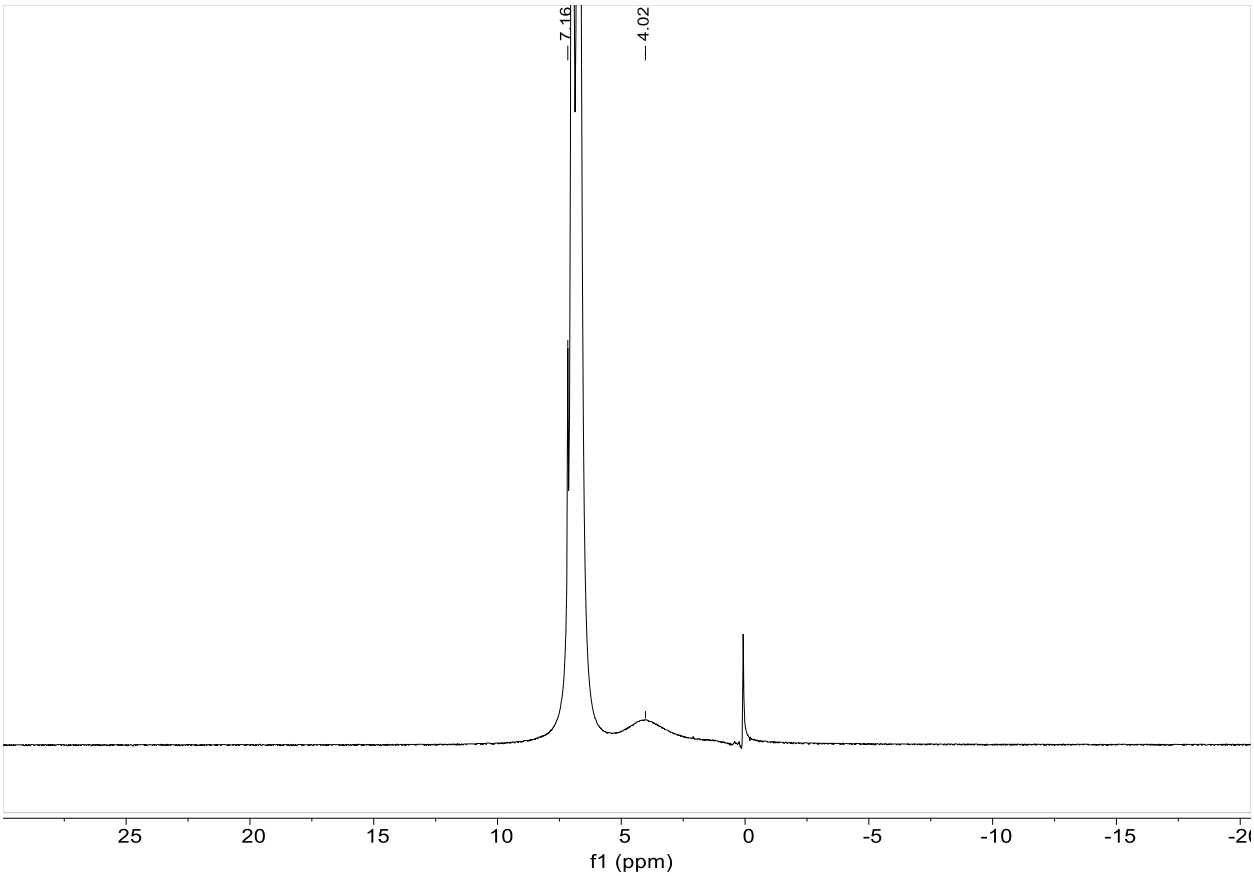

Figure 2.S17. ^{1}H-NMR Spectrum of $V\{N(SiMe_3)_2\}_3$ $(PhCN)_2$ in benzene-d_6 at 25 °C, 70 equivalents of PhCN added.

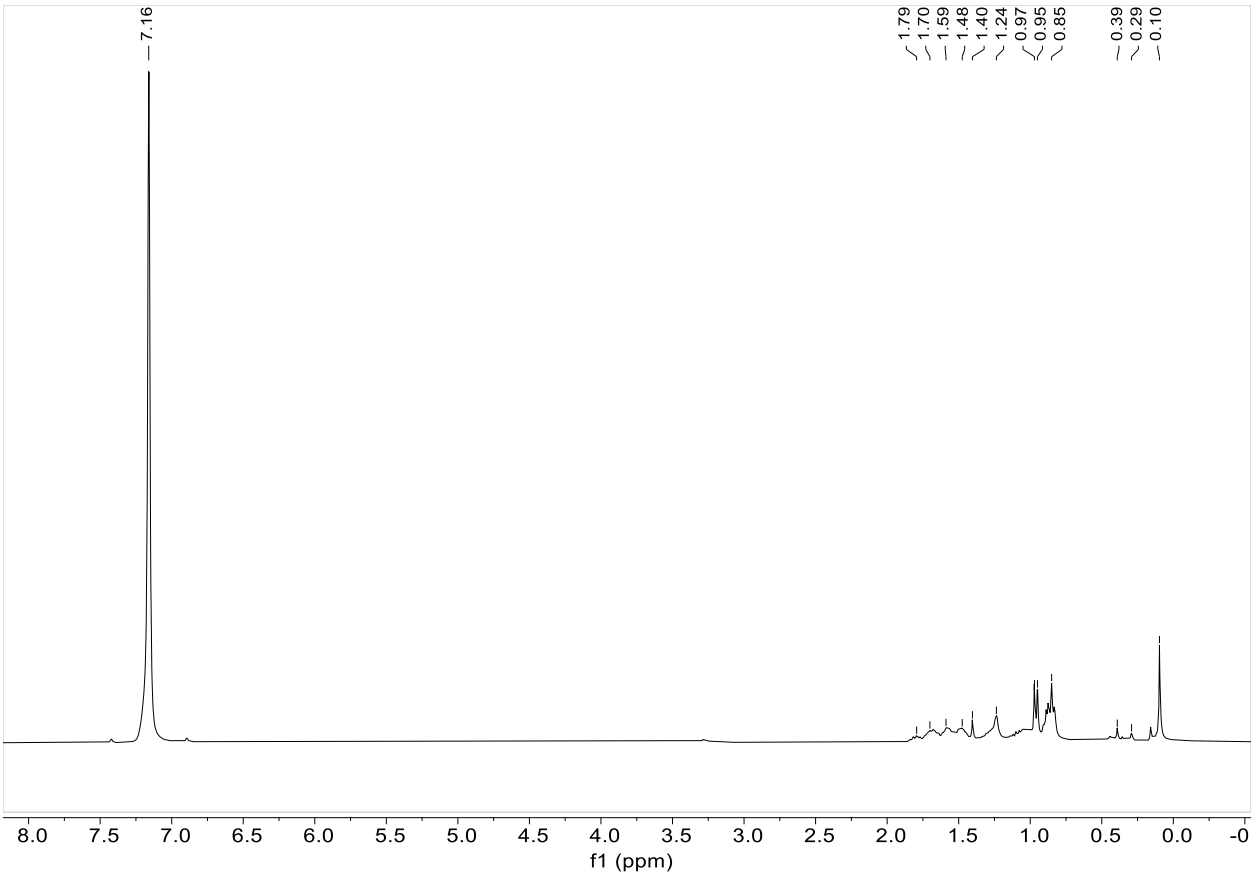

Figure 2.S18. ^{1}H-NMR Spectrum of $Ti\{N(SiMe_3)_2\}_3$ in benzene-d_6 at 25 °C

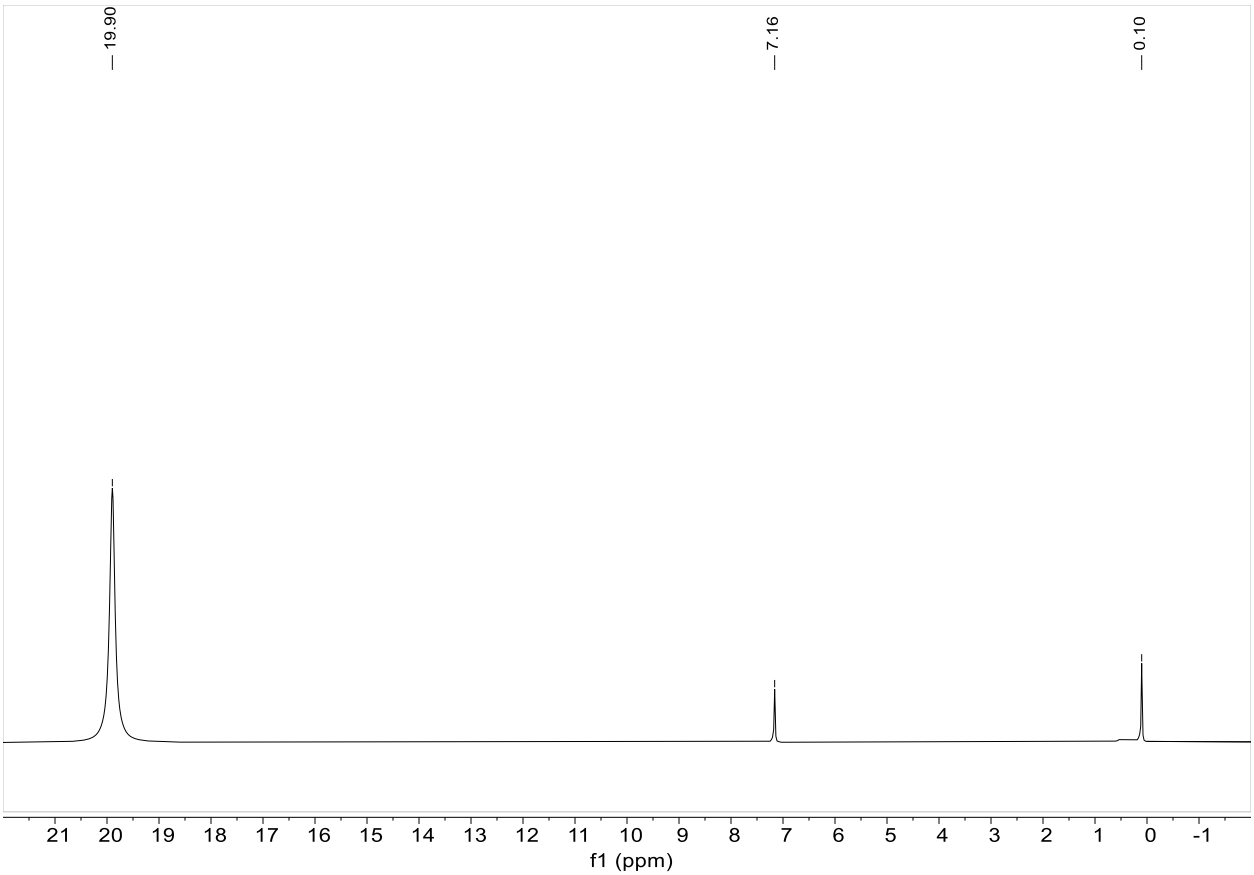

Figure 2.S19. ^{1}H-NMR Spectrum of V{N(SiMe$_3$)$_2$}$_3$ in benzene-d$_6$ at 25 °C. The proton NMR spectrum of V{N(SiMe3)2}3 contains a slight impurity of hexamethyldisilazane, removal of which is difficult to accomplish without causing decomposition of the vanadium complex (the metal amide is unstable at elevated temperature).

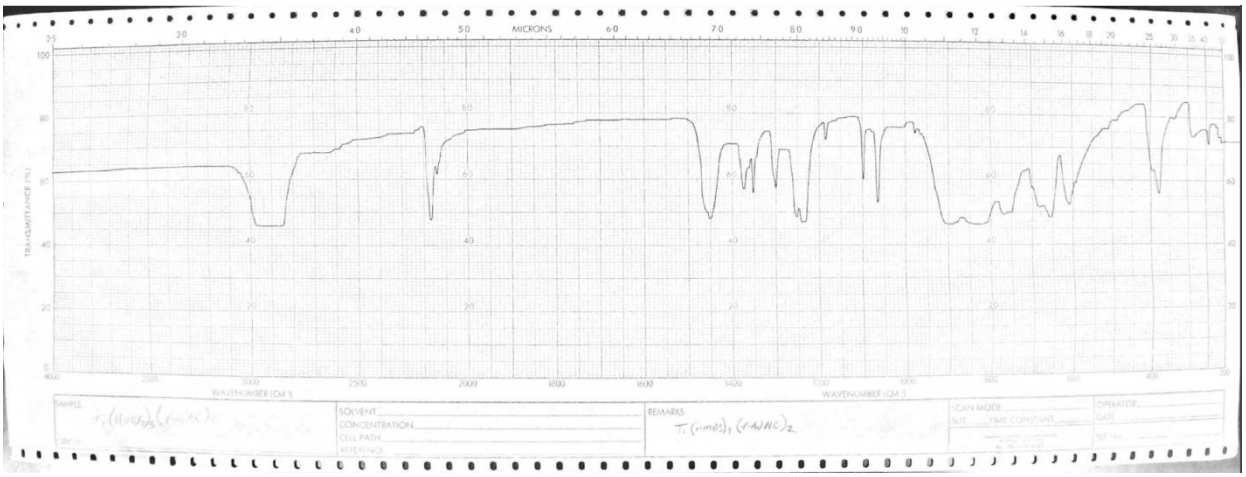

Figure 2.S20. Infrared Spectrum of $Ti\{N(SiMe_3)_2\}_3$ $(1\text{-AdNC})_2$ (**1**) (Nujol, CsI windows)

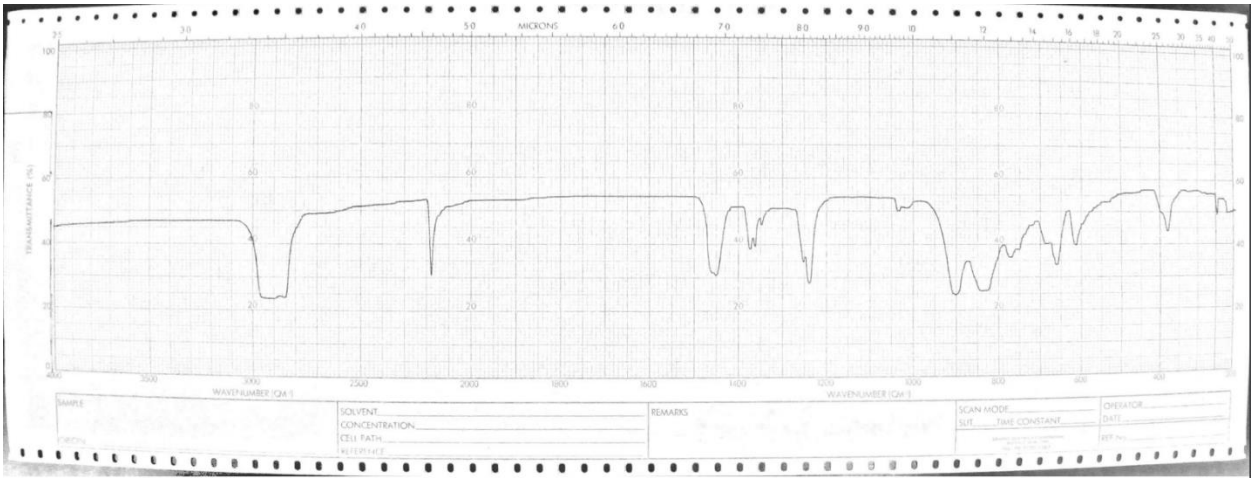

Figure 2.S21. Infrared Spectrum of $Ti\{N(SiMe_3)_2\}_3$ $(CyNC)_2$ (**2**) (Nujol, CsI windows)

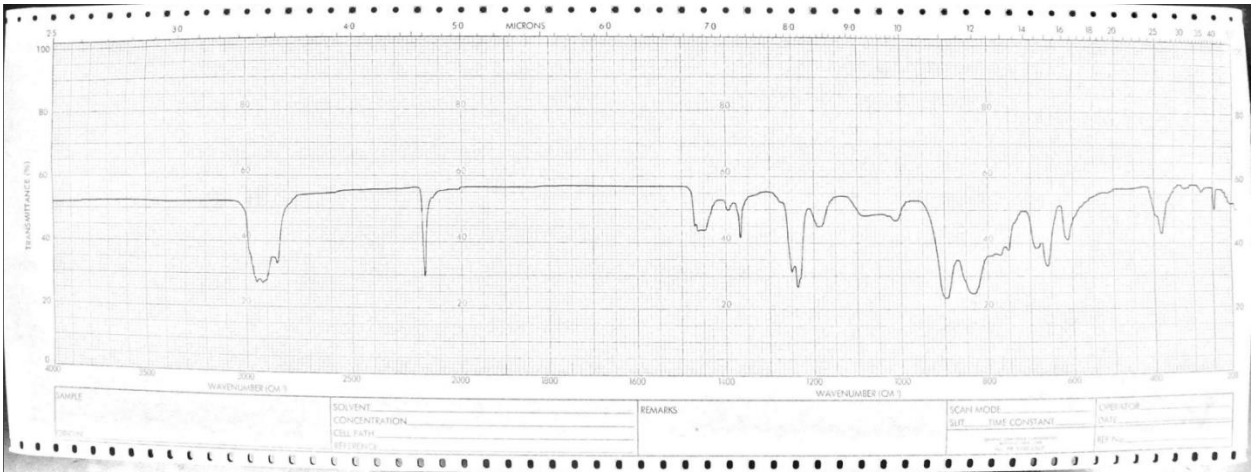

Figure 2.S22. Infrared Spectrum of $Ti\{N(SiMe_3)_2\}_3(Bu^tNC)_2$ (**3**) (Nujol, CsI windows)

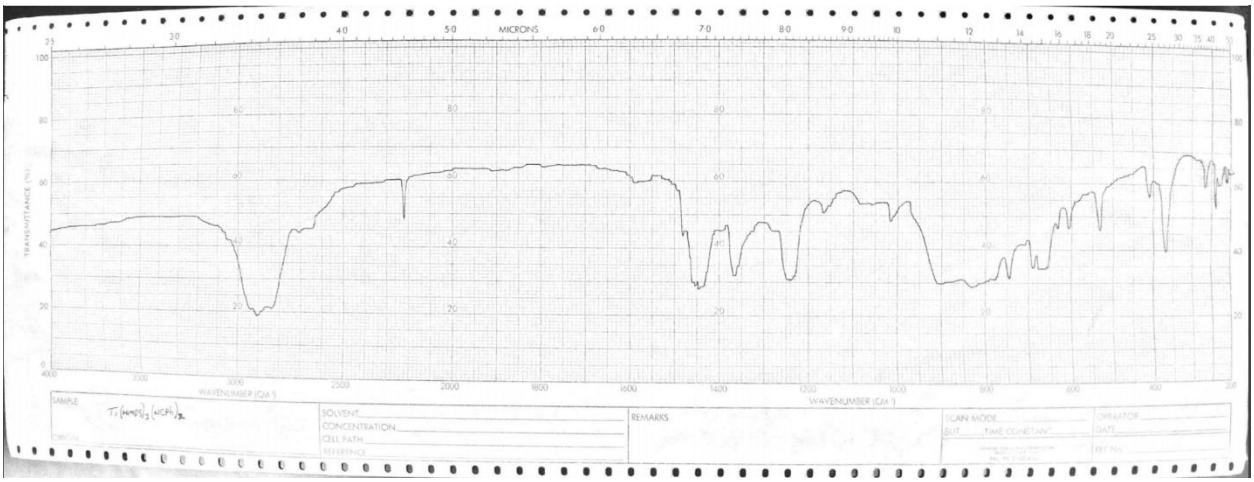

Figure 2.S23. Infrared Spectrum of $Ti\{N(SiMe_3)_2\}_3(PhCN)_2$ (**4**) (Nujol, CsI windows)

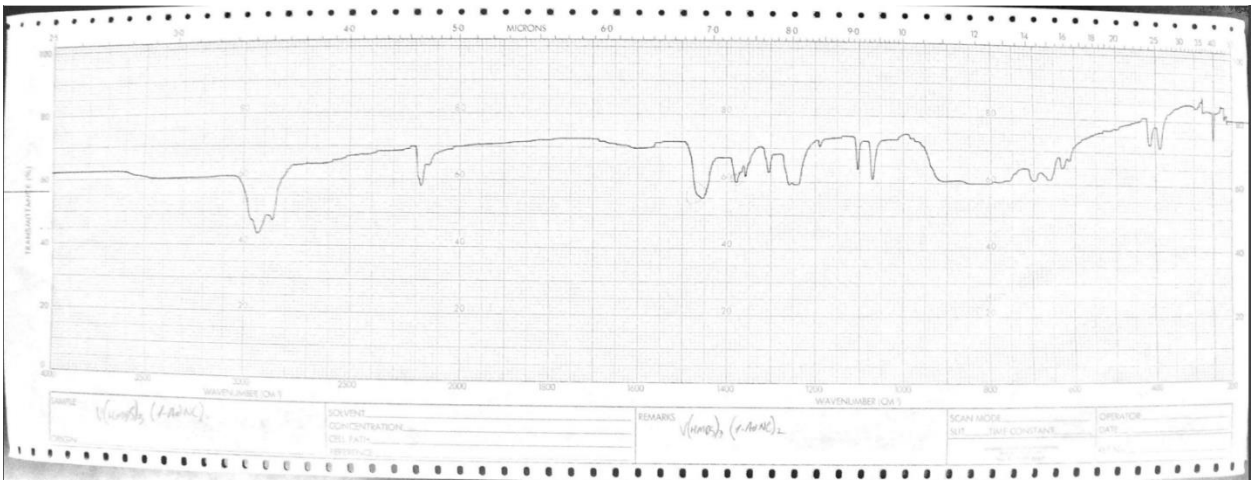

Figure 2.S24. Infrared Spectrum of $V\{N(SiMe_3)_2\}_3$ $(1\text{-AdNC})_2$ (**5**) (Nujol, CsI windows)

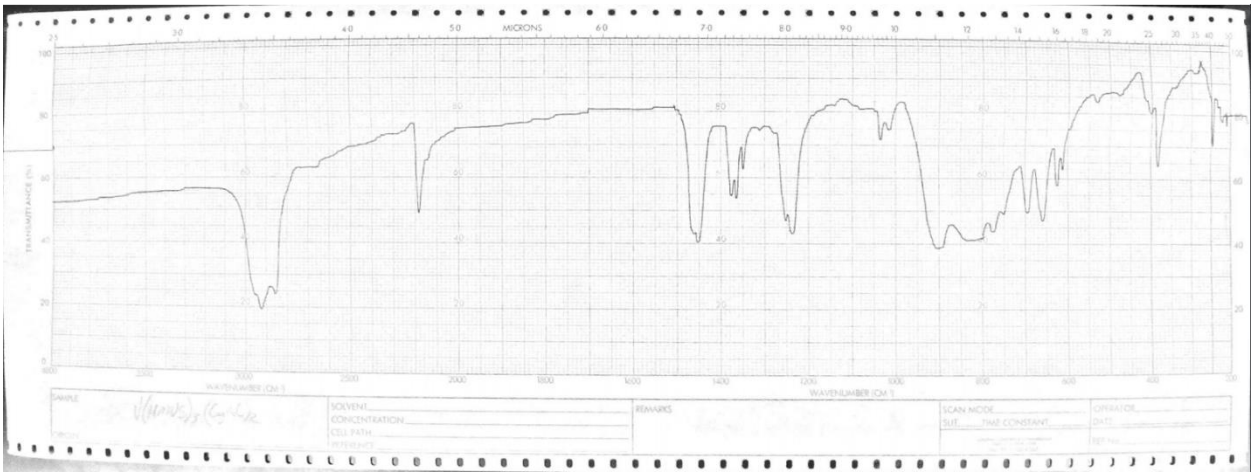

Figure 2.S25. Infrared Spectrum of $V\{N(SiMe_3)_2\}_3$ $(CyNC)_2$ (**6**) (Nujol, CsI windows)

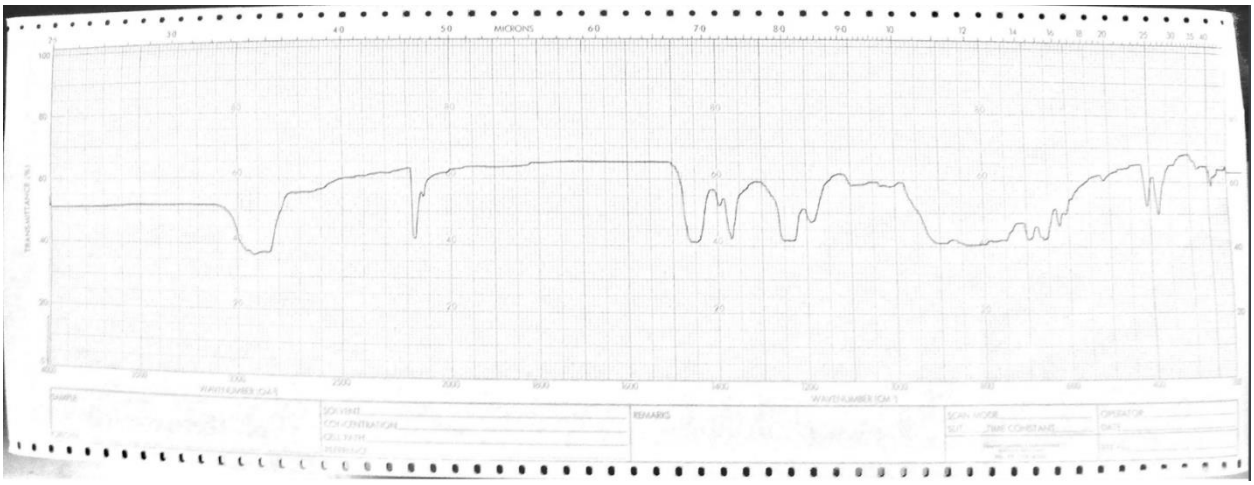

Figure 2.S26. Infrared Spectrum of $V\{N(SiMe_3)_2\}_3(Bu^tNC)_2$ (**7**) (Nujol, CsI windows)

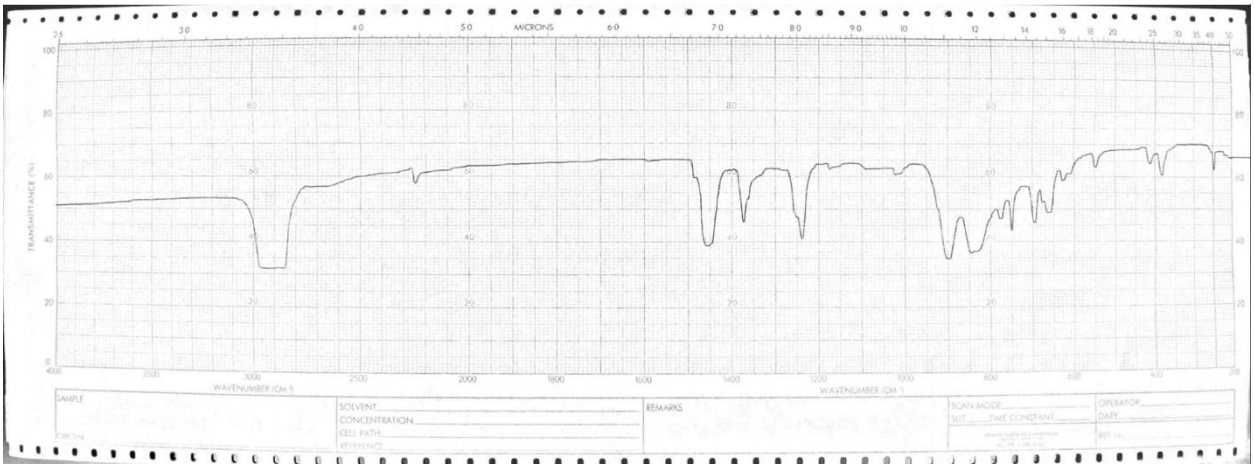

Figure 2.S27. Infrared Spectrum of $V\{N(SiMe_3)_2\}_3(PhCN)_2$ (**8**) (Nujol, CsI windows)

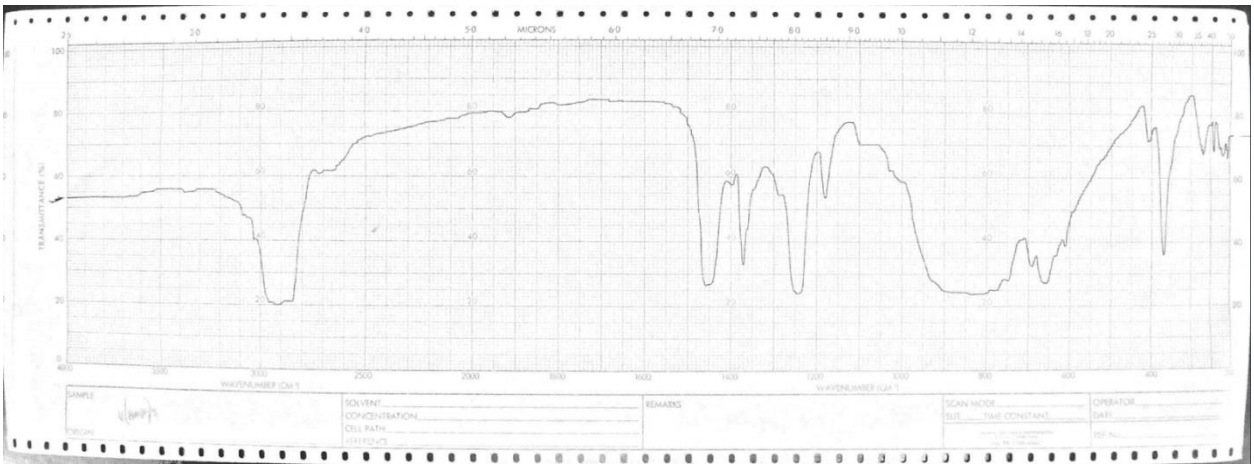

Figure 2.S28. Infrared Spectrum of $V\{N(SiMe_3)_2\}_3$ (Nujol, CsI windows)

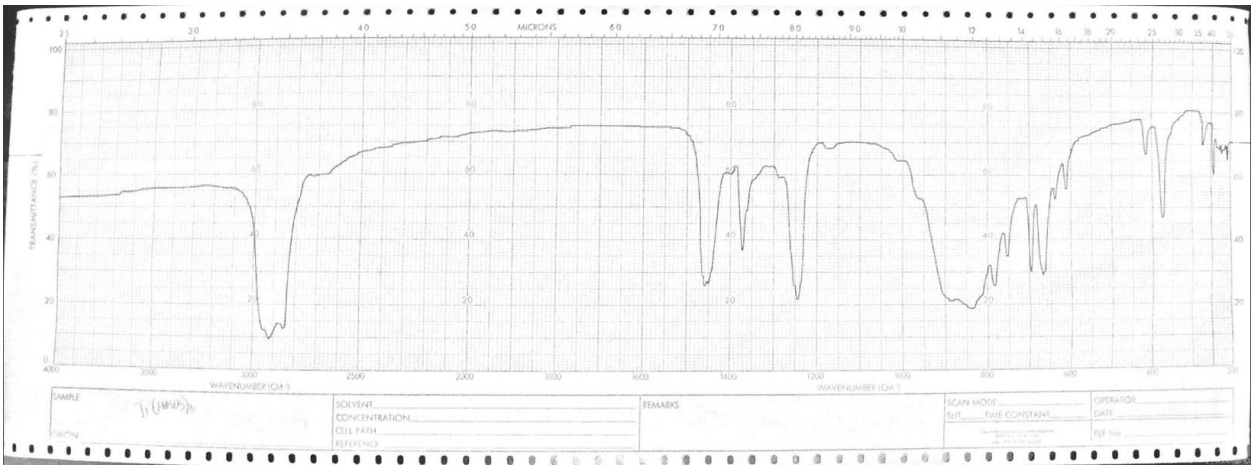

Figure 2.S29. Infrared Spectrum of $Ti\{N(SiMe_3)_2\}_3$ (Nujol, CsI windows)

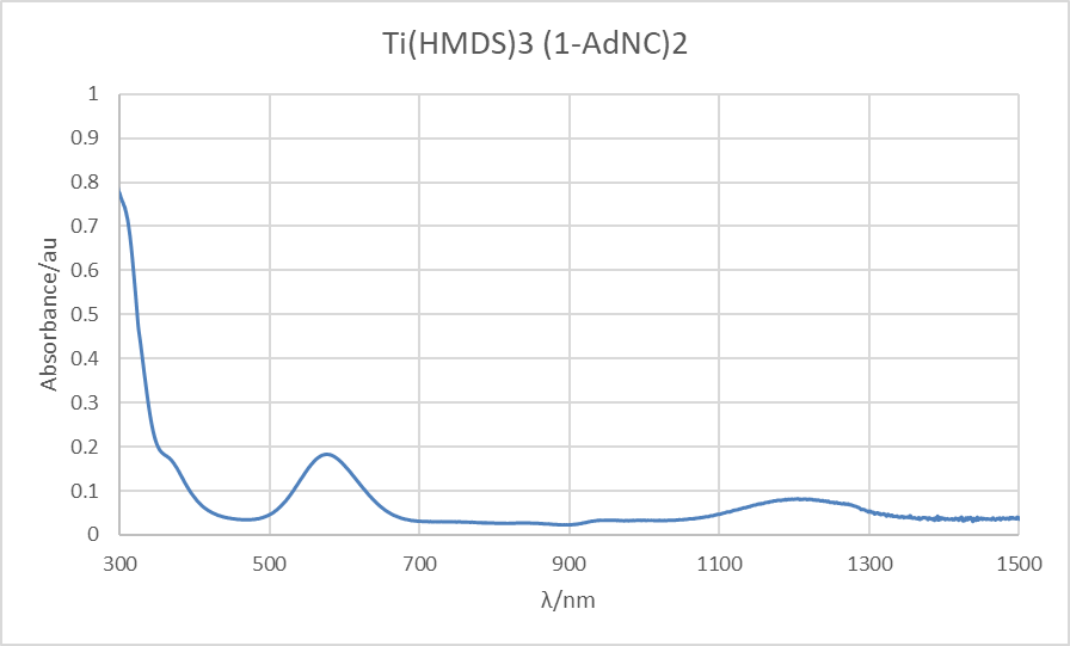

Figure 2.S30. UV-Vis spectrum of $Ti\{N(SiMe_3)_2\}_3$ $(1\text{-AdNC})_2$ (**1**) (0.34 mM, hexanes, 1 cm path length)

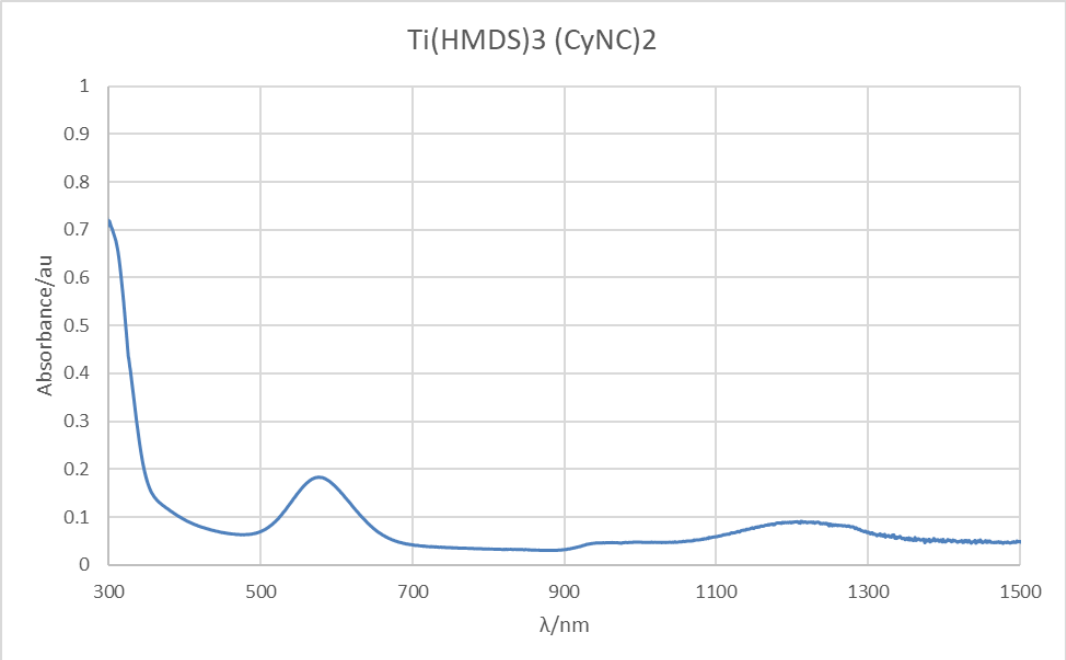

Figure 2.S31. UV-Vis spectrum of $Ti\{N(SiMe_3)_2\}_3$ $(CyNC)_2$ (**2**) (0.38 mM, hexanes, 1 cm path length)

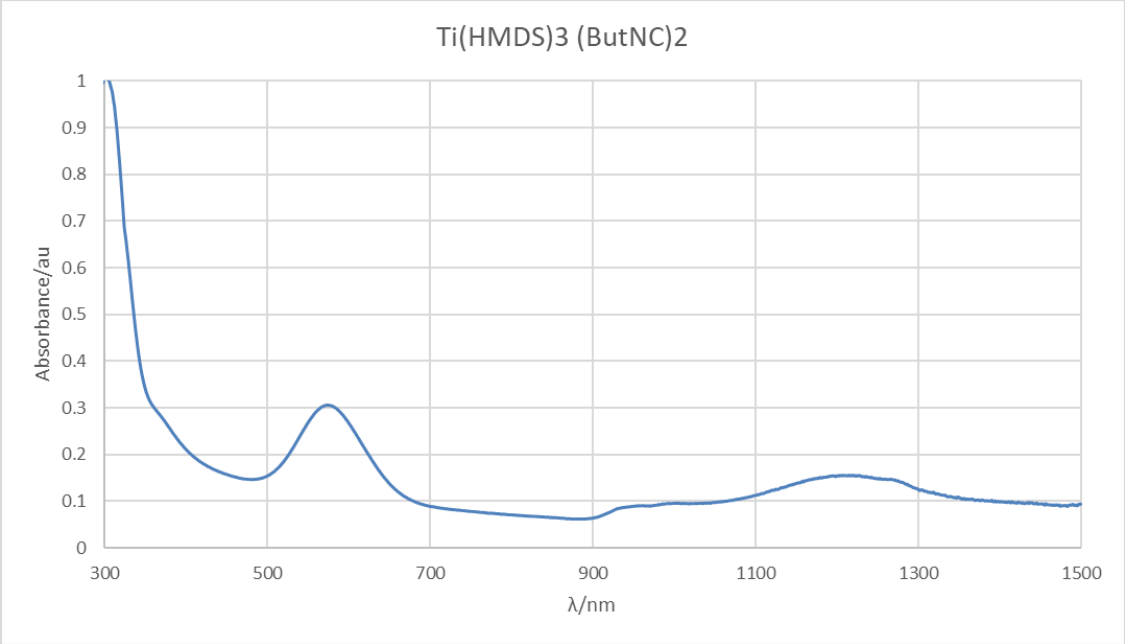

Figure 2.S32. UV-Vis spectrum of Ti{N(SiMe$_3$)$_2$}$_3$ (Bu^{t}NC)$_2$ (**3**) (0.41 mM, hexanes, 1 cm path length)

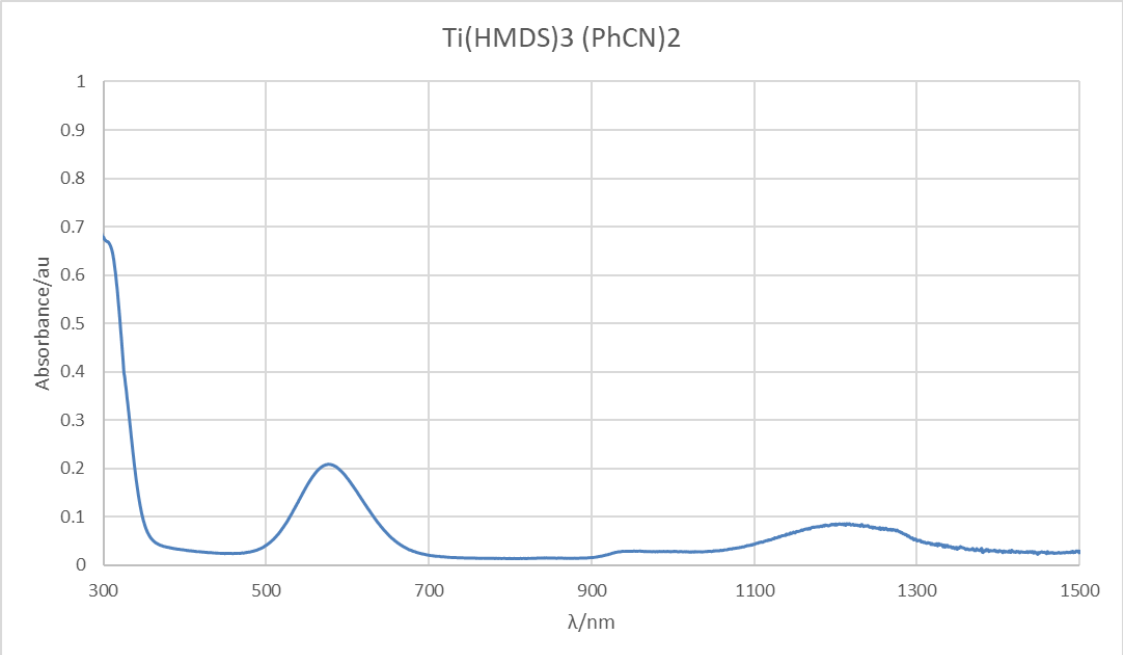

Figure 2.S33. UV-Vis spectrum of Ti{N(SiMe$_3$)$_2$}$_3$ (PhCN)$_2$ (**4**) (0.39 mM, hexanes, 1 cm path length)

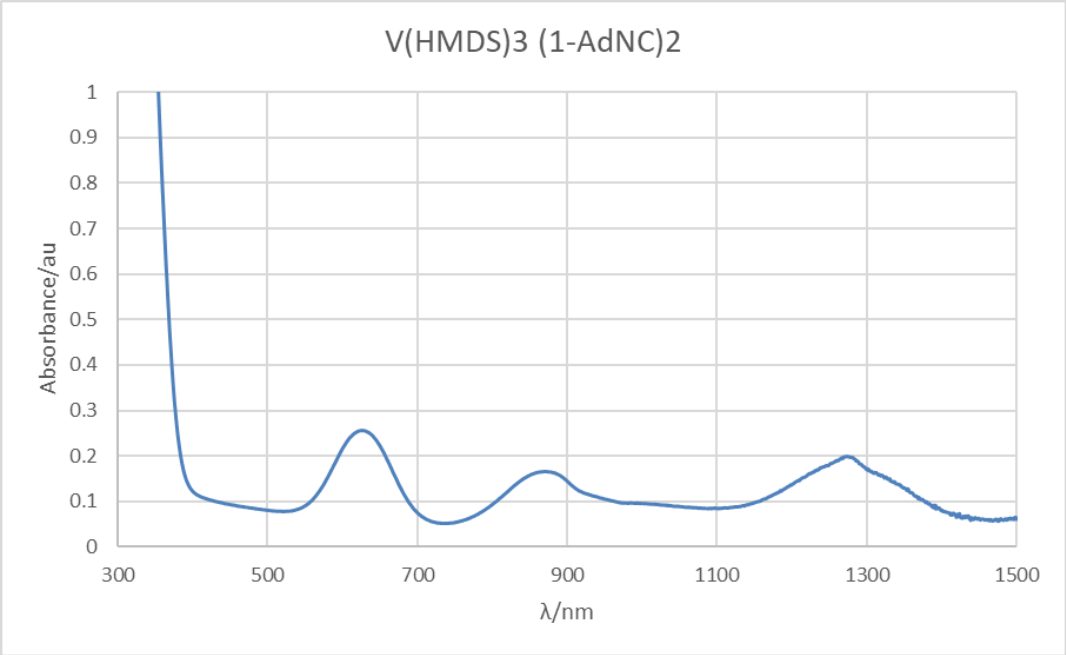

Figure 2.S34. UV-Vis spectrum of $V\{N(SiMe_3)_2\}_3$ $(1\text{-AdNC})_2$ (**5**) (0.33 mM, hexanes, 1 cm path length)

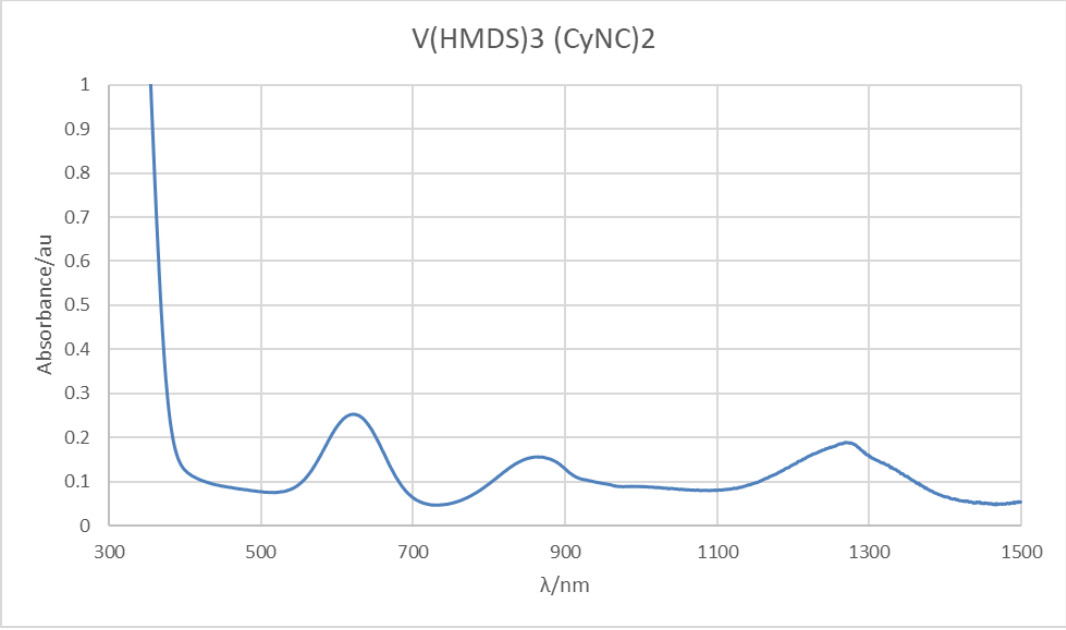

Figure 2.S35. UV-Vis spectrum of $V\{N(SiMe_3)_2\}_3$ $(CyNC)_2$ (**6**) (0.33 mM, hexanes, 1 cm path length)

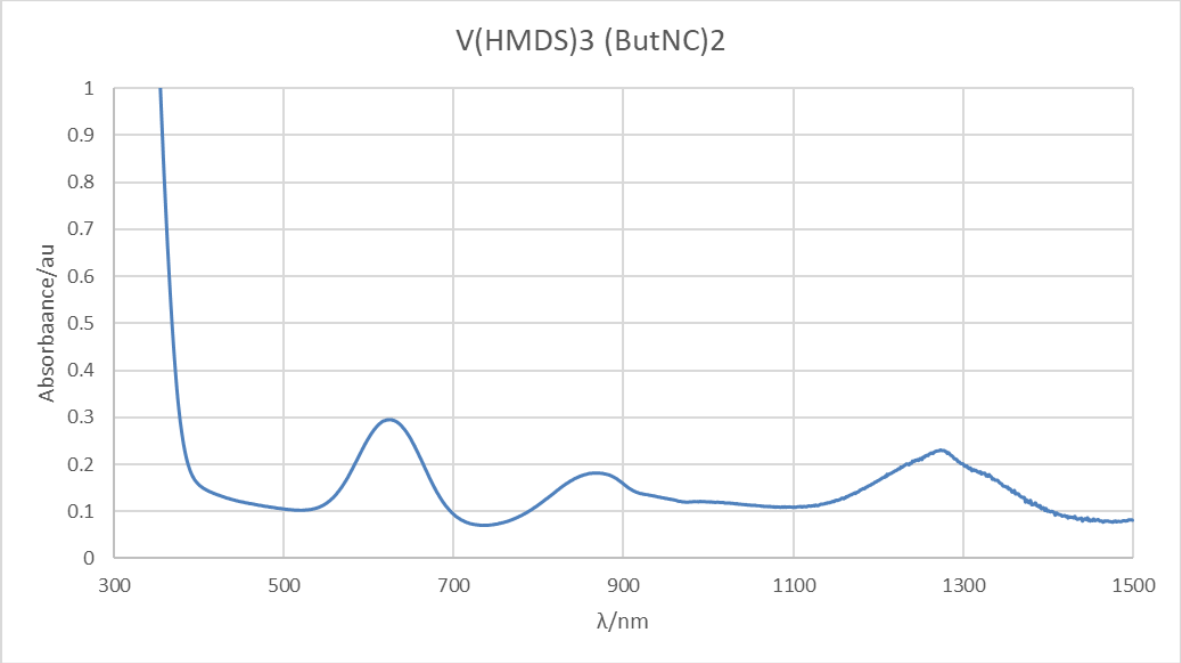

Figure 2.S36. UV-Vis spectrum of $V\{N(SiMe_3)_2\}_3$ $(Bu^tNC)_2$ (**7**) (0.41 mM, hexanes, 1 cm path length)

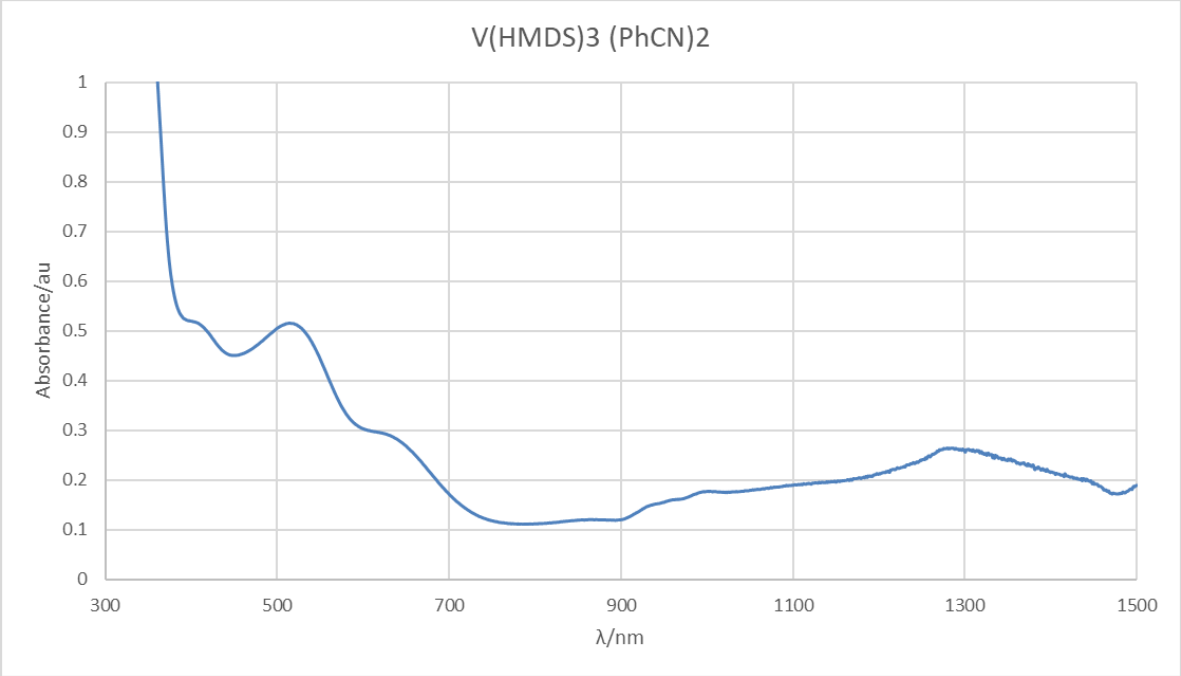

Figure 2.S37. UV-Vis spectrum of $V\{N(SiMe_3)_2\}_3$ $(PhCN)_2$ (**8**) (0.40 mM, hexanes, 1 cm path length)

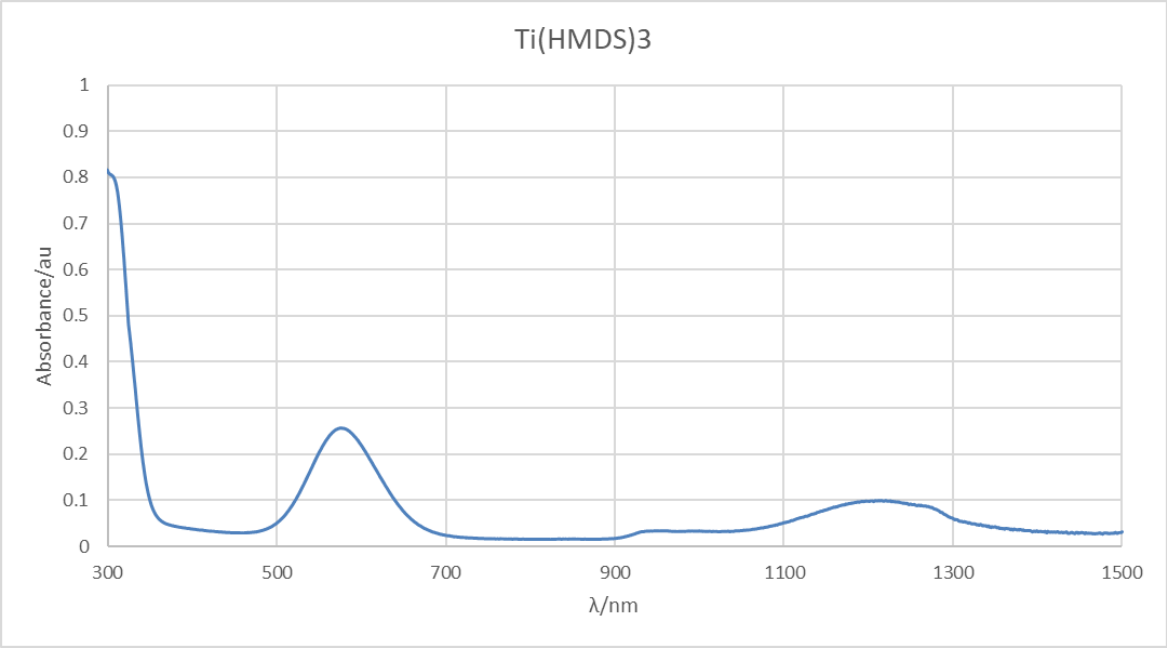

Figure 2.S38. UV-Vis spectrum of $Ti\{N(SiMe_3)_2\}_3$ (0.40 mM, hexanes, 1 cm path length)

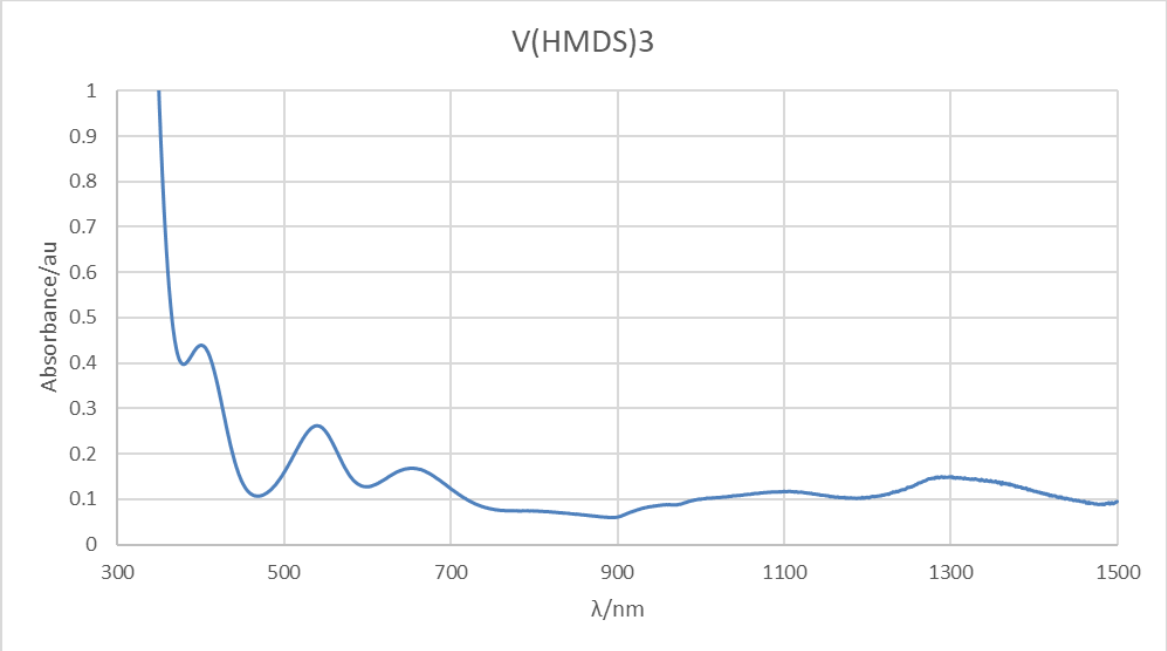

Figure 2.S39. UV-Vis spectrum of $V\{N(SiMe_3)_2\}_3$ (0.70 mM, hexanes, 1 cm path length)

Figure 2.S40. Photograph of V{N(SiMe$_3$) (1-AdNC)$_2$ (**5**) in solution (blue) and crystalline (red)

Figure 2.S40. Photograph of crystalline $V\{N(SiMe_3)_2\}_3$ $(PhCN)_2$

Figure 2.S41. Photograph of crystalline $Ti\{N(SiMe_3)_2\}_3$ $(1\text{-AdNC})_2$

Figure 2.S42. Photograph of crystalline $Ti\{N(SiMe_3)_2\}_3$

Chapter 3. Characterization of the "Absent" Vanadium Oxo V(=O){N(SiMe$_3$)$_2$}$_3$, Imido V(=NSiMe$_3$){N(SiMe$_3$)$_2$}$_3$, and Imido-Siloxy V(=NSiMe$_3$)(OSiMe$_3$){N(SiMe$_3$)$_2$}$_2$ Complexes Derived from V{N(SiMe$_3$)$_2$}$_3$ and Kinetic Study of the Spontaneous Conversion of the Oxo Complex into its Imido-Siloxy Isomer.

Cary R. Stennett, Thien H. Nguyen, and Philip P. Power*

This work is dedicated to the memory of Professor Richard A. Andersen, who made numerous important contributions to metal silylamide chemistry.

Reprinted with permission from *Inorg. Chem.* **2020**, 59, 15, 11079–11088.

Abstract.

The synthesis and characterization of V(=O){N(SiMe$_3$)$_2$}$_3$ (**1**), V(=NSiMe$_3$){N(SiMe$_3$)$_2$}$_3$ (**2**), and V(=NSiMe$_3$)(OSiMe$_3$){N(SiMe$_3$)$_2$}$_2$ (**3**) are described. Prior attempts to synthesize the vanadium(V) oxo complex **1** via salt metathesis of $VOCl_3$ with the lithium or sodium silylamide salt had yielded either the putative rearranged species V(=NSiMe$_3$)(OSiMe$_3$){N(SiMe$_3$)$_2$}$_2$ (**3**) or the oxo-bridged, dimetallic {(μ-O)$_2$V$_2$[N(SiMe$_3$)$_2$]$_4$}. We now show that complex **1** is available by treatment of the vanadium(III) tris(silylamide) V{N(SiMe$_3$)$_2$}$_3$ with iodosylbenzene. The imido complex **2** was obtained by treatment of V{N(SiMe$_3$)$_2$}$_3$ with trimethylsilyl azide. Sublimation of **1** formed complex **3**, which was determined to be V(=NSiMe$_3$)(OSiMe$_3$){N(SiMe$_3$)$_2$}$_2$ on the basis of infrared, electronic, ^{1}H, and ^{51}V NMR spectroscopies. Crystallographic disorder precluded a complete structural characterization of **3**, although a four-coordinate vanadium atom as well as severely disordered ligands were apparent. Comparison of the vibrational spectra of **1** and **2** allowed an unambiguous assignment of the V-O (995 cm^{-1}) and V-N$_{imide}$ (1060 cm^{-1}) stretching bands. The vibrational spectrum of complex **3** displayed strong absorbances at 1090 and 945 cm^{-1}, indicative of its metal imide and metal siloxide moieties. The ^{1}H NMR spectrum of **1** in deuterated benzene showed overlapping signals for the ligand protons proximal and distal to the oxo moiety at 0.52 and 0.38 ppm. The

^{1}H NMR spectrum of **2** in deuterated methylene chloride displayed distinct signals for the imido (0.41 ppm) and amido (0.35 ppm) protons, whereas ^{1}H NMR spectroscopy of **3** showed three signals in an intensity ratio consistent with the formula V(=NSiMe$_3$)(OSiMe$_3$){N(SiMe$_3$)$_2$}$_2$. ^{51}V NMR spectra of **1-3** revealed singlet resonances at -119 (**1**), -24 (**2**), and -279 (**3**) ppm. The electronic spectra of **1-3** displayed single absorbances in the charge transfer region, consistent with their d^0 electron configurations. Kinetic studies of the spontaneous conversion of complex **1** into **3** were used to determine the rate constants (ca. 0.0002 s^{-1} (63 °C), 0.0006 s^{-1} (73 °C), 0.002 (83 °C)) and activation energy (ca. 20 kcal/mol) of this first-order process.

Introduction.

Homoleptic metal bis(trimethysilyl)amide complexes M{N(SiMe$_3$)$_2$}$_n$ are of interest due to their low metal coordination numbers, ease of preparation and their broad use in synthesis.[1,2] Their utility as synthetic reagents has led to the ranking of the bis(trimethylsilyl)amide ligand among diisopropylamide and tetramethylpiperidide as the aptly-named 'utility amides.'[3] The ready availability and steric bulk of the -N(SiMe$_3$)$_2$ ligand makes it attractive for use in stabilizing low-coordinate metal complexes. Its large size inhibits association and generally confers high volatility on its metal complexes and hence their use as a volatile source of metal cations in atomic layer/chemical vapor deposition techniques,[4,5] as well as in the synthesis of nanoparticles.[6] These complexes have also been shown to be useful catalysts or precatalysts in some industrially important reactions.[7,8] Despite their long history and proven utility, recent work has shown that much of their chemistry remains unexplored and that there are inaccuracies in the original work on their synthesis and characterization. For instance, the earliest examples of divalent transition metal silylamido M{N(SiMe$_3$)$_2$}$_2$ complexes (M = Mn, Co, Ni), reported by Bürger and Wannagat in the 1960s,[9,10] were later shown to be THF complexes that arose from their synthesis in THF solvent.[11] Trivalent M(III) tris(silylamide) complexes M{N(SiMe$_3$)$_2$}$_3$ (M = Cr, Fe) were also first discovered by Bürger and Wannagat[9,10] and are now known for transition metals of the first row from scandium to cobalt,[12–17] many lanthanides,[12,18–24] and the actinides uranium, plutonium, and neptunium.[25–27] The synthesis, physical

properties and reactivity of the transition metal derivatives have been reviewed in two articles,[28,29] a book,[30] and an extensive chapter in a book series,[31] which also revealed instances of inaccurate characterization. For example, it was found recently that $V\{N(SiMe_3)_2\}_3$ had been originally mischaracterized as a brown crystalline solid, despite an accurate determination of its structural characteristics by X-ray crystallography.[1,32] The recent reinvestigation showed that it had a striking violet color and was readily characterizable by its ^{1}H-NMR, electronic, and infrared spectra.[14] These findings urged us to further investigate the chemistry of $V\{N(SiMe_3)_2\}_3$.

However, our investigation did not reveal the identity of the originally reported brown complex but suggested that it might be a vanadium(V) oxo species. Stable vanadium oxo complexes are commonplace (over 2400 structurally characterized vanadium complexes featuring a terminal oxide ligand are deposited in the CCDC),[33] so our initial hypothesis was that the brown complex may have formed by the reaction of $V\{N(SiMe_3)_2\}_3$ with adventitious oxygen. However, despite the large library of vanadium(V) oxo complexes, the simple oxo complex $V(=O)\{N(SiMe_3)_2\}_3$ (**1**) remained unknown. A survey of the literature revealed other unexplained results. Thus, at least two attempts to prepare this simple vanadium(V) oxo complex $V(=O)\{N(SiMe_3)_2\}_3$ (**1**) have appeared in the literature. In 1963, Bürger, Smrekar, and Wannagat reported that reaction of $VOCl_3$ with three equivalents of $NaN(SiMe_3)_2$ in ethereal solvent gave a green complex apparently consistent with the molecular formula of **1**.[34] However, the reported infrared spectrum of this complex showed no absorption indicative of a V-O multiple bond. It was concluded by the authors that a shift of one trimethylsilyl group from nitrogen to oxygen or interaction of $NaN(SiMe_3)_2$ with the V=O moiety of $VOCl_3$ had resulted in the formation of a siloxo/silylimido complex of the form $V(=NSiMe_3)(OSiMe_3)\{N(SiMe_3)_2\}_2$. A more recent paper by McCarley, Verkade, and coworkers in 1996 showed that reaction of $VOCl_3$ with three equivalents of $LiN(SiMe_3)_2$ in pentane or benzene gave the green dinuclear vanadium(IV) complex $\{(\mu\text{-}O)_2V_2[N(SiMe_3)_2]_4\}$.[35] Although prepared by very similar methods, the spectroscopic data indicate that the complex isolated by Bürger, Smrekar, and Wannagat[34] was distinct from the bridging oxo complex described by McCarley, Verkade and coworkers[35] despite both complexes

having a green color. In neither case was a terminal oxo group detected spectroscopically. Conversely, the niobium(V) congener $Nb(=O)\{N(SiMe_3)_2\}_3$ was successfully isolated by Hubert-Pfalzgraf and coworkers in 1988.[36] This complex was prepared in low yield by treatment of $(NbOCl_3)_n$ with $LiN(SiMe_3)_2$ or in significantly higher yield by reaction of $NbCl_4(THF)_2$ and $LiN(SiMe_3)_2$, which apparently proceeds by abstraction of an oxygen atom from the THF ligand of the niobium chloride. Given the large number of vanadium oxo complexes and the successful isolation of the aforementioned niobium oxo complex, we sought to isolate the 'missing' vanadium complex $V(=O)\{N(SiMe_3)_2\}_3$.

Herein we report the synthesis of $V(=O)\{N(SiMe_3)_2\}_3$ (**1**) and the related $V(=NSiMe_3)\{N(SiMe_3)_2\}_3$ (**2**) by treatment of $V\{N(SiMe_3)_2\}_3$ with iodosylbenzene or trimethylsilylazide, respectively. Complexes **1** and **2** were characterized by X-ray crystallography, as well as by ^1H, ^{51}V NMR, infrared, and electronic spectroscopies. Sublimation of a crude sample of **1** results in the formation of the complex $V(=NSiMe_3)(OSiMe_3)\{N(SiMe_3)_2\}_2$ (**3**), which was characterized spectroscopically. The X-ray crystallographic characterization of **3** was rendered incomplete by disorder. Complex **1** was also shown to convert spontaneously to complex **3** in solution or by thermolysis in the solid state, and a kinetic study was performed to estimate the activation energy of this transformation.

Experimental.

General considerations. All manipulations were performed by using modified Schlenk techniques or in a Vacuum Atmospheres drybox under nitrogen or argon. Solvents were dried and collected using an S2 Grubbs-type solvent purification system (Glass Contour) and degassed using the freeze, pump, thaw method. All physical measurements were obtained under strictly anaerobic and anhydrous conditions. IR spectra were recorded as Nujol mulls between CsI windows on a PerkinElmer 1430 spectrophotometer. UV–vis spectra were recorded as dilute hexane solutions in 3.5 mL quartz cuvettes using an OLIS modernized Cary 14 UV/vis/NIR spectrophotometer. ^1H NMR spectra were referenced to residual solvent signals. ^{51}V NMR spectra were referenced to an external standard of 90% vanadyl trichloride in deuterated toluene ($\delta = 0$). Melting points were determined on a Meltemp II apparatus in flame-sealed glass capillaries

and are uncorrected. Elemental analyses were not attempted due to the high air and moisture sensitivity of these complexes. $V\{N(SiMe_3)_2\}_3$[1,14] and iodosylbenzene[37,38] were prepared according to literature procedures. Trimethylsilyl azide was purified by distillation and stored overnight over 4 Å molecular sieves before use (caution: due to the risk of explosion, appropriate care should be taken when distilling trimethylsilyl azide).

Synthesis of $V(=O)\{N(SiMe_3)_2\}_3$ (1). A violet solution of $V\{N(SiMe_3)_2\}_3$ (0.5 g, 0.9 mmol) in ca. 20 mL of diethyl ether was added by cannula at room temperature to a stirred suspension of iodosylbenzene (0.42 g, 1.9 mmol) in ca. 20 mL of diethyl ether. The mixture was stirred overnight, and the resulting orange solution was filtered through Celite. The filtrate was concentrated under reduced pressure until the formation of small yellow crystals was observed. The solution was then warmed by hand to redissolve the crystals, whereupon the solution was re-cooled in a ca. -18 °C freezer for 24 hours to afford 0.16 g (30 %) of the product as yellow crystalline blocks that were suitable for X-ray crystallographic studies. M.p.: gradually became orange at 100-120 °C, decomposed at 237 °C. UV/Vis: λ/nm ($\varepsilon/M^{-1}cm^{-1}$): 343 (22000). IR (Nujol) $\tilde{\nu}$ [cm^{-1}] = 995 (νV=O). ^1H NMR (300 MHz, [D_6] benzene, 25 °C): δ = 0.52 ($SiMe_3$, 27H), 0.38 ($SiMe_3$, 27H). ^{51}V NMR (132 MHz, [D_2] methylene chloride, 25 °C): δ = -119 ($\Delta\nu_{1/2}$ = 133 Hz).

Synthesis of $V(=NSiMe_3)\{N(SiMe_3)_2\}_3$ (2). Trimethylsilyl azide (0.12 mL, 0.94 mmol) was added in one portion by syringe to a stirred violet solution of $V\{N(SiMe_3)_2\}_3$ (0.5 g, 0.94 mmol) in ca. 20 mL hexane at ca. -78 °C. The flask was then removed from the cold bath and stirring was continued at ambient temperature. Over one hour, the violet solution slowly became yellow with concomitant evolution of nitrogen gas. The hexane was then removed under reduced pressure to leave an oily residue, which was then dissolved in ca. 5 mL of diethyl ether to afford a yellow solution. The solution was then filtered and cooled overnight in a ca. -18 °C freezer to give 0.2 g of (40 %) of the product as yellow crystals that were suitable for X-ray diffraction studies. M.p.: 229 °C. UV/Vis: λ/nm ($\varepsilon/M^{-1}cm^{-1}$): 377 (6300). IR (Nujol) $\tilde{\nu}$ [cm^{-1}] = 1060 (νV=N). ^1H NMR (400 MHz, [D_6] benzene, 25 °C): δ = 0.47 ($SiMe_3$). ^1H NMR (300 MHz,

[D_2] methylene chloride, 25 °C): δ = 0.41 (s, -$NSiMe_3$, 9H), 0.35 (s, -$N(SiMe_3)_2$, 54H). ^{51}V NMR (132 MHz, [D_2] methylene chloride, 25 °C): δ = -24 ($\Delta\nu_{1/2}$ = 200 Hz).

Synthesis of V(=$NSiMe_3$)($OSiMe_3$){$N(SiMe_3)_2$}$_2$ (3). A violet solution of V{$N(SiMe_3)_2$}$_3$ (0.5 g, 0.94 mmol) in ca. 20 mL diethyl ether was added by cannula at room temperature to a stirred suspension of iodosylbenzene (0.21 g, 0.94 mmol) in ca. 20 mL diethyl ether, and the mixture was stirred overnight to give a dark yellow mixture. The solvent was removed under reduced pressure to give a yellow/brown residue. The crude residue was then sublimed (ca. 150 °C, 50 mTorr) to afford orange, crystalline **3**. The crystals were then collected and recrystallized from diethyl ether to give orange crystals suitable for X-ray crystallography. Complex **3** can be prepared in essentially quantitative yield by sublimation of a pure sample of **1** at 100 °C / 50 mTorr, or by heating powdered **1** to 100 °C for thirty minutes. The molecular structure of **3** was not definitively determined due to heavy crystallographic disorder in the ligand groups (see SI). M.p. 237 °C (dec.). UV/Vis: λ/nm (ε/$M^{-1}cm^{-1}$): 315 (5300). IR (Nujol) $\tilde{\nu}$ [cm^{-1}] = 1090 (νV=$NSiMe_3$), 945 (νV-$OSiMe_3$). ^{1}H NMR (300 MHz, [D_6] benzene, 25 °C): δ = 0.43 (s), 0.30 (m). ^{1}H NMR (400 MHz, [D_8] toluene, 25 °C): δ = 0.40 (s), 0.29 (m). ^{1}H NMR (400 MHz, [D_2] methylene chloride, 25 °C): δ = 0.29 (s, -$N(SiMe_3)_2$, 36H), 0.27 (s, =$NSiMe_3$, 9H), 0.23 (s, -$OSiMe_3$, 9H). ^{51}V NMR (132 MHz, [D_2] methylene chloride, 25 °C): δ = -279 ($\Delta\nu_{1/2}$ = 200 Hz).

X-ray Crystallography. Crystals of **1**-**3** were removed from the reaction flask under a flow of argon and covered in Paratone oil. Suitable crystals were selected, mounted on a MiTeGen MicroLoop, and then placed in the cold nitrogen stream of the diffractometer. Data collection was performed at 90 K using Mo Kα radiation (λ = 0.71073 Å) on a Bruker Apex II diffractometer. Absorption corrections were applied using SADABS.[39] Structure solution and refinement were performed within the Olex^2 GUI.[40] The structures were solved by intrinsic phasing using SHELXT[41] and refined by least-squares methods using SHELXL.[42] All non-hydrogen atoms were refined anisotropically. The structure of **1** was refined further by determination of the appropriate twin law and subsequent full matrix (BASF/TWIN) refinement.[42]

Although the data set for **3** was of high quality, the structure could be only partially solved due to extensive disorder.

Results and Discussion.

Synthesis. Several monomeric vanadium(V) complexes of formula $V(=O)L_3$ (L = monoanionic, unidentate ligand) featuring a terminal oxo ligand have been reported previously.[43–51] They were prepared by a variety of methods, including treatment of a vanadium(III) precursor with an oxidant (e.g. iodosylbenzene,[43] pyridine n-oxide,[45] or styrene oxide[52]), salt metathesis of an alkali metal complex or Grignard reagent and $VOCl_3$,[53] or, uniquely, by the passage of a hydrocarbon solution of a vanadium(IV) complex through a column of cellulose.[53] Previous experimental work has shown that $V(=O)\{N(SiMe_3)_2\}_3$ (**1**) is inaccessible through the salt metathesis route,[34,35] possibly due to the reactivity of the trimethylsilyl groups of the ligands toward metal oxo moieties. Furthermore, our own work has shown that the tris(silylamide) $V\{N(SiMe_3)_2\}_3$ is unreactive toward a variety of coordinating bases due to the steric crowding engendered by the three silylamide ligands, which increases the difficulty of addition reactions. Nonetheless, given the steric similarities between iodosylbenzene[54] and the isocyanide and nitrile bases which formed, albeit weak, complexes with $V\{N(SiMe_3)_2\}_3$,[55] it was thought possible that **1** would be formed via the reaction of iodosylbenzene with the vanadium trisamide.

The synthesis of complexes **1**-**3** is described in Scheme 3.1. The reaction of $V\{N(SiMe_3)_2\}_3$ with one equivalent of iodosylbenzene in diethyl ether followed by recrystallization of the crude product from the same solvent afforded pale yellow crystals of **1** in low yield. Improved yields of **1** were achieved by reaction of $V\{N(SiMe_3)_2\}_3$ with a twofold excess of iodosylbenzene. Given the success of this synthesis, we further sought to isolate the related imido complex $V\{=N(SiMe_3)\}\{N(SiMe_3)_2\}_3$ (**2**) in order to compare its structural and spectroscopic features with those of **1**. Treatment of $V\{N(SiMe_3)_2\}_3$ with one equivalent of trimethylsilyl azide in hexanes followed by recrystallization from diethyl ether afforded yellow crystals of **2** in modest yield. Complexes **1** and **2** are highly air and moisture sensitive, and their high solubility in hydrocarbon solvents resulted in relatively high crystallization losses and lower purified yields. Attempts

to form analogous oxo-complexes with later first-row transition metals (Cr, Mn, Fe, Co) were unsuccessful, likely for electronic reasons that we have described elsewhere.[55] Sublimation of the crude residue of the reaction of a stoichiometric equivalent of iodosyl benzene with $V\{N(SiMe_3)_2\}_3$ was attempted to improve the isolated yield of **1**. During this process, bright orange crystals of a new complex, **3**, were isolated. Our characterization of this complex is described in detail below.

Scheme 3.1: Synthesis of complexes **1**-**3**.

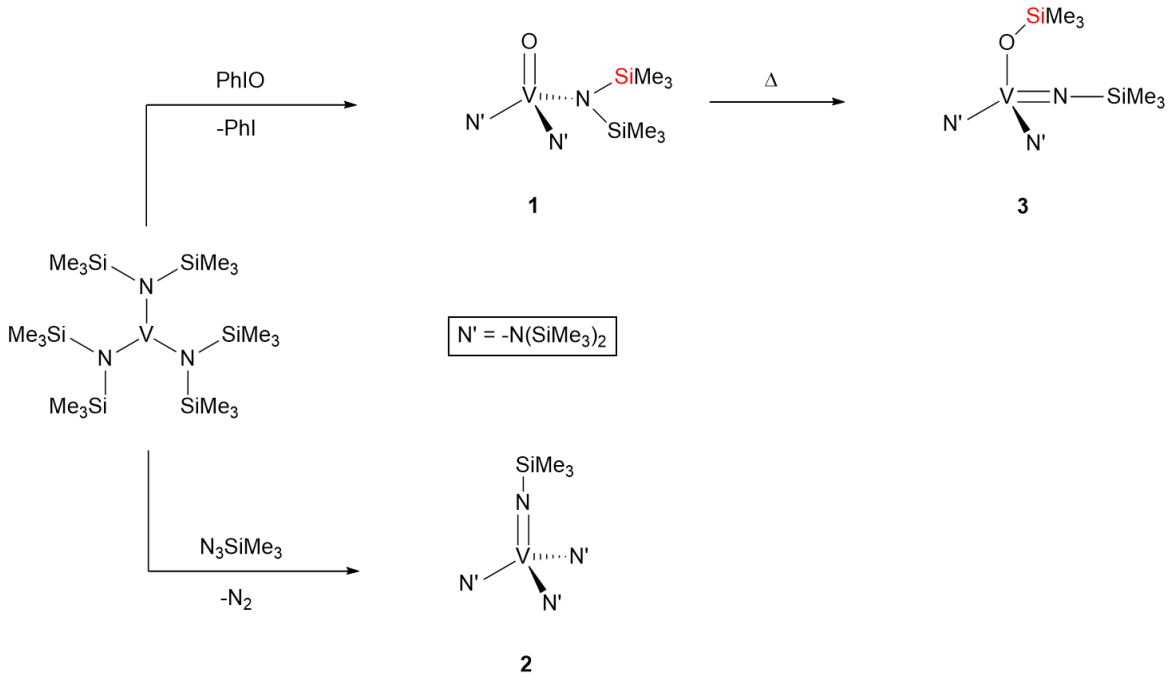

Structures. The molecular structures of **1** and **2** are shown in Figure 3.1, and important bond distances and angles are given in Table 3.1. Complex **1** crystallizes in the orthorhombic space group $Pca2_1$, while **2** crystallizes in the trigonal space group R3c. Complexes **1** and **2** crystallized as racemic mixtures of their Δ and Λ enantiomers. In each case, the geometry around vanadium approaches idealized tetrahedral, with τ_4 values of 0.92 (**1**) and 0.95 (**2**).[56] The average V-O bond length in **1** (1.598(1) Å) is comparable to those found in other vanadium(V) mono-oxo complexes (cf. $V(=O)\{OC(Bu^t)_2Me\}_3$ (1.605(1) Å),[43] $V(=O)\{N(3,5\text{-}Me_2\text{-}C_6H_3)(Bu^t)\}_3$ (1.590(3) Å),[45] $V(=O)(2,4,6\text{-}Me_3\text{-}C_6H_2)_3$ (1.578(4) Å)[50]). The analogous $V\text{-}N_{imide}$ bond length (1.672(4) Å) is slightly longer, which is consistent with the larger size of nitrogen versus oxygen[57] and with previously established trends between $V\text{-}O_{oxo}$ and $V\text{-}N_{imide}$ bond lengths in vanadium complexes sharing comparable ligand environments.[58] The $V\text{-}N_{imide}\text{-}Si$ bond angle in complex **2** is strictly linear as crystallographically required. The $V\text{-}N_{amide}$ bond lengths in **1** (1.899(1) Å) are shortened in comparison to that of the parent $V\{N(SiMe_3)_2\}_3$ complex (V-N = 1.9173(11) Å),[14] despite the higher coordination number but consistent with the decreased ionic radius of vanadium(V) (0.355 Å) versus that of vanadium(III) (0.640 Å).[59] It is worth mentioning that the related (although not strictly three-coordinate) vanadium(III) trisamide reported by Gambarotta and coworkers, $V\{N(1\text{-adamantyl})(3,5\text{-}Me_2\text{-}C_6H_3)\}_3$[60] has

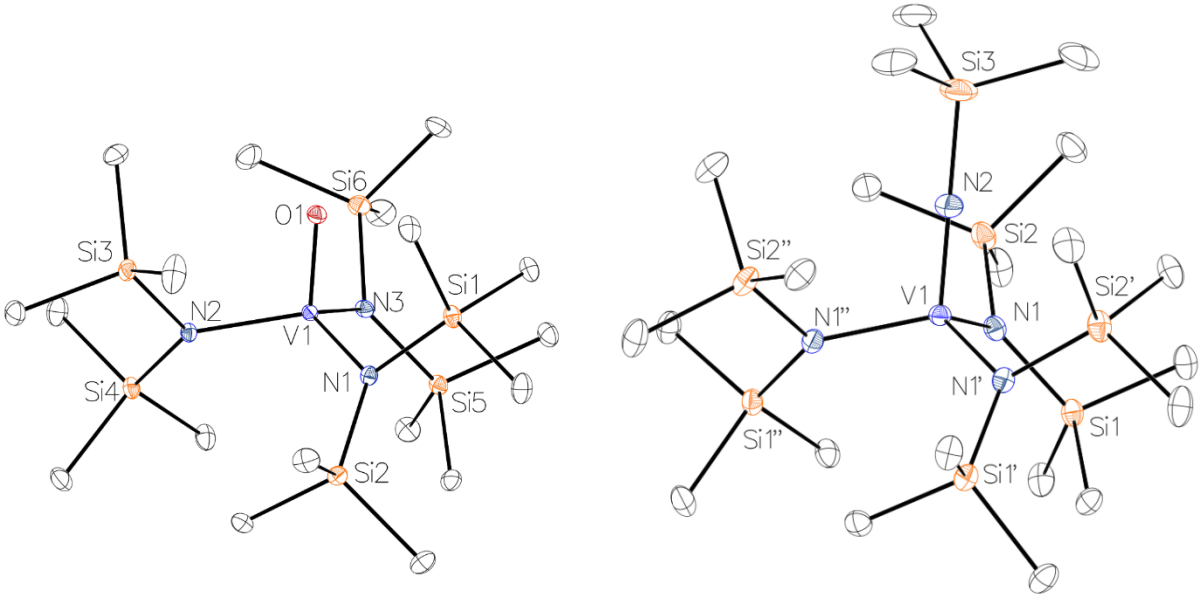

Figure 3.1: Molecular structures of **1** (left) and **2** (right). Thermal ellipsoids are shown at 30% probability. For clarity, hydrogen atoms are not shown. Selected bond distances and angles are given in Table 1.

V-N bond lengths of 1.945(3), 1.900(3), and 1.905(3) Å, the longest of which is associated with an interaction between the vanadium and an aryl group of one of the amido ligands. Oxidation of this complex with elemental sulfur or selenium results in the tetrahedrally coordinated sulfido or selenido complexes analogous to complex **1**. In agreement with what is shown in **1**, the average V-N bond distance in this complex is shortened upon oxidation to 1.892 Å. However, this trend is not observed in imido complex **2**, where the corresponding V-N_{amide} distance (1.923(2) Å) is slightly lengthened in comparison to that of the parent trisamide. However, $V\{N(SiMe_3)_2\}_3$ remains the sole example of a structurally characterized strictly three-coordinate homoleptic vanadium(III) trisamide,[14] making it difficult to establish a trend for V-N_{amide} bond length upon oxidation of such complexes.

While the diffraction data for complex **3** are of high technical quality (R_{int} = 0.0298, I/σ = 92.1), the similarity of the ligand group substitution in the molecule and the required symmetry of the space group ($P4_2/nmc$) resulted in extensive disorder that precluded a satisfactory determination of its molecular structure (see SI). This obstacle persisted across several data sets that were collected at a variety of temperatures, as well as after recrystallization of **3** from several solvents (hexane, toluene, benzene, diethyl ether, tetrahydrofuran). Despite this, it could be determined from the diffraction data that the molecule contains a single four-coordinate vanadium atom with a coordination environment of approximately tetrahedral geometry, and an average metal-ligand distance of 1.804(12) Å. This distance is similar to the average metal-ligand distance found in complex **1** (1.823(1) Å), but significantly shorter than that found in complex **2** (1.860(2) Å). Typical V-$OSiMe_3$ bond lengths range from ca. 1.74 to 1.83 Å[61,62]. Using these values and those determined experimentally in complexes **1** and **2**, a reasonable range for the average M-L bond length in **3,** assuming a structural formula of $V(=NSiMe_3)(OSiMe_3)\{N(SiMe_3)_2\}_2$, was between 1.80 and 1.84 Å. This range, and the experimentally determined value, agree with the presence of an -$OSiMe_3$ and an =$NSiMe_3$ ligand in complex **3.**

Table 3.1: Selected bond lengths (Å) and angles (°) for complexes 1 and 2.

	$V(=O)\{N(SiMe_3)_2\}_3$ (**1**)	$V\{=N(SiMe_3)\}\{N(SiMe_3)_2\}_3$ (**2**)
V-O (avg)	1.598(1)	-
$V\text{-}N_{imide}$	-	1.672(4)
$V\text{-}N_{amide}$ (avg)	1.899(1)	1.923(2)
N-V-O (avg)	103.09(5)	-
$N\text{-}V\text{-}N_{imide}$ (avg)	-	106.00(7)
N-V-N (avg)	115.03(6)	112.71(6)
Σ N-V-N	345.08(2)	338.13(6)

Spectroscopy. *Vibrational spectroscopy*. Vibrational spectroscopy studies of vanadium(V) complexes featuring a terminal oxo ligand have suggested that the presence of a stretching band in the region of ca. 900-1050 cm^{-1} can be taken as diagnostic of a terminal V-O bond.[63] The analogous $V\text{-}N_{imide}$ stretching frequency, however, is often difficult to determine due to the potential for strong coupling of the $M\text{-}N_{imide}$ stretching mode with other metal-ligand and N-R vibrations.[58] This difficulty has resulted in the absence of infrared spectra for many of the reported metal imido complexes, or, in many cases, the absence of assigned $M\text{-}N_{imide}$ stretches where such data are reported. The majority of reported $M\text{-}N_{imide}$ stretching bands appear in the range of 1100-1300 cm^{-1}, although assignment of these bands is a matter of some controversy.[58,64] This is exemplified by a report involving the study of ^{15}N labelled $Cp^*_2V{=}NPh$ which suggested that the band found in this region is due to the N-C stretching mode, and that the $V\text{-}N_{imide}$ stretching frequency may be as low as 934 cm^{-1}.[65] This assignment was made on the basis of the observed change in energy of the stretching bands associated with the imido ligand in $Cp^*_2V{=}NPh$ (1300, 934 cm^{-1}) when compared to the related complex $Cp^*_2V{=}N(2,6\text{-}Me_2\text{-}C_6H_3)$ (1293, 940 cm^{-1}). These changes are in agreement with the observed shortening of the V-N bond and lengthening of the N-C bond in the methyl substituted derivative. More recent studies involving metal alkyl/arylimide[66,67] and metal alkylidyne[68]

complexes have further corroborated this claim and suggest that these higher energy bands may be taken as a general fingerprint of such complexes, though they are not simple diatomic stretching modes.

Characteristic stretching frequencies of complexes **1**-**3** are given in Table 3.2. Given their similar ligand environments, we anticipated that the vibrational spectra of complexes **1** and **2** would permit assignment of these vibrational frequencies. The infrared spectrum of complex **1** contains the expected strong V-O stretching band which appears at 995 cm^{-1} in good agreement with values previously reported for related complexes.[43,44] The spectrum of complex **2** is very similar to that of **1**, differing only in the absence of the V-O stretching band and the appearance of a new band at 1060 cm^{-1}. The similarity of these two spectra allows the absorbance at 1060 cm^{-1} to be assigned as the $V\text{-}N_{imide}$ stretching band. Among the small number of structurally characterized vanadium trimethylsilylimido complexes, a lone report suggests that the $V\text{-}N_{imide}$ stretching band in $VCl_3(=NSiMe_3)$ is at 1104 cm^{-1}.[69] Several examples of other first-row transition metal trimethylsilylimido complexes are known, but the $M\text{-}N_{imide}$ stretching band is either not reported or not assigned. It is therefore difficult to establish a trend for these energies, but the absence of any lower frequency bands in the vibrational spectrum of imido complex **2** distinguishing it from oxo complex **1** indicates that the band at 1060 cm^{-1} is either the authentic $V\text{-}N_{imide}$ stretching band or that any other vibrations associated with this ligand are obscured by other bands found in the spectra of both complexes.

The vibrational spectrum of complex **3** lacks the characteristic V-O multiple bond stretching band found in oxo complex **1**, and instead shows two new bands at 1090 and 945 cm^{-1}. Additionally, the pair of metal amide stretching bands (A_1 and E) that are present in complexes **1** (A_1 = 430, E = 390 cm^{-1}) and **2** (A_1 = 440, E = 400 cm^{-1}) are absent in complex **3**. Instead, the spectrum of complex **3** features a single weak absorption at 400 cm^{-1}, suggesting that the threefold rotational symmetry of the $V\text{-}N_3$ moiety found in complexes **1** and **2** is absent in complex **3**. Along with an assignment of the 1090 cm^{-1} absorption to the $V\text{-}N_{imide}$ stretching band, these data (cf. NMR data below) suggest that $V(=NSiMe_3)(OSiMe_3)\{N(SiMe_3)_2\}_2$ is the most likely formulation of **3**. This is the same as that previously deduced (but not spectroscopically

demonstrated) by Bürger, Smrekar, and Wannagat to be the product of the reaction between $VOCl_3$ and three equivalents of $NaN(SiMe_3)_2$ and subsequent sublimation. While these data suggest that the identity of **3** is the same as that previously reported, the complex **3** that we isolated differs in several ways from that described earlier.[34] For example, our complex **3** has an orange color, whereas that reported earlier was described as having an "olive green" color.[34] Furthermore, the earlier reported infrared spectrum had stretching bands at 1117 and 986 cm^{-1}, which is in poor agreement with what we observe for complex **3**. However, as mentioned above, the identification of complex **3** as $V(=NSiMe_3)(OSiMe_3)\{N(SiMe_3)_2\}_2$ is further supported by NMR spectroscopy (vide infra).

Table 3.2: Selected Vibrational Frequencies (cm^{-1}) of Complexes 1-3

	$V\text{-}O_{oxo}$	$V\text{-}O_{siloxide}$	$V\text{-}N_{imide}$	$V\text{-}N_{amide}$
$V(=O)\{N(SiMe_3)_2\}_3$ (**1**)	995	-	-	430 (A_1), 390 (E)
$V(=NSiMe_3)\{N(SiMe_3)_2\}_3$ (**2**)	-	-	1060	440 (A_1), 400 (E)
$V(=NSiMe_3)(OSiMe_3)\{N(SiMe_3)_2\}_2$ (**3**)	-	945	1090	400

NMR and Electronic Spectroscopy. The ^{1}H NMR spectrum of oxo complex **1** in deuterated benzene shows two overlapping resonances corresponding to distal and proximal trimethylsilyl protons at 0.52 and 0.38 ppm that integrate in a 1:1 ratio. In contrast, free rotation of the bis(trimethylsilyl)amide ligands of the niobium analogue $Nb(=O)\{N(SiMe_3)_2\}_3$ results in a spectrum containing a single resonance at room temperature that resolves into two resonances at -11 °C.[36] That this behavior is not seen in the room temperature spectrum of complex **1** can be attributed to the significantly greater crowding due to the shorter M-N bond distances found in **1** (average V-N distance: 1.899(1) Å) in comparison to that found in the niobium analogue (average Nb-N distance: 2.020(1) Å). Unlike the spectrum of complex **1**, the ^{1}H-NMR spectrum of imido complex **2** in deuterated benzene contains a single unsymmetric resonance at 0.47 ppm. Closer examination indicated that this signal is likely comprised of at least two poorly resolved resonances, with a less intense signal slightly upfield of the main resonance at 0.47 ppm. To better resolve these signals,

we collected the spectrum of complex **2** in deuterated methylene chloride. Two signals were then apparent at 0.41 and 0.35 ppm and these integrated in a 1:6 ratio, indicating that the upfield signal corresponds to the six trimethylsilyl groups from the three amido ligands (54 protons), and the signal at 0.41 corresponds to those of the imido ligand (9 protons).

The ^{1}H-NMR spectrum of complex **3** in deuterated toluene displays a singlet resonance at 0.40 ppm and an overlapping pair of signals at 0.31 ($NSiMe_3$) and 0.29 ($OSiMe_3$) ppm. The assignment of the imido and siloxide protons was made on the basis of the chemical shifts of other vanadium complexes featuring these ligands.[70,71] The more intense signal at 0.40 ppm integrates with the less intense pair of signals in a 2:1 ratio. This spectrum is consistent with the proposed structure of **3** as $V(=NSiMe_3)(OSiMe_3)\{N(SiMe_3)_2\}_2$, which should have three distinct resonances; a signal for the amido trimethylsilyl protons (36 protons), as well as signals for the imido (9 protons) and siloxido (9 protons) ligands. As the chemical shift of the less intense pair of signals coincide with the chemical shift of a potential silicone grease impurity, the ^{1}H-NMR spectrum of **3** was recollected in deuterated methylene chloride. This spectrum contained three signals: an intense singlet at 0.29 ppm with a less intense shoulder at 0.27 ppm, and a singlet at 0.23 ppm of roughly the same intensity as the shoulder signal at 0.27 ppm. These data also agree with our formulation of **3** as $V(=NSiMe_3)(OSiMe_3)\{N(SiMe_3)_2\}_2$, as the overlapping signals at 0.29 and 0.27 ppm integrate with the resonance at 0.23 ppm in the expected 5:1 ratio.

Complexes **1**-**3** were further characterized by ^{51}V NMR and UV-visible spectroscopies. The ^{51}V NMR spectra of complexes **1**-**3** each featured a single resonance. These were observed at -119 (**1**), -24 (**2**), and -279 (**3**) ppm. The resonances of **1** and **2** appear at shifts comparable to the structurally similar five-coordinate oxido and imido complexes previously reported by Schrock.[72] The large upfield chemical shift of **1** in comparison to that of **2** agrees with the general observation that ^{51}V NMR signals of high valent vanadium complexes are typically shifted upfield as the metal is coordinated to more electronegative groups, a non-intuitive effect described elsewhere as an "inverse electronegativity dependence."[73,74] The signal due to **3** is observed furthest upfield, but in the absence of other reported shifts for similar compounds

it is difficult to draw useful conclusions. UV-vis spectroscopy revealed strong absorbances (ε = ca. 5000-6000 $M^{-1}cm^{-1}$) consistent with charge transfer transitions in the ultraviolet region of the spectrum, with complexes **1**, **2**, and **3** having maxima at 343, 377, and 315 nm, respectively. No weaker absorbances were detected in the visible region, consistent with the d^0 electron configuration of these complexes.

Conversion of Oxo Complex 1 to Siloxido Complex 3. Our attempts to characterize the oxo complex **1** were initially frustrated by its unusual solution behavior. Despite using crystalline **1** for sample preparation, the ^{1}H NMR spectrum of **1** was difficult to understand and contained far more resonances than predicted on the basis of its molecular structure. As described above, attempts to further purify **1** by sublimation resulted in the formation of the imido/siloxido complex **3**. Examination of the ^{1}H NMR spectrum of this complex revealed that complex **3** was the impurity consistently found in the ^{1}H NMR spectrum of oxo complex **1**. Further, we discovered that the spectrum of **1** was free of this impurity when the data were collected immediately after sample preparation, suggesting that conversion of complex **1** to complex **3** takes place in solution at a significant rate at ambient temperature.

Indeed, through several NMR experiments over a period of five days, **1** was shown to slowly convert to **3** at 25 °C in deuterated benzene by an apparent migration of a trimethylsilyl group from an amido ligand to the oxo moiety in **1** (see SI). Kinetic studies monitoring the relative concentration of **1** versus **3** by ^{1}H NMR spectroscopy were performed at 63, 73, and 83 °C. Using these data, we estimate the rate constants at these temperatures to be 0.0002, 0.0006, and 0.002 s^{-1}, respectively. A plot of the data showing this conversion at 73 °C is shown in Figure 3.2. Using an Arrhenius plot of these rate constants (ln(k) versus 1/T), we estimate the activation energy of this conversion to be ca. 20 kcal/mol (See SI). This activation energy is in good agreement with activation energies previously experimentally determined for the exchange of trimethylsilyl groups between nitrogen and oxygen in organic trimethylsilyl amides (15.0 to 22.1 kcal/mol),[75] lending further support to our identification of complex **3** as $V(=NSiMe_3)(OSiMe_3)\{N(SiMe_3)_2\}_2$.

It is worth noting here that this conversion apparently does not occur in the analogous niobium(V) oxo complex Nb(=O){N(SiMe$_3$)$_2$}$_3$.[36] The reported details of this complex are thorough, with its fluxionality in solution attributed to rotation of the bis(trimethylsilyl)amide ligands. However, no evidence of silyl migration was apparent from the data. This difference in stability is potentially a result of the significantly larger ionic radius of four coordinate niobium(V) (0.48 Å) versus that of vanadium (0.355 Å). This ultimately results in a closer approach of the proximal silicon atoms to oxygen in the case of complex **1** (average Si-O distance = 3.105(1) Å) when compared to that of the niobium complex (average Si-O distance = 3.228(2) Å). Further, we do not discount the possibility that this transformation may be thermodynamically disfavored in the niobium complex owing to the anticipated increased strength of the

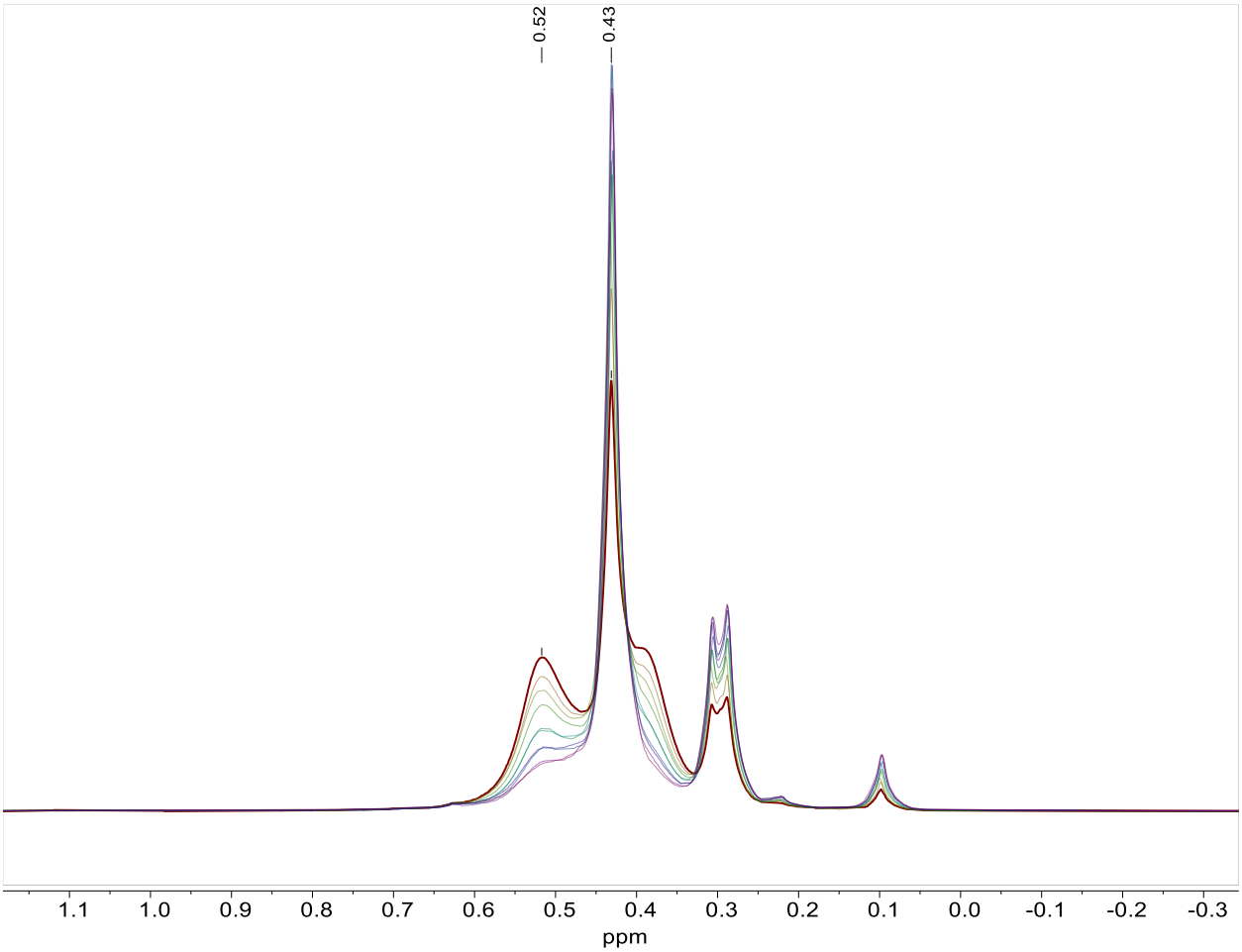

Figure 3.2: Conversion of V(=O){N(SiMe$_3$)$_2$}$_3$ (**1**) to V(=N(SiMe$_3$)$_2$(OSiMe$_3$){N(SiMe$_3$)$_2$}$_2$ (**3**) in deuterated benzene at 73 °C. Data were collected from 30 minutes (red trace) to 120 minutes (violet trace) in 10 minute intervals.

Nb-O bond in comparison to that of complex **1**. This difference in stability is further underlined by the behavior of complex **1** in the solid state. During melting point analysis of complex **1**, the yellow powder was shown to slowly turn orange between 100 and 120 °C and decompose at an identical temperature (237 °C) to a sample of freshly prepared complex **3**. The identity of the complex formed by this thermolysis was further verified by its ^{1}H NMR spectrum, which displayed identical features to that of an authentic sample of complex **3**.

Conclusion.

Our investigations[14] to determine the nature of the "brown" complex previously described as $V\{N(SiMe_3)_2\}_3$[1,32] led us to reexamine the chemistry of the authentic tris(silylamide) complex. Despite the ubiquity of vanadium oxo complexes and previous efforts over several decades,[34,35] $V(=O)\{N(SiMe_3)_2\}_3$ (**1**) had remained unknown. While early reports indicated that salt metathesis of $MN(SiMe_3)_2$ (M = Li, Na) and $VOCl_3$ did not yield **1**,[34,35] we have shown that it is available through reaction of iodosylbenzene with $V\{N(SiMe_3)_2\}_3$. Additionally, treatment of the trisamide with trimethylsilyl azide was shown to form the imido complex $V\{=NSiMe_3\}\{N(SiMe_3)_2\}_3$ (**2**). The similarity of the vibrational spectra of complexes **1** and **2** allowed unambiguous assignment of the V-O and V-N_{imide} stretching bands (995 and 1060 cm^{-1}, respectively), where extensive vibrational coupling in other complexes has made assignment of the M-N_{imide} stretching band difficult.[58] The electronic spectra of complexes **1**-**3** show strong absorbances in the charge transfer region of the spectrum, consistent with their d^0 electron count. The thermal decomposition of the oxo-complex **1** afforded the putative vanadium imide/siloxide **3**. This ready conversion of **1** to **3** may partially explain the absence of $V(=O)\{N(SiMe_3)_2\}_3$ in the literature and the apparent difficulty in early attempts at its synthesis. Although it could not be structurally characterized in full detail owing to disorder, the partial structure obtained and the spectroscopic features of **3** identify it as a product of a migration of a trimethylsilyl group from nitrogen to oxygen in complex **1** as previously posited by Bürger, Smrekar, and Wannagat.[34] Additionally, the experimentally determined activation energy of the conversion of complex **1** to complex **3** by migration of an amido silyl group to oxygen agrees well with activation energies

determined for this transformation in other molecules containing these moieties.[75] Nonetheless, the IR spectroscopic and color differences between orange **3** and the olive-green color of the species reported earlier are less easily reconciled. The orange color of **3** arises from the tailing of the charge transfer bands into the visible region, and there are no bands in the visible portion of the spectrum. This is consistent with its d^0, V(V) formulation, whereas the olive-green color of '$V(=NSiMe_3)(OSiMe_3)\{N(SiMe_3)_2\}_2$' reported earlier is suggestive of absorption in the visible region possibly arising from d-d transitions thereby implying a vanadium oxidation state less than (V). The latter scenario is therefore inconsistent with the formulation that was given but may be consistent with that of $\{(\mu\text{-}O)_2V_2[N(SiMe_3)_2]_4\}$[35] which was synthesized by a very similar route and described as a green crystalline material. The pursuit of complex **1** was one of the original justifications for this work, but it is obviously not the "brown" complex originally described by Bradley and coworkers as $V\{N(SiMe_3)_2\}_3$.[1,32] Nonetheless, the isolation of the complexes described here has further underlined the fact that $M\{N(SiMe_3)_2\}_3$ complexes have a far richer chemistry than previously suspected on the basis of their high steric crowding.

Associated Content.

Supporting information.

The Supporting Information, including spectra (NMR, infrared, UVVis), crystallographic data, and photographs of materials is available free of charge on the ACS Publications website at https://doi.org/10.1021/acs.inorgchem.0c01572. CCDC entries 1960615 and 1970454 contain the supplementary crystallographic data of complexes **1** and **2**. These data can be obtained free of charge via www.ccdc.cam.ac.uk/data_request/cif, or by emailing data_request@ccdc.cam.ac.uk, or by contacting The Cambridge Crystallographic Data Centre, 12 Union Road, Cambridge CB2 1EZ, UK; fax: + 44 1223 336033.

Author Information.

Corresponding author

*pppower@ucdavis.edu

ORCID

Cary R. Stennett: 0000-0002-2727-5747

Thien H. Nguyen: 0000-0002-4566-7728

Philip P. Power: 0000-0002-6262-3209

Notes

The authors declare no competing financial interest.

Acknowledgements

We wish to acknowledge the US National Science Foundation (CHE-1565501) for support of this work and for the purchase of a dual-source X-ray diffractometer (CHE-0840444). The authors also thank Dr. Jeffrey Walton for assistance in the acquisition of ^{51}V NMR spectra.

References.

(1) Bradley, D. C.; Copperthwaite, R. G.; Extine, M. W.; Reichert, W. W.; Chisholm, M. H. Transition Metal Complexes of Bis(Trimethyl-Silyl)Amine (1,1,1,3,3,3-Hexamethyldisilazane). *Inorg. Synth.* **1978**, *18*, 112–120.

(2) Andersen, R. A.; Bryan, A. M.; Faust, M.; Power, P. P. Divalent Manganese, Iron, and Cobalt Bis(Trimethylsilyl)Amido Derivatives and Their Tetrahydrofuran Complexes. *Inorg. Synth.* **2018**, *37*, 1–14.

(3) Mulvey, R. E.; Robertson, S. D. Synthetically Important Alkali-Metal Utility Amides: Lithium, Sodium, and Potassium Hexamethyldisilazides, Diisopropylamides, and Tetramethylpiperidides. *Angew. Chem. Int. Ed.* **2013**, *52*, 11470–11487.

(4) Ponraj, J. S.; Attolini, G.; Bosi, M. Review on Atomic Layer Deposition and Applications of Oxide Thin Films. *Crit. Rev. Solid State Mater. Sci.* **2013**, *38*, 203–233.

(5) Baxter, D. V; Chisholm, M. H.; Gama, G. J.; Hector, A. L.; Parkin, I. P. Low Pressure Chemical Vapor Deposition of Metallic Films of Iron, Manganese, Cobalt, Copper, Germanium and Tin Employing Bis(Trimethyl)Silylamido Complexes, $M(N(SiMe_3)_2)_n$. *Chem. Vap. Deposition* **1995**, *1*, 49–51.

(6) Cormary, B.; Dumestre, F.; Liakakos, N.; Soulantica, K.; Chaudret, B. Organometallic Precursors of Nano-Objects, a Critical View. *Dalton Trans.* **2013**, *42*, 12546–12553.

(7) Yang, J.; Tilley, T. D. Efficient Hydrosilylation of Carbonyl Compounds with the Simple Amide Catalyst $[Fe\{N(SiMe_3)_2\}_2]$. *Angew. Chem. Int. Ed.* **2010**, *49*, 10186–10188.

(8) Gieshoff, T. N.; Chakraborty, U.; Villa, M.; Jacobi von Wangelin, A. Alkene Hydrogenations by Soluble Iron Nanocluster Catalysts. *Angew. Chem. Int. Ed.* **2017**, *56*, 3585–3589.

(9) Bürger, H.; Wannagat, U. Silylamido-Derivate von Eisen Und Kobalt. *Monatsh. Chem.* **1963**, *94*, 1007–1012.

(10) Bürger, H.; Wannagat, U. Silylamido-Verbindungen von Chrom, Mangan, Nickel Und Kupfer. *Monatsh. Chem.* **1964**, *95*, 1099–1102.

(11) Bryan, A. M.; Long, G. J.; Grandjean, F.; Power, P. P. Synthesis, Spectroscopic Characterization, and Determination of the Solution Association Energy of the Dimer [Co{N(SiMe3)2}2]2: Magnetic Studies of Low-Coordinate Co(II) Silylamides [Co{N(SiMe$_3$)$_2$}$_2$L] (L = PMe$_3$, Pyridine, and THF) and Related Species That Reveal Evidence of Very Large Zero-Field Splittings. *Inorg. Chem.* **2013**, *52*, 12152–12160.

(12) Ghotra, J. S.; Hursthouse, M. B.; Welch, A. J. Three-Co-Ordinate Scandium(III) and Europium(III); Crystal and Molecular Structures of Their Trishexamethyldisilylamides. *J. Chem. Soc., Chem. Commun.* **1973**, 669–670.

(13) Putzer, M. A.; Magull, J.; Goesmann, H.; Neumüller, B.; Dehnicke, K. Synthese, Eigenschaften Und Kristallstrukturen Der Titan(III)-Amido-Komplexe Ti[N(SiMe$_3$)$_2$]$_3$, [TiCl$_2${N(SiMe$_3$)$_2$}(THF)$_2$] Und [Na(12-Krone-4)$_2$][TiCl$_2${N(SiMe$_3$)$_2$}$_2$]. *Chem. Ber.* **1996**, *129*, 1401–1405.

(14) Wagner, C. L.; Phan, N. A.; Fettinger, J. C.; Berben, L. A.; Power, P. P. New Characterization of V{N(SiMe$_3$)$_2$}$_3$: Reductions of Tris[Bis(Trimethylsilyl)Amido]Vanadium(III) and -Chromium(III) To Afford the Reduced Metal(II) Anions [M{N(SiMe$_3$)$_2$}$_3$]$^-$ (M = V and Cr). *Inorg. Chem.* **2019**, *58*, 6095–6101.

(15) Köhn, R. D.; Kociok-Köhn, G.; Haufe, M. The Chemistry of 1,3,5-Triazacyclohexane Complexes, 3. High Yield Synthesis of [Cr{N(SiMe$_3$)$_2$}$_3$] and Accurate Structure Determination by Cocrystallization with Me$_6$Si$_2$. *Chem. Ber.* **1996**, *129*, 25–27.

(16) Ellison, J. J.; Power, P. P.; Shoner, S. C. First Examples of Three-Coordinate Manganese(III) and Cobalt(III): Synthesis and Characterization of the Complexes M[N(SiMe$_3$)$_2$]$_3$ (M = Mn or Co). *J. Am. Chem. Soc.* **1989**, *111*, 8044–8046.

(17) Hursthouse, M. B.; Rodesiler, P. F. Crystal and Molecular Structure of Tris(Hexamethyldisilylamido)Iron(III). *J. Chem. Soc. Dalton Trans.* **1972**, 2100–2102.

(18) Rees, W. S. J.; Just, O.; Van Derveer, D. S. Molecular Design of Dopant Precursors for Atomic Layer Epitaxy of SrS:Ce. *J. Mater. Chem.* **1999**, *9*, 249–252.

(19) Andersen, R. A.; Templeton, D. H.; Zalkin, A. Structure of Tris(Bis(Trimethylsilyl)Amido)Neodymium(III), $Nd[N(Si(CH_3)_3)_2]_3$. *Inorg. Chem.* **1978**, *17*, 2317–2319.

(20) Brady, E. D.; Clark, D. L.; Gordon, J. C.; Hay, P. J.; Keogh, D. W.; Poli, R.; Scott, B. L.; Watkin, J. G. Tris(Bis(Trimethylsilyl)Amido)Samarium: X-Ray Structure and DFT Study. *Inorg. Chem.* **2003**, *42*, 6682–6690.

(21) Hitchcock, P. B.; Hulkes, A. G.; Lappert, M. F.; Li, Z. Cerium(III) Dialkyl Dithiocarbamates from $[Ce\{N(SiMe_3)_2\}_3]$ and Tetraalkylthiuram Disulfides, and $[Ce(K_2\text{-}S_2CNEt_2)_4]$ from the CeIII Precursor; TbIII and NdIII Analogues. *Dalton Trans.* **2004**, No. 1, 129–136.

(22) Herrmann, W. A.; Anwander, R.; Munck, F. C.; Scherer, W.; Dufaud, V.; Huber, N. W.; Artus, G. R. J. Lanthanoiden-Komplexe, IX [1]. Reaktivitätsbestimmender Einfluß Der Ligandenkonstitution Bei Seltenerdamiden: Herstellung Und Struktur Sterisch Überladener Alkoxid-Komplexe / Lanthanoid Complexes, IX [1]. Reactivity Control of Lanthanoid Amides through Li. *Z. Naturforsch., B: Chem. Sci.* **1994**, *49*, 1789.

(23) Bienfait, A. M.; Wolf, B. M.; Törnroos, K. W.; Anwander, R. Trivalent Rare-Earth-Metal Bis(Trimethylsilyl)Amide Halide Complexes by Targeted Oxidations. *Inorg. Chem.* **2018**, *57*, 5204–5212.

(24) Niemeyer, M. Synthesis and Structural Characterization of Several Ytterbium Bis(Trimethylsilyl)Amides Including Base-Free $[Yb\{N(SiMe_3)_2\}_2(\mu\text{-}Cl)]_2$ — A Coordinatively Unsaturated Complex with Additional Agostic Yb···(H_3C—Si) Interactions. *Z. Anorg. Allg. Chem.* **2002**, *628*, 647–657.

(25) Avens, L. R.; Bott, S. G.; Clark, D. L.; Sattelberger, A. P.; Watkin, J. G.; Zwick, B. D. A Convenient Entry into Trivalent Actinide Chemistry: Synthesis and Characterization of $AnI_3(THF)_4$ and $An[N(SiMe_3)_2]_3$ (An = U, Np, Pu). *Inorg. Chem.* **1994**, *33*, 2248–2256.

(26) Stewart, J. L.; Andersen, R. A. Trivalent Uranium Chemistry: Molecular Structure of $[(Me_3Si)_2N]_3U$. *Polyhedron* **1998**, *17*, 953–958.

(27) Gaunt, A. J.; Enriquez, A. E.; Reilly, S. D.; Scott, B. L.; Neu, M. P. Structural Characterization of $Pu[N(SiMe_3)_2]_3$, a Synthetically Useful Nonaqueous Plutonium(III) Precursor. *Inorg. Chem.* **2008**, *47*, 26–28.

(28) Eller, P. G.; Bradley, D. C.; Hursthouse, M. B.; Meek, D. W. Three Coordination in Metal Complexes. *Coord. Chem. Rev.* **1977**, *24*, 1–95.

(29) Alvarez, S. Bonding and Stereochemistry of Three-Coordinated Transition Metal Compounds. *Coord. Chem. Rev.* **1999**, *193–195*, 13–41.

(30) Lappert, M. F.; Power, P. P.; Protchenko, A.; Seeber, A. *Metal Amide Chemistry*; Chichester, U.K. : Wiley: Chichester, U.K., 2009.

(31) Cummins, C. C. Three-Coordinate Complexes of "Hard" Ligands: Advances in Synthesis, Structure and Reactivity. *Prog. Inorg. Chem.* **1997**, *47*, 685–836.

(32) Alyea, E. C.; Bradley, D. C.; Copperthwaite, R. G. Three-Co-Ordinated Transition Metal Compounds. Part I. The Preparation and Characterization of Tris(Bistrimethylsilylamido)-Derivatives of Scandium, Titanium, Vanadium, Chromium, and Iron. *J. Chem. Soc. Dalton Trans.* **1972**, No. 14, 1580–1584.

(33) Groom, C. R.; Bruno, I. J.; Lightfoot, M. P.; Ward, S. C. The Cambridge Structural Database. *Acta Crystallogr. Sect. B* **2016**, *72*, 171–179.

(34) Bürger, H.; Smrekar, O.; Wannagat, U. Silylamido-Verbindungen Des Vanadiums. *Monatsh. Chem.* **1964**, *95*, 292–302.

(35) Duan, Z.; Schmidt, M.; Young, V. G.; Xie, X.; McCarley, R. E.; Verkade, J. G. The Novel Bis(Oxo-Bridged) Dinuclear Vanadium(IV) Complex $\{(\mu\text{-}O)_2V_2[N(SiMe_3)_2]_4\}$: An Unexpected Reaction Product. *J. Am. Chem. Soc.* **1996**, *118*, 5302–5303.

(36) Hubert-Pfalzgraf, L. G.; Tsunoda, M.; Le Borgne, G. Synthesis and Crystal Structure of Tris[Bis(Trimethylsilyl)Amido]Oxoniobium(V): A Four-Co-Ordinated Oxo Niobium Precursor. *J. Chem. Soc. Dalton Trans.* **1988**, No. 2, 533–535.

(37) Zhao, X.-F.; Zhang, C. Iodobenzene Dichloride as a Stoichiometric Oxidant for the Conversion of Alcohols into Carbonyl Compounds; Two Facile Methods for Its Preparation. *Synthesis* **2007**, *2007*, 551–557.

(38) Lucas, H. J.; Kennedy, E. R.; Formo, M. W. Iodosobenzene. *Org. Synth.* **1942**, *22*, 70.

(39) Sheldrick, G. M. *SADABS*; University of Göttingen, Germany, 1996.

(40) Dolomanov, O. V; Bourhis, L. J.; Gildea, R. J.; Howard, J. A. K.; Puschmann, H. *OLEX*^{2}: A Complete Structure Solution, Refinement and Analysis Program. *J. Appl. Crystallogr.* **2009**, *42*, 339–341.

(41) Sheldrick, G. M. SHELXT - Integrated Space-Group and Crystal-Structure Determination. *Acta Crystallogr. Sect. A Found. Crystallogr.* **2015**, *A71*, 3–8.

(42) Sheldrick, G. M. Crystal Structure Refinement with SHELXL. *Acta Crystallogr. Sect. C, Struct. Chem.* **2015**, *C71*, 3–8.

(43) Groysman, S.; Villagrán, D.; Nocera, D. G. Pseudotetrahedral d^0, d^1, and d^2 Metal−Oxo Cores within a Tris(Alkoxide) Platform. *Inorg. Chem.* **2010**, *49*, 10759–10761.

(44) Henderson, R. A.; Hughes, D. L.; Janas, Z.; Richards, R. L.; Sobota, P.; Szafert, S. Preparation and Crystal Structures of the Mononuclear Vanadium Phenoxide Complexes $[VCl(OC_6H_3Pr^i_2\text{-}2,6)_2(C_4H_8O)_2]$ and $[VO(OC_6H_3Pr^i_2\text{-}2,6)_3]$: Procatalysts for Ethylene Polymerisation. *J. Organomet. Chem.* **1998**, *554*, 195–201.

(45) Palluccio, T. D.; Rybak-Akimova, E. V; Majumdar, S.; Cai, X.; Chui, M.; Temprado, M.; Silvia, J. S.; Cozzolino, A. F.; Tofan, D.; Velian, A.; Cummins, C. C.; Captain, B.; Hoff, C. D. Thermodynamic and Kinetic Study of Cleavage of the N–O Bond of N-Oxides by a Vanadium(III) Complex: Enhanced Oxygen Atom Transfer Reaction Rates for Adducts of Nitrous Oxide and Mesityl Nitrile Oxide. *J. Am. Chem. Soc.* **2013**, *135*, 11357–11372.

(46) Hillerns, F.; Olbrich, F.; Behrens, U.; Rehder, D. Tris(Cyclopentanolato)Oxovanadium(V): A Model for the Transition State of Enzymatic Phosphoester Cleavage. *Angew. Chem. Int. Ed. English* **1992**, *31*, 447–448.

(47) Feher, F. J.; Walzer, J. F. Synthesis and Characterization of Vanadium-Containing Silsesquioxanes. *Inorg. Chem.* **1991**, *30*, 1689–1694.

(48) Huang, M.; DeKock, C. W. Triphenylsiloxy Complexes. A Novel Compound Containing a Molybdenum(VI)-Phosphorus Bond: Dioxo(Triphenylphosphine)Bis(Triphenylsiloxo)Molybdenum. *Inorg. Chem.* **1993**, *32*, 2287–2291.

(49) Viasus, C. J.; Alderman, N. P.; Licciulli, S.; Korobkov, I.; Gambarotta, S. Radical Behavior of CO2 versus Its Deoxygenation Promoted by Vanadium Aryloxide Complexes: How the Geometry of Intermediate CO_2-Adducts Determines the Reactivity. *Chem. – A Eur. J.* **2017**, *23*, 17269–17278.

(50) Ruiz, J.; Vivanco, M.; Floriani, C.; Chiesi-Villa, A.; Guastini, C. Oxovanadium(V) and Oxovanadium(IV) Organometallic Compounds from Direct Oxidation of the Corresponding Vanadium(III) Precursors: The X-Ray Structure of Tris-Mesityl Oxovanadium(V). *J. Chem. Soc., Chem. Commun.* **1991**, No. 11, 762–764.

(51) Spandl, J.; Brüdgam, I.; Hartl, H. Synthese, Struktur Und Reaktionen von Vanadiumsäureestern $VO(OR)_3$: Umesterung Und Reaktion Mit Oxalsäure. *Zeitschrift für Anorg. und Allg. Chemie* **2000**, *626*, 2125–2132.

(52) Ishida, Y.; Kawaguchi, H. Methylene-Linked Anilide—Bis(Aryloxide) Ligands: Lithium, Sodium, Potassium, Chromium(III), and Vanadium(III) Ligation. *Inorg. Chem.* **2014**, *53*, 6775–6787.

(53) Mowat, W.; Shortland, A.; Yagupsky, G.; Hill, N. J.; Yagupsky, M.; Wilkinson, G. Elimination Stabilized Alkyls. Part I. Chromium, Molybdenum, Tungsten, and Vanadium. *J. Chem. Soc. Dalton Trans.* **1972**, No. 4, 533–542.

(54) Wegeberg, C.; Frankær, C. G.; McKenzie, C. J. Reduction of Hypervalent Iodine by Coordination to Iron(III) and the Crystal Structures of PhIO and $PhIO_2$. *Dalton Trans.* **2016**, *45*, 17714–17722.

(55) Stennett, C. R.; Fettinger, J. C.; Power, P. P. Unexpected Coordination Complexes of the Metal Tris-Silylamides $M\{N(SiMe_3)_2\}_3$ (M = Ti, V). *Inorg. Chem.* **2020**, *59*, 1871–1882.

(56) Yang, L.; Powell, D. R.; Houser, R. P. Structural Variation in Copper(I) Complexes with Pyridylmethylamide Ligands: Structural Analysis with a New Four-Coordinate Geometry Index, τ_4. *Dalton Trans.* **2007**, No. 9, 955–964.

(57) Pyykkö, P.; Atsumi, M. Molecular Single-Bond Covalent Radii for Elements 1–118. *Chem. – A Eur. J.* **2009**, *15*, 186–197.

(58) Nugent, W. A.; Haymore, B. L. Transition Metal Complexes Containing Organoimido (NR) and Related Ligands. *Coord. Chem. Rev.* **1980**, *31*, 123–175.

(59) Shannon, R. D. Revised Effective Ionic Radii and Systematic Studies of Interatomic Distances in Halides and Chalcogenides. *Acta Crystallogr. Sect. A* **1976**, *32*, 751–767.

(60) Ruppa, K. B. P.; Desmangles, N.; Gambarotta, S.; Yap, G.; Rheingold, A. L. Preparation and Characterization of a Homoleptic Vanadium(III) Amide Complex and Its Transformation into Terminal

Chalcogenide Derivatives $[(3,5\text{-}Me_2Ph)AdN]_3VE$ (E = S, Se; Ad = Adamantyl). *Inorg. Chem.* **1997**, *36*, 1194–1197.

(61) Witt, M.; Roesky, H. W.; Noltemeyer, M.; Sheldrick, G. M. Synthesis and Structure of $[ClV(OSiMe_3)N_2PPh_2]_2$, the First Cyclodimetallaphosphazene–an Eight-Membered Planar Unsaturated Heterocycle. *Angew. Chem. Int. Ed. English* **1988**, *27*, 850–851.

(62) Danopoulos, A. A.; Hay-Motherwell, R. S.; Wilkinson, G.; Sweet, T. K. N.; Hursthouse, M. B. Synthesis and X-Ray Crystal Structures of Imido and Isodiazene Complexes of Vanadium, Niobium and Tantalum. *Polyhedron* **1997**, *16*, 1081–1088.

(63) Griffith, W. P. Transition Metal Oxo Complexes. *Coord. Chem. Rev.* **1970**, *5*, 459–517.

(64) Nugent, W. A. *Metal-Ligand Multiple Bonds : The Chemistry of Transition Metal Complexes Containing Oxo, Nitrido, Imido, Alkylidene, or Alkylidyne Ligands*; Mayer, J. M., Ed.; Wiley: New York, 1988.

(65) Osborne, J. H.; Trogler, W. C. Assignment of Metal-Nitrogen Stretching Frequencies in Metal Nitrene Complexes. *Inorg. Chem.* **1985**, *24*, 3098–3099.

(66) Heinselman, K. S.; Miskowski, V. M.; Geib, S. J.; Wang, L. C.; Hopkins, M. D. Molecular Structures and FT-Raman Spectroscopy of Luminescent Niobium and Tantalum Arylimido Compounds. *Inorg. Chem.* **1997**, *36*, 5530–5538.

(67) Mehn, M. P.; Brown, S. D.; Jenkins, D. M.; Peters, J. C.; Que, L. Vibrational Spectroscopy and Analysis of Pseudo-Tetrahedral Complexes with Metal Imido Bonds. *Inorg. Chem.* **2006**, *45*, 7417–7427.

(68) Manna, J.; Dallinger, R. F.; Miskowski, V. M.; Hopkins, M. D. Vibrational Spectroscopy and Normal-Mode Analysis of Tungsten−Methylidyne Complexes. Insight into the Nature of the M⋮CH Bonds. *J. Phys. Chem. B* **2000**, *104*, 10928–10939.

(69) Schweda, E.; Scherfise, K. D.; Dehnicke, K. Trimethylsilyl-Imido-Vanadiumtrichlorid, Me3Si-N≡VCl_3 Synthese, Eigenschaften Und Kristallstruktur. *Zeitschrift für Anorg. und Allg. Chemie* **1985**, *528*, 117–124.

(70) Nugent, W. A.; Harlow, R. L. Stable First-Row Transition Metal Alkylimido Complexes; X-Ray Crystal and Molecular Structure of N-(1-Adamantylimido)Tris(Trimethylsiloxy)Vanadium(V). *J. Chem. Soc., Chem. Commun.* **1979**, No. 7, 342–343.

(71) Kilgore, U. J.; Sengelaub, C. A.; Fan, H.; Tomaszewski, J.; Karty, J. A.; Baik, M.-H.; Mindiola, D. J. A Transient Vanadium(III) Neopentylidene Complex. Redox Chemistry and Reactivity of the V═CHtBu Functionality. *Organometallics* **2009**, *28*, 843–852.

(72) Cummins, C. C.; Schrock, R. R.; Davis, W. M. Synthesis of Terminal Vanadium(V) Imido, Oxo, Sulfido, Selenido, and Tellurido Complexes by Imido Group or Chalcogenide Atom Transfer to Trigonal Monopyramidal V[N_3N] (N_3N = $[(Me_3SiNCH_2CH_2)_3N]^{3-}$). *Inorg. Chem.* **1994**, *33*, 1448–1457.

(73) Rehder, D. A Survey of Vanadium-51 NMR Spectroscopy. *Bull. Magn. Reson.* **1982**, *4*, 33–83.

(74) Rehder, D. Vanadium NMR of Organovanadium Complexes. *Coord. Chem. Rev.* **2008**, *252*, 2209–2223.

(75) Yoder, C. H.; Copenhafer, W. C.; DuBeshter, B. Structure of Trimethylsilyl Amides. *J. Am. Chem. Soc.* **1974**, *96*, 4283–4286.

Supporting Information.

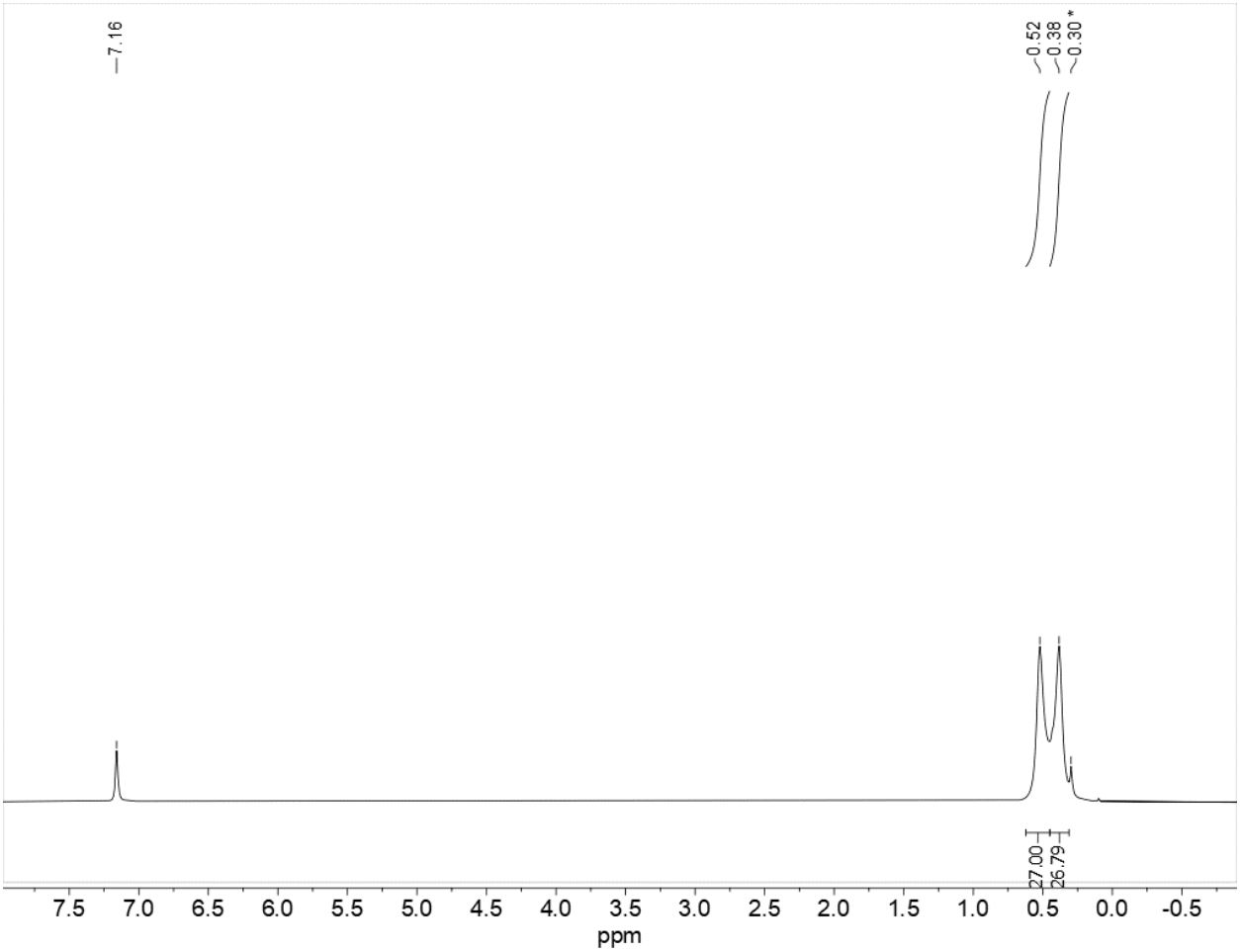

Figure 3.S1. ^{1}H-NMR spectrum of V(=O){N(SiMe$_3$)$_2$}$_3$ (**1**) in [D$_6$] benzene at 25 °C. The signal at 0.30 marked with an asterisk is a minor impurity of silicone grease.

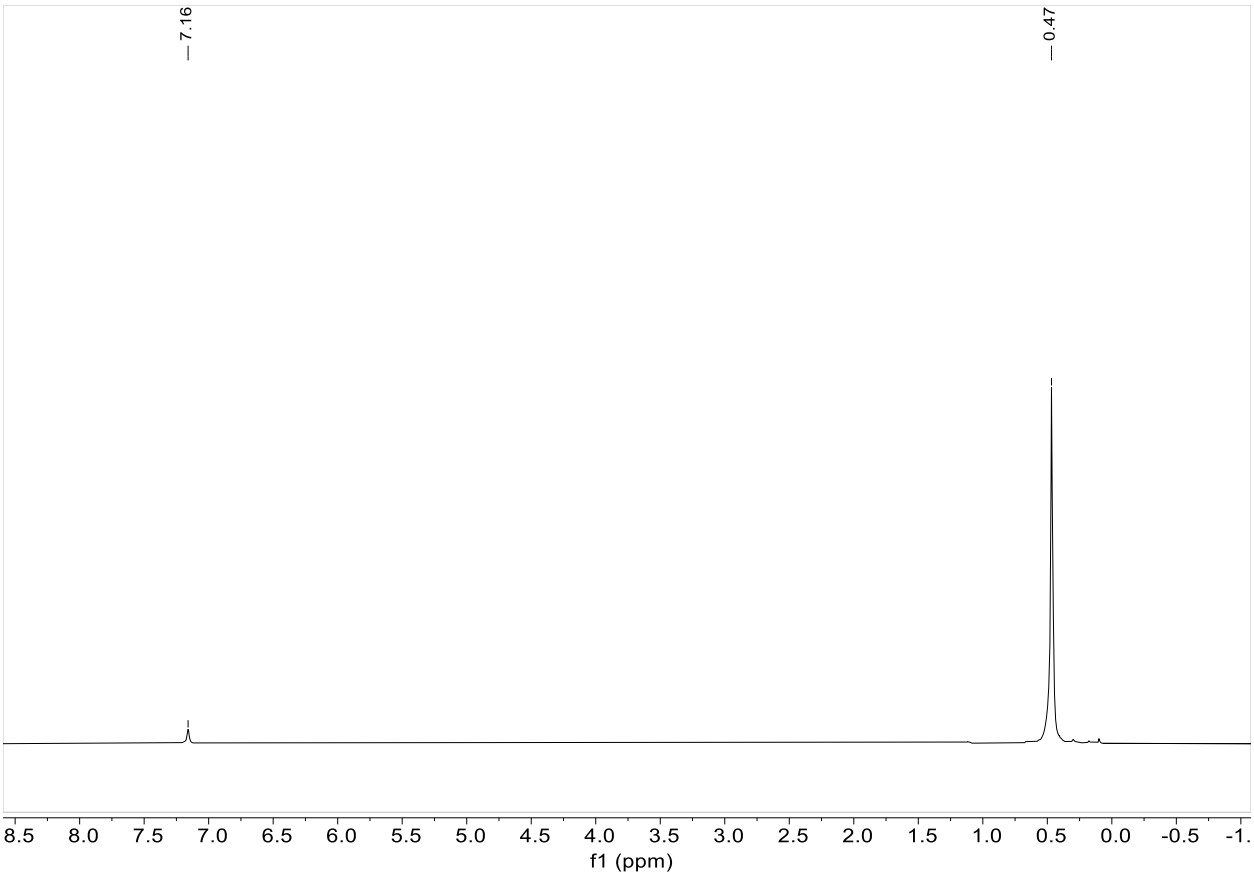

Figure 3.S2. ^{1}H-NMR spectrum of V{=N(SiMe$_3$)$_2$}{N(SiMe$_3$)$_2$}$_3$ (**2**) in [D$_6$] benzene at 25 °C.

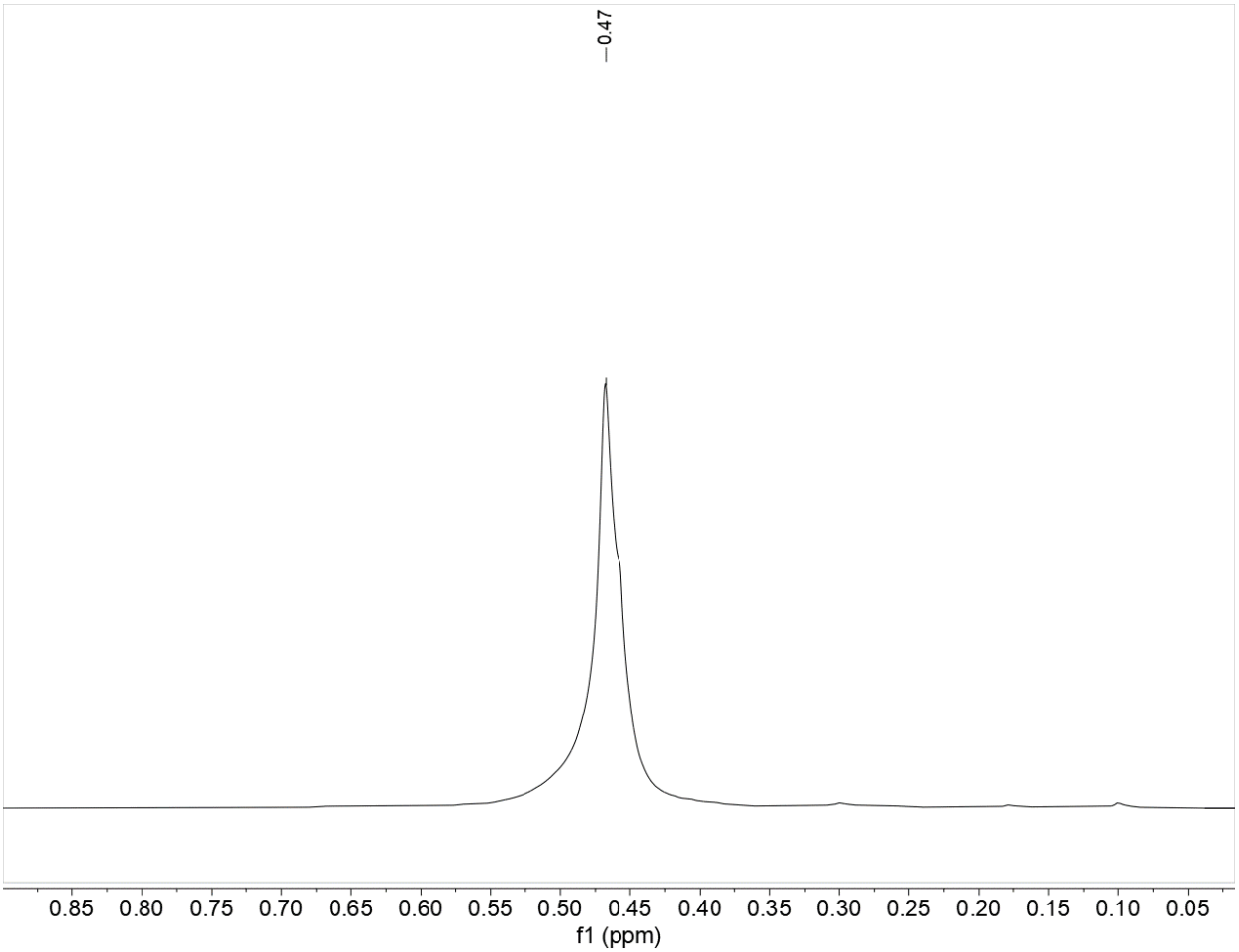

Figure 3.S3. Expanded scale ^{1}H-NMR spectrum of V{=N(SiMe$_3$)$_2$}{N(SiMe$_3$)$_2$}$_3$ (**2**) in [D$_6$] benzene showing the unsymmetric signal shape at 25 °C.

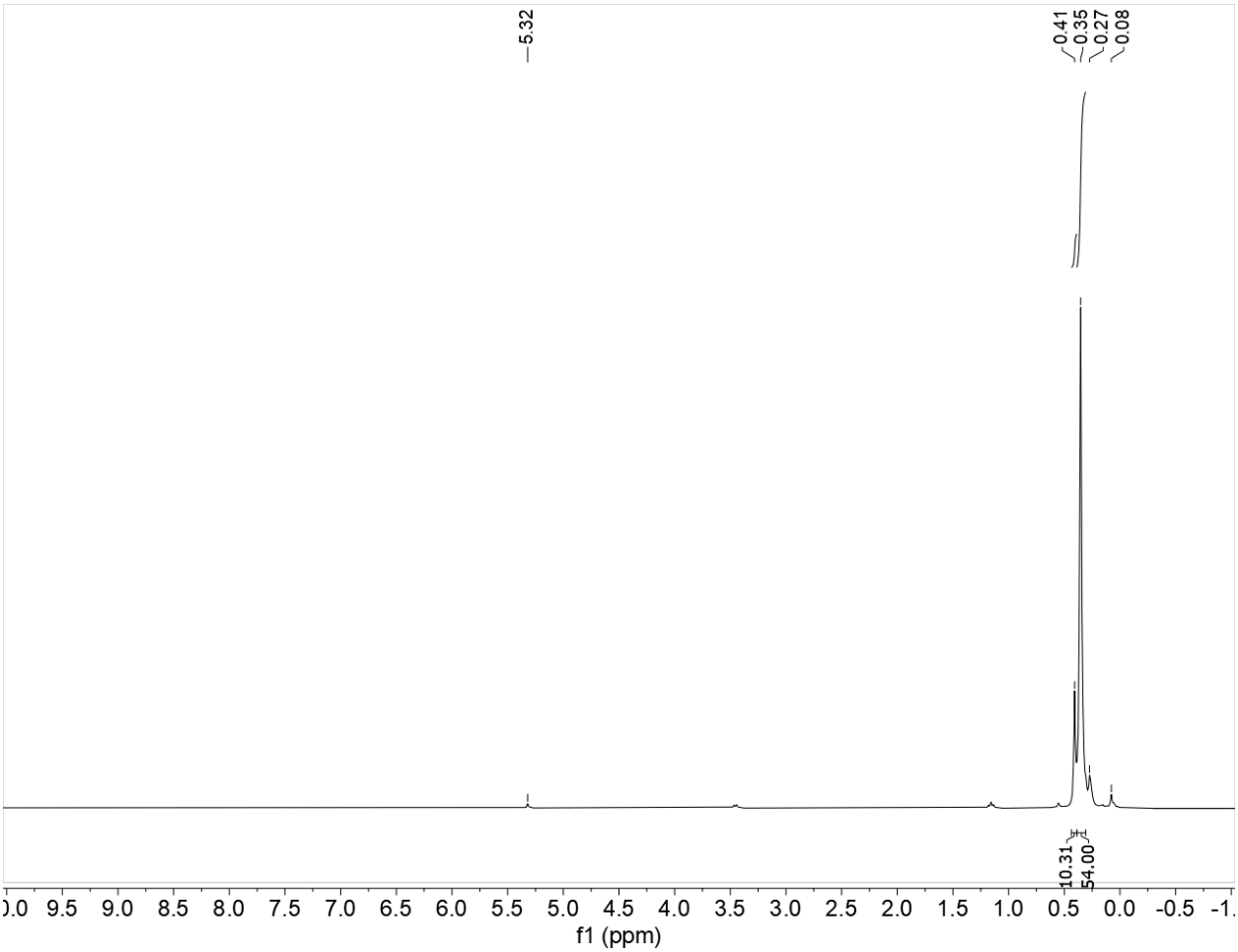

Figure 3.S4. ^{1}H-NMR spectrum of V{=N(SiMe$_3$)$_2$}{N(SiMe$_3$)$_2$}$_3$ (**2**) in [D$_2$] methylene chloride at 25 °C

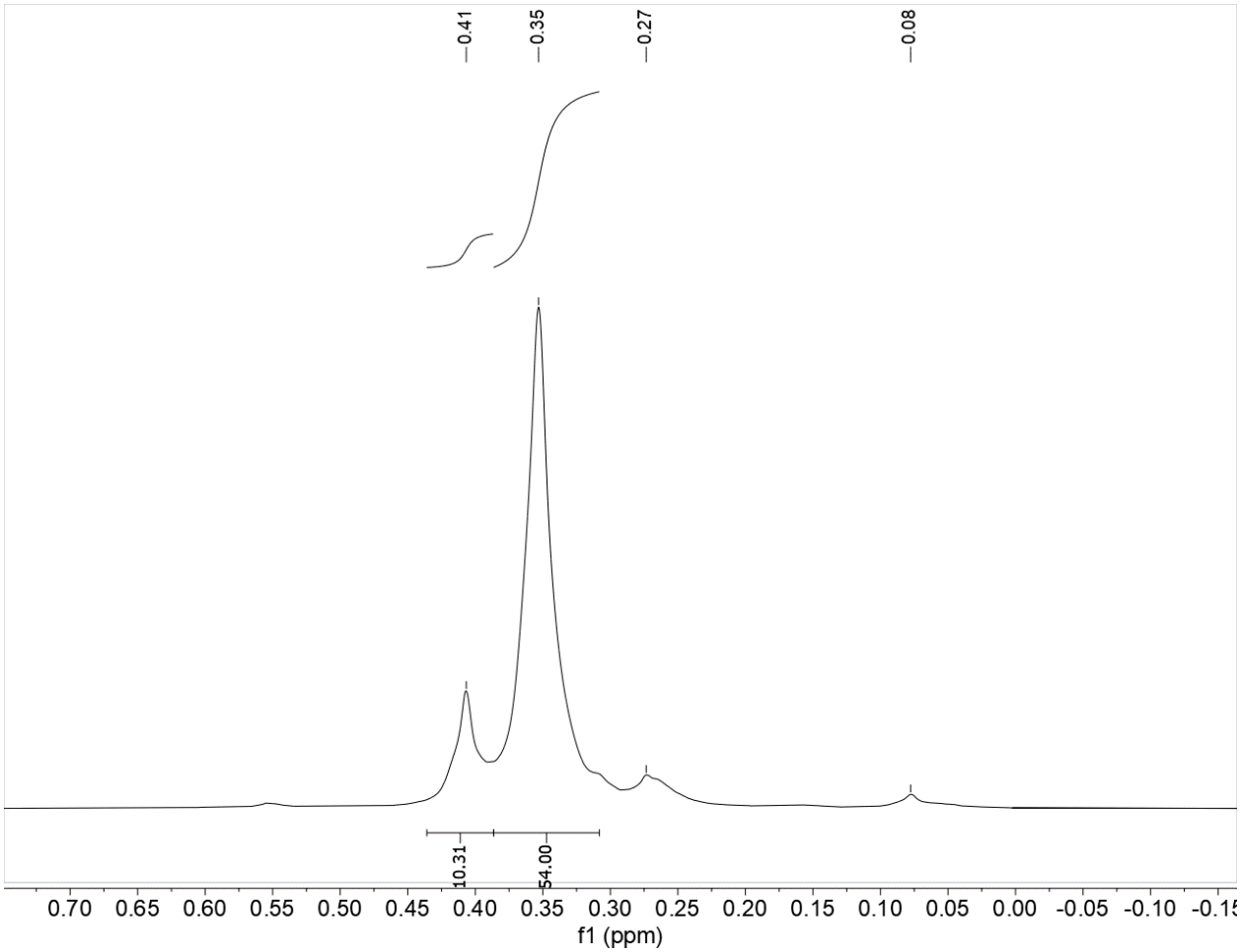

Figure 3.S5. Expanded scale ^{1}H-NMR spectrum of V{=N(SiMe$_3$)$_2$}{N(SiMe$_3$)$_2$}$_3$ (**2**) in [D$_2$] methylene chloride at 25 °C.

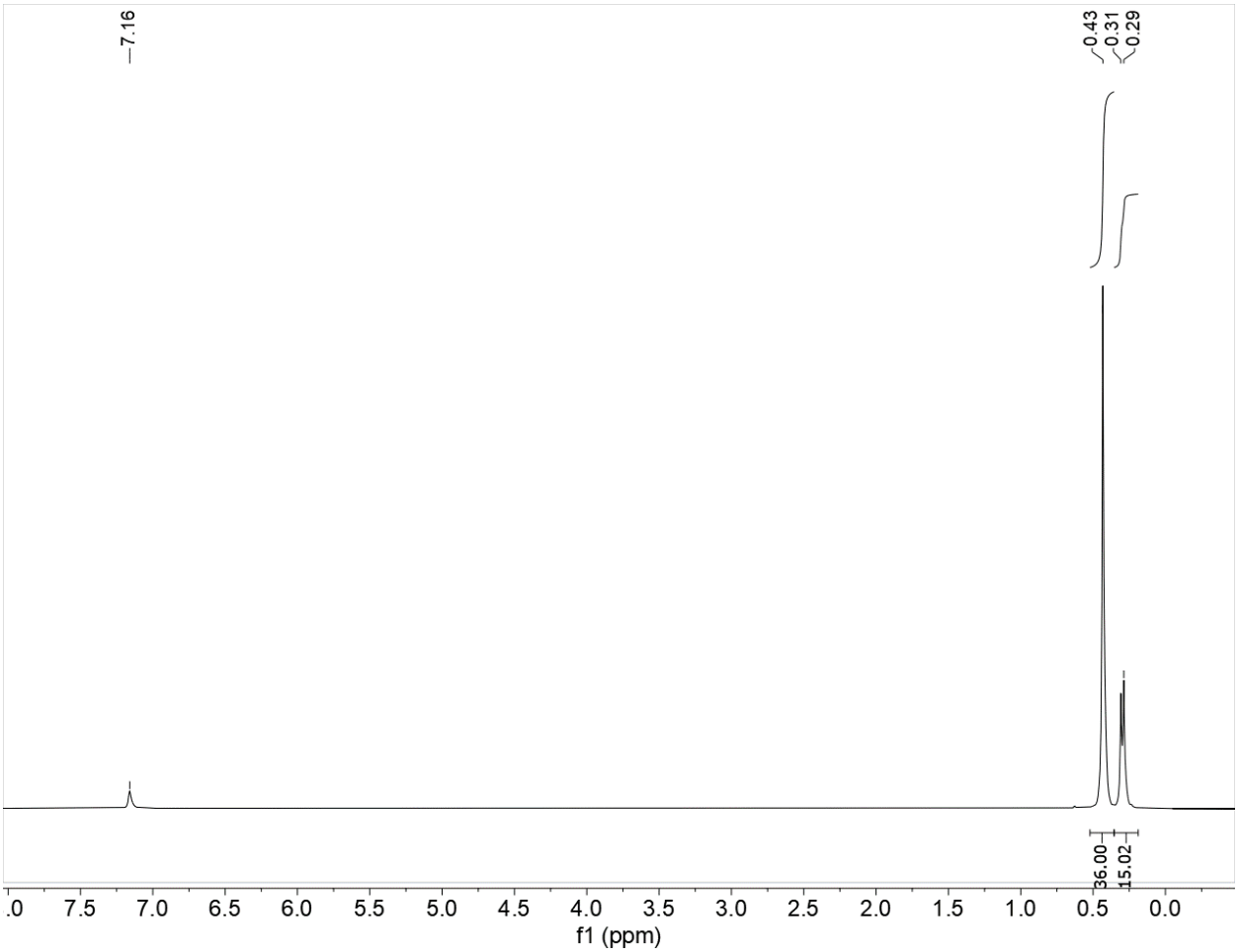

Figure 3.S6. ^{1}H-NMR spectrum of complex **3** in [D_6] benzene at 25 °C.

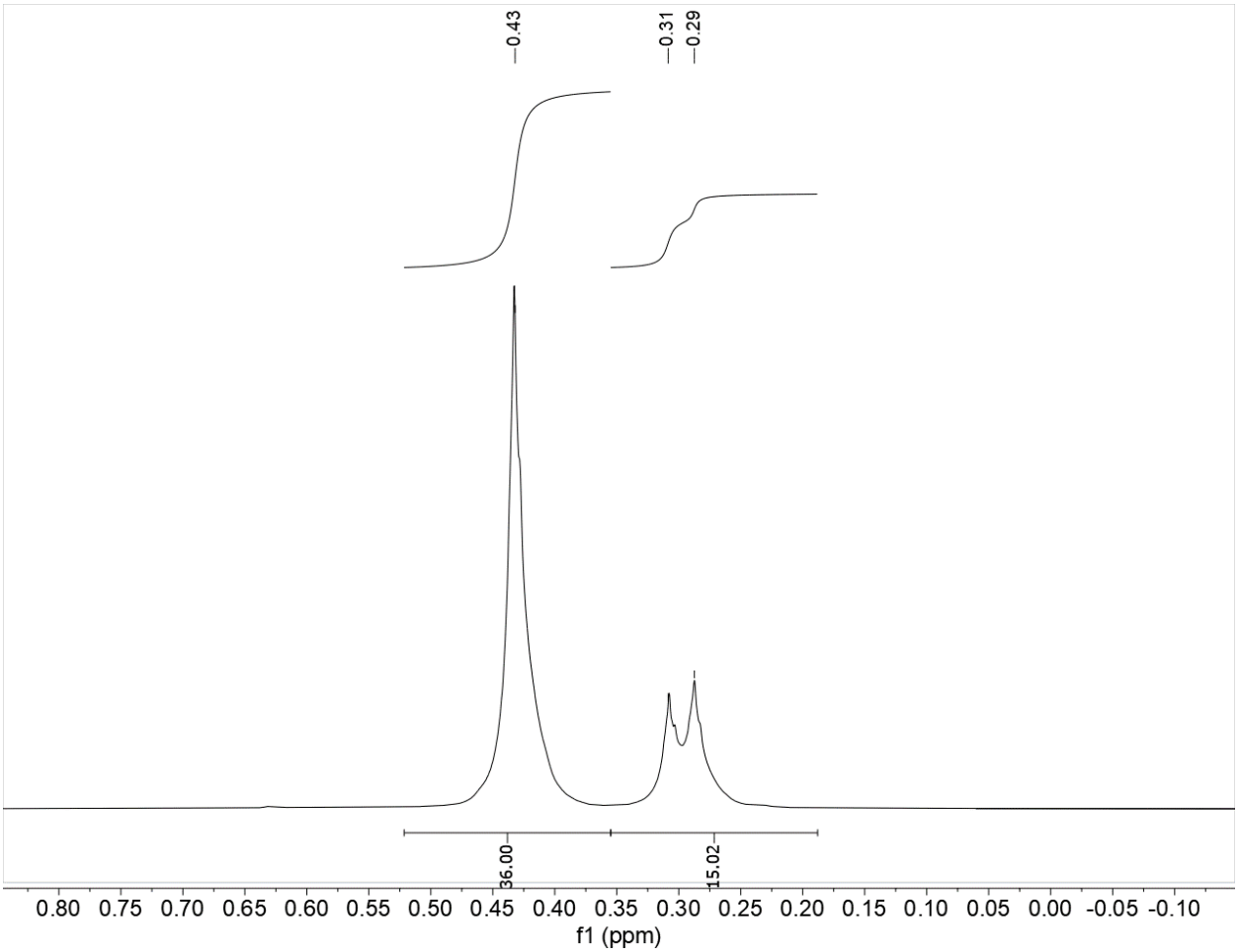

Figure 3.S7. Expanded scale ^{1}H-NMR spectrum of complex **3** in [D_6] benzene at 25 °C. ^{1}H-NMR spectrum of 3 in deuterated benzene appears to contain overlapping signals and potentially silicone grease; spectra were therefore also collected in other solvents.

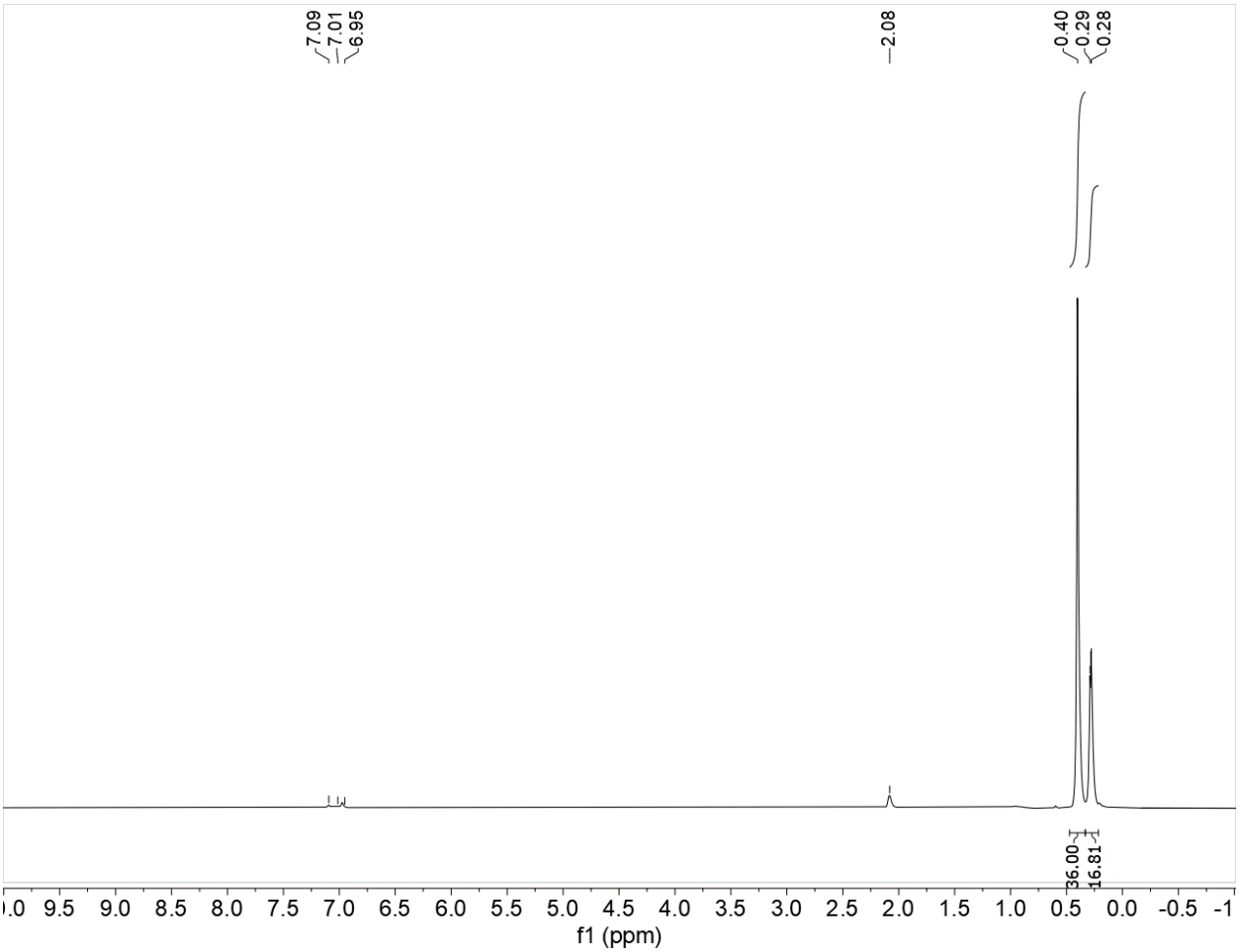

Figure 3.S8. ^{1}H-NMR spectrum of complex **3** in [D_8] toluene at 25 °C.

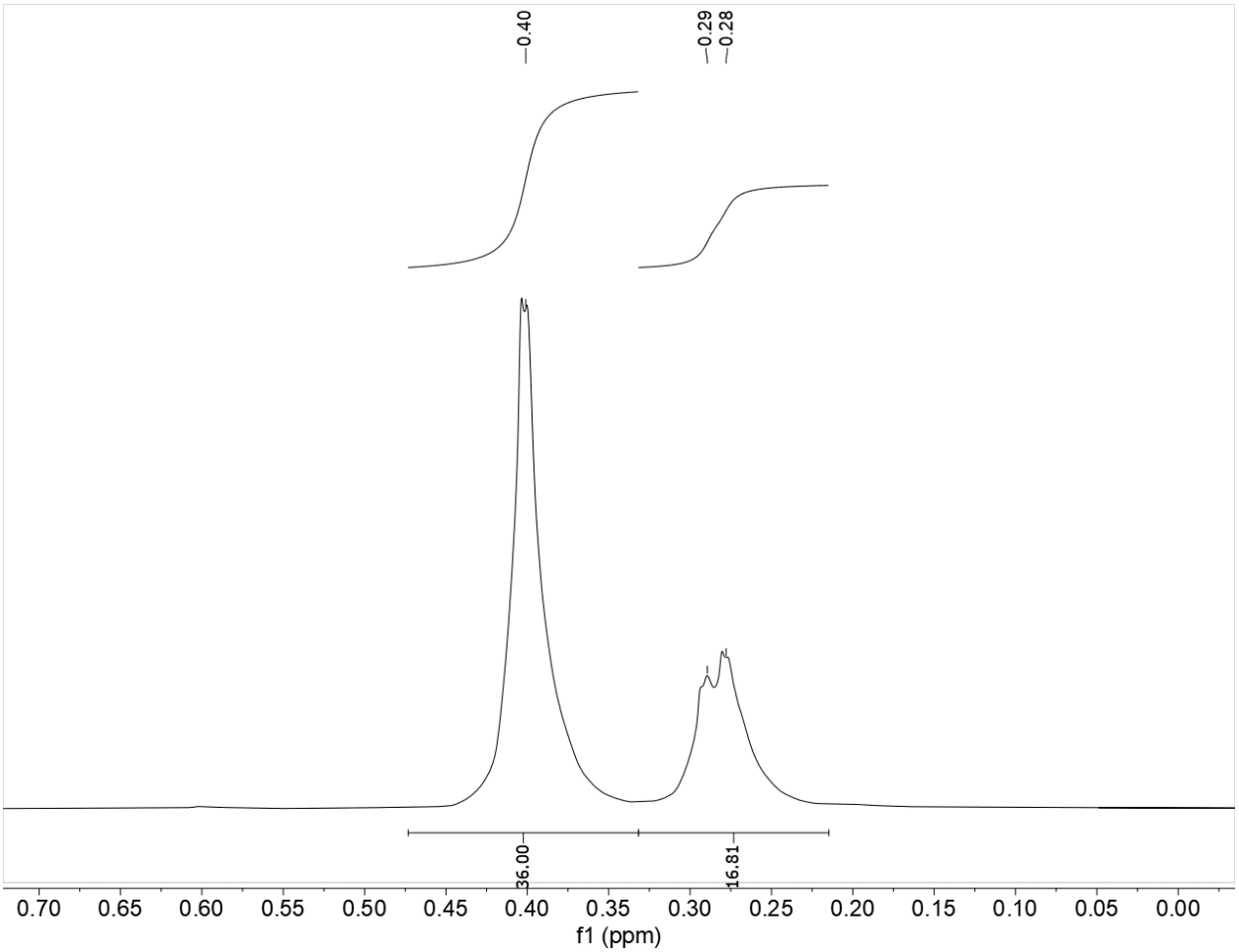

Figure 3.S9. Expanded scale ^{1}H-NMR spectrum of complex **3** in [D_8] toluene at 25 °C

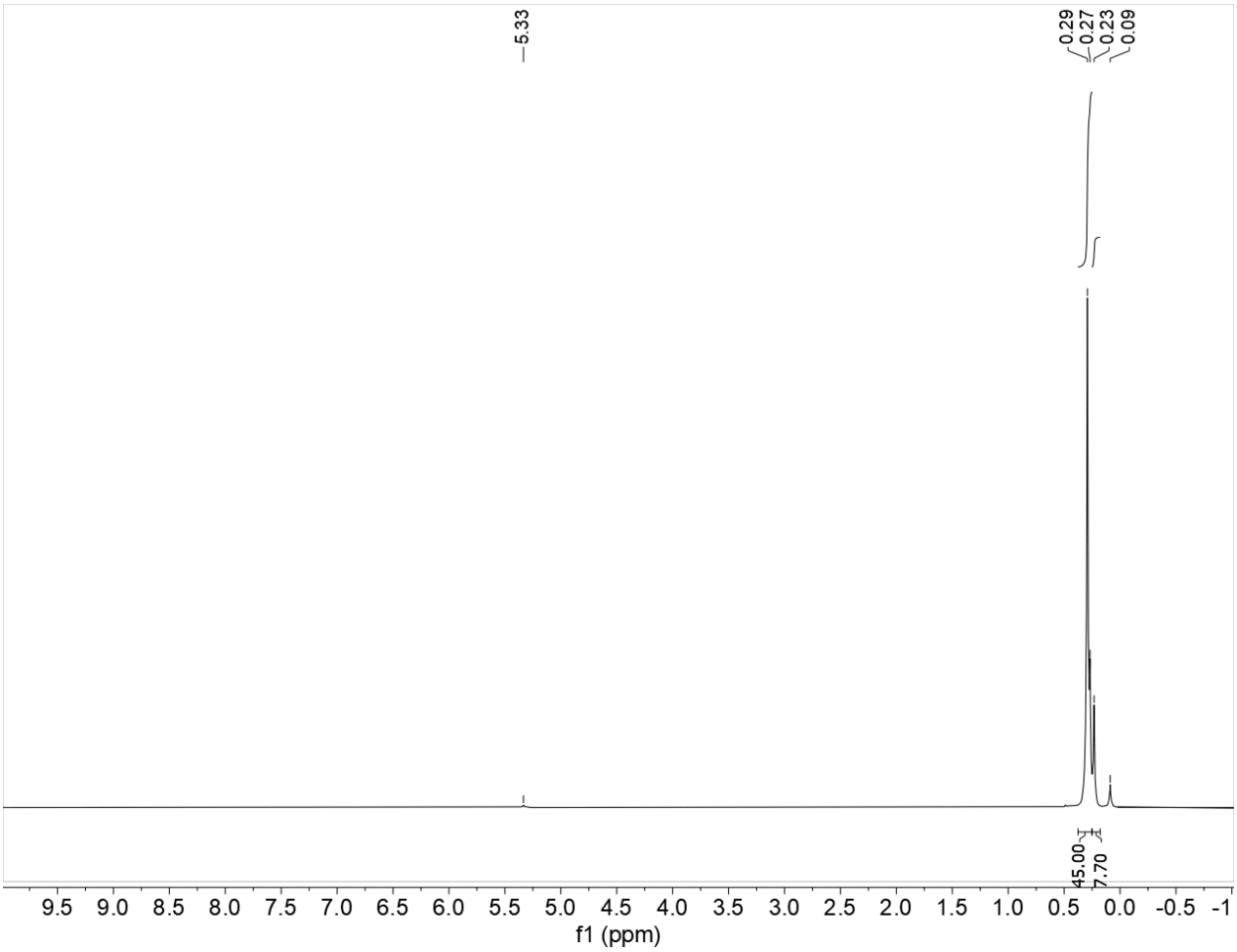

Figure 3.S10. ^{1}H-NMR spectrum of complex **3** in [D_2] methylene chloride at 25 °C.

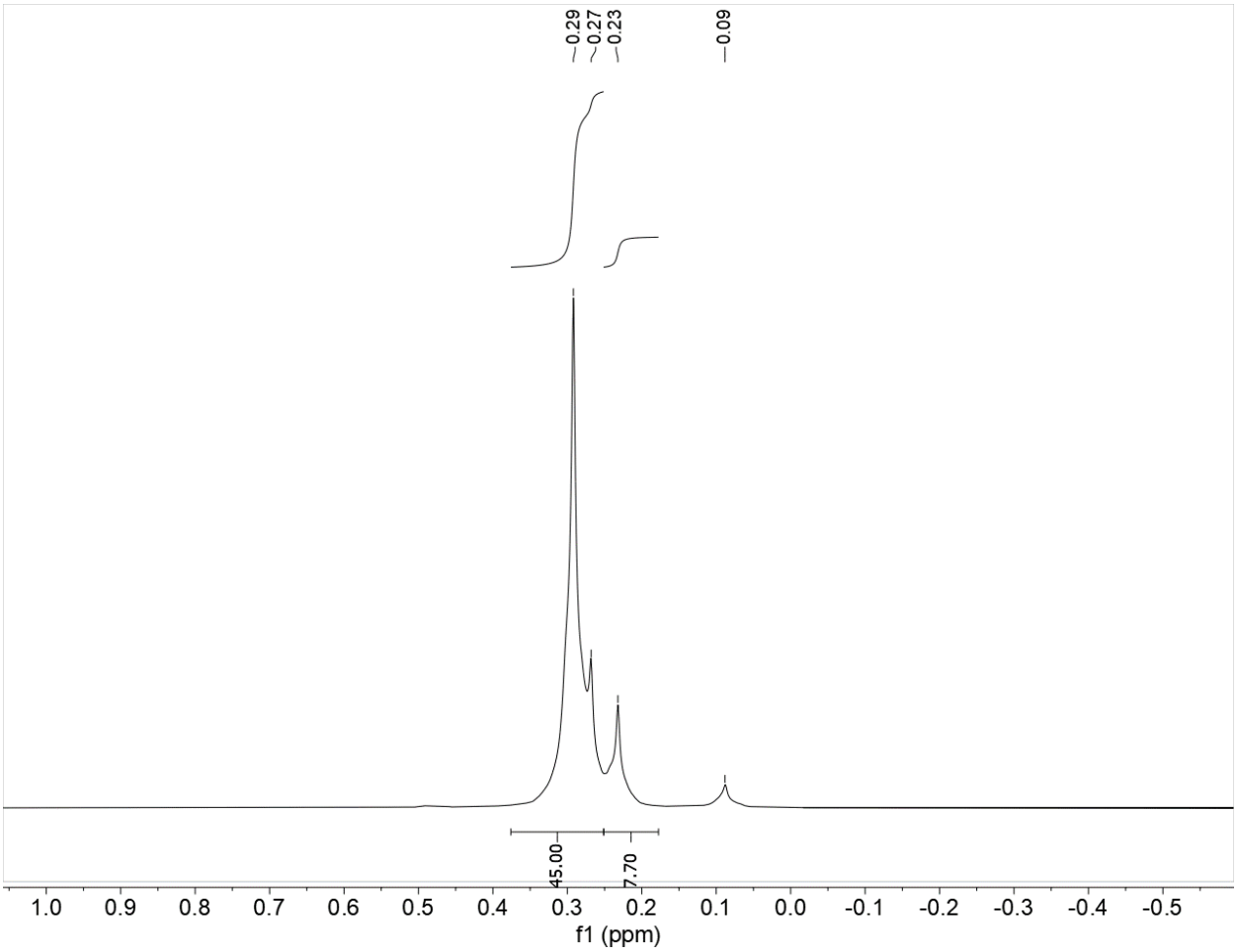

Figure 3.S11. Expanded scale ^{1}H-NMR spectrum of complex **3** in [D_2] methylene chloride at 25 °C

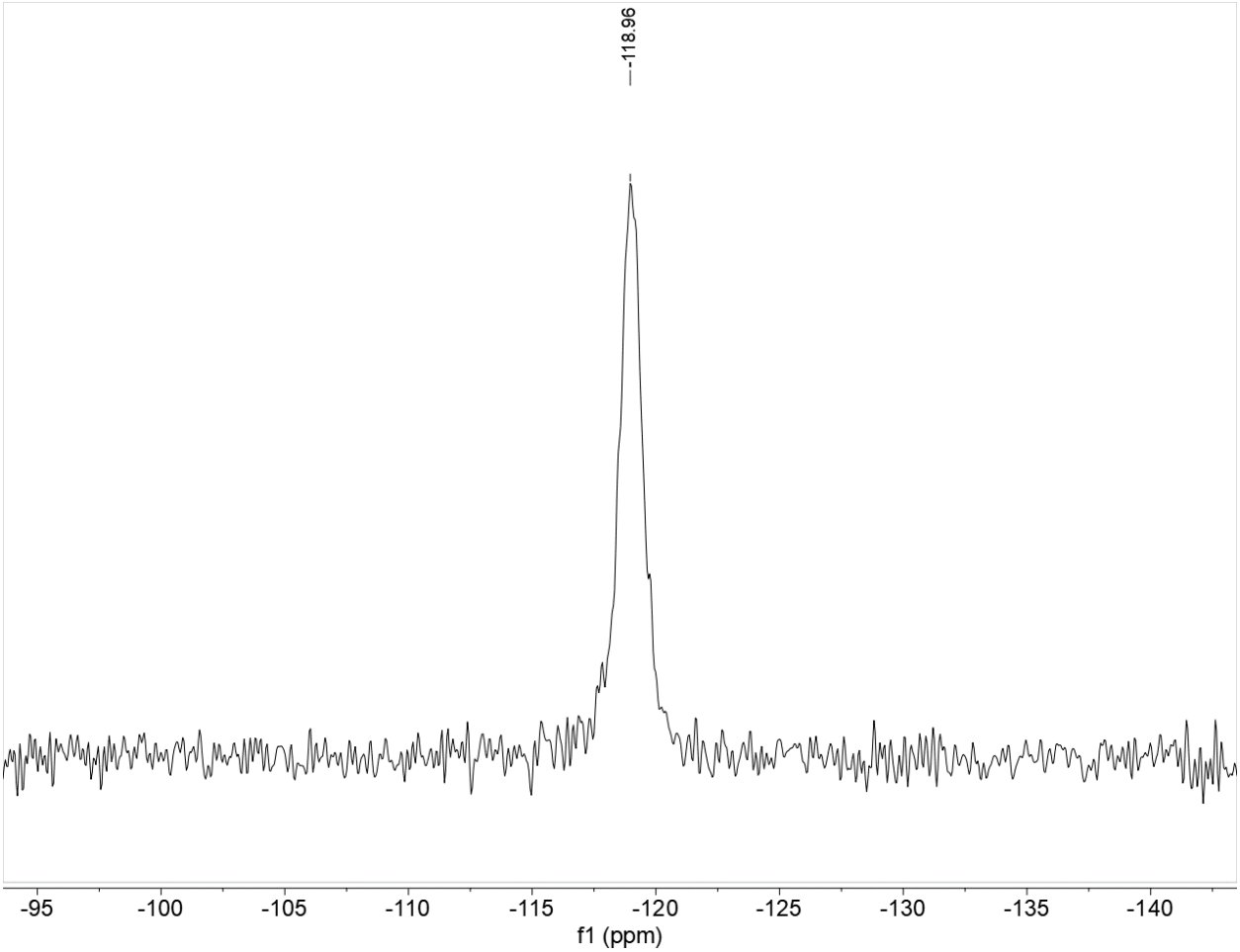

Figure 3.S12. ^{51}V-NMR spectrum of V(=O){N(SiMe$_3$)$_2$}$_3$ (**1**) in [D$_8$] toluene at 25 °C.

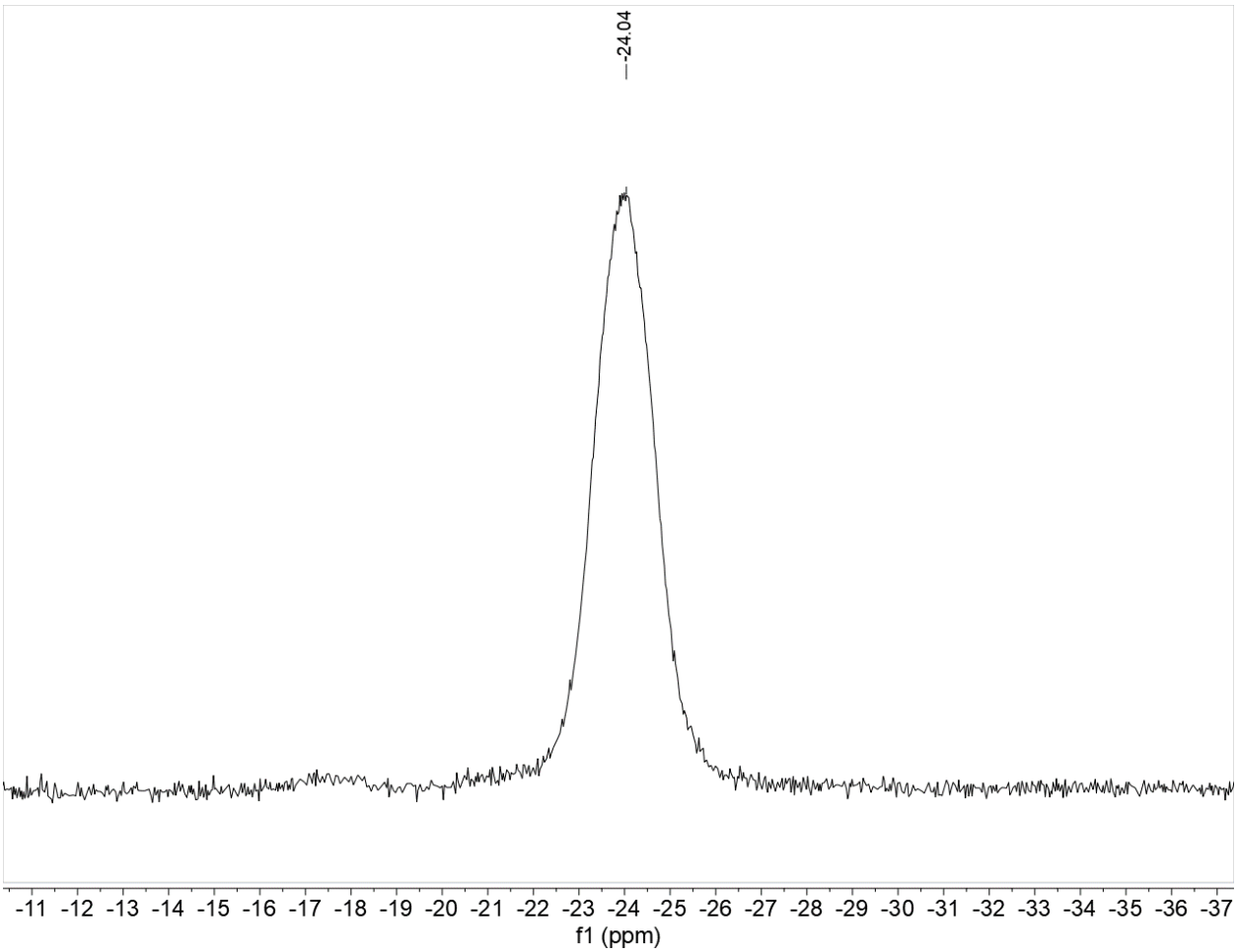

Figure 3.S13. ^{51}V-NMR spectrum of V{=N(SiMe$_3$)$_2$}{N(SiMe$_3$)$_2$}$_3$ (**2**) in [D$_2$] methylene chloride at 25 °C.

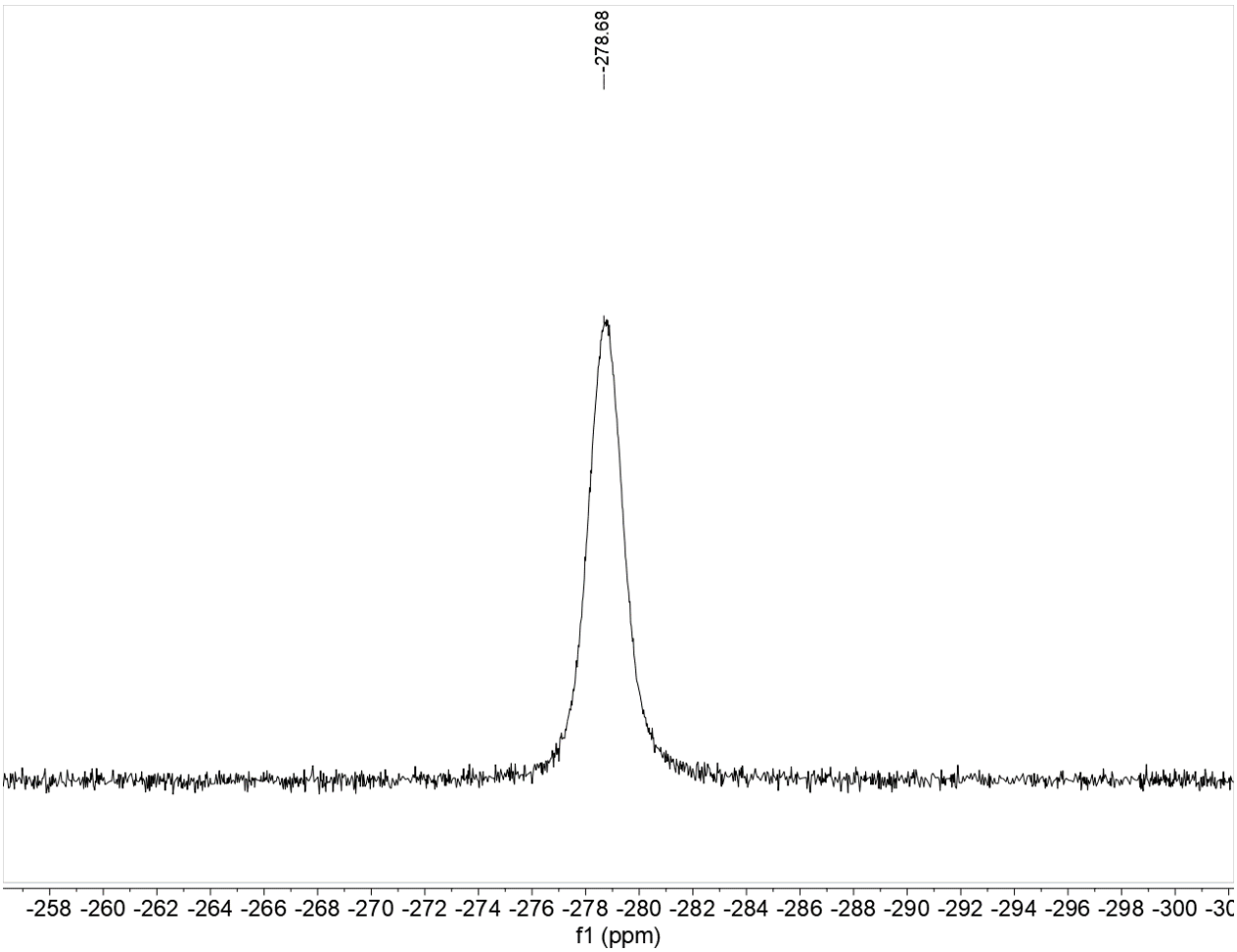

Figure 3.S14. ^{51}V-NMR spectrum of complex **3** in [D_2] methylene chloride at 25 °C.

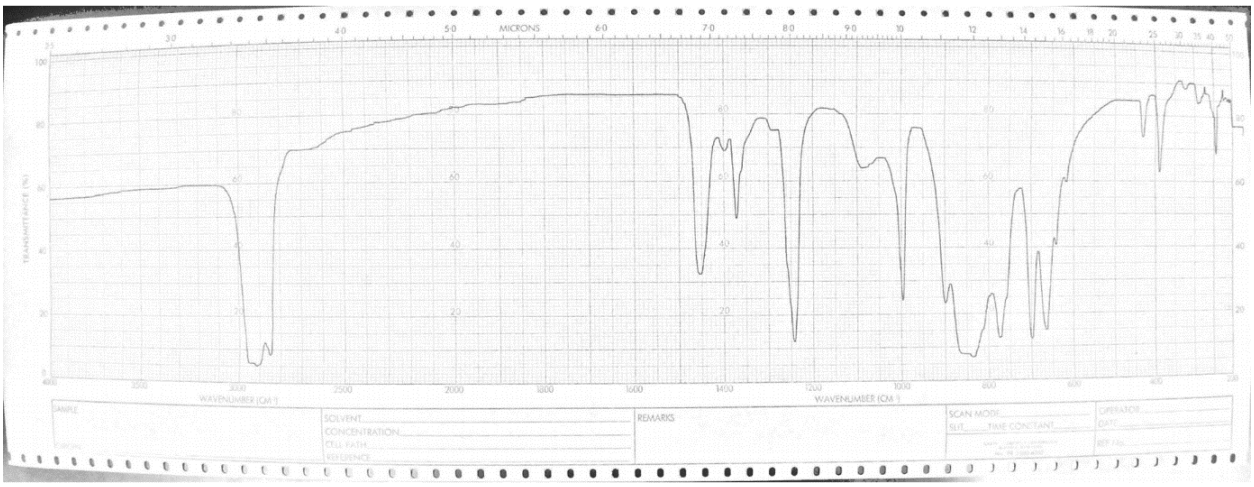

Figure 3.S15. Infrared spectrum of $V(=O)\{N(SiMe_3)_2\}_3$ (**1**) (Nujol, CsI windows)

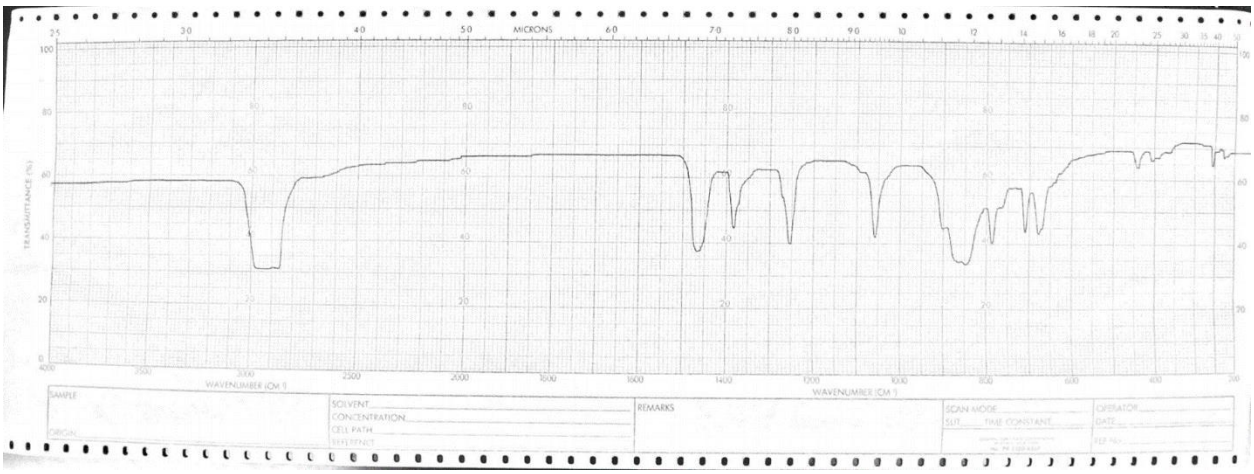

Figure 3.S16. Infrared spectrum of $V\{=N(SiMe_3)_2\}\{N(SiMe_3)_2\}_3$ (**2**) (Nujol, CsI windows)

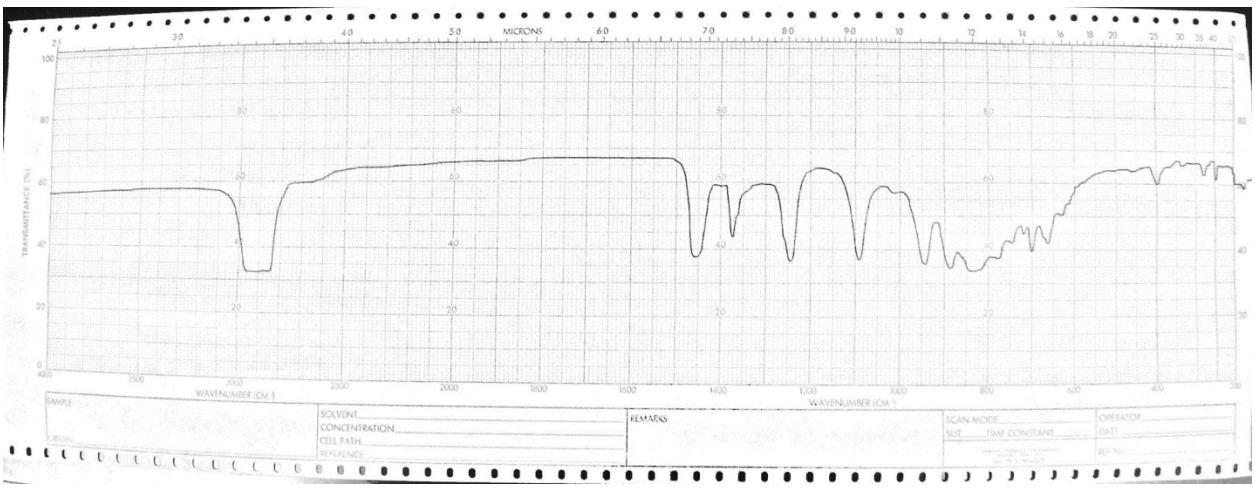

Figure 3.S17. Infrared spectrum of **3** (Nujol, CsI windows)

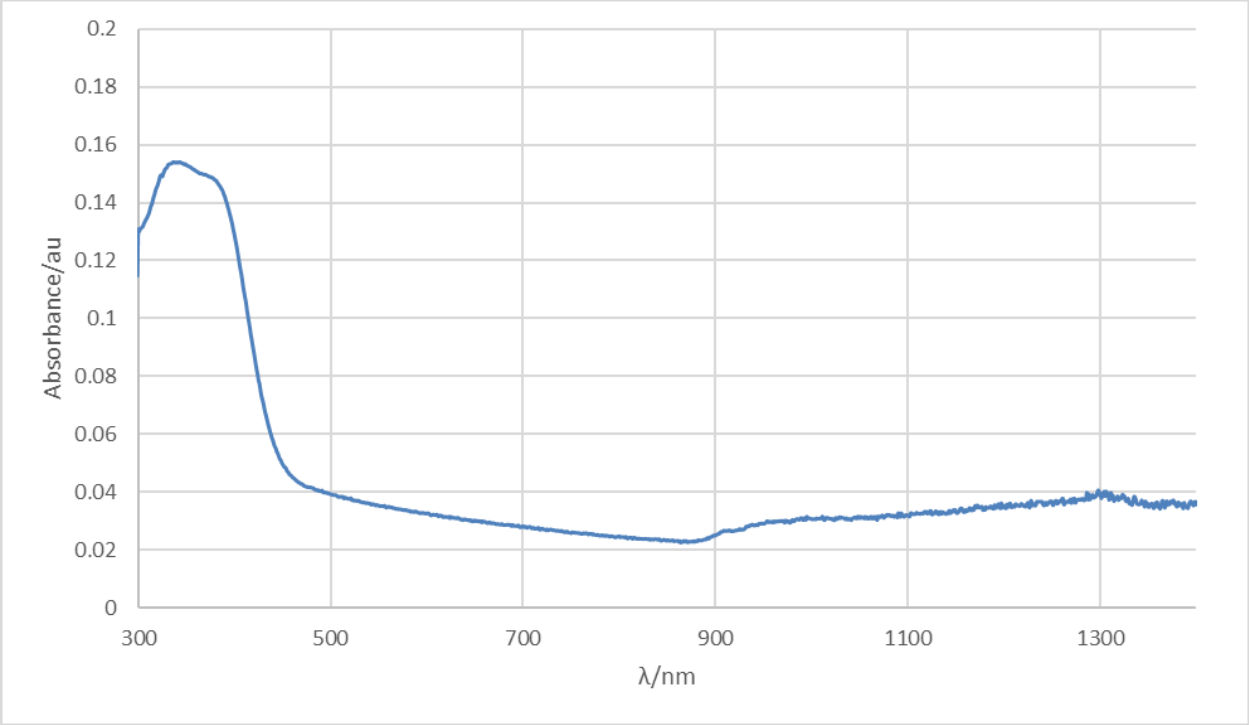

Figure 3.S18. UV-Vis spectrum of V(=O){N(SiMe$_3$)$_2$}$_3$ (**1**) (7 µM, hexanes, 1 cm path length**)**

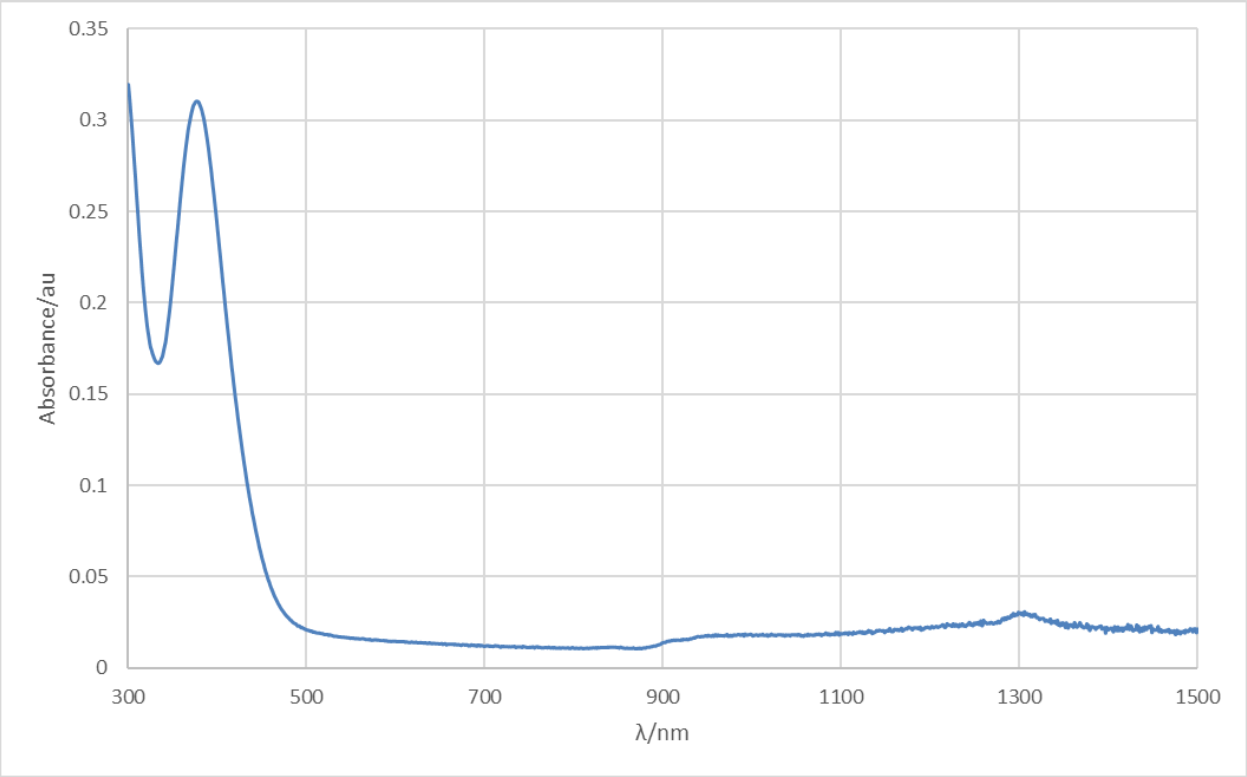

Figure 3.S19. UV-Vis spectrum of $V(=NSiMe_3)\{N(SiMe_3)_2\}_3$ (**2**) (49 μM, hexanes, 1 cm path length).

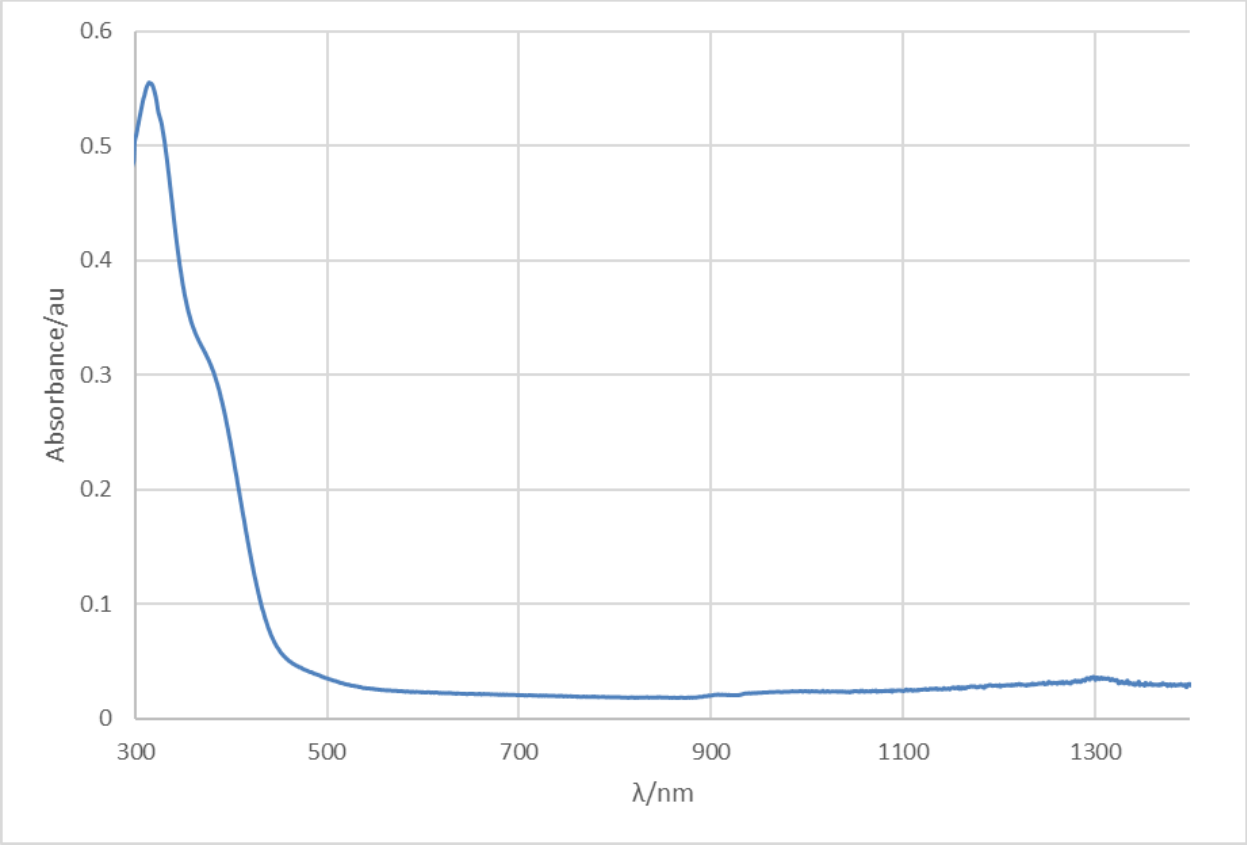

Figure 3.S20. UV-Vis spectrum of complex **3** (104 μM, hexanes, 1 cm path length).

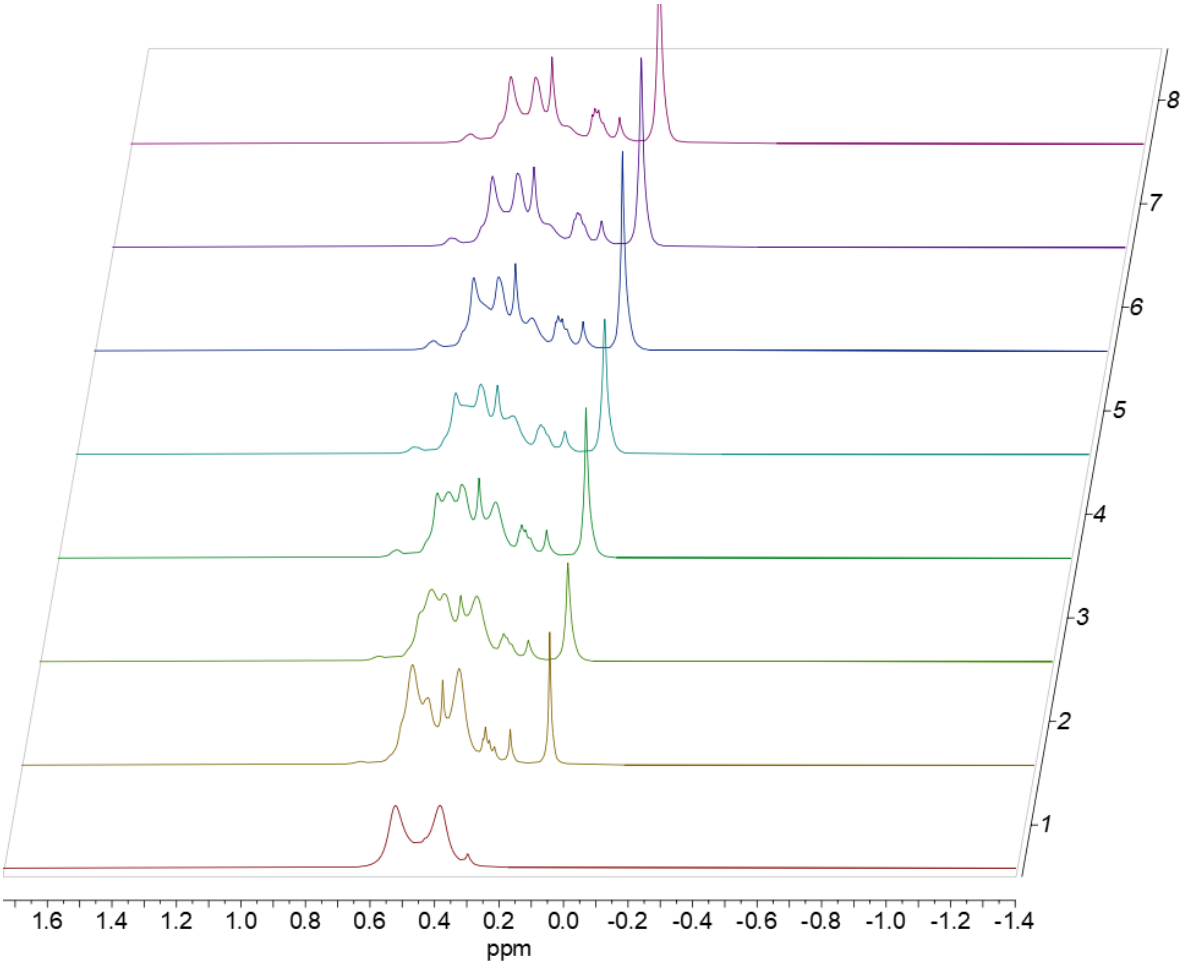

Figure 3.S21. Conversion of complex **1** to complex **3** (in [D_6] benzene, 25 °C. Note: The growth of the signal at 0.10 ppm (hexamethyldisilazane) suggests decomposition of **1** by adventitious water. This figure is provided to show only the conversion of **1** to **3** at ambient temperature as indicated by the growth of signals at 0.43 and 0.30 ppm. Information on the rate and activation energy are taken from studies at elevated temperature (vide infra).

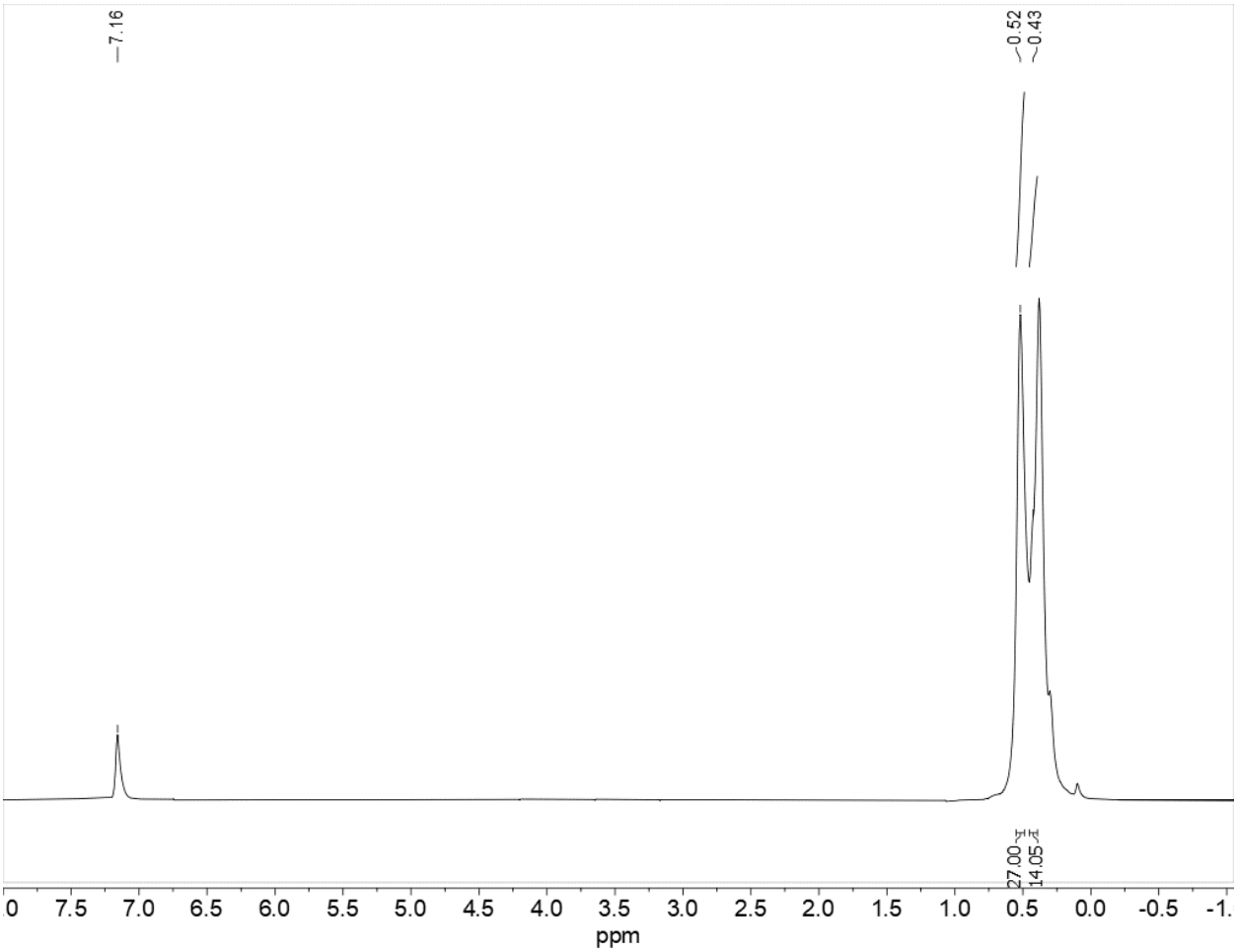

Figure 3.S22. Conversion of Complex **1** to Complex **3** (in [D_6] benzene, 63 °C, 5 minutes).

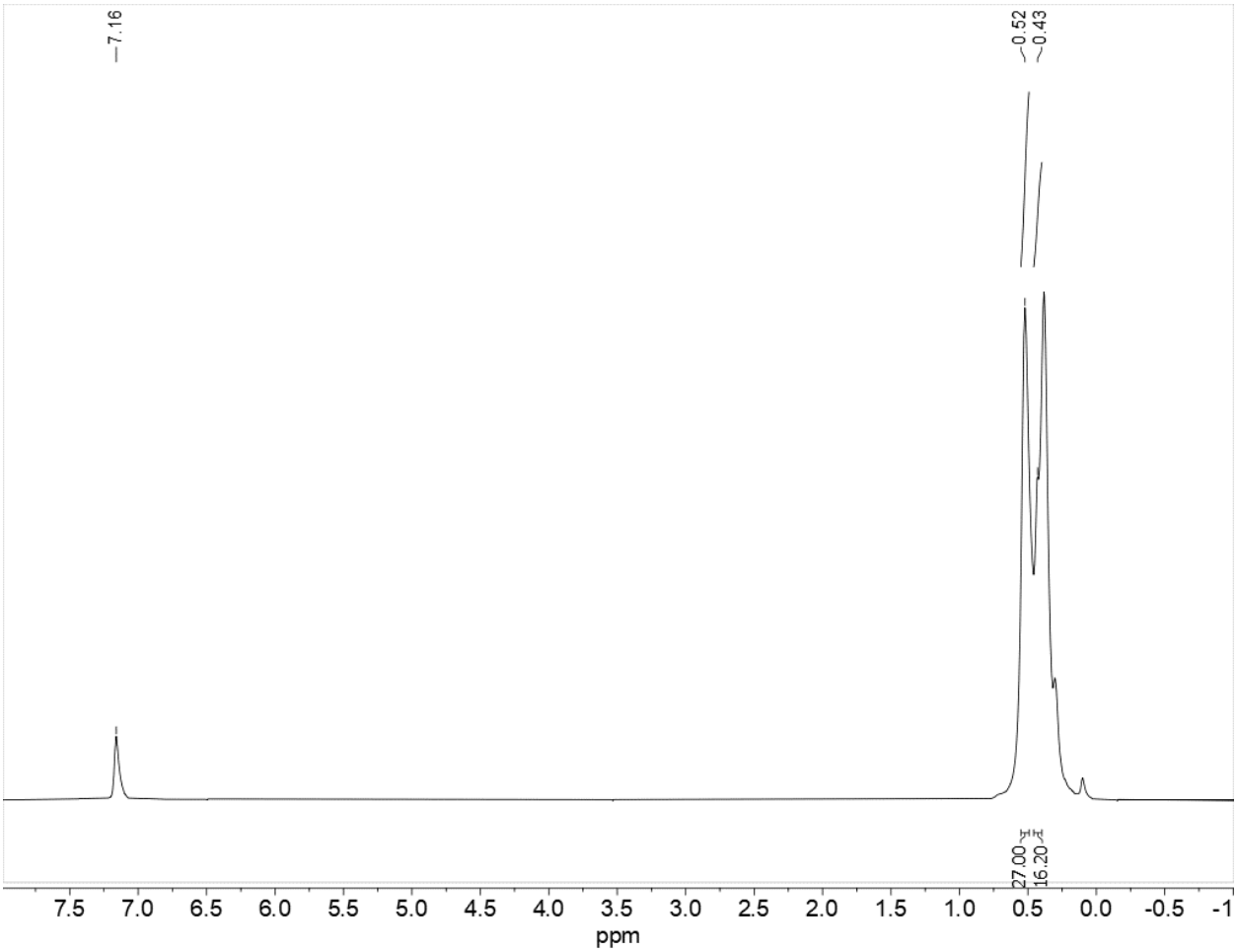

Figure 3.S23. Conversion of Complex **1** to Complex **3** (in [D_6] benzene, 63 °C, 10 minutes).

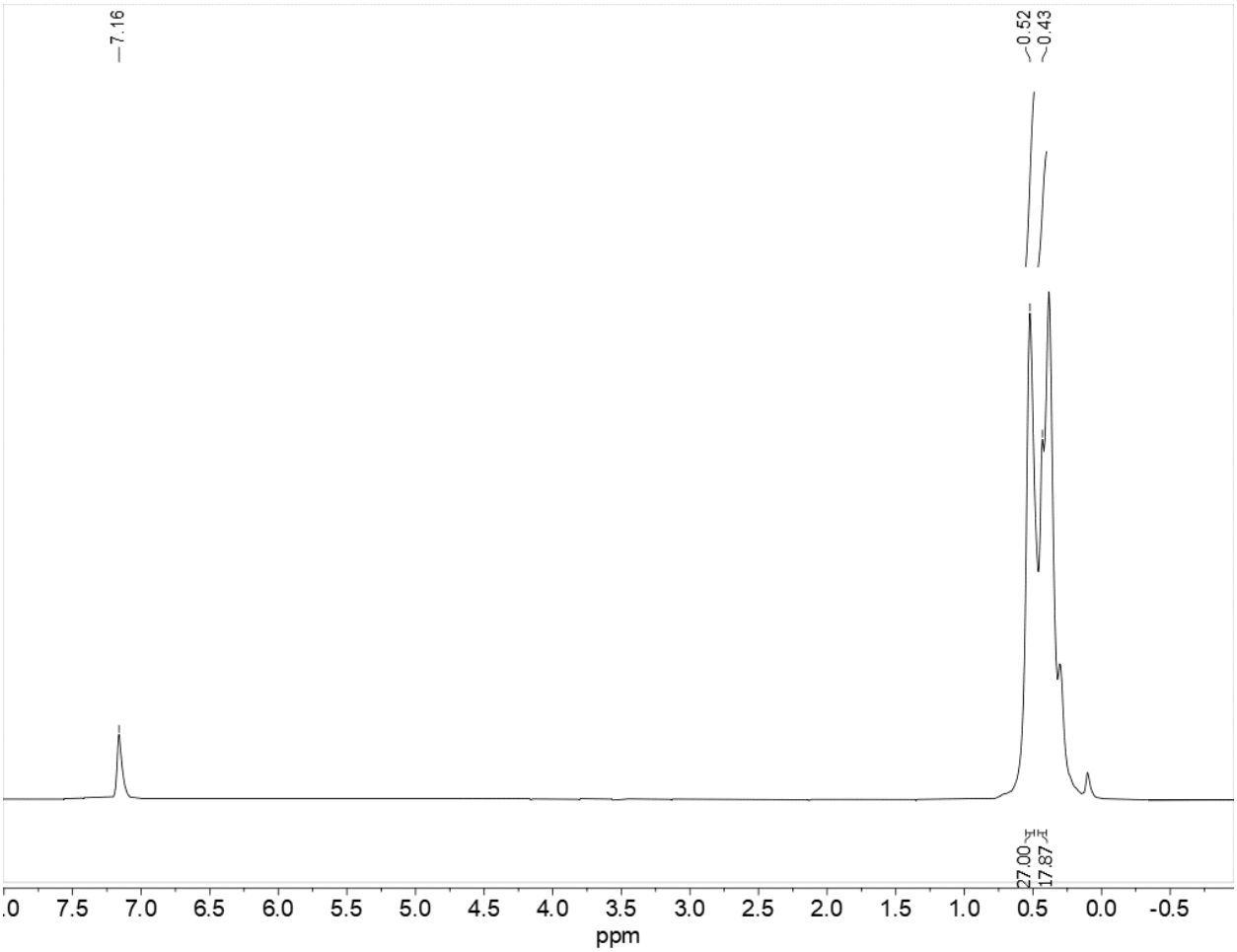

Figure 3.S24. Conversion of Complex **1** to Complex **3** (in [D_6] benzene, 63 °C, 15 minutes).

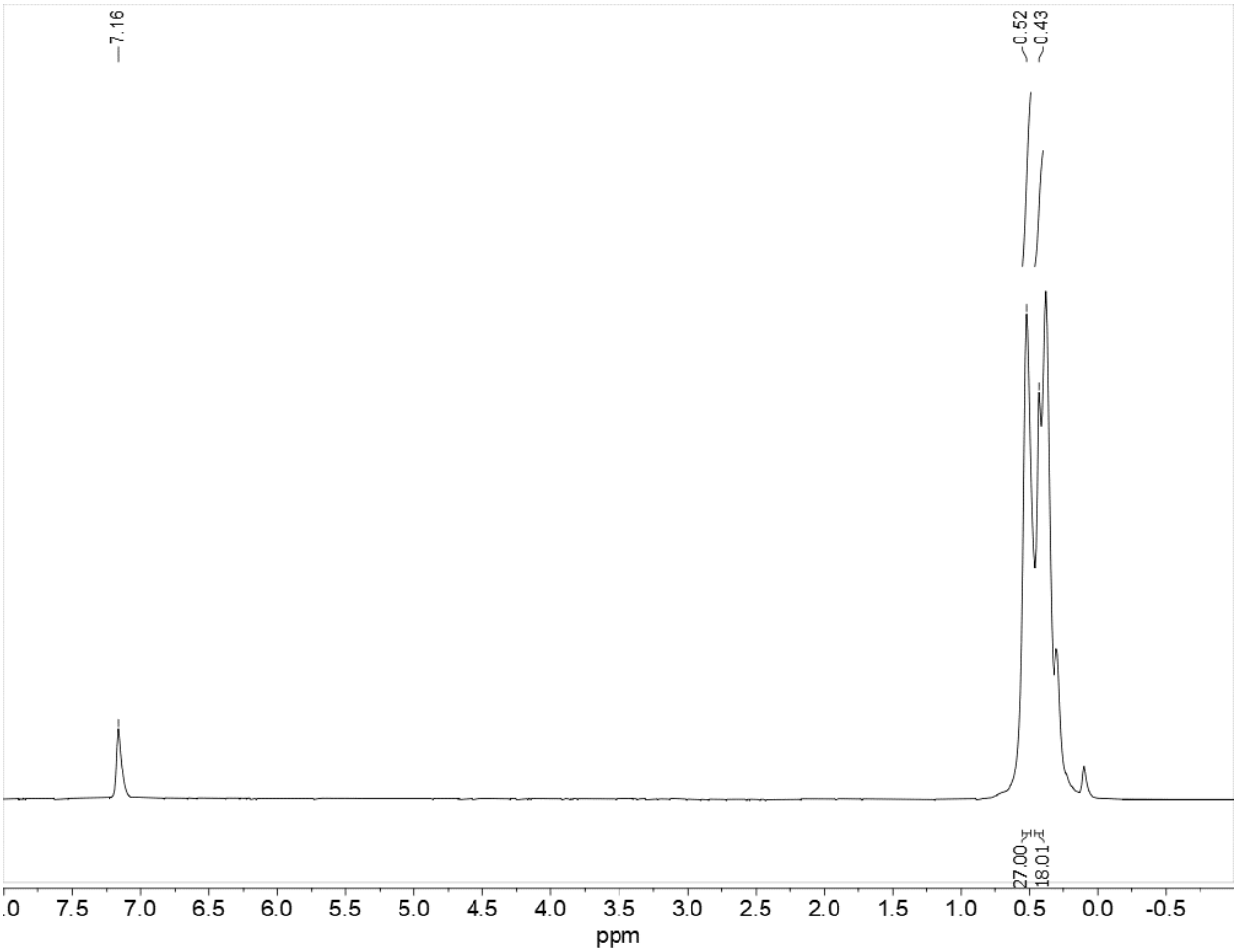

Figure 3.S25. Conversion of Complex **1** to Complex **3** (in [D_6] benzene, 63 °C, 20 minutes).

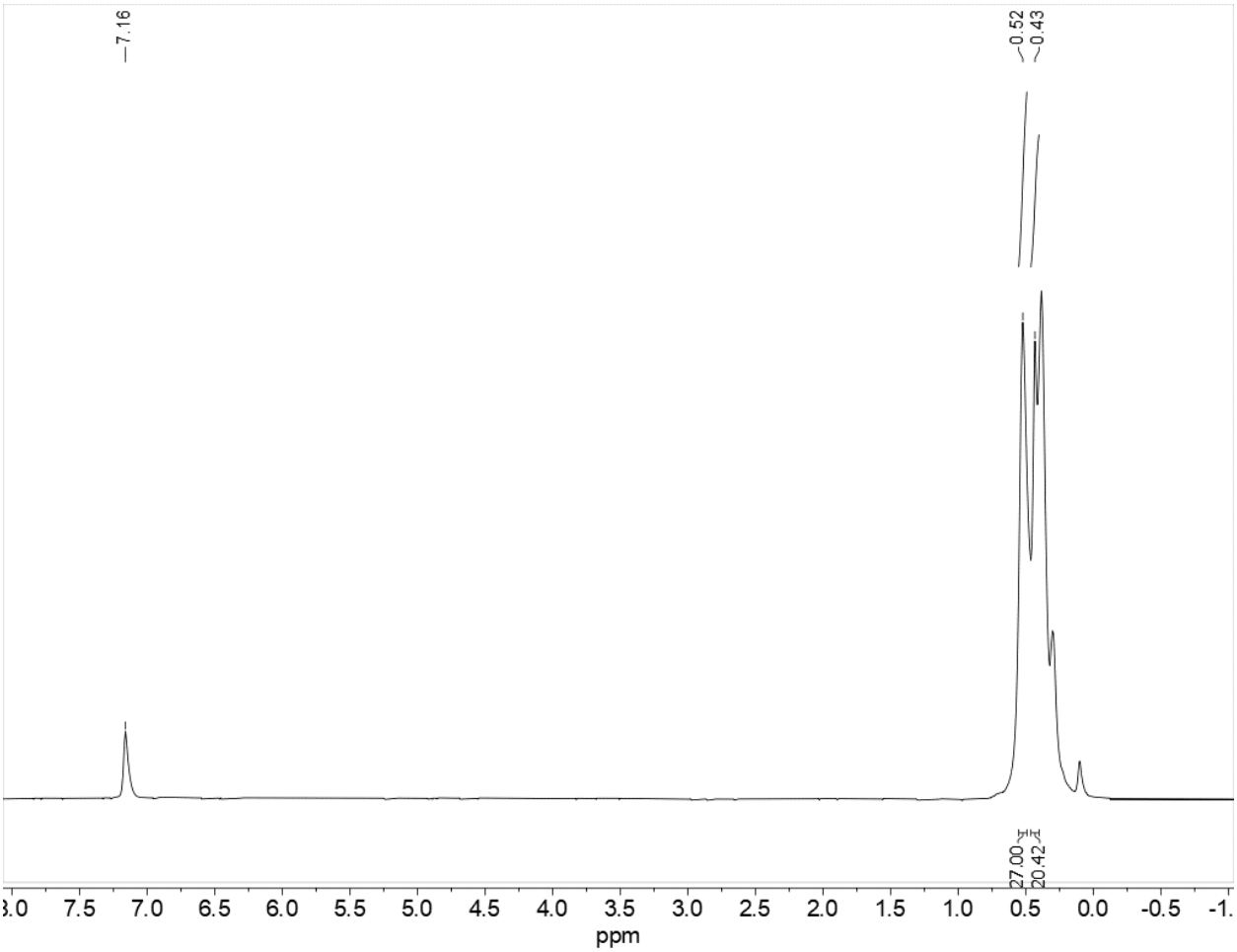

Figure 3.S26. Conversion of Complex **1** to Complex **3** (in [D_6] benzene, 63 °C, 25 minutes).

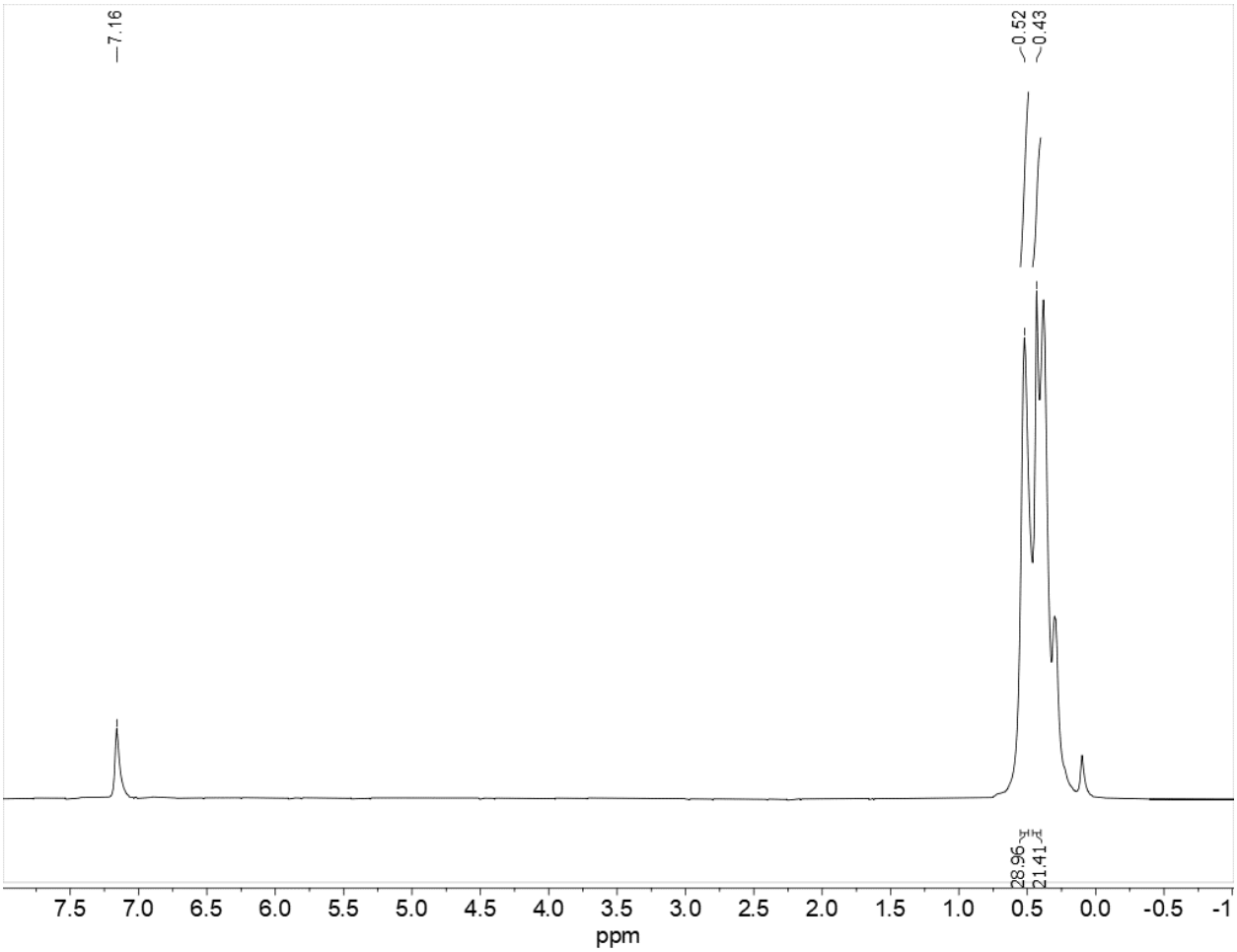

Figure 3.S27. Conversion of Complex **1** to Complex **3** (in [D_6] benzene, 63 °C, 30 minutes).

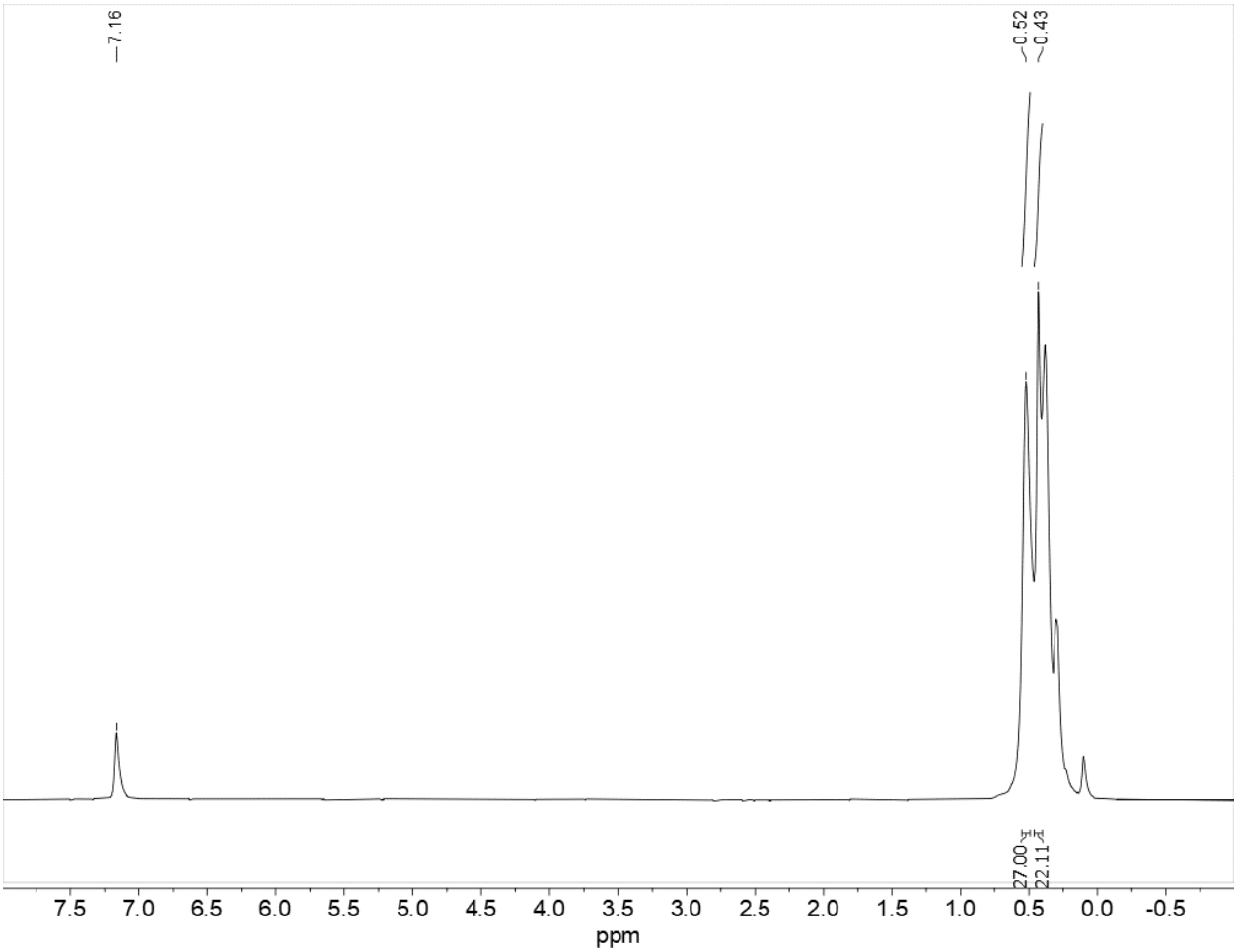

Figure 3.S28. Conversion of Complex **1** to Complex **3** (in [D_6] benzene, 63 °C, 35 minutes).

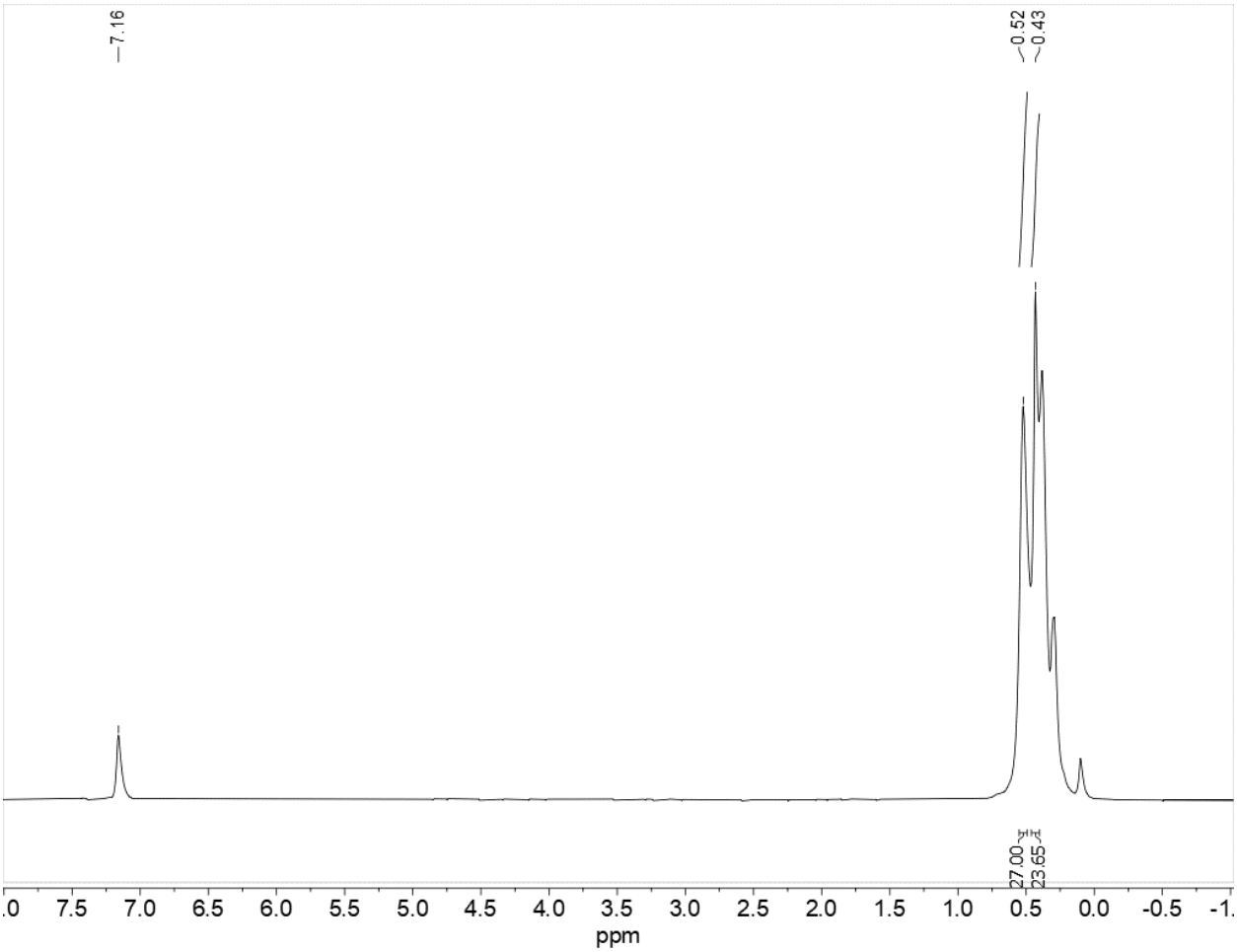

Figure 3.S29. Conversion of Complex **1** to Complex **3** (in [D_6] benzene, 63 °C, 40 minutes).

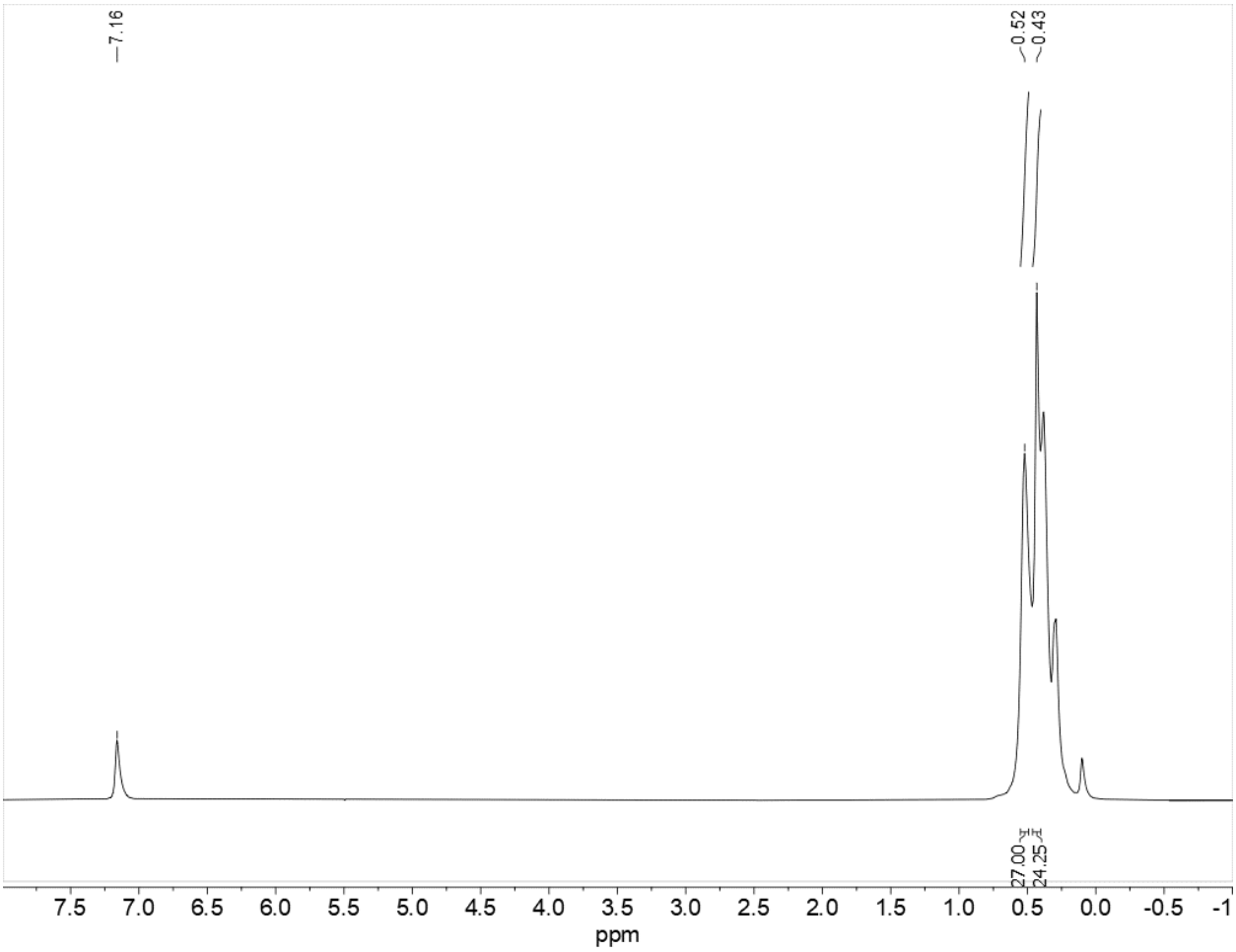

Figure 3.S30. Conversion of Complex **1** to Complex **3** (in [D_6] benzene, 63 °C, 45 minutes).

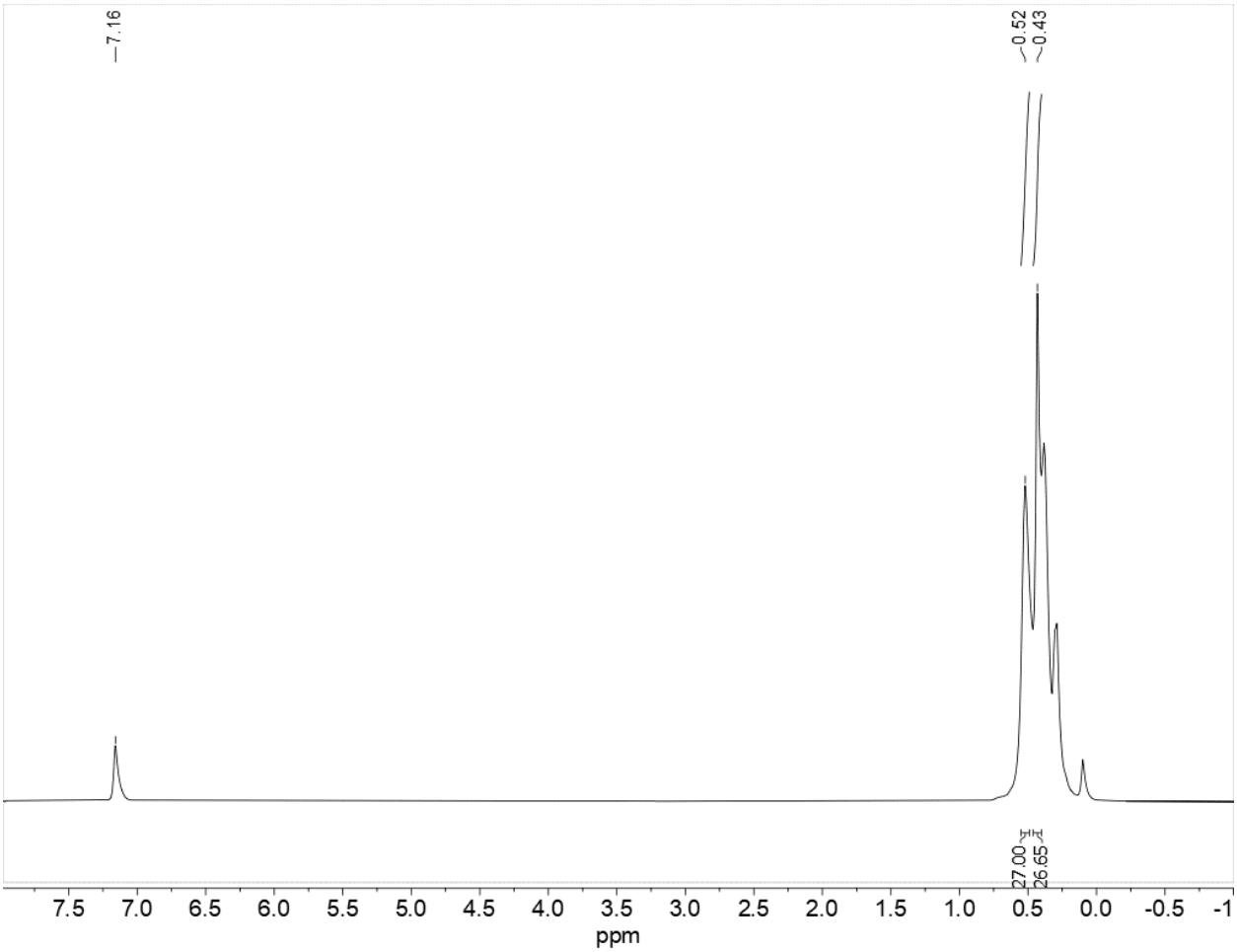

Figure 3.S31. Conversion of Complex **1** to Complex **3** (in [D_6] benzene, 63 °C, 50 minutes).

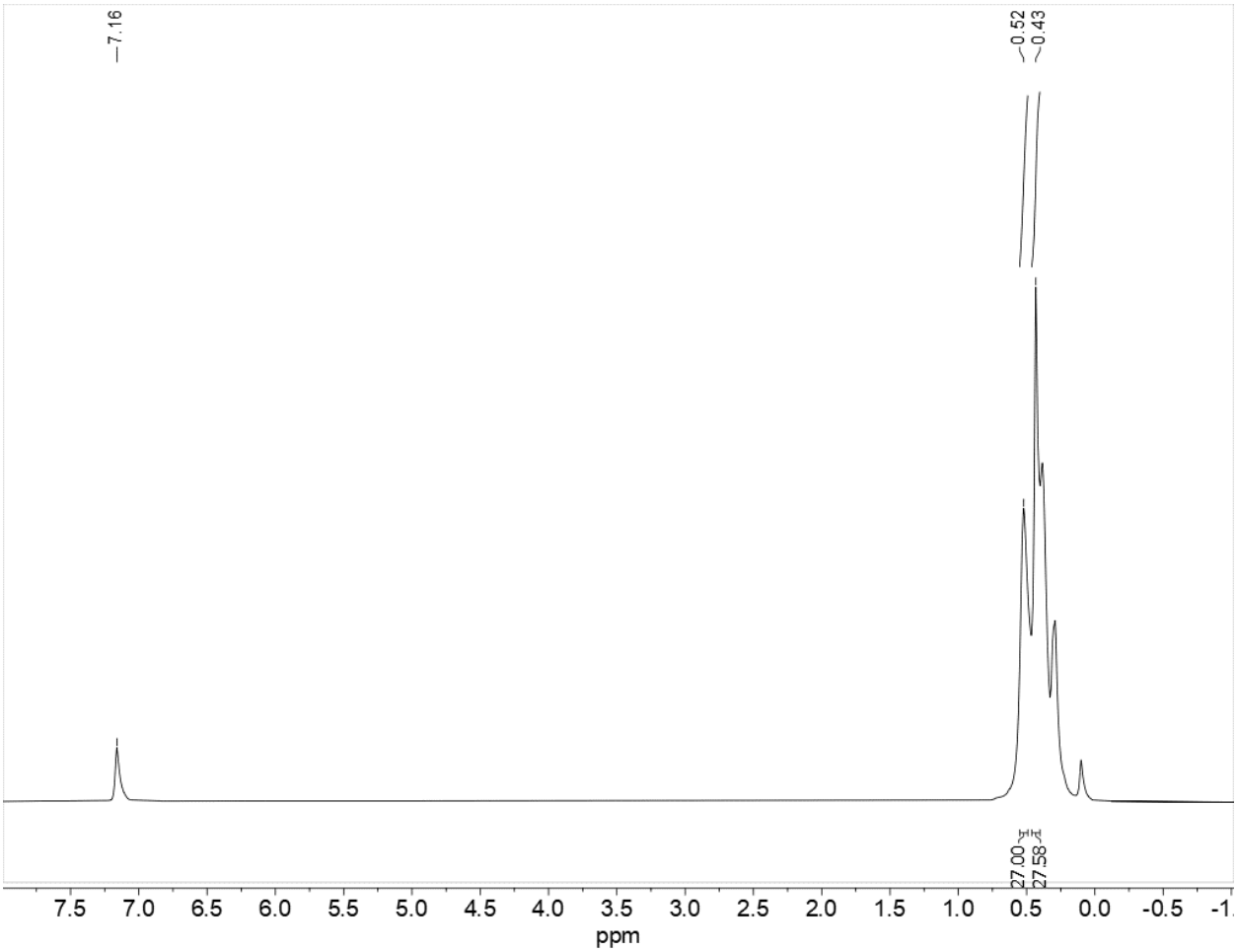

Figure 3.S32. Conversion of Complex **1** to Complex **3** (in [D_6] benzene, 63 °C, 55 minutes).

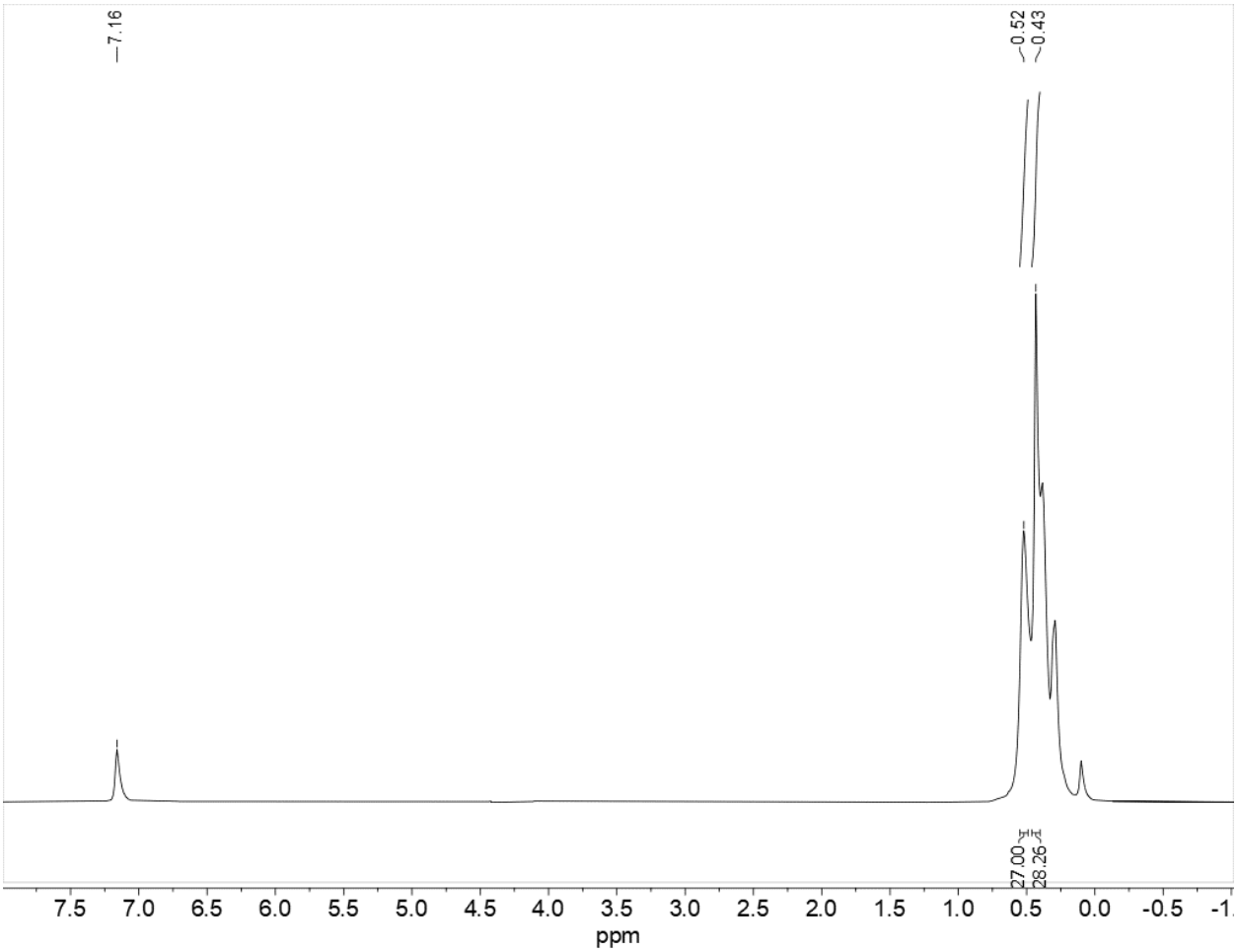

Figure 3.S33. Conversion of Complex **1** to Complex **3** (in [D_6] benzene, 63 °C, 60 minutes).

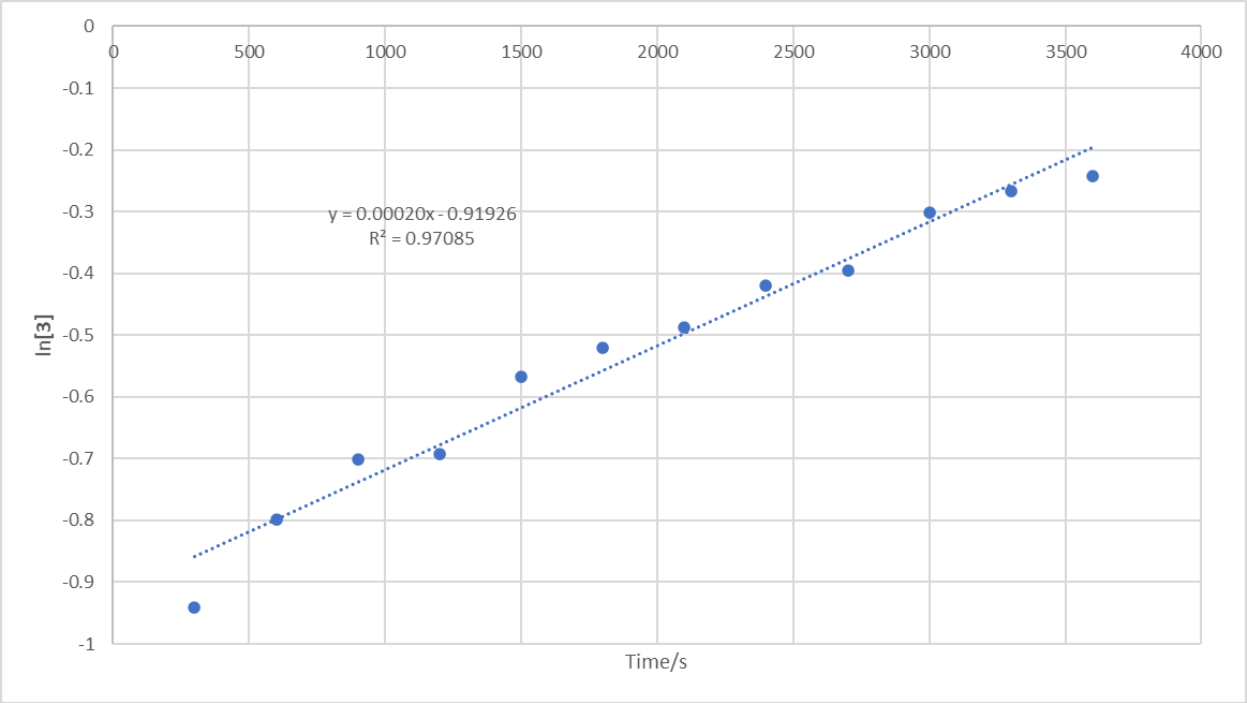

Figure 3.S34. Plot of ln[**3**] vs. Time at 63 °C. Note: Concentration of **3** is given relative to concentration of **1** (the signal at 0.52 was normalized to a constant integration value of 27 trimethylsilyl protons (one molecule of V(=O){N(SiMe$_3$)$_2$}$_3$), and the integration of the signal at 0.43 was treated as a fraction of the 36 trimethylsilyl amido protons of **3**).

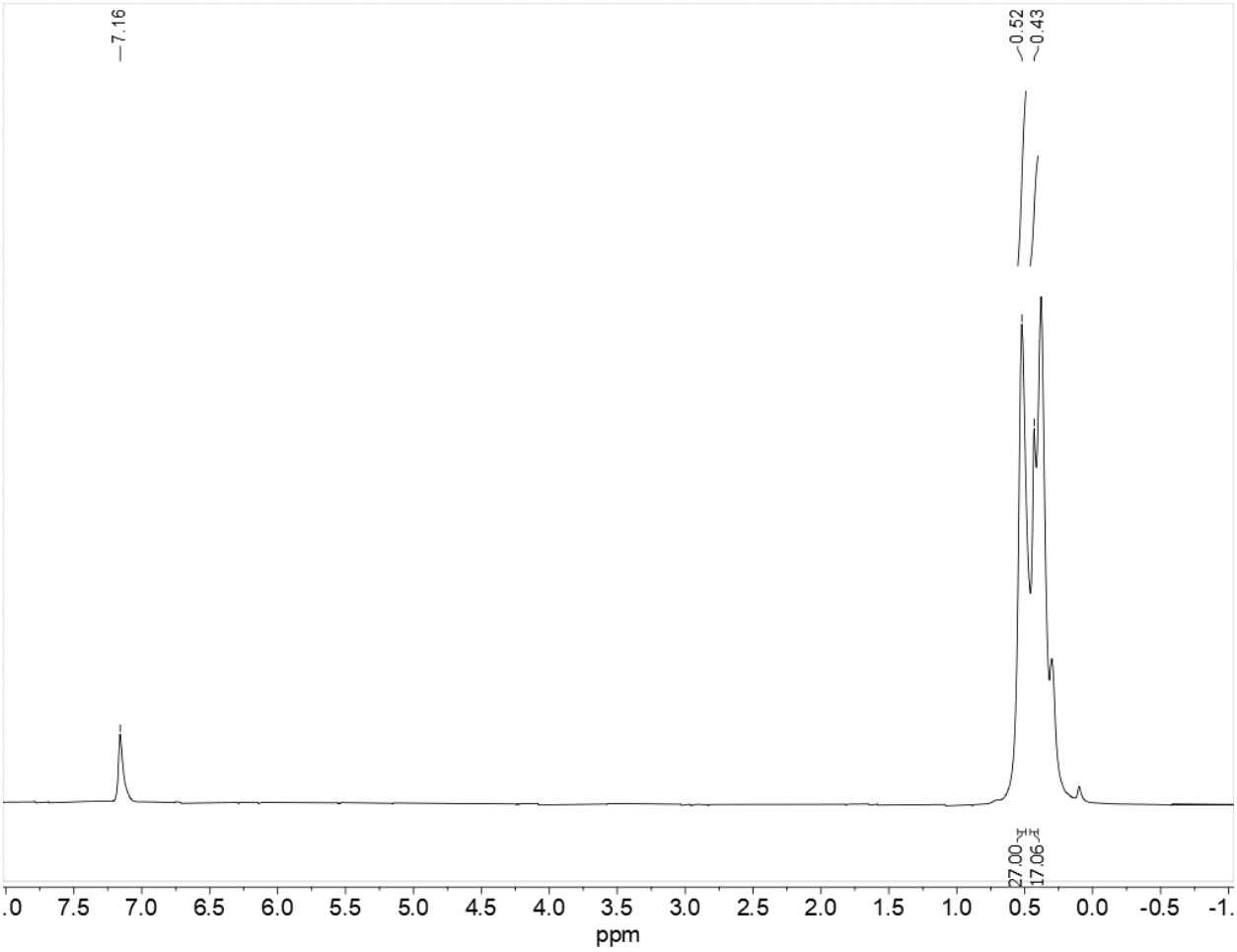

Figure 3.S35. Conversion of Complex **1** to Complex **3** (in [D_6] benzene, 73 °C, 5 minutes).

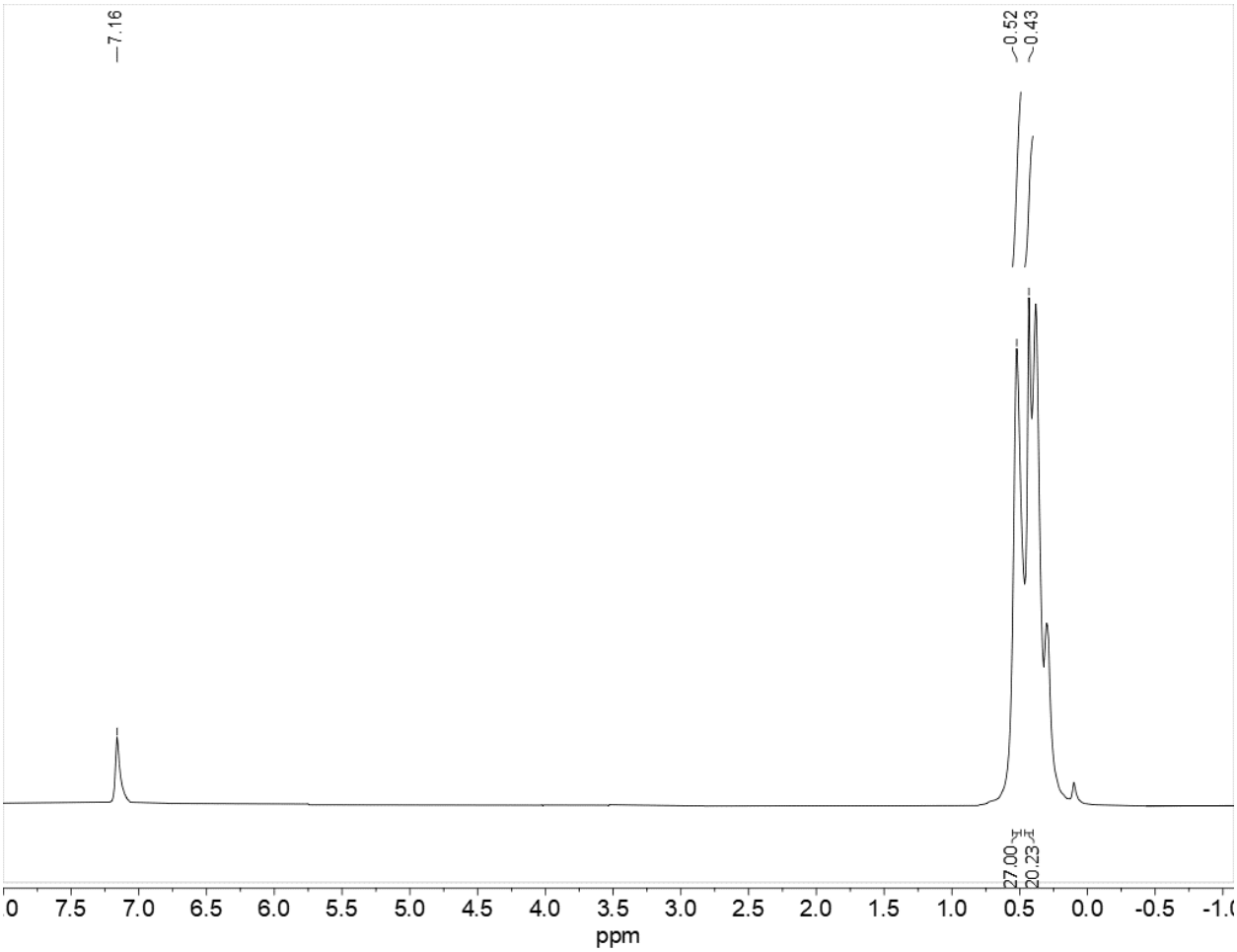

Figure 3.S36. Conversion of Complex **1** to Complex **3** (in [D_6] benzene, 73 °C, 10 minutes).

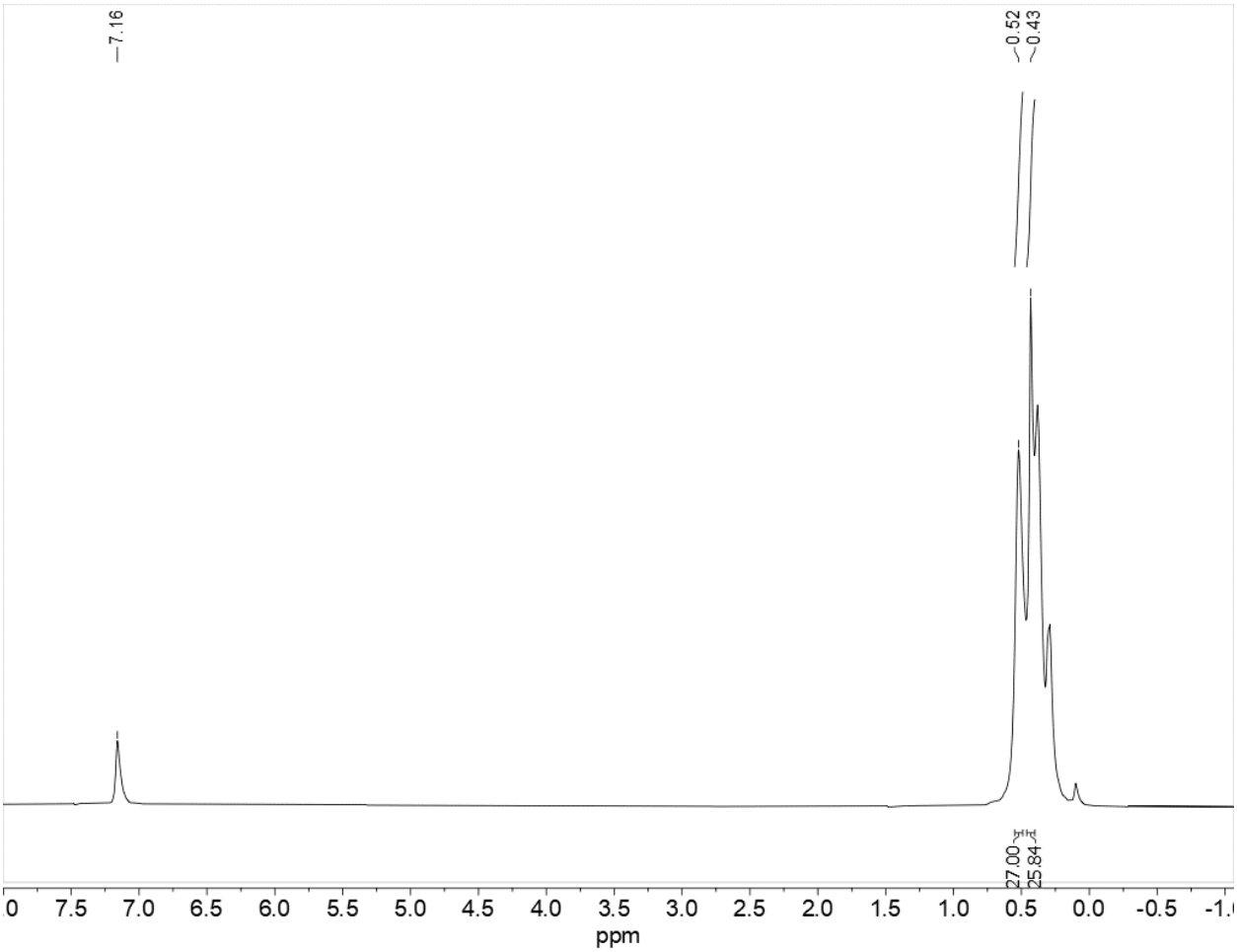

Figure 3.S37. Conversion of Complex **1** to Complex **3** (in [D_6] benzene, 73 °C, 15 minutes).

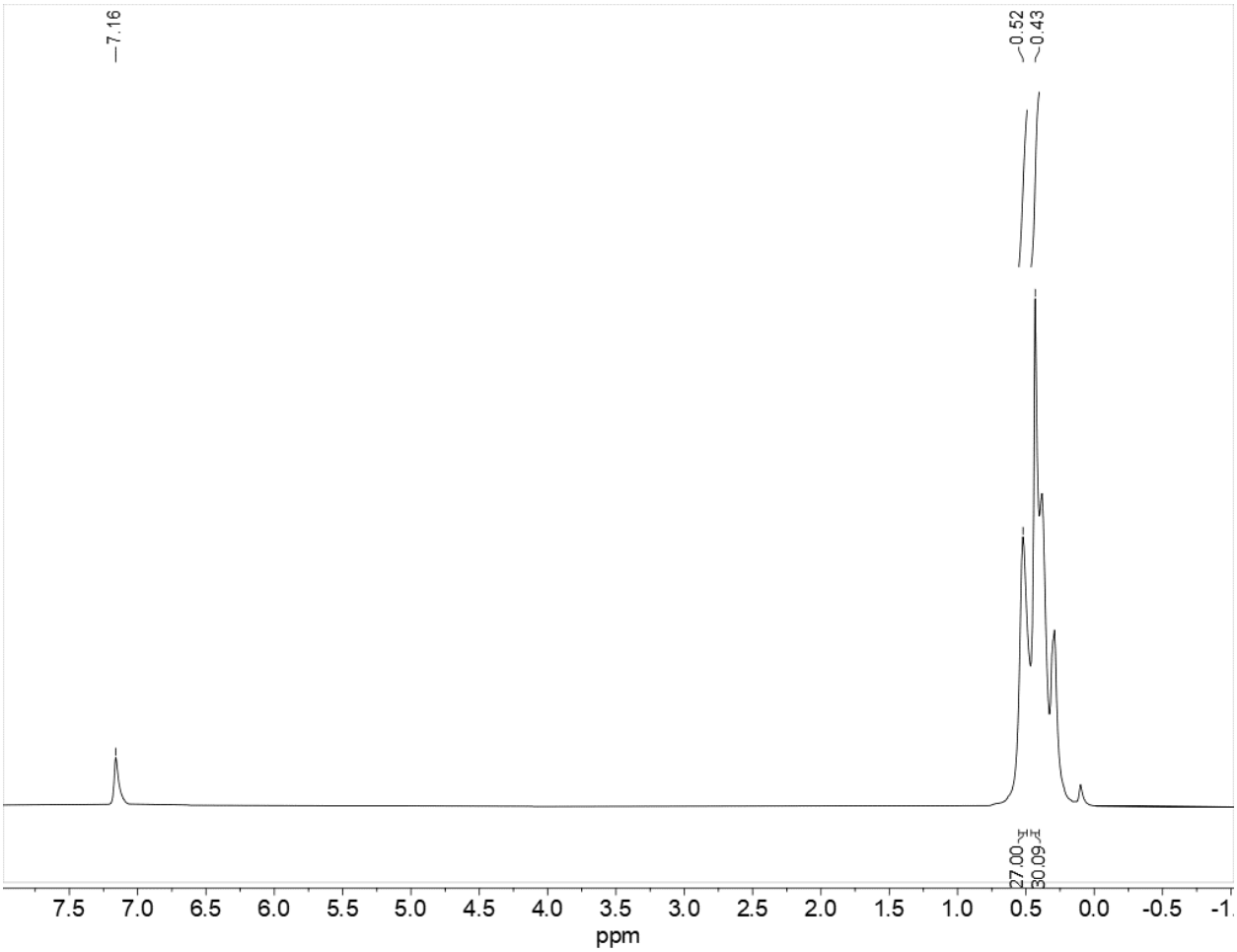

Figure 3.S38. Conversion of Complex **1** to Complex **3** (in [D_6] benzene, 73 °C, 20 minutes).

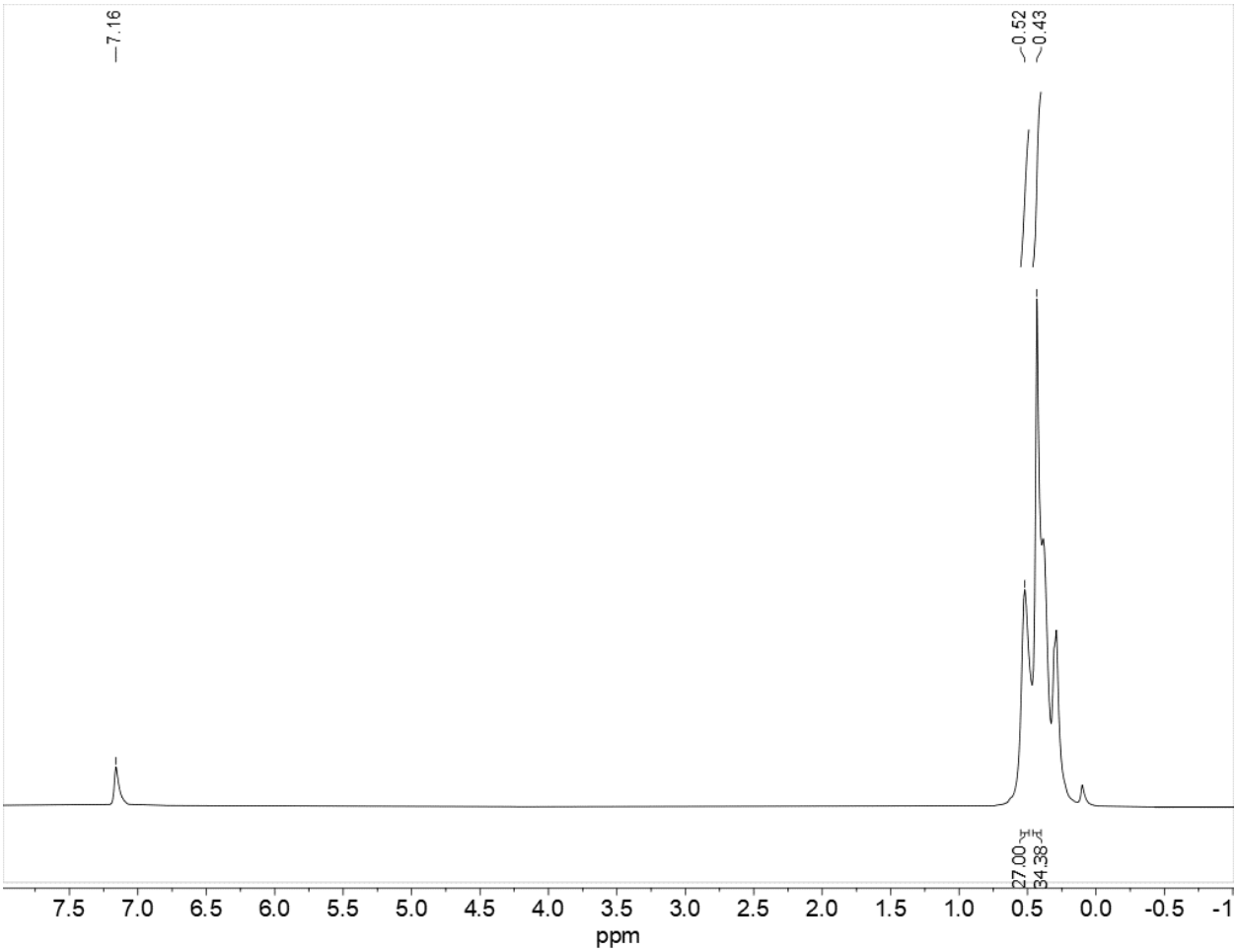

Figure 3.S39. Conversion of Complex **1** to Complex **3** (in [D_6] benzene, 73 °C, 25 minutes).

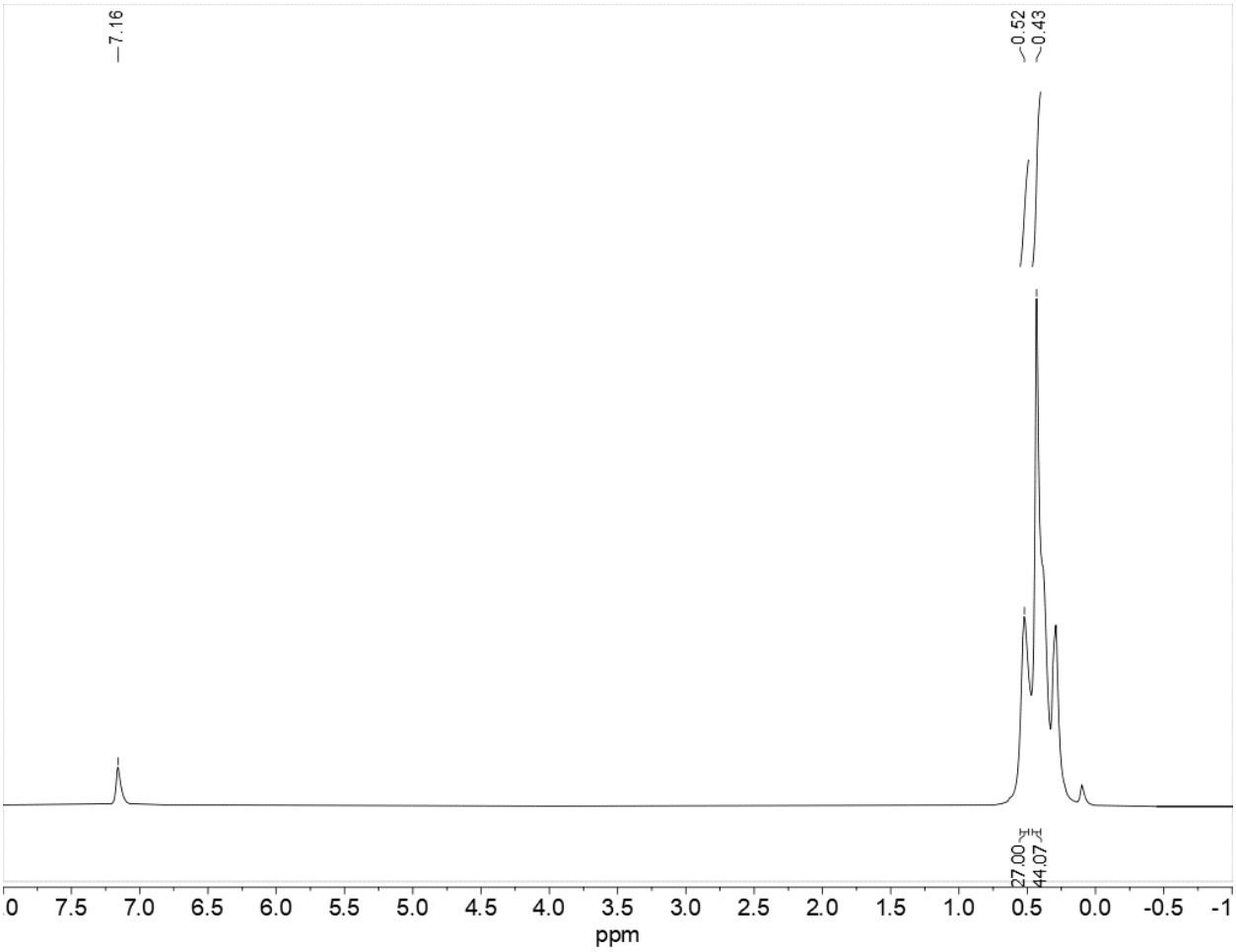

Figure 3.S40. Conversion of Complex **1** to Complex **3** (in [D_6] benzene, 73 °C, 30 minutes).

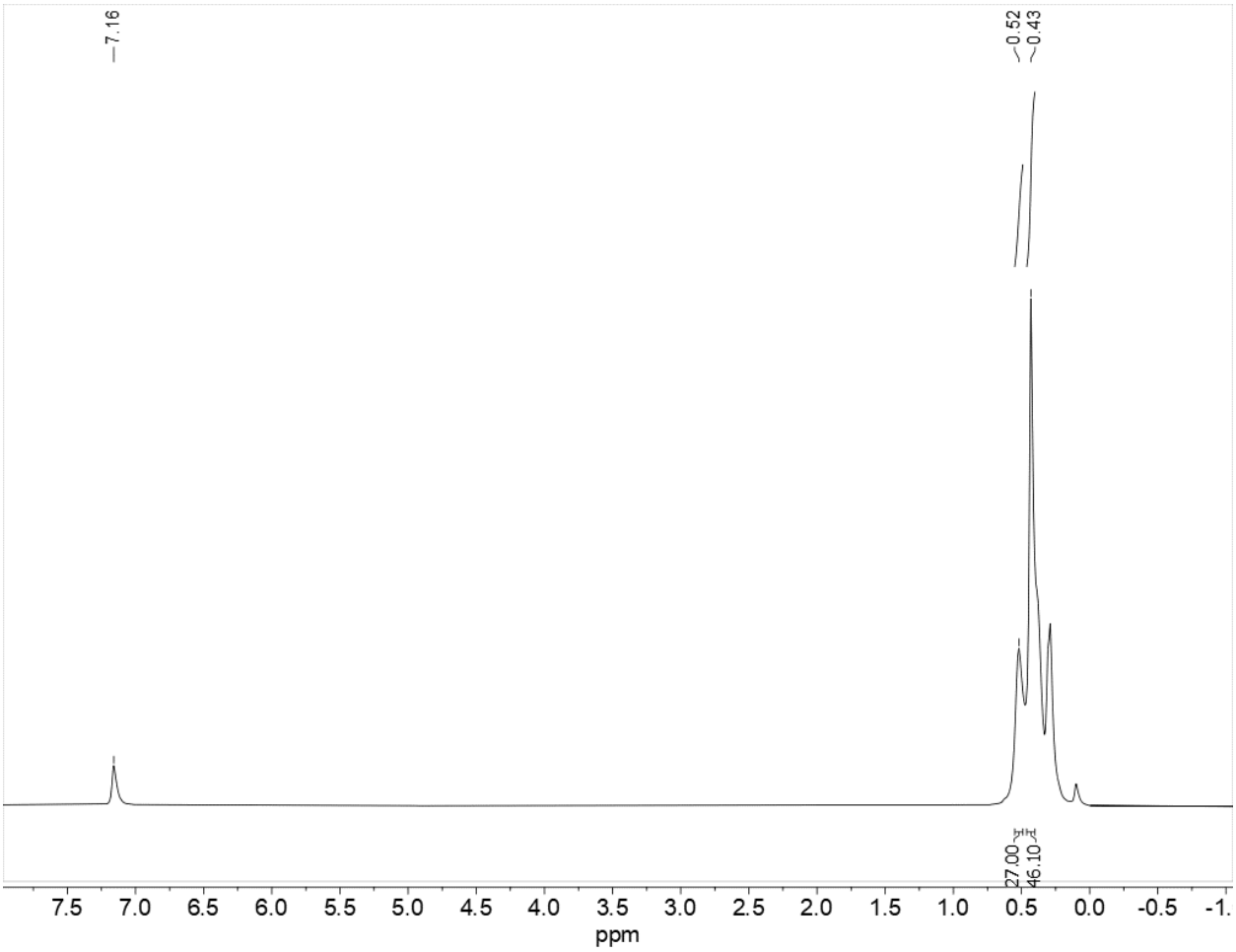

Figure 3.S41. Conversion of Complex **1** to Complex **3** (in [D_6] benzene, 73 °C, 35 minutes).

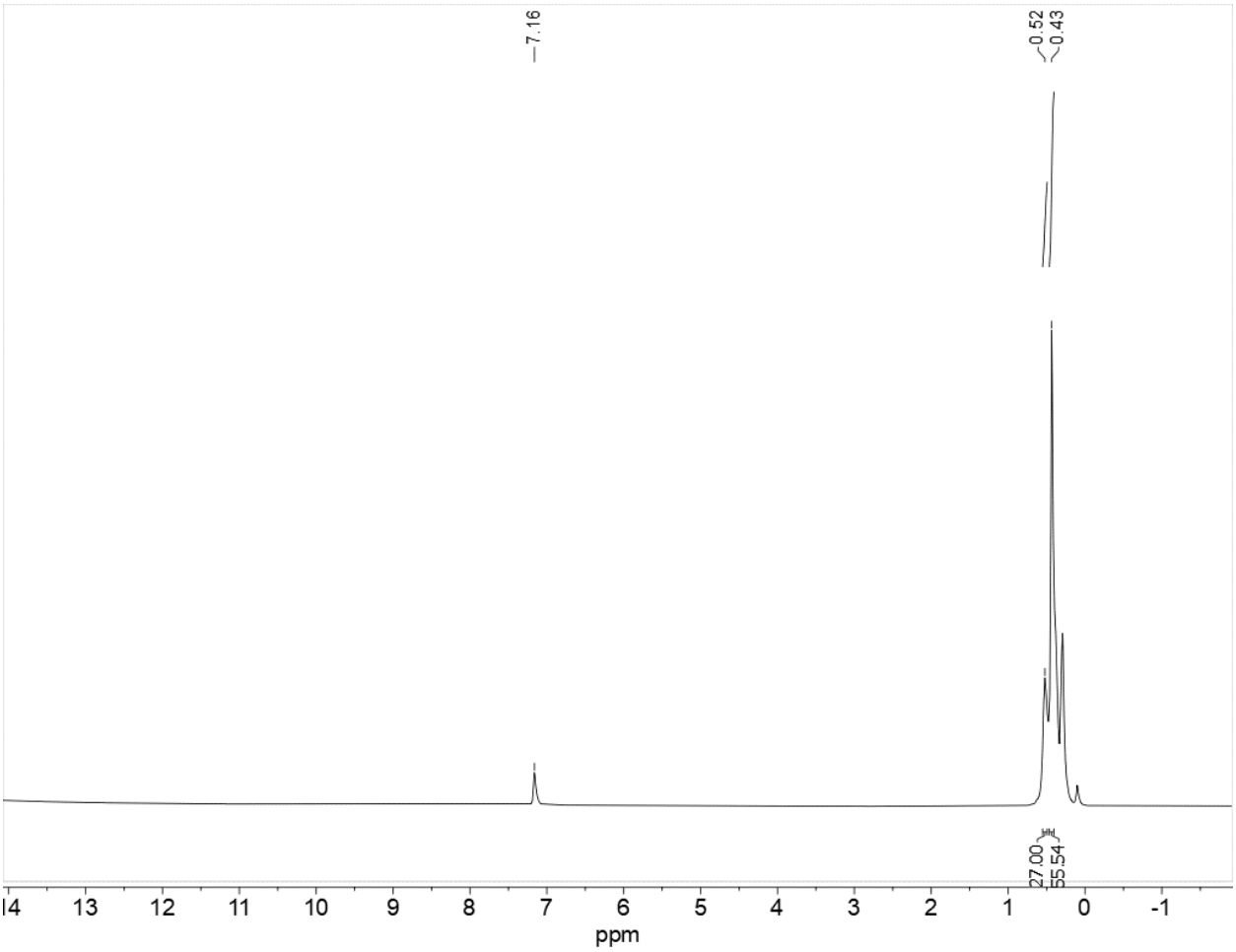

Figure 3.S42. Conversion of Complex **1** to Complex **3** (in [D_6] benzene, 73 °C, 40 minutes).

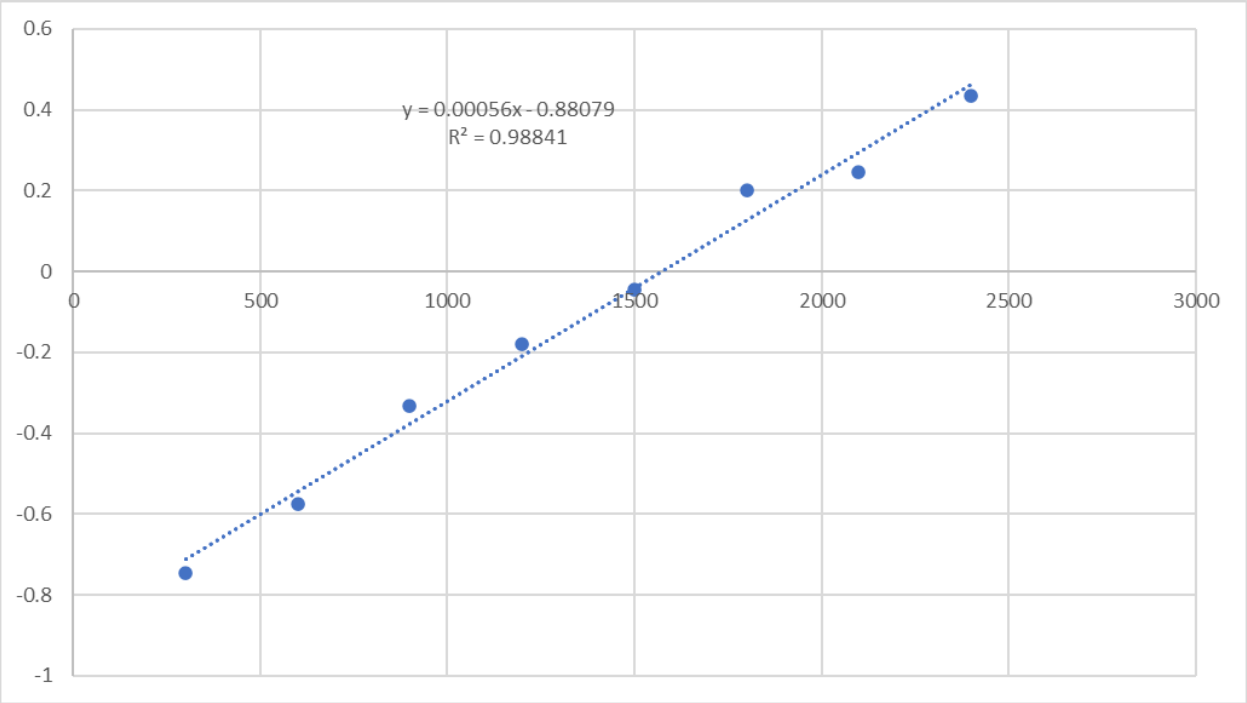

Figure 3.S43. Plot of ln[**3**] vs. Time at 73 °C. Note: Concentration of **3** is given relative to concentration of **1** (the signal at 0.52 was normalized to a constant integration value of 27 trimethylsilyl protons (one molecule of $V(=O)\{N(SiMe_3)_2\}_3$), and the integration of the signal at 0.43 was treated as a fraction of the 36 trimethylsilyl amido protons of **3**).

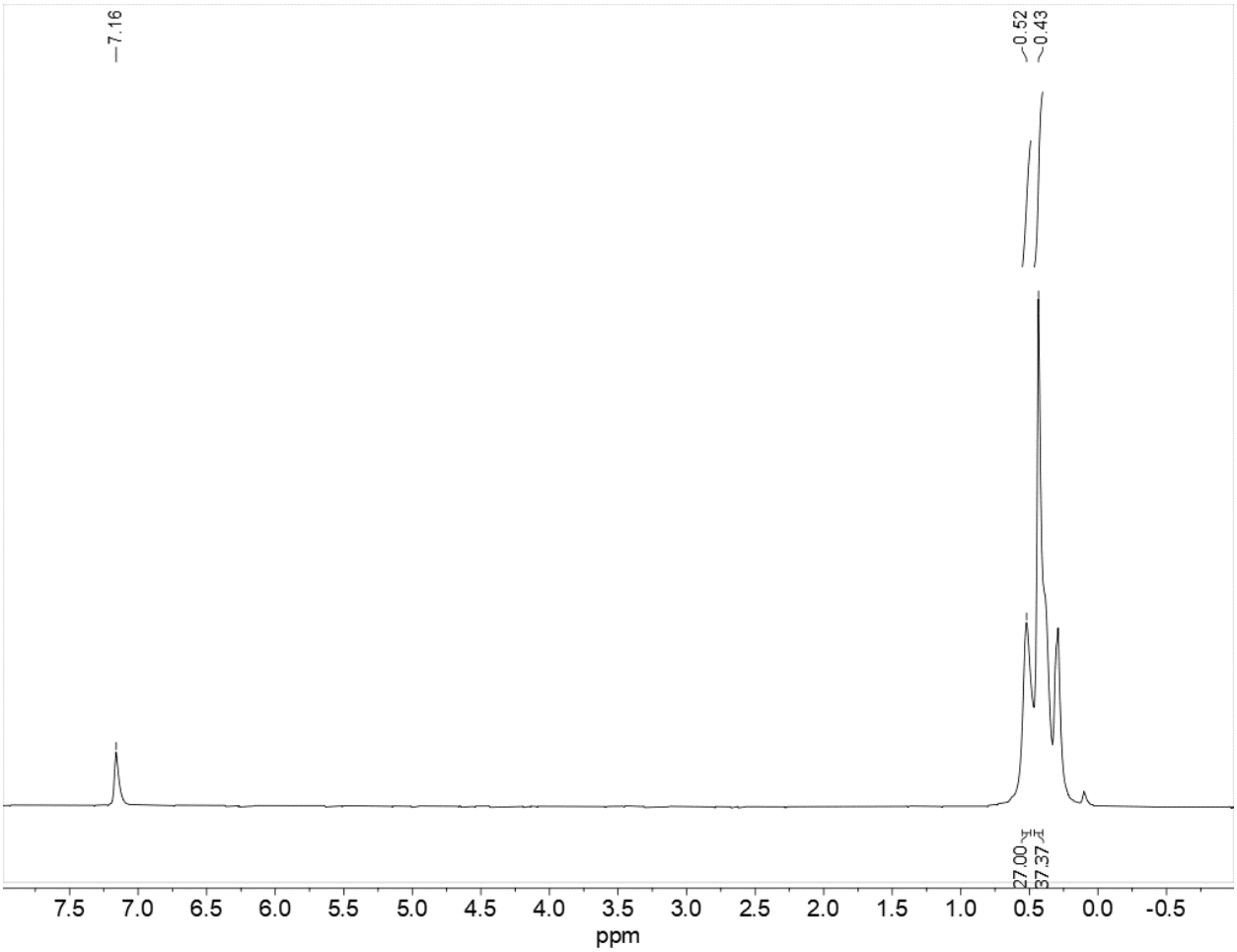

Figure 3.S44. Conversion of Complex **1** to Complex **3** (in [D_6] benzene, 83 °C, 10 minutes).

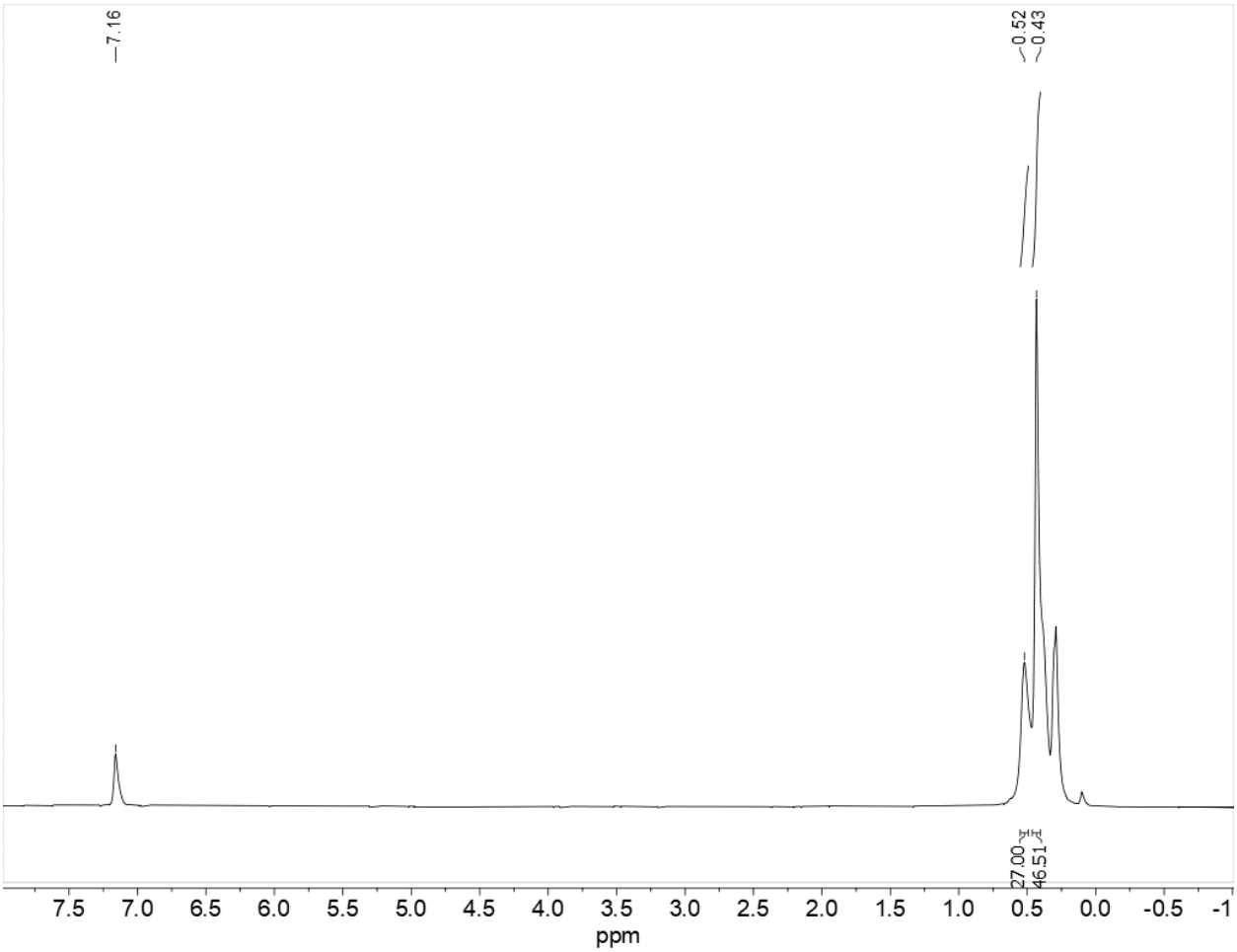

Figure 3.S45. Conversion of Complex **1** to Complex **3** (in [D_6] benzene, 83 °C, 12 minutes).

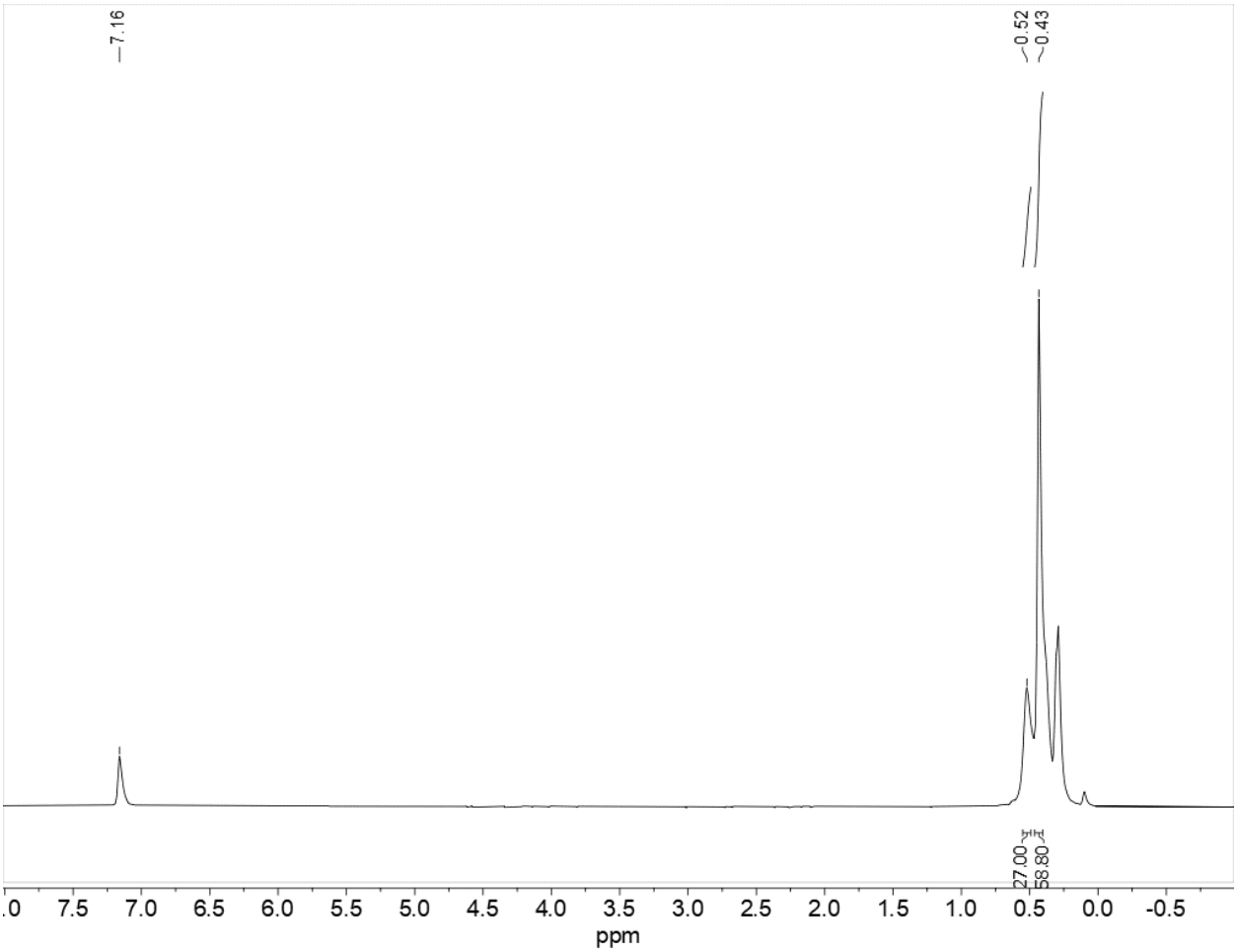

Figure 3.S46. Conversion of Complex **1** to Complex **3** (in [D_6] benzene, 83 °C, 14 minutes)

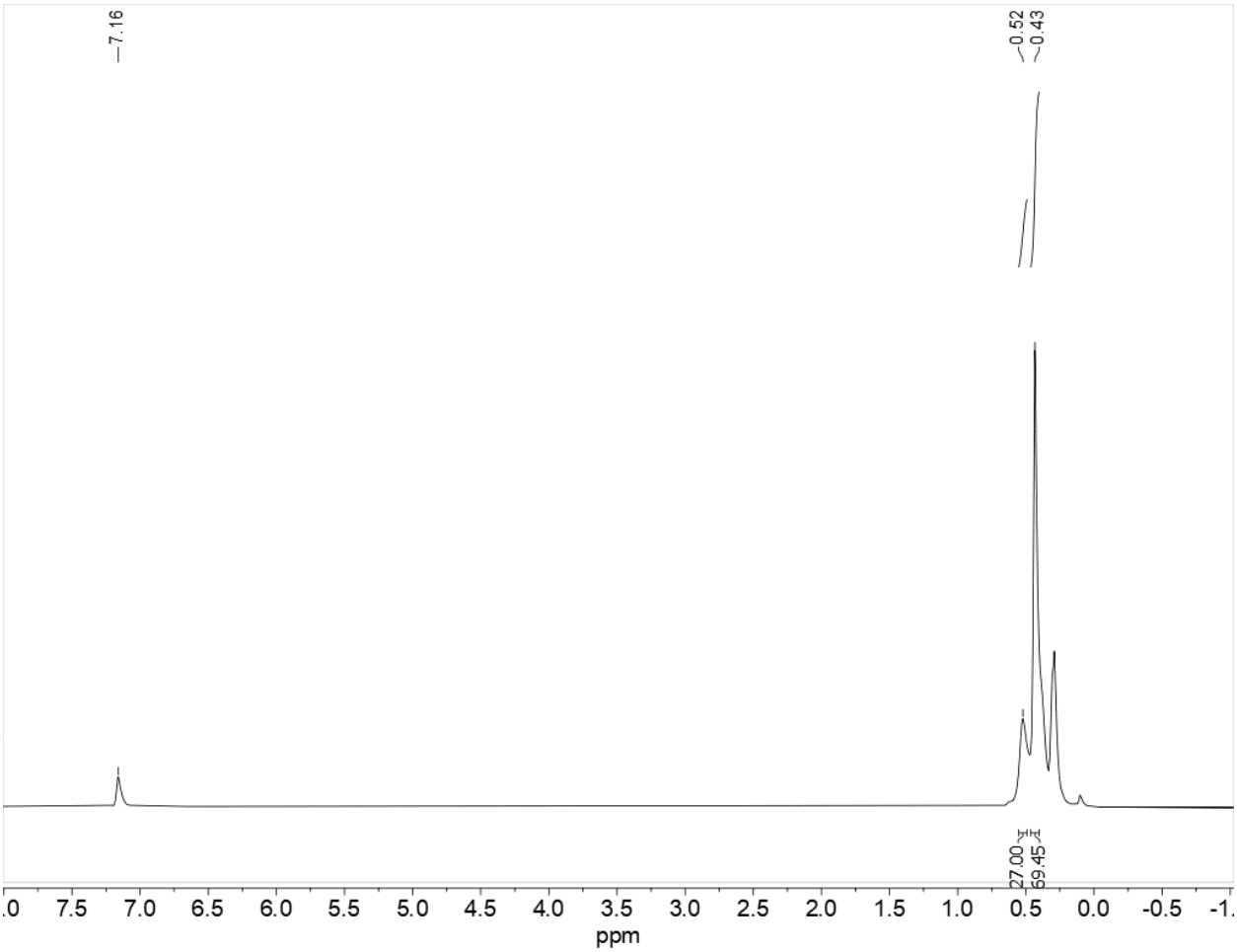

Figure 3.S47. Conversion of Complex **1** to Complex **3** (in [D_6] benzene, 83 °C, 16 minutes).

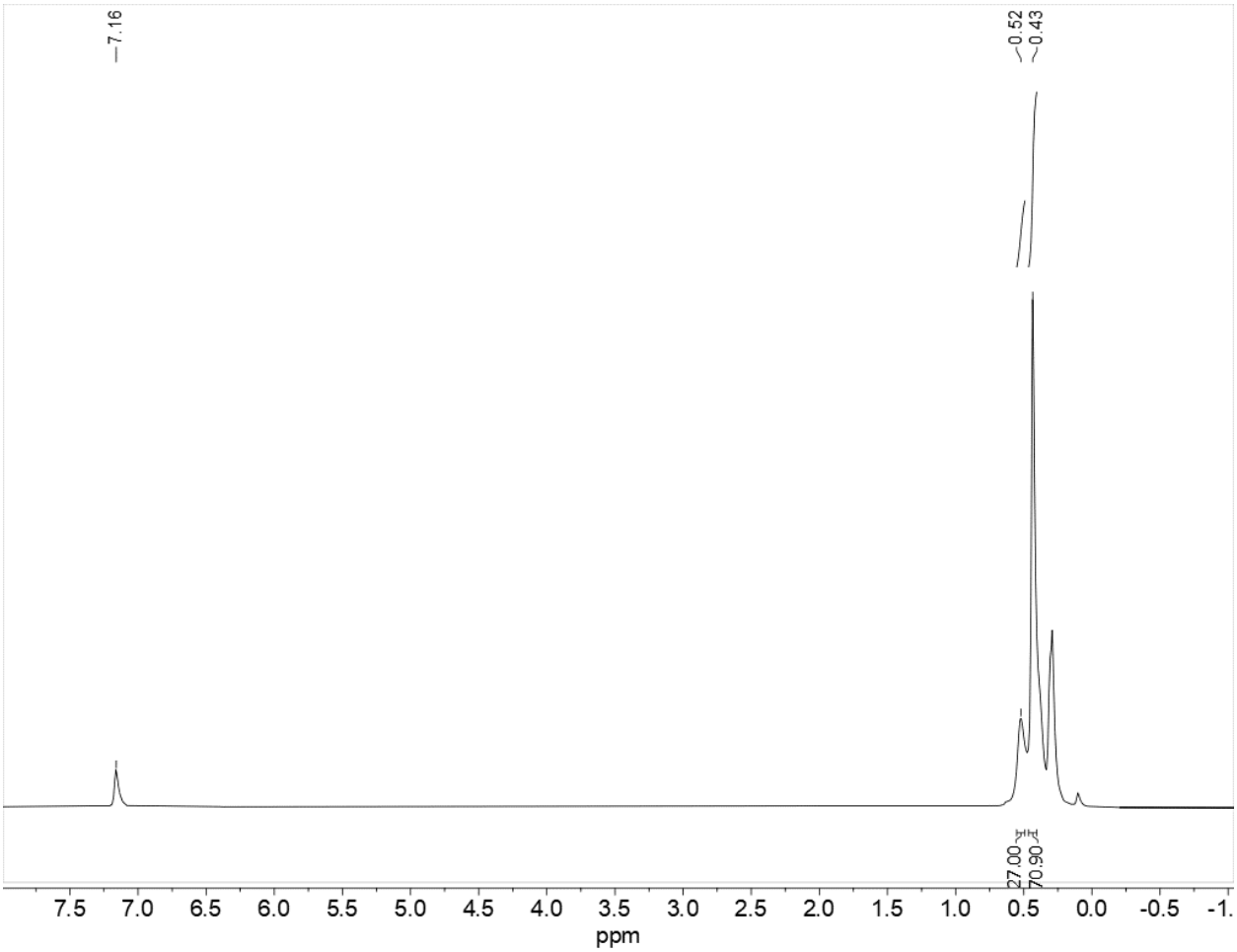

Figure 3.S48. Conversion of Complex **1** to Complex **3** (in [D_6] benzene, 83 °C, 18 minutes).

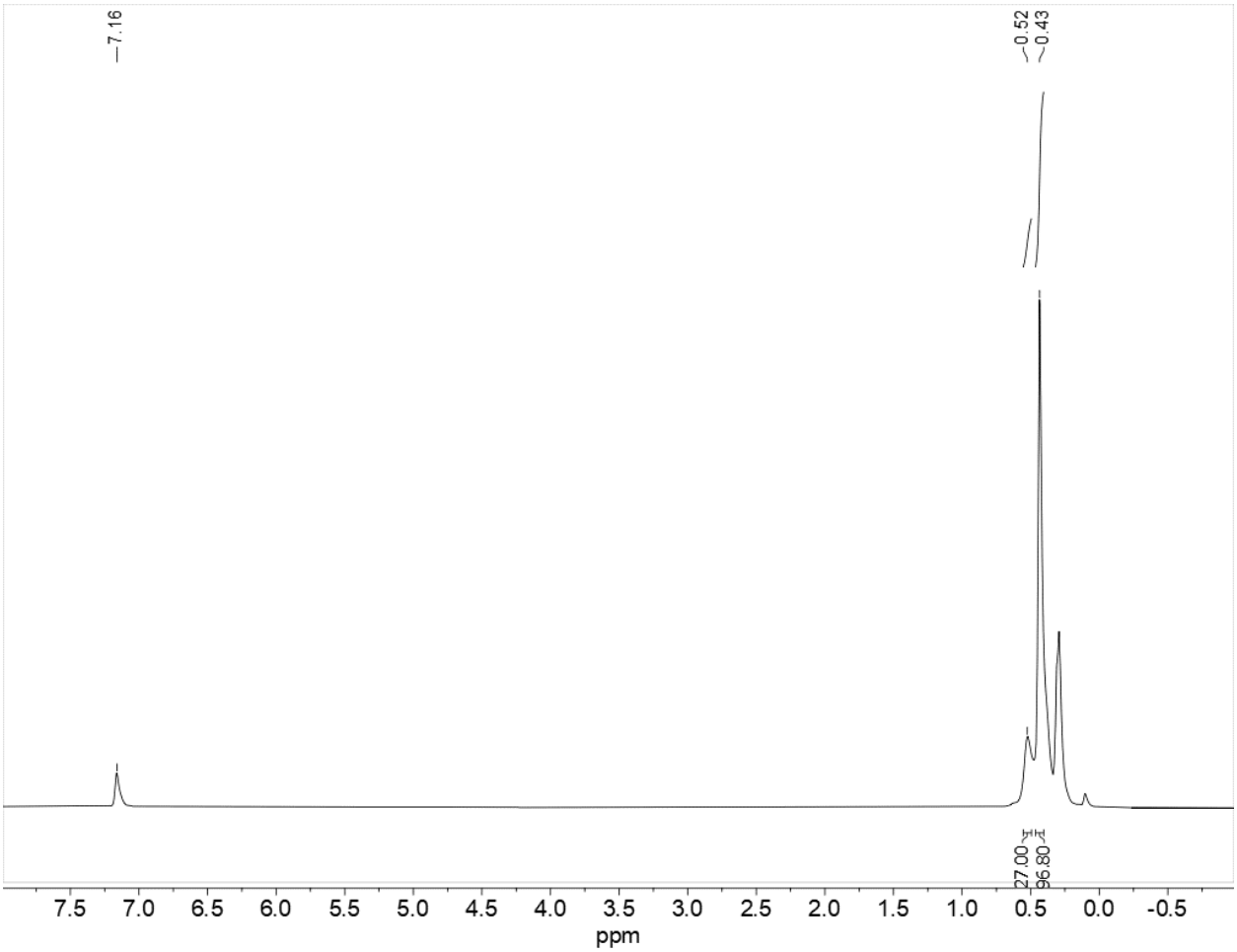

Figure 3.S49. Conversion of Complex **1** to Complex **3** (in [D_6] benzene, 83 °C, 20 minutes).

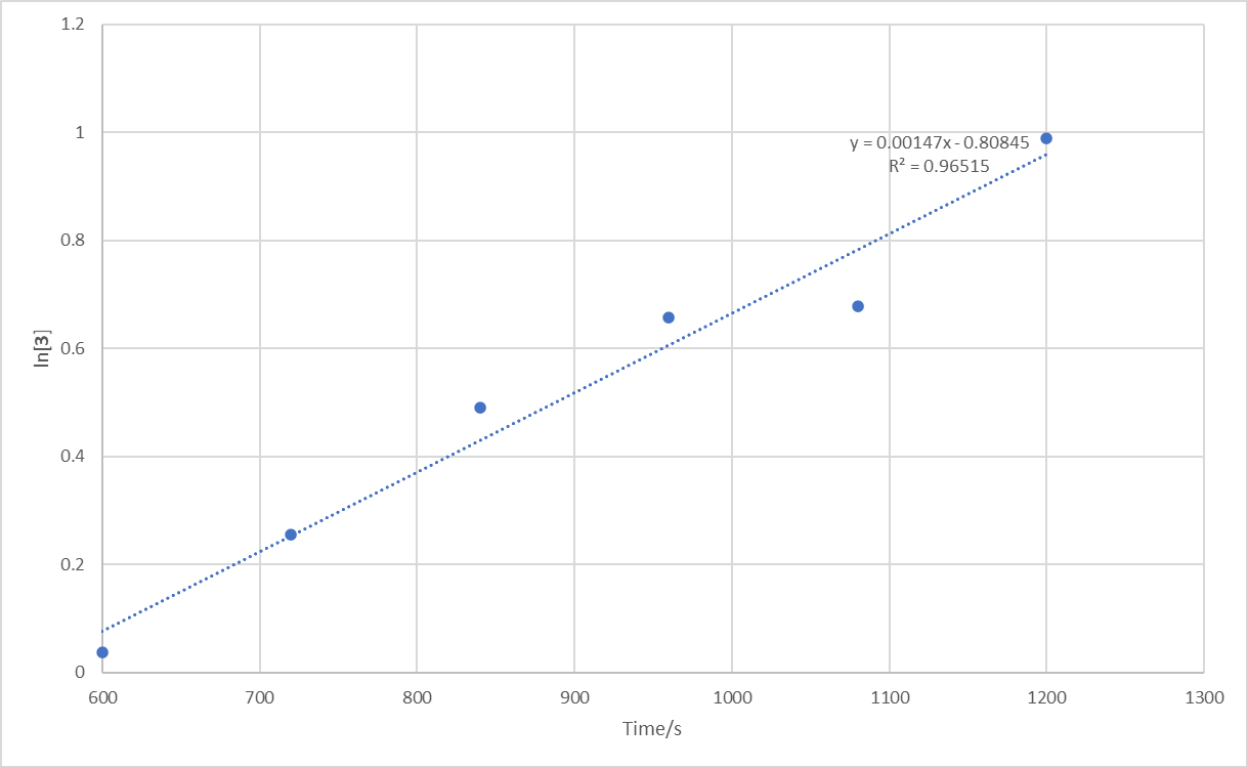

Figure 3.S50. Plot of ln[**3**] vs. Time at 83 °C. Note: Concentration of **3** is given relative to concentration of **1** (the signal at 0.52 was normalized to a constant integration value of 27 trimethylsilyl protons (one molecule of V(=O){N(SiMe$_3$)$_2$}$_3$), and the integration of the signal at 0.43 was treated as a fraction of the 36 trimethylsilyl amido protons of **3**).

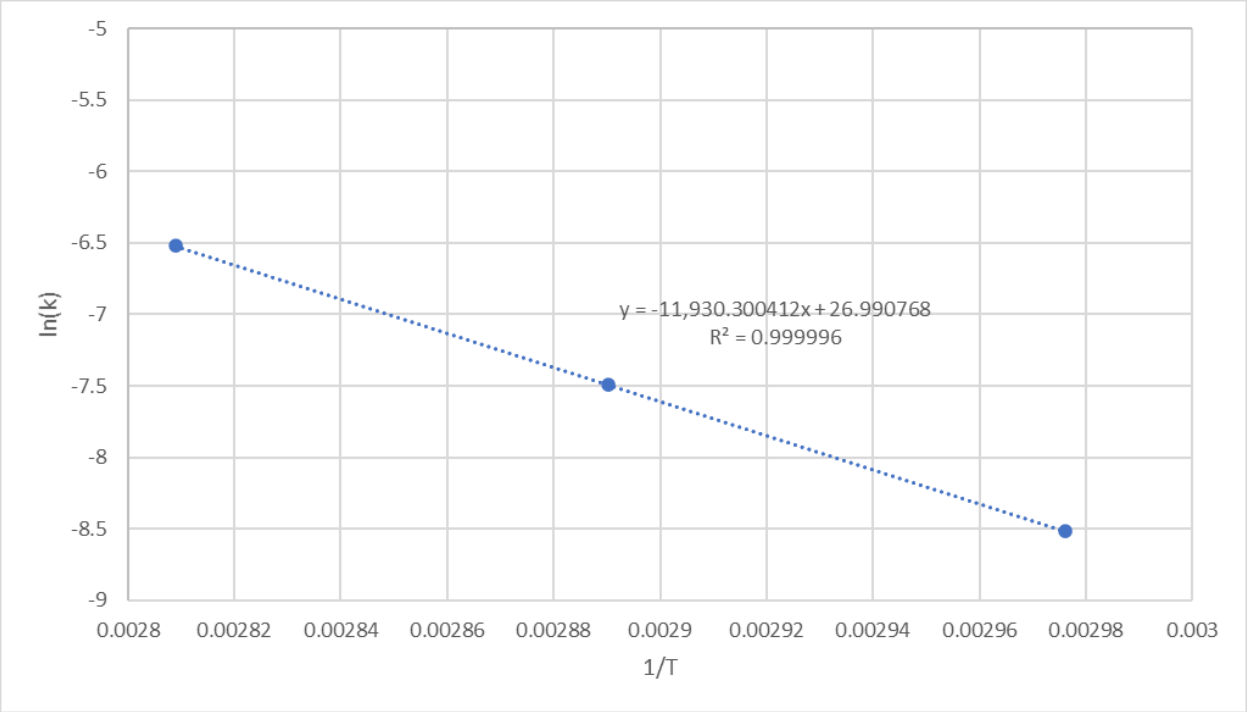

Figure 3.S51. Arrhenius plot of ln(k) vs. 1/T at 63, 73, and 83 °C. Note: The slope of the fitted line was taken to be E_a/R ($R = 8.314$ J mol^{-1} K^{-1}), with E_a given in units of joules/mole. This value of E_a converts to 23.706 kcal/mol.

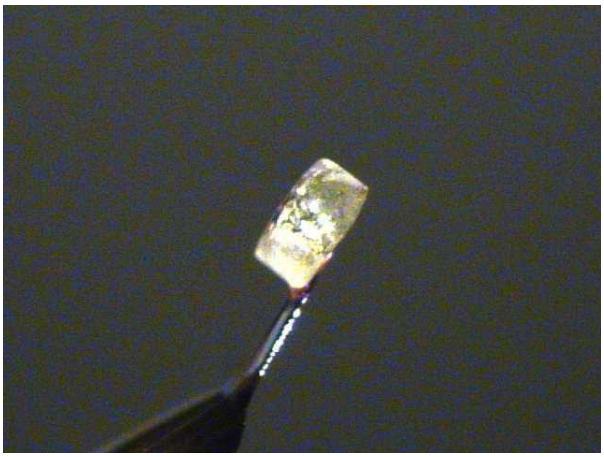

Figure 3.S52. Photograph of Crystalline **1**.

Figure 3.S53. Photograph of Crystalline **2**.

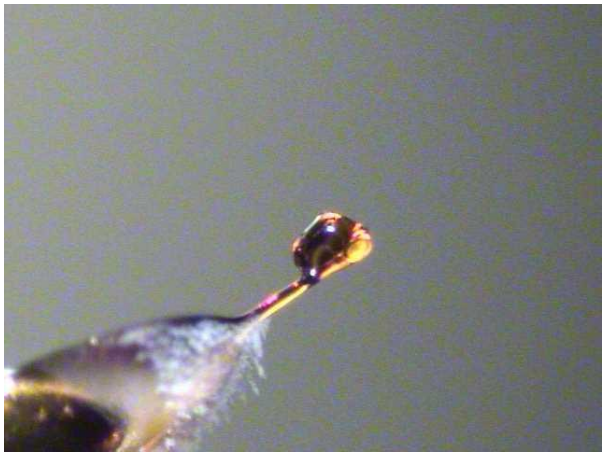

Figure 3.S54. Photograph of Crystalline **3.**

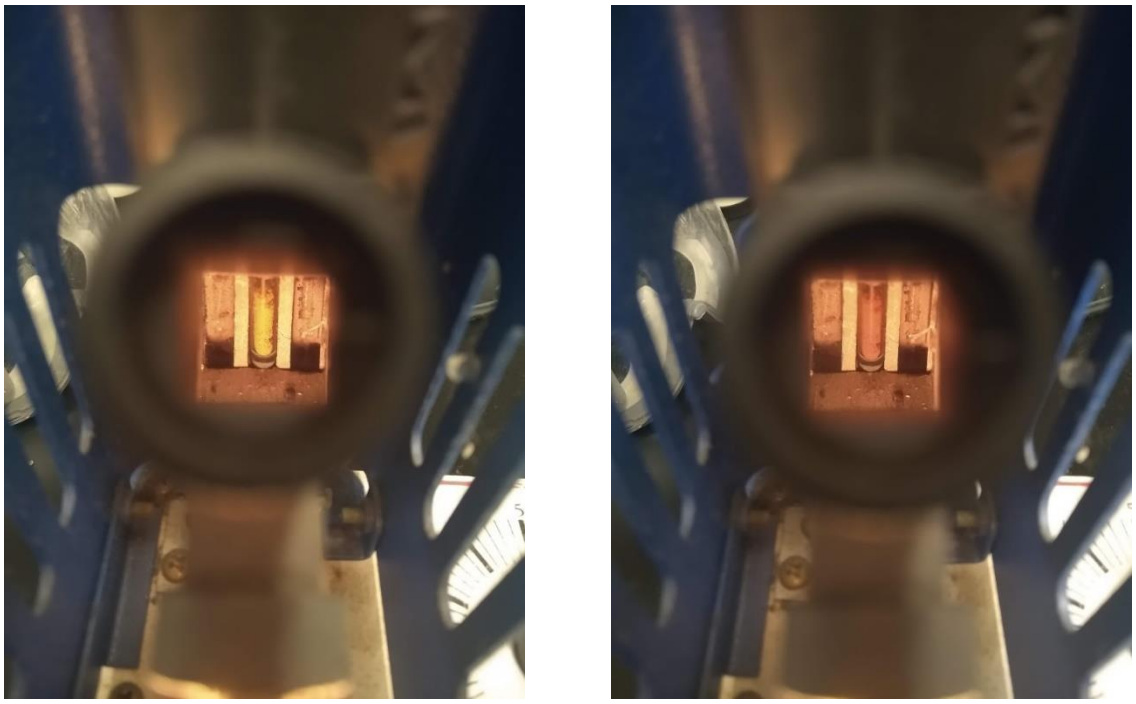

Figure 3.S55. Images of solid complex **1** at ambient temperature (left) and 130 °C (right). Note: yellow $V(=O)\{N(SiMe_3)_2\}_3$ (**1**) slowly converts to orange $V(=NSiMe_3)(OSiMe_3)\{N(SiMe_3)_2\}_3$ (**3**) over a temperature range of 100-120 °C and then decomposes at 237 °C, identical to the decomposition temperature of a separately prepared sample of **3**.

Table 3.S1. Crystallographic and Data Collection Parameters of Complex **1.**

Empirical formula	$C_{18}H_{54}N_3OSi_6V$
Formula weight	548.12
Temperature/K	90
Crystal system	orthorhombic
Space group	$Pca2_1$
a/Å	21.1735(13)
b/Å	14.9625(9)
c/Å	19.7373(12)
α/°	90
β/°	90
γ/°	90
Volume/Å^3	6252.9(7)
Z	8
ρ_{calc}g/cm^3	1.164
μ/mm^{-1}	0.562
F(000)	2384.0
Crystal size/mm^3	0.423 × 0.236 × 0.196
Radiation	MoKα (λ = 0.71073)
2Θ range for data collection/°	2.722 to 61.102
Index ranges	$-30 \leq h \leq 30$, $-21 \leq k \leq 21$, $-28 \leq l \leq 27$
Reflections collected	101910
Independent reflections	19088 [R_{int} = 0.0448, R_{sigma} = 0.0348]
Data/restraints/parameters	19088/1/560
Goodness-of-fit on F^2	1.083
Final R indexes [I>=2σ (I)]	R_1 = 0.0342, wR_2 = 0.0751
Final R indexes [all data]	R_1 = 0.0413, wR_2 = 0.0791
Largest diff. peak/hole / e Å^{-3}	0.63/-0.40
Flack parameter	-0.001(6)

Table 3.S2. Crystallographic and Data Collection Parameters of Complex **2.**

Empirical formula	$C_{21}H_{63}N_4Si_7V$
Formula weight	619.33
Temperature/K	90
Crystal system	trigonal
Space group	R3c
a/Å	17.0117(4)
b/Å	17.0117(4)
c/Å	21.4631(5)
α/°	90
β/°	90
γ/°	120
Volume/Å^3	5379.2(3)
Z	6
ρ_{calc}g/cm^3	1.147
μ/mm^{-1}	0.527
F(000)	2028.0
Crystal size/mm^3	0.153 × 0.143 × 0.128
Radiation	MoKα (λ = 0.71073)
2Θ range for data collection/°	4.696 to 61.36
Index ranges	$-24 \leq h \leq 24$, $-24 \leq k \leq 23$, $-30 \leq l \leq 30$
Reflections collected	26529
Independent reflections	3703 [R_{int} = 0.0483, R_{sigma} = 0.0345]
Data/restraints/parameters	3703/1/107
Goodness-of-fit on F^2	1.061
Final R indexes [I>=2σ (I)]	R_1 = 0.0344, wR_2 = 0.0767
Final R indexes [all data]	R_1 = 0.0418, wR_2 = 0.0815
Largest diff. peak/hole / e Å^{-3}	0.38/-0.26
Flack parameter	0.012(12)

Chapter 4. Reductions of $M\{N(SiMe_3)_2\}_3$ (M = V, Cr, Fe): Terminal and Bridging Low-Valent First-Row Transition Metal Hydrido Complexes, and "Metallo-Transamination."

Cary R. Stennett,[a] Clifton L. Wagner,[a] James C. Fettinger,[a] Petra Vasko,[b,*] and Philip P. Power[a,*]

a) Department of Chemistry, University of California, Davis, One Shields Avenue, Davis, California 95616, United States

b) Department of Chemistry, Nanoscience Center, University of Jyväskylä, P.O. Box 35, FI-40014, Jyväskylä, Finland

Reprinted with permission from *Inorg. Chem.* **2021**, 60, 15, 11401–11411.

Abstract.

The reaction of the vanadium(III) tris(silylamide) $V\{N(SiMe_3)_2\}_3$ with $LiAlH_4$ in diethyl ether gives the highly unstable mixed-metal polyhydride $[V(\mu_2\text{-}H)_6[Al\{N(SiMe_3)_2\}_2]_3][Li(OEt_2)_3]$ (**1**), which was structurally characterized. Alternatively, performing the same reaction in the presence of 12-crown-4 affords a rare example of a structurally verified vanadium terminal hydride complex, $[VH\{N(SiMe_3)_2\}_3][Li(12\text{-crown-}4)_2]$ (**2**). The corresponding deuteride **2D** was also prepared using $LiAlD_4$. In contrast, no hydride complexes were isolated by reaction of $M\{N(SiMe_3)_2\}_3$ (M = Cr, Fe) with $LiAlH_4$ and 12-crown-4. Instead, these reactions afforded the anionic metal(II) complexes $[M\{N(SiMe_3)_2\}_3][Li(12\text{-crown-}4)_2]$ (**3**, M = Cr or **4**, M = Fe). Reaction of the iron(III) tris(silylamide) $Fe\{N(SiMe_3)_2\}_3$ with lithium aluminium hydride without a crown ether gives the "hydrido inverse crown" complex $[Fe(\mu_2\text{-}H)\{N(SiMe_3)_2\}_2(\mu_2\text{-}Li)]_2$ (**5**), while treatment of the same trisamide with alane trimethylamine complex gives the iron(II) polyhydride complex $Fe(\mu_2\text{-}H)_6[Al\{N(SiMe_3)_2\}_2]_2[Al\{N(SiMe_3)_2\}(NMe_3)]$ (**6**). Complexes **2**-**6** were characterized by X-ray crystallography, as well as by infrared, electronic, and ^1H and ^{13}C (complex **6**) NMR spectroscopies. Complexes **1** and **6** are apparently formed by an unusual "metallo-transamination" process.

Introduction.

Prompted by observations that were at variance with literature reports, recent work in this laboratory has revisited the chemistry of first-row transition metal $M\{N(SiMe_3)_2\}_2$ and $M\{N(SiMe_3)_2\}_3$ complexes. These were first reported in the early 1960s by Bürger and Wannagat[1,2] and later studied extensively by Bradley and Hursthouse.[3–7] Currently, three-coordinate transition metal $M\{N(SiMe_3)_2\}_3$ complexes are known for the first-row metals from scandium through cobalt,[1–3,8–13] several lanthanides,[8,14–20] as well as plutonium and uranium.[21,22] Our recent finding[10] that the complex $V\{N(SiMe_3)_2\}_3$ had been initially mischaracterized in the 1970s[3,4,7] led us to reexamine first-row transition metal $M\{N(SiMe_3)_2\}_3$ complexes. Advances in techniques for the handling and characterization of such complexes has allowed the development of the coordination chemistry for the titanium and vanadium tris(silylamide) complexes,[23] as well as the isolation of several high valent vanadium complexes that were unknown despite earlier efforts to synthesize them.[24–26] As described in these reports, attempts to extend this chemistry to other first-row transition metal $M\{N(SiMe_3)_2\}_3$ complexes (M = Cr, Mn, Fe, Co) were largely unsuccessful. However, isolation of the chromium(II) complex $[K(18\text{-crown-}6)(Et_2O)_2][Cr\{N(SiMe_3)_2\}_3]$ by reduction of $Cr\{N(SiMe_3)_2\}_3$ suggested that the later metal tris(silylamide) complexes may be useful synthons for lower valent species.[10]

Transition metal hydride complexes have long been an important class of compounds. First reported by Hieber and Leutert in 1931, the isolation of $Fe(CO)_4(H)_2$ marked the beginning of the study of transition metal hydrides.[27] More recent work has focused on the use of first-row transition metal hydrides as cost effective and environmentally benign substitutes in reactions typically catalyzed by precious metals. Efforts toward this objective have been reviewed recently by several authors.[28–31] In many of these reactions, the formation of a transient hydride complex is implicated as a critical step in the catalytic cycle.[32] The development of new classes transition metal hydrides and an understanding of their chemistry is therefore of importance for many areas of chemistry. Recent exploratory research by the groups of Ohki and Jacobi von Wangelin has shown that unusual high nuclearity iron[33,34] and cobalt[35] hydride complexes

may be formed by reduction of the divalent $M\{N(SiMe_3)_2\}_2$ complexes with group 13 element hydrides. However, despite their ready availability, the chemistry of the related metal(III) complexes $M\{N(SiMe_3)_2\}_3$ remains relatively unexplored.

Herein, we show that the reaction of $V\{N(SiMe_3)_2\}_3$ with lithium aluminium hydride affords the highly unstable complex $[V(\mu_2\text{-}H)_6[Al\{N(SiMe_3)_2\}_2]_3][Li(OEt_2)_3]$ (**1**), which was characterized structurally. Performing the same reaction in the presence of 12-crown-4 gives the unusual monohydride $[VH\{N(SiMe_3)_2\}_3][Li(12\text{-crown-}4)_2]$ (**2**). The corresponding deuteride **2D** was isolated by reaction of $V\{N(SiMe_3)_2\}_3$ with $LiAlD_4$. In contrast, we show also that the same reaction using $M\{N(SiMe_3)_2\}_3$ (M = Cr, Fe) gives no hydride complexes, but afford the anionic metal(II) species $[M\{N(SiMe_3)_2\}_3][Li(12\text{-crown-}4)_2]$ (**3**, M = Cr or **4**, M = Fe). Alternatively, the reaction of $Fe\{N(SiMe_3)_2)_3$ with $LiAlH_4$ in the absence of a crown ether afforded the so-called "hydrido inverse crown"[36] complex $[Fe(\mu_2\text{-}H)\{N(SiMe_3)_2\}_2(\mu_2\text{-}Li)]_2$ (**5**). Additionally, treatment of $Fe\{N(SiMe_3)_2\}_3$ with $AlH_3(NMe_3)$ gives the polyhydride $Fe(\mu_2\text{-}H)_6[Al\{N(SiMe_3)_2\}_2]_2[Al\{N(SiMe_3)_2\}(NMe_3)]$ (**6**), which is structurally similar to the anion of polyhydride **1**. Complexes **2**-**6** were characterized by X-ray crystallography, their solution magnetic moments, and by ^1H, ^{13}C (complex **6**) NMR, infrared, and electronic spectroscopies. Additionally, the identities of monohydride **2** and deuteride **2D** were further confirmed by comparison of their computed vibrational spectra with those obtained experimentally.

Experimental Details.

General considerations. All manipulations were performed by using modified Schlenk techniques or in a Vacuum Atmospheres drybox under argon. Solvents were dried and collected using an S2 Grubbs-type solvent purification system (Glass Contour) and degassed using the freeze, pump, thaw method. All physical measurements were obtained under strictly anaerobic and anhydrous conditions. IR spectra were recorded as Nujol mulls between CsI windows on a PerkinElmer 1430 spectrophotometer. UV–vis spectra were recorded as dilute diethyl ether (**1**-**4**) or hexane (**5**, **6**) solutions in 3.5 mL quartz cuvettes using an OLIS modernized Cary 14 UV/vis/NIR spectrophotometer. ^1H and ^{13}C NMR spectra were internally

referenced to residual solvent signals. Melting points were determined on a Meltemp II apparatus in flame-sealed glass capillaries equipped with a partial immersion thermometer. Complexes **1-6** melt (or decompose) over narrow temperature ranges (1-2 °C), which indicated their high purity. Solution magnetic moments were determined by the Evans method in deuterated THF and corrected using the appropriate diamagnetic constants.[37,38] Elemental analyses were not attempted due to the high air and moisture sensitivity of these complexes. Additionally, their high silicon content has been shown elsewhere to result in erroneous analytical values for carbon and nitrogen, making accurate combustion analysis of these complexes difficult or impossible to obtain.[11,20,39] $M\{N(SiMe_3)_2\}_3$ (M = Ti, V, Cr, Fe) complexes were prepared according to literature methods.[7,10] Lithium aluminium hydride was purified by extraction of the crude material in dry, degassed diethyl ether and recrystallization from the same solvent.[40] The alane-trimethylamine complex was freshly prepared by reaction of recrystallized lithium aluminium hydride with trimethylammonium chloride and purified by sublimation.[41]

$[V(\mu_2\text{-}H)_6[Al\{N(SiMe_3)_2\}_2]_3]\ [Li(OEt_2)_3]$ (1). A solution of lithium aluminium hydride (0.036 g, 0.94 mmol) in ca. 20 mL of diethyl ether was added dropwise to a cooled (-78 °C), violet solution of $V\{N(SiMe_3)_2\}_3$ (0.50 g, 0.94 mmol) in ca. 10 mL of diethyl ether with stirring over 15 minutes. The mixture became dark blue. The mixture was allowed to reach room temperature over one hour with stirring. The dark blue solution was then stored in a freezer cooled to ca. -30 °C. Dark blue/green crystals that were suitable for X-ray diffraction studies grew overnight. Redissolving or otherwise manipulating the crystalline material resulted in immediate loss of gas and decomposition of the product, a characteristic that precluded its complete characterization.

$[VH\{N(SiMe_3)_2\}_3][Li(12\text{-crown-}4)_2]$ (2). A solution of lithium aluminium hydride (0.124 g, 3.27 mmol) in 30 mL of diethyl ether was added dropwise to a cooled (-78 °C), violet solution of $V\{N(SiMe_3)_2\}_3$ (1.74 g, 3.27 mmol) and 12-crown-4 (1.06 mL 6.54 mmol) in 10 mL of diethyl ether with stirring over 20 minutes. The mixture became dark blue. After stirring at this temperature for 20 minutes, the mixture was allowed to reach ambient temperature and stirred for a further 30 minutes. The dark blue solution was

filtered, and the filtrate was concentrated to ca. 20 mL and stored at ca. -30 °C. 0.94 g (1.05 mmol, 32%) of large, dark blue crystals of **2**. Crystals that were suitable for X-ray diffraction studies grew from the solution after storage for one week. M.p. 178-180 °C (dec.). UV/Vis (diethyl ether): λ/nm (ε/$M^{-1}cm^{-1}$): 616 (570), 676 (470). IR (Nujol) $\tilde{\nu}$ [cm^{-1}] = 1575 (br, νV-H), 370 (νV-N_3). ^{1}H NMR (600 MHz, THF-D_8, 298 K): δ = 4.82 ($SiMe_3$, $\Delta\nu_{1/2}$ = 430 Hz), 3.65 (OCH_2, $\Delta\nu_{1/2}$ = 4 Hz). μ_{eff}: 3.0 μ_B.

[VD{N(SiMe$_3$)$_2$}$_3$][Li(12-crown-4)$_2$] (2D). In a preparation analogous to that of **2**, a solution of lithium aluminium deuteride (0.079 g, 1.88 mmol) in ca. 30 mL of diethyl ether was added dropwise to a cooled (-78 °C), violet solution of V{N($SiMe_3$)$_2$}$_3$ (1.00 g, 1.88 mmol) and 12-crown-4 (0.61 mL 3.76 mmol) in ca. 10 mL of diethyl ether with stirring over 20 minutes. The mixture became dark blue. After stirring at this temperature for 20 minutes, the mixture was allowed to reach ambient temperature and stirred for a further 30 minutes. The dark blue solution was filtered, and the filtrate was concentrated to ca. 20 mL and stored at ca. -30 °C. After overnight storage, 0.29 g (0.32 mmol) of **2D** were isolated as small, dark blue crystals suitable for X-ray diffraction studies. An additional 0.35 g (0.39 mmol) of **2D** grew from the mother liquor after storage for one week at ca. -30 °C (overall yield: 38%). M.p. 172-174 °C (dec.). UV/Vis (diethyl ether): λ/nm (ε/$M^{-1}cm^{-1}$): 617 (670), 676 (shoulder, 530). IR (Nujol) $\tilde{\nu}$ [cm^{-1}] = 440 (br, δV-D), 370 (νV-N_3). ^{1}H NMR (600 MHz, THF-D_8, 298 K): δ = 4.74 ($SiMe_3$, $\Delta\nu_{1/2}$ = 470 Hz), 3.65 (OCH_2, $\Delta\nu_{1/2}$ = 4 Hz). μ_{eff}: 2.9 μ_B.

[Cr{N(SiMe$_3$)$_2$}$_3$][Li(12-crown-4)$_2$] (3). A solution of lithium aluminium hydride (0.036 g, 0.94 mmol) in ca. 30 mL of diethyl ether was added dropwise to a cooled (-78 °C), bright green solution of Cr{N($SiMe_3$)$_2$}$_3$ (0.5 g, 0.94 mmol) and 12-crown-4 (0.3 mL 1.9 mmol) in ca. 10 mL of diethyl ether with stirring over 20 minutes. The mixture was warmed to ambient temperature and stirred for four hours. A large amount of gray precipitate formed, and the solution became colorless. The mixture was filtered, and the solution was concentrated to ca. 2 mL and stored in a freezer cooled to ca. -30 °C. 0.26 g (0.29 mmol, 31%) of large, very pale green crystals that were suitable for X-ray diffraction studies grew from the solution after 6 hours. M.p. 182-184 °C (dec.). UV/Vis (diethyl ether): λ/nm (ε/$M^{-1}cm^{-1}$): 325 (shoulder,

600), 824 (140). IR (Nujol) $\tilde{\nu}$ [cm^{-1}] = 395 (shoulder, ν_{as}Cr-N), 355 (s, ν_sCr-N). ^{1}H NMR (600 MHz, THF-D_8, 298 K): δ = 28.63 ($SiMe_3$, $\Delta\nu_{1/2}$ = 540 Hz), 3.65 (OCH_2, $\Delta\nu_{1/2}$ = 5 Hz). μ_{eff} = 4.3 μ_B.

[Fe{N(SiMe$_3$)$_2$}$_3$][Li(12-crown-4)$_2$] (4). In a preparation analogous to that of **3**, a solution of lithium aluminium hydride (0.036 g, 0.94 mmol) in ca. 30 mL of diethyl ether was dropwise added to a cooled (-78 °C), bright green solution of Fe{$N(SiMe_3)_2$}$_3$ (0.5 g, 0.94 mmol) and 12-crown-4 (0.3 mL 1.9 mmol) in ca. 10 mL of diethyl ether with stirring over 20 minutes. The mixture was warmed to ambient temperature and stirred for four hours. A large amount of gray precipitate formed, and the solution became colorless. The mixture was filtered, and the solution was concentrated to ca. 2 mL and stored in a freezer at ca. -30 °C. 0.21 g (0.23 mmol, 25%) of large, very pale green crystals that were suitable for X-ray diffraction studies grew from the solution after 6 hours. M.p. 225-227 °C (dec.). UV/Vis (diethyl ether): λ/nm (ε/$M^{-1}cm^{-1}$): 892 (120). IR (Nujol) $\tilde{\nu}$ [cm^{-1}] = 390 (shoulder, ν_{as}Fe-N), 360 (ν_sFe-N). ^{1}H NMR (600 MHz, THF-D_8, 298 K): δ = 3.58 (shoulder overlapping THF signal, OCH_2), -2.53 ($SiMe_3$, $\Delta\nu_{1/2}$ = 650 Hz). μ_{eff} = 5.5 μ_B.

[Fe(μ$_2$-H){N(SiMe$_3$)$_2$}$_2$(μ$_2$-Li)]$_2$ (5). A dark green solution of Fe{$N(SiMe_3)_2$}$_3$ (0.5 g, 0.9 mmol) in ca. 30 mL diethyl ether was added over 30 minutes to a cold (0 °C), stirred solution of lithium aluminium hydride (0.034 g, 0.9 mmol) in the ca. 10 mL of the same solvent. The mixture was then allowed to slowly warm to ambient temperature and stirred at this temperature overnight, giving a colorless solution with a tan precipitate. The solvent was then removed under reduced pressure and the residue was extracted in ca. 20 mL of hexanes. This mixture was filtered, and the filtrate was concentrated to ca. 15 mL and stored overnight at ca. -30 °C to afford 0.05 g (7%) of pale green, almost colorless crystals of complex **5** that were suitable for X-ray diffraction studies. M.p. 82-84 °C (dec.). IR (Nujol) $\tilde{\nu}$ [cm^{-1}] = 410 (νFe-N), 360 (νFe-N). ^{1}H NMR (600 MHz, C_6D_6, 298 K): δ = 17.87 ($\Delta\nu_{1/2}$ = 1160 Hz), 1.38 ($\Delta\nu_{1/2}$ = 110 Hz), -2.53 ($\Delta\nu_{1/2}$ = 2400 Hz). μ_{eff} = 6.0 μ_B (3.0 μ_B per Fe atom).

Fe(μ$_2$-H)$_6$[Al{N(SiMe$_3$)$_2$}$_2$]$_2$[Al{N(SiMe$_3$)$_2$}(NMe$_3$)] (6). Alane-trimethylamine complex (0.17 g, 1.91 mmol) was suspended in ca. 20 mL hexane and added dropwise over 10 minutes to a stirred solution

of $Fe\{N(SiMe_3)_2\}_3$ (0.50 g, 0.93 mmol) in ca. 20 mL of the same solvent at ca. -78 °C. The mixture was stirred for a further 10 minutes at ca. -78 °C, allowed to warm to ambient temperature and stirred at this temperature for 12 h to give an orange solution with a beige precipitate. The solution was filtered, concentrated under reduced pressure to ca. 20 mL, and stored overnight at ca. 5 °C to give crystals of complex **6** as orange blocks that were suitable for X-ray diffraction studies. Yield: 0.17 g (0.17 mmol, 18 %); mp 178-179 °C (dec.). UV/Vis: λ/nm (ε/$M^{-1}cm^{-1}$): 342 (350), 410 (290). IR (Nujol) $\tilde{\nu}$ [cm^{-1}] = 1635 (shoulder, νAl-H), 1600 (νAl-H), 1520 (w, νFe-H), 450 (νAl-NMe_3) 415 (ν_{as}Al-$N(SiMe_3)_2$), 365 (ν_sAl-$N(SiMe_3)_2$). ^{1}H NMR (399.8 MHz, C_6D_6, 298 K): δ = 2.06 (s, 9H, NMe_3), 0.61 (s, 36H, $SiMe_3$), 0.51 (s, 18H, $SiMe_3$), 0.45 (s, 18H, $SiMe_3$), 0.29 (s, 9H, $SiMe_3$), 0.25 (s, 9H, $SiMe_3$), -17.15 (s, 1H, μ-H), -17.52 (s, 2H, μ-H), -18.05 (s, 1H, μ-H), -18.46 (s, 1H, μ-H), -18.99 (s, 1H, μ-H). $^{13}C\{^1H\}$ NMR (100.5 MHz, C_6D_6, 298 K): δ = 49.97 (NMe_3), 7.69 ($SiMe_3$), 7.32 ($SiMe_3$), 6.93 ($SiMe_3$), 6.33 ($SiMe_3$), 6.03 ($SiMe_3$).

Additional reactions of other $M\{N(SiMe_3)_2\}_3$ complexes (M = Ti, V, Cr). $M\{N(SiMe_3)_2\}_3$ (M = Ti, V, Cr) was reacted with AlH_3NMe_3 in the same conditions described for the preparation of **6**. No new complexes were isolated. The reaction of intense blue solutions of $Ti\{N(SiMe_3)_2\}_3$ in several solvents with either $LiAlH_4$ or $AlH_3(NMe_3)$ resulted in no color change, and $Ti\{N(SiMe_3)_2\}_3$ was the only product isolated from these reactions. Similarly, no new products were observed in the reaction of violet $V\{N(SiMe_3)_2\}_3$ with $AlH_3(NMe_3)_2$, or in the reactions of green $Cr\{N(SiMe_3)_2\}_3$ with $LiAlH_4$ (in the absence of a crown ether) or with $AlH_3(NMe_3)$.

X-ray Crystallography. Crystals were removed from the Schlenk flask under a flow of argon and covered in Paratone oil. Suitable crystals were selected, mounted on a MiTeGen MicroLoop, and then placed in the cold nitrogen stream of the diffractometer. Data collection was performed at 190 K using Mo Kα radiation (λ = 0.71073 Å) or Cu Kα radiation (λ = 1.5406 Å) on a Bruker Apex Duo diffractometer. Absorption corrections were applied using SADABS.[42] The structures were solved by intrinsic phasing using SHELXT[43] and refined by least-squares methods using SHELXL[44] in the Olex2 GUI.[45] The positions

of the hydrides in complexes **1**, **2**, **2D**, **5**, and **6** were located in the Fourier difference map and were refined isotropically. All other non-hydrogen atoms were refined anisotropically.

Computational Details. All computational work reported here was carried out at the density functional theory (DFT) level with Gaussian16 (Revision C.01) program package.[46] The gas phase geometry optimizations were performed with the PBE1PBE exchange correlation functional[47–49] using Def2-TZVP basis sets[50,51] with Grimme's empirical dispersion correction (DFT-D3)[52,53] and an ultrafine integration grid. The nature of stationary points found (minimum) was confirmed by full frequency calculations. NBO analyses were performed with the NBO 7.0 program.[54]

Results and Discussion

Synthesis. The syntheses described herein are summarized in Scheme 4.1. Addition of one equivalent of lithium aluminium hydride to a deep violet solution of $V\{N(SiMe_3)_2\}_3$ at ca. -78 °C resulted in an immediate color change of the solution to dark blue. Overnight cooling of this mixture to ca. -30 °C afforded dark blue crystals of the vanadium/aluminium polyhydride **1**. Complex **1** proved exceptionally difficult to handle, and the yield of this reaction could not be determined. Loss of gas from the crystalline material was immediately observed upon covering the crystals with Paratone oil prior to an X-ray diffraction study, and the material was observed to quickly change from a dark blue to a brown color while selecting an appropriate crystal for the study. Similarly, application of low pressure on **1** or its redissolution resulted in its immediate decomposition. These characteristics precluded the complete characterization of **1**. Our attempts to optimize the conditions of this reaction to improve the yield or better understand its stoichiometry were unsuccessful. Nevertheless, the X-ray diffraction study of **1** revealed a very unusual anionic polyhydride structure (vide infra) that we attempted to stabilize so that we might study its characteristics further. Noting that this structure contained a lithium cation solvated by diethyl ether molecules, we reasoned that capture of the cation by a crown ether might improve the stability of the ionic complex. However, while addition of one equivalent of lithium aluminium hydride to a cold (-78 °C) 1:2 mixture of $V\{N(SiMe_3)_2\}_3$ and 12-crown-4 in diethyl ether afforded a blue solution similar to that found

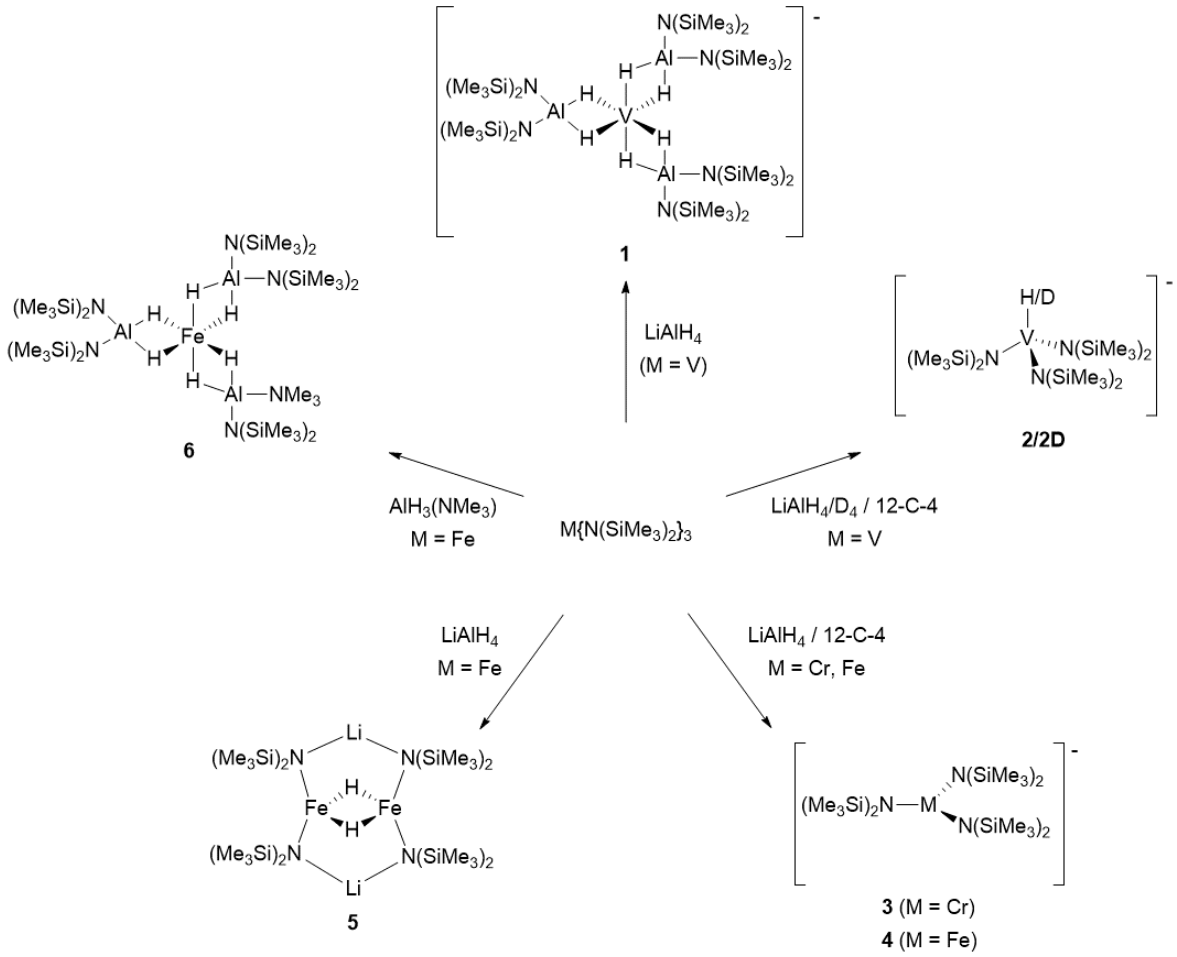

Scheme 4.1. Overview of the synthetic routes used for complexes **1**-**6**. The cations are not shown for clarity.

during the preparation of **1**, this synthesis gave the ionic monohydride complex [V{N(SiMe$_3$)$_2$}$_3$(H)][Li(12-crown-4)$_2$] (**2**). Complex **2** proved far more stable than **1**, and its complete characterization, along with that of its deuteride analog **2D**, is described in detail herein.

As several other first-row transition metal M{N(SiMe$_3$)$_2$}$_3$ complexes (M = Ti, Cr, Fe) are also readily available in high yield,[7] we sought to extend this chemistry to these metals as well. Strangely, addition of lithium aluminium hydride to a cold (-78 °C) 1:2 mixture of bright green Cr{N(SiMe$_3$)$_2$}$_3$ and 12-crown-4 did not result in an immediate change in the color of the solution as was observed in the case of vanadium. Rather, this reaction required extended stirring (4 hours) at ambient temperature before the

formation of a gray precipitate and the complete loss of color of the solution was observed. Concentration of this filtered solution afforded no hydride complex, but instead gave large, pale green crystals of the ionic chromium(II) trisamide $[Cr\{N(SiMe_3)_2\}_3][Li(12\text{-crown-}4)_2]$ (**3**). Likewise, treatment of the iron(III) amide $Fe\{N(SiMe_3)_2\}_3$ with $LiAlH_4$ in the presence of 12-crown-4 gave the anionic iron(II) trisamide $[Fe\{N(SiMe_3)_2\}_3][Li(12\text{-crown-}4)_2]$ (**4**). Although no hydride complexes of chromium or iron were formed during these reactions, the spectroscopic features of complexes **3** and **4** proved useful in confirming the presence of the hydride ligand in complex **2** (vide infra).

Addition of one equivalent of lithium aluminium hydride to a cold (-78 °C) diethyl ether solution of $Fe\{N(SiMe_3)_2\}_3$ in the absence of a crown ether followed by overnight stirring at ambient temperature afforded a pale green solution with a brown precipitate. Filtration, followed by concentration and overnight storage of the filtrate at ca. -20 °C, afforded crystals of the iron/lithium hydride complex **5** in low yield. Complex **5** is a solvent-free example of the "inverse hydrido crown" complexes previously reported by Mulvey and coworkers.[36] These complexes are more generally synthesized by reaction of an alkyl metal(II) complex (Mg, Mn) with a group 1 organometallic complex and the appropriate amine (diisopropylamine or 1,1,1,3,3,3-hexamethyldisilazane). Alternatively, $[M\{N(SiMe_3)_2\}_2MgBu^n]$ could be formed in situ by reaction of the alkali metal amide $MN(SiMe_3)_2$ (M = Li, Na, or K) with dibutylmagnesium and hexamethyldisilazane, which was subsequently reacted with phenylsilane to give the mixed-metal dihydride.[55] In each of these cases, it is worth noting that the hydrides are formed by metathesis, and not by a reduction of any of the metal species involved. In contrast, dimeric **5** was produced by one-electron reduction of the iron(III) tris(silylamide) $Fe\{N(SiMe_3)_2\}_3$ via treatment with one equivalent of lithium aluminium hydride to give the iron(II) complex. Thus, while the aforementioned complexes were exclusively synthesized from divalent metal reagents, complex **5** represents the first instance of their formation by reduction of a metal(III) amide.

The isolation of these hydride species encouraged us to further explore complexes accessible by reduction of $Fe\{N(SiMe_3)_2\}_3$ with other main group element hydrides. Treatment of $Fe\{N(SiMe_3)_2\}_3$ with

two equivalents of freshly prepared alane-trimethylamine complex suspended in hexanes gave the orange-colored iron(II) hydride complex **6**. The structure of **6** is strikingly similar to that of the anion of **1** (vide infra), having been formed by an apparent transamination of the amide groups of $Fe\{N(SiMe_3)_2\}_3$ to the aluminium atom. The formation of transition metal polyhydrides by reaction of group 13 hydrides with transition metal silylamides is not without precedent. As reported by Ohki in 2016, treatment of the divalent cobalt amide complex $Co\{N(SiMe_3)_2\}_2$ with an equivalent of pinacolborane yielded the hydride cluster $Co_7H_6\{N(SiMe_3)_2\}_6$ along with formation of the cobalt(I) tetramer $[CoN(SiMe_3)_2\}_4$.[35] It was further shown in papers by Ohki[34] and Jacobi von Wangelin[33] that treatment of the related divalent iron amide $Fe\{N(SiMe_3)_2\}_2$ with either pinacolborane or diisobutylaluminium hydride gave hydride clusters similar to what was shown for cobalt. In contrast to these results, reduction of trivalent $Fe\{N(SiMe_3)_2\}_3$ with $AlH_3(NMe_3)$ gave the mixed metal polyhydride complex **6**, which incorporates three aluminium atoms in its structure. Complex **6** bears some resemblance to the $[FeH_6][MgX(THF)_2]_4$ complex originally reported by Gibbins in 1977, which was prepared by reaction of $FeCl_3$ with phenylmagnesium bromide and excess hydrogen.[56] However, the heteroleptic ligand environment of **6** and the coordination geometry at the aluminium atoms results in several substantial structural and spectroscopic differences (vide infra).

Structures.

The mixed-metal vanadium/aluminium hydride complex **1** (Figure 4.1) is formed by apparent transfer of the amido groups of $V\{N(SiMe_3)_2\}_3$ to the aluminium atom of $LiAlH_4$. The anion of the vanadium(II) complex **1** features a distorted octahedral geometry around the vanadium atom which is coordinated by six hydrogens that bridge to three aluminium atoms. The complex crystallizes as a racemic mixture of its Δ and Λ isomers. The positions of the hydrogen atoms bound to vanadium were located in

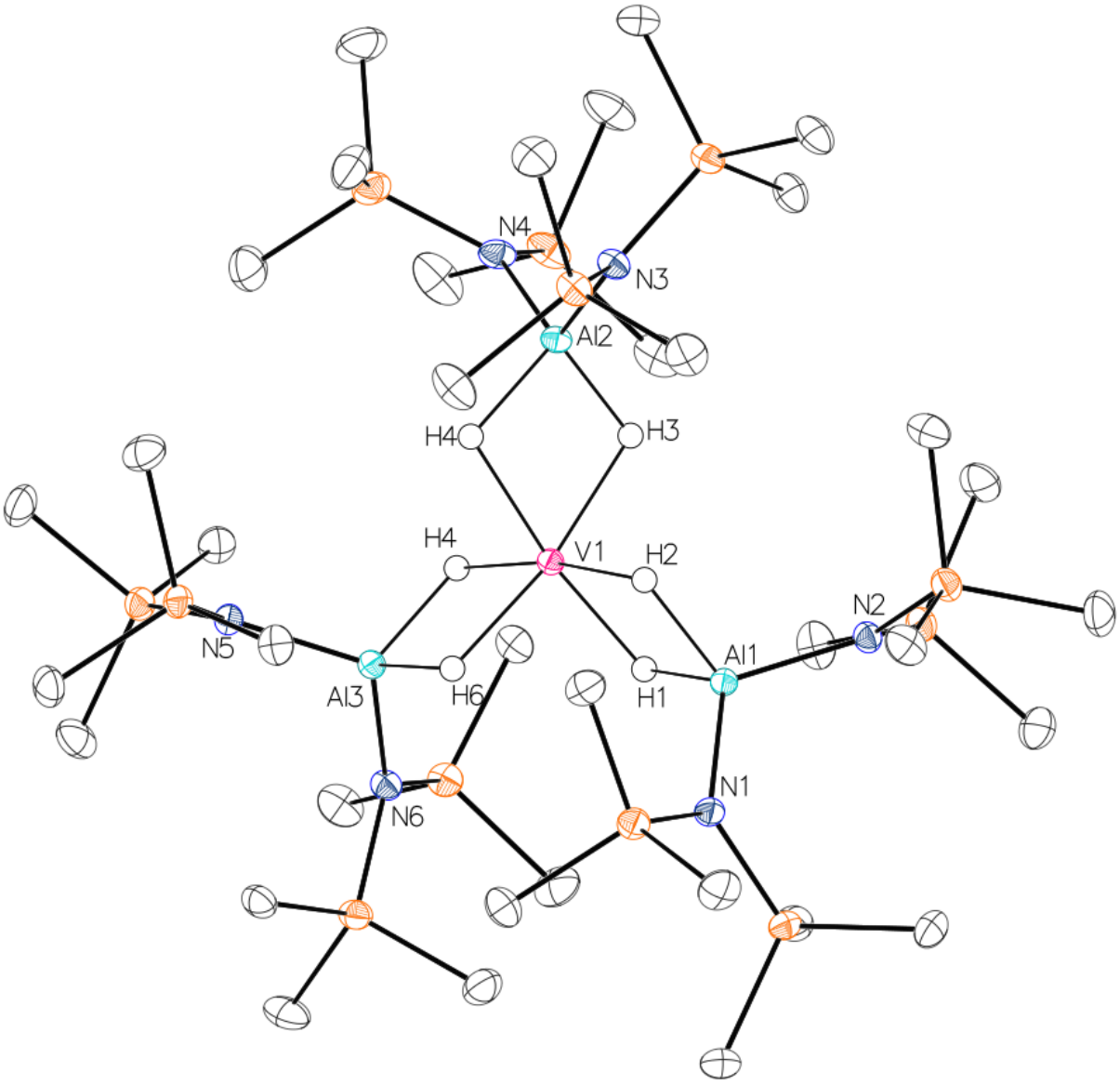

Figure 4.1: Molecular structure of the Δ isomer of the anion of **1** with ellipsoids shown at 30% probability. Non-hydride hydrogen atoms are not shown for clarity.

the Fourier difference map and refined isotropically. The V-H distances range from 1.83(2) to 1.86(2) Å, in good agreement with those found in other vanadium hydride complexes featuring μ_2 bridging hydrides.[57–59] The Al-H distances range from 1.64(2) to 1.68(2) Å. The vanadium and aluminium atoms are coplanar, with Al-V-Al angles ranging from 119.501(17)° to 120.562(17)° and V-Al distances ranging from 2.6632(6) to 2.6726(5) Å. These distances are near the sum of the single bonded covalent radii of vanadium and aluminium (2.60 Å)[60]. However, there are no structurally characterized examples of complexes featuring bonds between vanadium and aluminium, so conclusions about the nature of any possible interaction between the two metals are difficult to make based on the structural data alone. The anion in complex **1** was therefore optimized computationally and its structure examined. The optimized geometry of the anion is in good agreement with the experimentally obtained parameters. The V-H distances range from 1.86 to 1.89 Å, and the V-Al distances are calculated at 2.4919, 2.4961 and 2.5424 Å, which are slightly shorter than observed in the solid-state structure. However, the calculated Wiberg bond indices for the V-Al bonds are 0.201, 0.206 and 0.185, which indicates only weak interactions between the two different metals.[61]

The geometry at the four coordinate vanadium atom in the anion of complex **2** (Figure 4.2) is highly distorted tetrahedral, with N-V-N angles ranging from 117.86(5)° to 119.48(5)° and V-N distances ranging from 1.9995(13) to 2.0064(14) Å. These V-N distances are slightly shorter than the those found in the related $[V\{N(SiMe_3)_2\}_3]^-$, which range from 2.0186(11) to 2.0346(10) Å.[10] Considering the synthetic route, these features suggested to us that what we initially thought was a vacant coordination site might in fact contain a hydride ligand, and examination of the Fourier difference map revealed this to be the case. The position of the hydride ligand was refined isotropically, and the V-H distance was determined to be 1.58(2) Å. This distance is in approximate agreement with the distances found in the few vanadium complexes

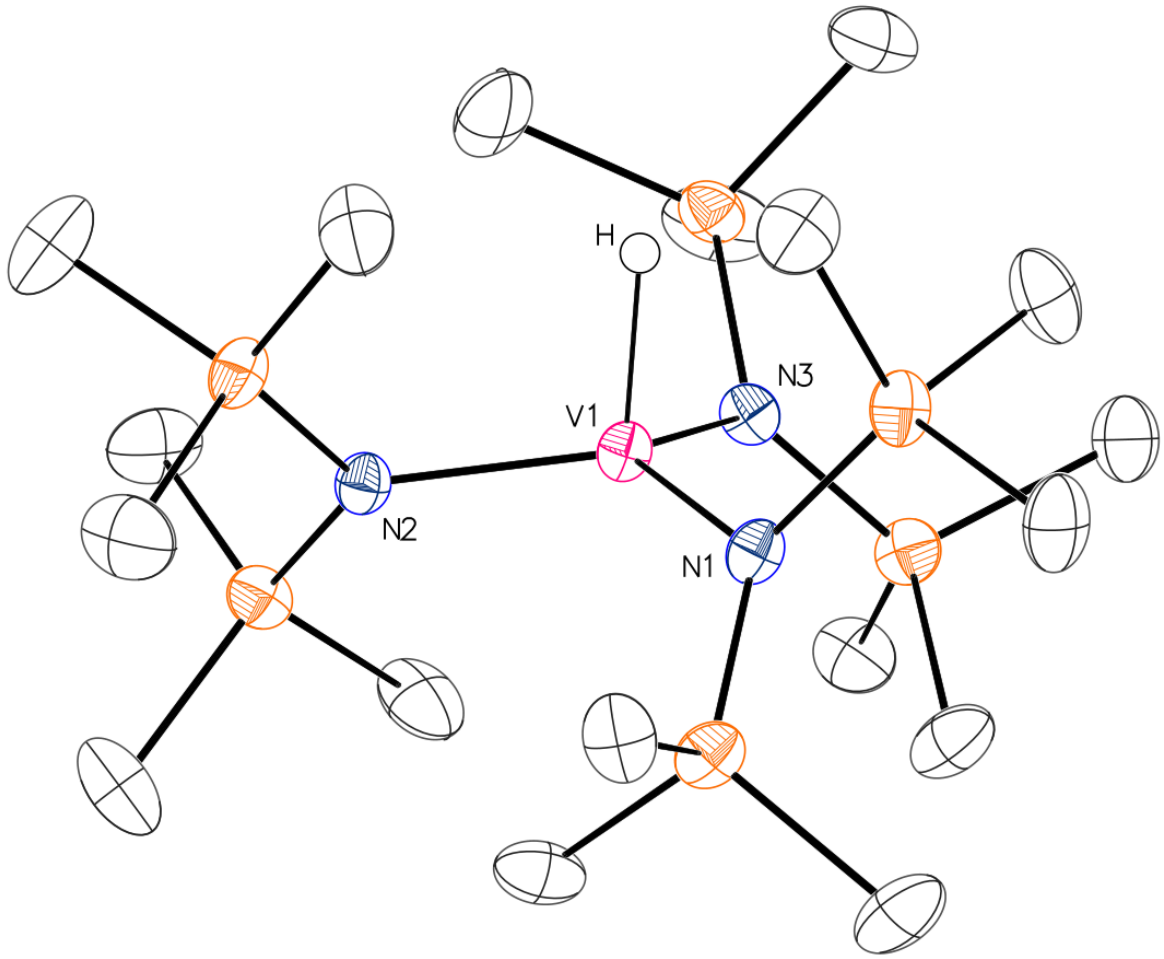

Figure 4.2: Molecular structure of the Δ isomer of the anion of **2** with ellipsoids shown at 30% probability. All non-hydride hydrogen atoms are not shown for clarity.

featuring a terminal hydride ligand for which structural data are available (cf. 1.55(9) Å in the neutral V(I) complex $HV(CO)_4(Ph_2PCH_2CH_2PPh_2)$ and 1.58 Å in the anionic V(I) complex $[CpV(CO)_3H]^-$).[62,63]

As described above, treatment of either $Cr\{N(SiMe_3)_2\}_3$ or $Fe\{N(SiMe_3)_2\}_3$ with one equivalent of $LiAlH_4$ gave the isostructural anionic metal(II) trisamide complexes **3** and **4**, respectively (Figures 4.3 and 4.4), rather than a hydride complex. The structures of these species are comparable to the previously reported anionic complexes featuring the $[K(18\text{-crown-6})]^+$ cation, and are thus not discussed further.[10,64]

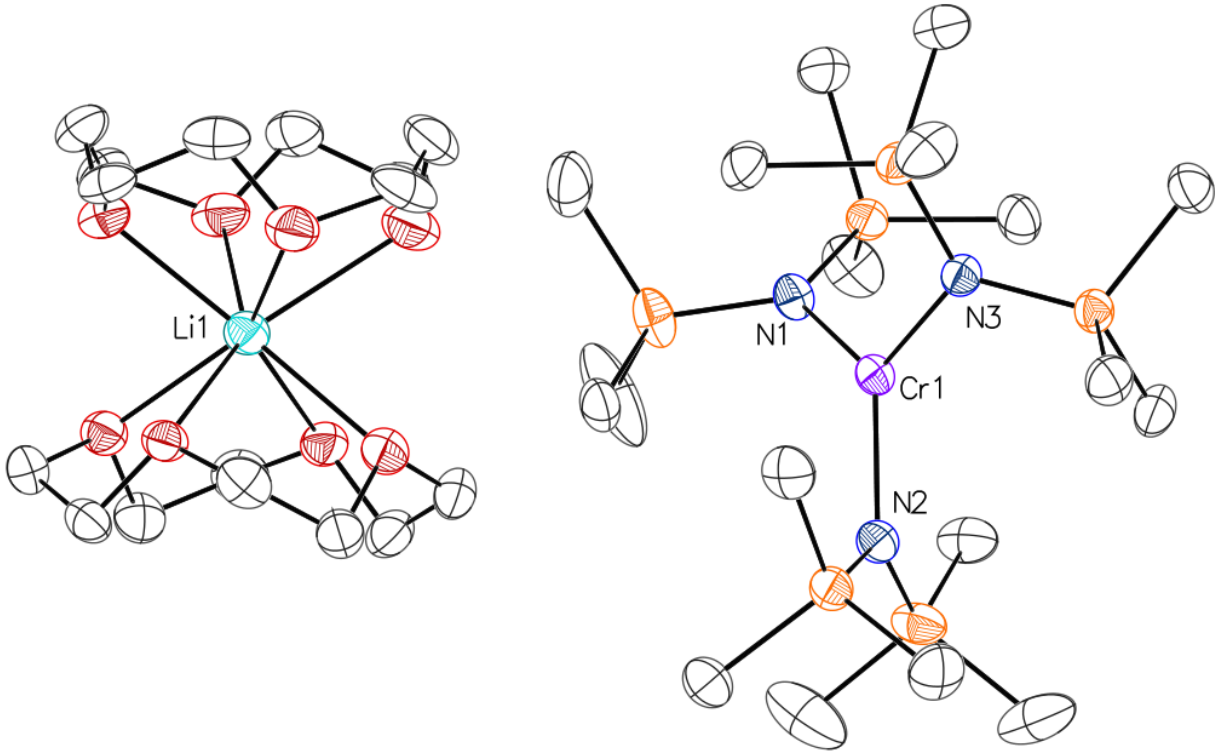

Figure 4.3: Molecular structure of the Δ isomer of **3** with ellipsoids shown at 30% probability. All non-hydride hydrogen atoms are not shown for clarity. Selected bond lengths (Å) and angles (°): Cr1-N1: 2.043(3), Cr1-N2: 2.050(3), Cr1-N3: 2.041(2), N1-Cr1-N2: 126.83(11), N2-Cr1-N3: 116.93(10), N3-Cr1-N1: 116.24(10).

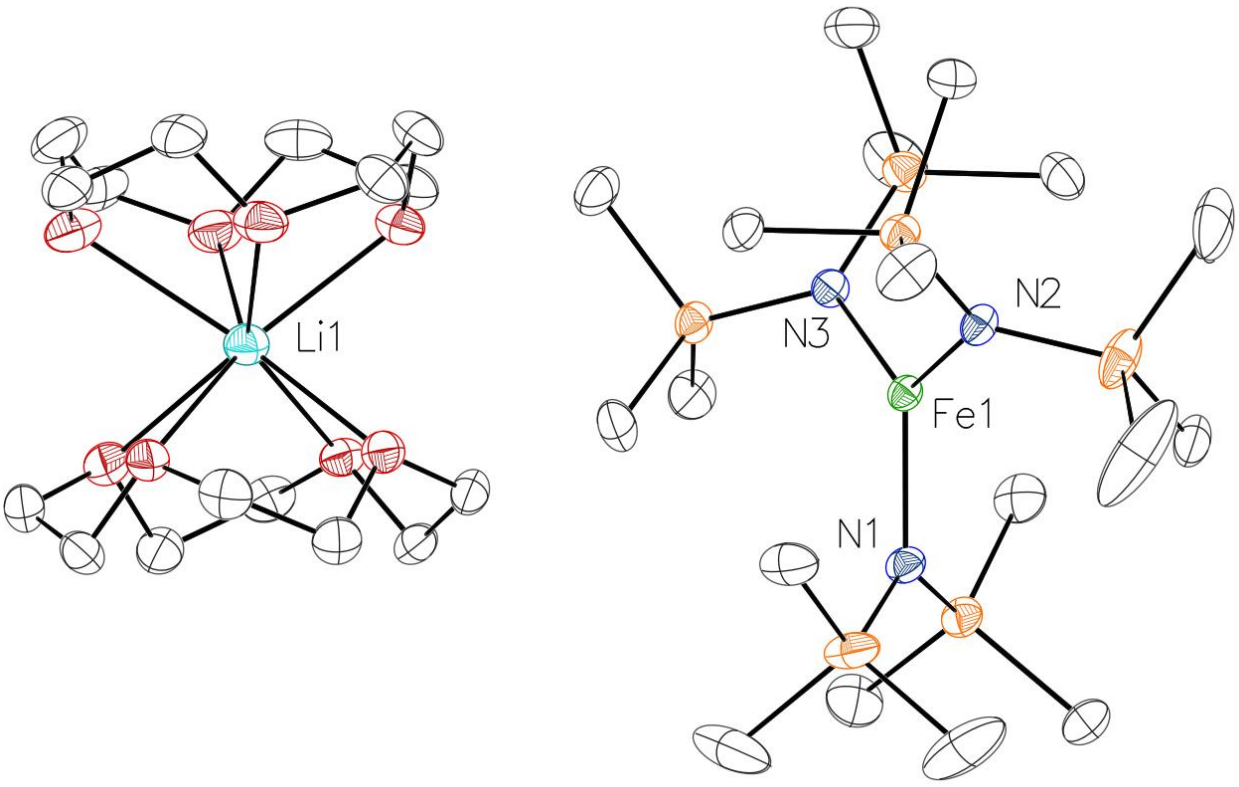

Figure 4.4: Molecular structure of the Δ isomer of **4** with ellipsoids shown at 30% probability. All non-hydride hydrogen atoms are not shown for clarity. Selected bond lengths (Å) and angles (°): Fe1-N1: 1.9993(15), Fe1-N2: 1.9871(15), Fe1-N3: 1.9941(14), N1-Fe1-N2: 120.49(7), N2-Fe1-N3: 119.36(6), N3-Fe1-N1: 120.15(6).

The structure of complex **5** (Figure 4.5) resembles the previously reported hydrido 'inverse crown' complexes which were first reported by Mulvey in 2002.[65] These complexes typically consist of a bimetallic magnesium/alkali metal core,[36,55,65,66] with the notable exception of the manganese/sodium complex $[Na_2Mn_2(\mu\text{-}H)_2\{N(iPr)_2\}_4]\cdot 2$ toluene discovered serendipitously in 2009 during attempts to metallate ferrocene with manganese.[67] The iron hydride complex **5** (Figure 1) crystallizes in the space group P2/n and has identical unit cell parameters to those of the tetrameric transition metal(I) silylamide complexes $\{MN(SiMe_3)_2\}_4$ (M = Co, Ni, Cu, Ag).[35,68–70] Like these complexes, **5** is comprised of four metal atoms in a planar arrangement bridged by four silylamide ligands having coplanar nitrogen atoms. In contrast to the referenced structures, the metal sites in complex **5** are occupied with equal probability by lithium and iron

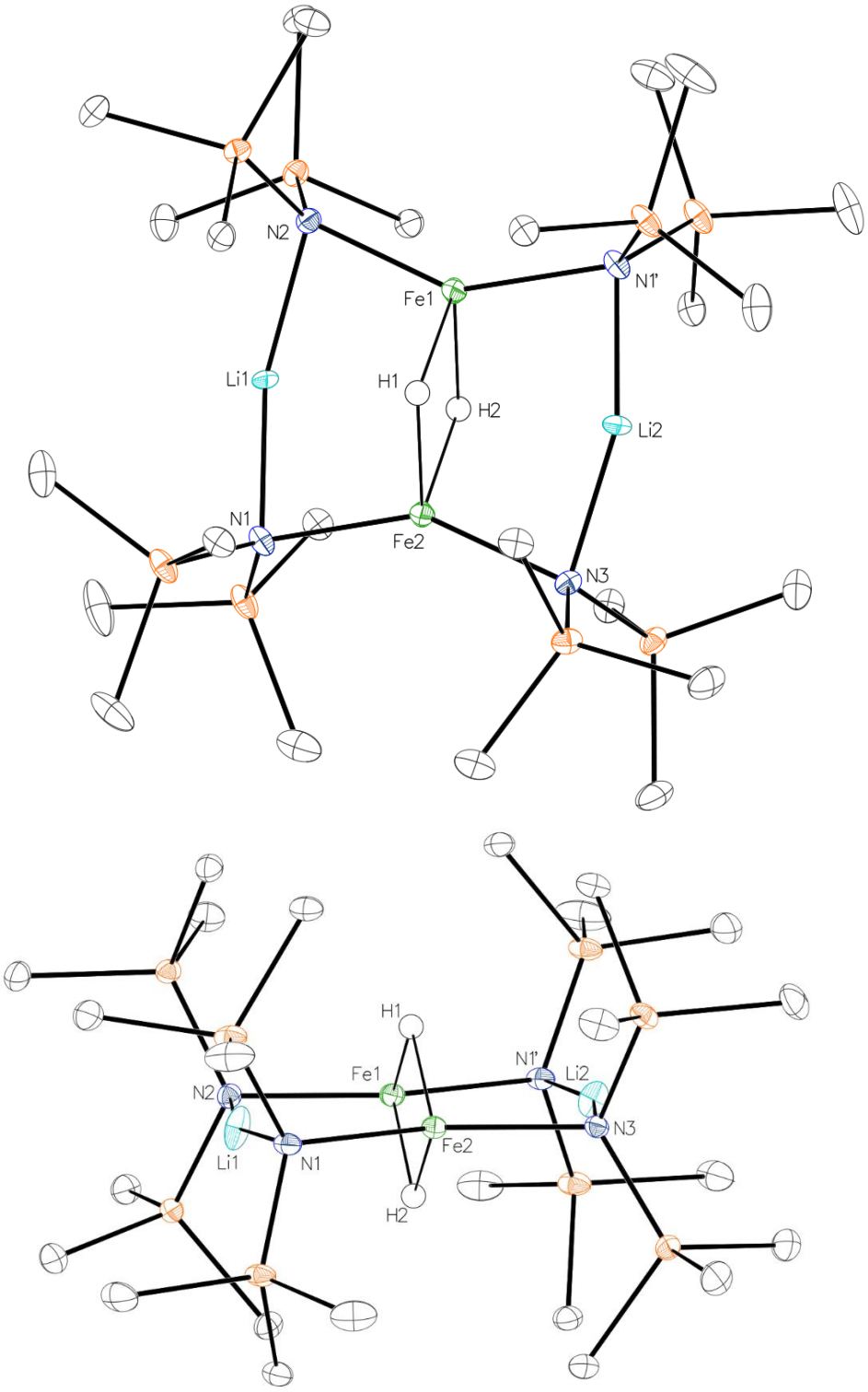

Figure 4.5: Top: Molecular structure of **5** with thermal ellipsoids shown at 30% probability. For clarity, hydrogens other than those bridging the iron atoms are not shown. Bottom: Alternate view of **5** showing the out of plane character of the bridging hydrogen atoms.

atoms. As such, the metal sites shown in Figure 5 have half occupancy as required by crystallographic symmetry. The planar $Fe_2Li_2N_4$ core of **5** differs from the similar manganese/sodium hydride structure previously reported by Blair and Mulvey, where the two alkali metals lie out of the Mn_2N_4 plane in a 'chair' fashion and are each η^3 coordinated by a toluene molecule.[67] The bridging hydrides of complex **5** are located 1.06(2) Å above and below the center of the metal-nitrogen plane. The Fe-H bond distances differ from each other only slightly, and range from 1.71(2) to 1.76(2) Å. The transannular Fe-Fe distance of 2.7523(6) Å suggests little, if any, interaction between the two metals.

The neutral iron hexahydride complex **6** (Figure 4.6) crystallizes as a racemic mixture of its Δ and Λ isomers. The coordination of the iron atom in **6** bears a striking resemblance to that of the vanadium atom in the anion of **1**, differing only in the substitution of one $-N(SiMe_3)_2$ group for a trimethylamine at one aluminium atom, thus making it a neutral iron (II) complex. This structural motif suggests that **1** and **6** were formed by a similar mechanism (i.e., transamination of the amide groups of $Fe\{N(SiMe_3)_2\}_3$ from iron to aluminium). The asymmetric unit contains the two enantiomers, neither of which possess any crystallographically required symmetry. The ligand environment at iron is that of a distorted octahedron, with Fe-H distances ranging from 1.52(3) to 1.65(3) Å and an average Fe-H distance of 1.59(1) Å. The H-Fe-H angles range from 83.1(18)° to 97.1(18)°. The Al-H distances range from 1.68(3) to 1.82(3) Å with an average Al-H distance of 1.72(1) Å. The H-Al-H angles range from 82.0(13)° to 87.4(17)°. The Fe-H bond lengths in **6** are notably shorter than those found in **5**, despite the higher coordination number of iron in complex **6**. The iron and aluminium atoms are nearly coplanar, with the iron atom only slightly out of the plane formed by the three aluminium atoms in both enantiomers (Fe-plane distances: 0.0119(6) and 0.0364(6) Å). The Fe-Al distances in **6** are quite short, ranging from 2.2879(8) to 2.4033(8) Å with an average length of 2.3337(3) Å. This length is shorter than the sum of the single bonded covalent radii of iron and aluminium (2.42 Å)[71] and similar in length to complexes having an Fe-Al bond, suggestive of some interaction between iron and aluminium (cf. cyclopentadienyl iron complexes by Aldridge (Fe-Al lengths ranging from 2.343 to 2.480 Å),[72] Driess (Fe-Al = 2.483 Å),[73] and Nöth (Fe-Al = 2.45 Å)[74]). The

calculated geometry for complex **6** is in good agreement with the experimental structure: the Fe-Al bond distances range from 2.2622 to 2.3833 Å. However, close inspection of the calculated Wiberg bond indices revealed only minor interaction between the metals (WBI for Fe-Al: 0.1563, 0.1410 and 0.1401), similar to the anion of **1**.[61] It is worth noting here that the structure of **6** differs substantially from that of $[FeH_6][MgX(THF)_2]_4$ of Bau and Gibbins.[75,76] The most obvious structural differences between these two molecules is the number of metal atoms surrounding the central iron (3 aluminium atoms in **6** versus 4 magnesium atoms in $[FeH_6][MgX(THF)_2]_4$), and the geometry around the main group metals (distorted tetrahedral in **6** versus distorted octahedral in $[FeH_6][MgX(THF)_2]_4$). The chirality of complex **6** arises from these significant differences. In the structure of $[FeH_6][MgX(THF)_2]_4$, the authors note that the Mg-H bond length (2.045(18) Å) is significantly longer than that found in MgH_2 (1.95 Å), a feature that suggests primarily ionic Mg-H bonding. However, the corresponding average Al-H distance in **6** (1.76(1) Å) is very similar to the Al-H distance found in the crystal structure of aluminium hydride (1.72(1) Å),[77] which suggests that these interactions are largely covalent. The average Fe-H distance in **6** (1.59(1) Å), is similar to that found in $[FeH_6][MgX(THF)_2]_4$ (1.609(2) Å), suggesting similar Fe-H interactions between the two molecules.

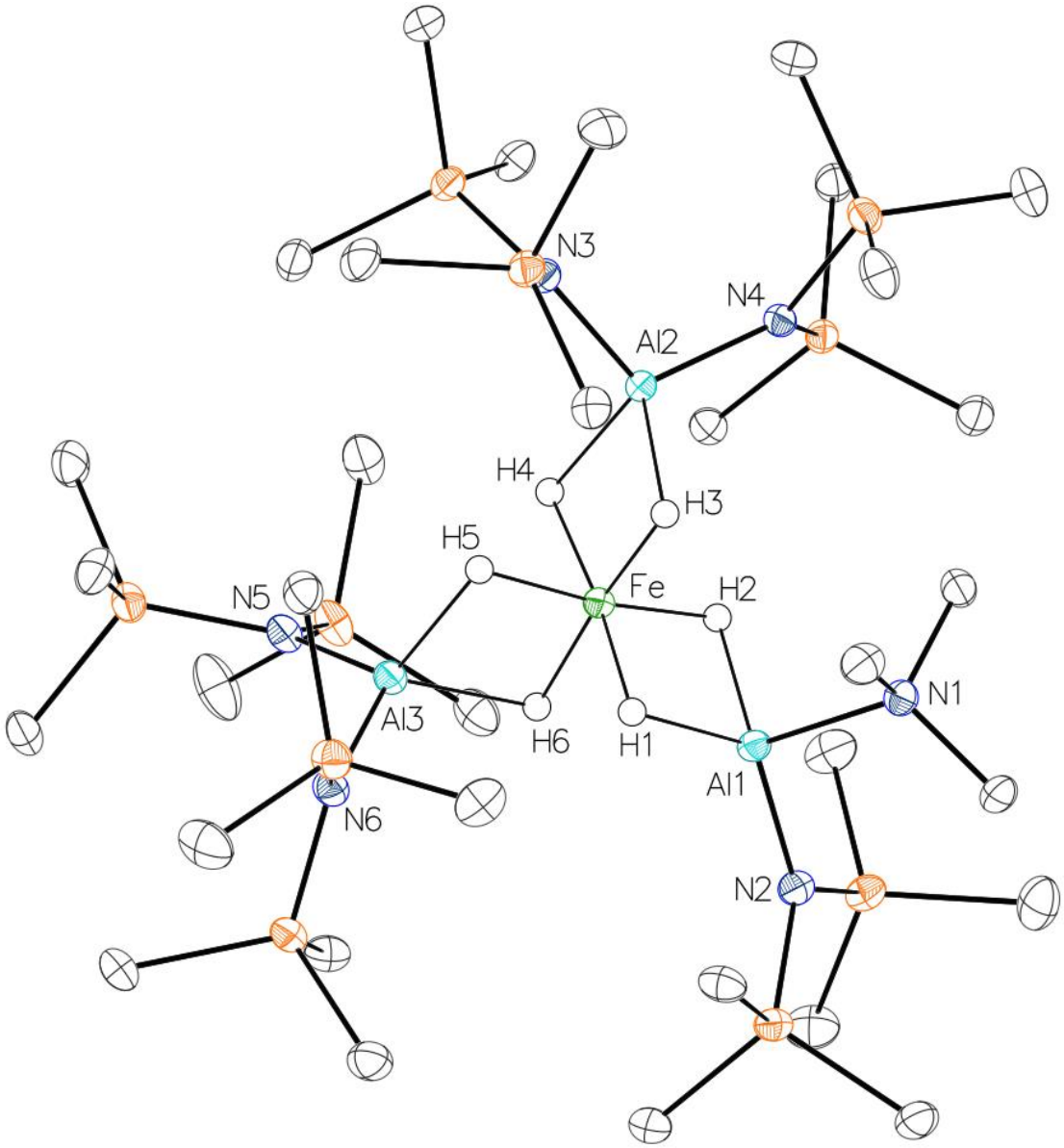

Figure 4.6: Molecular structure of the Λ isomer of **6**. Thermal ellipsoids (except bridging hydrides) are shown at 30% probability. For clarity, non-hydride hydrogen atoms are not shown.

Spectroscopy.

NMR Spectroscopy. The ^{1}H NMR spectrum of paramagnetic **2** is quite simple, showing a very broad ($\Delta\nu_{1/2}$ = 450 Hz) resonance at 4.74 ppm in deuterated THF attributable to the protons of the trimethylsilyl groups of the amide ligands. A much sharper ($\Delta\nu_{1/2}$ = 5 Hz) resonance found at 3.65 ppm was

attributed to the protons of the crown ether bound to the lithium cation. No signal was found for the hydride ligand in the proton NMR spectrum of **2**, which is perhaps unsurprising given its proximity to the paramagnetic vanadium atom. The effective magnetic moment of **2** was determined by the Evans' method to be 3.0 μ_B, which is in good agreement with its assignment as a high spin vanadium(III) ion, and indicative of the presence of a hydride ligand. The proton NMR spectrum of deuterated **2D** was identical to that of **2**, and the effective magnetic moment was found to be 2.9 μ_B. No signal for the deuteride ligand was located in the ^{2}H NMR spectrum of 2D, however.

Like complex **2**, the ^{1}H NMR spectrum of chromium(II) trisamido complex **3** features a broad resonance attributable to the trimethylsilyl protons, which was observed at 28.63 ppm, and a much sharper signal at 3.65 ppm was assigned to the protons of the crown ether. The corresponding signals in the ^{1}H NMR spectrum of iron complex **4** were observed at -2.53 and 3.58 ppm, respectively. These shifts are in good agreement with those previously published for the analogous chromium and iron salts featuring the $[K(18\text{-crown-6})]^+$ cation.[10,64] However, in contrast to the high spin metal(III) nature of complex **2**, the effective magnetic moments of complexes **3** and **4** (4.3 and 5.5 μ_B, respectively) clearly show them to be high spin metal(II) complexes.

The proton NMR spectrum of diamagnetic complex **6** agrees with its crystal structure and its identification as a low spin iron(II) complex, having sharp resonances appearing in the expected regions (Figure 4.7). A resonance at 2.06 ppm was assigned to the nine protons of the trimethylamine coordinated to aluminium. Five resonances integrating in a 4:2:2:1:1 ratio were assigned to the trimethylsilyl protons. Similarly, five upfield resonances integrating in in 1:2:1:1:1 ratio were assigned to the bridging hydrides. The splitting of these signals is attributable to the lower symmetry in the molecule due to the presence of the trimethylamine donor molecule bound to one of the aluminium atoms (cf. the ^{1}H-NMR spectrum of highly symmetric $[FeH_6][MgX(THF)_2]_4$, which features two hydride resonances that coalesce at 40 °C). This effect is also apparent in the ^{13}C NMR spectrum, which indicates that the molecule possesses six

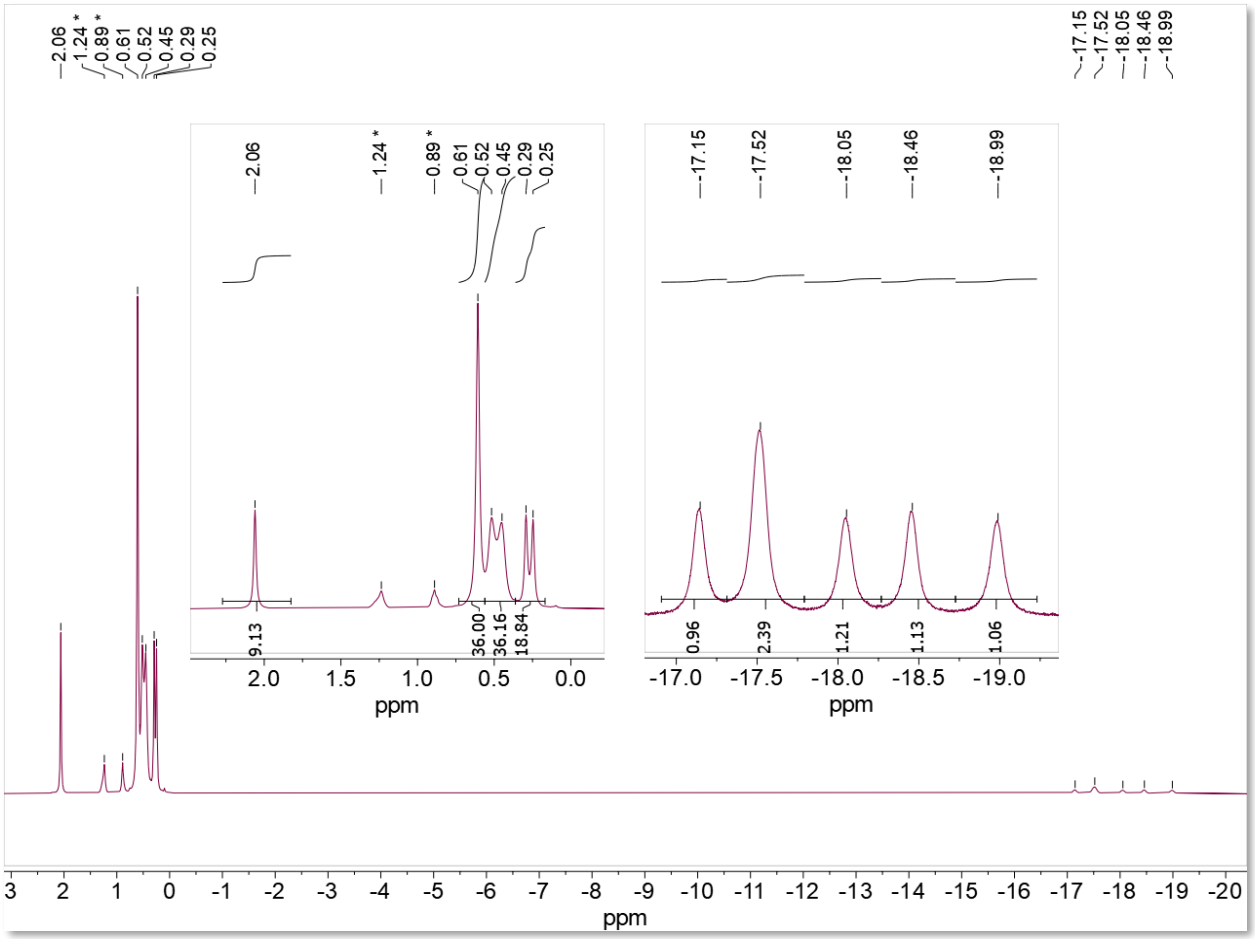

Figure 4.7: ^{1}H NMR spectrum of **6**. Left inset: detail of trimethylamine (2.06 ppm) and trimethylsilyl (0.61-0.25 ppm) resonances. Right inset: detail of bridging hydride resonances. Asterisks indicate resonances of residual hexanes.

magnetically distinct carbon environments (one trimethylamine ligand and five bis(trimethylsilyl) amide ligands).

Vibrational Spectroscopy. Comparison of the vibrational spectrum of vanadium hydride **2** with those of metal(II) trisamides **3** and **4** confirms the presence of a hydride ligand in **2**. Although these spectra are very similar, the infrared spectrum of hydride **2** displays a broad absorbance at 1575 cm^{-1}, a feature that is not present in the spectra of either **3** or **4**. We tentatively assigned this absorbance to the terminal V-H stretching mode, as terminal $\upsilon_{M\text{-}H}$ stretching absorbances are typically found in the region of 2200 to 1600 cm^{-1}.[78,79] This assignment was confirmed by comparison of the vibrational spectrum of **2** with the spectrum of the analogous deuteride **2D**, where the absorbance at 1575 cm^{-1} is absent (Figure 4.8). We also noted the presence of a new broad absorbance at 440 cm^{-1} in the spectrum of **2D** that is not present in the spectrum of the hydride **2**. Based on the difference in reduced mass between **2** and **2D**, we anticipated that the absorbance corresponding to the terminal V-D stretching mode would be found at ca. 1100 cm^{-1}. We therefore assigned the absorbance at 440 cm^{-1} to the $\delta_{V\text{-}D}$ rocking mode. These assignments were further corroborated by the calculated spectra of the anions of **2** and **2D** (see SI), which predicted energies of 1647 ($\nu_{V\text{-}H}$) and 593-636 cm^{-1} ($\delta_{V\text{-}H}$) for **2**, and 1177 ($\nu_{V\text{-}D}$) and 410-449 cm^{-1} ($\delta_{V\text{-}D}$) for **2D**, in good agreement with the energies found experimentally. The V-H rocking mode and the V-D stretching mode both appear in regions of their respective spectra that are dominated by other absorbances (an observation that has been described elsewhere).[80] However, careful examination of the spectra reveals features at the energies predicted by the calculated spectra that are attributable to these vibrations, namely a shoulder at ca. 1110 cm^{-1} in the spectrum of **2D** (the V-D stretching mode) and the obscuring of absorbances from ca. 500-700 cm^{-1} in the spectrum of **2** (which are quite sharp in the spectrum of **2D**).

No obvious Fe-H vibrational modes are observed in the infrared spectrum of **5**, although bands attributable to the metal-amide vibrations are apparent in the 350 to 450 cm^{-1} range. In contrast, the infrared spectrum of complex **6** shows a strong absorbance at 1600 cm^{-1} with a weaker shoulder at 1635 cm^{-1}. Bands in this region have previously been shown to be diagnostic for the presence of bridging hydrides in simple

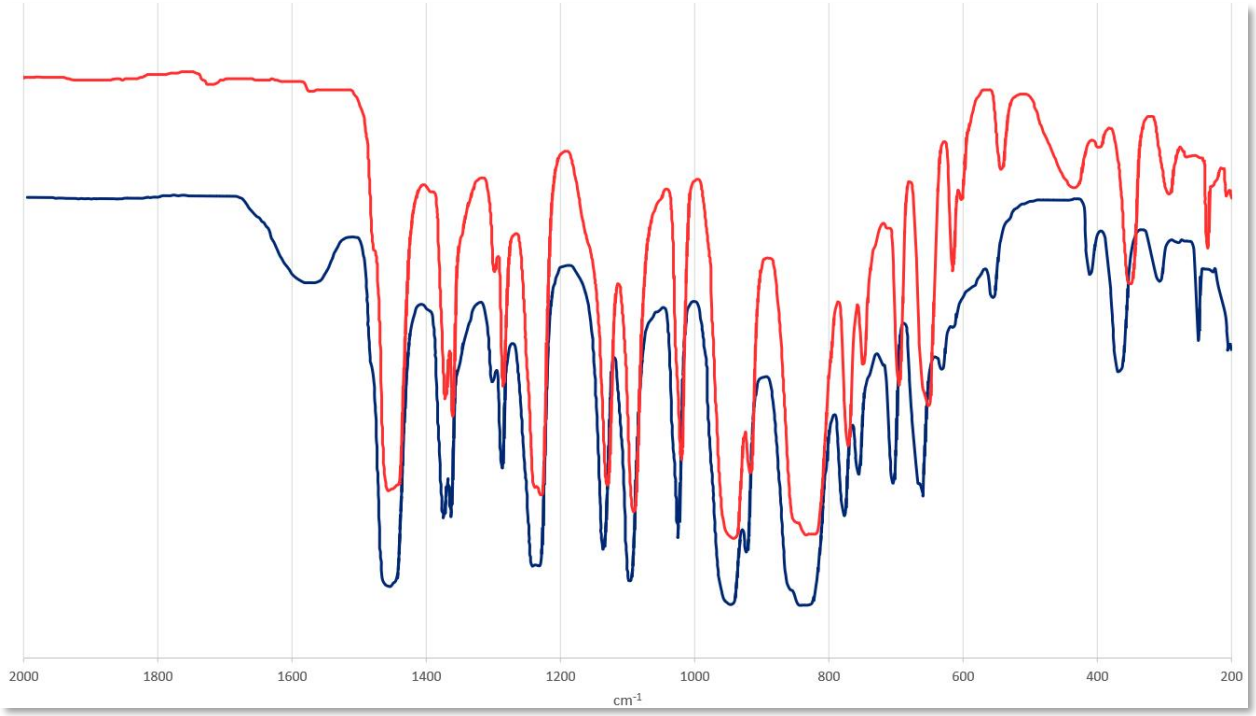

Figure 4.8: Vibrational spectra of **2** (blue trace) and **2D** (red trace). The V-H stretching mode in **2** is observed at 1575 cm^{-1}. The corresponding V-D mode is observed as a shoulder at ca. 1175 cm^{-1} in the spectrum of **2D**. The V-D rocking mode is clearly visible as a broad absorbance at 440 cm^{-1}, while the corresponding V-H bending mode is obscured by other absorbances present from ca. 575 to 650 cm^{-1}.

aluminium complexes.[81] Less obvious, however, is any Fe-H stretching band. Iron hydride stretching bands appear over a wide frequency range, and are often quite weak.[32] A report by Linn and Gibbins describing the vibrational spectroscopy of the $[FeH_6]^{4-}$ anion indicated that the Fe-H stretching vibrations appeared at 1569 and 1523 cm^{-1}.[82] We therefore assign the weak absorbance at 1520 cm^{-1} in the spectrum of **6** to an Fe-H stretching mode. In the far infrared, complex **6** shows absorbances attributed to the Al-$N(SiMe_3)_2$ vibrations at 365 cm^{-1} and 415 cm^{-1}, and the Al-NMe_3 vibration at 450 cm^{-1}. These energies are in good agreement with Al-N stretching bands found in the complexes $Al\{N(SiMe_3)_2\}_3$[83] and $AlH_3(NMe_3)$.[81]

Conclusion.

$M\{N(SiMe_3)_2\}_3$ (M = V, Cr, Fe) complexes were shown to react differently with lithium aluminium hydride. In the case of vanadium, the unstable ionic vanadium(II) polyhydride **1** was formed. Carrying out this reaction in the presence of 12-crown-4 gives the unusual vanadium(III) terminal hydride **2**. Preparation of the analogous deuteride **2D** and comparison of its spectroscopic data with that of **2** confirmed the

presence of the hydride ligand that was located crystallographically, and the computed vibrational spectra of these complexes were shown to agree well with experiment. In contrast, when M = Cr or Fe, the analogous terminal hydrides are not formed. Instead, these reactions give the anionic metal(II) amide complexes $[M\{N(SiMe_3)_2\}_3][Li(12\text{-crown-}4)_2]$ (**3**, M = Cr or **4**, M = Fe). Mixed-metal hydrido complexes $[Fe(\mu_2\text{-}H)\{N(SiMe_3)_2\}_2(\mu_2\text{-}Li)]_2$ (**5**) and $Fe(\mu_2\text{-}H)_6[Al\{N(SiMe_3)_2\}_2]_2[Al\{N(SiMe_3)_2\}(NMe_3)]$ (**6**) were prepared by reaction of $Fe\{N(SiMe_3)_2\}_3$ with $LiAlH_4$ or AlH_3NMe_3, respectively. Complex **5** is an example of a growing class of 'hydrido inverse crown' complexes, suggesting that complexes of this form may be accessible for more combinations of alkali metal and a second divalent metal. Complexes **1** and **6** are rare examples of vanadium or iron coordinated exclusively by hydrogen, with NBO analyses indicating only weak interactions between the transition metal and aluminium. The synthesis of these complexes further underlines that, despite initial reports, $M\{N(SiMe_3)_2\}_3$ complexes display a very rich chemistry.

Associated Content.

Supporting information.

The Supporting Information, including spectra (NMR, infrared, UV-Vis), crystallographic data, xyz-coordinates of the optimized structures and photographs of material is available free of charge on the ACS Publications website at https://doi.org/10.1021/acs.inorgchem.1c01399. CCDC entries 2058689 (**1**), 2070539 (**2**), 2074655 (**2D**), 2070550 (**3**), 2071502 (**4**), 1970388 (**5**), and 1970386 (**6**) contain the supplementary crystallographic data of the complexes described here. These data can be obtained free of charge via www.ccdc.cam.ac.uk/data_request/cif, by emailing data_request@ccdc.cam.ac.uk, or by contacting The Cambridge Crystallographic Data Centre, 12 Union Road, Cambridge CB2 1EZ, UK; fax: + 44 1223 336033.

Author Information.

Corresponding author

*pppower@ucdavis.edu

*petra.vasko@jyu.fi

ORCID

Cary R. Stennett: 0000-0002-2727-5747

James C. Fettinger: 0000-0002-6428-4909

Petra Vasko: 0000-0003-4202-6869

Philip P. Power: 0000-0002-6262-3209

Notes

The authors declare no competing financial interest.

Acknowledgements

We wish to acknowledge the US National Science Foundation (CHE-1565501) for support of this work and for the purchase of a dual-source X-ray diffractometer (CHE-0840444). PV would like to thank Academy of Finland (project number 314794) for funding.

References.

(1) Bürger, H.; Wannagat, U. Silylamido-Derivate von Eisen und Kobalt. *Monatsh. Chem.* **1963**, *94*, 1007–1012.

(2) Bürger, H.; Wannagat, U. Silylamido-Verbindungen von Chrom, Mangan, Nickel und Kupfer. *Monatsh. Chem.* **1964**, *95*, 1099–1102.

(3) Alyea, E. C.; Bradley, D. C.; Copperthwaite, R. G. Three-Co-Ordinated Transition Metal Compounds. Part I. The Preparation and Characterization of Tris(Bistrimethylsilylamido)-Derivatives of Scandium, Titanium, Vanadium, Chromium, and Iron. *J. Chem. Soc. Dalton Trans.* **1972**, 1580–1584.

(4) Alyea, E. C.; Bradley, D. C.; Copperthwaite, R. G.; Sales, K. D. Three-Co-Ordinated Transition-Metal Compounds. Part II. Electronic Spectra and Magnetism of Tris(Bistrimethylsilylamido)Derivatives of Scandium, Titanium, Vanadium, Chromium, and Iron. *J. Chem. Soc. Dalton Trans.* **1973**, 185–191.

(5) Bradley, D. C. Steric Control of Metal Coordination. *Chem. Br.* **1975**, *11*, 393–397.

(6) Eller, P. G.; Bradley, D. C.; Hursthouse, M. B.; Meek, D. W. Three Coordination in Metal Complexes. *Coord. Chem. Rev.* **1977**, *24*, 1–95.

(7) Bradley, D. C.; Copperthwaite, R. G.; Extine, M. W.; Reichert, W. W.; Chisholm, M. H. Transition Metal Complexes of Bis(Trimethyl-Silyl)Amine (1,1,1,3,3,3-Hexamethyldisilazane). In *Inorganic Syntheses*; 1978; Vol. 18, 112–120.

(8) Ghotra, J. S.; Hursthouse, M. B.; Welch, A. J. Three-Co-Ordinate Scandium(III) and Europium(III); Crystal and Molecular Structures of Their Trishexamethyldisilylamides. *J. Chem. Soc., Chem. Commun.* **1973**, 669–670.

(9) Putzer, M. A.; Magull, J.; Goesmann, H.; Neumüller, B.; Dehnicke, K. Synthese, Eigenschaften und Kristallstrukturen Der Titan(III)-Amido-Komplexe $Ti[N(SiMe_3)_2]_3$, $[TiCl_2\{N(SiMe_3)_2\}(THF)_2]$ und $[Na(12\text{-Krone-}4)_2][TiCl_2\{N(SiMe_3)_2\}_2]$. *Chem. Ber.* **1996**, *129*, 1401–1405.

(10) Wagner, C. L.; Phan, N. A.; Fettinger, J. C.; Berben, L. A.; Power, P. P. New Characterization of $V\{N(SiMe_3)_2\}_3$: Reductions of Tris[Bis(Trimethylsilyl)Amido]Vanadium(III) and -Chromium(III) To Afford the Reduced Metal(II) Anions $[M\{N(SiMe_3)_2\}_3]^-$ (M = V and Cr). *Inorg. Chem.* **2019**,

58, 6095–6101.

(11) Köhn, R. D.; Kociok-Köhn, G.; Haufe, M. The Chemistry of 1,3,5-Triazacyclohexane Complexes, 3. High Yield Synthesis of $[Cr\{N(SiMe_3)_2\}_3]$ and Accurate Structure Determination by Cocrystallization with Me_6Si_2. *Chem. Ber.* **1996**, *129*, 25–27.

(12) Ellison, J. J.; Power, P. P.; Shoner, S. C. First Examples of Three-Coordinate Manganese(III) and Cobalt(III): Synthesis and Characterization of the Complexes $M[N(SiMe_3)_2]_3$ (M = Mn or Co). *J. Am. Chem. Soc.* **1989**, *111*, 8044–8046.

(13) Hursthouse, M. B.; Rodesiler, P. F. Crystal and Molecular Structure of Tris(Hexamethyldisilylamido)Iron(III). *J. Chem. Soc. Dalton Trans.* **1972**, 2100–2102.

(14) Rees, W. S. J.; Just, O.; Van Derveer, D. S. Molecular Design of Dopant Precursors for Atomic Layer Epitaxy of SrS:Ce. *J. Mater. Chem.* **1999**, *9*, 249–252.

(15) Andersen, R. A.; Templeton, D. H.; Zalkin, A. Structure of Tris(Bis(Trimethylsilyl)Amido)Neodymium(III), $Nd[N(Si(CH_3)_3)_2]_3$. *Inorg. Chem.* **1978**, *17*, 2317–2319.

(16) Brady, E. D.; Clark, D. L.; Gordon, J. C.; Hay, P. J.; Keogh, D. W.; Poli, R.; Scott, B. L.; Watkin, J. G. Tris(Bis(Trimethylsilyl)Amido)Samarium: X-Ray Structure and DFT Study. *Inorg. Chem.* **2003**, *42*, 6682–6690.

(17) Hitchcock, P. B.; Hulkes, A. G.; Lappert, M. F.; Li, Z. Cerium(III) Dialkyl Dithiocarbamates from $[Ce\{N(SiMe_3)_2\}_3]$ and Tetraalkylthiuram Disulfides, and $[Ce(K_2\text{-}S_2CNEt_2)_4]$ from the Ce^{III} Precursor; Tb^{III} and Nd^{III} Analogues. *Dalton Trans.* **2004**, No. 1, 129–136.

(18) Herrmann, W. A.; Anwander, R.; Munck, F. C.; Scherer, W.; Dufaud, V.; Huber, N. W.; Artus, G. R. J. Lanthanoiden-Komplexe, IX [1]. Reaktivitätsbestimmender Einfluß Der Ligandenkonstitution Bei Seltenerdamiden: Herstellung Und Struktur Sterisch Überladener Alkoxid-Komplexe /

Lanthanoid Complexes, IX [1]. Reactivity Control of Lanthanoid Amides through Li. *Z. Naturforsch., B: Chem. Sci.* **1994**, *49*, 1789.

(19) Bienfait, A. M.; Wolf, B. M.; Törnroos, K. W.; Anwander, R. Trivalent Rare-Earth-Metal Bis(Trimethylsilyl)Amide Halide Complexes by Targeted Oxidations. *Inorg. Chem.* **2018**, *57*, 5204–5212.

(20) Niemeyer, M. Synthesis and Structural Characterization of Several Ytterbium Bis(Trimethylsilyl)Amides Including Base-Free $[Yb\{N(SiMe_3)_2\}_2(\mu\text{-}Cl)]_2$ — A Coordinatively Unsaturated Complex with Additional Agostic Yb···(H_3C—Si) Interactions. *Z. Anorg. Allg. Chem.* **2002**, *628*, 647–657.

(21) Gaunt, A. J.; Enriquez, A. E.; Reilly, S. D.; Scott, B. L.; Neu, M. P. Structural Characterization of $Pu[N(SiMe_3)_2]_3$, a Synthetically Useful Nonaqueous Plutonium(III) Precursor. *Inorg. Chem.* **2008**, *47*, 26–28.

(22) Stewart, J. L.; Andersen, R. A. Trivalent Uranium Chemistry: Molecular Structure of $[(Me_3Si)_2N]_3U$. *Polyhedron* **1998**, *17*, 953–958.

(23) Stennett, C. R.; Fettinger, J. C.; Power, P. P. Unexpected Coordination Complexes of the Metal Tris-Silylamides $M\{N(SiMe_3)_2\}_3$ (M = Ti, V). *Inorg. Chem.* **2020**, *59*, 1871–1882.

(24) Stennett, C. R.; Nguyen, T. H.; Power, P. P. Characterization of the "Absent" Vanadium Oxo $V(=O)\{N(SiMe_3)_2\}_3$, Imido $V(=NSiMe_3)\{N(SiMe_3)_2\}_3$, and Imido-Siloxy $V(=NSiMe_3)(OSiMe_3)\{N(SiMe_3)_2\}_2$ Complexes Derived from $V\{N(SiMe_3)_2\}_3$ and Kinetic Study of the Spontaneous Conversion of the Oxo Complex into Its Imido-Siloxy Isomer. *Inorg. Chem.* **2020**, *59*, 11079–11088.

(25) Bürger, H.; Smrekar, O.; Wannagat, U. Silylamido-Verbindungen Des Vanadiums. *Monatsh. Chem.* **1964**, *95*, 292–302.

(26) Duan, Z.; Schmidt, M.; Young, V. G.; Xie, X.; McCarley, R. E.; Verkade, J. G. The Novel Bis(Oxo-Bridged) Dinuclear Vanadium(IV) Complex $\{(\mu\text{-}O)_2V_2[N(SiMe_3)_2]_4\}$: An Unexpected Reaction Product. *J. Am. Chem. Soc.* **1996**, *118*, 5302–5303.

(27) Hieber, W.; Leutert, F. Zur Kenntnis Des Koordinativ Gebundenen Kohlenoxyds: Bildung von Eisencarbonylwasserstoff. *Naturwissenschaften* **1931**, *19*, 360–361.

(28) Bolm, C.; Legros, J.; Le Paih, J.; Zani, L. Iron-Catalyzed Reactions in Organic Synthesis. *Chem. Rev.* **2004**, *104*, 6217–6254.

(29) Fürstner, A.; Martin, R. Advances in Iron Catalyzed Cross Coupling Reactions. *Chem. Lett.* **2005**, *34*, 624–629.

(30) Correa, A.; García Mancheño, O.; Bolm, C. Iron-Catalysed Carbon–Heteroatom and Heteroatom–Heteroatom Bond Forming Processes. *Chem. Soc. Rev.* **2008**, *37*, 1108–1117.

(31) Enthaler, S.; Junge, K.; Beller, M. Sustainable Metal Catalysis with Iron: From Rust to a Rising Star? *Angew. Chem. Int. Ed.* **2008**, *47*, 3317–3321.

(32) Nakazawa, H.; Itazaki, M. Fe–H Complexes in Catalysis BT - Iron Catalysis: Fundamentals and Applications; Plietker, B., Ed.; Springer Berlin Heidelberg: Berlin, Heidelberg, 2011; pp 27–81.

(33) Gieshoff, T. N.; Chakraborty, U.; Villa, M.; Jacobi von Wangelin, A. Alkene Hydrogenations by Soluble Iron Nanocluster Catalysts. *Angew. Chem. Int. Ed.* **2017**, *56*, 3585–3589.

(34) Araake, R.; Sakadani, K.; Tada, M.; Sakai, Y.; Ohki, Y. $[Fe_4]$ and $[Fe_6]$ Hydride Clusters Supported by Phosphines: Synthesis, Characterization, and Application in N_2 Reduction. *J. Am. Chem. Soc.* **2017**, *139*, 5596–5606.

(35) Ohki, Y.; Shimizu, Y.; Araake, R.; Tada, M.; Sameera, W. M. C.; Ito, J.-I.; Nishiyama, H. $Co_6H_8(P^iPr_3)_6$: A Cobalt Octahedron with Face-Capping Hydrides. *Angew. Chem. Int. Ed.* **2016**, *55*, 15821–15825.

(36) Andrikopoulos, P. C.; Armstrong, D. R.; Kennedy, A. R.; Mulvey, R. E.; O'Hara, C. T.; Rowlings, R. B. Synthesis, Structure and Theoretical Studies of the Hydrido Inverse Crown $[K_2Mg_2(N^iPr_2)_4(\mu\text{-}H)_2\cdot(Toluene)_2]$: A Rare Example of a Molecular Magnesium Hydride with a Mg-$(\mu\text{-}H)_2$-Mg Double Bridge. *Eur. J. Inorg. Chem.* **2003**, *2003*, 3354–3362.

(37) Evans, D. F. 400. The Determination of the Paramagnetic Susceptibility of Substances in Solution by Nuclear Magnetic Resonance. *J. Chem. Soc.* **1959**, No. 0, 2003–2005.

(38) Bain, G. A.; Berry, J. F. Diamagnetic Corrections and Pascal's Constants. *J. Chem. Educ.* **2008**, *85*, 532.

(39) Bradley, D. C.; Chudzynska, H.; Backer-Dirks, J. D. J.; Hursthouse, M. B.; Ibrahim, A. A.; Motevalli, M.; Sullivan, A. C. Synthesis, Photochemistry and X-Ray Crystal Structures of the Methyltris[Bis(Trimethylsilyl)Amido] Compounds $MeTi[N(SiMe_3)_2]_3$ and $MeZr[N(SiMe_3)_2]_3$. *Polyhedron* **1990**, *9*, 1423–1427.

(40) Ruff, J. K. The Amine Complexes of Aluminum Hydride. III. Substitution Reactions. *J. Am. Chem. Soc.* **1961**, *83*, 1798–1800.

(41) Ruff, J. K.; Parry, R. W.; Smith, W. L. Trimethylamine–Aluminum Hydride and Trimethylamine–Aluminum Chloride Dihydride (Trimethylamine-Aluane and Trimethylamine-Chloroaluane). *Inorg. Synth.* **1967**, *9*, 30–37.

(42) Sheldrick, G. M. *SADABS*; University of Göttingen, Germany, 1996.

(43) Sheldrick, G. M. SHELXT - Integrated Space-Group and Crystal-Structure Determination. *Acta Crystallogr. Sect. A Found. Crystallogr.* **2015**, *A71*, 3–8.

(44) Sheldrick, G. M. Crystal Structure Refinement with SHELXL. *Acta Crystallogr. Sect. C, Struct. Chem.* **2015**, *C71*, 3–8.

(45) Dolomanov, O. V; Bourhis, L. J.; Gildea, R. J.; Howard, J. A. K.; Puschmann, H. *OLEX2*: A

Complete Structure Solution, Refinement and Analysis Program. *J. Appl. Crystallogr.* **2009**, *42*, 339–341.

(46) Frisch, M. J.; Trucks, G. W.; Schlegel, H. B.; Scuseria, G. E.; Robb, M. A.; Cheeseman, J. R.; Scalmani, G.; Barone, V.; Petersson, G. A.; Nakatsuji, H.; Li, X.; Caricato, M.; Marenich, A. V.; Bloino, J.; Janesko, B. G.; Gomperts, R.; Mennucci, B.; Hratchian, H. P.; Ortiz, J. V.; Izmaylov, A. F.; Sonnenberg, J. L.; Williams-Young, D.; Ding, F.; Lipparini, F.; Egidi, F.; Goings, J.; Peng, B.; Petrone, A.; Henderson, T.; Ranasinghe, D.; Zakrzewski, V. G.; Gao, J.; Rega, N.; Zheng, G.; Liang, W.; Hada, M.; Ehara, M.; Toyota, K.; Fukuda, R.; Hasegawa, J.; Ishida, M.; Nakajima, T.; Honda, Y.; Kitao, O.; Nakai, H.; Vreven, T.; Throssell, K.; Montgomery, J. A., Jr.; Peralta, J. E.; Ogliaro, F.; Bearpark, M. J.; Heyd, J. J.; Brothers, E. N.; Kudin, K. N.; Staroverov, V. N.; Keith, T. A.; Kobayashi, R.; Normand, J.; Raghavachari, K.; Rendell, A. P.; Burant, J. C.; Iyengar, S. S.; Tomasi, J.; Cossi, M.; Millam, J. M.; Klene, M.; Adamo, C.; Cammi, R.; Ochterski, J. W.; Martin, R. L.; Morokuma, K.; Farkas, O.; Foresman, J. B.; Fox, D. J. Gaussian 16, Revision C.01, Gaussian, Inc., Wallingford CT, 2016.

(47) Perdew, J. P.; Burke, K.; Ernzerhof, M. Generalized Gradient Approximation Made Simple. *Phys. Rev. Lett.* **1996**, *77*, 3865–3868.

(48) Perdew, J. P.; Ernzerhof, M.; Burke, K. Rationale for Mixing Exact Exchange with Density Functional Approximations. *J. Chem. Phys.* **1996**, *105*, 9982–9985.

(49) Adamo, C.; Barone, V. Toward Reliable Density Functional Methods without Adjustable Parameters: The PBE0 Model. *J. Chem. Phys.* **1999**, *110*, 6158–6170.

(50) Weigend, F.; Ahlrichs, R. Balanced Basis Sets of Split Valence, Triple Zeta Valence and Quadruple Zeta Valence Quality for H to Rn: Design and Assessment of Accuracy. *Phys. Chem. Chem. Phys.* **2005**, *7*, 3297–3305.

(51) Weigend, F. Accurate Coulomb-Fitting Basis Sets for H to Rn. *Phys. Chem. Chem. Phys.* **2006**, *8*,

1057–1065.

(52) Grimme, S.; Antony, J.; Ehrlich, S.; Krieg, H. A Consistent and Accurate Ab Initio Parametrization of Density Functional Dispersion Correction (DFT-D) for the 94 Elements H-Pu. *J. Chem. Phys.* **2010**, *132*, 154104.

(53) Grimme, S.; Ehrlich, S.; Goerigk, L. Effect of the Damping Function in Dispersion Corrected Density Functional Theory. *J. Comput. Chem.* **2011**, *32*, 1456–1465.

(54) Glendening, E. D.; Badenhoop, J. K.; Reed, A. E.; Carpenter, J. E.; Bohmann, J. A.; Morales, C. M.; Karafiloglou, P.; Landis, C. R.; Weinhold, F. NBO 7.0. University of Wisconson: Madison, WI 2018.

(55) Liptrot, D. J.; Hill, M. S.; Mahon, M. F. Heterobimetallic S-Block Hydrides by σ-Bond Metathesis. *Chem. Eur. J.* **2014**, *20*, 9871–9874.

(56) Gibbins, S. G. Formation and Isolation of $FeH_6Mg_4X_4(C_4H_8O)_8$. *Inorg. Chem.* **1977**, *16*, 2571–2576.

(57) P. Clancy, G.; C. S. Clark, H.; K. B. Clentsmith, G.; Geoffrey N. Cloke, F.; B. Hitchcock, P. Vanadium(III) Complexes Incorporating the Silylamino(Disilylamido) Ligand $[(Me_3Si)N\{CH_2CH_2N(SiMe_3)\}_2]^{2-}$ $[N\{N''\}_2]^{2-}$. Synthesis and Crystal Structure of the Dimeric, Non-Metallocene Vanadium(III) Hydride $[\{V(N\{N''\}_2)\}_2(\mu\text{-}H)_2]$. *J. Chem. Soc. Dalton Trans.* **1999**, 3345–3347.

(58) P. Gerlach, C.; Arnold, J. Synthesis of $N(SiMe_3)_2$ Supported Vanadium(III) Complexes, Including Hydrocarbyl, Tetrahydroborate and Azaalkenylidene Derivatives†. *J. Chem. Soc. Dalton Trans.* **1997**, 4795–4806.

(59) Aharonian, G.; Feghali, K.; Gambarotta, S.; Yap, G. P. A. Stability of Trivalent Vanadium Alkyl and Hydride Supported by a Chelating Phosphinimido Ligand. *Organometallics* **2001**, *20*, 2616–2622.

(60) Pyykkö, P. Additive Covalent Radii for Single-, Double-, and Triple-Bonded Molecules and Tetrahedrally Bonded Crystals: A Summary. *J. Phys. Chem. A* **2015**, *119*, 2326–2337.

(61) Wiberg, K. B. Application of the Pople-Santry-Segal CNDO Method to the Cyclopropylcarbinyl and Cyclobutyl Cation and to Bicyclobutane. *Tetrahedron* **1968**, *24*, 1083–1096.

(62) Greiser, T.; Puttfarcken, U.; Rehder, D. The Molecular Structure of Tetracarbonylhydrido(1,1,4,4-Tetraphenyl-1,4-Diphosphabutane)Vanadium(+I), $HV(CO)_4(Ph_2PCH_2CH_2PPh_2)$. *Transit. Met. Chem.* **1979**, *4*, 168–171.

(63) Kuo, J. L.; Gunasekara, T.; Hansen, A.; Vibbert, H. B.; Bohle, F.; Norton, J. R.; Grimme, S.; Quinlivan, P. J. Thermodynamics of $H^+/H^\bullet/H^-/e^-$ Transfer from $[CpV(CO)_3H]^-$: Comparisons to the Isoelectronic $CpCr(CO)_3H$. *Organometallics* **2019**, *38*, 4319–4328.

(64) Werncke, C. G.; Müller, I. The Ambiguous Behaviour of Diphosphines towards the Quasilinear Iron(I) Complex $[Fe(N(SiMe_3)_2)_2]^-$ – Between Inertness, P–C Bond Cleavage and C–C Double Bond Isomerisation. *Chem. Commun.* **2020**, *56*, 2268–2271.

(65) Gallagher, D. J.; Henderson, K. W.; Kennedy, A. R.; O'Hara, C. T.; Mulvey, R. E.; Rowlings, R. B. Hydride Encapsulation in S-Block Metal Inverse Crown Chemistry. *Chem. Commun.* **2002**, 376–377.

(66) Graham, D. V; Kennedy, A. R.; Mulvey, R. E.; O'Hara, C. T. A Polymeric Solvent-Free Variant of a Hydridomagnesium Inverse Crown. *Acta Crystallogr. Sect. C* **2006**, *62*, m366--m368.

(67) Blair, V. L.; Carrella, L. M.; Clegg, W.; Klett, J.; Mulvey, R. E.; Rentschler, E.; Russo, L. Structural and Magnetic Insights into the Trinuclear Ferrocenophane and Unexpected Hydrido Inverse Crown Products of Alkali-Metal-Mediated Manganation(II) of Ferrocene. *Chem. – A Eur. J.* **2009**, *15*, 856–863.

(68) Faust, M.; Bryan, A. M.; Mansikkamäki, A.; Vasko, P.; Olmstead, M. M.; Tuononen, H. M.;

Grandjean, F.; Long, G. J.; Power, P. P. The Instability of Ni{N(SiMe$_3$)$_2$}$_2$: A Fifty Year Old Transition Metal Silylamide Mystery. *Angew. Chem. Int. Ed.* **2015**, *54*, 12914–12917.

(69) James, A. M.; Laxman, R. K.; Fronczek, F. R.; Maverick, A. W. Phosphorescence and Structure of a Tetrameric Copper(I)−Amide Cluster. *Inorg. Chem.* **1998**, *37*, 3785–3791.

(70) Hitchcock, P. B.; Lappert, M. F.; Pierssens, L. J.-M. Synthesis and X-Ray Molecular Structures of the Silver(I) Amides [{Ag[μ-N(SiMe$_3$)$_2$]}$_4$] and [{Ag[μ-NCMe$_2$(CH$_2$)$_3$CMe$_2$]}$_4$]. *Chem. Commun.* **1996**, 1189–1190.

(71) Pyykkö, P.; Atsumi, M. Molecular Single-Bond Covalent Radii for Elements 1–118. *Chem. – A Eur. J.* **2009**, *15*, 186–197.

(72) Riddlestone, I. M.; Urbano, J.; Phillips, N.; Kelly, M. J.; Vidovic, D.; Bates, J. I.; Taylor, R.; Aldridge, S. Salt Metathesis for the Synthesis of M–Al and M–H–Al Bonds. *Dalton Trans.* **2013**, *42*, 249–258.

(73) Tan, G.; Szilvási, T.; Inoue, S.; Blom, B.; Driess, M. An Elusive Hydridoaluminum(I) Complex for Facile C–H and C–O Bond Activation of Ethers and Access to Its Isolable Hydridogallium(I) Analogue: Syntheses, Structures, and Theoretical Studies. *J. Am. Chem. Soc.* **2014**, *136*, 9732–9742.

(74) Anand, B. N.; Krossing, I.; Nöth, H. Synthesis and X-Ray Crystal Structure of (Tmp)$_2$Al−Fe(Cp)(CO)$_2$: An Alanyl-Containing Iron Complex with a Tricoordinated Aluminum Atom. *Inorg. Chem.* **1997**, *36*, 1979–1981.

(75) Bau, R.; Ho, D. M.; Gibbins, S. G. The Binary Metal Hydrido Anion Hexahydroferrate(4-). X-Ray Structural Characterization. *J. Am. Chem. Soc.* **1981**, *103*, 4960–4962.

(76) Bau, R.; Chiang, M. Y.; Ho, D. M.; Gibbins, S. G.; Emge, T. J.; Koetzle, T. F. X-Ray and Neutron Diffraction Studies of the Polyhydrido Complex FeH$_6$Mg$_4$Br$_{3.5}$Cl$_{0.5}$(C$_4$H$_8$O)$_8$: Discussion of Binary Transition-Metal Hydride Anions of the Type [MHx]$^{N-}$. *Inorg. Chem.* **1984**, *23*, 2823–2829.

(77) Turley, J. W.; Rinn, H. W. Crystal Structure of Aluminum Hydride. *Inorg. Chem.* **1969**, *8*, 18–22.

(78) Nakamoto, K. *Infrared and Raman Spectra of Inorganic and Coordination Compounds : Applications in Coordination, Organometallic, and Bioinorganic Chemistry*; John Wiley & Sons, Incorporated: New York, UNITED STATES, 2009.

(79) Belkova, N. V; Epstein, L. M.; Filippov, O. A.; Shubina, E. S. IR Spectroscopy of Hydrides and Its Application to Hydrogen Bonding and Proton Transfer Studies. In *Spectroscopic Properties of Inorganic and Organometallic Compounds: Techniques, Materials and Applications, Volume 43*; The Royal Society of Chemistry, 2012; Vol. 43, pp 1–28.

(80) Choukroun, R.; Lorber, C.; Vendier, L.; Lepetit, C. Vanadocene-Mediated Ionization of Water in the Aqua Species $[H_2O{\cdot}B(C_6F_5)_3]$: Structural Characterization of the Hydride and Hydroxide Complexes $[Cp_2V(\mu\text{-}H)B(C_6F_5)_3]$ and $[Cp_2V(\mu\text{-}OH)B(C_6F_5)_3]$. *Organometallics* **2006**, *25*, 1551–1553.

(81) Humphries, T. D.; Munroe, K. T.; Decken, A.; McGrady, G. S. Lewis Base Complexes of AlH_3: Prediction of Preferred Structure and Stoichiometry. *Dalton Trans.* **2013**, *42*, 6965–6978.

(82) Linn Donald E.; Gibbins, S. G. Solution Spectroscopic and Chemical Properties of the Complex Hydride $[FeH_6]^{4-}$. *Inorg. Chem.* **1997**, *36*, 3461–3465.

(83) Bürger, H.; Cichon, J.; Goetze, U.; Wannagat, U.; Wismar, H. J. Beiträgezur Chemie Der Silicium-Stickstoff-Verbindungen: CVII. Darstellung, Schwingungsspektren Und Normalkoordinatenanalyse von Disilylamiden Der 3. Gruppe: $M[N(SiMe_3)_2]_3$ Mit M = Al, Ga Und In. *J. Organomet. Chem.* **1971**, *33*, 1–12.

Supporting information

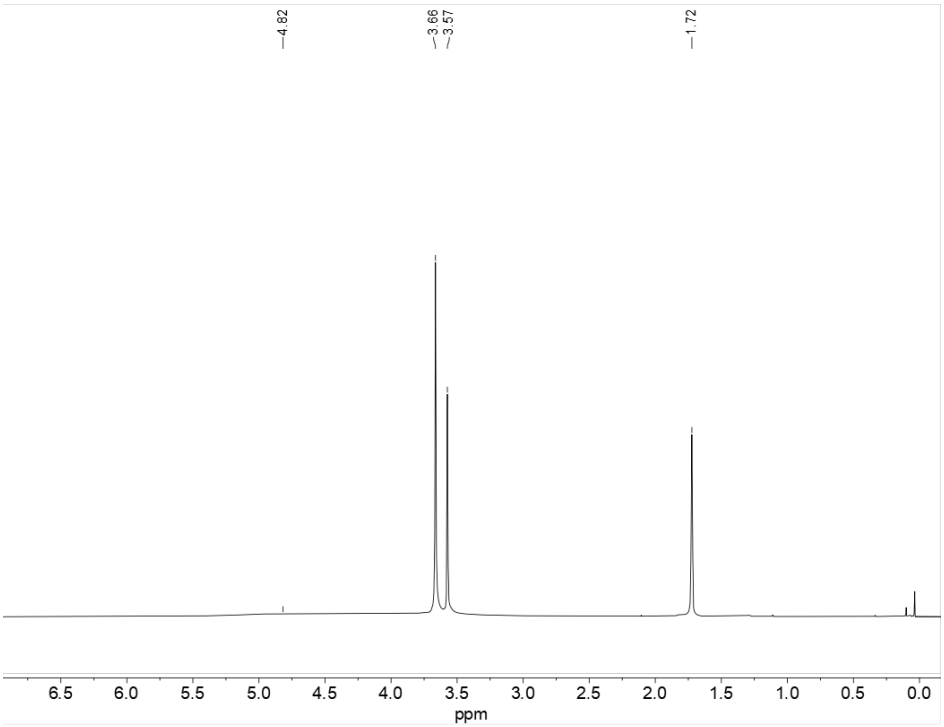

Figure 4.S1: ^{1}H-NMR spectrum of [VH{N(SiMe$_3$)$_2$}$_3$][Li(12-crown-4)$_2$] (**2**) in THF-D$_8$.

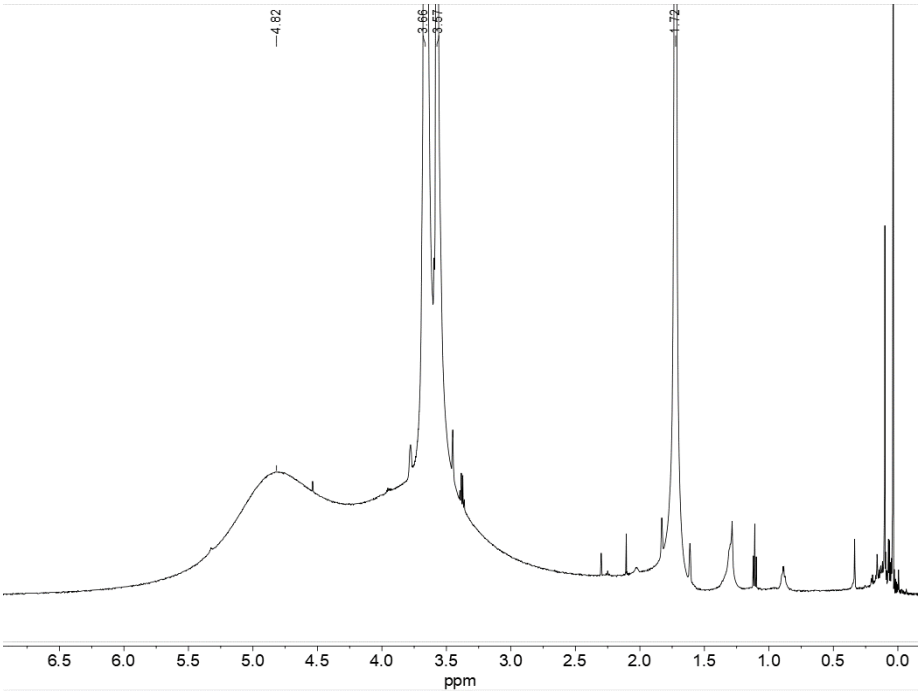

Figure 4.S2: ^{1}H-NMR spectrum of [VH{N(SiMe$_3$)$_2$}$_3$][Li(12-crown-4)$_2$] (**2**) in THF-D$_8$ (magnified).

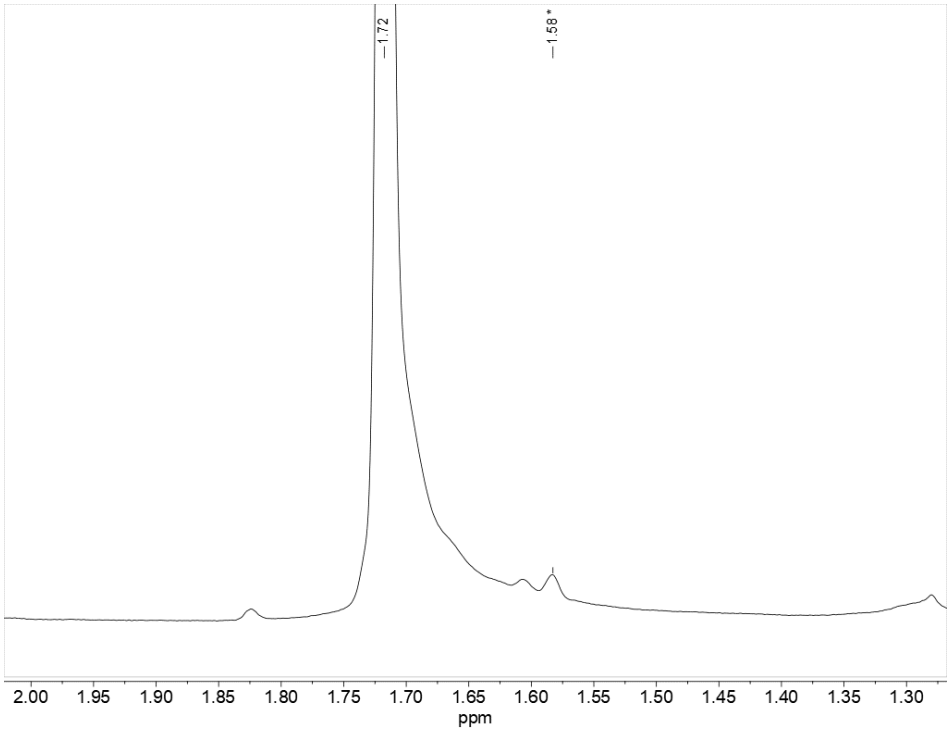

Figure 4.S3: ^{1}H-NMR spectrum of [VH{N(SiMe$_3$)$_2$}$_3$][Li(12-crown-4)$_2$] (**2**) in THF-D$_8$ (Evans' method). Signal at 1.58 ppm is due to THF-D$_8$ in capillary for magnetic moment measurement.

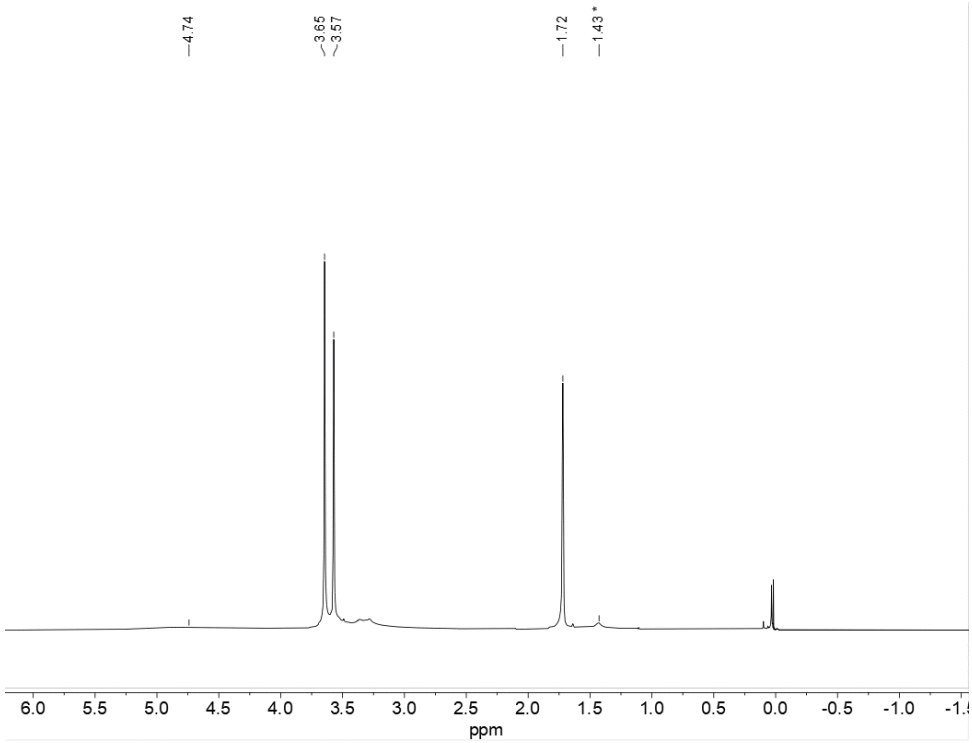

Figure 4.S4: ^{1}H-NMR spectrum of [VD{N(SiMe$_3$)$_2$}$_3$][Li(12-crown-4)$_2$] (**2D**) in THF-D$_8$. The signal at 1.43 ppm is due to THF-D$_8$ in capillary for magnetic moment measurement.

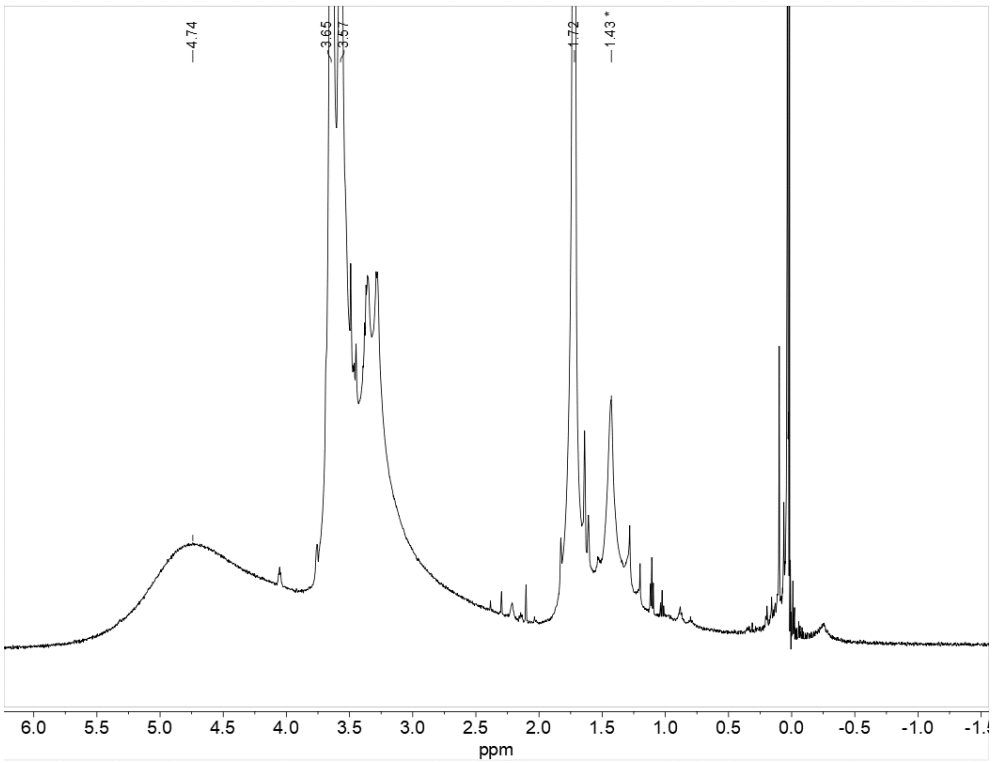

Figure 4.S5: ^{1}H-NMR spectrum of [VD{N(SiMe$_3$)$_2$}$_3$][Li(12-crown-4)$_2$] (**2D**) in THF-D$_8$ (magnified).

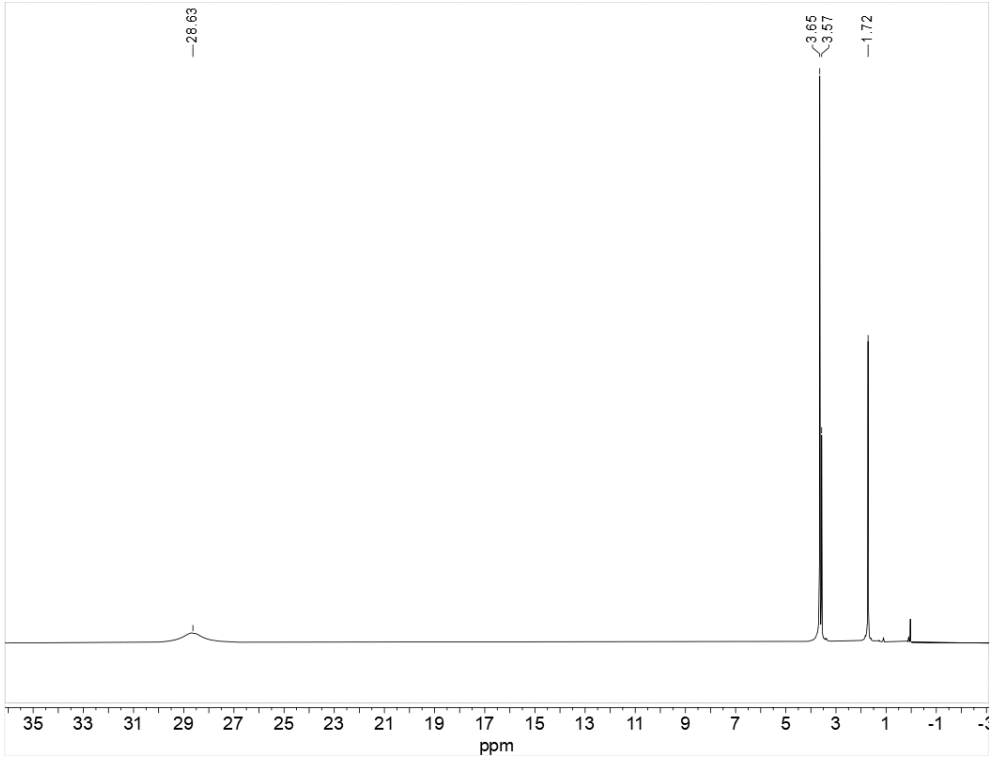

Figure 4.S6: ^{1}H-NMR spectrum of [Cr{N(SiMe$_3$)$_2$}$_3$][Li(12-crown-4)$_2$] (**3**) in THF-D$_8$.

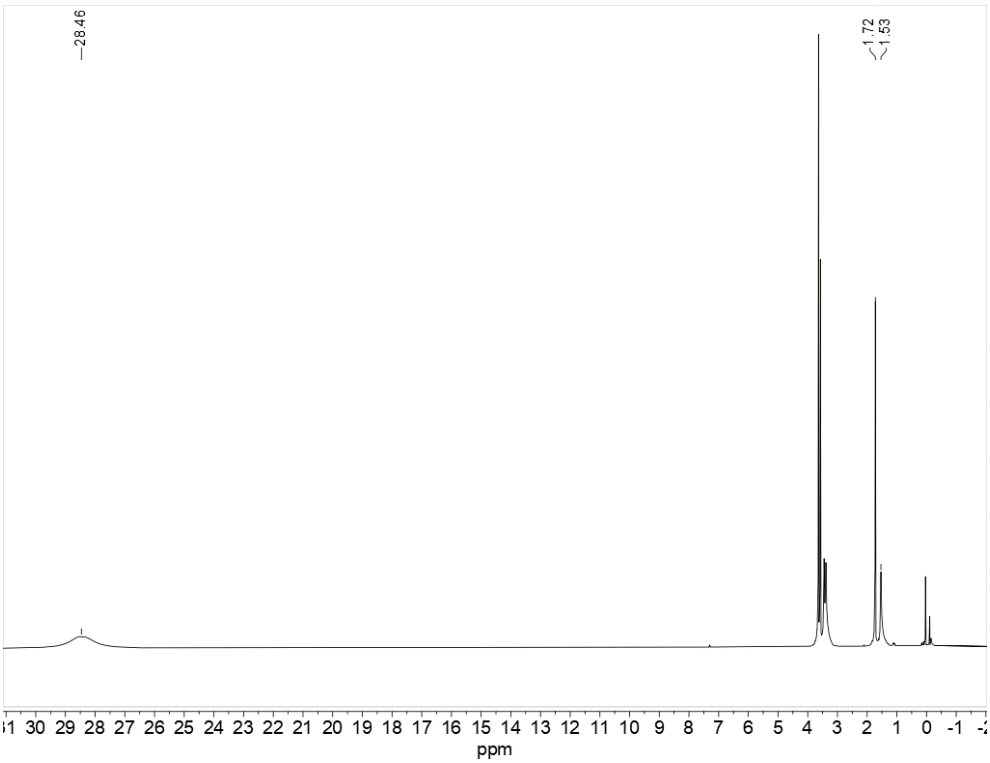

Figure 4.S7: ^{1}H-NMR spectrum of [Cr{N(SiMe$_3$)$_2$}$_3$][Li(12-crown-4)$_2$] (**3**) in THF-D$_8$ (Evans' method). The signal at 1.53 ppm is due to THF-D$_8$ in capillary for magnetic moment measurement.

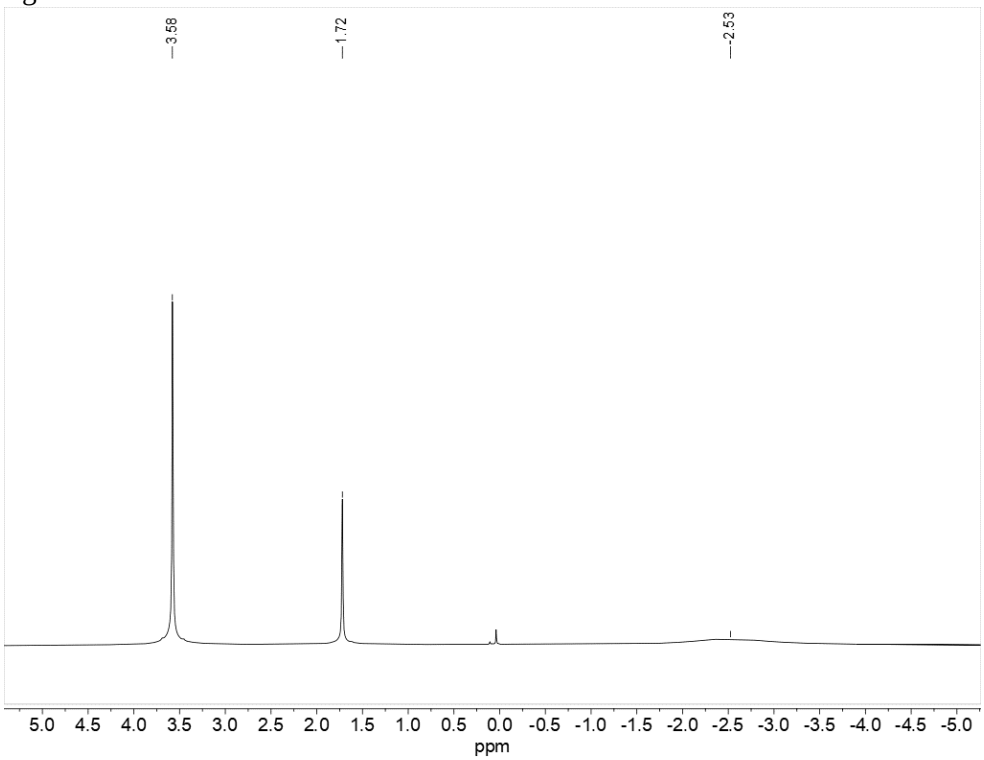

Figure 4.S8: ^{1}H-NMR spectrum of [Fe{N(SiMe$_3$)$_2$}$_3$][Li(12-crown-4)$_2$] (**4**) in THF-D$_8$.

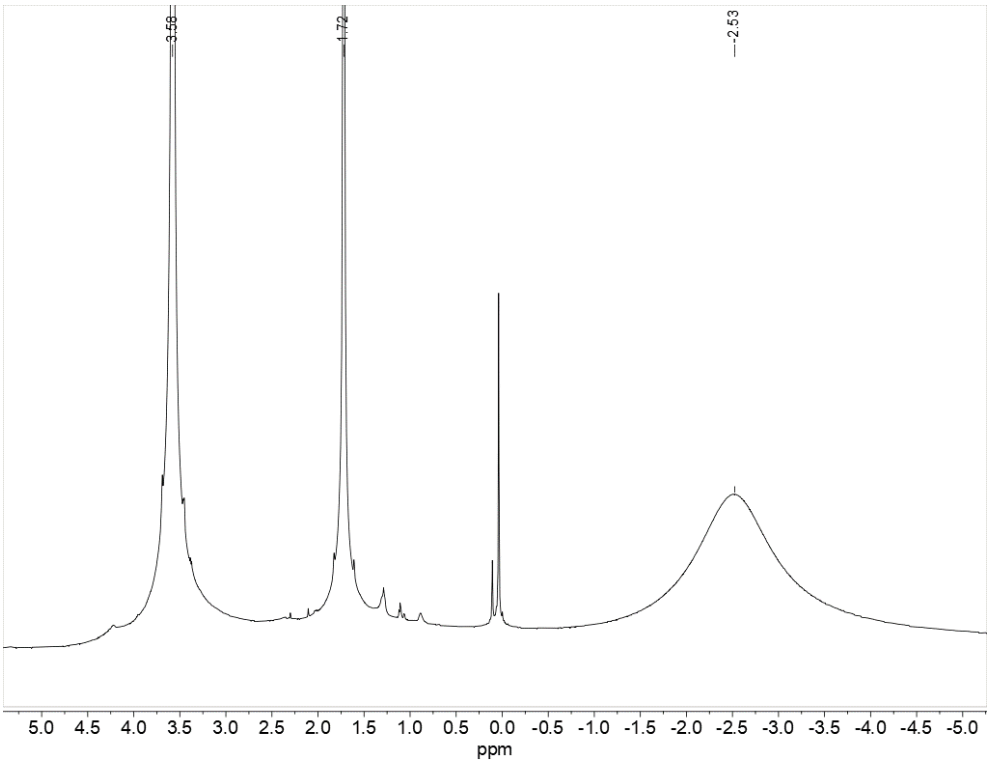

Figure 4.S9: ^{1}H-NMR spectrum of [Fe{N(SiMe$_3$)$_2$}$_3$][Li(12-crown-4)$_2$] (**4**) in THF-D$_8$ (magnified).

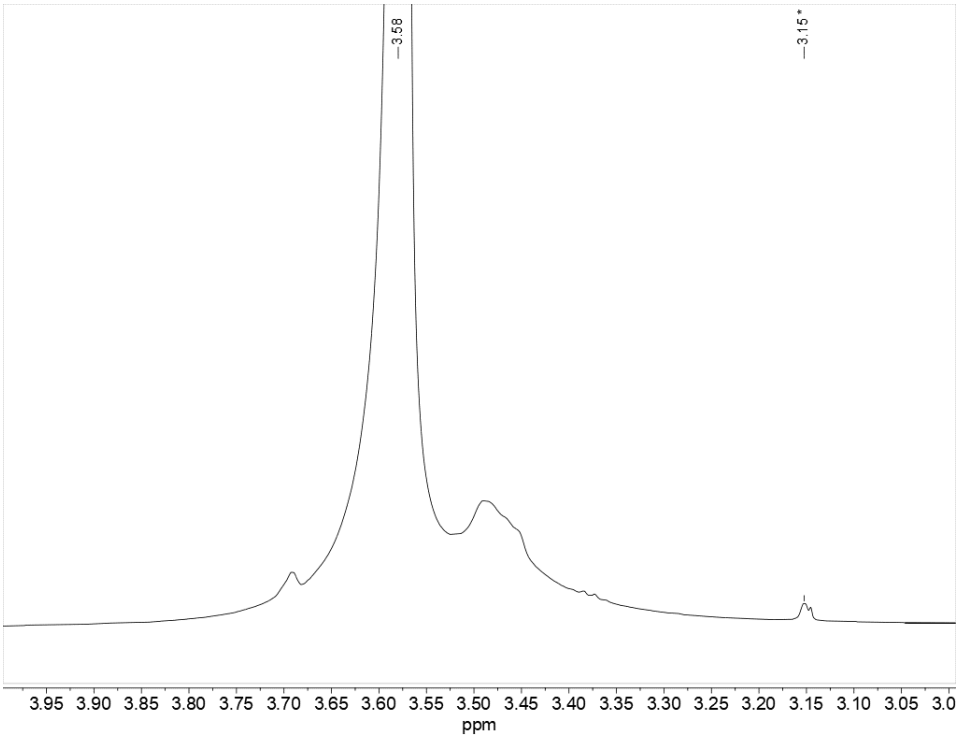

Figure 4.S10: ^{1}H-NMR spectrum of [Fe{N(SiMe$_3$)$_2$}$_3$][Li(12-crown-4)$_2$] (**4**) in THF-D$_8$ (Evans' method). The signal at 3.15 ppm is due to THF-D$_8$ in capillary for magnetic moment measurement.

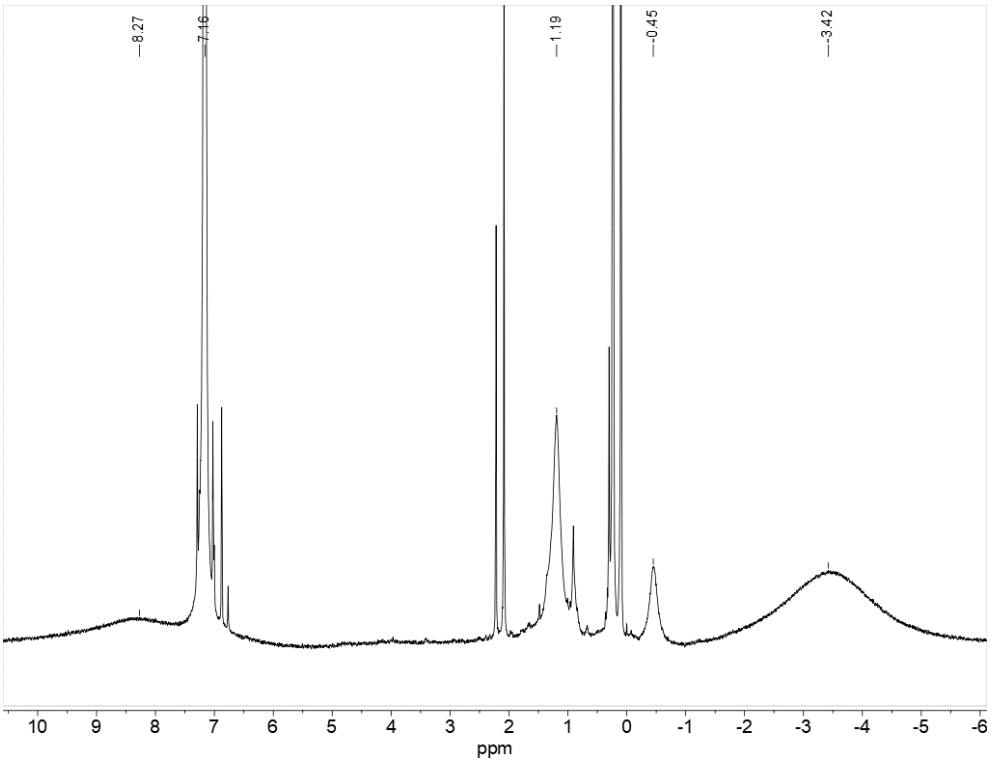

Figure 4.S11: ^{1}H-NMR spectrum of [Fe(μ$_2$-H){N(SiMe$_3$)$_2$}$_2$(μ$_2$-Li)]$_2$ (**5**) in benzene-D$_6$.

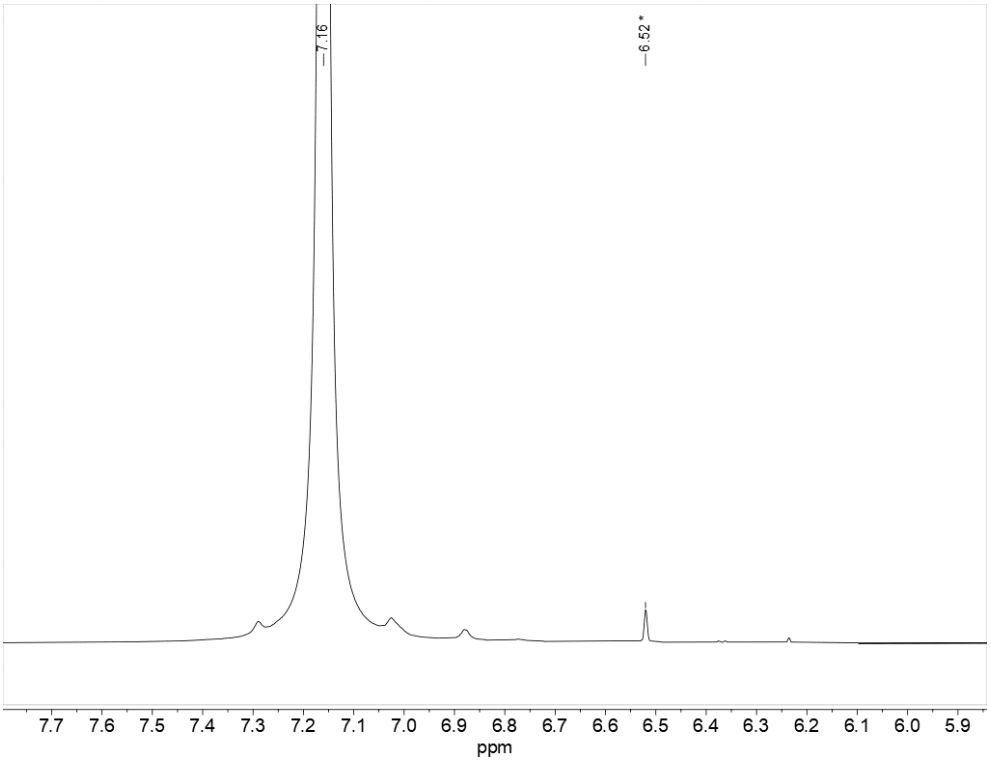

Figure 4.S12: ^{1}H-NMR spectrum of [Fe(μ$_2$-H){N(SiMe$_3$)$_2$}$_2$(μ$_2$-Li)]$_2$ (**5**) in benzene-D$_6$. (Evans' method). The signal at 6.52 ppm is due to benzene-D$_6$ in capillary for magnetic moment measurement.

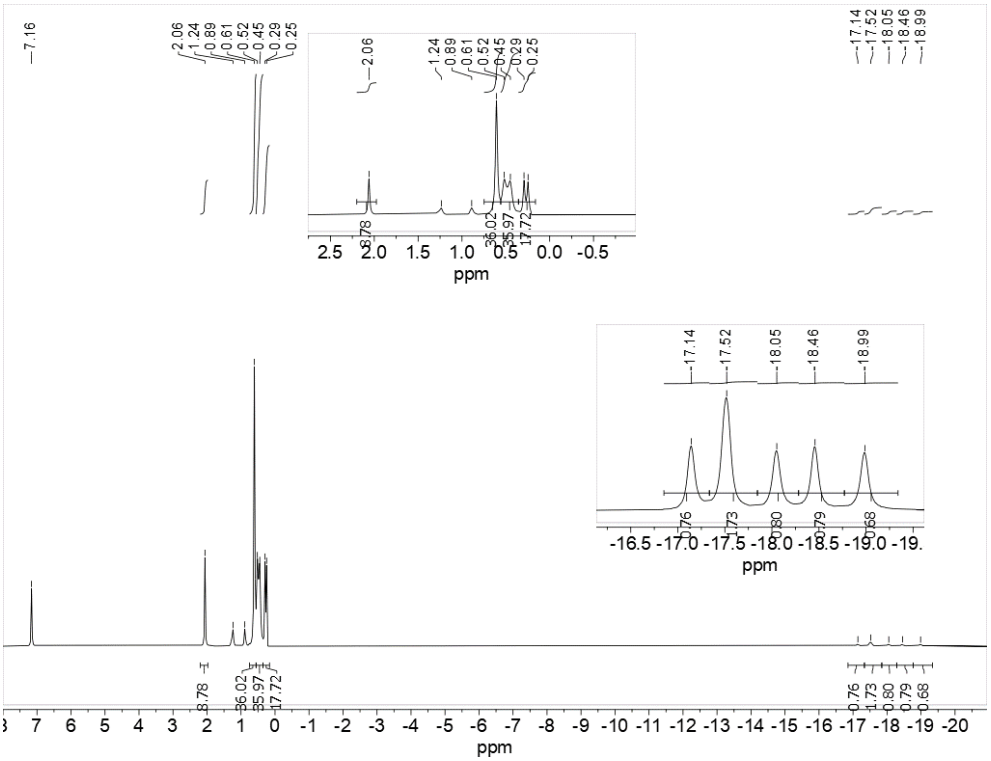

Figure 4.S13: ^{1}H-NMR spectrum of $Fe(\mu_2\text{-}H)_6[Al\{N(SiMe_3)_2\}_2]_2$ $[Al\{N(SiMe_3)_2\}(NMe_3)]$ (**6**) in benzene-D_6.

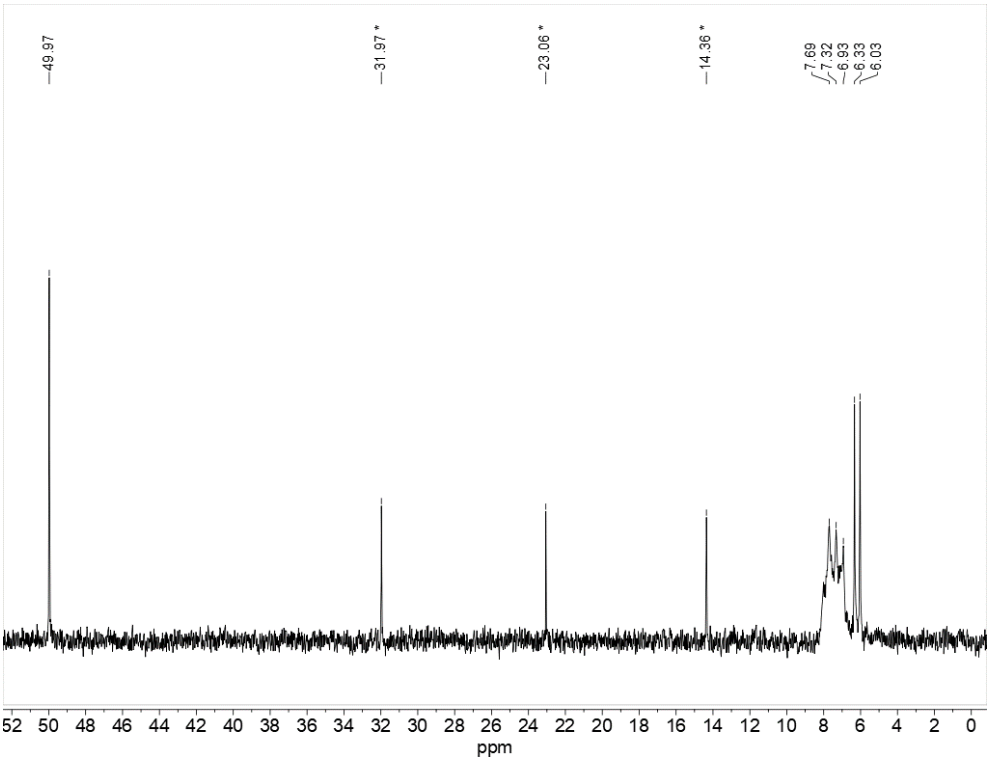

Figure 4.S14: ^{13}C-NMR spectrum of $Fe(\mu_2\text{-}H)_6[Al\{N(SiMe_3)_2\}_2]_2$ $[Al\{N(SiMe_3)_2\}(NMe_3)]$ (**6**) in benzene-D_6. Signals marked with an asterisk are due to residual hexanes.

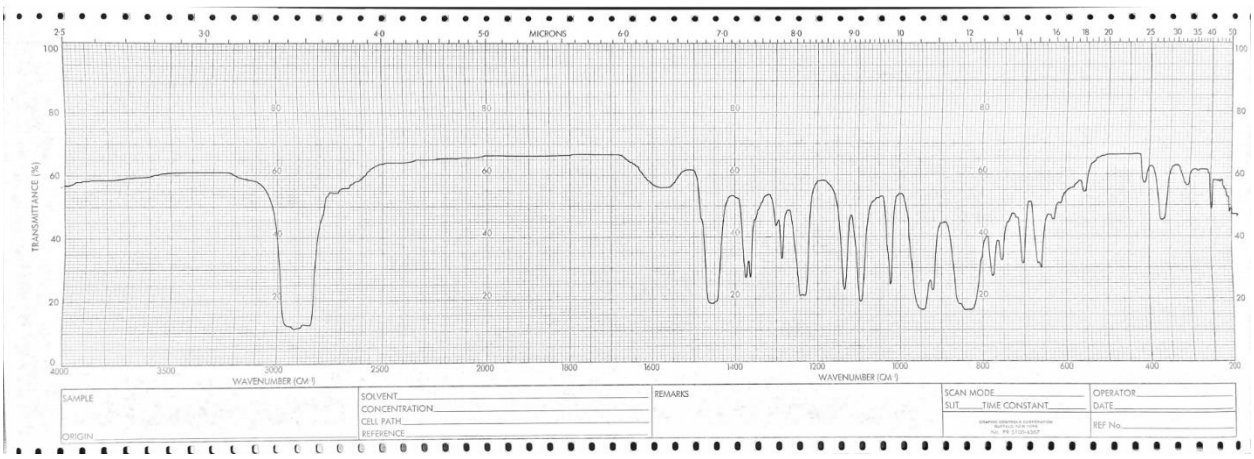

Figure 4.S15: Infrared spectrum of $[VH\{N(SiMe_3)_2\}_3][Li(12\text{-crown-}4)_2]$ (**2**) (Nujol mull, CsI windows)

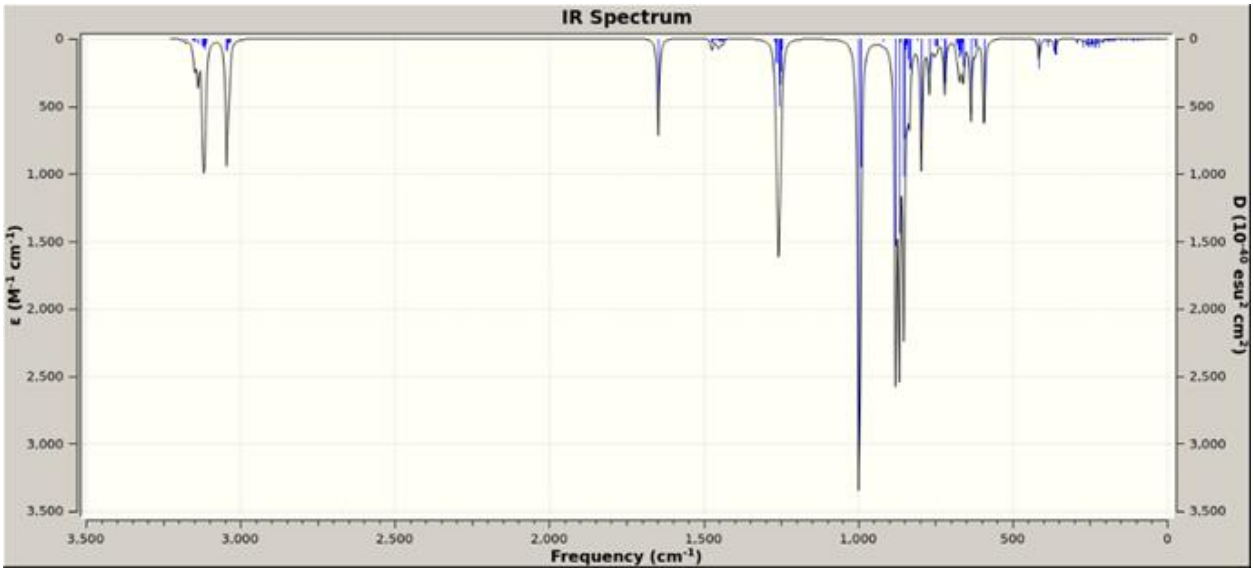

Figure 4.S16: Calculated infrared spectrum of the anion $[VH\{N(SiMe_3)_2\}_3]^-$ (**2**)

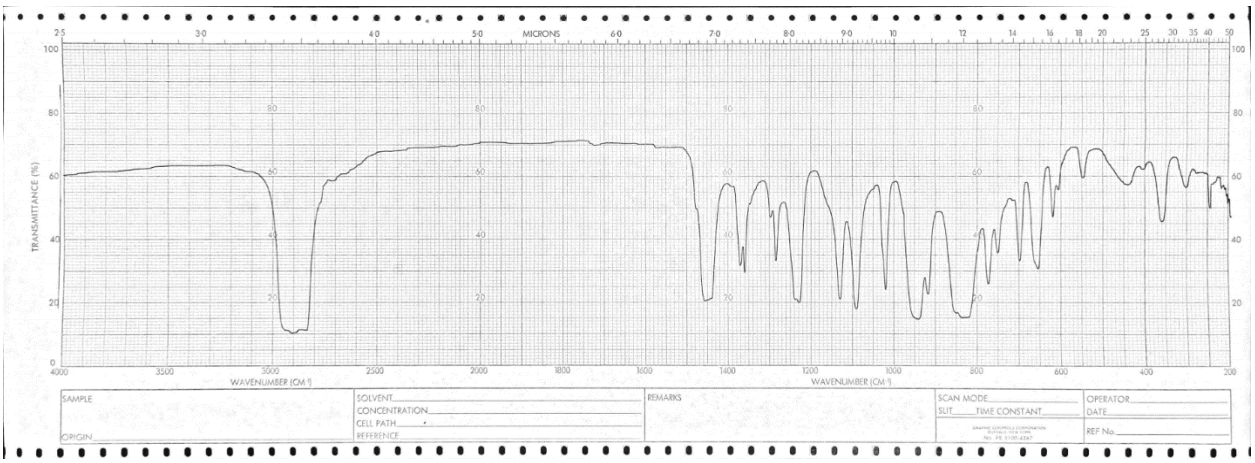

Figure 4.S17: Infrared spectrum of [VD{N(SiMe$_3$)$_2$}$_3$][Li(12-crown-4)$_2$] (**2D**) (Nujol mull, CsI windows)

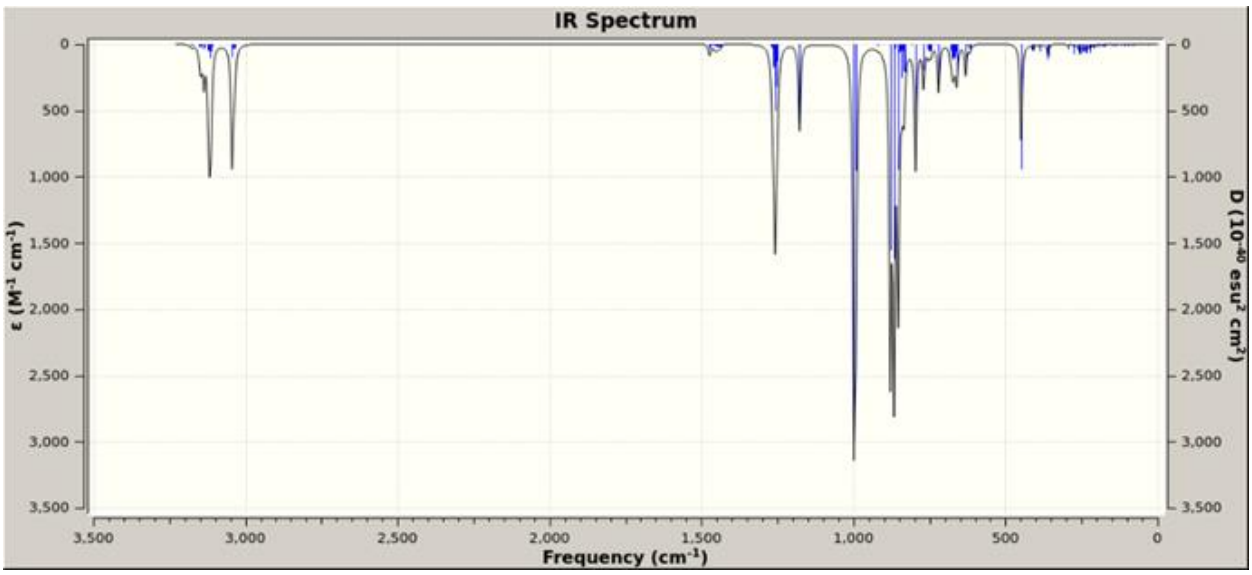

Figure 4.S18: Calculated infrared spectrum of the anion [VD{N(SiMe$_3$)$_2$}$_3$]$^-$ (**2D**)

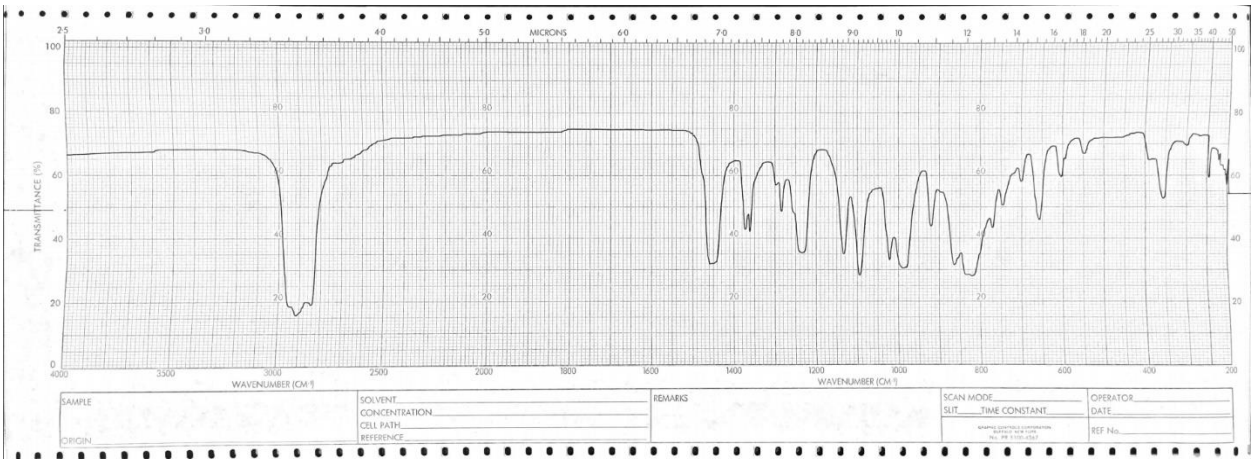

Figure 4.S19: Infrared spectrum of $[Cr\{N(SiMe_3)_2\}_3][Li(12\text{-crown-}4)_2]$ (**3**) (Nujol mull, CsI windows)

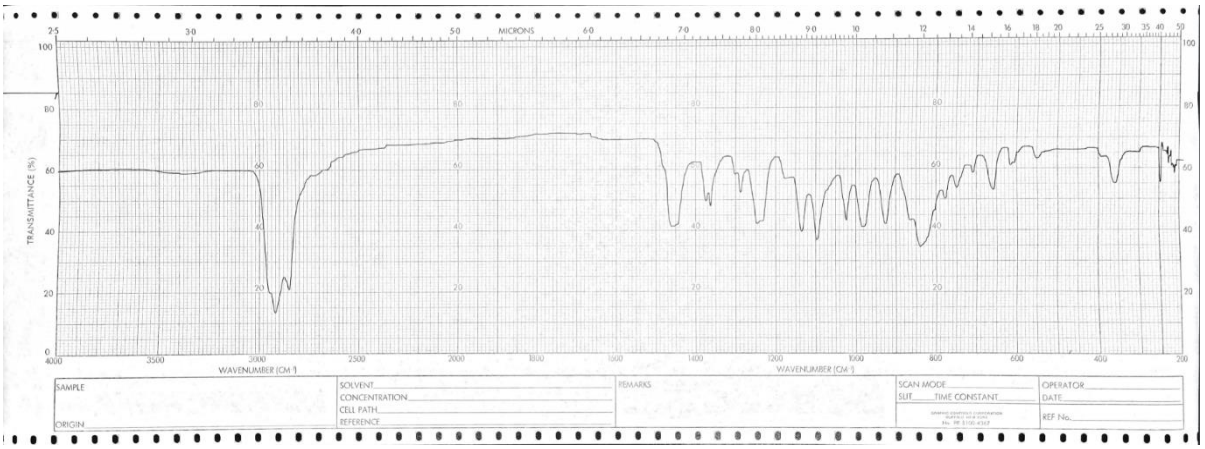

Figure 4.S20: Infrared spectrum of $[Fe\{N(SiMe_3)_2\}_3][Li(12\text{-crown-}4)_2]$ (**4**) (Nujol mull, CsI windows)

Figure 4.S21: Infrared spectrum of $[Fe(\mu_2\text{-}H)\{N(SiMe_3)_2\}_2(\mu_2\text{-}Li)]_2$ (**5**) (Nujol mull, CsI windows)

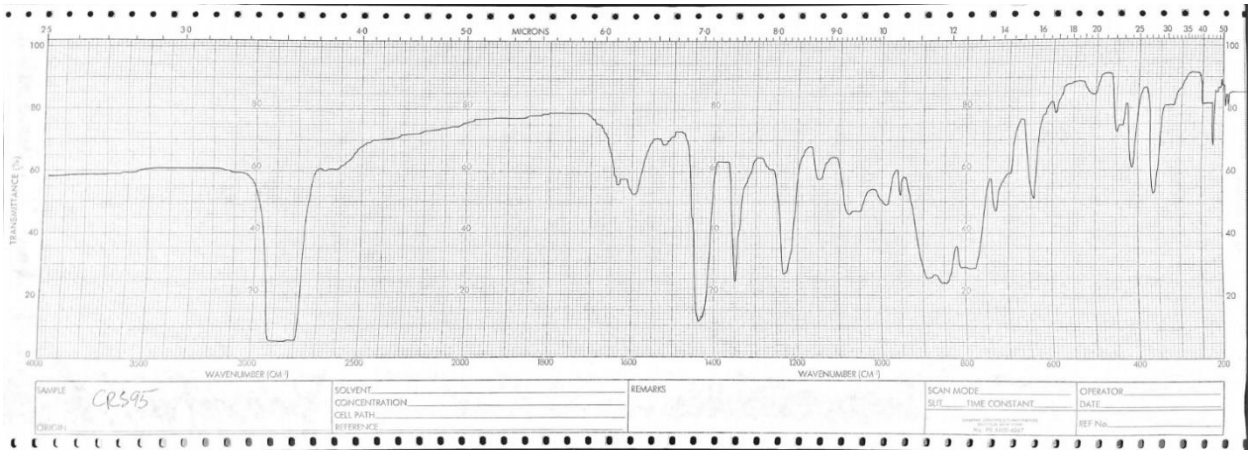

Figure 4.S22: Infrared spectrum of $Fe(\mu_2\text{-}H)_6[Al\{N(SiMe_3)_2\}_2]_2[Al\{N(SiMe_3)_2\}(NMe_3)]$ (**6**) (Nujol mull, CsI windows)

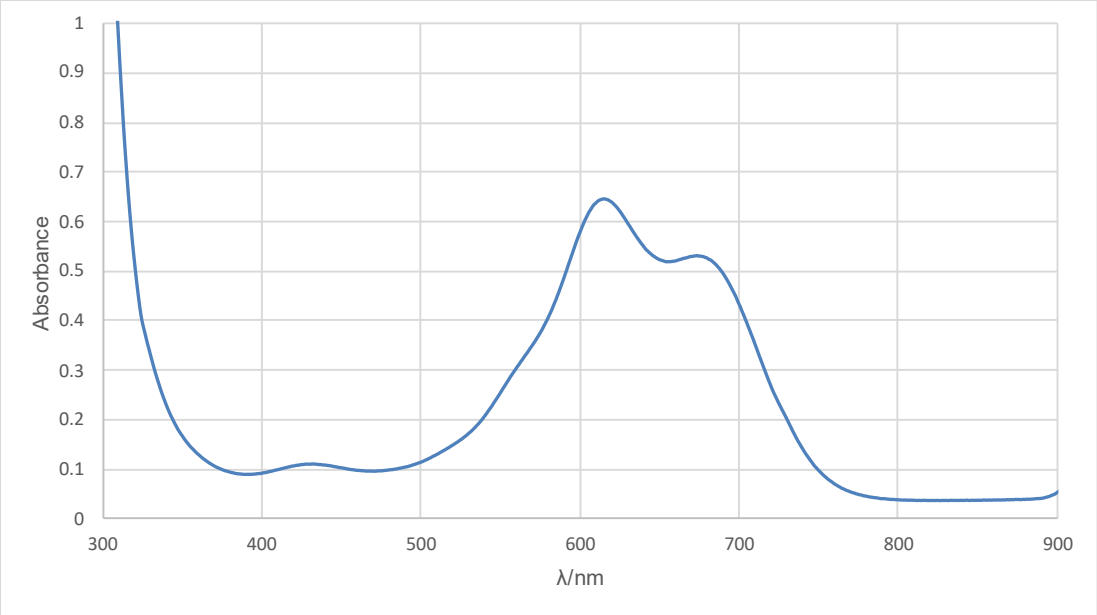

Figure 4.S23: UV-Vis spectrum of [VH{N(SiMe$_3$)$_2$}$_3$][Li(12-crown-4)$_2$] (**2**) at 25 °C (1.1 mM in diethyl ether, 1 cm path length).

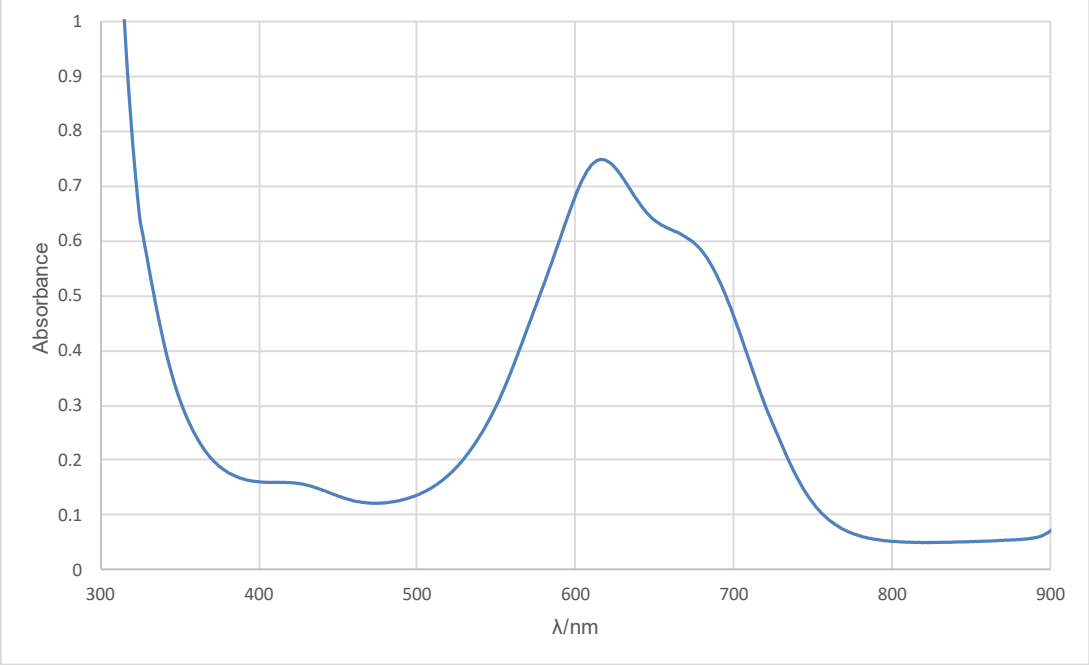

Figure 4.S24: UV-Vis spectrum of [VD{N(SiMe$_3$)$_2$}$_3$][Li(12-crown-4)$_2$] (**2D**) at 25 °C (1.1 mM in diethyl ether, 1 cm path length).

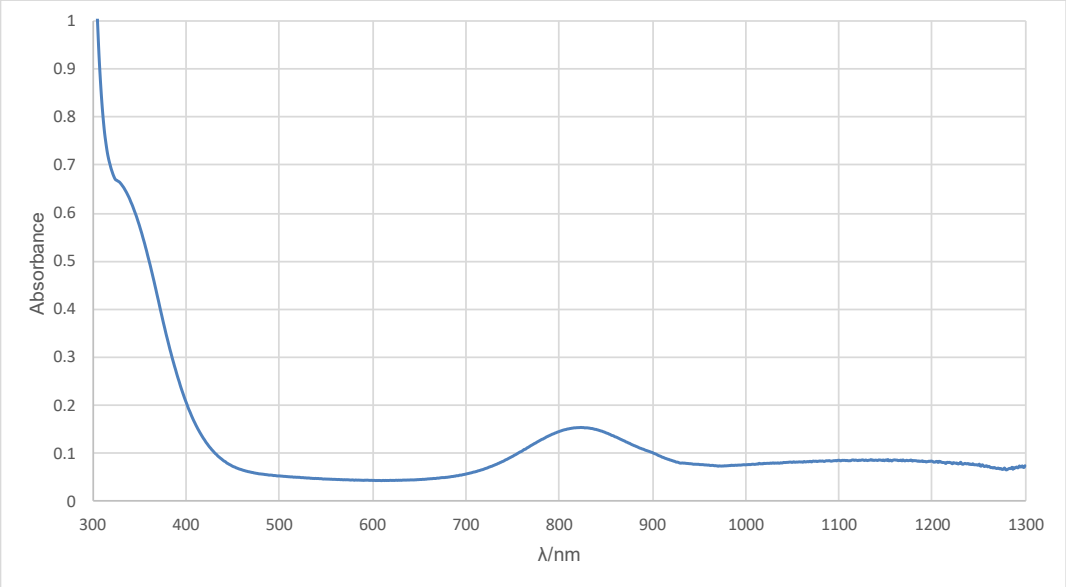

Figure 4.S25: UV-Vis spectrum of [Cr{N(SiMe$_3$)$_2$}$_3$][Li(12-crown-4)$_2$] (**3**) at 25 °C (1.1 mM in hexanes, 1 cm path length)

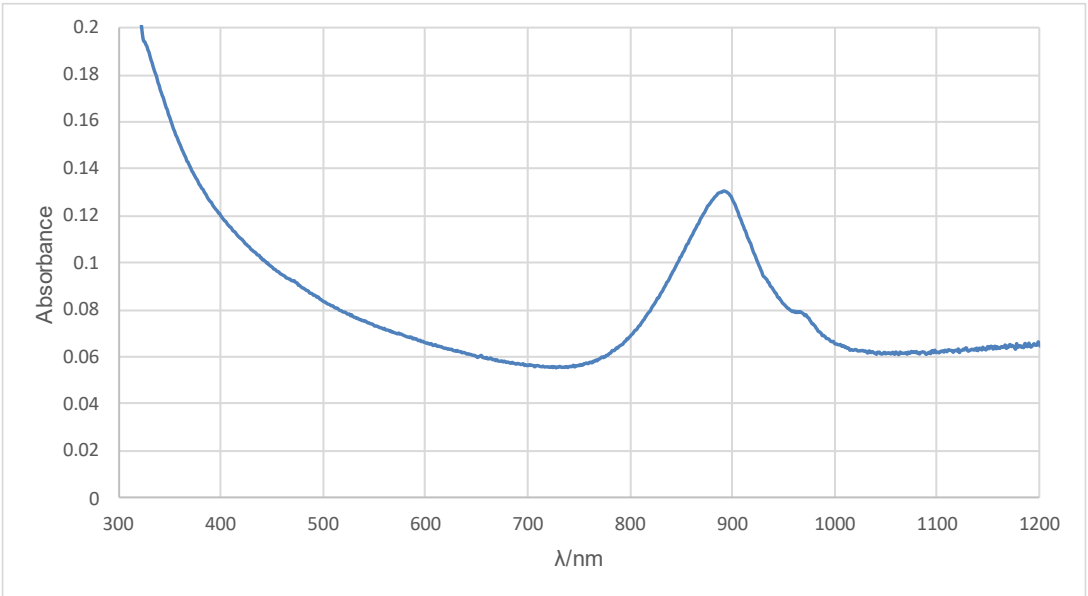

Figure 4.S26: UV-Vis spectrum of [Fe{N(SiMe$_3$)$_2$}$_3$][Li(12-crown-4)$_2$] (**4**) at 25 °C (1.1 mM in hexanes, 1 cm path length)

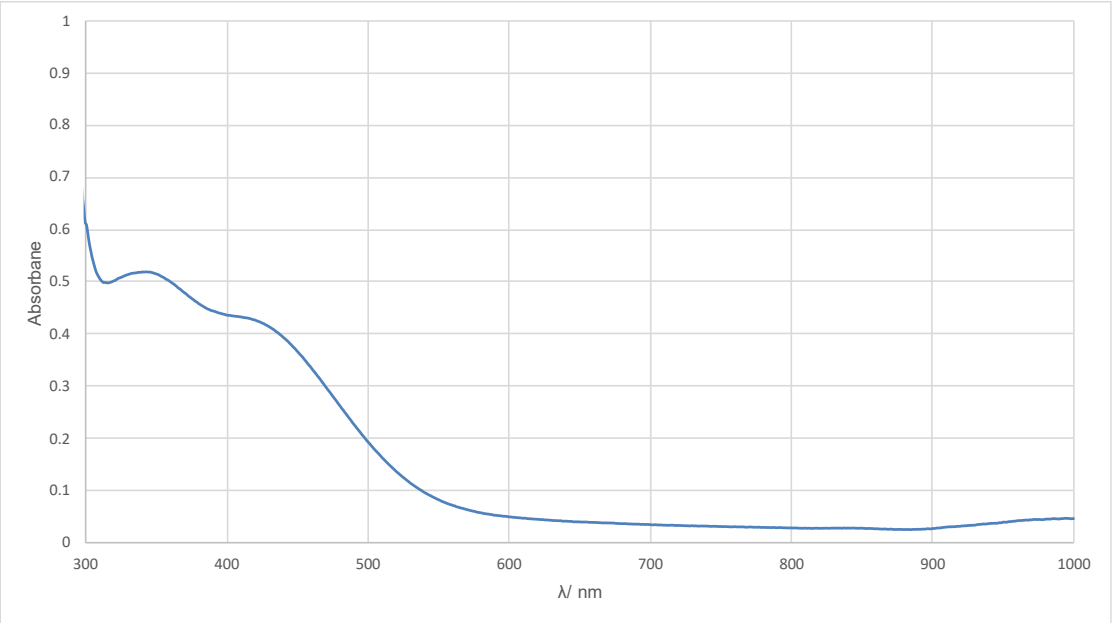

Figure 4.S27: UV-Vis spectrum of $Fe(\mu_2\text{-}H)_6[Al\{N(SiMe_3)_2\}_2]_2[Al\{N(SiMe_3)_2\}(NMe_3)]$ (**6**) at 25 °C (1.5 mM in hexanes, 1 cm path length)

Table 4.S1: Crystallographic and X-ray Data Collection Parameters of Complex **1**

Empirical formula	$C_{54}H_{150}Al_3LiN_6O_3Si_{12}V$
Formula weight	1407.69
Temperature/K	90.15
Crystal system	monoclinic
Space group	P2/c
a/Å	25.863(2)
b/Å	14.8207(13)
c/Å	25.578(2)
α/°	90
β/°	113.7981(11)
γ/°	90
Volume/Å^3	8970.4(13)
Z	4
ρ_{calc}g/cm^3	1.042
μ/mm^{-1}	0.336
F(000)	3092.0
Crystal size/mm^3	0.772 × 0.626 × 0.52
Radiation	MoKα (λ = 0.71073)
2Θ range for data collection/°	3.252 to 61.27
Index ranges	$-37 \leq h \leq 37$, $-21 \leq k \leq 21$, $-36 \leq l \leq 36$
Reflections collected	104006
Independent reflections	27610 [R_{int} = 0.0426, R_{sigma} = 0.0351]
Data/restraints/parameters	27610/42/869
Goodness-of-fit on F^2	1.036
Final R indexes [I>=2σ (I)]	R_1 = 0.0481, wR_2 = 0.1205
Final R indexes [all data]	R_1 = 0.0647, wR_2 = 0.1319
Largest diff. peak/hole / e Å^{-3}	1.32/-0.51

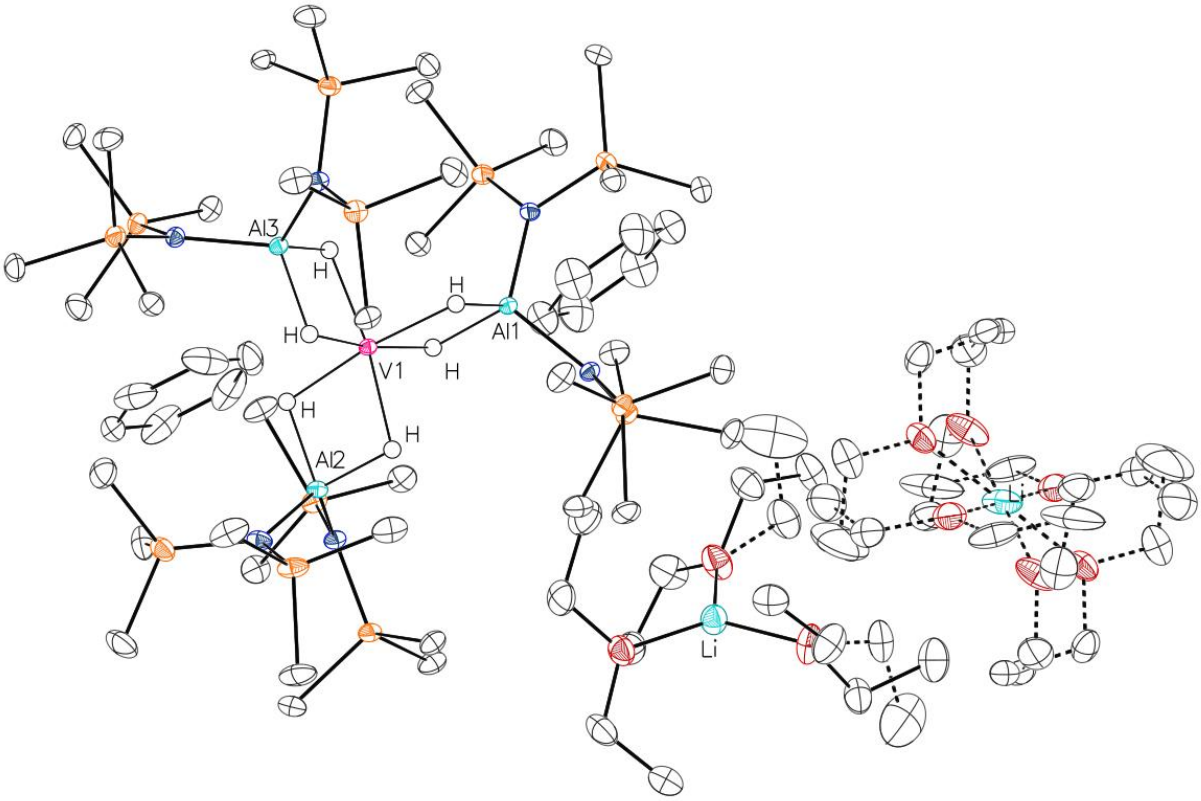

Figure 4.S28: Molecular structure of **1** showing $Li(OEt_2)_3$ cations (each of ½ occupancy in the crystal) and solvent of crystallization.

Table 4.S2: Crystallographic and X-ray Data Collection Parameters of Complex **2**

Empirical formula	$C_{34}H_{87}LiN_3O_8Si_6V$
Formula weight	892.48
Temperature/K	190
Crystal system	monoclinic
Space group	$P2_1/c$
a/Å	10.7353(3)
b/Å	29.7282(9)
c/Å	16.3760(5)
α/°	90
β/°	93.5020(10)
γ/°	90
Volume/Å3	5216.5(3)
Z	4
ρcalcg/cm3	1.136
μ/mm-1	3.250
F(000)	1944.0
Crystal size/mm3	0.661 × 0.509 × 0.158
Radiation	CuKα (λ = 1.54178)
2Θ range for data collection/°	5.946 to 136.71
Index ranges	$-12 \leq h \leq 11$, $-35 \leq k \leq 35$, $-19 \leq l \leq 19$
Reflections collected	67726
Independent reflections	9322 [Rint = 0.0368, Rsigma = 0.0229]
Data/restraints/parameters	9322/25/612
Goodness-of-fit on F2	1.046
Final R indexes [I>=2σ (I)]	R1 = 0.0354, wR2 = 0.1050
Final R indexes [all data]	R1 = 0.0365, wR2 = 0.1062
Largest diff. peak/hole / e Å-3	0.46/-0.33

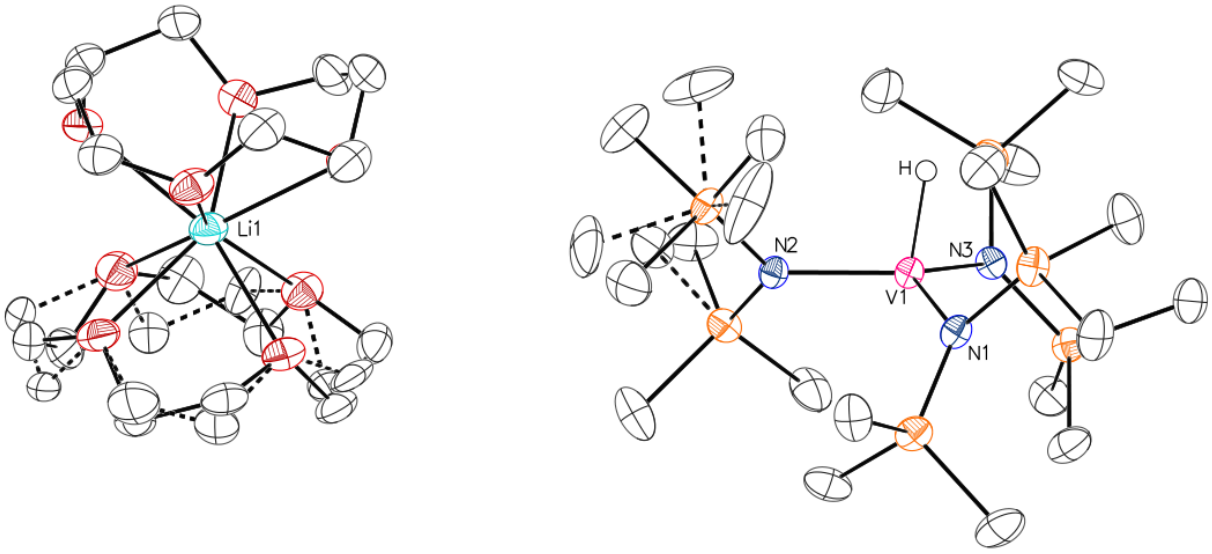

Figure 4.S29: Molecular structure of **2** showing Li(12-crown-4) cation and modeled disorder.

Table 4.S3: Crystallographic and X-ray Data Collection Parameters of Complex **2D**

Empirical formula	$C_{34}H_{86}DLiN_3O_8Si_6V$
Formula weight	893.49
Temperature/K	190.15
Crystal system	monoclinic
Space group	$P2_1/c$
a/Å	10.7648(10)
b/Å	29.768(3)
c/Å	16.4193(13)
α/°	90
β/°	93.443(5)
γ/°	90
Volume/Å^3	5252.1(8)
Z	4
ρ_{calc}g/cm^3	1.130
μ/mm^{-1}	3.228
F(000)	1944.0
Crystal size/mm^3	0.444 × 0.265 × 0.221
Radiation	CuKα (λ = 1.54178)
2Θ range for data collection/°	5.938 to 144.696
Index ranges	$-13 \leq h \leq 12$, $-36 \leq k \leq 36$, $-20 \leq l \leq 20$
Reflections collected	33086
Independent reflections	10352 [R_{int} = 0.0450, R_{sigma} = 0.0414]
Data/restraints/parameters	10352/335/678
Goodness-of-fit on F^2	1.039
Final R indexes [I>=2σ (I)]	R_1 = 0.0487, wR_2 = 0.1372
Final R indexes [all data]	R_1 = 0.0536, wR_2 = 0.1430
Largest diff. peak/hole / e Å^{-3}	0.73/-0.54

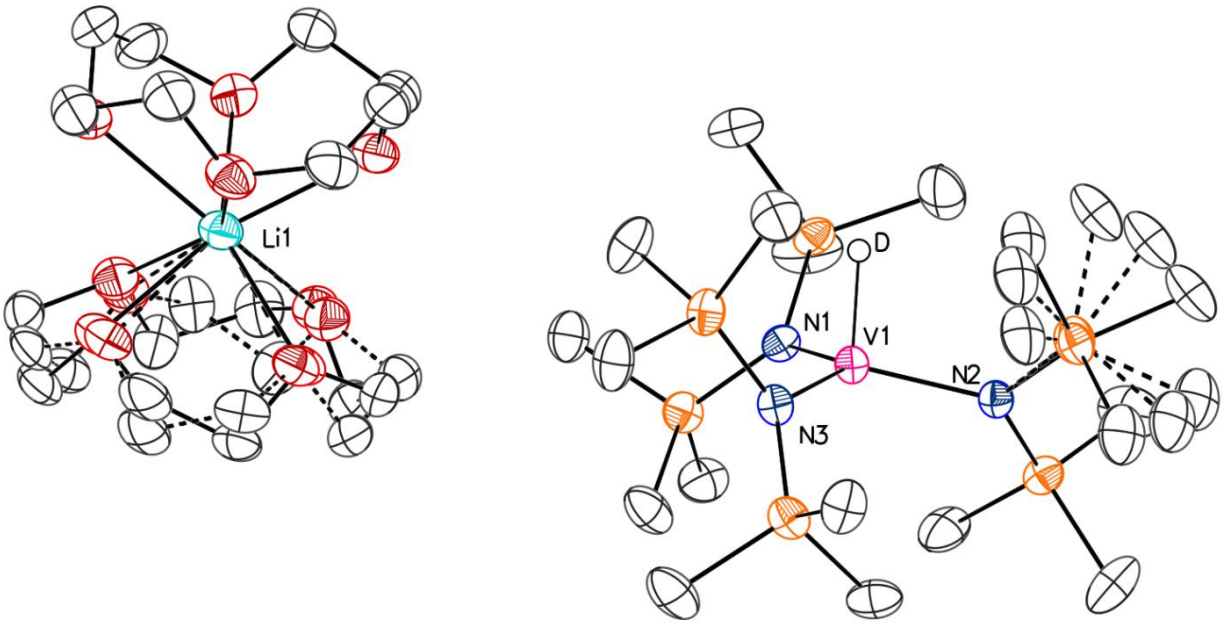

Figure 4.S30: Molecular structure of **2D** showing Li(12-crown-4) cation and modeled disorder.

Table 4.S4: Crystallographic and X-ray Data Collection Parameters of Complex **3**

Empirical formula	$C_{38}H_{96}CrLiN_3O_9Si_6$
Formula weight	966.65
Temperature/K	190.15
Crystal system	triclinic
Space group	P-1
a/Å	11.9331(15)
b/Å	13.5968(18)
c/Å	18.7871(19)
α/°	90.568(9)
β/°	104.363(9)
γ/°	99.895(9)
Volume/Å^3	2904.6(6)
Z	2
ρ_{calc}g/cm^3	1.105
μ/mm^{-1}	3.158
F(000)	1056.0
Crystal size/mm^3	0.397 × 0.38 × 0.319
Radiation	CuKα (λ = 1.54178)
2Θ range for data collection/°	4.862 to 144.9
Index ranges	$-14 \leq h \leq 14$, $-16 \leq k \leq 15$, $-23 \leq l \leq 23$
Reflections collected	20889
Independent reflections	11480 [R_{int} = 0.0265, R_{sigma} = 0.0410]
Data/restraints/parameters	11480/283/763
Goodness-of-fit on F^2	1.077
Final R indexes [I>=2σ (I)]	R_1 = 0.0535, wR_2 = 0.1470
Final R indexes [all data]	R_1 = 0.0625, wR_2 = 0.1593
Largest diff. peak/hole / e Å^{-3}	0.45/-0.47
Empirical formula	$C_{38}H_{96}CrLiN_3O_9Si_6$

Table 4.S5: Crystallographic and X-ray Data Collection Parameters of Complex **4**

Empirical formula	$C_{38}H_{96}FeLiN_3O_9Si_6$
Formula weight	970.50
Temperature/K	190.15
Crystal system	triclinic
Space group	P-1
a/Å	11.9969(3)
b/Å	13.5747(4)
c/Å	18.7390(5)
α/°	90.0948(15)
β/°	104.6492(15)
γ/°	100.3333(15)
Volume/Å^3	2901.09(14)
Z	2
ρ_{calc}g/cm^3	1.111
μ/mm^{-1}	0.427
F(000)	1060.0
Crystal size/mm^3	0.384 × 0.376 × 0.279
Radiation	MoKα (λ = 0.71073)
2Θ range for data collection/°	3.054 to 61.122
Index ranges	$-17 \leq h \leq 17$, $-19 \leq k \leq 19$, $-26 \leq l \leq 26$
Reflections collected	34230
Independent reflections	17725 [R_{int} = 0.0278, R_{sigma} = 0.0410]
Data/restraints/parameters	17725/211/684
Goodness-of-fit on F^2	1.048
Final R indexes [I>=2σ (I)]	R_1 = 0.0406, wR_2 = 0.1029
Final R indexes [all data]	R_1 = 0.0661, wR_2 = 0.1153
Largest diff. peak/hole / e Å^{-3}	0.59/-0.36

Table 4.S6: Crystallographic and X-ray Data Collection Parameters of Complex **5**

Empirical formula	$C_{24}H_{74}Fe_2Li_2N_4Si_8$
Formula weight	769.17
Temperature/K	90.15
Crystal system	monoclinic
Space group	P2/n
a/Å	9.2300(8)
b/Å	13.5763(12)
c/Å	17.7458(16)
α/°	90
β/°	90.8610(10)
γ/°	90
Volume/Å^3	2223.5(3)
Z	2
ρ_{calc}g/cm^3	1.149
μ/mm^{-1}	0.887
F(000)	832.0
Crystal size/mm^3	0.318 × 0.175 × 0.13
Radiation	MoKα (λ = 0.71073)
2Θ range for data collection/°	3 to 61.1
Index ranges	$-13 \leq h \leq 13$, $-19 \leq k \leq 19$, $-25 \leq l \leq 25$
Reflections collected	35628
Independent reflections	6828 [R_{int} = 0.0342, R_{sigma} = 0.0260]
Data/restraints/parameters	6828/0/216
Goodness-of-fit on F^2	1.110
Final R indexes [I>=2σ (I)]	R_1 = 0.0341, wR_2 = 0.0838
Final R indexes [all data]	R_1 = 0.0478, wR_2 = 0.0903
Largest diff. peak/hole / e Å^{-3}	0.38/-0.46

Table 4.S7: Crystallographic and X-ray Data Collection Parameters of Complex **6**

Empirical formula	$C_{72}H_{224}N_{12}Al_6Si_{20}Fe_2$
Formula weight	2094.00
Temperature/K	90(2)
Crystal system	monoclinic
Space group	$P2_1/n$
a/Å	25.656(2)
b/Å	11.8558(13)
c/Å	42.028(5)
α/°	90
β/°	94.994(11)
γ/°	90
Volume/Å^3	12735(2)
Z	4
ρ_{calc}g/cm^3	1.092
μ/mm^{-1}	4.316
F(000)	4600.0
Crystal size/mm^3	0.304 × 0.115 × 0.093
Radiation	CuKα (λ = 1.54178)
2Θ range for data collection/°	4.204 to 139.074
Index ranges	$-30 \leq h \leq 30$, $-13 \leq k \leq 14$, $-50 \leq l \leq 50$
Reflections collected	61888
Independent reflections	22850 [R_{int} = 0.0498, R_{sigma} = 0.0493]
Data/restraints/parameters	22850/14/1158
Goodness-of-fit on F^2	1.013
Final R indexes [I>=2σ (I)]	R_1 = 0.0409, wR_2 = 0.0977
Final R indexes [all data]	R_1 = 0.0544, wR_2 = 0.1049
Largest diff. peak/hole / e Å^{-3}	0.92/-0.35

Figure 4.S31: Photographs of crystalline (left) and powdered (right) $[VH\{N(SiMe_3)_2\}_3][Li(12\text{-crown-}4)_2]$ (**2**).

Figure 4.S32: Photographs of crystalline (left) and powdered (right) [VD{N(SiMe3)2}3][Li(12-crown-4)2] (**2D**).

Figure 4.S33: Photograph of powdered $Fe(\mu_2\text{-}H)_6[Al\{N(SiMe_3)_2\}_2]_2[Al\{N(SiMe_3)_2\}(NMe_3)]$ (**6**)

Table 4.S8. xyz-coordinates for the optimized structures

Anion **1**

172

V	-0.020929	-0.003998	-0.038759
Si	0.691273	5.177643	-0.190091
Si	0.445988	3.607764	-2.707128
Si	4.251731	2.530875	0.168802
Si	2.773997	2.435776	2.744248
Si	3.025731	-2.136270	-2.707326
Si	4.236910	-3.182401	-0.179943
Si	0.107180	-4.840501	0.170014
Si	0.823148	-3.570275	2.735519
Si	-4.927024	-2.051641	-0.113265
Si	-3.436196	-1.571710	-2.653277
Si	-3.603911	1.215802	2.683274
Si	-4.353580	2.393410	0.073175
Al	1.217991	2.162166	0.020036
Al	1.368479	-2.072647	-0.038992
Al	-2.561938	-0.085021	-0.010717
H	-0.201966	1.635221	0.825337
H	-0.067660	-1.658243	-0.895895
C	0.065397	4.979480	1.566719
H	-0.909938	4.490876	1.569446
H	-0.043006	5.962942	2.035624
H	0.739823	4.390981	2.185721

N	0.770699	3.670973	-1.016103
C	-0.505160	6.425247	-0.956978
H	-0.297506	6.661078	-2.002155
H	-0.434827	7.356186	-0.383802
H	-1.533474	6.064700	-0.884791
N	2.757598	2.545407	1.025123
C	2.353290	6.061013	-0.085380
H	3.071113	5.436533	0.449968
H	2.252681	7.008374	0.454686
H	2.758965	6.276791	-1.077663
N	2.922628	-2.452219	-1.015314
C	1.444330	4.912534	-3.652656
H	1.314008	5.924559	-3.262878
H	1.142274	4.917758	-4.705294
H	2.509982	4.672772	-3.610195
N	0.912530	-3.572652	1.016313
C	-1.366824	3.876157	-3.145443
H	-1.974662	3.102626	-2.670560
H	-1.498203	3.785841	-4.228948
H	-1.754983	4.846496	-2.833342
N	-3.652947	-1.277104	-0.968316
C	0.855465	1.976663	-3.526326
H	1.880915	1.637056	-3.380746
H	0.680595	2.083650	-4.602774
H	0.195148	1.193798	-3.153569
N	-3.657984	1.096900	0.965924

C	5.564839	3.654064	0.939483
H	5.229276	4.692847	0.993664
H	6.464688	3.621900	0.315914
H	5.848222	3.336122	1.945613
C	4.066084	3.127416	-1.599165
H	3.368215	2.511428	-2.167615
H	5.039866	3.069899	-2.096317
H	3.708794	4.156079	-1.640302
C	5.014437	0.818463	0.070811
H	5.429389	0.505818	1.030882
H	5.818895	0.793706	-0.670764
H	4.257751	0.087353	-0.225070
C	4.032249	1.192478	3.401115
H	3.831947	0.197751	2.997090
H	3.951827	1.134259	4.491471
H	5.064080	1.456239	3.156325
C	1.133901	1.898481	3.464732
H	0.305765	2.570777	3.239502
H	1.228007	1.821007	4.553015
H	0.872671	0.916859	3.067644
C	3.235145	4.085853	3.549434
H	4.257007	4.381743	3.301593
H	3.163119	4.000583	4.639061
H	2.570794	4.892274	3.230785
C	3.648891	-3.649649	-3.661399
H	4.612798	-4.021981	-3.307505

H	3.756643	-3.396440	-4.721479
H	2.924832	-4.464963	-3.583916
C	4.174835	-0.705528	-3.129729
H	3.816854	0.206021	-2.646306
H	4.175888	-0.534671	-4.211280
H	5.204077	-0.872757	-2.808129
C	1.390345	-1.683449	-3.492791
H	0.650114	-2.484271	-3.472058
H	1.565120	-1.410029	-4.538746
H	0.961851	-0.822299	-2.980559
C	4.118047	-5.060988	-0.107560
H	3.210895	-5.351877	0.425412
H	4.978117	-5.484801	0.421343
H	4.083511	-5.499702	-1.108581
C	4.375645	-2.562408	1.584670
H	4.616431	-1.498776	1.593793
H	5.174485	-3.097952	2.108069
H	3.457367	-2.703000	2.151226
C	5.931035	-2.794140	-0.925348
H	6.040436	-3.096813	-1.968271
H	6.690433	-3.325863	-0.341612
H	6.143423	-1.725041	-0.854757
C	0.681308	-4.971258	-1.610891
H	0.492982	-4.052187	-2.166617
H	0.127530	-5.775866	-2.105177
H	1.748029	-5.187016	-1.673369

C	-1.756689	-4.625733	0.119152
H	-2.215952	-4.840433	1.085738
H	-2.201529	-5.295296	-0.623277
H	-2.007265	-3.597961	-0.156046
C	0.422178	-6.555514	0.908189
H	1.486224	-6.805387	0.916200
H	-0.093453	-7.299032	0.290830
H	0.043009	-6.652935	1.927983
C	2.042044	-4.797152	3.506490
H	1.821994	-5.822718	3.201590
H	1.979486	-4.748566	4.598935
H	3.072742	-4.579997	3.218231
C	-0.871881	-4.068225	3.403551
H	-1.640957	-3.388524	3.029199
H	-0.860873	-3.991649	4.495832
H	-1.163668	-5.088136	3.143618
C	1.139225	-1.902284	3.522960
H	2.085798	-1.439625	3.245449
H	1.119002	-2.019510	4.611949
H	0.344698	-1.211036	3.238123
C	-5.415071	-3.739490	-0.812980
H	-5.724089	-3.718560	-1.859517
H	-6.254673	-4.123673	-0.223435
H	-4.586668	-4.444782	-0.714943
C	-6.509913	-1.030215	-0.058459
H	-6.314846	-0.077328	0.437607

H	-7.294017	-1.553771	0.498534
H	-6.886761	-0.822208	-1.063735
C	-4.447508	-2.431889	1.660188
H	-3.586871	-3.102223	1.684638
H	-5.279442	-2.924820	2.173895
H	-4.193864	-1.537934	2.226341
C	-2.769696	-3.288952	-3.046108
H	-1.786681	-3.411308	-2.586468
H	-2.650386	-3.397285	-4.129347
H	-3.410658	-4.096502	-2.689678
C	-2.238973	-0.423976	-3.523228
H	-2.474910	0.636281	-3.429658
H	-2.243248	-0.679511	-4.589016
H	-1.230266	-0.573662	-3.139750
C	-5.071632	-1.386984	-3.594863
H	-5.878827	-2.000270	-3.188144
H	-4.928905	-1.673206	-4.642328
H	-5.400759	-0.344743	-3.574142
C	-2.331507	0.112940	3.504307
H	-2.434999	-0.947879	3.276838
H	-2.412764	0.240601	4.589460
H	-1.331100	0.417115	3.194363
C	-5.281938	0.804776	3.459409
H	-6.048854	1.520473	3.154237
H	-5.206592	0.835654	4.551733
H	-5.627410	-0.191191	3.173748

C	-3.180244	2.945920	3.309333
H	-2.194066	3.248100	2.949765
H	-3.147730	2.933028	4.403802
H	-3.901209	3.708495	3.006103
C	-5.988665	3.014263	0.795823
H	-6.738289	2.219698	0.837073
H	-6.376787	3.811041	0.152193
H	-5.875404	3.426515	1.801058
C	-4.760564	1.894155	-1.688192
H	-3.875352	1.570542	-2.236999
H	-5.180693	2.756096	-2.216461
H	-5.483672	1.078559	-1.713262
C	-3.218011	3.884593	-0.039947
H	-3.163357	4.427232	0.905764
H	-3.562090	4.579913	-0.811754
H	-2.207151	3.559743	-0.299369
H	1.420958	-0.671075	0.958616
H	-1.416821	-0.753403	0.989294
H	1.387739	0.788011	-1.002382
H	-1.484315	0.648470	-1.046902

Anion **2**

83

V	0.00020	0.00008	-0.22846
H	0.00088	0.00021	-1.90138

Si	2.82004	-0.99564	-1.22059
Si	2.82247	0.69216	1.25682
Si	-0.54621	2.94052	-1.21935
Si	-2.01190	2.09765	1.25613
Si	-2.27442	-1.94242	-1.21908
Si	-0.81041	-2.79227	1.25415
N	1.97319	-0.15121	0.02440
N	-0.85573	1.78439	0.02478
N	-1.11742	-1.63282	0.02419
C	3.07937	0.00255	-2.79427
H	2.11760	0.26047	-3.24272
H	3.65518	-0.58232	-3.51911
H	3.62508	0.92934	-2.59757
C	1.26975	3.01927	-1.67598
H	1.83523	3.48242	-0.86338
H	1.41032	3.62906	-2.57411
H	1.68627	2.03040	-1.85894
C	1.98045	-2.60662	-1.68119
H	2.09549	-3.32908	-0.86915
H	2.44110	-3.03245	-2.57827
H	0.91657	-2.47181	-1.86773
C	4.55392	-1.55587	-0.69655
H	5.01268	-2.07152	-1.54702
H	4.50508	-2.26737	0.13174
H	5.22146	-0.74245	-0.40566
C	4.11119	1.88956	0.56847

H	4.90675	1.37041	0.02895
H	4.57642	2.45115	1.38517
H	3.65674	2.60340	-0.12069
C	3.76245	-0.39845	2.48020
H	3.09040	-1.07621	3.01048
H	4.25140	0.24068	3.22339
H	4.53588	-0.99740	1.99666
C	1.65913	1.72343	2.30654
H	1.15065	2.47665	1.70460
H	2.22603	2.22458	3.09763
H	0.88830	1.11534	2.78820
C	-1.53689	2.66597	-2.79519
H	-1.27815	1.70402	-3.24279
H	-1.31636	3.45696	-3.51956
H	-2.61287	2.67522	-2.60133
C	-0.92917	4.72238	-0.69637
H	-1.96775	4.89387	-0.40685
H	-0.71098	5.37697	-1.54698
H	-0.28952	5.03644	0.13244
C	-1.53759	3.45535	2.48134
H	-0.61677	3.20948	3.01409
H	-2.33737	3.56120	3.22231
H	-1.40156	4.42434	1.99836
C	-2.32545	0.57386	2.30434
H	-2.72261	-0.24303	1.70164
H	-3.04410	0.81398	3.09444

H	-1.41409	0.21028	2.78728
C	-1.54281	-2.66755	-2.79349
H	-0.83849	-1.96438	-3.24310
H	-2.33845	-2.87310	-3.51717
H	-1.01373	-3.60403	-2.59734
C	-3.24817	-0.40849	-1.67847
H	-3.93380	-0.14955	-0.86762
H	-3.84464	-0.59161	-2.57787
H	-2.59905	0.44611	-1.86030
C	-3.62793	-3.16115	-0.69241
H	-3.25898	-4.14635	-0.40072
H	-4.30509	-3.30020	-1.54198
H	-4.21805	-2.76084	0.13598
C	-0.42328	-4.50658	0.56147
H	-1.27434	-4.93589	0.02773
H	-0.16312	-5.19110	1.37545
H	0.41710	-4.46864	-0.13383
C	-2.22181	-3.05910	2.48141
H	-2.46725	-2.13846	3.01468
H	-1.91319	-3.80511	3.22177
H	-3.13030	-3.42467	1.99996
C	0.66878	-2.30601	2.30037
H	1.57399	-2.24348	1.69623
H	0.81955	-3.04950	3.08960
H	0.53146	-1.33501	2.78433
C	-3.69222	2.61689	0.56657

H	-3.63997	3.56752	0.03080
H	-4.41258	2.73555	1.38255
H	-4.08180	1.86886	-0.12607

Complex **6**

158

Fe	-0.03202	0.35603	-0.16186
Si	3.66057	3.56745	-0.80692
Si	2.10825	4.18108	1.71791
Si	1.80466	-4.30270	1.48568
Si	0.97782	-2.05527	3.20138
Si	2.48368	-2.05223	-2.73138
Si	4.44760	-1.57845	-0.49759
Si	-3.11079	-1.89570	-2.57196
Si	-3.68498	-2.68277	0.24523
Si	-4.89192	1.64327	-0.51607
Si	-3.51778	1.93078	2.12254
Al	0.87386	2.40306	-0.48846
Al	1.46566	-1.46883	0.16482
Al	-2.37204	-0.00101	-0.12378
N	-0.20267	3.55300	-1.79102
N	2.19664	3.46194	0.12928
N	1.39372	-2.60741	1.59538
N	2.81184	-1.71264	-1.05837
N	-3.11841	-1.48727	-0.88405
N	-3.52905	1.28572	0.50609

C	-1.46687	3.87470	-1.09980
H	-1.97710	2.96253	-0.79241
H	-2.11331	4.45540	-1.76514
H	-1.24754	4.47092	-0.21503
C	0.46927	4.81549	-2.13610
H	0.73902	5.34978	-1.22771
H	-0.19877	5.43035	-2.74732
H	1.37641	4.60891	-2.70006
C	-0.50095	2.81682	-3.03373
H	0.42776	2.56568	-3.54629
H	-1.11987	3.43754	-3.68887
H	-1.02518	1.89563	-2.79538
C	4.04777	5.29257	-1.44182
H	3.21196	5.75434	-1.97101
H	4.88419	5.22562	-2.14466
H	4.34731	5.96961	-0.64100
C	5.15268	3.00244	0.17035
H	5.36055	3.68262	1.00044
H	6.04044	2.98512	-0.46819
H	5.01493	2.00176	0.58332
C	3.43573	2.46673	-2.30699
H	3.19187	1.43821	-2.03545
H	4.36255	2.43371	-2.88617
H	2.66002	2.82360	-2.99144
C	0.31448	4.49696	2.15919
H	-0.12251	5.28855	1.54379

H	0.24661	4.82752	3.19943
H	-0.30967	3.60509	2.07239
C	2.97887	5.84185	1.76857
H	4.06128	5.75570	1.65084
H	2.79544	6.29933	2.74546
H	2.60701	6.52814	1.00413
C	2.85935	3.09000	3.03093
H	2.30142	2.15812	3.13222
H	2.84405	3.59542	4.00100
H	3.89628	2.83606	2.80100
C	0.59278	-5.40916	2.40444
H	0.51746	-5.20024	3.47215
H	0.93629	-6.44330	2.29772
H	-0.40754	-5.34499	1.97282
C	3.51117	-4.68989	2.18379
H	4.23001	-3.88973	2.00525
H	3.90444	-5.59816	1.71727
H	3.47085	-4.86516	3.25983
C	1.74648	-4.92006	-0.27835
H	0.75480	-4.77458	-0.71187
H	1.94892	-5.99529	-0.27299
H	2.48062	-4.43901	-0.92336
C	-0.82418	-2.37564	3.59544
H	-1.45895	-1.93537	2.82649
H	-1.09713	-1.93216	4.55722
H	-1.05131	-3.44229	3.63413

C	1.32448	-0.23596	3.47070
H	2.37084	-0.01004	3.25368
H	1.14566	-0.00626	4.52543
H	0.69531	0.41466	2.86791
C	2.01490	-2.88023	4.53916
H	1.87757	-3.95785	4.62717
H	1.72555	-2.43423	5.49609
H	3.08032	-2.68473	4.39436
C	0.89238	-3.01895	-2.95891
H	1.06053	-4.09019	-2.84515
H	0.49909	-2.84570	-3.96384
H	0.11456	-2.72301	-2.25459
C	3.82799	-3.10480	-3.51781
H	4.80305	-2.61613	-3.56189
H	3.52635	-3.32836	-4.54599
H	3.94925	-4.05637	-2.99516
C	2.32102	-0.51210	-3.79503
H	1.52225	0.13532	-3.42618
H	2.06800	-0.80800	-4.81764
H	3.24460	0.06799	-3.83252
C	4.43036	-0.86686	1.24223
H	3.86520	0.06967	1.28720
H	5.45343	-0.64751	1.56142
H	3.99209	-1.55463	1.96755
C	5.49125	-0.41497	-1.54329
H	5.44908	-0.65789	-2.60734

H	6.53643	-0.49768	-1.22908
H	5.19257	0.62567	-1.42433
C	5.38082	-3.20953	-0.48627
H	4.75384	-4.04965	-0.18821
H	6.22180	-3.15646	0.21188
H	5.78828	-3.42953	-1.47508
C	-4.80824	-1.67578	-3.34906
H	-5.54274	-2.33871	-2.88633
H	-4.76269	-1.92360	-4.41412
H	-5.18023	-0.65432	-3.25859
C	-2.64561	-3.68990	-2.88966
H	-1.66045	-3.94665	-2.50088
H	-2.62492	-3.85349	-3.97165
H	-3.36897	-4.39143	-2.47053
C	-1.90386	-0.84998	-3.56891
H	-2.26138	0.16643	-3.74585
H	-1.78397	-1.31865	-4.55038
H	-0.92162	-0.79056	-3.10048
C	-4.14805	-1.85315	1.86199
H	-3.37508	-1.20471	2.27831
H	-4.35119	-2.62102	2.61392
H	-5.04808	-1.25086	1.73251
C	-2.35180	-3.95083	0.59333
H	-2.16279	-4.58816	-0.27249
H	-2.63753	-4.59448	1.43022
H	-1.41421	-3.45438	0.85615

C	-5.24217	-3.57867	-0.30429
H	-6.07645	-2.88627	-0.43885
H	-5.52594	-4.28725	0.48026
H	-5.12105	-4.14657	-1.22763
C	-6.22967	0.33783	-0.43074
H	-5.83628	-0.63276	-0.73375
H	-7.06198	0.59115	-1.09372
H	-6.62464	0.24579	0.58414
C	-4.31934	1.81758	-2.29869
H	-3.76968	2.75129	-2.43757
H	-5.18319	1.84281	-2.96893
H	-3.68186	0.99825	-2.62884
C	-5.71163	3.29423	-0.14455
H	-6.15610	3.35750	0.84979
H	-6.51907	3.42607	-0.87204
H	-5.02086	4.13196	-0.26291
C	-5.09205	1.51198	3.06068
H	-5.99665	1.80656	2.52410
H	-5.09440	2.03803	4.02025
H	-5.15853	0.44214	3.26698
C	-3.35979	3.80721	2.17172
H	-2.55823	4.17254	1.52910
H	-3.11736	4.11251	3.19415
H	-4.28083	4.31521	1.88578
C	-2.09040	1.29116	3.15101
H	-2.06815	0.20656	3.26061

H	-2.18531	1.71819	4.15427
H	-1.12455	1.59554	2.74846
H	-1.18936	0.67609	-1.20554
H	-0.99951	-0.28343	0.95222
H	-0.30308	1.76833	0.58709
H	0.98260	0.89292	-1.31246
H	0.04745	-1.08525	-0.82035
H	1.22797	0.16771	0.79021

Chapter 5. Hydrides, Halides, and Polymers: Some Unexpected Intermediates on the Routes to First-Row Transition Metal M{N(SiMe$_3$)$_2$}$_n$ (n = 2, 3) Complexes.

Cary R. Stennett and Philip P. Power*

Department of Chemistry, University of California, Davis, One Shields Avenue, Davis, California 95616, United States

Reprinted with permission from *Inorg. Chem*. https://pubs.acs.org/doi/10.1021/acs.inorgchem.1c03065

Abstract.

The reaction of 2 equiv. of LiN(SiMe$_3$)$_2$·Et$_2$O with TiCl$_3$(NMe$_3$)$_2$ or VCl$_3$(NMe$_3$)$_2$ afforded the dimeric, halide bridged complexes [Ti(μ-Cl){N(SiMe$_3$)$_2$}$_2$]$_2$ (**1**) or [V(μ-Cl){N(SiMe$_3$)$_2$}$_2$]$_2$ (**2**) in moderate yields. The reduction of titanium complex **1** with 3 equiv. of 5 % (wt.) Na/NaCl gave the mixed metal titanium/sodium hydride cluster Ti$_2$(μ-H)$_2$N(SiMe$_3$)$_2$}$_3${N(SiMe$_3$)(SiMe$_2$*C*H)}(Na) (**3**), which was formed by activation of two C-H bonds at a single methyl group of one of the bis(trimethylsilyl)amide ligands. Attempts to form the analogous vanadium complex by reduction of **2** gave only intractable products. Treatment of Co{N(SiMe$_3$)$_2$}$_2$ with 1 equiv. of BrN(SiMe$_3$)$_2$ (which was previously shown to give the unique three-coordinate cobalt(III) trisamide Co{N(SiMe$_3$)$_2$}$_3$) afforded the polymeric [(μ-Br)Co{μ-N(SiMe$_3$)(SiMe$_2$CH$_2$CH$_2$Me$_2$Si)(Me$_3$Si)μ-N}Co(μ-Br)]$_\infty$ (**4**) as a second product, which was shown by a structural analysis to possess a carbon-carbon bond formed between the two ligands. Attempts to isolate manganese and iron complexes analogous to **4** were unsuccessful. The role of bromine in these reactions was further studied by examining the reaction of 0.5 equiv. of elemental bromine with [Mn{N(SiMe$_3$)$_2$}$_2$]$_2$ or [Co{N(SiMe$_3$)$_2$}$_2$]$_2$, which for manganese was shown to give the previously reported manganese trisamide Mn{N(SiMe$_3$)$_2$}$_3$, but for cobalt gives the dimeric amide-bridged [Co(Br){μ-N(SiMe$_3$)$_2$}]$_2$ (**5**).

Introduction.

The use of the bulky bis(trimethylsilyl)amide ligand (-$N(SiMe_3)_2$) to stabilize low-coordinate molecular complexes of transition metals began in the 1960s with the synthesis of divalent $M\{N(SiMe_3)_2\}_2$ (M = Mn, Co, Ni) and trivalent $M\{N(SiMe_3)_2\}_3$ (M = Cr, Fe) by Bürger and Wannagat.[1,2] Later work by Bradley and Hursthouse in the 1970s revealed the three-coordinate monomeric molecular structures and explored the chemical and physical properties of the trivalent $M\{N(SiMe_3)_2\}_3$ complexes of first-row transition metals.[3–5] Since then, homoleptic $M\{N(SiMe_3)_2\}_n$ (n = 2 or 3) complexes have been reported and structurally characterized for the first-row transition metals from scandium to cobalt,[3,6–16] as well as several lanthanides[6,17–24] and actinides,[25–28] establishing the bis(trimethylsilyl)amide ligand as one of the most widely used and economical of uninegative bulky ligands.[29,30]

Recent work in this laboratory revisited the chemistry of first-row transition metal $M\{N(SiMe_3)_2\}_n$ (n = 1, 2, or 3) complexes. These studies resulted in the isolation and characterization of tetrameric $\{NiN(SiMe_3)_2\}_4$, the first example of a complex of this type to possess an open-shell electron configuration, as well as the unstable dimeric Ni(II) complex $[Ni\{N(SiMe_3)_2\}_2]_2$.[10] The structural and spectroscopic characterization and exploration of the redox chemistry of $V\{N(SiMe_3)_2\}_3$ (which had been previously mischaracterized) were also described.[13] A coordination chemistry was initiated for the titanium and vanadium tris(silylamide) complexes (previously thought not possible due to steric crowding) to give $M\{N(SiMe_3)_2\}_3L_2$ (L = a nitrile or isocyanide ligand) complexes.[31] Additionally, the isolation of a new vanadium(V) oxy silylamide complex, e.g. $V(=O)\{N(SiMe_3)_2\}_3$, that was absent from the literature despite several attempts to isolate it,[32] and the synthesis of several unusual metal hydride complexes that are available by reduction of $M\{N(SiMe_3)_2\}_3$ complexes were described.[33]

During this work, two observations for these silylamide complexes became a focus of interest. First, it is notable that while divalent $M\{N(SiMe_3)_2\}_2$ complexes have been described for the mid and late transition metals from chromium to nickel (although only as base-stabilized complexes in the case of chromium), no such complexes have been described for titanium or vanadium.[7,9,10,15,34–37] Second, we noted

that while the most recently reported trivalent $M\{N(SiMe_3)_2\}_3$ (M = Mn, Co) complexes were obtained by the reaction of $BrN(SiMe_3)_2$ with the corresponding divalent $M\{N(SiMe_3)_2\}_2$ species, the fate of the bromine in these reactions was not well understood.[16] Attempts to resolve these outstanding questions about the chemistry of these molecules are described here.

Herein, we report the preparation of $[Ti(\mu\text{-}Cl)\{N(SiMe_3)_2\}_2]_2$ (**1**) and $[V(\mu\text{-}Cl)\{N(SiMe_3)_2\}_2]_2$ (**2**) by the reaction of 2 eq. of $LiN(SiMe_3)_2{\cdot}Et_2O$ with the corresponding $MCl_3(NMe_3)_2$ salt. While **1** had been previously structurally characterized, we report here its rational synthesis together with its spectroscopic characterization. In an attempted preparation of the titanium complex "$Ti\{N(SiMe_3)_2\}_2$," **1** was treated with 5 % (wt.) Na/NaCl. This afforded the mixed-valent titanium(III/IV) hydride complex $Ti_2(\mu\text{-}H)_2\{N(SiMe_3)_2\}_3\{N(SiMe_3)(SiMe_2CH)\}(Na)$ (**3**). The analogous reduction of $[V(\mu\text{-}Cl)\{N(SiMe_3)_2\}_2]_2$ (**2**) afforded only an intractable mixture of products. The reaction of $[Co\{N(SiMe_3)_2\}_2]_2$ with $BrN(SiMe_3)_2$ afforded the expected trisamide $Co\{N(SiMe_3)_2\}_3$, but workup of the mother liquor gave the cobalt amide/halide polymer $[(\mu\text{-}Br)Co\{\mu\text{-}N(SiMe_3)(SiMe_2CH_2CH_2Me_2Si)(Me_3Si)\mu\text{-}N\}Co(\mu\text{-}Br)]_\infty$ (**4**) in low yield. In contrast, treatment of $[Co\{N(SiMe_3)_2\}_2]_2$ with elemental bromine gave the dimeric $[Co(Br)\{\mu\text{-}N(SiMe_3)_2\}]_2$ (**5**), while the only product isolated from the corresponding treatment of $[Mn\{N(SiMe_3)_2\}_2]_2$ with elemental bromine was, unexpectedly, the trisamide $Mn\{N(SiMe_3)_2\}_3$.

Experimental.

General Considerations. All manipulations were performed by using modified Schlenk techniques or in a Vacuum Atmospheres drybox under nitrogen or argon. Solvents were dried and collected using an S2 Grubbs-type solvent purification system (Glass Contour) and degassed using the freeze, pump, thaw method. All physical measurements were recorded under strictly anaerobic and anhydrous conditions. IR spectra were recorded as Nujol mulls between CsI windows on a PerkinElmer 1430 spectrophotometer. UV–vis spectra were recorded as dilute hexane solutions in 3.5 mL quartz cuvettes using an OLIS modernized Cary 14 UV/vis/NIR spectrophotometer. ^1H NMR spectra were referenced to residual solvent signals. Magnetic moments were determined by Evans' method and corrected using the appropriate

diamagnetic constants.[38,39] Melting points were determined in flame-sealed glass capillaries using a Meltemp II apparatus equipped with a partial immersion thermometer. Due to the high air and moisture sensitivity and high silicon content of the complexes, elemental analyses were not attempted. $TiCl_3(NMe_3)_2$,[5] $VCl_3(NMe_3)_2$,[5] $LiN(SiMe_3)_2{\cdot}(OEt_2)$,[40] 5 wt. % Na/NaCl,[41] $[Mn\{N(SiMe_3)_2\}_2]_2$,[40] $[Co\{N(SiMe_3)_2\}_2]_2$,[40] and $BrN(SiMe_3)_2$[42] were prepared via literature procedures.

Synthesis of $[Ti(\mu\text{-}Cl)\{N(SiMe_3)_2\}_2]_2$ (1). $LiN(SiMe_3)_2{\cdot}(OEt_2)$ (2.0 g, 8.3 mmol) in ca. 50 mL of diethyl ether was added by cannula to a stirred suspension of $TiCl_3(NMe_3)_2$ (1.12 g, 4.14 mmol) in ca. 10 mL of diethyl ether cooled to ca. 0 °C. When the addition was complete, the resulting suspension was allowed to warm to room temperature. The mixture became bright green upon stirring overnight. The diethyl ether was removed under low pressure, and the residue was extracted in hexanes and filtered through a Celite padded frit. The filtrate was concentrated under reduced pressure until the formation of small green crystals was observed. The solution was then gently warmed by hand to redissolve the crystals, and it was then cooled in a ca. -18 °C freezer for 24 hours to afford 0.58 g (35 %) of the product as bright green crystalline plates. The unit cell determined by single crystal X-ray crystallography was consistent with that previously reported for **1** (see below). M.p.: 145-147 (dec.). ^{1}H NMR (600 MHz, [D_6] benzene, 25 °C): δ = 3.38 (s, $\Delta\nu_{1/2}$ = 90 Hz). UV/Vis: λ/nm (ε/$M^{-1}cm^{-1}$): 359 (4000) 733 (400). IR (Nujol) $\tilde{\nu}$ [cm^{-1}] = 405 (ν_sTi-N), 380 (ν_{as}Ti-N), 310 (νTi-Cl). μ_{eff} = 3.0 μ_B.

Synthesis of $[V(\mu\text{-}Cl)\{N(SiMe_3)_2\}_2]_2$ (2). In a preparation analogous to that of complex **1**, $LiN(SiMe_3)_2{\cdot}(OEt_2)$ (2.0 g, 8.3 mmol) in ca. 50 mL of diethyl ether was added by cannula to a stirred suspension of $VCl_3(NMe_3)_2$ (1.14 g, 4.14 mmol) in ca. 10 mL of diethyl ether cooled to 0 °C. When the addition was complete, the resulting red suspension was allowed to warm to room temperature. After overnight stirring, the mixture had become dark blue. The diethyl ether was removed under low pressure, and the residue was extracted in hexanes and filtered through a Celite padded frit. The filtrate was concentrated under reduced pressure until the formation of small blue crystals was observed. The solution was then gently warmed by hand to redissolve the crystals, whereupon the solution was re-cooled in a ca. -

18 °C freezer for 24 hours to afford 0.51 g (30 %) of the product as dark blue/violet dichroic crystalline plates that were suitable for X-ray crystallographic studies. M.p.: 123-125 °C (dec.). ^{1}H NMR (600 MHz, [D_6] benzene, 25 °C): δ = 7.18 (s, $\Delta\nu_{1/2}$ = 380 Hz). UV/Vis: λ/nm (ε/$M^{-1}cm^{-1}$): 329 (4000), 556 (400), 617 (500), 716 (400). IR (Nujol) $\tilde{\nu}$ [cm^{-1}] = 405 ν_sV-N), 380 (ν_{as}V-N), 300 (νV-Cl). μ_{eff} = 5.0 μ_B.

Synthesis of $Ti_2(\mu\text{-}H)_2\{N(SiMe_3)_2\}_3\{N(SiMe_3)(SiMe_2CH)\}(Na)$ (3). 2.0 g (2.5 mmol) of $[Ti(Cl)\{N(SiMe_3)_2\}_2]_2$ (**1**) in ca. 30 mL of diethyl ether was added dropwise over ca. 15 min. to a stirred slurry of 2.7 g (5.9 mmol) of 5 wt. % Na/NaCl in ca. 20 mL of diethyl ether cooled to ca. -78 °C. Stirring was continued, and the mixture was allowed to slowly warm to ambient temperature overnight. The solvent was then removed under reduced pressure and the residue was extracted in ca. 40 mL of hexanes. The mixture was filtered, and the dark green filtrate was concentrated to ca. 15 mL. Overnight storage of this solution at ca. – 30 °C afforded 0.5 g (0.7 mmol, 30 %) of dark green, almost black crystals of **3** that were suitable for X-ray diffraction studies. M.p.: 121-122 °C (dec.). ^{1}H NMR (600 MHz, [D_6] benzene, 25 °C): δ = 0.97 (s, $\Delta\nu_{1/2}$ = 55 Hz, $SiMe_3$). UV/Vis: λ/nm (ε/$M^{-1}cm^{-1}$): 395 (3000), 604 (500). IR (Nujol) $\tilde{\nu}$ [cm^{-1}] = 375 (νV-N), 300. μ_{eff} = 1.8 μ_B.

Synthesis of $[(\mu\text{-}Br)Co\{\mu\text{-}N(SiMe_3)(SiMe_2CH_2CH_2Me_2Si)(Me_3Si)\mu\text{-}N\}Co(\mu\text{-}Br)]_\omega$ (4). The trisamide $Co\{N(SiMe_3)_2\}_3$ was prepared as previously described[16] by addition of $BrN(SiMe_3)_2$ (1.2 g, 5.3 mmol) to a solution of 2.0 g (2.6 mmol) of $[Co\{N(SiMe_3)_2\}_2]_2$ in ca. 50 mL of toluene cooled to ca. 0 °C. The solution was stirred overnight at ambient temperature and subsequently concentrated under reduced pressure to ca. 15 mL. Overnight storage of this solution at ca. -20 °C afforded a mass of dark green crystalline needles of $Co\{N(SiMe_3)_2\}_3$. The solvent was separated from the green crystalline material and stored at ambient temperature for one week to afford a small quantity of small orange crystals of polymeric **4** that were suitable for study by X-ray crystallography. Despite multiple attempts, a larger amount of **4** could not be isolated, and the complex has therefore been only structurally characterized.

Synthesis of $[Co(Br)\{\mu\text{-}N(SiMe_3)_2\}]_2$ (5). Elemental bromine (0.21 g, 1.3 mmol) was added in one portion by syringe to a room temperature green solution of $[Co\{N(SiMe_3)_2\}_2]_2$ (1.0 g, 1.3 mmol) in ca. 30

mL of toluene and the solution was stirred overnight. Orange/yellow crystals that were suitable for X-ray diffraction studies grew spontaneously on the wall of the flask when concentrating the solution under reduced pressure. The solution was further concentrated to ca. 15 mL and gently warmed (ca. 40 °C) to dissolve the precipitated material. Overnight storage at ca. -20 °C gave 0.13 g (0.2 mmol) of orange/yellow crystals of **5** that were suitable for X-ray diffraction studies. Storage of the mother liquor at ca. -20 °C for one week afforded an additional 0.4 g (0.7 mmol) of crystalline material (overall yield: 68%). M.p.: 160 °C (dec). UV/Vis: λ/nm (ε/$M^{-1}cm^{-1}$): 370 (1300), 437 (800), 503 (1400). IR (Nujol) $\tilde{\nu}$ [cm^{-1}]: 485 (νCo-N), 285 (νCo-Br). ^{1}H NMR (399.8 MHz, C_6H_6, 298 K): δ = -5.13 ($\Delta\nu_{1/2}$ = 38 Hz $SiMe_3$). $\mu_{eff.}$ 3.8 μ_B.

Alternate Synthesis of Mn{N(SiMe$_3$)$_2$}$_3$. Bromine (0.21 g, 1.3 mmol) was added in one portion by syringe to a room temperature solution of [Mn{N(SiMe$_3$)$_2$}$_2$]$_2$ (1.0 g, 1.3 mmol) in ca. 30 mL of toluene with stirring. The solution immediately turned dark violet. After stirring overnight, the solution was concentrated to ca. 15 mL and stored at ca. -18 °C to give violet needles of Mn{N(SiMe$_3$)$_2$}$_3$. The infrared spectrum and unit cell data agreed with the previously published data for Mn{N(SiMe$_3$)$_2$}$_3$.[16]

X-ray Crystallography. Crystals of **2-5** were removed from the reaction flask under a flow of argon and covered in Paratone oil. Suitable crystals were selected, mounted on a MiTeGen MicroLoop, and then placed in the cold nitrogen stream of the diffractometer. Data collection was performed at 90 K using Mo Kα radiation (λ = 0.71073 Å, complexes **2**, **4**, and **5**) or CuKα (λ = 1.54178 Å, complex **3**) on a Bruker Apex II diffractometer. Absorption corrections were applied using SADABS.[43] Structure solution and refinement were performed within the Olex2 GUI.[44] The structures were solved by intrinsic phasing using SHELXT[45] and refined by least-squares methods using SHELXL.[46] All non-hydrogen atoms were refined anisotropically. The positions of the hydrogen atoms bound to titanium in **3** and the methylene hydrogen atoms in **4** were located in the difference map and refined freely. The structure of **5** was refined further by determination of the appropriate twin law and subsequent full matrix (BASF/TWIN) refinement.[46]

Results and Discussion.

Synthesis.

The divalent complexes $M\{N(SiMe_3)_2\}_2$ of the mid and late first-row transition metals (M = Mn, Fe, Co) are prepared in a simple manner by reaction of 2 equivalents of the alkali metal amide with the appropriate metal dihalide in diethyl ether and subsequent low-pressure distillation of the crude product.[40] The highly unstable divalent nickel amide may be prepared analogously.[10] Although a few Lewis base stabilized complexes of $Cr\{N(SiMe_3)_2\}_2$ are known,[34–37] no $M\{N(SiMe_3)_2\}_2$ complexes have been reported for the earlier transition metals titanium or vanadium. Our initial attempts to prepare $V\{N(SiMe_3)_2\}_2$ by reaction of the vanadium(II) salt $VI_2(THF)_4$ with 2 equivalents of $LiN(SiMe_3)_2(OEt_2)$ were unsuccessful, giving only intractable oils as products. We therefore sought to prepare the divalent complexes from trivalent precursors by reduction. We also note that the structure of $[Ti(\mu\text{-}Cl)\{N(SiMe_3)_2\}_2]_2$ (**1**) was reported in 2017.[47] It was prepared by reaction of $TiCl_4$ with 2 equivalents of $LiN(SiMe_3)_2$. Having ready access to trivalent $TiCl_3(NMe_3)_2$, we synthesized complex **1** in a rational manner by reaction of $TiCl_3(NMe_3)_2$ with two equivalents of $LiN(SiMe_3)_2(OEt_2)$ in diethyl ether (Scheme 5.1). Filtration and subsequent crystallization of the residue from hexanes afforded bright green, crystalline **1** in moderate yield. An analogous synthesis using $VCl_3(NMe_3)_2$ gave blue/purple dichroic crystals of $[V(\mu\text{-}Cl)\{N(SiMe_3)_2\}_2]_2$ (**2**) in slightly lower yield. It should also be noted that the monomeric THF complex $V\{N(SiMe_3)_2\}_2(Cl)\cdot THF$ was prepared previously by Gambarotta in 1994.[48]

Scheme 5.1. The synthetic route used for the preparation of complexes **1** (M = Ti) and **2** (M = V).

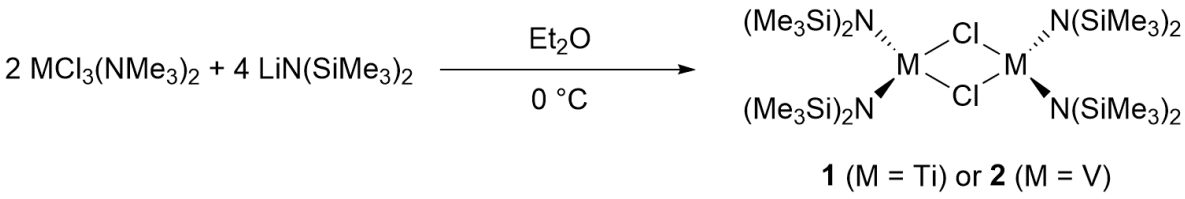

With the trivalent Ti and V complexes **1** and **2** in hand, we attempted to prepare their respective divalent $M\{N(SiMe_3)_2\}_2$ complexes by reduction. Our lab has recently developed a preference for using 5 % (wt.) sodium on sodium chloride as a reductant, given its ease of preparation and storage[41] and the recent success we have had in isolating other long-sought complexes using this reductant.[49] Thus, treatment of titanium complex **1** with a slight excess of Na/NaCl in diethyl ether (Scheme 5.2) resulted in the formation of a very dark green mixture. Filtration, removal of the solvent, and recrystallization of the resulting residue from a concentrated hexanes solution afforded a large amount of dark green, nearly black crystals. A structural study revealed that the resulting complex was not of the form $M\{N(SiMe_3)_2\}_2$. Instead, the titanium/sodium hydride cluster **3** was formed, which results from activation of two C-H moieties of a single methyl group (vide infra). In contrast, several attempts to isolate a product from the analogous reaction using the vanadium halide complex **2** as the starting material resulted only in the formation of intractable mixtures.

Scheme 5.2. Synthesis of the titanium hydride complex **3.**

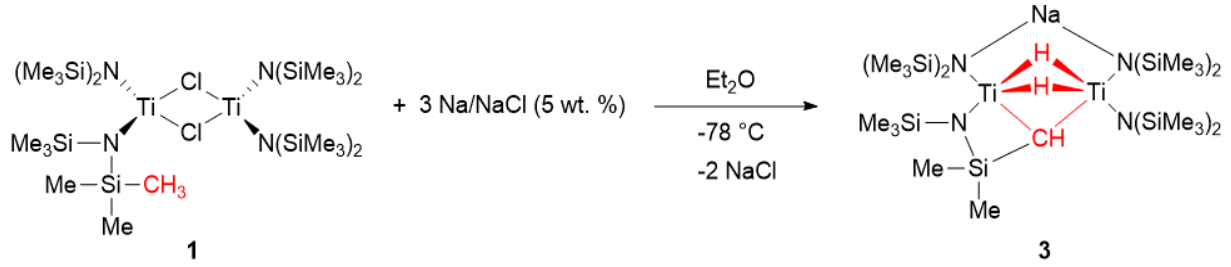

We further sought an increased understanding of the fate of the bromine atom from $BrN(SiMe_3)_2$ as well as its role in the formation of $M\{N(SiMe_3)_2\}_3$ complexes of the later transition metals manganese and cobalt. Currently, there are no convenient sources of Mn(III) or Co(III) halides that are synthetically useful or commercially available. Thus, the trivalent silylamide complexes of manganese or cobalt were prepared by oxidation of their divalent $M\{N(SiMe_3)_2\}_2$ complexes with $BrN(SiMe_3)_2$ as described in the initial report.[16] Although these reactions afforded the trivalent $M\{N(SiMe_3)_2\}_3$ complexes in moderate yields, this synthetic route implies the formation of an additional, unknown product containing bromine. To identify this product, we first performed the synthesis of $Co\{N(SiMe_3)_2\}_3$ as previously described.

Having separated the crystals of $Co\{N(SiMe_3)_2\}_3$, storage of the mother liquor for two weeks at room temperature afforded orange crystals of the cobalt polymer **4** in low yield (Scheme 5.3). Examination of the structure of **4** (vide infra) indicated that it is formed by H abstraction from two methyl groups of two bis(trimethylsilyl)amide ligands with concomitant elimination of bis(trimethylsilyl)amine and formation of an ethylene bridge. Although uncommon, similar coupling of methylene units in this ligand has been previously described in nearly simultaneous reports by the groups of Hayton and Ephritikine.[50–52] In these reports, a four-membered metallacycle of the form $U\{N(SiMe_3)SiMe_2CH_2\}$ was treated with iodine[51,52] or iodotrimethylsilane,[50] which resulted in the cleavage of the U-CH_2 bonds of two metallacycles and subsequent coupling of the methylene carbons. Given these results, and the fact that $M\{N(SiMe_3)_2$ moieties are known to react with hexamethyldisilazide to form four-membered metallacycles with concomitant formation of bis(trimethylsilyl)amine (cf. early work by Gambarotta and Dehnicke),[48,53,54] we suggest that the formation of **4** may proceed through such a metallacyclic intermediate, although we cannot be certain of this without further investigations. To date, attempts to isolate the corresponding manganese or iron products in an analogous way have been unsuccessful.

Scheme 5.3. Synthesis of cobalt complexes **4** and **5**.

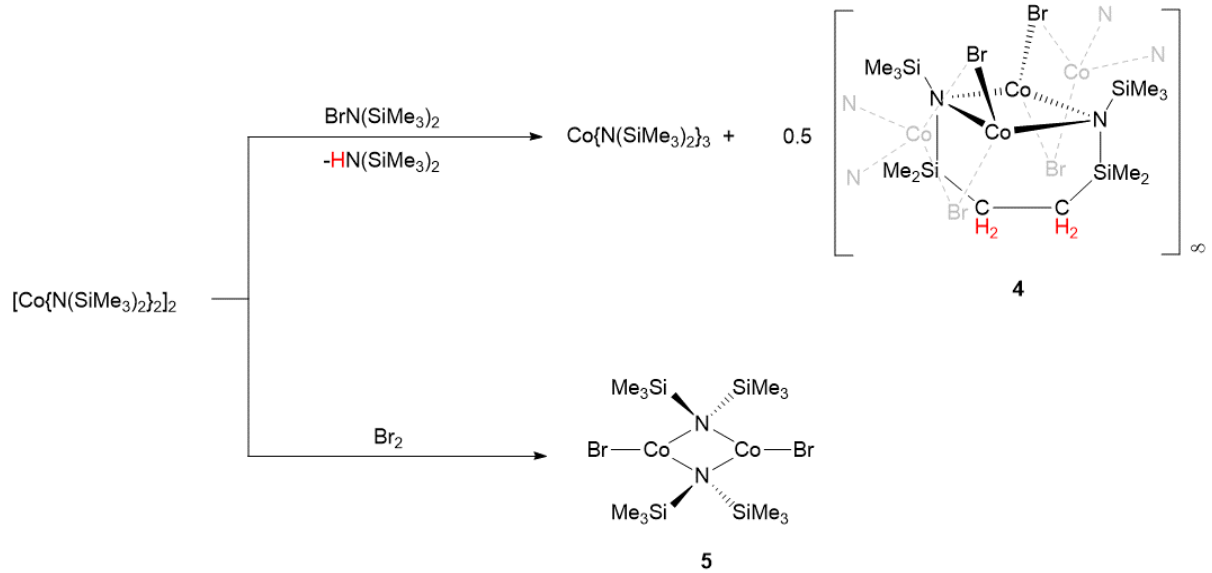

Although isolation of the cobalt polymer **4** provided information about the other products that are formed during these syntheses, the route by which either $Co\{N(SiMe_3)_2\}_3$ or polymer **4** is formed remained

unclear. We treated divalent $Co\{N(SiMe_3)_2\}_2$ with elemental bromine (Scheme 3) to better understand the role of bromine in the formation of these complexes. Addition of 0.5 equivalents of Br_2 to a cooled (0 °C) toluene solution of $Co\{N(SiMe_3)_2\}_2$ resulted in the formation of orange/yellow crystals that grew spontaneously from the reaction mixture upon standing overnight at ambient temperature. The product was identified by X-ray crystallography as dimeric $[Co(Br)\{\mu\text{-}N(SiMe_3)_2\}]_2$ (**5**). Unexpectedly, the only isolated product of the analogous reaction of $Mn\{N(SiMe_3)_2\}_2$ and 0.5 eq. of Br_2 was violet crystalline needles of the previously reported trisamide $Mn\{N(SiMe_3)_2\}_3$, which was also verified by X-ray crystallography.[16]

Structures.

Dimeric $[V(\mu\text{-}Cl)\{N(SiMe_3)_2\}_2]_2$ (**2**, Figure 5.1) is isostructural to its titanium analogue, **1**, which was previously reported by Le Roux and coworkers in 2017.[47] Like **1**, it has an essentially planar V_2Cl_2 core (sum of interior angles = 359.7(1)°) in which the vanadium atoms are symmetrically bridged by the chlorine atoms. The average V-Cl distance is 2.3806(7) Å, and the average V-N distance is 1.912(2) Å. The transannular V-V distance of 3.517(1) Å is quite long (cf. the single bonded covalent radius of vanadium of 1.34 Å),[55] suggesting very little bonding interaction between the two metal atoms. Surprisingly, complexes **1** and **2** are the only structurally characterized examples of trivalent first-row transition metal

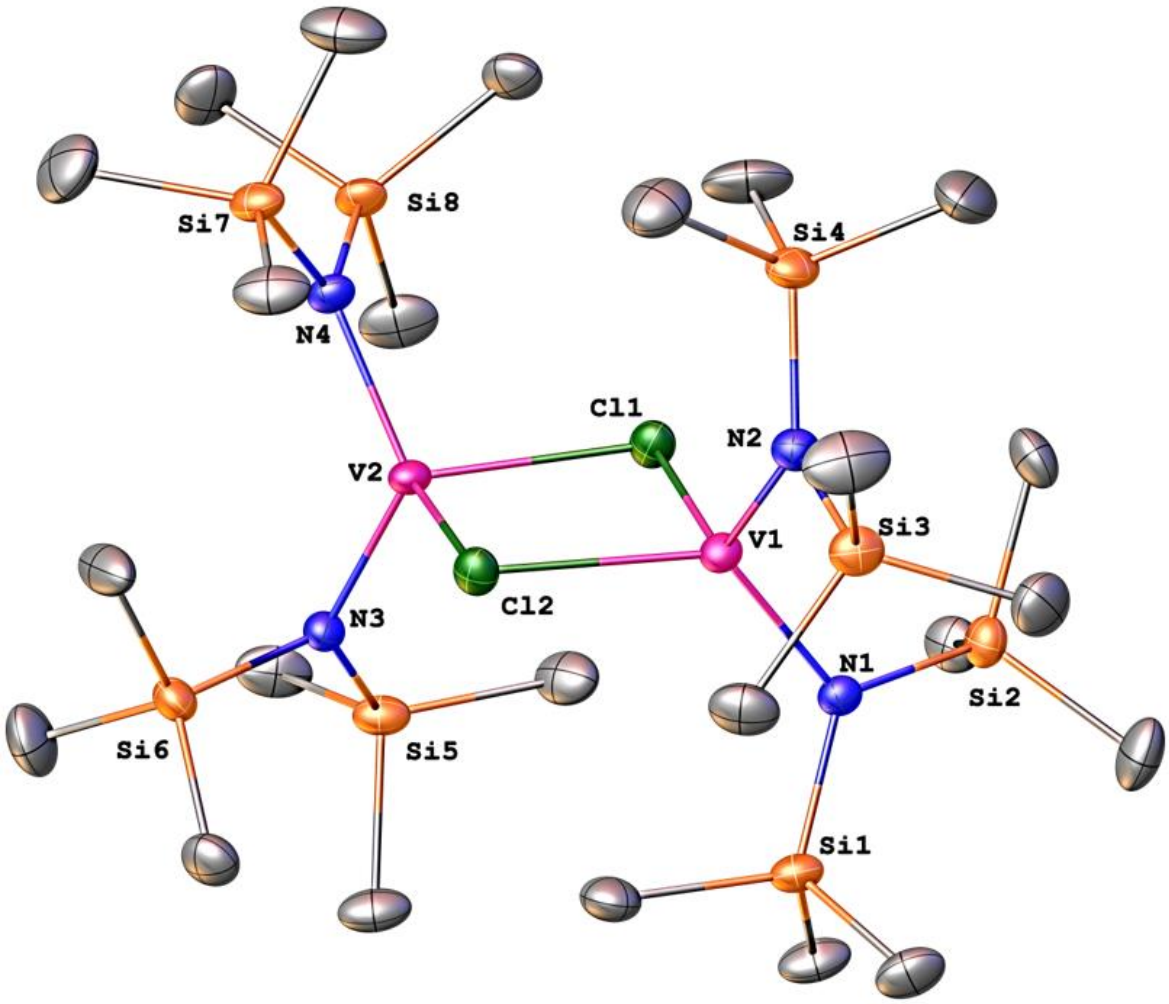

Figure 5.1. Molecular structure of $[V(\mu\text{-}Cl)\{N(SiMe_3)_2\}_2]_2$ (**2**) with thermal ellipsoids shown at 30% probability. Hydrogen atoms and site disorder at one trimethylsilyl group (Si8) are not shown. Selected distances (Å) and angles (°): V1-V2 :3.517(1), V1-Cl1: 2.388(1), V1-Cl2: 2.384(1), V2-Cl1: 2.370(1), V2-Cl2: 2.381(1), V1-N1: 1.916(4), V1-N2: 1.901(4), V2-N3: 1.914(4), V2-N4: 1.915(4), V1-Cl1-V2: 95.35(5), V1-Cl2-V2: 95.15(5), Cl1-V1-Cl2: 84.41(5), Cl1-V2-Cl2: 84.86(5), N1-V1-N2: 115.36(17), N3-V2-N4: 123.02(17).

$[M(\mu\text{-}X)\{N(SiMe_3)_2\}_2]_2$ (X = halide) complexes, so comparisons with such complexes of the later transition elements is not possible at present.

The structure of the titanium/sodium hydride complex **3** (Figure 5.2) bears some resemblance to the "hydrido inverse crown" complexes (cf. $[Na_2Mg_2\{N(Pr^i)_2\}_4(\mu\text{-}H)_2\cdot(toluene)_2]$) originally reported by Mulvey and coworkers.[56] We recently reported that the donor solvent-free iron/lithium inverse crown could be prepared by reaction of $Fe\{N(SiMe_3)_2\}_3$ with lithium aluminium hydride,[33] and the isolation of

titanium/sodium **3** further highlights that this structural motif is likely accessible for a variety of metals. The structure of **3** suggests that the reduction of $[Ti(\mu\text{-}Cl)\{N(SiMe_3)_2\}_2]_2$ (**1**) with sodium metal may transiently form a divalent "$Ti\{N(SiMe_3)_2\}_2$" species that then subsequently reacts with ligand CH moieties to form the hydride complex **3**. This type of activation of the bis(trimethylsilyl) ligand has been described on several occasions previously,[12,48,54,57,58] although such reactivity had not been shown to result in the formation of a hydride complex as in **3**.

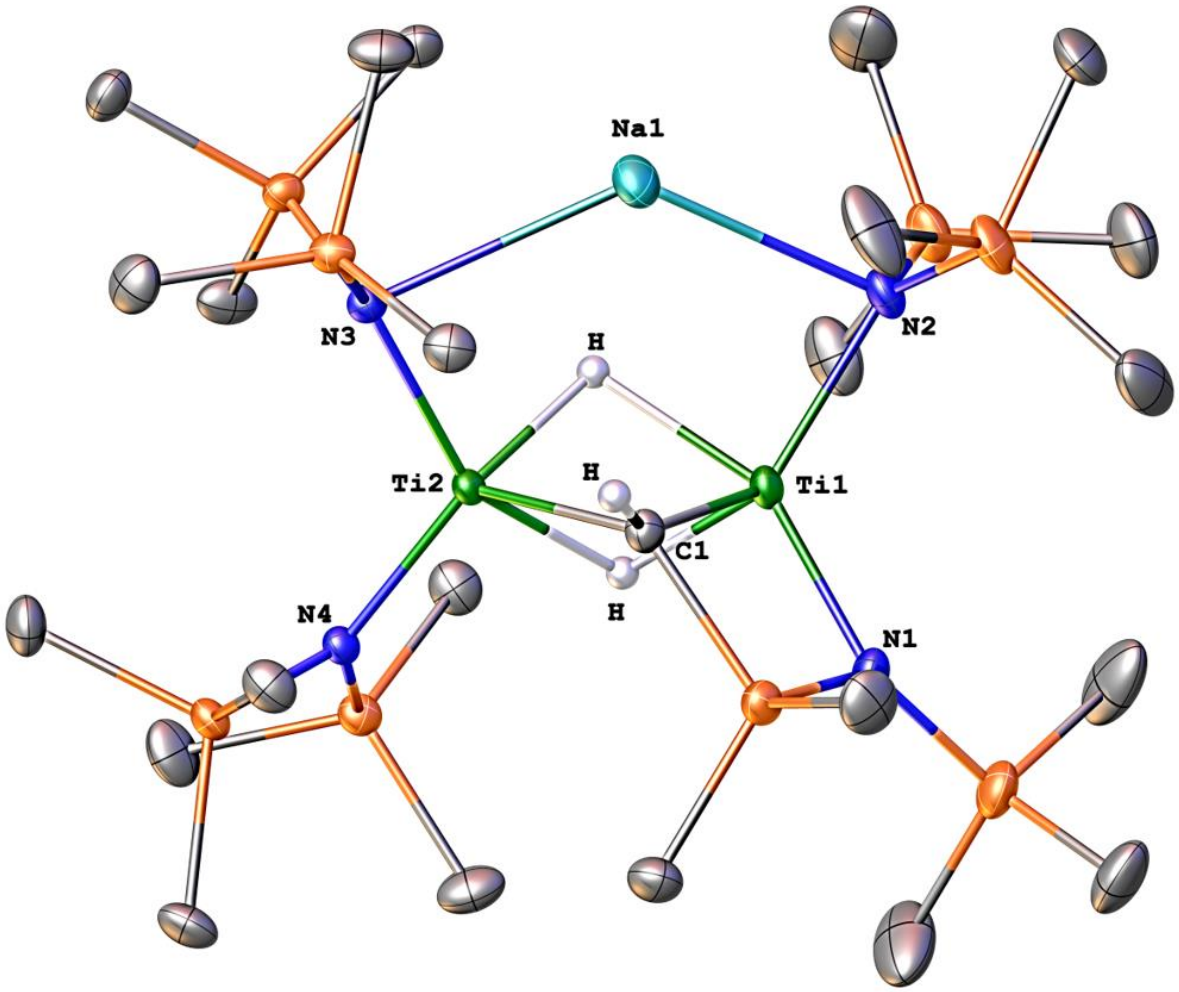

Figure 5.2. The molecular structure of **3** with thermal ellipsoids shown at 30% probability. For clarity, all hydrogens other than bridging hydrides H1 and H2 and alkynyl hydrogen H3 are not shown. Selected bond distances (Å) and angles (°): Ti1-Ti2: 2.6923(4), Ti-H1: 1.96(2), Ti1-H2: 1.73(2), Ti2-H1: 1.74(2), Ti2-H2: 1.94(2), Ti1-C1: 2.115(2), Ti2-C1: 2.001(2), Ti1-N1: 1.9795(13), Ti1-N2: 2.0573(13), Ti2-N3: 2.0439(15), Ti2-N4: 1.9404(15), Na1-N2: 2.6649(15), Na1-N3: 2.6071(17), Ti1-H1-Ti2: 93.1(9), Ti1-H2-Ti2: 94.2(10), Ti1-C1-Ti2: 81.64(7), N1-Ti1-N2: 118.04(5), N3-Ti2-N4: 118.42(6), N2-Na1-N3: 130.29(5).

The diffraction data collected for **3** were of sufficient quality that the positions of bridging hydrides, as well as that of the alkynyl hydrogen atom, were found in the Fourier difference map and refined freely rather than calculated. The Ti-H distances range from 1.73(2) to 1.96(2) Å (average Ti-H distance: 1.84(1) Å). The average Ti-H distance is comparable to that observed in other titanium(III) bridging hydride complexes, for example $\{TiH(NN_2)\}_2$ (average Ti-H distance: 1.83(2) Å, NN_2 = the chelating diamidoammine ligand $[(Me_3SiNCH_2CH_2)_2NSiMe_3]^{2-}$).[59] The Ti-Ti distance of 2.6923(4) Å in **3** is exceptionally short (cf. the single bonded covalent radius of titanium of 1.36 Å).[55] Among non-metallocene bridging hydrido complexes of titanium, the dimeric titanium(III) complex $[Li_3(thf)_2(Et_2O)$- $\{Ti(^tBu$-$L)\}_2(\mu$-$H)_3]$ (^{t}Bu-L = the tridentate aryloxide ligand 2,6-bis(4-*tert*-butyl-6-methylsalicyl)-4-*tert*-butylphenolate) and the dinitrogen dititanium hydride complex $\{[(^{acri}PNP)Ti]_2(\mu_2$-$\eta^1$:$\eta^2$-$N_2)(\mu$-$H)_2\}$ (^{acri}PNP=4,5-bis(diisopropylphosphino)-2,7,9,9-tetramethyl-9*H*-acridin-10-ide) possess comparable Ti-Ti distances of 2.621(1) and 2.703(1) Å, respectively.[60,61] In these complexes, their diamagnetism and the short Ti-Ti distances were taken to be indicative of the presence of a single Ti-Ti covalent bond in the former case, and possible antiferromagnetic coupling in the latter. However, unlike the aforementioned complexes, examination of the structure and magnetic properties (vide infra) of **3** indicates that it is a mixed valent Ti(III)/Ti(IV) complex (although, given their identical ligand environments, assignment of the oxidation states of the individual metals is not possible). Thus, the short Ti-Ti distance in **3** is unlikely to be due to a covalent interaction between the two metals.

The structure of the cobalt polymer **4** is shown in Figure 5.3. The polymer consists of infinite chains of dimers related by an inversion center that lies in the Co_2Br_2 ring, such that the ethylene bridge appears on alternating sides of the chain. The nitrogen atoms of the Co_2N_2 core of the dimer of **4** are disposed slightly out of plane (sum of interior angles = 358.11(4)°) toward the ethylene bridge. The transannular Co-Co distance of 2.783(1) Å (cf. the single bonded covalent radius of cobalt of 1.11 Å)[55] is longer than that found in the divalent amide $[Co\{N(SiMe_3)_2\}_2]_2$ (Co-Co distance = 2.583(1) Å).[9,62] The average transannular Co-Co distance across the Co_2Br_2 ring in the polymer is 3.7257(1) Å, which is somewhat longer than that

typically found in Co(II) complexes featuring bridging bromide atoms. The C-C distance of 1.548(9) Å between methylene carbons in the ethylene bridge indicated the presence of a bond between these atoms. In support of this, the diffraction data of **4** were of sufficient quality that the positions of the two H atoms bound to each methylene carbon were found in the difference map and refined freely.

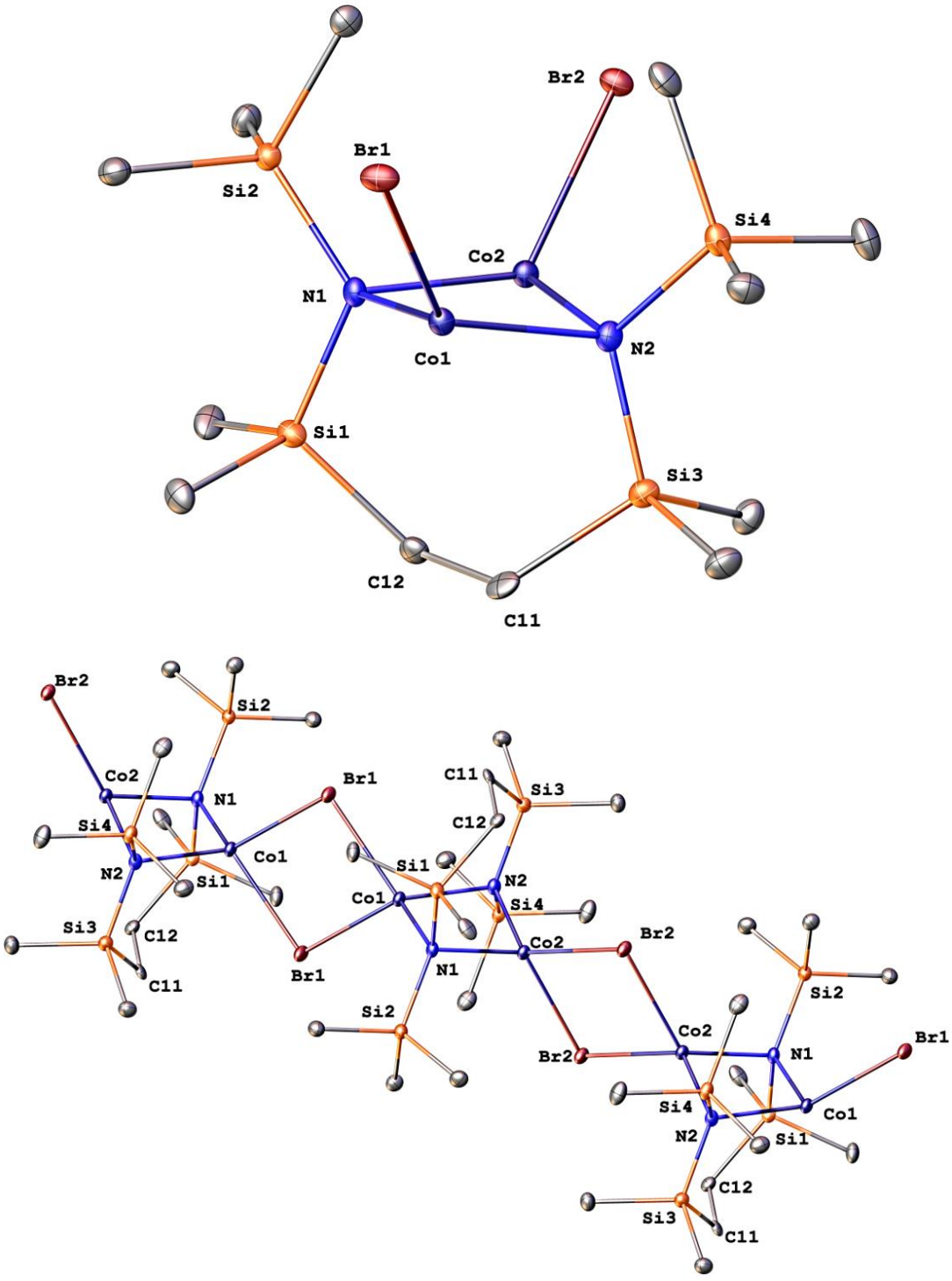

Figure 5.3. Structures of the dimer unit (top) and polymer (bottom) form of complex **4**. Thermal ellipsoids are shown at 30% probability. Hydrogen atoms are not shown. Selected distances (Å) and angles (°): Co1-Co2: 2.783(1), Co1-Co1: 3.743(2), Co2-Co2: 3.780(2), Co1-Br1: 2.498(1), Co2-Br2: 2.506(1), Co1-N1: 2.039(5), Co1-N2: 2.044(5), Co2-N1: 2.046(5), Co2-N2: 2.041(5), C11-C12: 1.549(9), Co1-N1-Co2: 85.90(19), Co1-N2-Co2: 85.88(19), N1-Co1-N2: 93.23(19), N1-Co2-N2: 93.10(19), Co1-Br1-Co1: 96.74(3), Br1-Co1-Br1: 83.26(3), Co2-Br2-Co2: 97.42(3), Br2-Co2-Br2: 82.58(3).

The molecular structure of dimeric $[Co(Br)\{\mu\text{-}N(SiMe_3)_2\}]_2$ (**5**) is shown in Figure 5.4. The structure of **5** features cobalt atoms bridged exclusively by amido groups and consists of a planar Co_2N_2 core (sum of internal angles = 359.97(3)°). The transannular Co-Co separation of 2.4827(7) Å is slightly shorter than that found in the cobalt(II) amide dimer $[Co\{N(SiMe_3)_2\}_2]_2$ (2.583(1) Å), and much shorter than for the amide bridged cobalt atoms in polymeric **4**. Complex **5** has an unusual structural motif wherein the bromine atoms are bound terminally, rather than bridging, to the cobalt atoms. Complexes of the form $\{M(\mu\text{-}X)L\}_2$ (M = a transition metal, X = a halide, L = a uninegative ligand) are commonplace, but there is apparently only a single additional example of a $\{M(\mu\text{-}L)X\}_2$ complex wherein the halide is terminally

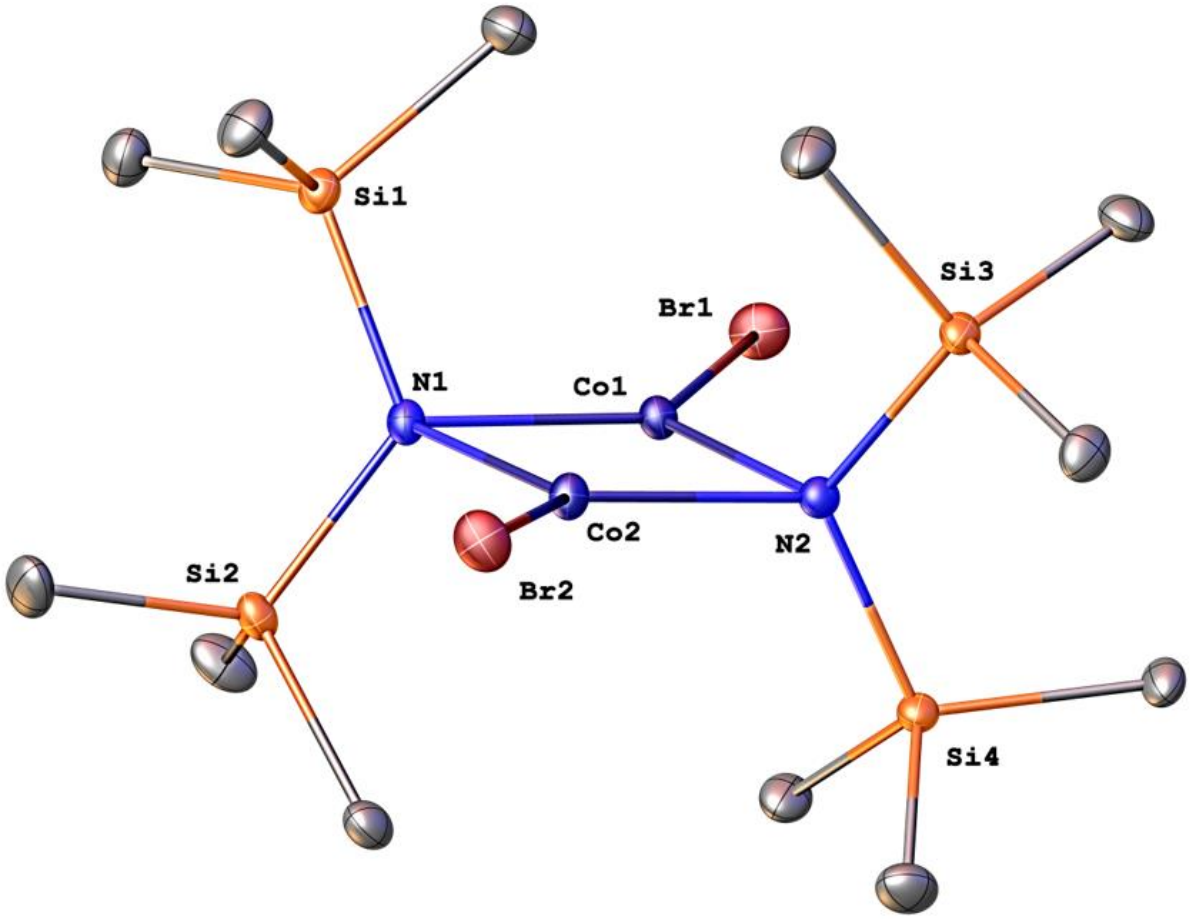

Figure 5.4. The molecular structure of $[Co(Br)\{\mu\text{-}N(SiMe_3)_2\}]_2$ (**5**) with thermal ellipsoids drawn at 30% probability. Hydrogen atoms are not shown. Selected bond distances (Å) and angles (°): Co1-N1: 1.986(3), Co1-N2: 1.986(3), Co2-N1: 1.989(3), Co2-N2: 1.976(3), Co1-Co2: 2.4827(7), N1-N2: Co1-Br1: 2.3148(6), Co2-Br2: 2.3075(6), N1-Co1-N2: 102.41(13), N1-Co2-N2: 102.66(13), Co1-N1-Co2: 77.31(11), Co1-N2-Co2: 77.59(12).

bound to an open-shell transition metal when a bridging mode would otherwise be possible.[63] That complexes **1** and **2** feature bridging halides suggests that the terminal binding of the halide in complex **5** may be connected to its synthetic route, rather than any property of the ligands (MX_3 complexes binding halide ligands were used in the synthesis of **1** and **2**, whereas the halide was added to a metal amide complex in the case of **5**).

Spectroscopy.

Infrared Spectroscopy. $[Ti(\mu\text{-}Cl)\{N(SiMe_3)_2\}_2]_2$ (**1**) and $[V(\mu\text{-}Cl)\{N(SiMe_3)_2\}_2]_2$ (**2**) have essentially identical vibrational spectra, as expected for these similar molecules. The absorbances found at 405 and 380 cm^{-1} are similar in energy to M-N stretching bands found in other first-row transition metal complexes featuring the $-N(SiMe_3)_2$ ligand.[3] We have tentatively assigned the absorbance at ca. 300 cm^{-1} as a M-Cl stretching band, which is in good agreement with that found for other transition metal complexes having bridging halide ligands.[64]

The vibrational spectrum of the titanium halide complex **3** displays a single absorbance in the M-N stretching region at 375 cm^{-1}. No bands attributable to a Ti-H stretching vibration were immediately apparent. However, close examination revealed an absorbance of medium intensity at 1350 cm^{-1} which overlaps with an absorbance associated with the mineral oil medium. Absorbances in this region have previously been attributed to bridging Ti-H stretching modes in titanocene hydrides and amido titanium hydrides. Additionally, this absorbance was not found in the spectra of the halide complexes **1** or **2**, so we have tentatively assigned this absorbance to the bridging Ti-H stretching mode in **3**.

While the vibrational spectrum of $[Co(Br)\{\mu\text{-}N(SiMe_3)_2\}]_2$ (**5**) displays a sharp absorbance at 1250 cm^{-1} which is common in complexes binding the bis(trimethylsilyl)amide ligand,[3] it differs somewhat from the spectra of **1** and **2** (and other silylamide complexes) in the far infrared region. Here, a single absorbance at 475 cm^{-1} was attributed to a Co-N stretching mode of **5**. This absorbance is somewhat higher in energy than that typically found in similar amido complexes. It is also noteworthy that there is only a single

absorbance attributable to this vibration in the spectrum, an observation that we attribute to the presence of fewer amido ligands in **5** (and thus fewer possible vibrations) in comparison to **1** or **2**. A single strong absorbance at 270 cm^{-1} was attributed to a Co-Br stretching mode, which agrees with absorbances found in other complexes with terminal bromide ligands.[64]

NMR Spectroscopy. $[Ti(\mu\text{-}Cl)\{N(SiMe_3)_2\}_2]_2$ (**1**), $[V(\mu\text{-}Cl)\{N(SiMe_3)_2\}_2]_2$ (**2**), and $[Co(Br)\{\mu\text{-}N(SiMe_3)_2\}]_2$ (**5**) have simple ^1H NMR spectra, with single broad signals attributed to the trimethylsilyl protons at 3.38 (**1**), 7.13 (**2**), and -5.12 ppm (**5**) ppm. A second, less intense, broadened signal also appeared at 19.81 ppm in the ^1H NMR spectrum of **2**, which is indicative of the presence of a slight impurity of the trisamide $V\{N(SiMe_3)_2\}_3$.[13,31] The effective magnetic moments of dimeric **1**, **2**, and **5** were determined by Evans' method to be 3.0, 5.0, and 3.8 μ_B, respectively. For **1** and **2**, these values are only slightly lower than the predicted spin only values, suggesting little antiferromagnetic coupling or orbital contribution to their magnetic moments. The linewidth of the ^1H NMR signal of **1** ($\Delta\nu_{1/2}$ = 90 Hz) is narrower than that of **2** ($\Delta\nu_{1/2}$ = 380 Hz), in agreement with its lower effective magnetic moment. In contrast, the magnetic moment of **5** is significantly lower than predicted for a high-spin, three-coordinate d^7 complex, indicating a significant degree of antiferromagnetic coupling between the unpaired spins two metal atoms.

Although the titanium hydride **3** should, in principle, have a more complicated ^1H NMR spectrum than **1** or **2**, only a single paramagnetically broadened signal was observed at 0.97 ppm. Given the proximity of the hydrides and the alkynyl ligand to the metal atoms, these signals are likely too broad to be detected. The effective magnetic moment of **3** was determined by Evans' method to be 1.8 μ_B, indicating the presence of a single unpaired electron in **3**. This value, along with the structure of **3**, identifies **3** as a mixed-valent Ti(III/IV) complex.

Conclusion.

The dimeric complex [Ti(μ-Cl){N(SiMe$_3$)$_2$}$_2$]$_2$ (**1**), the structure of which was recently reported,[47] was shown to be accessible in moderate yield by the reaction of 2 eq. of LiN(SiMe$_3$)$_2$·(OEt$_2$) with TiCl$_3$(NMe$_3$)$_2$. This preparative route was also proven to be applicable to the vanadium analogue [V(μ-Cl){N(SiMe$_3$)$_2$}$_2$]$_2$ (**2**), which is isostructural to **1**. An attempt to isolate a "Ti{N(SiMe$_3$)$_2$}$_2$" complex by reduction of **1** with Na/NaCl resulted instead in the formation of the unusual mixed-metal, mixed-valent Ti(III/IV) hydride complex **3**. The analogous reaction using [V(μ-Cl){N(SiMe$_3$)$_2$}$_2$]$_2$ (**2**) gave only intractable mixtures. Looking to the later transition metals, we have identified the cobalt polymer **4** as a byproduct of the preparation of Co{N(SiMe$_3$)$_2$}$_3$ by reaction of BrN(SiMe$_3$)$_2$ with [Co{N(SiMe$_3$)$_2$}$_2$]$_2$. Although **4** could only be characterized structurally, its identification suggests a plausible fate for the bromine atom in the previously reported synthesis of Co{N(SiMe$_3$)$_2$}$_3$.[16] In further exploring the role of bromine in these reactions, we showed that the reaction of elemental bromine with [Mn{N(SiMe$_3$)$_2$}$_2$]$_2$ unexpectedly afforded Mn{N(SiMe$_3$)$_2$}$_3$ as the only isolable product, while the analogous reaction with [Co{N(SiMe$_3$)$_2$}$_2$]$_2$ instead gave the amido halide complex [Co(Br){μ-N(SiMe$_3$)$_2$}]$_2$ (**5**).

Associated Content.

Supporting information.

The Supporting Information, including spectra (NMR, infrared, UV-Vis), crystallographic data, and photographs of material is available free of charge on the ACS Publications website at https://pubs.acs.org/doi/10.1021/acs.inorgchem.1c03065. CCDC entries 2049999 (**2**), 2061661 (**3**), 2094541 (**4**), and 2094540 (**5**) contain the supplementary crystallographic data of the complexes described here. These data can be obtained free of charge via www.ccdc.cam.ac.uk/data_request/cif, by emailing data_request@ccdc.cam.ac.uk, or by contacting The Cambridge Crystallographic Data Centre, 12 Union Road, Cambridge CB2 1EZ, UK; fax: + 44 1223 336033.

Author Information.

Corresponding author

*pppower@ucdavis.edu

ORCID

Cary R. Stennett: 0000-0002-2727-5747

Philip P. Power: 0000-0002-6262-3209

Notes

The authors declare no competing financial interest.

Acknowledgements

The authors wish to acknowledge the US National Science Foundation (CHE-1565501) for support of this work and for the purchase of a dual-source X-ray diffractometer (CHE-0840444).

References.

(1) Bürger, H.; Wannagat, U. Silylamido-Verbindungen von Chrom, Mangan, Nickel und Kupfer. *Monatsh. Chem.* **1964**, *95*, 1099–1102.

(2) Bürger, H.; Wannagat, U. Silylamido-Derivate von Eisen und Kobalt. *Monatsh. Chem.* **1963**, *94*, 1007–1012.

(3) Alyea, E. C.; Bradley, D. C.; Copperthwaite, R. G. Three-Co-Ordinated Transition Metal Compounds. Part I. The Preparation and Characterization of Tris(Bistrimethylsilylamido)-Derivatives of Scandium, Titanium, Vanadium, Chromium, and Iron. *J. Chem. Soc. Dalton Trans.* **1972**, 1580–1584.

(4) Alyea, E. C.; Bradley, D. C.; Copperthwaite, R. G.; Sales, K. D. Three-Co-Ordinated Transition-Metal Compounds. Part II. Electronic Spectra and Magnetism of Tris(Bistrimethylsilylamido) Derivatives of Scandium, Titanium, Vanadium, Chromium, and Iron. *J. Chem. Soc. Dalton Trans.* **1973**, 185–191.

(5) Bradley, D. C.; Copperthwaite, R. G.; Extine, M. W.; Reichert, W. W.; Chisholm, M. H. Transition Metal Complexes of Bis(Trimethyl-Silyl)Amine (1,1,1,3,3,3-Hexamethyldisilazane). *Inorganic Syntheses*; **1978**; Vol. 18, pp 112–120.

(6) Ghotra, J. S.; Hursthouse, M. B.; Welch, A. J. Three-Co-Ordinate Scandium(III) and Europium(III); Crystal and Molecular Structures of Their Trishexamethyldisilylamides. *J. Chem. Soc., Chem. Commun.* **1973**, 669–670.

(7) Olmstead, M. M.; Power, P. P.; Shoner, S. C. Three-Coordinate Iron Complexes: X-Ray Structural Characterization of the Iron Amide-Bridged Dimers $[Fe(NR_2)_2]_2$ (R = $SiMe_3$, C_6H_5) and the Adduct Fe[$N(SiMe_3)_2$]2(THF) and Determination of the Association Energy of the Monomer $Fe\{N(SiMe_3)_2\}_2$ in Solution. *Inorg. Chem.* **1991**, *30*, 2547–2551.

(8) Hursthouse, M. B.; Rodesiler, P. F. Crystal and Molecular Structure of Tris(Hexamethyldisilylamido)Iron(III). *J. Chem. Soc. Dalton Trans.* **1972**, 2100–2102.

(9) Murray, B. D.; Power, P. P. Three-Coordinate Metal Amides of Manganese(II) and Cobalt(II): Synthesis and X-Ray Structure of the First Tris(Silylamide) of Manganese and the x-Ray Crystal Structures of [M2(N(SiMe3)2)4] (M = Mn, Co). *Inorg. Chem.* **1984**, *23*, 4584–4588.

(10) Faust, M.; Bryan, A. M.; Mansikkamäki, A.; Vasko, P.; Olmstead, M. M.; Tuononen, H. M.; Grandjean, F.; Long, G. J.; Power, P. P. The Instability of $Ni\{N(SiMe_3)_2\}_2$: A Fifty Year Old Transition Metal Silylamide Mystery. *Angew. Chem. Int. Ed.* **2015**, *54*, 12914–12917.

(11) Woen, D. H.; Chen, G. P.; Ziller, J. W.; Boyle, T. J.; Furche, F.; Evans, W. J. Solution Synthesis, Structure, and CO2 Reduction Reactivity of a Scandium(II) Complex, $\{Sc[N(SiMe_3)_2]_3\}^-$. *Angew. Chem. Int. Ed.* **2017**, *56*, 2050–2053.

(12) Putzer, M. A.; Magull, J.; Goesmann, H.; Neumüller, B.; Dehnicke, K. Synthese, Eigenschaften Und Kristallstrukturen Der Titan(III)-Amido-Komplexe $Ti[N(SiMe_3)_2]_3$, $[TiCl_2\{N(SiMe_3)_2\}(THF)_2]$ und $[Na(12\text{-Krone-}4)_2][TiCl_2\{N(SiMe_3)_2\}_2]$. *Chem. Ber.* **1996**, *129*, 1401–1405.

(13) Wagner, C. L.; Phan, N. A.; Fettinger, J. C.; Berben, L. A.; Power, P. P. New Characterization of $V\{N(SiMe_3)_2\}_3$: Reductions of Tris[Bis(Trimethylsilyl)Amido]Vanadium(III) and -Chromium(III) To Afford the Reduced Metal(II) Anions $[M\{N(SiMe_3)_2\}_3]^-$ (M = V and Cr). *Inorg. Chem.* **2019**, *58*, 6095–6101.

(14) Köhn, R. D.; Kociok-Köhn, G.; Haufe, M. The Chemistry of 1,3,5-Triazacyclohexane Complexes, 3. High Yield Synthesis of $[Cr\{N(SiMe_3)_2\}_3]$ and Accurate Structure Determination by Cocrystallization with Me_6Si_2. *Chem. Ber.* **1996**, *129*, 25–27.

(15) Bradley, D. C.; Hursthouse, M. B.; Abdul Malik, K. M.; Möseler, R. The Crystal Molecular Structure of "Bis(Hexamethyldisilylamido) Manganese." *Transit. Met. Chem.* **1978**, *3*, 253–254.

(16) Ellison, J. J.; Power, P. P.; Shoner, S. C. First Examples of Three-Coordinate Manganese(III) and Cobalt(III): Synthesis and Characterization of the Complexes $M[N(SiMe_3)_2]_3$ (M = Mn or Co). *J. Am. Chem. Soc.* **1989**, *111*, 8044–8046.

(17) Bradley, D. C.; Ghotra, J. S.; Hart, F. A. Low Co-Ordination Numbers in Lanthanide and Actinide Compounds. Part I. The Preparation and Characterization of Tris{bis(Trimethylsilyl)-Amido}lanthanides. *J. Chem. Soc. Dalton Trans.* **1973**, No. 10, 1021–1023.

(18) Rees, W. S. J.; Just, O.; Van Derveer, D. S. Molecular Design of Dopant Precursors for Atomic Layer Epitaxy of SrS:Ce. *J. Mater. Chem.* **1999**, *9*, 249–252.

(19) Andersen, R. A.; Templeton, D. H.; Zalkin, A. Structure of Tris(Bis(Trimethylsilyl)Amido)Neodymium(III), $Nd[N(Si(CH_3)_3)_2]_3$. *Inorg. Chem.* **1978**, *17*, 2317–2319.

(20) Brady, E. D.; Clark, D. L.; Gordon, J. C.; Hay, P. J.; Keogh, D. W.; Poli, R.; Scott, B. L.; Watkin, J. G. Tris(Bis(Trimethylsilyl)Amido)Samarium: X-Ray Structure and DFT Study. *Inorg. Chem.* **2003**, *42*, 6682–6690.

(21) Hitchcock, P. B.; Hulkes, A. G.; Lappert, M. F.; Li, Z. Cerium(III) Dialkyl Dithiocarbamates from $[Ce\{N(SiMe_3)_2\}_3]$ and Tetraalkylthiuram Disulfides, and $[Ce(K_2\text{-}S_2CNEt_2)_4]$ from the Ce^{III} Precursor; Tb^{III} and Nd^{III} Analogues. *Dalton Trans.* **2004**, 129–136.

(22) Herrmann, W. A.; Anwander, R.; Munck, F. C.; Scherer, W.; Dufaud, V.; Huber, N. W.; Artus, G. R. J. Lanthanoiden-Komplexe, IX [1]. Reaktivitätsbestimmender Einfluß der Ligandenkonstitution Bei Seltenerdamiden: Herstellung und Struktur Sterisch Überladener Alkoxid-Komplexe / Lanthanoid Complexes, IX [1]. Reactivity Control of Lanthanoid Amides through Ligand Effects: Synthesis and Structures of Sterically Congested Alkoxy Complexes. *Z. Naturforsch., B: Chem. Sci.* **1994**, *49*, 1789.

(23) Bienfait, A. M.; Wolf, B. M.; Törnroos, K. W.; Anwander, R. Trivalent Rare-Earth-Metal Bis(Trimethylsilyl)Amide Halide Complexes by Targeted Oxidations. *Inorg. Chem.* **2018**, *57*, 5204–5212.

(24) Niemeyer, M. Synthesis and Structural Characterization of Several Ytterbium Bis(Trimethylsilyl)Amides Including Base-Free $[Yb\{N(SiMe_3)_2\}_2(\mu\text{-}Cl)]_2$ — A Coordinatively Unsaturated Complex with Additional Agostic $Yb\cdots(H_3C—Si)$ Interactions. *Z. Anorg. Allg. Chem.* **2002**, *628*, 647–657.

(25) Andersen, R. A. Tris((Hexamethyldisilyl)Amido)Uranium(III): Preparation and Coordination Chemistry. *Inorg. Chem.* **1979**, *18*, 1507–1509.

(26) Avens, L. R.; Bott, S. G.; Clark, D. L.; Sattelberger, A. P.; Watkin, J. G.; Zwick, B. D. A Convenient Entry into Trivalent Actinide Chemistry: Synthesis and Characterization of AnI3(THF)4 and An[N(SiMe$_3$)$_2$]$_3$ (An = U, Np, Pu). *Inorg. Chem.* **1994**, *33*, 2248–2256.

(27) Stewart, J. L.; Andersen, R. A. Trivalent Uranium Chemistry: Molecular Structure of [(Me$_3$Si)$_2$N]$_3$U. *Polyhedron* **1998**, *17*, 953–958.

(28) Gaunt, A. J.; Enriquez, A. E.; Reilly, S. D.; Scott, B. L.; Neu, M. P. Structural Characterization of Pu[N(SiMe$_3$)$_2$]$_3$, a Synthetically Useful Nonaqueous Plutonium(III) Precursor. *Inorg. Chem.* **2008**, *47*, 26–28.

(29) Lappert, M. F.; Power, P. P.; Protchenko, A.; Seeber, A. *Metal Amide Chemistry*; Chichester, U.K. : Wiley: Chichester, U.K., 2009.

(30) Mulvey, R. E.; Robertson, S. D. Synthetically Important Alkali-Metal Utility Amides: Lithium, Sodium, and Potassium Hexamethyldisilazides, Diisopropylamides, and Tetramethylpiperidides. *Angew. Chem. Int. Ed.* **2013**, *52*, 11470–11487.

(31) Stennett, C. R.; Fettinger, J. C.; Power, P. P. Unexpected Coordination Complexes of the Metal Tris-Silylamides M{N(SiMe$_3$)$_2$}$_3$ (M = Ti, V). *Inorg. Chem.* **2020**, *59*, 1871–1882.

(32) Stennett, C. R.; Nguyen, T. H.; Power, P. P. Characterization of the "Absent" Vanadium Oxo V(═O){N(SiMe$_3$)$_2$}$_3$, Imido V(═NSiMe$_3$){N(SiMe$_3$)$_2$}$_3$, and Imido-Siloxy V(═NSiMe$_3$)(OSiMe$_3$){N(SiMe$_3$)$_2$}$_2$ Complexes Derived from V{N(SiMe$_3$)$_2$}$_3$ and Kinetic Study of the Spontaneous Conversion of the Oxo Complex into Its Imido-siloxy Isomer. *Inorg. Chem.* **2020**, *59*, 11079–11088.

(33) Stennett, C. R.; Wagner, C. L.; Fettinger, J. C.; Vasko, P.; Power, P. P. Reductions of M{N(SiMe$_3$)$_2$}$_3$ (M = V, Cr, Fe): Terminal and Bridging Low-Valent First-Row Transition Metal Hydrido Complexes and "Metallo-Transamination." *Inorg. Chem.* **2021**, *60*, 11401–11411.

(34) Bradley, D. C.; Hursthouse, M. B.; Newing, C. W.; Welch, A. J. Square Planar and Tetrahedral Chromium(II) Complexes; Crystal Structure Determinations. *J. Chem. Soc., Chem. Commun.* **1972**, No. 9, 567–568.

(35) Zhou, W.; Desnoyer, A. N.; Bailey, J. A.; Patrick, B. O.; Smith, K. M. Direct Synthesis of Ligand-Based Radicals by the Addition of Bipyridine to Chromium(II) Compounds. *Inorg. Chem.* **2013**, *52*, 2271–2273.

(36) König, S. N.; Schädle, C.; Maichle-Mössmer, C.; Anwander, R. Silylamide Complexes of Chromium(II), Manganese(II), and Cobalt(II) Bearing the Ligands $N(SiHMe_2)_2$ and $N(SiPhMe_2)_2$. *Inorg. Chem.* **2014**, *53*, 4585–4597.

(37) Deng, Y.-F.; Han, T.; Wang, Z.; Ouyang, Z.; Yin, B.; Zheng, Z.; Krzystek, J.; Zheng, Y.-Z. Uniaxial Magnetic Anisotropy of Square-Planar Chromium(II) Complexes Revealed by Magnetic and HF-EPR Studies. *Chem. Commun.* **2015**, *51*, 17688–17691.

(38) Evans, D. F. 400. The Determination of the Paramagnetic Susceptibility of Substances in Solution by Nuclear Magnetic Resonance. *J. Chem. Soc.* **1959**, No. 0, 2003–2005.

(39) Bain, G. A.; Berry, J. F. Diamagnetic Corrections and Pascal's Constants. *J. Chem. Educ.* **2008**, *85*, 532.

(40) Andersen, R. A.; Bryan, A. M.; Faust, M.; Power, P. P. Divalent Manganese, Iron, and Cobalt Bis(Trimethylsilyl)Amido Derivatives and Their Tetrahydrofuran Complexes. *Inorg. Synth.* **2018**, *37*, 1–14.

(41) Hicks, J.; Juckel, M.; Paparo, A.; Dange, D.; Jones, C. Multigram Syntheses of Magnesium(I) Compounds Using Alkali Metal Halide Supported Alkali Metals as Dispersible Reducing Agents. *Organometallics* **2018**, *37*, 4810–4813.

(42) Lorberth, J. Zur Synthese Kovalenter Zinn-Stickstoff-Verbindungen. *J. Organomet. Chem.* **1969**, *19*, 435–438.

(43) Sheldrick, G. M. *SADABS*; University of Göttingen, Germany, 1996.

(44) Dolomanov, O. V; Bourhis, L. J.; Gildea, R. J.; Howard, J. A. K.; Puschmann, H. *OLEX2*: A Complete Structure Solution, Refinement and Analysis Program. *J. Appl. Crystallogr.* **2009**, *42*, 339–341.

(45) Sheldrick, G. M. SHELXT - Integrated Space-Group and Crystal-Structure Determination. *Acta Crystallogr. Sect. A Found. Crystallogr.* **2015**, *A71*, 3–8.

(46) Sheldrick, G. M. Crystal Structure Refinement with SHELXL. *Acta Crystallogr. Sect. C, Struct. Chem.* **2015**, *C71*, 3–8.

(47) Quadri, C. C.; Törnroos, K. W.; Le Roux, E. Di-μ-Chlorido-Bis-{bis-[N,N-Bis-(Tri-methyl-sil-yl)Amido]-titanium(III)}. *IUCrData* **2017**, *2*, x171488.

(48) Berno, P.; Gambarotta, S. Reactivity of a Four-Membered Vanadacycle Ring Supported by Bulky Silazanate. Regioselective Hydrogenation of Pyridine. *Organometallics* **1994**, *13*, 2569–2571.

(49) Queen, J. D.; Lehmann, A.; Fettinger, J. C.; Tuononen, H. M.; Power, P. P. The Monomeric Alanediyl :$AlAr^{i}Pr_8$ ($Ar^{i}Pr_8$ = C_6H-2,6-(C_6H_2-2,4,6-Pr^{i}_3)2-3,5-Pr^{i}_2): An Organoaluminum(I) Compound with a One-Coordinate Aluminum Atom. *J. Am. Chem. Soc.* **2020**, *142*, 20554–20559.

(50) Fortier, S.; Kaltsoyannis, N.; Wu, G.; Hayton, T. W. Probing the Reactivity and Electronic Structure of a Uranium(V) Terminal Oxo Complex. *J. Am. Chem. Soc.* **2011**, *133*, 14224–14227.

(51) Bénaud, O.; Berthet, J.-C.; Thuéry, P.; Ephritikhine, M. Iodide, Azide, and Cyanide Complexes of (N,C), (N,N), and (N,O) Metallacycles of Tetra- and Pentavalent Uranium. *Inorg. Chem.* **2011**, *50*, 12204–12214.

(52) Bénaud, O.; Berthet, J.-C.; Thuéry, P.; Ephritikhine, M. Towards High-Valent Uranium Compounds from Metallacyclic Uranium(Iv) Precursors. *Chem. Commun.* **2011**, *47*, 9057–9059.

(53) Putzer, M. A.; Neumüller, B.; Dehnicke, K.; Magull, J. Synthese Und Kristallstrukturen der Amido-Komplexe $[Na(12\text{-Krone-4})_2][M\{N(SiMe_3)_2\}_3]$ mit M = Mn, Fe Und Co. *Chem. Ber.* **1996**, *129*, 715–719.

(54) Karl, M.; Harms, K.; Seybert, G.; Massa, W.; Fau, S.; Frenking, G.; Dehnicke, K. Die Deprotonierung Silylierter Amido-Komplexe von Seltenerdelementen. *Zeitschrift für Anorg. und Allg. Chemie* **1999**, *625*, 2055–2063.

(55) Pyykkö, P. Additive Covalent Radii for Single-, Double-, and Triple-Bonded Molecules and Tetrahedrally Bonded Crystals: A Summary. *J. Phys. Chem. A* **2015**, *119*, 2326–2337.

(56) Gallagher, D. J.; Henderson, K. W.; Kennedy, A. R.; O'Hara, C. T.; Mulvey, R. E.; Rowlings, R. B. Hydride Encapsulation in S-Block Metal Inverse Crown Chemistry. *Chem. Commun.* **2002**, No. 4, 376–377.

(57) Putzer, M. A.; Neumüller, B.; Dehnicke, K. $[Li(12\text{-Krone-4})\{(Me_3Si)_2N\}_2TiCH_2SiMe_2NSiMe_3]$ – Ein Ionenpaar Mit Gestreckter Li–C–Ti-Achse. *Zeitschrift für Anorg. und Allg. Chemie* **1998**, *624*, 1087–1088.

(58) Cosham, S. D.; Johnson, A. L.; Kociok-Köhn, G.; Molloy, K. C. Synthesis, Structural and Thermal Characterisation of Titanium Silylamido Complexes. *J. Organomet. Chem.* **2014**, *772–773*, 27–33.

(59) Love, J. B.; Clark, H. C. S.; Cloke, F. G. N.; Green, J. C.; Hitchcock, P. B. A Non-Metallocene Hydride of Titanium(III). *J. Am. Chem. Soc.* **1999**, *121*, 6843–6849.

(60) Matsuo, T.; Kawaguchi, H. Triple-Hydrogen-Bridged Dititanium(III) and Dizirconium(IV) Aryloxide Complexes. *Organometallics* **2003**, *22*, 5379–5381.

(61) Mo, Z.; Shima, T.; Hou, Z. Synthesis and Diverse Transformations of a Dinitrogen Dititanium Hydride Complex Bearing Rigid Acridane-Based PNP-Pincer Ligands. *Angew. Chem. Int. Ed.* **2020**, *59*, 8635–8644.

(62) Bryan, A. M.; Long, G. J.; Grandjean, F.; Power, P. P. Synthesis, Spectroscopic Characterization, and Determination of the Solution Association Energy of the Dimer $[Co\{N(SiMe_3)_2\}_2]_2$: Magnetic Studies of Low-Coordinate Co(II) Silylamides $[Co\{N(SiMe_3)_2\}_2L]$ (L = PMe_3, Pyridine, and THF) and Related Species That Reveal Evidence of Very Large Zero-Field Splittings. *Inorg. Chem.* **2013**, *52*, 12152–12160.

(63) Jones, P. G.; Daniliuc, C.-G.; Glöckner, A.; Tamm, M. CCDC 2051640: Experimental Crystal Structure Determination. **2020**.

(64) Nakamoto, K. *Infrared and Raman Spectra of Inorganic and Coordination Compounds : Applications in Coordination, Organometallic, and Bioinorganic Chemistry*; John Wiley & Sons, Incorporated: New York, UNITED STATES, 2009.

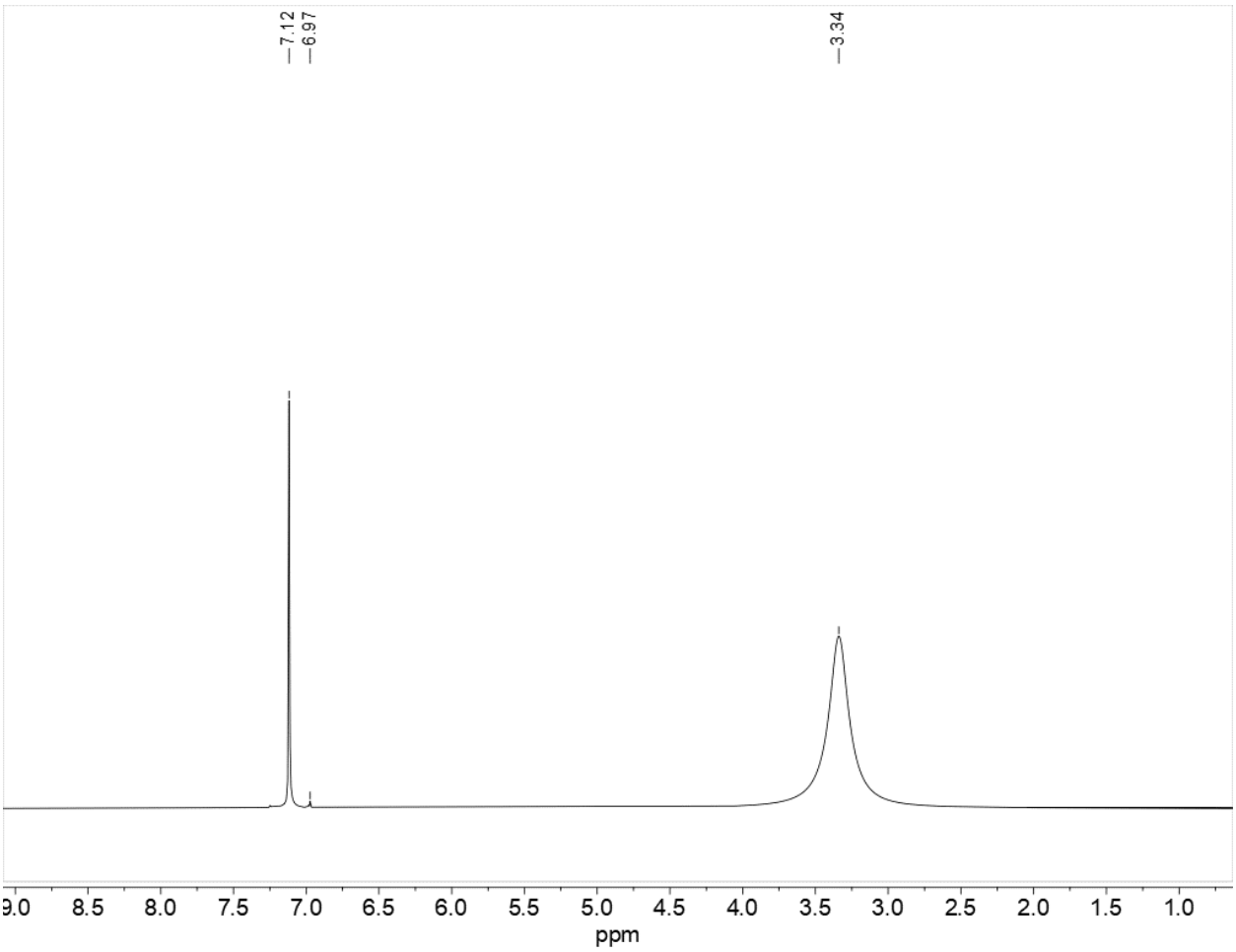

Figure 5.S1. ^{1}H NMR spectrum of $[Ti(\mu\text{-}Cl)\{N(SiMe_3)_2\}_2]_2$ (**1**) (Benzene D_6, 49 mM). The signal at 6.91 ppm is due to the capillary of deuterated benzene used for magnetic moment determination.

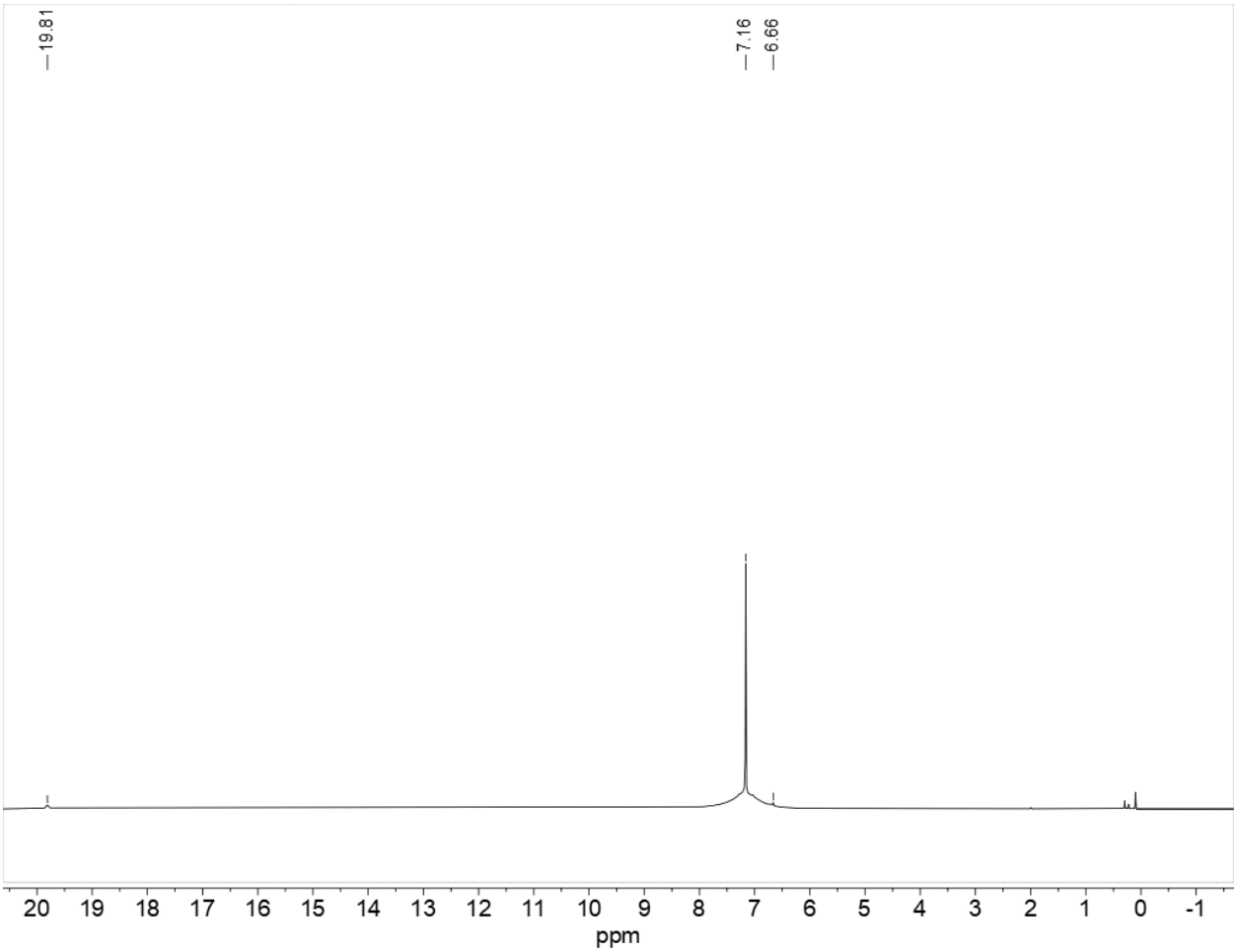

Figure 5.S2. ^{1}H NMR spectrum of [V(μ-Cl){N(SiMe$_3$)$_2$}$_2$]$_2$ (**2**) (Benzene D$_6$, 49 mM). The signal at 6.66 ppm is due to the capillary of deuterated benzene used for magnetic moment determination.

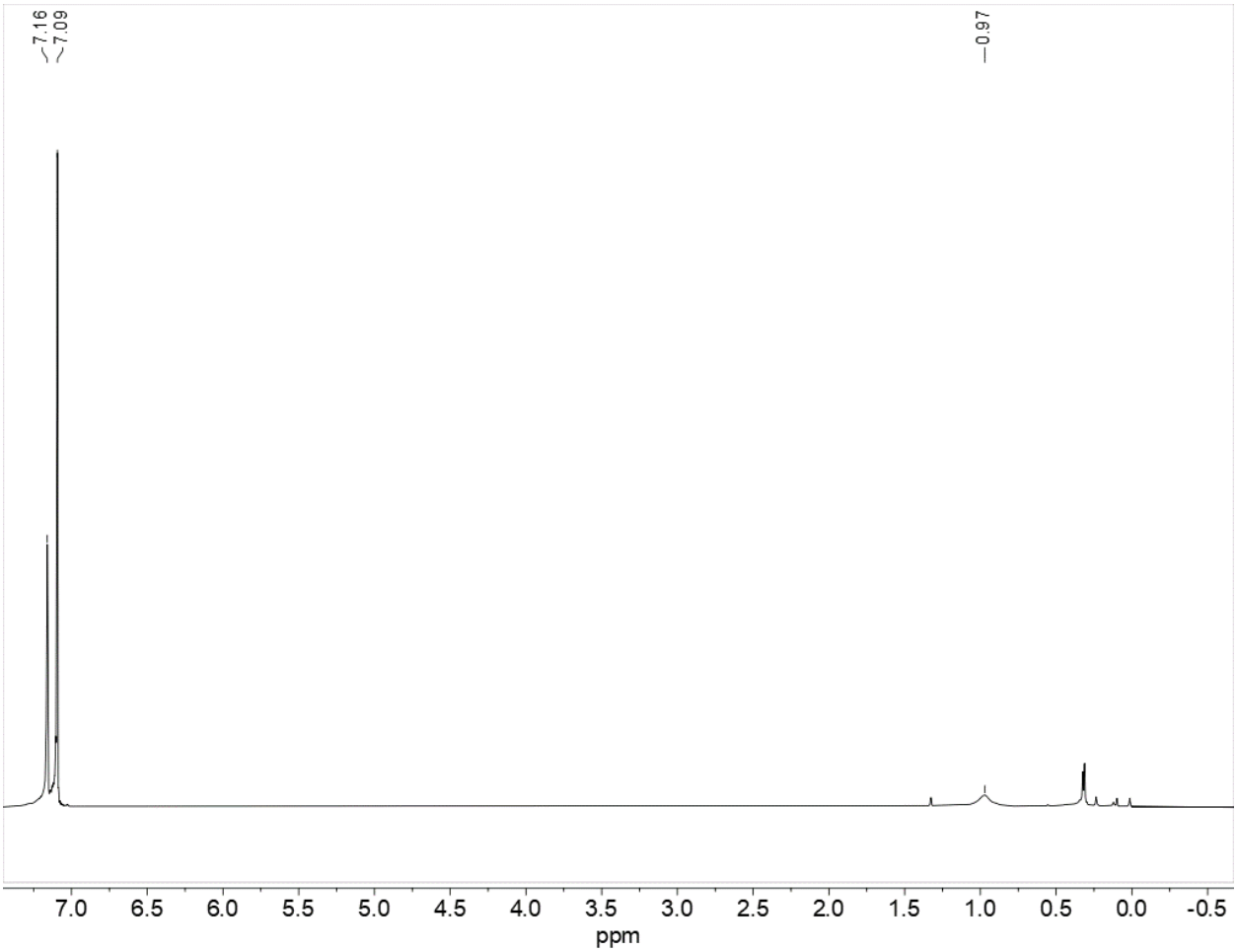

Figure 5.S3. ^{1}H NMR spectrum of $Ti_2(\mu\text{-}H)_2\{N(SiMe_3)_2\}_3\{N(SiMe_3)(SiMe_2CH)\}(Na)$ (**3**) (Benzene D_6, 49 mM). The signal at 7.09 ppm is due to the capillary of deuterated benzene used for magnetic moment determination.

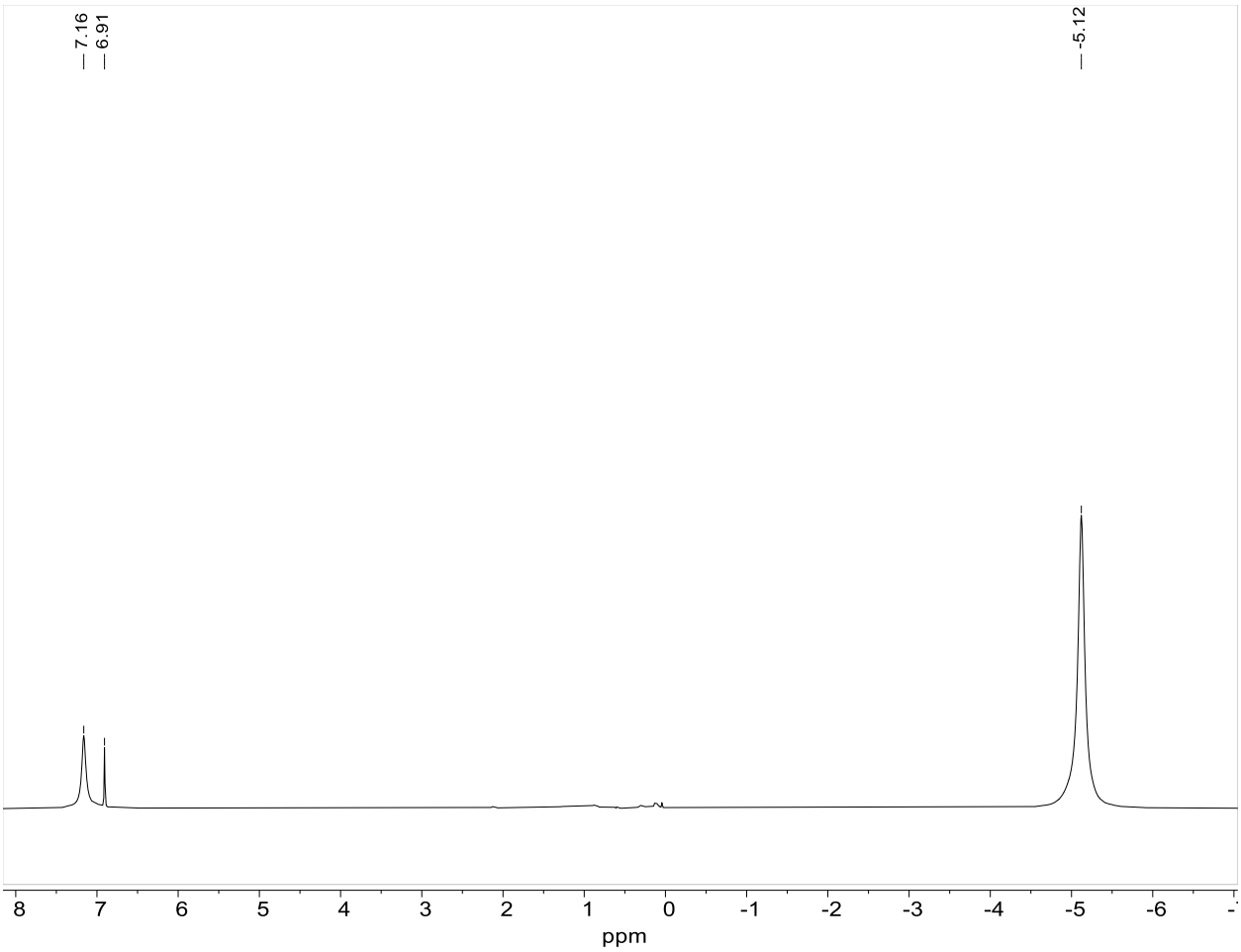

Figure 5.S4. ^{1}H NMR spectrum of [Co(Br){μ-N(SiMe$_3$)$_2$}]$_2$ (**5**) (Benzene D$_6$, 46.8 mM). The signal at 6.91 ppm is due to the capillary of deuterated benzene used for magnetic moment determination.

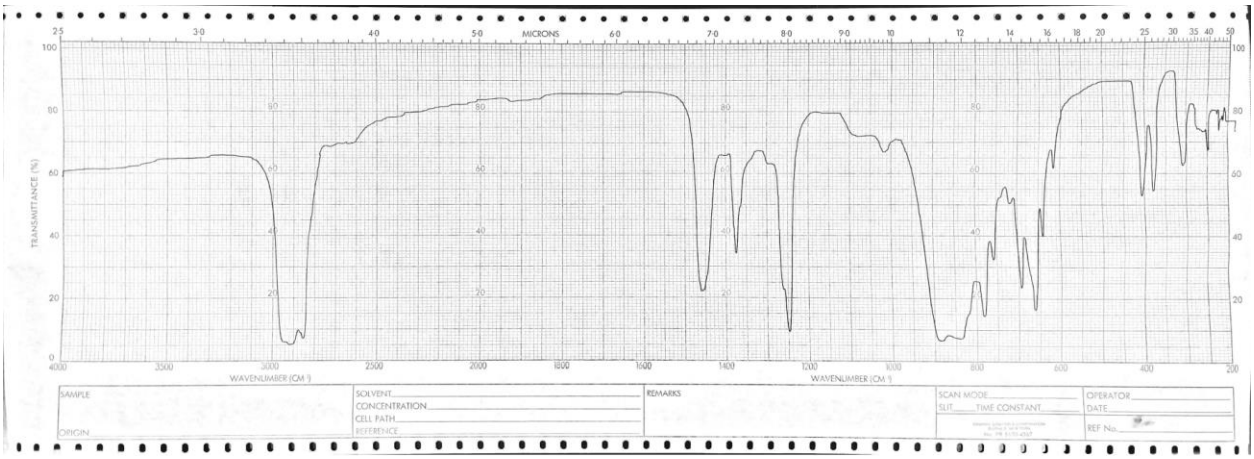

Figure 5.S5. Infrared spectrum of $[Ti(\mu\text{-}Cl)\{N(SiMe_3)_2\}_2]_2$ (**1**).

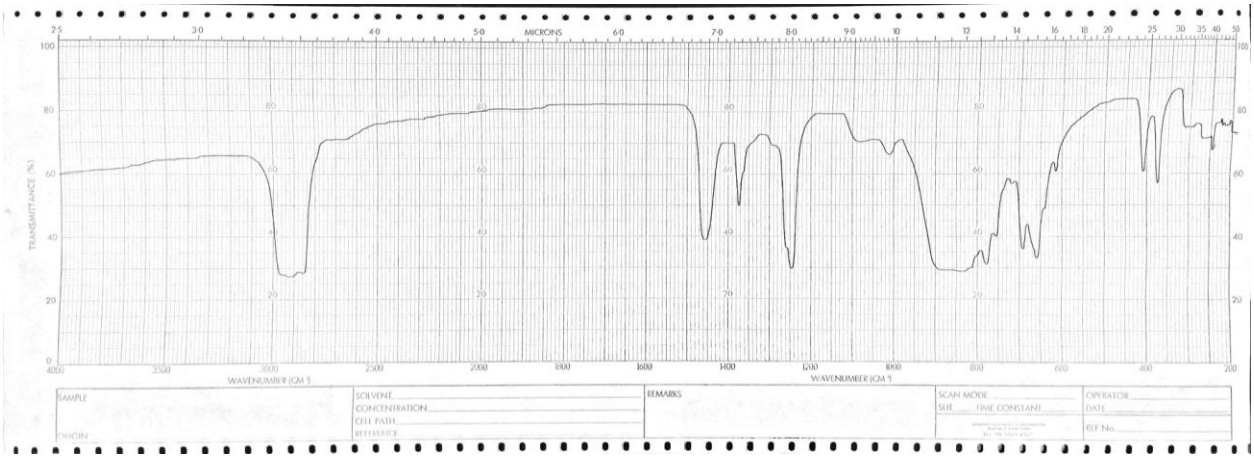

Figure 5.S6. Infrared spectrum of $[V(\mu\text{-}Cl)\{N(SiMe_3)_2\}_2]_2$ (**2**).

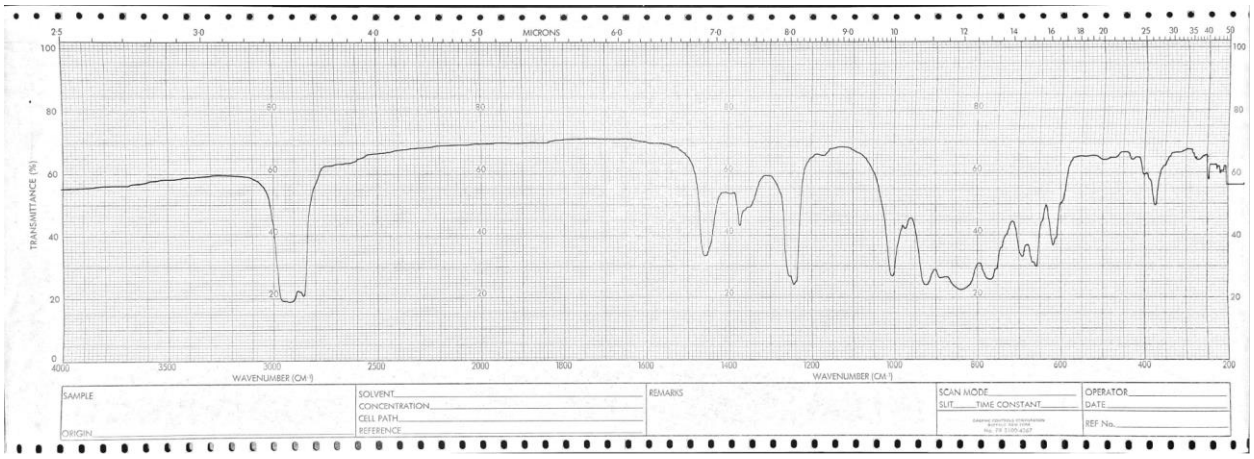

Figure 5.S7. Infrared spectrum of $Ti_2(\mu\text{-}H)_2\{N(SiMe_3)_2\}_3\{N(SiMe_3)(SiMe_2CH)\}(Na)$ (**3**).

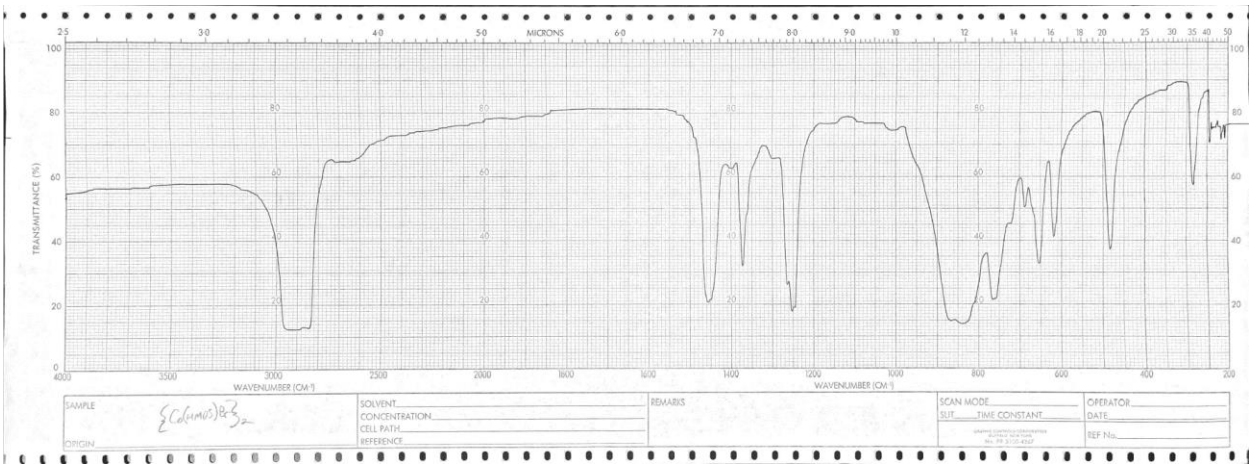

Figure 5.S8. Infrared spectrum of $[Co(Br)\{\mu\text{-}N(SiMe_3)_2\}]_2$ (**5**).

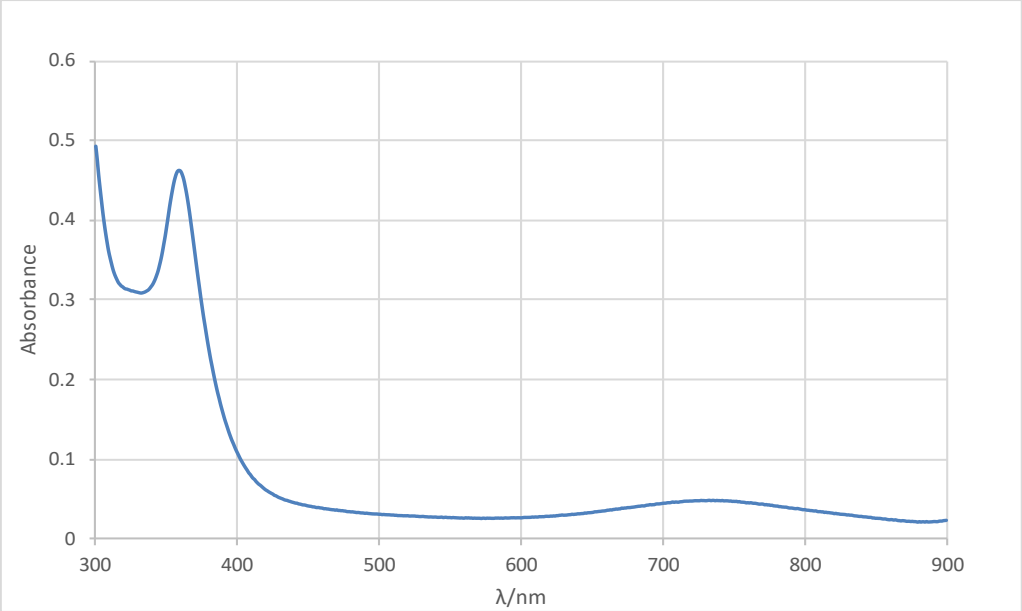

Figure 5.S9. UV-vis spectrum of [Ti(μ-Cl){N(SiMe$_3$)$_2$}$_2$]$_2$ (**1**) (hexanes, 120 μM, 1 cm path length).

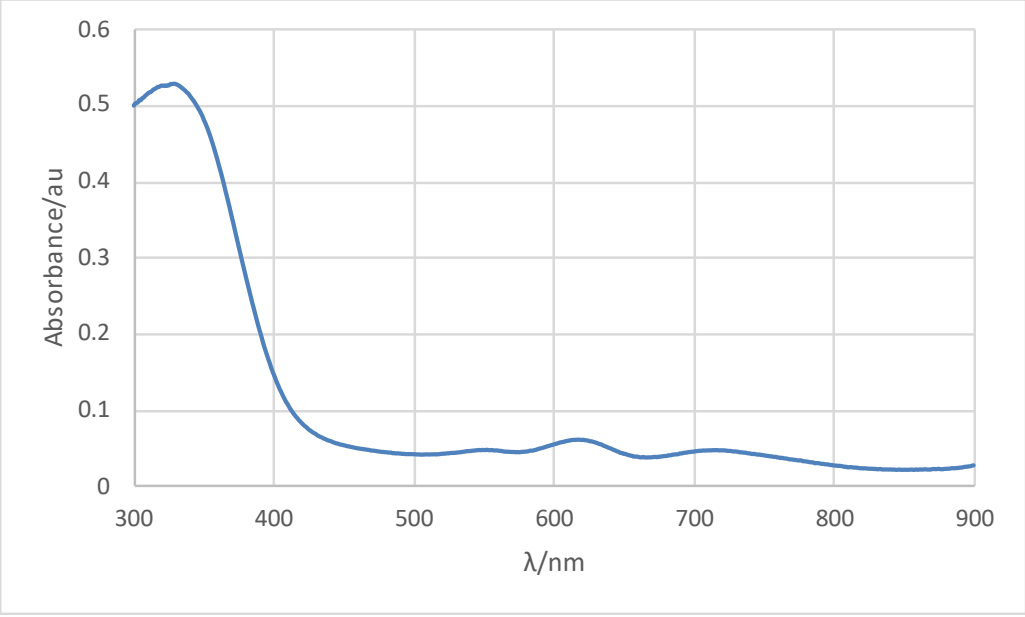

Figure 5.S10. UV-vis spectrum of [V(μ-Cl){N(SiMe$_3$)$_2$}$_2$]$_2$ (**2**) (hexanes, 120 μM, 1 cm path length).

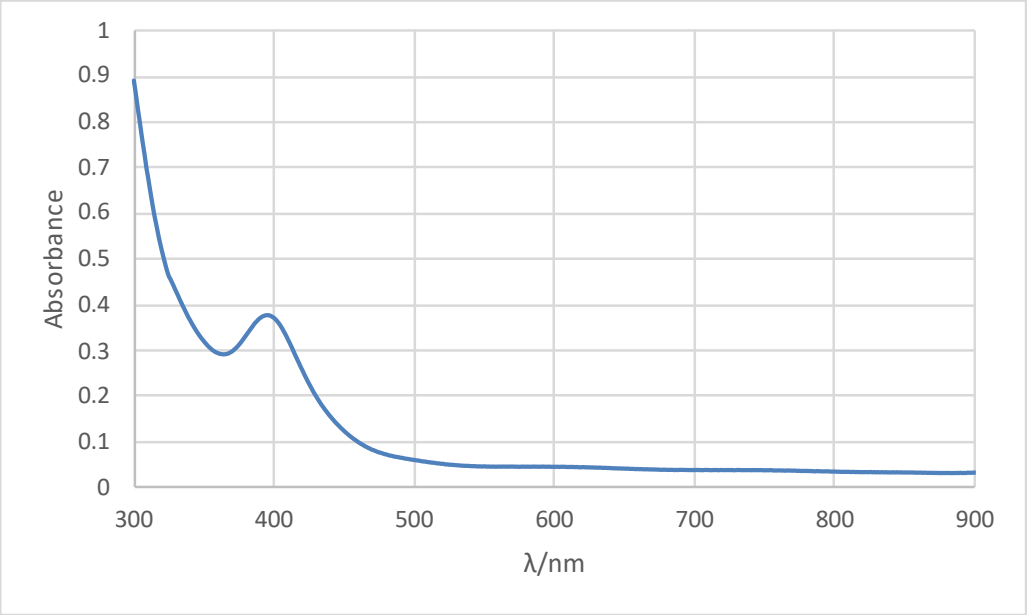

Figure 5.S11. UV-vis spectrum of $Ti_2(\mu\text{-}H)_2\{N(SiMe_3)_2\}_3\{N(SiMe_3)(SiMe_2CH)\}(Na)$ (**3**) (hexanes, 125 μM, 1 cm path length).

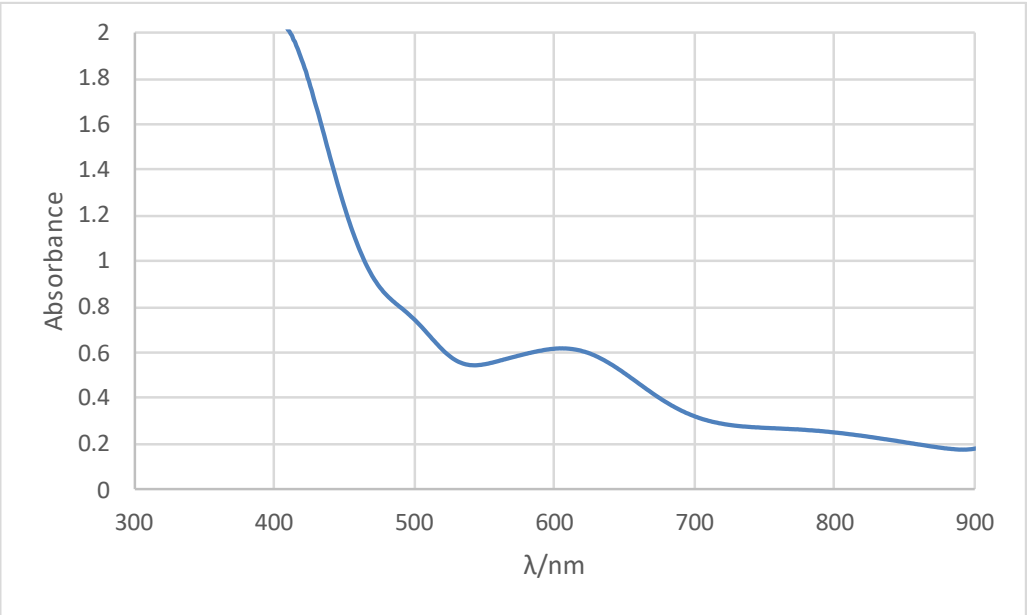

Figure 5.S12. UV-vis spectrum of $Ti_2(\mu\text{-}H)_2\{N(SiMe_3)_2\}_3\{N(SiMe_3)(SiMe_2CH)\}(Na)$ (**3**) (hexanes, 1.25 mM, 1 cm path length).

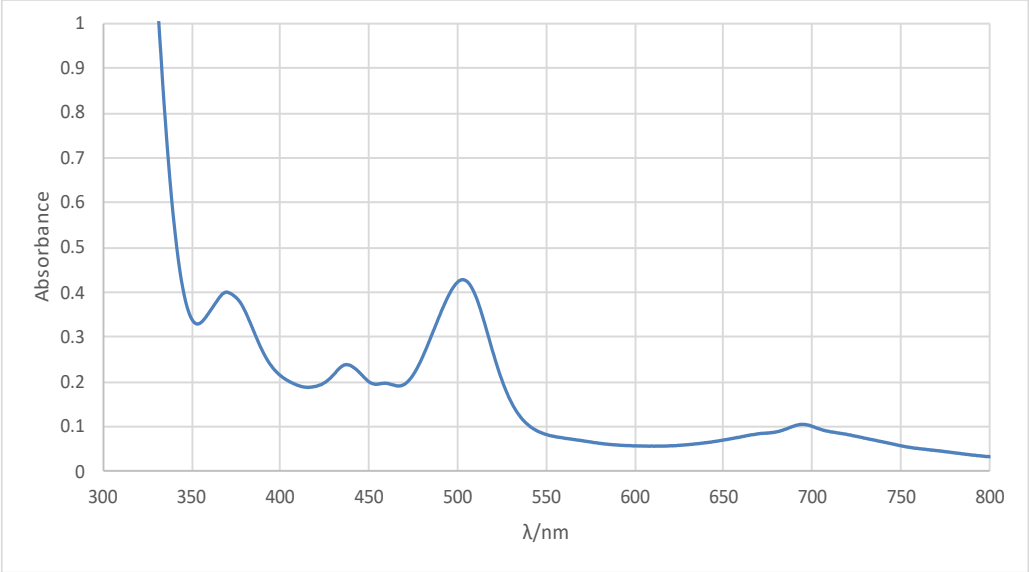

Figure 5.S13. UV-vis spectrum of $[Co(Br)\{\mu\text{-}N(SiMe_3)_2\}]_2$ (**5**) (hexanes, 300 μM, 1 cm path length).

Table 5.S1. X-ray Data Collection Parameters and Crystallographic Details of $[V(\mu\text{-}Cl)\{N(SiMe_3)_2\}_2]_2$ (**2**)

Empirical formula	$C_{24}H_{72}Cl_2N_4Si_8V_2$
Formula weight	814.35
Temperature/K	296.15
Crystal system	triclinic
Space group	P-1
a/Å	8.9594(3)
b/Å	11.6544(4)
c/Å	24.2269(8)
α/°	93.318(2)
β/°	97.079(2)
γ/°	112.001(2)
Volume/Å^3	2312.66(14)
Z	2
ρ_{calc}g/cm^3	1.169
μ/mm^{-1}	0.747
F(000)	872.0
Crystal size/mm^3	0.295 × 0.279 × 0.132
Radiation	MoKα (λ = 0.71073)
2Θ range for data collection/°	1.704 to 55.214
Index ranges	$-11 \leq h \leq 11$, $-15 \leq k \leq 15$, $-31 \leq l \leq 31$
Reflections collected	38433
Independent reflections	10664 [R_{int} = 0.0373, R_{sigma} = 0.0377]
Data/restraints/parameters	10664/10/424
Goodness-of-fit on F^2	1.149
Final R indexes [I>=2σ (I)]	R_1 = 0.0673, wR_2 = 0.1520
Final R indexes [all data]	R_1 = 0.0824, wR_2 = 0.1577
Largest diff. peak/hole / e Å^{-3}	0.46/-0.47

Table 5.S2. X-ray Data Collection Parameters and Crystallographic Details of $Ti_2(\mu\text{-}H)_2\{N(SiMe_3)_2\}_3\{N(SiMe_3)(SiMe_2CH)\}(Na)$**3**

Empirical formula	$C_{24}H_{72}N_4NaSi_8Ti_2$
Formula weight	760.36
Temperature/K	190
Crystal system	monoclinic
Space group	$P2_1/n$
a/Å	11.2782(3)
b/Å	24.9533(7)
c/Å	16.9821(5)
α/°	90
β/°	109.1960(10)
γ/°	90
Volume/Å^3	4513.5(2)
Z	4
ρ_{calc}g/cm^3	1.119
μ/mm^{-1}	5.282
F(000)	1644.0
Crystal size/mm^3	0.506 × 0.443 × 0.321
Radiation	CuKα (λ = 1.54178)
2Θ range for data collection/°	6.552 to 136.704
Index ranges	$-13 \leq h \leq 13$, $-30 \leq k \leq 29$, $-18 \leq l \leq 19$
Reflections collected	59399
Independent reflections	8150 [R_{int} = 0.0411, R_{sigma} = 0.0240]
Data/restraints/parameters	8150/0/387
Goodness-of-fit on F^2	1.050
Final R indexes [I>=2σ (I)]	R_1 = 0.0290, wR_2 = 0.0784
Final R indexes [all data]	R_1 = 0.0295, wR_2 = 0.0787
Largest diff. peak/hole / e Å^{-3}	0.36/-0.39

Table 5.S3. X-ray Data Collection Parameters and Crystallographic Details of $[(\mu\text{-Br})Co\{\mu\text{-N}(SiMe_3)(SiMe_2CH_2CH_2Me_2Si)(Me_3Si)\mu\text{-N}\}Co(\mu\text{-Br})]_\infty$ (**4**)

Empirical formula	$C_{12}H_{34}Br_2Co_2N_2Si_4$
Formula weight	596.45
Temperature/K	90
Crystal system	triclinic
Space group	P-1
a/Å	9.3878(8)
b/Å	10.9140(9)
c/Å	12.9888(10)
α/°	96.817(3)
β/°	106.968(3)
γ/°	110.135(3)
Volume/Å^3	1158.95(17)
Z	2
ρ_{calc}g/cm^3	1.709
μ/mm^{-1}	5.084
F(000)	600.0
Crystal size/mm^3	0.101 × 0.098 × 0.033
Radiation	MoKα (λ = 0.71073)
2Θ range for data collection/°	3.38 to 61.096
Index ranges	$-13 \leq h \leq 13$, $-15 \leq k \leq 15$, $-18 \leq l \leq 18$
Reflections collected	26635
Independent reflections	7059 [R_{int} = 0.1021, R_{sigma} = 0.1180]
Data/restraints/parameters	7059/0/225
Goodness-of-fit on F^2	1.032
Final R indexes [I>=2σ (I)]	R_1 = 0.0603, wR_2 = 0.1096
Final R indexes [all data]	R_1 = 0.1244, wR_2 = 0.1326
Largest diff. peak/hole / e Å^{-3}	1.00/-1.13

Table 5.S4. X-ray Data Collection Parameters and Crystallographic Details of $[Co(Br)\{\mu\text{-}N(SiMe_3)_2\}]_2$ (**5**).

Empirical formula	$C_{12}H_{36}Br_2Co_2N_2Si_4$
Formula weight	598.47
Temperature/K	90
Crystal system	orthorhombic
Space group	$Pca2_1$
a/Å	13.7041(5)
b/Å	14.9425(6)
c/Å	12.6019(5)
α/°	90
β/°	90
γ/°	90
Volume/Å^3	2580.54(17)
Z	4
ρ_{calc}g/cm^3	1.540
μ/mm^{-1}	4.566
F(000)	1208.0
Crystal size/mm^3	0.185 × 0.069 × 0.059
Radiation	MoKα (λ = 0.71073)
2Θ range for data collection/°	2.726 to 61.286
Index ranges	$-19 \leq h \leq 19$, $-21 \leq k \leq 21$, $-17 \leq l \leq 18$
Reflections collected	51347
Independent reflections	7668 [R_{int} = 0.0552, R_{sigma} = 0.0464]
Data/restraints/parameters	7668/1/212
Goodness-of-fit on F^2	1.048
Final R indexes [I>=2σ (I)]	R_1 = 0.0306, wR_2 = 0.0581
Final R indexes [all data]	R_1 = 0.0407, wR_2 = 0.0611
Largest diff. peak/hole / e Å^{-3}	0.67/-0.60
Flack parameter	0.027(8)

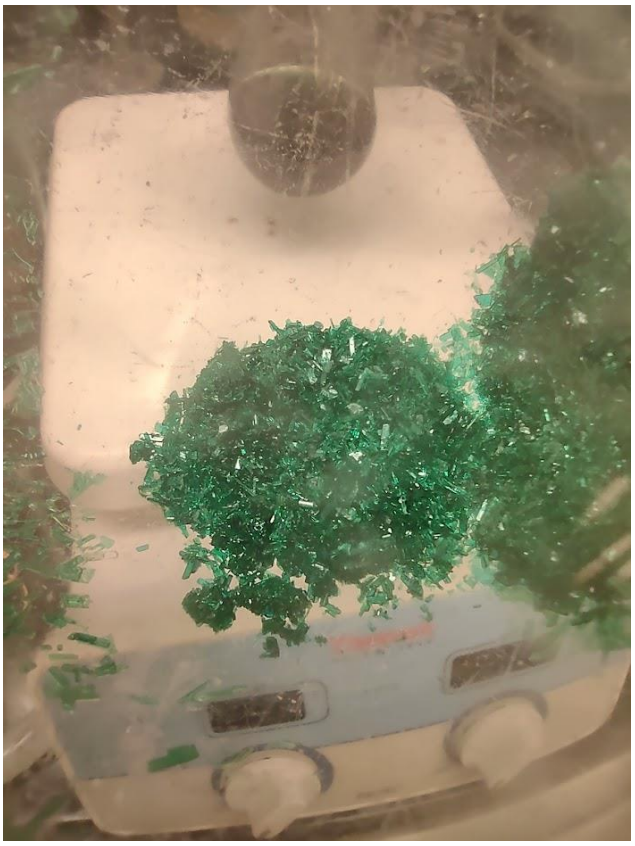

Figure 5.S14. Photograph of crystalline $[Ti(\mu\text{-}Cl)\{N(SiMe_3)_2\}_2]_2$ (**1**)

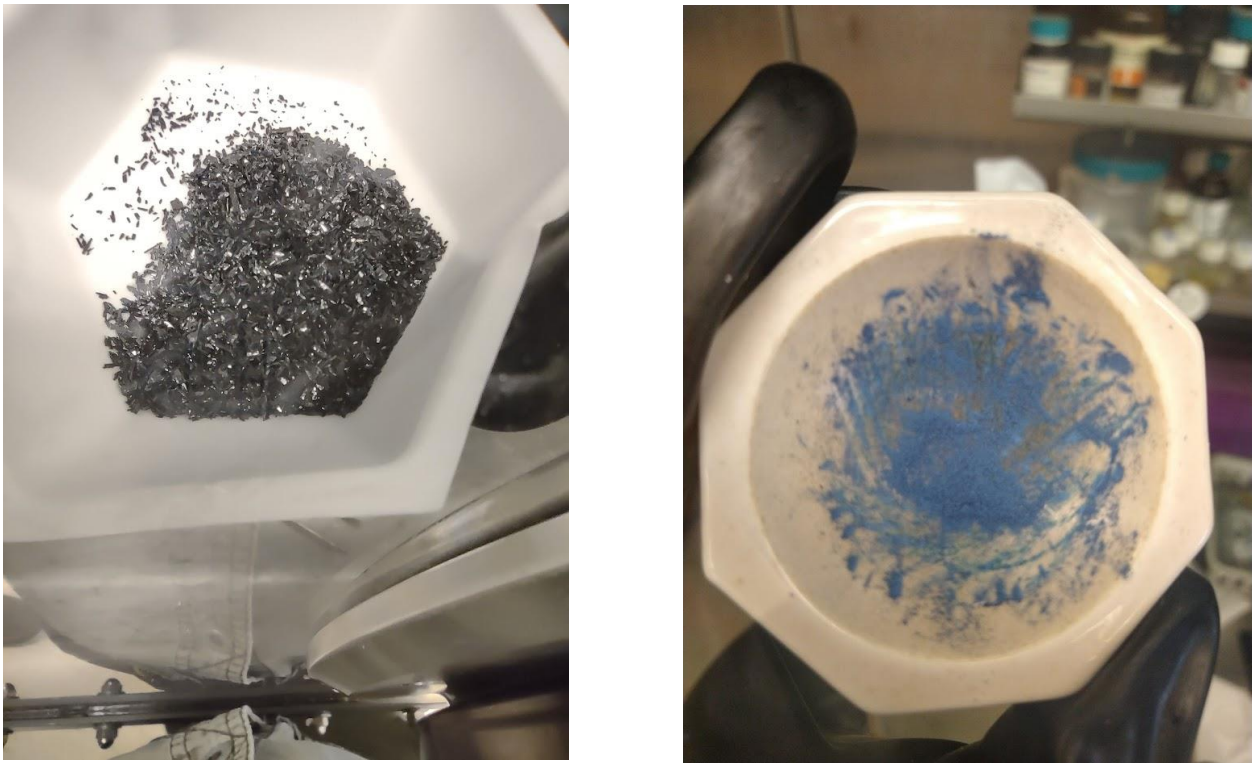

Figure 5.S15. Photograph of crystalline (left) and powdered (right) $[V(\mu\text{-}Cl)\{N(SiMe_3)_2\}_2]_2$ (**2**).

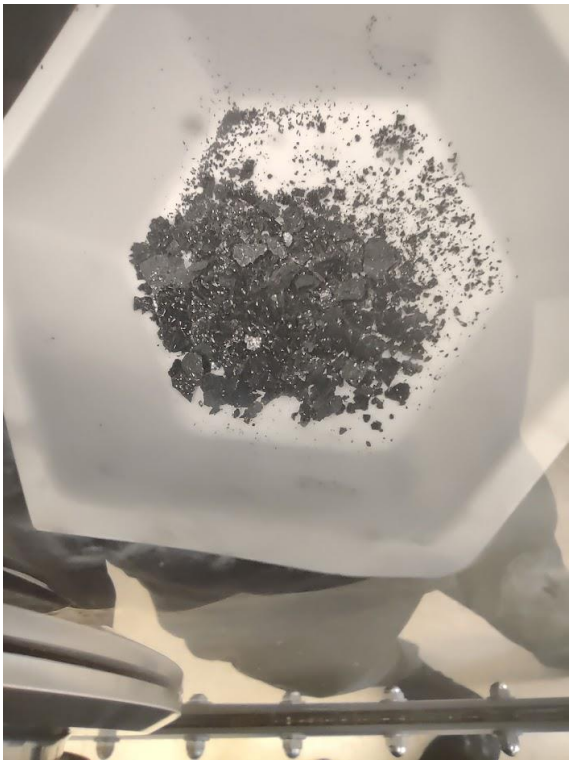

Figure 5.S16. Photograph of crystalline (left) and powdered (right) $Ti_2(\mu\text{-}H)_2\{N(SiMe_3)_2\}_3\{N(SiMe_3)(SiMe_2CH)\}(Na)$ (**3**).

Chapter 6. Low-Coordinate Iron Chalcogenolates and Their Complexes with Diethyl Ether and Ammonia

Cary R. Stennett, James C. Fettinger, and Philip P. Power*

Department of Chemistry, University of California, Davis, One Shields Avenue, Davis, California 95616, United States

This work is dedicated to the memory of Professor Richard H. Holm, a pioneer in the chemistry of iron-sulfur complexes.

Reprinted with permission from *Inorg. Chem.* **2021**, 60, 9, 6712–6720.

Abstract

Treatment of $Fe\{N(SiMe_3)_2\}_2$ with two equivalents of the appropriate phenol or thiol affords the dimers $\{Fe(OC_6H_2\text{-}2,6\text{-}Bu^t_2\text{-}4\text{-}Me)_2\}_2$ (**1**) and $\{Fe(OC_6H_3\text{-}2,6\text{-}Bu^t_2)_2\}_2$ (**2**), or the monomeric $Fe\{SC_6H_3\text{-}2,6\text{-}(C_6H_3\text{-}2,6\text{-}Pr^i_2)_2\}_2$ (**3**). Recrystallization of **1** or **2** from diethyl ether gives the corresponding three-coordinate ether complexes $Fe(OC_6H_3\text{-}2,6\text{-}Bu^t_2\text{-}4\text{-}Me)_2(OEt_2)$ (**4**) and $Fe(OC_6H_3\text{-}2,6\text{-}Bu^t_2)_2(OEt_2)$ (**5**). In contrast, no diethyl ether complex is formed by the dithiolate **3**. The ^{1}H-NMR spectra of **4** and **5** show equilibria between the ether complexes and the base-free dimers. Comparison of these spectra with those of the dimeric **1** and **2** allows unambiguous assignment of the paramagnetically shifted signals. Treatment of **1** with excess ammonia gives the tetrahedral diammine $Fe(OC_6H_2\text{-}2,6\text{-}Bu^t_2\text{-}4\text{-}Me)_2(NH_3)_2$ (**6**). Ammonia is strongly coordinated by **6**, with no apparent loss of ammine ligand either in solution or upon heating under low pressure. In contrast, significantly weaker ammonia coordination is observed when dithiolate **3** is treated with excess ammonia, which gives the diammine $Fe\{SC_6H_3\text{-}2,6\text{-}(2,6\text{-}Pr^i_2\text{-}C_6H_3)_2\}_2(NH_3)_2$ (**7**). Complex **7** readily loses ammonia either in solution or under reduced pressure to give the monoammine complex $Fe\{SC_6H_3\text{-}2,6\text{-}(2,6\text{-}Pr^i_2\text{-}C_6H_3)_2\}_2(NH_3)$ (**8**). The weak binding of ammonia by iron thiolate **7**

reflects the likely behavior of the proposed iron-sulfur active site in nitrogenases, where release of ammonia is required to close the catalytic cycle.

Introduction

Low-coordinate, homoleptic complexes of iron(II) bound to the chalcogenides oxygen or sulfur remain quite scarce despite established routes for their preparation and the ready availability of suitable ligands that might stabilize them.[1,2] For example, dimeric chalcogenolate complexes featuring three-coordinate iron are accessible when ligands of sufficient size are used. The first complex of this type, $\{Fe(SC_6H_2\text{-}2,4,6\text{-}Bu^t_3)_2\}_2$, its manganese and cobalt analogues, the analogous iron aryloxide complex, $\{Fe(OC_6H_2\text{-}2,4,6\text{-}Bu^t_3)_2\}_2$, the thiolate complex $\{Fe(SC_6H_2\text{-}2,4,6\text{-}Ph_3)_2\}_2$ and a structurally similar boryloxide complex $[Fe\{OB(C_6H_2\text{-}2,4,6\text{-}Me_3)_2\}_2]_2$ were reported in the early 1990s.[1–4] The isolation of monomeric chalcogenolate complexes of iron(II) becomes possible when ligands of even greater steric demand are employed as in $Fe\{SC_6H_3\text{-}2,6\text{-}(C_6H_2\text{-}2,4,6\text{-}Me_3)_2\}_2$ and $Fe\{OC_6H_3(C_6H_3\text{-}2,6\text{-}Pr^i_2)_2\}_2$ which were reported in 1994 and 2009, respectively.[5,6]

Since these early reports, a few further monomeric and dimeric homoleptic $Fe(ER)_2$ (E = O, S) complexes of iron(II) have been structurally characterized. For example: $[Fe\{SC_6H_3\text{-}2,6\text{-}(SiMe_3)_2\}_2]_2$ by Henkel,[7] $[Fe(SC_6H_3\text{-}2,6\text{-}(C_6H_5)_2\}_2]_2$ and $[Fe\{SC_6H_3\text{-}2,6\text{-}(4\text{-}Me\text{-}C_6H_4)_2\}_2]_2$ by Tatsumi,[8] and $\{Fe(SSiBu^t_3)_2\}_2$ reported by Wolczanski.[9] No newer dimeric complexes of this type featuring iron bound to oxygen have been reported. More recent reports of monomeric $Fe(ER)_2$ (E = O, S) chalcogenolates are similarly scarce. Examples include $Fe\{SC_6H_3\text{-}2,6\text{-}(2,4,6\text{-}Pr^i_3\text{-}C_6H_2)_2\}_2$ and $Fe\{SC_6H_3\text{-}(2,6\text{-}Pr^i_2\text{-}C_6H_3)\}_2$ reported by this group in 2005 and 2018, respectively,[10,11] $Fe\{SC_6H_3\text{-}2,6\text{-}(2,6\text{-}Me_2\text{-}C_6H_3)_2\}_2$ and $Fe[SC_6H_2\text{-}2,4,6\text{-}\{CH(SiMe_3)_2\}_2]_2$ by Tatsumi in 2007 and 2018,[8,12] and $Fe\{OC_6H_3\text{-}2,6\text{-}(1\text{-}Ad)_2\text{-}4\text{-}Me\}_2$ and $Fe\{OC_6H_3\text{-}2,6\text{-}(1\text{-}Ad)_2\text{-}4\text{-}Pr^i\}_2$ by Kawaguchi in 2011.[13] However, the chemistry of these complexes remains poorly explored.

This lack of reactivity studies is in contrast to the comparatively well explored chemistry of the related iron(II) amido complexes.[14–16] In the original report on $\{Fe(OC_6H_2\text{-}2,4,6\text{-}Bu^t_3)_2\}_2$, a survey of the available structural data suggested that the Fe-O bonding is primarily ionic.[1] We therefore sought to examine the potentially different coordination chemistry of iron(II) chalcogenolates. Herein we report the synthesis and structural and spectroscopic characterization of two new dimeric iron aryloxide complexes, $\{Fe(OC_6H_2\text{-}2,6\text{-}Bu^t_2\text{-}4\text{-}Me)_2\}_2$ (**1**) and $\{Fe(OC_6H_3\text{-}2,6\text{-}Bu^t_2)_2\}_2$ (**2**), and a more efficient preparation of the monomeric thiolate complex $Fe\{SC_6H_3\text{-}2,6\text{-}(2,6\text{-}Pr^i_2\text{-}C_6H_3)_2\}_2$ (**3**). Recrystallization of complexes **1** or **2** from diethyl ether gives $Fe(OC_6H_2\text{-}2,6\text{-}Bu^t_2\text{-}4\text{-}Me)_2(OEt_2)$ (**4**) or $Fe(OC_6H_3\text{-}2,6\text{-}Bu^t_2)_2(OEt_2)$ (**5**), which are rare examples of complexes of iron that coordinate diethyl ether. A comparative study of the ^{1}H-NMR spectra of paramagnetic aryloxide complexes **1**, **2**, **4**, and **5** enables complete assignment of their respective ^{1}H-NMR spectra. Treatment of aryloxide **1** with excess ammonia gives the bisammine complex $Fe\{(OC_6H_2\text{-}2,6\text{-}Bu^t_2\text{-}4\text{-}Me)_2\}_2(NH_3)_2$ (**6**), which features strong coordination of ammonia. In contrast, we show that the treatment of the monomeric thiolate complex **3** with excess ammonia gives the bisammine species $Fe\{SC_6H_3\text{-}2,6\text{-}(2,6\text{-}Pr^i_2\text{-}C_6H_3)_2\}_2(NH_3)_2$ (**7**), which readily dissociates one of its ammonia molecules in solution. Similarly, brief exposure of **7** to reduced pressure affords the monoammine complex $Fe\{SC_6H_3\text{-}2,6\text{-}(2,6\text{-}Pr^i_2\text{-}C_6H_3)_2\}_2(NH_3)$ (**8**). Extended heating of **8** under reduced pressure removes the remaining ammine ligand to yield uncomplexed **3**.

Experimental

General Considerations. All manipulations were performed by using modified Schlenk techniques or in a Vacuum Atmospheres glove box under an atmosphere of dry argon. Solvents were dried and collected using a S2 Grubbs-type[17] solvent purification system (Glass Contour) and degassed using the freeze, pump, thaw method. All physical measurements were obtained under strictly anaerobic and anhydrous conditions. IR spectra were recorded as Nujol mulls between CsI windows on a Perkin-Elmer 1430 spectrophotometer. UV-visible spectra were recorded as dilute hexane solutions in 3.5 mL quartz cuvettes using an OLIS modernized Cary 14 UV/VIS/NIR spectrophotometer. Melting points of samples

in flame-sealed capillaries were determined using a Meltemp II apparatus equipped with a partial immersion thermometer. Magnetic susceptibility data were collected by the Evans' method using the indicated deuterated solvent and were corrected using the appropriate diamagnetic constants.[18,19] $[Fe\{N(SiMe_3)_2\}_2]_2$ and HSAr [Ar =C_6H_3-2,6-(2,6-$^iPr_2$-C_6H_3)$_2$] were prepared according to literature procedures.[20,21] The substituted phenols were purchased from Sigma Aldrich and purified by recrystallization from hexanes after overnight storage as a solution in the same solvent over 4 Å molecular sieves.

$\{Fe(OC_6H_2$-2,6-Bu^t_2-4-$Me)_2\}_2$ (1). Complex **1** was prepared by using a modified procedure previously reported for the preparation of $\{Fe(OC_6H_2$-2,4,6-$Bu^t_3)_2\}_2$.[1] A solution of 2,6-di-tert-butyl-4-methylphenol (3.5 g, 16 mmol) in hexanes (ca. 50 mL) was added dropwise to a stirred, green solution of $Fe\{N(SiMe_3)_2\}_2$ (3.0 g, 8.0 mmol) in hexanes (ca. 20 mL) at room temperature and the mixture was stirred overnight to give a dark yellow solution. The solvent was removed under reduced pressure to give a yellow residue. Pumping was continued for 30 minutes with gentle heating (ca. 50 °C), after which the residue was extracted in hexanes (ca. 50 mL). Filtration through a Celite padded frit, followed by concentration to ca. 20 mL under reduced pressure and storage overnight at ca. -30 °C yielded 3.3 g (84%) of the product as amber crystals. M.p. 243-245 °C (dec.). UV/Vis: λ/nm (ε/$M^{-1}cm^{-1}$): 389 (2000), 275 (shoulder, 8000), 239 (11000). IR (Nujol) $\tilde{\nu}$ [cm^{-1}] = 3650w, 1660w, br, 1310w, 1260w, 1230w, 1190w, 1155w, 930w, 915w, 880w, 8602, 620w, 570w, 460w, 390w. ^{1}H NMR (400 MHz, [D_6] benzene, 25 °C): δ = 106.66 (*m*-H, terminal, $\Delta\nu_{1/2}$ = 110 Hz), 95.55 (*p*-Me, terminal, $\Delta\nu_{1/2}$ = 50 Hz), 30.23 (*p*-Me, bridging, $\Delta\nu_{1/2}$ = 12 Hz), 16.82 (*o*-Bu^t, bridging, $\Delta\nu_{1/2}$ = 720 Hz), 7.92 (*m*-H, bridging, $\Delta\nu_{1/2}$ = 50 Hz), -29.40 (o-Bu^t, terminal, $\Delta\nu_{1/2}$ = 860 Hz). μ_{eff}: 3.6 μ_B.

$\{Fe(OC_6H_3$-2,6-$Bu^t_2)_2\}_2$ (2). Solid 2,6-di-tert-butylphenol (2.2 g, 10.6 mmol) and $Fe\{N(SiMe_3)_2\}_2$ (2.0 g, 5.3 mmol) were combined in a 100 mL Schlenk flask. The reactants were then melted by external heating (ca. 50 °C) until they combined to form a solid yellow mass. The flask was then briefly evacuated for five minutes to remove the eliminated $HN(SiMe_3)_2$. Hexanes (ca. 25 mL) were added, and gentle heating was resumed with stirring until the reactants had completely dissolved. Stirring was discontinued and the

reaction was allowed to come to room temperature. The flask was then stored overnight at ca. 5 °C to yield 1.2 g (47 %) of the product **2** as yellow crystals. M.p 218-221°C. UV/Vis: λ/nm (ε/$M^{-1}cm^{-1}$): 381 (6000), 300 (10,000). IR (Nujol) $\tilde{\nu}$ [cm^{-1}] = 3650w, 3185w, 3085w, 2710w, 2510w, 1910w, 1890m, 1780w, 1690m, 1630m, 1580s, sh, 1530w, 1255s, br, 1180s, br, 1105s, br, 1020m, sh, 945w, 915w, 880s, sh, 840s ,sh, 800s, sh, 740s, sh, 670s, sh, 635s, sh, 580m, sh, 540, sh, 450s, 410s, 310s. ^{1}H NMR (400 MHz, [D_6] benzene, 25 °C): δ = 105.84 (*m*-H, terminal, $\Delta\nu_{1/2}$ = 133 Hz), 16.59 (*o*-Bu^t, bridging, $\Delta\nu_{1/2}$ = 686 Hz), 7.62 (*m*-H, bridging, $\Delta\nu_{1/2}$ = 56 Hz), -18.39 (*p*-H, terminal, $\Delta\nu_{1/2}$ = 38 Hz), -24.33 (*o*-Bu^t, terminal, $\Delta\nu_{1/2}$ = 892 Hz), -59.09 (*p*-H, bridging, $\Delta\nu_{1/2}$ = 47 Hz). μ_{eff}: 3.3 μ_B.

Fe{SC$_6$H$_3$-2,6-(C$_6$H$_3$-2,6-Pr$^i_2$)$_2$}$_2$ (3). Complex **3** was prepared in a manner analogous to that used for complex **1**. A solution of HSC$_6$H$_3$-2,6-(C$_6$H$_3$-2,6-Pr$^i_2$)$_2$}$_2$ (7.4 g, 17.3 mmol) in hexanes (ca. 50 mL) was added dropwise to a stirred solution of Fe{N(SiMe$_3$)$_2$}$_2$ (3.3 g, 8.6 mmol) in hexanes (ca. 20 mL) and the mixture was stirred overnight. The solvent was then removed under reduced pressure to afford a dark red residue. The residue was dissolved in ca. 50 mL of diethyl ether, and the solvent was removed under reduced pressure until a large amount of red, microcrystalline material formed. The red crystals were then separated by cannula, washed with cold diethyl ether, and residual solvent was removed under reduced pressure to give 3.0 g of **3**. An additional 1.9 g of **3** was collected by recrystallization upon storage of the mother liquor for one week at -18 °C (overall yield: 4.9 g, 62%). M.p: > 260 °C. UV/Vis: λ/nm (ε/$M^{-1}cm^{-1}$): 330 (4000), 457 (3000). IR (Nujol) $\tilde{\nu}$ [cm^{-1}] = 1570w, 1310m, 1180w, 1100m, 1040w, 930w, 800s, 760s, 700m, sh, 600w, 580w, 550w, 480m, 400m, 350m. ^{1}H NMR (400 MHz, [D_6] benzene, 25 °C): δ = 56.26 (4H, $\Delta\nu_{1/2}$ = 37 Hz), 25.66 (8H, $\Delta\nu_{1/2}$ = 165 Hz), 2.64 (24H, -CH(C<u>H</u>$_3$)$_2$, $\Delta\nu_{1/2}$ = 24 Hz), -19.51 (2H, *p*-H, central ring, $\Delta\nu_{1/2}$ = 24 Hz), -21.41 (24H, -CH(C<u>H</u>$_3$)$_2$, $\Delta\nu_{1/2}$ = 121 Hz), -21.70 (8H, $\Delta\nu_{1/2}$ = 136 Hz), -23.17 (4H, $\Delta\nu_{1/2}$ = 96 Hz). μ_{eff}: 5.1 μ_B.

Fe(OC$_6$H$_3$-2,6-Bu$^t_2$-4-Me)$_2$(OEt$_2$) (4). 2,6-di-tert-butyl-4-methylphenol (1.1 g, 5.3 mmol) and Fe{N(SiMe$_3$)$_2$}$_2$ (1.0 g, 2.6 mmol) were combined as solids in a 50 mL flask. The flask was then evacuated, and the solids were gently warmed (ca. 50 °C) with stirring for 30 minutes to give a fine yellow powder.

The powder was extracted in ca. 20 mL of diethyl ether. Overnight cooling of this solution at ca. 0 °C gave 0.45 g of yellow/green crystals of **4** that were suitable for X-ray diffraction studies. A second collection of crystals grown from the mother liquor afforded an additional 0.30 g of the product (overall yield: 0.75 g, 51%). M.p: 231 °C. UV/Vis: λ/nm (ε/$M^{-1}cm^{-1}$): 313 (shoulder, 3000), 394 (2000). IR (Nujol) $\tilde{\nu}$ [cm^{-1}] = 1730w, 1400s, 1340m, 1250s, 1190m, 1170m, sh, 1100m, sh, 1090m, sh, 1070m, 1050m, 1030m, 1000m, sh, 930w, 890w, 850s, 810m, sh, 790m, 760m, 560m, 340m, sh, 320m, 280w. ^{1}H NMR (400 MHz, [D_6] benzene, 25 °C): δ = 86.90 (*m*-H, $\Delta\nu_{1/2}$ = 113 Hz), 81.11 (*p*-Me, $\Delta\nu_{1/2}$ = 54 Hz), -19.38 (*o*-Bu^t, $\Delta\nu_{1/2}$ = 765 Hz), other signals are due to the presence the dimer **1**. μ_{eff}: 5.1 μ_B.

Fe(OC_6H_3-2,6-Bu^t_2)$_2$(OEt_2) (5). A solution of 2,6-di-tert-butylphenol (2.2 g, 10.6 mmol) in hexanes (ca. 50 mL) was added dropwise to a stirred solution of Fe{$N(SiMe_3)_2$}$_2$ (2.0 g, 5.3 mmol) in hexanes (ca. 20 mL) at room temperature and the mixture was stirred overnight. The solvent was then removed under reduced pressure to afford a yellow residue. Evacuation was continued for 30 minutes with gentle heating (50 °C), whereupon the residue was extracted in diethyl ether (ca. 50 mL). The solution was filtered through a Celite-padded frit and concentrated until a large amount of yellow precipitate had formed. The flask was gently warmed by hand until the solid had redissolved, and the flask was placed in an ice bath for 1 h to yield 1.4 g (50%) of the product as pale yellow/green crystals. M.p: 129-131 °C. UV/Vis: λ/nm (ε/$M^{-1}cm^{-1}$): 383 (700), 300 (shoulder, 4000), 270 (16000). IR (Nujol) $\tilde{\nu}$ [cm^{-1}] = 3650w, 1910w, 1840w, 1580s, sh, 1260s, br, 1210w, 1190m, br, 1150m, sh, 1120m, 1100m, 1030s, 930w, sh, 880s, 820m, sh, 800m, sh, 780w, 750s, sh, 680s, sh, 550m, 460s, 380s, 320m, sh, 270w. ^{1}H NMR (400 MHz, [D_6] benzene, 25 °C): δ = 84.95 (*m*-H, $\Delta\nu_{1/2}$ = 91 Hz), -18.77 (*o*-Bu^t, $\Delta\nu_{1/2}$ = 858 Hz), -23.35 (*p*-H, $\Delta\nu_{1/2}$ = 50 Hz), other signals are due to the presence the dimer **2**. μ_{eff}: 5.4 μ_B.

Fe(OC_6H_2-2,6-Bu^t_2-4-Me)$_2$(NH_3)$_2$ (6). Anhydrous ammonia (ca. 30 mL, dried over sodium) was condensed onto solid **1** (0.6 g, 0.6 mmol) cooled in a bath of liquid nitrogen. The flask was then removed from the cold bath and allowed to warm to room temperature with stirring while the excess ammonia was allowed to evaporate. Any residual ammonia was then removed under reduced pressure, leaving 0.56 g (87

%) of the colorless bisammine complex. Recrystallization of a concentrated solution of **6** in diethyl ether afforded colorless crystals of **6** that were suitable for single crystal X-ray diffraction studies. M.p. 167-170 °C (dec.). IR (Nujol) $\tilde{\nu}$ [cm^{-1}] = 3630w, 3340w, br, 3245w, 1610w, 1300w, 1250w, 1220w, 1145w, 1110w, 1080w, 1010w, 850w, 765w, 755w, 610w, 440w. ^{1}H NMR (400 MHz, [D_6] benzene, 25 °C): δ = 52.93 (*m*-H, $\Delta\nu_{1/2}$ = 122 Hz), 51.17 (*p*-CH_3, $\Delta\nu_{1/2}$ = 56 Hz), -1.34 (*o*-Bu^t, $\Delta\nu_{1/2}$ = 1067 Hz). μ_{eff}: 6.1 μ_B.

Fe{SC_6H_3-2,6-(2,6-^{i}Pr$_2$-C_6H_3)$_2$}$_2$(NH_3)$_2$ (7). Anhydrous ammonia (ca. 30 mL, dried over sodium) was condensed onto a red solution of **3** (1.0 g, 1.0 mmol) in ca. 30 mL diethyl ether cooled to ca. -78 °C. The mixture was stirred for one hour after which time the flask was removed from the cold bath, allowed to warm to room temperature with stirring. The excess ammonia was allowed to evaporate, giving a light brown solution. The solvent was removed under reduced pressure until a solid began to form on the wall of the flask. The mixture was then gently warmed (ca. 40°C) to dissolve the solid. Storage of this solution for one week at room temperature afforded colorless single crystals of the bisammine complex **7** that were suitable for X-ray diffraction studies.

Fe{SC_6H_3-2,6-(2,6-^{i}Pr$_2$-C_6H_3)$_2$}$_2$(NH_3) (8). Anhydrous ammonia (ca. 30 mL, dried over sodium) was condensed onto solid **3** (1.5 g, 1.6 mmol) cooled in a dry ice/ethanol bath. The flask was then removed from the cold bath and allowed to warm to room temperature with stirring, whereupon the excess ammonia was allowed to evaporate, leaving a colorless powder. The residual ammonia was removed under reduced pressure, which resulted in a color change from colorless to bright yellow. The yellow powder was dissolved in ca. 20 mL of diethyl ether. Slow removal of the solvent under reduced pressure resulted in the formation of small yellow crystals. The solvent volume was further reduced until only a small amount of liquid (ca. 5 mL) remained above the solid. The solid product was then separated by cannula and washed with cold diethyl ether. Removal of residual solvent under reduced pressure afforded 1.4 g (1.5 mmol, 92 %) of the monoammine complex **8.** Crystals suitable for X-ray diffraction studies were grown from a concentrated solution of **8** in diethyl ether after overnight storage at room temperature. M.p 202-208 °C (dec.). UV/Vis: λ/nm ($\varepsilon/M^{-1}cm^{-1}$): 400 (500). IR (Nujol) $\tilde{\nu}$ [cm^{-1}] = 3300w, 1550m, sh, 1230m, sh, 1200m, sh, 1140m,

1090m, 1020m, 910m, 780s, 745s, 680m, sh, 560m, br, 450m, sh, 275w, br. ^{1}H NMR (400 MHz, [D$_6$] benzene, 25 °C): δ = 33.93 ($\Delta\nu_{1/2}$ = 150 Hz), 1.88 (-CH(C<u>H</u>$_3$)$_2$, $\Delta\nu_{1/2}$ = 33 Hz), -2.38 (-CH(C<u>H</u>$_3$)$_2$, $\Delta\nu_{1/2}$ = 147 Hz), -27.28 ($\Delta\nu_{1/2}$ = 71 Hz). μ_{eff}: 4.4 μ_B.

Results and Discussion.

The syntheses described herein are summarized in Scheme 6.1. Complexes **1**-**3** were synthesized by treatment of [Fe{N(SiMe$_3$)$_2$}$_2$]$_2$ with the appropriate phenol or thiol. This route was used in preference to the salt metathesis approach (treatment of the metal halide with the alkali metal salt of the thiolate or phenolate), as the protonolysis route has been shown to be high yielding and avoid the formation a product incorporating alkali metal ions.[1,22] Treatment of [Fe{N(SiMe$_3$)$_2$}$_2$]$_2$ with four equivalents of the corresponding phenol readily afforded the yellow/amber-colored dimers {Fe(OC$_6$H$_2$-2,6-Bu$^t_2$-4-Me-C$_6$H$_2$)$_2$}$_2$ (**1**, Figure 6.1) and {Fe(OC$_6$H$_2$-2,6-Bu$^t_2$)$_2$}$_2$ (**2**, Figure 6.2). Complexes **1** and **2** are structurally

Scheme 6.1: Overview of the routes used in this work for the synthesis of low valent iron chalcogenolates and their diethyl ether or ammonia complexes.

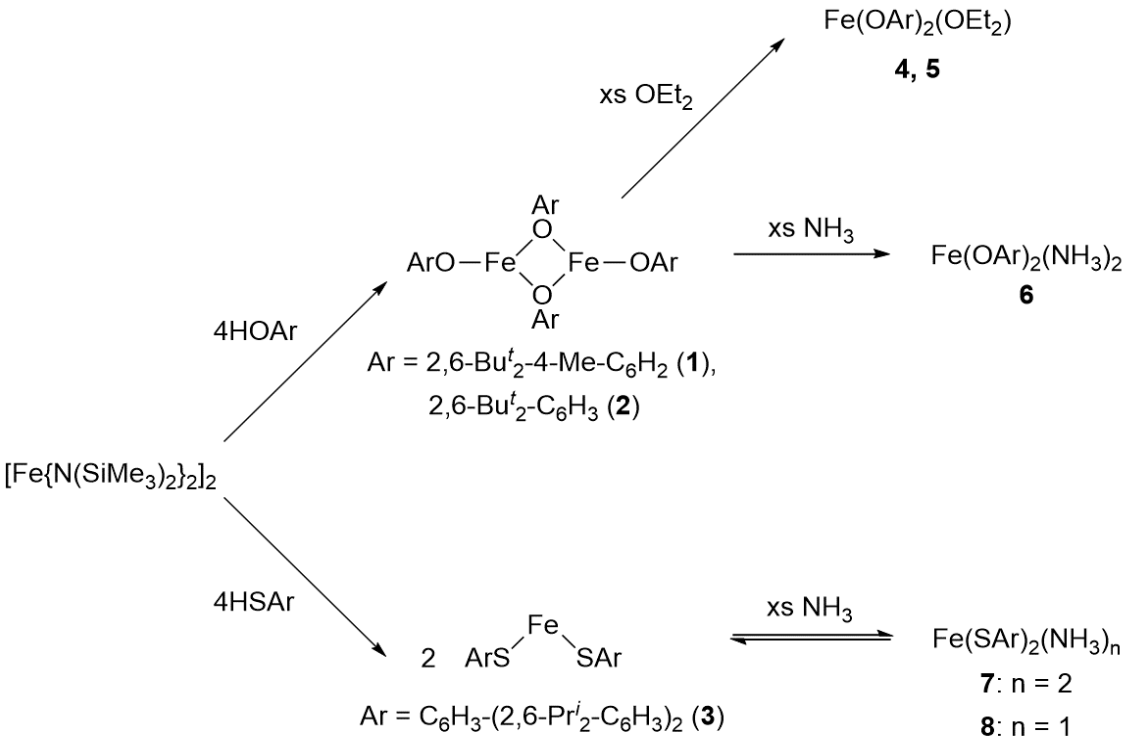

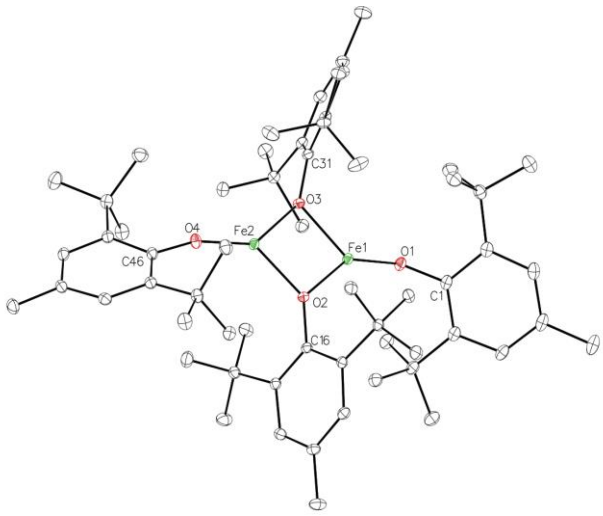

Figure 6.1*:* Molecular structure of **1** with thermal ellipsoids shown at 30% probability. For clarity, hydrogen atoms are not shown. Selected bond lengths (Å) and angles (°): Fe1-O1: 1.8267(10), Fe1-O2: 2.0127(9), Fe1:-O3: 2.0391(9), Fe2-O2: 1.9752(9), Fe2-O3: 1.9874(9), Fe2-O4: 1.8069(10); O1-Fe1-O2: 145.02(4), O1-Fe1-O3: 134.91(4), O2-Fe1-O3: 79.91(4), O2-Fe2-O3: 82.10(4), O4-Fe2-O2: 135.72(4), O4-Fe2-O3: 142.07(4), Fe1-O2-Fe2: 99.53(4), Fe1-O3-Fe2: 98.23(4), Fe1-O1-C1: 142.51(9), Fe1-O2-C16: 127.12(8), Fe1-O3-C31: 118.63(8), Fe2-O2-C16: 133.03(8), Fe2-O3-C31: 142.96(8), Fe2-O4-C46: 162.93(9).

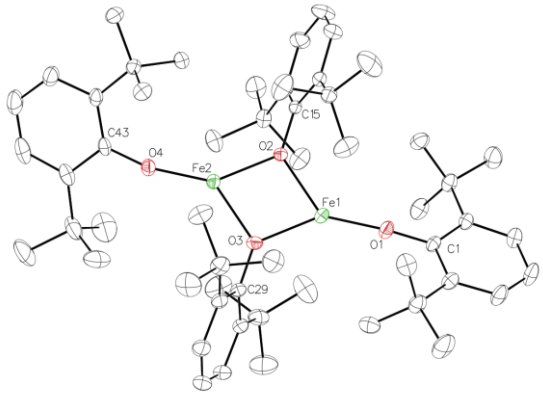

Figure 6.2: Molecular structure of **2**, with thermal ellipsoids shown at 30% probability. Hydrogen atoms are not shown for clarity. Selected bond lengths (Å) and angles (°): Fe1-O1: 1.8093(15), Fe1-O2: 2.0365(13), Fe1:-O3: 2.0007(14), Fe2-O2: 2.0044(13), Fe2-O3: 2.0382(13), Fe2-O4: 1.8159(14); O1-Fe1-O2: 134.90(6), O1-Fe1-O3: 145.16(6), O2-Fe1-O3: 79.87(5), O2-Fe2-O3: 79.74(5), O4-Fe2-O2: 144.93(6), O4-Fe2-O3: 135.31(6), Fe1-O2-Fe2: 100.16(5), Fe1-O3-Fe2: 100.22(6), Fe1-O1-C1: 175.28(14), Fe1-O2-C15: 129.63(8), Fe1-O3-C29: 131.87(12), Fe2-O2-C15: 130.19(11), Fe2-O3-C29: 127.89(12), Fe2-O4-C43: 161.91(13).

similar to the previously synthesized homoleptic aryloxide of iron(II), $\{Fe(OC_6H_2\text{-}2,4,6\text{-}Bu^t_3)_2\}_2$[1] and feature planar Fe coordination as well as a planar Fe_2O_2 cores. The internal O-Fe-O angles at the iron atoms are near 100° whereas those at the bridging oxygens are near 80°. The external O-Fe-O angles can differ by up to 10° at each iron atom. The complexes contain unusually wide Fe-O-C angles in the terminally

bound ligands, the widest of which is found in complex **2** (Figure 6.2), wherein one of the terminal Fe-O-C angles has an almost linear value of 175.28(14)°.

Initially, attempts to crystallize **2** using several solvents proved difficult. We tested diethyl ether as a solvent for the crystallization of complexes **1** and **2** and this resulted in the formation of the monomeric complexes **4** and **5** (Figures 6.3 and 6.4). Complexes **4** and **5** are relatively rare examples of neutral iron complexes coordinating diethyl ether (ca. a dozen such complexes are currently structurally characterized), all of which feature polydentate co-ligands, except the bis(diethyl ether) complex of $FeCl_3$.[23,24,33–35,25–32] **4** and **5** each coordinate a single ether molecule to produce essentially planar coordination of the iron by three oxygen atoms with dissimilar O-Fe-O angles caused by the different ligand sizes. These angles range from 103.62(8)° to 146.12(8)° in **4** and from 102.93(4)° to 153.86(5)° in **5**, with the widest angles observed between the oxygens of the terminal aryloxide ligands. Like the terminal Fe-O-C_{aryl} angles in the dimers **1** and **2**, the monomers **4** and **5** feature wide Fe-O-C_{aryl} angles that range from 149.62(9)° to 161.62(16)°.

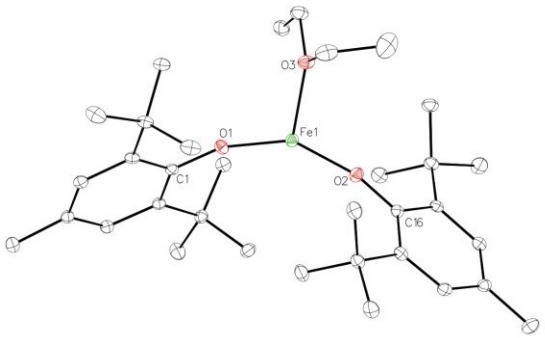

Figure 6..3: Molecular structure of **4**, with thermal ellipsoids shown at 30% probability. Hydrogen atoms are not shown for clarity. Selected bond lengths (Å) and angles (°): Fe1-O1: 1.8196(15), Fe1-O2: 1.8190(17), Fe2-O3: 2.0745(18), O1-Fe1-O2: 146.12(8), O1-Fe1-O3: 110.14(7), O2-Fe1-O3: 103.62(8), Fe1-O1-C1: 157.25(17), Fe1-O2-C16: 161.62(16).

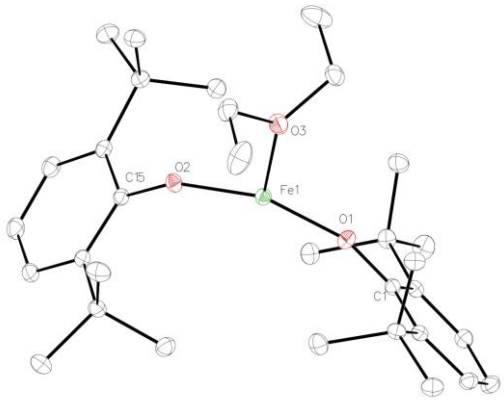

Figure 6.4: Molecular structure of **5**, with thermal ellipsoids shown at 30% probability. Hydrogen atoms are not shown for clarity. Selected bond lengths (Å) and angles (°): Fe1-O1: 1.8207(9), Fe1-O2: 1.8250(10), Fe2-O3: 2.0391(10), O1-Fe1-O2: 153.86(5), O1-Fe1-O3: 102.93(4), O2-Fe1-O3: 103.21(4), Fe1-O1-C1: 156.98(9), Fe1-O2-C15: 149.62(9).

The ^{1}H-NMR spectra of **1** and **2** (Figure 5) show the highly broadened and shifted signals expected for these paramagnetic species.[1] The spectra feature three pairs of signals corresponding to protons of the *ortho*, *meta*, and *para* substituents of the terminal and bridging aryloxide ligands. While the relative intensities of the signals allow assignment of the signals of the pairs of the terminal and bridging ligands, it is not possible to distinguish the signals of the terminal and bridging ligands by these spectra alone. The ^{1}H-NMR spectrum of **5** in deuterated benzene shows clear evidence of some loss of diethyl ether and partial formation of the dimer **2** in solution. As shown in Figure 5, the six paramagnetically shifted signals of the dimer appear in this spectrum, along with three signals attributable to the protons of the substituted aryl groups of the monomer. Accurate determination of the extent to which **5** dimerizes in solution is not possible using these data due to signal broadening and overlap, but examination of their relative signal intensities suggests that **2** and **5** exist in a near 1:1 ratio in benzene solution at ambient temperature (Figure 6.5).

Considering that there must be a 1:2 ratio of the dimer **2** to diethyl ether in solution (cf. Figure 5, top), this implies an equilibrium constant of ca. 4 and a ΔG of ca. -3 kJ/mol for this process at 25 °C. The ^{1}H-NMR spectrum of monomeric **5** shows that its signals are similarly shifted in comparison to one set of signals attributed to the aryl ligands of **2**. Since **5** contains only terminal aryloxide ligands, the signals of the bridging and terminal ligands of **2** can be unambiguously assigned by this comparison. With this information in hand, **1** was also treated with diethyl ether to give the corresponding three-coordinate monomer **4**. Using the same reasoning that used for the spectra of **2** and **5**, the ^{1}H-NMR signals of the terminal and bridging ligands of **1** were assigned by comparison with the spectrum of **4.**

The magnetic moments of **1** and **2** were determined by the Evans method to be 3.6 and 3.3 μ_B, respectively, consistent with previously reported values for homoleptic aryloxide and amide dimers of

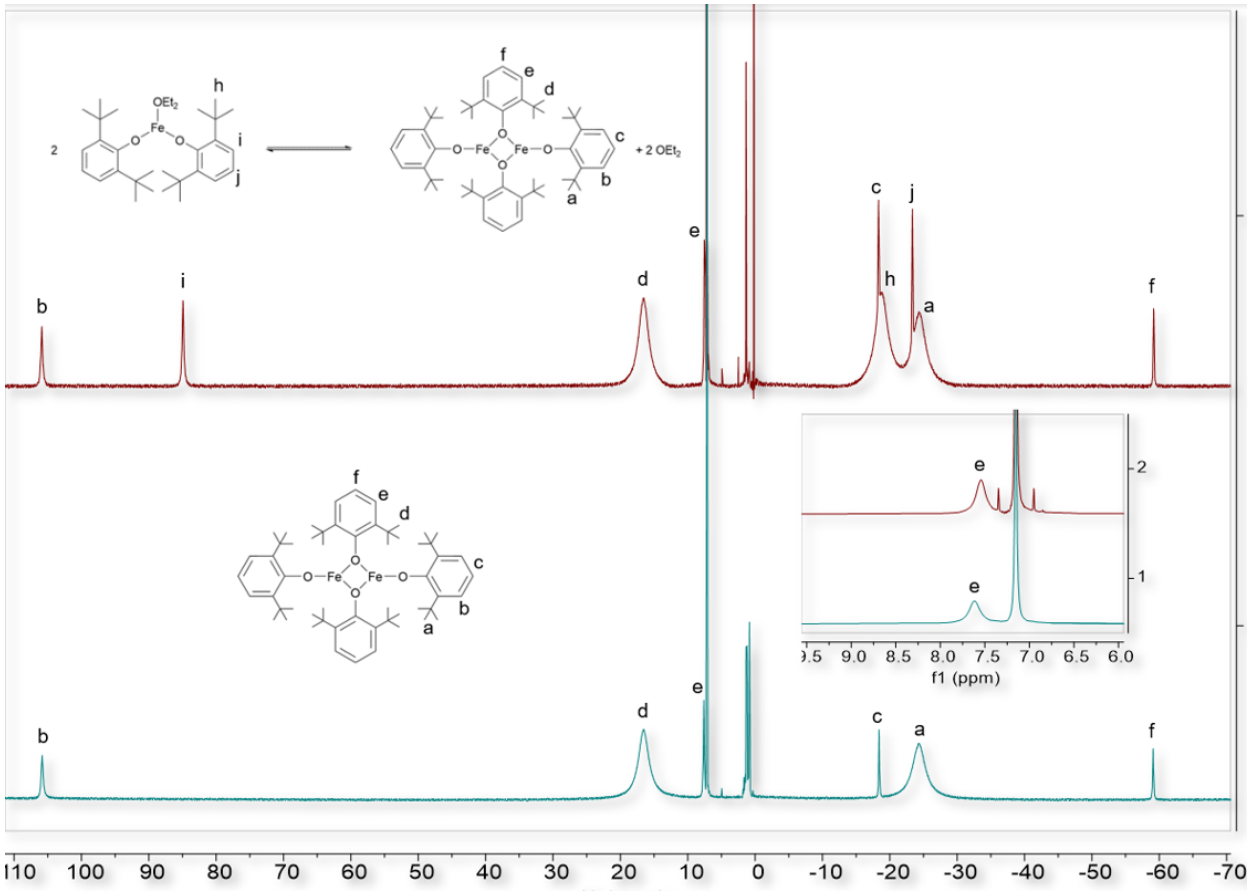

Figure 6.5: Proton NMR spectra of **2** (bottom) and **5** in equilibrium with **2** (top). For clarity, the region containing signal **e** has been detailed in the inset. As complex **5** contains no bridging ligands, comparison of signals with similar chemical shifts of **2** and **5** (e.g., signals **a** and **h** in the top spectrum) allows unambiguous assignment of bridging and terminal signals of **2**.

iron(II) (cf. $\{Fe(OC_6H_2\text{-}2,4,6\text{-}Bu^t_3)_2\}_2$ (3.4 μ_B)[1] and $[Fe\{N(SiMe_3)_2\}_2]_2$ (3.5 μ_B)[36]). Such low μ_{eff} values indicate that the high spin iron atoms of **1** and **2** are likely antiferromagnetically coupled.[1,36] Highlighting this notion are the much higher magnetic moments of the monomers **4** (5.1 μ_B) and **5** (5.4 μ_B), though an accurate determination of the magnetic moment by this method is not possible due to the equilibrium between the monomeric and dimeric complexes in solution. However, these values are close to those of other monomeric, low-coordinate complexes of iron(II), including the complexes $Fe\{N(SiMe_3)_2\}_2(THF)$ and $Fe\{N(SiMe_3)_2\}_2(PCy_3)$ (5.44 and 5.73 μ_B, respectively),[37] and $Fe(OCPh_3)_2(THF)_2$ (5.2 μ_B).[1] Comparing these values to the spin-only magnetic moment of 4.90 μ_B for the Fe(II) ion ($\mu_{eff} = [n(n+2)]^{1/2}\ \mu_B$, where n is the number of unpaired electrons) indicates a significant orbital angular momentum contribution to the effective magnetic moment of these complexes.

Given the high affinity of complexes **1** and **2** for the weakly Lewis basic diethyl ether, we sought to examine their ability to coordinate other weak bases. Although ammonia is among the earliest recorded ligands to be used in coordination chemistry[38] and one of the most common of ligands used in transition metal chemistry (cf. nearly 2500 structurally characterized transition metal complexes of ammonia entered in the CCDC database),[39] there are only 35 structurally characterized complexes in which ammonia is coordinated to iron. Previous work by this group has shown that treatment of homoleptic iron and manganese aryls with ammonia resulted in the formation of parent metal amides with arene elimination, rather than the isolation of ammonia complexes.[40] Aryloxide complexes of iron, however, have been shown to display primarily ionic bonding to the metal,[1] a condition that could favor coordination of ammonia rather than amide formation.

Our hypothesis regarding the stability of the ammonia complexes was shown to be correct, as treatment of **1** with anhydrous ammonia gives the colorless bisammine complex **6**, shown in Figure 6. The unit cell of **6** contains one molecule of **6** which has no crystallographically required symmetry as well as d half of a molecule of **6**, the iron atom of which lies on a twofold rotational axis that generates the complete molecule. The ligands of **6** form a distorted tetrahedron, with L-Fe-L angles ranging from 94.58(6)° to 136.58(5)°. Similar to **4** and **5**, complex **6** features wide Fe-O-C_{aryl} angles that are comparable to the terminal Fe-O-C_{aryl} angles found in **1** and **2**. The widest of these found in **6** is nearly linear at 174.55(10)°. The coordination of ammonia by **6** is in contrast to the behavior of the iron(II) amide $Fe\{N(SiMe_3)_2\}_2$, which yielded only intractable solids during our attempts to study its reactivity with ammonia. Complex **6** is a rare example of a species in which iron coordinates more than one ammine ligand; only three other examples of monomeric iron complexes coordinating two or more ammine ligands have been identified crystallographically.[41–43] Unlike the spectra of complexes **4** and **5**, the ^{1}H-NMR spectrum of **6** clearly shows the presence of a monomeric diaryloxide species in solution, with no evidence of the presence of dimeric **1**. The spectrum of **6** contains a single set of paramagnetically shifted signals attributable to the protons of the substituted aryl group, rather than the pairs of signals attributable to the bridging and terminal ligands present in the spectra of dimers **1** and **2**. The monomeric character of **6** in solution is further supported by comparison of its significantly higher magnetic moment (6.1 μ_B) with that of aryloxide dimers **1** and **2** (3.6 and 3.3 μ_B, respectively), indicating the absence of any antiferromagnetic coupling in **6**. An extremely broadened signal at -53.96 ppm is attributed to the coordinated ammonia. The intensity of this signal seems to indicate the presence of only a

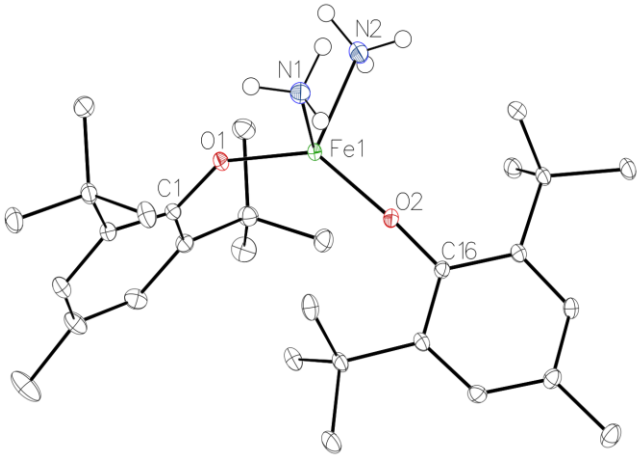

Figure 6.6: Molecular structure of **6**. For clarity, all non-ammonia hydrogen atoms are not shown. Selected bond lengths (Å) and angles (°): Fe1-O1: 1.8835(10), Fe1-O2: 1.8812(10), Fe1-N1: 2.1547(14), Fe1-N2: 2.1842(14); O1-Fe1-O2: 136.58(5), N1-Fe1-O1: 108.16(5), N2-Fe1-O1: 100.69(5), N1-Fe1-O2: 97.90(5), N2-Fe1-O2: 111.38(5), N1-Fe1-N2: 94.58(6), Fe1-O1-C1: 143.47, Fe1-O2-C16: 174.55(10).

single ammine ligand, though its low relative intensity could be due either to the loss of one ammine ligand in solution or to the extensive broadening of the signal resulting from the proximity of the ammine group to the paramagnetic iron atom of complex **6**.

Complex **6** is stable and has relatively strong ammonia complexation, since heating the crystalline material to 45°C under reduced pressure (ca. 60 mTorr) for two hours leaves the complex unaltered. In an attempt to exploit this strong complexation and examine the reactivity of the ammine, complex **6** was treated with one equivalent of t-BuLi at 0°C. However, the only isolable product of this reaction has been the lithium salt of the phenol, presumably resulting from the cleavage of the Fe-O bond and subsequent formation of an unstable metal alkyl complex. Hydrogen atom abstraction was also attempted by treatment of complex **6** with one equivalent of the tri-*tert*-butylphenoxy radical, though we were unable to isolate the expected tris-aryloxide iron product of this reaction.

Having shown that these iron(II) aryloxides strongly complex ammonia, we examined the corresponding behavior of a low-coordinate iron thiolate complex. Given that iron is bonded to sulfur in the proposed active site of nitrogenase enzymes,[44] and that low-coordinate iron complexes show some relevance as synthetic models of nitrogenase,[45] we hypothesized that a bulky iron(II) thiolate might also be capable of complexing ammonia. In an analogous preparation to that of **1**, the monomeric complex $Fe(SAr)_2$ [Ar = C_6H_3-2,6-(C_6H_3-2,6-Pr^i_2)$_2$] (**3**) was prepared in order to examine its ability to coordinate ammonia. Using the method of protonolysis, **3** was prepared in higher yield than that previously reported for the salt metathesis of $FeCl_2$ and NaSAr.[11]

Treatment of a solution of **3** in diethyl ether with anhydrous ammonia gave the colorless bisammine complex **7** shown in Figure 7. The iron atom of **7** has a distorted tetrahedral geometry, with L-Fe-L angles ranging from 87.90(11)° to 119.91(4)°. As expected, the Fe-S-C_{aryl} angles in **7** (110.50(13)° and 123.52(12)°) are narrower than any of the corresponding Fe-O-C_{aryl} angles in **4** and **5** or the terminal Fe-O-C_{aryl} angles in **1** and **2**, a consequence of the increased p character of the bonding orbitals in sulfur compared to oxygen. Despite the relevance of iron-sulfur moieties to the biological reduction of dinitrogen to

ammonia, other ammonia complexes of iron that are bound to ligands that bind through sulfur atoms are surprisingly scarce: $L(NH_3)FeSFe(NH_3)L$ (L = $[HC(CMeN[2,6\text{- diisopropylphenyl}])_2]^-$,[46] the tripodal ligand complex $[NEt_4][Fe(PS3'')(NH_3)]$ ($PS3'' = P(C_6H_3\text{-}3\text{-}Me_3Si\text{-}2\text{-}S)_3$,[47] the complex $[Fe(NH_3)(`N_HS_4')]$, (‘N_HS_4’ = the dianion of 2,2’-bis[(2- mercaptophenyl)thio]diethylamine),[48] and the recently reported polymeric complexes $_\infty{}^1[Fe(NH_3)(SPh)(\mu\text{-}SPh)]$ and $_\infty{}^1[(\mu\text{-}SPh)Fe(NH_3)_2(\mu\text{-}SPh)_2Fe(\mu\text{-}SPh)]$[49] represent the complete list of such structurally characterized complexes.

Alternatively, addition of liquid ammonia to solid **3** initially gave colorless **7**, but evacuation of the flask immediately gave a bright yellow powder. Recrystallization of the yellow powder afforded the monoammine complex **8** shown in Figure **8**. Complex **8** is a unique example of a three-coordinate, open shell transition metal ammine complex. The interaction between the iron atom and the flanking aryl ring observed originally in **3** (Fe-centroid distance: 2.15269(6) Å)[11] is disrupted by the coordination of the ammine ligand in **8** (Fe-centroid distance: 2.9129(4) Å, shortest Fe-C distance: 2.8314(2) Å). The resulting three-coordinate iron atom assumes a slightly pyramidalized geometry, with the sum of the interligand angles at iron being ca. 351 °.

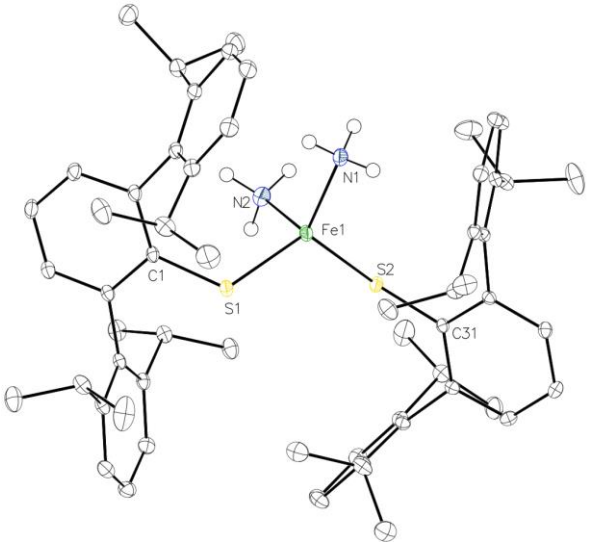

Figure 6.7: Molecular structure of **7**. For clarity, all non-ammonia hydrogens are not shown. Selected bond lengths (Å) and angles (°): Fe1-S1: 2.2947(11), Fe1-S2: 2.2993(10), Fe1-N1: 2.102(4), Fe1-N2: 2.165(4); S1-Fe1-S2: 119.91(4), S1-Fe1-N1: 114.33(12), S1-Fe1-N2: 117.34(11), S2-Fe1-N1: 103.00(11), S2-Fe1-N2: 87.90(11), Fe1-S1-C1: 110.50(13), Fe1-S2-C31: 123.52(12).

Loss of an ammine ligand by **7** to form the monoammine **8** is also effected by dissolving **7** in deuterated benzene. Comparison of the room temperature ^{1}H-NMR spectra of samples of **7** and **8** shows that they have identical spectral features, indicating preferential formation of the monoammine complex in solution. This weak coordination of a second ammine ligand by **7** has hindered complete characterization of the complex, as the material immediately loses ammonia to form **8** when not in the presence of an excess of ammonia. Such behavior of iron dithiolates is consistent with the reversible coordination of primary amines ($PhNH_2$ or Bu^tNH_2) by the dimer $Fe_2(\mu\text{-}STriph)_2(STriph)_2$ previously shown to occur upon application of low pressure or dissolving of the ammine complex.[50] However, this behavior differs from the stronger coordination of ammonia by aryloxide complex **6**, which remains unchanged upon either dissolving or heating the ammine complex under low pressure. It is likely that the high electronegativity of the oxygen ligand induces greater positive charge character at iron and hence greater Lewis acidity and stronger coordination by ammonia. Additionally, the 'hard' aryloxide ligands form primarily ionic bonds with iron, resulting in a substantial partial positive charge on the metal and strong binding of ammonia.[1] This is in contrast to the 'soft' and less electronegative thiolate ligands which form significantly more covalent bonds with iron, thereby weakening the interaction with ammonia in these complexes. The stronger Lewis acidity of aryloxides **1** and **2** is also highlighted by their binding of diethyl ether when crystallized from this solvent, whereas such complexes are not formed by the iron thiolates.

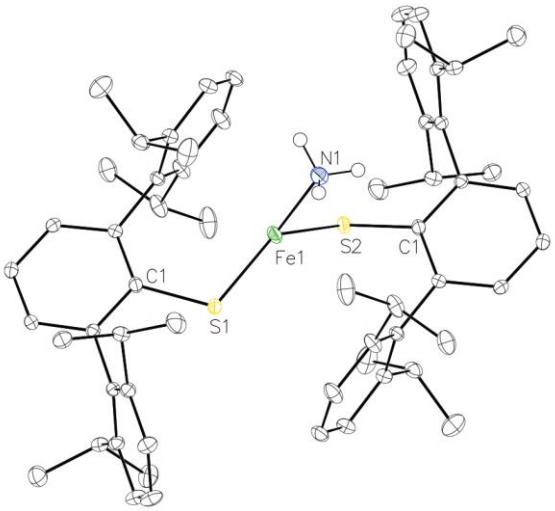

Figure 6.8: Molecular structure of **8**. The FeS_2N core is disordered over two sites related by a crystallographically imposed inversion center. For clarity, one of the half-occupied FeS_2N sites and all non-ammonia hydrogens are not shown. Selected bond lengths (Å) and angles (°): Fe1-S1: 2.2794(9), Fe1-S2: 2.2829(11), Fe1-N1: 2.129(3); S1-Fe1-S2: 141.18(3), S1-Fe1-N1: 112.54(9), S2-Fe1-N1: 97.06(9), Fe1-S1-C1: 110.11(6), Fe1-S2-C1: 106.28(7).

The reversible coordination of ammonia at the iron atom of **7** is a relatively rare occurrence at ambient temperature. Peters' $[PhBP^{mter}_3]Fe(\eta^2\text{-}N_2H_3)(NH_3)$ complex is apparently the only example of a structurally characterized iron ammine complex that loses ammonia by simple application of vacuum.[51] Among well-defined iron ammine complexes, other processes resulting in the release of ammonia include thermal decomposition of the complex as in the case of $[Fe(NH_3)_6](BH_4)_2$,[41] replacement of an ammine ligand by a stronger base such as acetonitrile,[47] application of heat and low pressure,[52] or redox-induced expulsion of an ammine ligand.[53] This weak binding of ammonia is consistent with the dearth of structurally characterized ammine complexes of iron thiolates. Furthermore, such weak binding of ammonia by **7** is probably necessary in the final step of the enzymatic reduction of dinitrogen to ammonia at the proposed iron-sulfur active site of nitrogenases, as release of the ammonia thus formed is required to complete the catalytic cycle.[54]

Conclusion

Iron chalcogenolate complexes **1**-**3** have provided new insight into the coordination chemistry of low-coordinate, low-valent iron complexes. The formation of monomeric complexes **4** and **5** upon coordination of diethyl ether by iron aryloxide dimers **1** and **2** provides unusual examples of coordination of diethyl ether by iron. Furthermore, comparison of the paramagnetic NMR spectra of the dimers **1** and **2** with their monomeric diethyl ether complexes **4** and **5** permits unambiguous assignment of their respective proton signals. Reaction of the iron aryloxide dimer **1** with anhydrous ammonia affords the four-coordinate bisammine complex **6**, an unusual example of a monomeric iron species complexing more than a single ammine ligand. Complex **6** was shown to strongly coordinate the two ammine ligands, with no apparent ammine dissociation after extended heating under low pressure. Treatment of the iron dithiolate **3** with excess ammonia affords the distorted tetrahedral geometry bisammine complex **7**, which readily loses ammonia to form the three-coordinate ammine complex **8**.

Associated Content.

Supporting information

The Supporting Information, including spectra (NMR, infrared, UVVis), crystallographic data, and photographs of bulk material is available free of charge on the ACS Publications website at https://doi.org/10.1021/acs.inorgchem.1c00539. CCDC entries 1973414 (**1**), 1974996 (**2**), 1973418 (**4**), 1973415 (**5**), 1973419 (**6**), 1973416 (**7**), 1973417 (**8**) contain the supplementary crystallographic data for this work. These data can be obtained free of charge via www.ccdc.cam.ac.uk/data_request/cif, or by emailing data_request@ccdc.cam.ac.uk, or by contacting The Cambridge Crystallographic Data Centre, 12 Union Road, Cambridge CB2 1EZ, UK; fax: + 44 1223 336033.

Author Information.

Corresponding author

*pppower@ucdavis.edu

ORCID

Cary R. Stennett: 0000-0002-2727-5747

James C. Fettinger: 0000-0002-6428-4909

Philip P. Power: 0000-0002-6262-3209

Notes

The authors declare no competing financial interest.

Acknowledgements

The authors wish to acknowledge the US National Science Foundation (CHE-1565501) for support of this work and for the purchase of a dual-source X-ray diffractometer (CHE-0840444).

References

(1) Bartlett, R. A.; Ellison, J. J.; Power, P. P.; Shoner, S. C. Synthesis and Characterization of the Homoleptic Aryloxides $[M\{O(2,4,6\text{-Tert-}Bu_3C_6H_2)\}_2]_2$ (M = Manganese, Iron), the Adducts $[Mn(OCPh_3)_2(Py)_2]$ and $[Fe(OCPh_3)_2(THF)_2]$, and the Mixed Complex $[Fe\{N(SiMe_3)_2\}\{\mu\text{-}O(2,4,6\text{-Tert-}Bu_3C_6H_2)\}]_2$: Evidence for Primaril. *Inorg. Chem.* **1991**, *30*, 2888–2894.

(2) Power, P. P.; Shoner, S. C. The Neutral Transition Metal Thiolates $[M(SAr)_2]_2$ (M = Mn, Fe or Co, Ar = 2,4,6-*t*-$Bu_3C_6H_2$). *Angew. Chem. Int. Ed.* **1991**, *30*, 330–332.

(3) Ruhlandt-Senge, K.; Power, P. P. The Synthesis and Characterization of Metal Derivatives of the New, Conveniently Prepared, Bulky Thiolato Ligand 2,4,6-Triphenylbenzenethiol. *Bull. Soc. Chim. Fr.* **1993**, *129*, 594–598.

(4) Chen, H.; Power, P. P.; Shoner, S. C. Synthesis and Spectroscopic and X-Ray Structural Characterization of the First Homoleptic Transition-Metal Boryloxides $[Mn(OBTrip_2)(\mu\text{-}OBTrip_2)]_2$ and $[Fe(OBMes_2)(\mu\text{-}OBMes_2)]_2$. *Inorg. Chem.* **1991**, *30*, 2884–2888.

(5) Ellison, J. J.; Ruhlandt-Senge, K.; Power, P. P. Synthesis and Characterization of Thiolato Complexes with Two-Coordinate Iron(II). *Angew. Chem. Int. Ed. English* **1994**, *33*, 1178–1180.

(6) Ni, C.; Power, P. P. Insertion Reactions of a Two-Coordinate Iron Diaryl with Dioxygen and Carbon Monoxide. *Chem. Commun.* **2009**, No. 37, 5543–5545.

(7) Hauptmann, R.; Kliß, R.; Schneider, J.; Henkel, G. Koordinativ Ungesättigte Eisen-Chalkogenolat-Komplexe Mit Trigonalplanaren Ligandensphären – Synthese, Eigenschaften Und Reaktionen Mit Stickstoff- Und Sauerstoff-Donormolekülen. *Zeitschrift für Anorg. und Allg. Chemie* **1998**, *624*, 1927–1936.

(8) Ohta, S.; Ohki, Y.; Ikagawa, Y.; Suizu, R.; Tatsumi, K. Synthesis and Characterization of Heteroleptic Iron(II) Thiolate Complexes with Weak Iron–Arene Interactions. *J. Organomet. Chem.*

2007, *692*, 4792–4799.

(9) Sydora, O. L.; Henry, T. P.; Wolczanski, P. T.; Lobkovsky, E. B.; Rumberger, E.; Hendrickson, D. N. Aggregation of [(^{t}Bu$_3$SiS)MX]: Structures of {[Br$_2$Fe(μ-SSitBu_3)$_2$FeBr(THF)]Na(THF)$_4$}$_\infty$, Cis-[(THF)FeI]$_2$(μ-SSitBu_3)$_2$, [(^{t}Bu$_3$SiS)Fe]$_2$(μ-SSitBu_3)$_2$, and Comparative Structure and Magnetism Studies of [(^{t}Bu$_3$SiS)MX]$_n$ (M = Fe, Co, X = Cl, n = 12; M = Fe, Ni, X = B. *Inorg. Chem.* **2006**, *45*, 609–626.

(10) Nguyen, T.; Panda, A.; Olmstead, M. M.; Richards, A. F.; Stender, M.; Brynda, M.; Power, P. P. Synthesis and Characterization of Quasi-Two-Coordinate Transition Metal Dithiolates M(SAr*)$_2$ (M = Cr, Mn, Fe, Co, Ni, Zn; Ar* = C$_6$H$_3$-2,6(C$_6$H$_2$-2,4,6-Pr$^i_3$)$_2$. *J. Am. Chem. Soc.* **2005**, *127*, 8545–8552.

(11) Pratt, J.; Bryan, A. M.; Faust, M.; Boynton, J. N.; Vasko, P.; Rekken, B. D.; Mansikkamäki, A.; Fettinger, J. C.; Tuononen, H. M.; Power, P. P. Effects of Remote Ligand Substituents on the Structures, Spectroscopic, and Magnetic Properties of Two-Coordinate Transition-Metal Thiolate Complexes. *Inorg. Chem.* **2018**, *57*, 6491–6502.

(12) Moula, G.; Matsumoto, T.; Miehlich, M. E.; Meyer, K.; Tatsumi, K. Synthesis of an All-Ferric Cuboidal Iron–Sulfur Cluster [Fe$^{III}_4$S$_4$(SAr)$_4$]. *Angew. Chem. Int. Ed.* **2018**, *57*, 11594–11597.

(13) Hatanaka, T.; Miyake, R.; Ishida, Y.; Kawaguchi, H. Synthesis of Two-Coordinate Iron Aryloxides and Their Reactions with Organic Azide: Intramolecular C–H Bond Amination. *J. Organomet. Chem.* **2011**, *696*, 4046–4050.

(14) Olmstead, M. M.; Power, P. P.; Shoner, S. C. Three-Coordinate Iron Complexes: X-Ray Structural Characterization of the Iron Amide-Bridged Dimers [Fe(NR$_2$)$_2$]$_2$ (R = SiMe$_3$, C$_6$H$_5$) and the Adduct Fe[N(SiMe$_3$)$_2$]$_2$(THF) and Determination of the Association Energy of the Monomer Fe{N(SiMe$_3$)$_2$}$_2$ in Solution. *Inorg. Chem.* **1991**, *30*, 2547–2551.

(15) Lin, C.-Y.; Fettinger, J. C.; Power, P. P. Reversible Complexation of Lewis Bases to Low-Coordinate Fe(II), Co(II), and Ni(II) Amides: Influence of the Metal, Donor Ligand, and Amide Substituent on Binding Constants. *Inorg. Chem.* **2017**, *56*, 9892–9902.

(16) Broere, D. L. J.; Čorić, I.; Brosnahan, A.; Holland, P. L. Quantitation of the THF Content in $Fe[N(SiMe_3)_2]_2 \cdot xTHF$. *Inorg. Chem.* **2017**, *56*, 3140–3143.

(17) Pangborn, A. B.; Giardello, M. A.; Grubbs, R. H.; Rosen, R. K.; Timmers, F. J. Safe and Convenient Procedure for Solvent Purification. *Organometallics* **1996**, *15*, 1518–1520.

(18) Evans, D. F. 400. The Determination of the Paramagnetic Susceptibility of Substances in Solution by Nuclear Magnetic Resonance. *J. Chem. Soc.* **1959**, No. 0, 2003–2005.

(19) Bain, G. A.; Berry, J. F. Diamagnetic Corrections and Pascal's Constants. *J. Chem. Educ.* **2008**, *85*, 532.

(20) Andersen, R. A.; Bryan, A. M.; Faust, M.; Power, P. P. Divalent Manganese, Iron, and Cobalt Bis(Trimethylsilyl)Amido Derivatives and Their Tetrahydrofuran Complexes. *Inorg. Synth.* **2018**, *37*, 1–14.

(21) Barnett, B. R.; Mokhtarzadeh, C. C.; Figueroa, J. S.; Lummis, P.; Wang, S.; Queen, J. D.; Gavenonis, J.; Schüwer, N.; Tilley, T. D.; Boynton, J. N.; Power, P. P.; Ditri, T. B.; Weidemann, N.; Barnett, B. R.; Agnew, D. W.; Figueroa, J. S.; Smith, P. W.; Ditri, T. B.; Barnett, B. R.; Carpenter, A. E.; Mokhtarzadeh, C. C.; Agnew, D. W.; Figueroa, J. S.; Smith, P. W.; Pratt, J. K.; Power, P. P.; Mendelson, N. D.; Figueroa, J. S.; Queen, J. D.; Power, P. P.; Agnew, D. W.; Carpenter, A. E.; Figueroa, J. S. Terphenyl Ligands and Complexes. *Inorg. Synth.* **2018**, *37*, 85–122.

(22) Sigel, G. A.; Bartlett, R. A.; Decker, D.; Olmstead, M. M.; Power, P. P. Synthesis and Spectroscopic and X-Ray Structural Characterization and Dynamic Solution Behavior of the Neutral Cobalt(II) Alkoxides $[Co\{OC(C_6H_{11})_3\}_2]_2.CH_3OH \cdot 1/2C_6H_{12} \cdot THF$, $[Co(OCPh_3)_2]_2 \cdot n\text{-}C_6H_{14}$,

[$Co(OSiPh_3)_2(THF)]_2$, and $Co(OCPh_3)_2(THF)_2$. *Inorg. Chem.* **1987**, *26*, 1773–1780.

(23) Bellows, S. M.; Brennessel, W. W.; Holland, P. L. Effects of Ligand Halogenation on the Electron Localization, Geometry and Spin State of Low-Coordinate (β-Diketiminato)Iron Complexes. *Eur. J. Inorg. Chem.* **2016**, *2016*, 3344–3355.

(24) Lee, W.-T.; Zeller, M.; Lugosan, A. Bis(Triazenide), Tris(Triazenide), and Lantern-Type of Triazenide Iron Complexes: Synthesis and Structural Characterization. *Inorg. Chim. Acta* **2018**, *477*, 109–113.

(25) Searles, K.; Fortier, S.; Khusniyarov, M. M.; Carroll, P. J.; Sutter, J.; Meyer, K.; Mindiola, D. J.; Caulton, K. G. A Cis-Divacant Octahedral and Mononuclear Iron(IV) Imide. *Angew. Chem. Int. Ed.* **2014**, *53*, 14139–14143.

(26) Hennessy, E. T.; Betley, T. A. Complex N-Heterocycle Synthesis via Iron-Catalyzed, Direct C–H Bond Amination. *Science* **2013**, *340*, 591–595.

(27) Bouwkamp, M. W.; Bart, S. C.; Hawrelak, E. J.; Trovitch, R. J.; Lobkovsky, E.; Chirik, P. J. Square Planar Bis(Imino)Pyridine Iron Halide and Alkyl Complexes. *Chem. Commun.* **2005**, No. 27, 3406–3408.

(28) Vela, J.; Smith, J. M.; Yu, Y.; Ketterer, N. A.; Flaschenriem, C. J.; Lachicotte, R. J.; Holland, P. L. Synthesis and Reactivity of Low-Coordinate Iron(II) Fluoride Complexes and Their Use in the Catalytic Hydrodefluorination of Fluorocarbons. *J. Am. Chem. Soc.* **2005**, *127*, 7857–7870.

(29) Jellema, E.; Sciarone, T. J. J.; Navarrete, N. M.; Hettinga, M. J.; Meetsma, A.; Hessen, B. Reactivity of Paramagnetic FeII–Bis(Amidinate) Complexes. *Eur. J. Inorg. Chem.* **2011**, *2011*, 91–100.

(30) Müller, H.; Seidel, W.; Görls, H. Zur Chemie Des Dimesityleisens. XI. Reaktion von Dimesityleisen Mit β-Diketonen – Strukturen von Bis(Diethylether)-Bis(1,3-Diphenylpropan-1,3-Dionato)Eisen(II) Und Poly[Bis(2,2,6,6-Tetramethylheptan-3,5-Dionato)Eisen(II)-μ-(1,4-

Dioxan)]. *Zeitschrift für Anorg. und Allg. Chemie* **1997**, *623*, 155–158.

(31) Xiao, J.; Deng, L. Iron-Mediated C–H Bond Amination by Organic Azides on a Tripodal Bis(Anilido)Iminophosphorane Platform. *Dalton Trans.* **2013**, *42*, 5607–5610.

(32) Hakey, B. M.; Darmon, J. M.; Zhang, Y.; Petersen, J. L.; Milsmann, C. Synthesis and Electronic Structure of Neutral Square-Planar High-Spin Iron(II) Complexes Supported by a Dianionic Pincer Ligand. *Inorg. Chem.* **2019**, *58*, 1252–1266.

(33) Spandl, J.; Kusserow, M.; Brüdgam, I. Alkoxo-Verbindungen Des Dreiwertigen Eisen: Synthese Und Charakterisierung von [Fe2(O^tBu)$_6$], [$Fe_2Cl_2(O^tBu)_4$], [$Fe_2Cl_4(O^tBu)_2$] Und [$N(NBu)_4]_2[Fe_6OCl_6(OMe)_{12}$]. *Zeitschrift für Anorg. und Allg. Chemie* **2003**, *629*, 968–974.

(34) King, E. R.; Hennessy, E. T.; Betley, T. A. Catalytic C−H Bond Amination from High-Spin Iron Imido Complexes. *J. Am. Chem. Soc.* **2011**, *133*, 4917–4923.

(35) Hennessy, E. T.; Liu, R. Y.; Iovan, D. A.; Duncan, R. A.; Betley, T. A. Iron-Mediated Intermolecular N-Group Transfer Chemistry with Olefinic Substrates. *Chem. Sci.* **2014**, *5*, 1526–1532.

(36) Andersen, R. A.; Faegri, K.; Green, J. C.; Haaland, A.; Lappert, M. F.; Leung, W. P.; Rypdal, K. Synthesis of Bis[Bis(Trimethylsilyl)Amido]Iron(II). Structure and Bonding in M[$N(SiMe_3)_2]_2$ (M = Manganese, Iron, Cobalt): Two-Coordinate Transition-Metal Amides. *Inorg. Chem.* **1988**, *27*, 1782–1786.

(37) Eichhöfer, A.; Lan, Y.; Mereacre, V.; Bodenstein, T.; Weigend, F. Slow Magnetic Relaxation in Trigonal-Planar Mononuclear Fe(II) and Co(II) Bis(Trimethylsilyl)Amido Complexes—A Comparative Study. *Inorg. Chem.* **2014**, *53*, 1962–1974.

(38) Werner, A. Beitrag Zur Konstitution Anorganischer Verbindungen. *Z. Anorg. Allg. Chem.* **1893**, *3*, 267–330.

(39) Groom, C. R.; Bruno, I. J.; Lightfoot, M. P.; Ward, S. C. The Cambridge Structural Database. *Acta*

Crystallogr. Sect. B **2016**, *72*, 171–179.

(40) Ni, C.; Lei, H.; Power, P. P. Reaction of M(II) Diaryls (M = Mn or Fe) with Ammonia to Afford Parent Amido Complexes. *Organometallics* **2010**, *29*, 1988–1991.

(41) Roedern, E.; Jensen, T. R. Ammine-Stabilized Transition-Metal Borohydrides of Iron, Cobalt, and Chromium: Synthesis and Characterization. *Inorg. Chem.* **2015**, *54*, 10477–10482.

(42) Tomyn, S.; Haukka, M.; Nedelkov, R. Diammine{N-[2-(Hy-droxy-imino)-propion-yl]-N'-[2-(Oxidoimino)-propion-yl]Propane-1,3-Diaminido-[Kappa]4N,N',N'',N'''}iron(III). *Acta Crystallogr. Sect. E* **2012**, *68*, m1568--m1569.

(43) McQuarters, A. B.; Goodrich, L. E.; Goodrich, C. M.; Lehnert, N. Disproportionation of O-Benzylhydroxylamine Catalyzed by a Ferric Bis-Picket Fence Porphyrin Complex. *Zeitschrift für Anorg. und Allg. Chemie* **2013**, *639*, 1520–1526.

(44) Kirn, J.; Rees, D. C. Crystallographic Structure and Functional Implications of the Nitrogenase Molybdenum–Iron Protein from Azotobacter Vinelandii. *Nature* **1992**, *360*, 553–560.

(45) Holland, P. L. Low-Coordinate Iron Complexes as Synthetic Models of Nitrogenase. *Can. J. Chem.* **2005**, *83*, 296–301.

(46) Vela, J.; Stoian, S.; Flaschenriem, C. J.; Münck, E.; Holland, P. L. A Sulfido-Bridged Diiron(II) Compound and Its Reactions with Nitrogenase-Relevant Substrates. *J. Am. Chem. Soc.* **2004**, *126*, 4522–4523.

(47) Chang, Y.-H.; Chan, P.-M.; Tsai, Y.-F.; Lee, G.-H.; Hsu, H.-F. Catalytic Reduction of Hydrazine to Ammonia by a Mononuclear Iron(II) Complex on a Tris(Thiolato)Phosphine Platform. *Inorg. Chem.* **2014**, *53*, 664–666.

(48) Sellmann, D.; Soglowek, W.; Knoch, F.; Ritter, G.; Dengler, J. Transition-Metal Complexes with Sulfur Ligands. 88. Dependence of Spin State, Structure, and Reactivity of [FeII(L) ('N_H)S_4')]

Complexes on the Coligand L (L = CO, N_2H_2, N_2H_4, NH_3, Pyridine, $NHCH_3NH_2$, CH_3OH, THF, $P(OCH_3)_3$, $P(OPh)_3$): Model Complexes for iron nitrogenases ('N_HS_4'$^{2-}$ = dianion of 2,2'-bis[(2-mercaptophenyl)thio]diethylamine). *Inorg. Chem.* **1992**, *31*, 3711–3717.

(49) Eichhöfer, A.; Buth, G. 1-D Polymeric Iron(II) Thiolato Complexes: Synthesis, Structure, and Properties of $_\infty^1$[$Fe(SR)_2$] (R = Ph, Mes), $_\infty^1$[$Fe(NH_3)(SPh)(\mu\text{-}SPh)$] and $_\infty^1$[$(\mu\text{-}SPh)Fe(NH_3)_2(\mu\text{-}SPh)_2Fe(\mu\text{-}SPh)$]. *Eur. J. Inorg. Chem.* **2019**, *2019*, 639–646.

(50) Zdilla, M. J.; Verma, A. K.; Lee, S. C. Reactivity of a Sterically Hindered Fe(II) Thiolate Dimer with Amines and Hydrazines. *Inorg. Chem.* **2008**, *47*, 11382–11390.

(51) Saouma, C. T.; Lu, C. C.; Peters, J. C. Mononuclear Five- and Six-Coordinate Iron Hydrazido and Hydrazine Species. *Inorg. Chem.* **2012**, *51*, 10043–10054.

(52) Saouma, C. T.; Moore, C. E.; Rheingold, A. L.; Peters, J. C. A Five-Coordinate Phosphino/Acetate Iron(II) Scaffold That Binds N_2, N_2H_2, N_2H_4, and NH_3 in the Sixth Site. *Inorg. Chem.* **2011**, *50*, 11285–11287.

(53) Lee, Y.; Mankad, N. P.; Peters, J. C. Triggering N_2 Uptake via Redox-Induced Expulsion of Coordinated NH3 and N2 Silylation at Trigonal Bipyramidal Iron. *Nature Chem.* **2010**, *2*, 558.

(54) Hoffman, B. M.; Lukoyanov, D.; Yang, Z.-Y.; Dean, D. R.; Seefeldt, L. C. Mechanism of Nitrogen Fixation by Nitrogenase: The Next Stage. *Chem. Rev.* **2014**, *114*, 4041–4062.

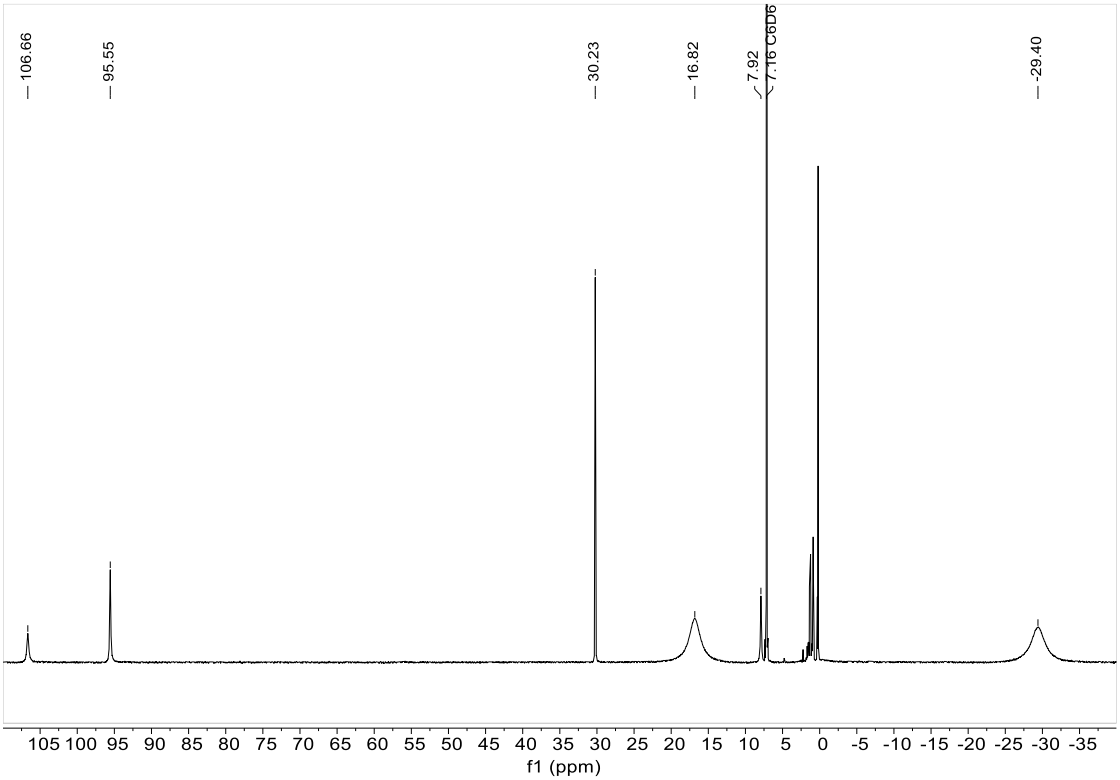

Figure 6.S1: ^{1}H-NMR spectrum of {Fe(OC_6H_2-2,6-Bu^t_2-4-Me)$_2$}$_2$ (**1**) in [D_6] benzene at 25 °C

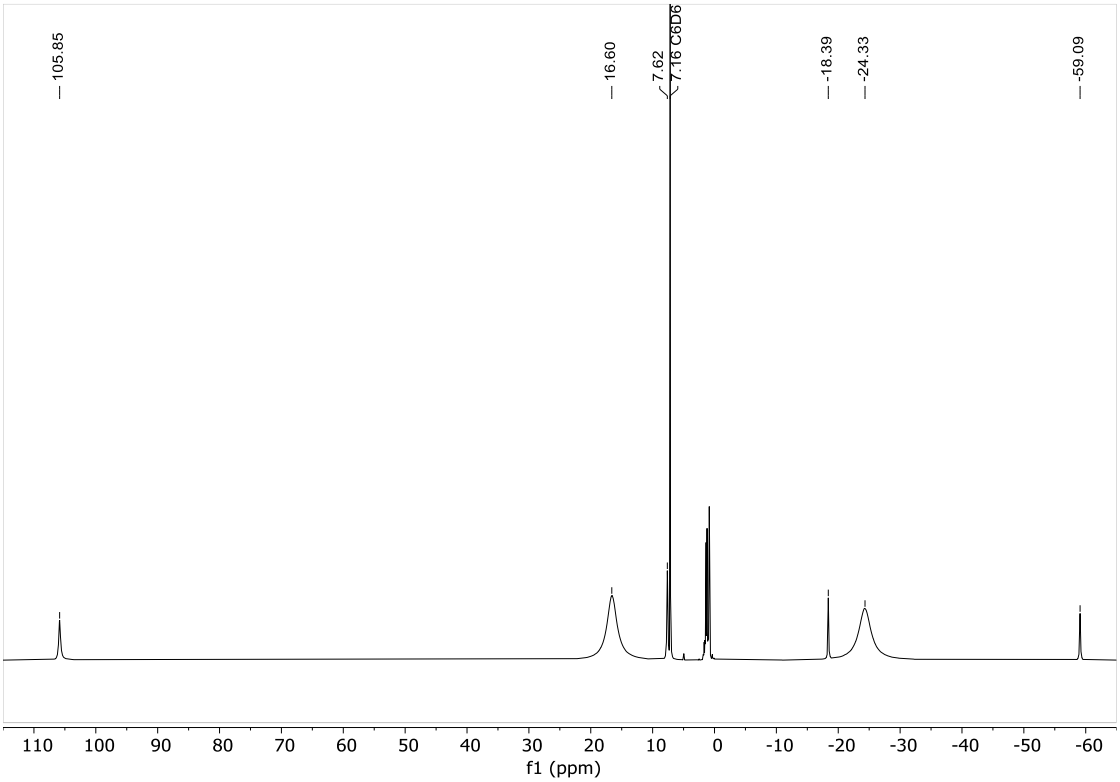

Figure 6.S2: ^{1}H-NMR spectrum of {Fe(OC_6H_3-2,6-Bu^t_2)$_2$}$_2$ (**2**) in [D_6] benzene at 25 °C

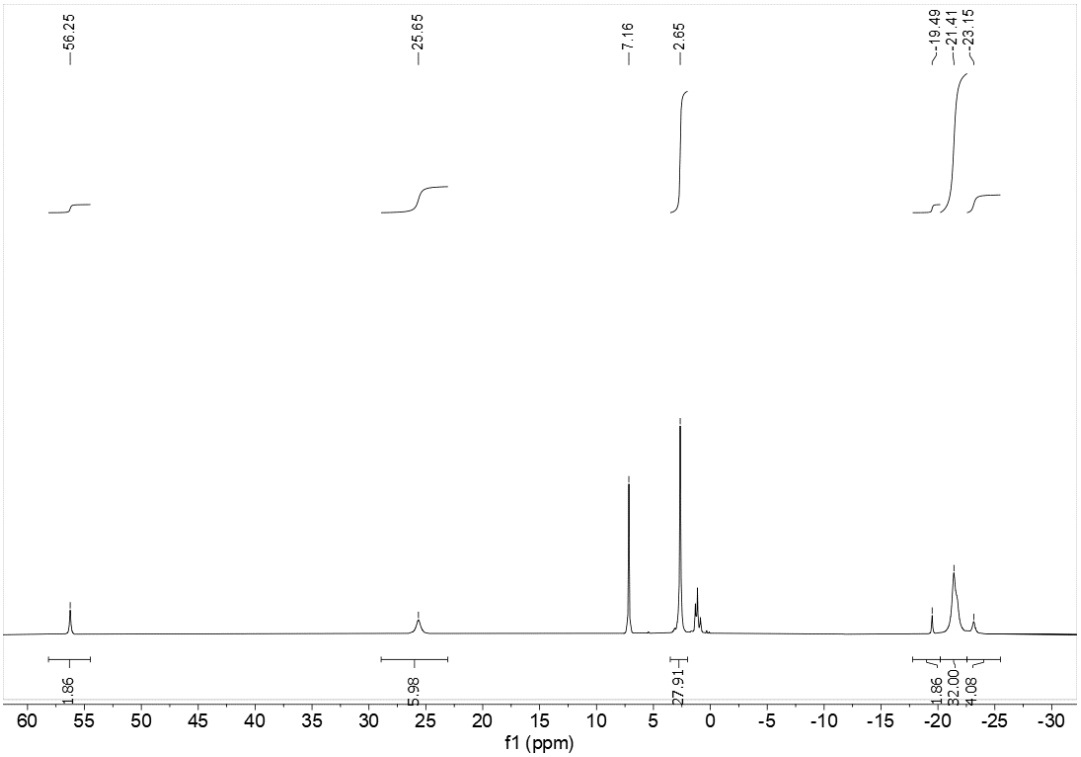

Figure 6.S3: ^{1}H-NMR spectrum of Fe{SC_6H_3-2,6-(C_6H_3-2,6-Pr^i_2)$_2$}$_2$ (**3**) in [D_6] benzene at 25 °C

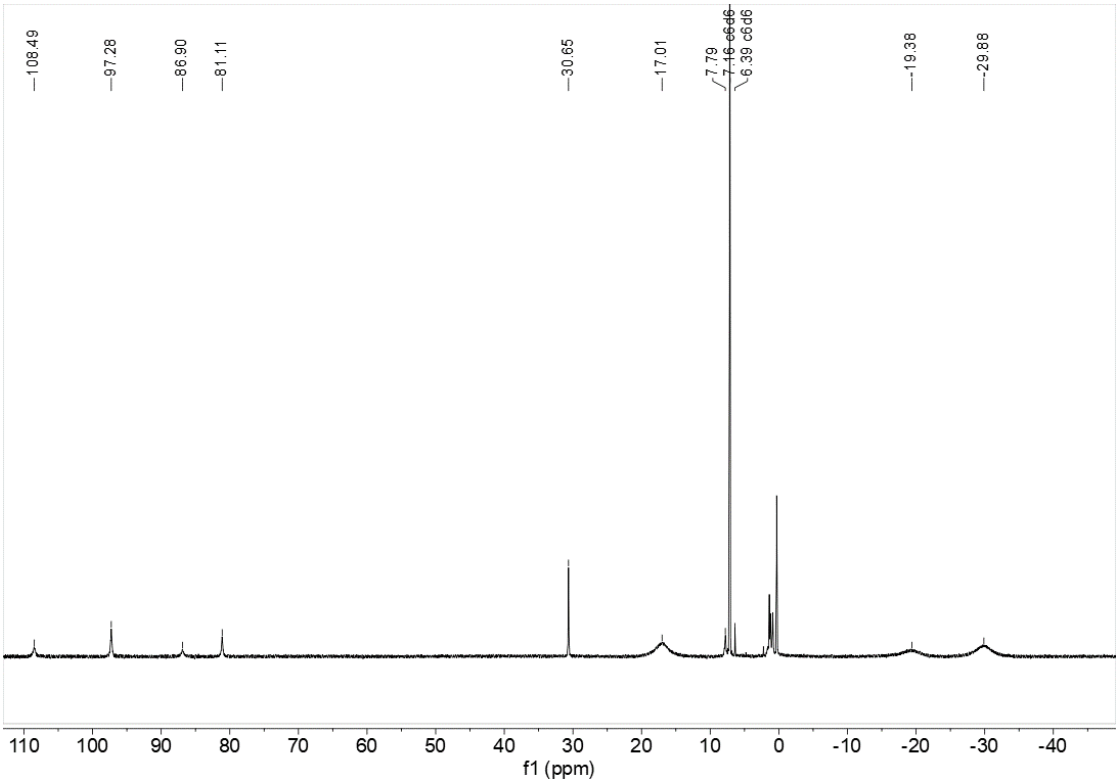

Figure 6.S4: ^{1}H-NMR spectrum of Fe(OC_6H_2-2,6-Bu^t_2-4-Me)$_2$(OEt_2) (**4**) in equilibrium with **1** in [D_6] benzene at 25 °C. Signal at 6.39 is due to deuterated benzene used for Evans' method.

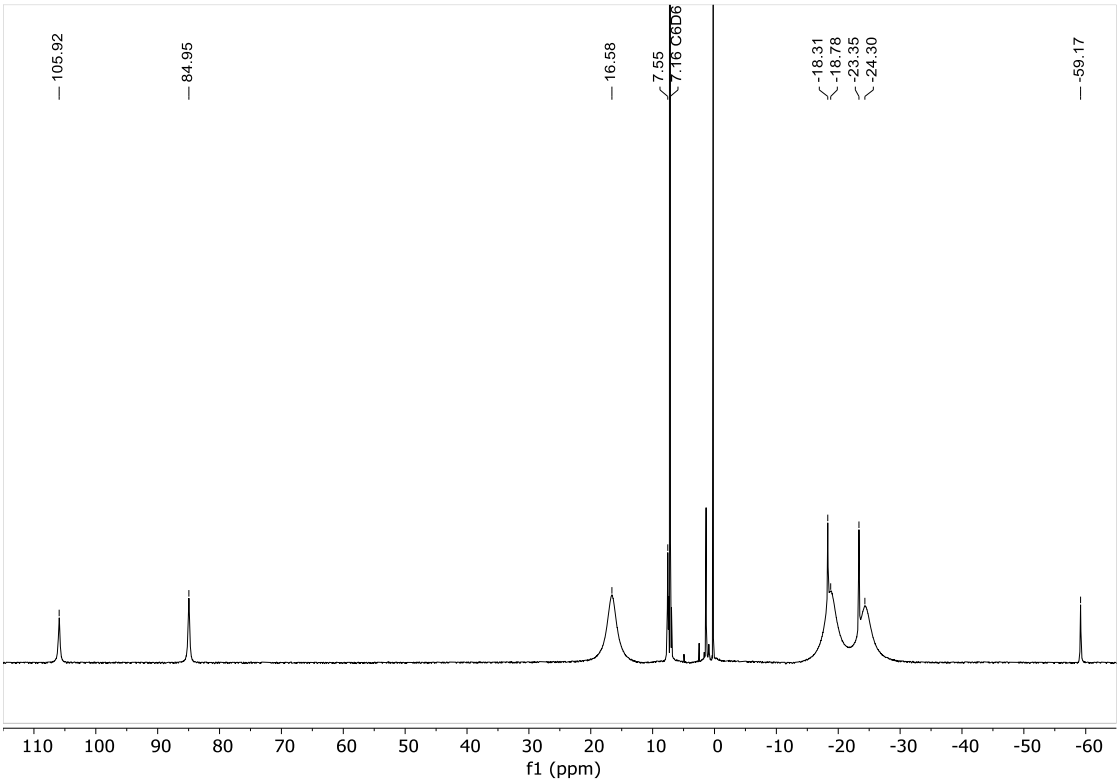

Figure 6.S5: ^{1}H-NMR spectrum of $Fe(OC_6H_3\text{-}2,6\text{-}Bu^t_2)_2(OEt_2)$ (**5**) in equilibrium with (**2**) in [D_6] benzene at 25 °C

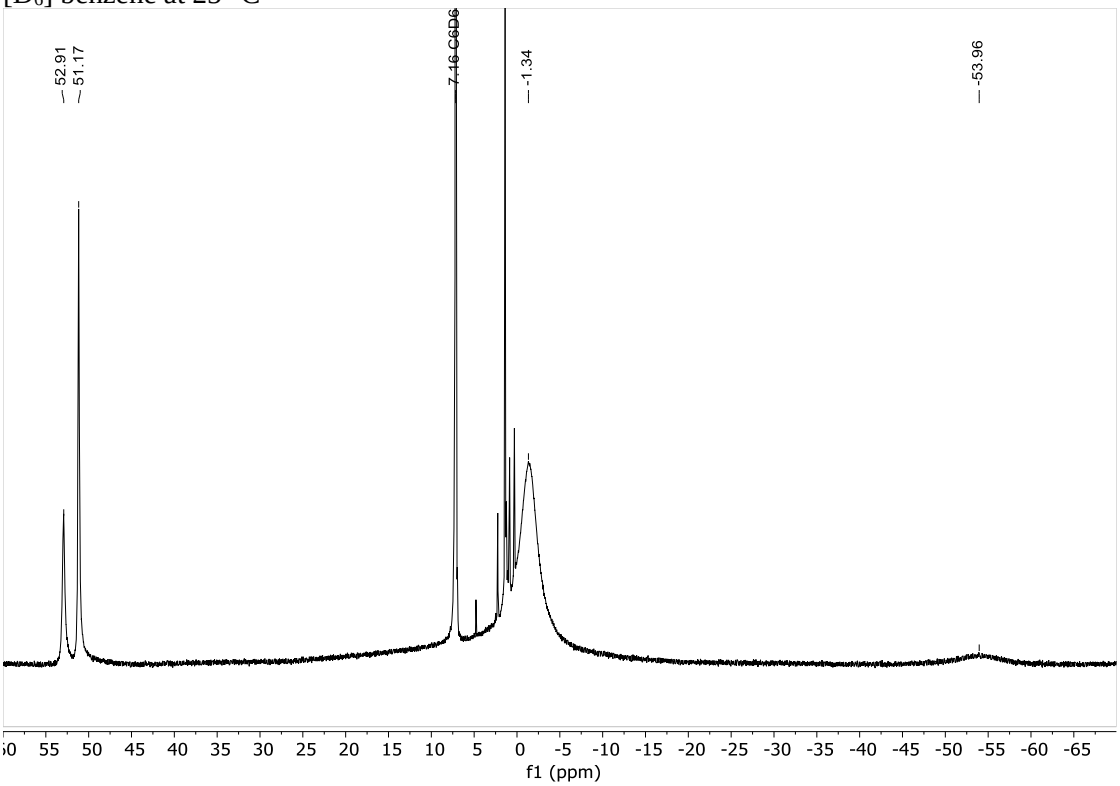

Figure S6: ^{1}H-NMR spectrum of $Fe(OC_6H_2\text{-}2,6\text{-}Bu^t_2\text{-}4\text{-}Me)_2(NH_3)_2$ (**6**) in [D_6] benzene at 25 °C

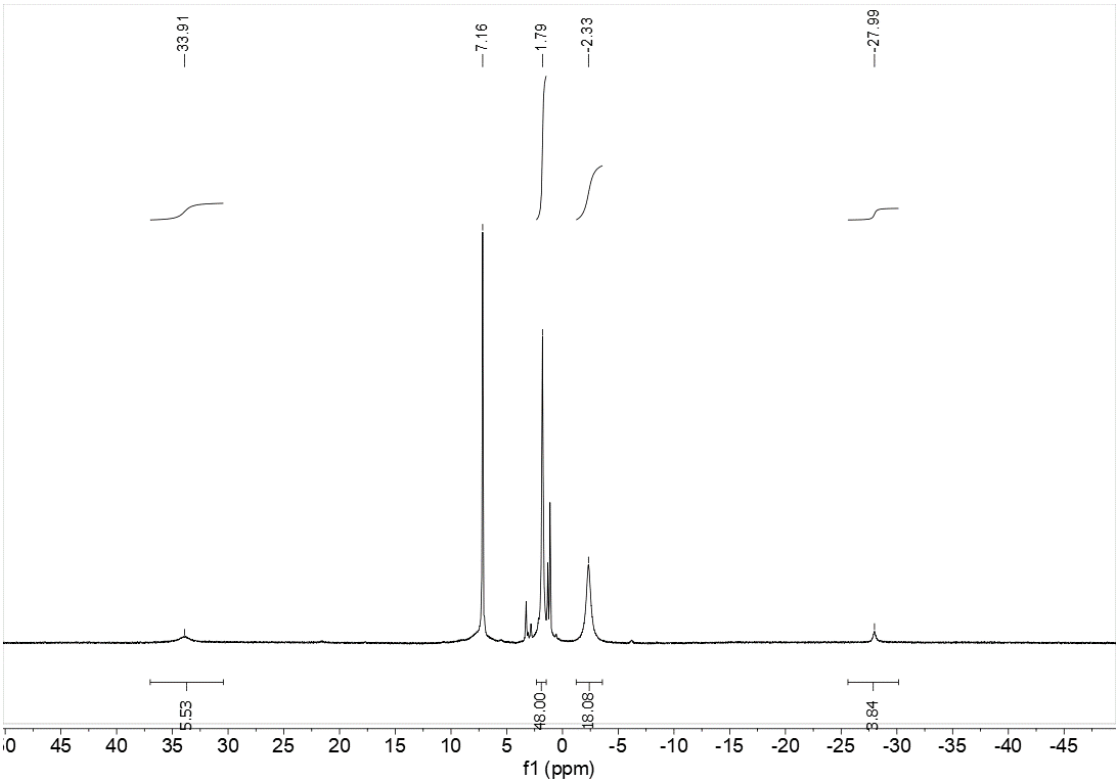

Figure 6.S7: ^{1}H-NMR spectrum of Fe{SC_6H_3-2,6-(C_6H_3-2,6-Pr^{i}_2)$_2$}$_2$(NH_3) (**8**) in [D_6] benzene at 25 °C

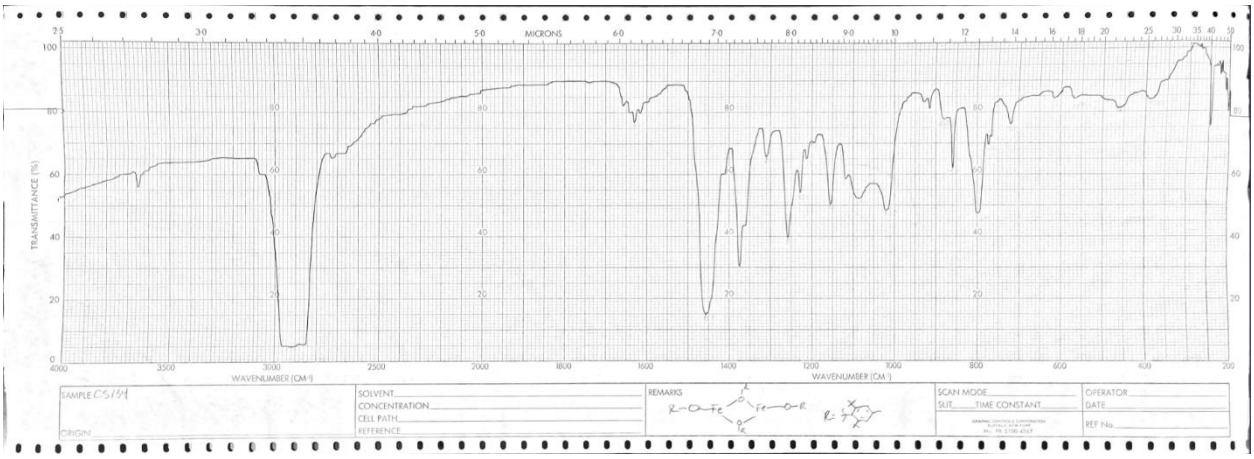

Figure 6.S8: Infrared spectrum of $\{Fe(OC_6H_2\text{-}2,6\text{-}Bu^t_2\text{-}4\text{-}Me)_2\}_2$ (**1**) (Nujol mull, CsI windows)

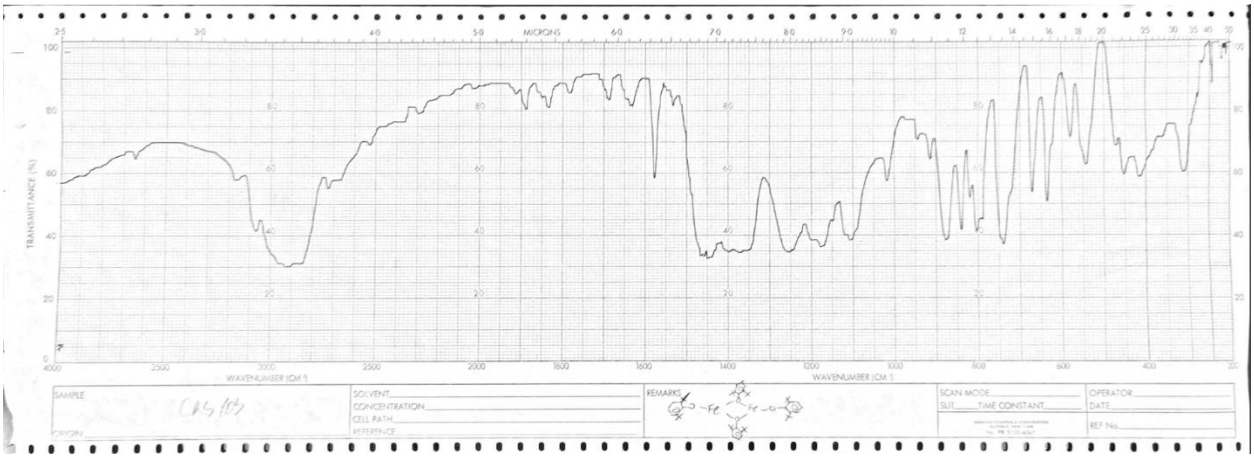

Figure 6.S9: Infrared spectrum of $\{Fe(OC_6H_3\text{-}2,6\text{-}Bu^t_2)_2\}_2$ (**2**) (Nujol mull, CsI windows)

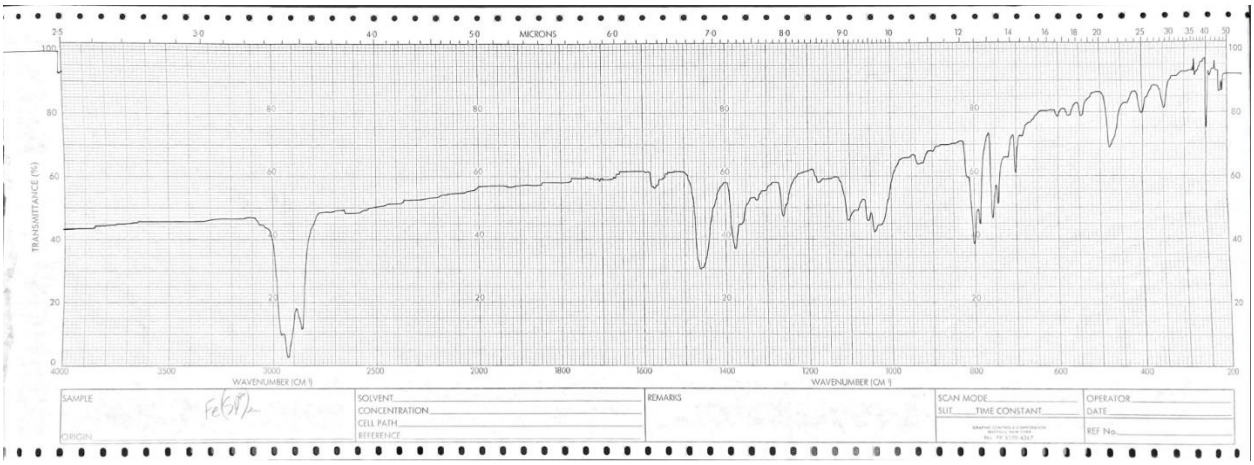

Figure 6.S10: Infrared spectrum of $Fe\{SC_6H_3\text{-}2,6\text{-}(C_6H_3\text{-}2,6\text{-}Pr^i_2)_2\}_2$ (**3**) (Nujol mull, CsI windows)

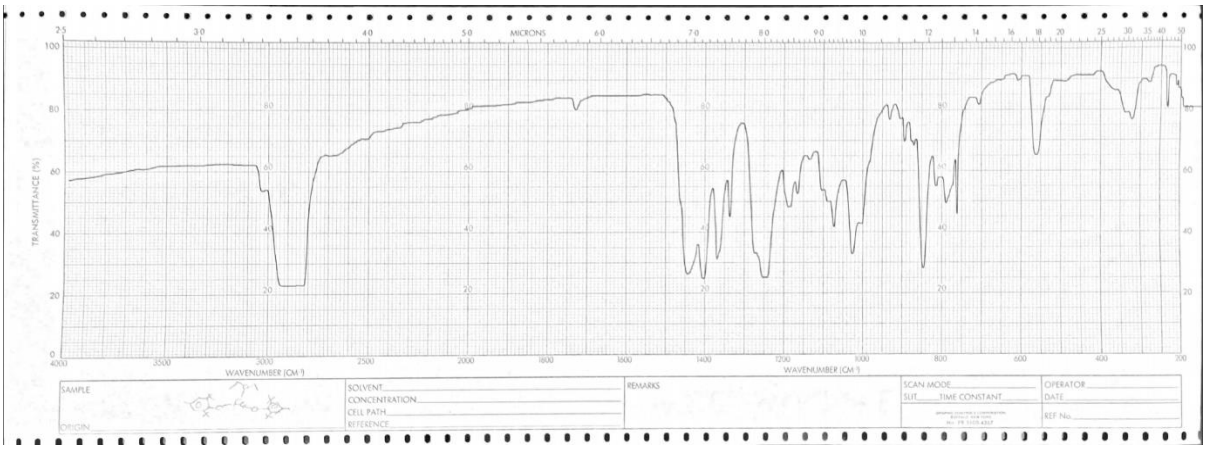

Figure 6.S11: Infrared spectrum of $Fe(OC_6H_2\text{-}2,6\text{-}Bu^t_2\text{-}4\text{-}Me)_2(OEt_2)$ (**4**) (Nujol mull, CsI windows)

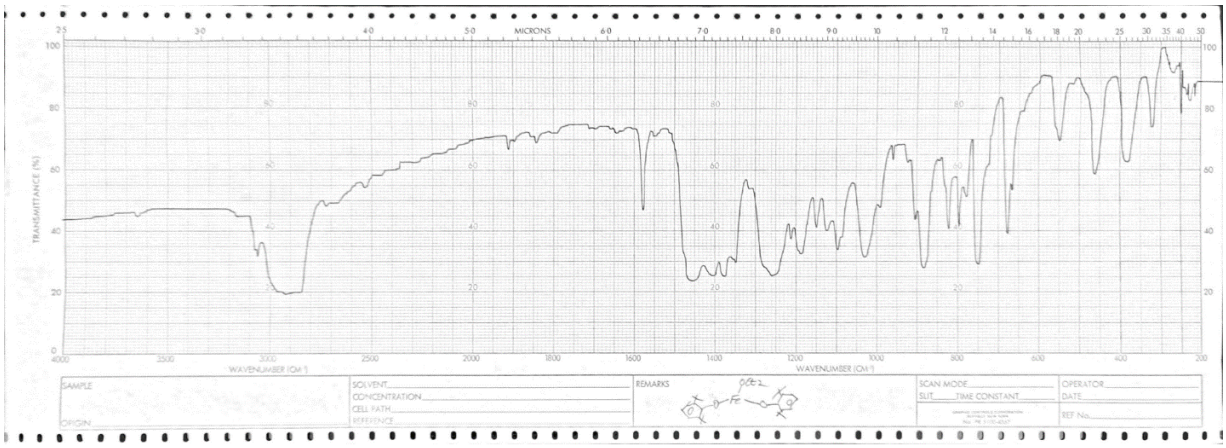

Figure 6.S12: Infrared spectrum of $Fe(OC_6H_2\text{-}2,6\text{-}Bu^t_2)_2(OEt_2)$ (**5**) (Nujol mull, CsI windows)

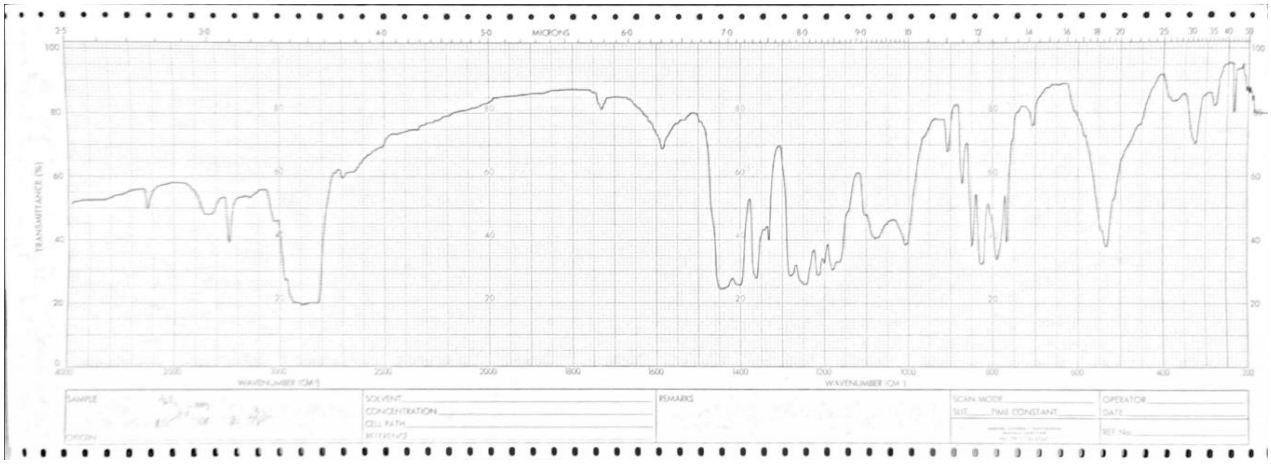

Figure 6.S13: Infrared spectrum of $Fe(OC_6H_2\text{-}2,6\text{-}Bu^t_2\text{-}4\text{-}Me)_2(NH_3)_2$ (**6**) (Nujol mull, CsI windows)

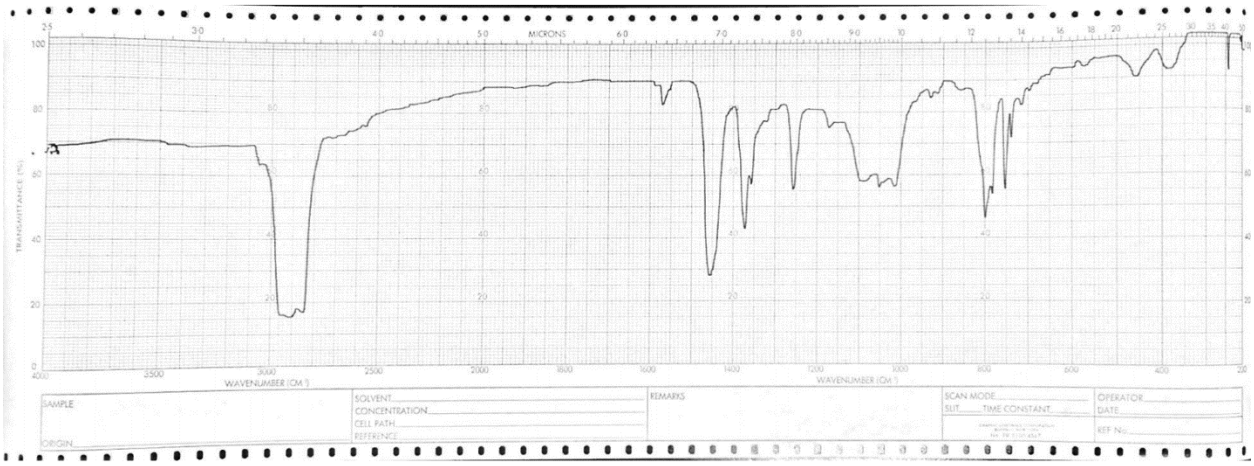

Figure 6.S14: Infrared spectrum of $Fe\{SC_6H_3\text{-}2,6\text{-}(C_6H_3\text{-}2,6\text{-}Pr^i_2)_2\}_2(NH_3)_2$ (**7**) (Nujol mull, CsI windows)

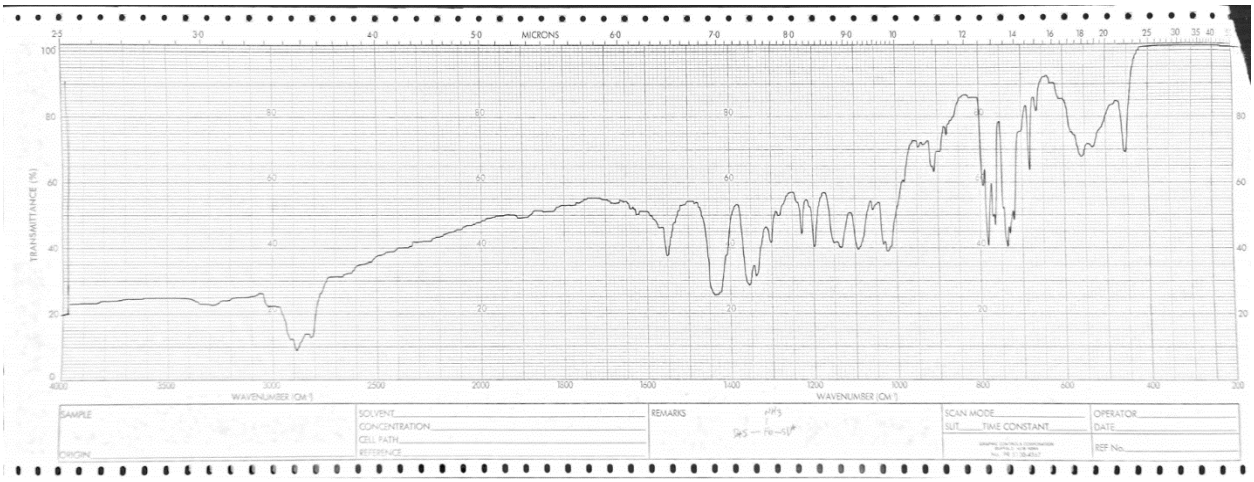

Figure 6.S15: Infrared spectrum of $Fe\{SC_6H_3\text{-}2,6\text{-}(C_6H_3\text{-}2,6\text{-}Pr^i_2)_2\}_2(NH_3)$ (**8**) (Nujol mull, CsI windows)

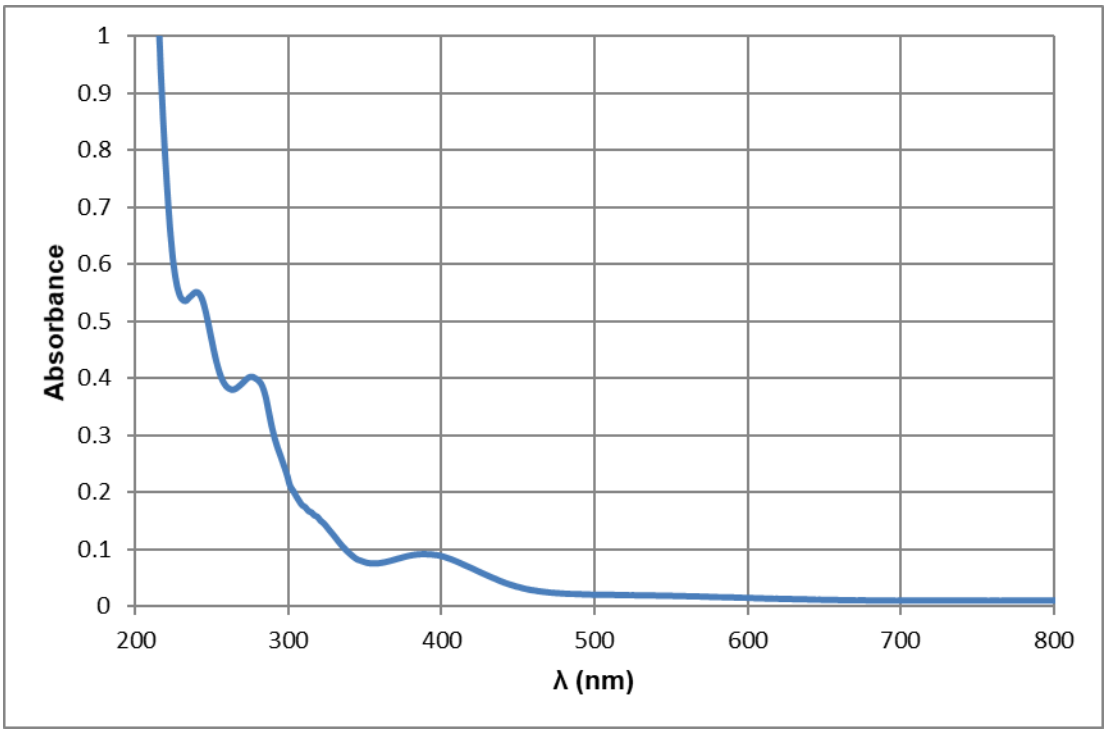

Figure 6.S16: UV-Vis spectrum of $\{Fe(OC_6H_2\text{-}2,6\text{-}Bu^t_2\text{-}4\text{-}Me)_2\}_2$ (**1**) at 25 °C (50 μM in hexanes, 1 cm path length)

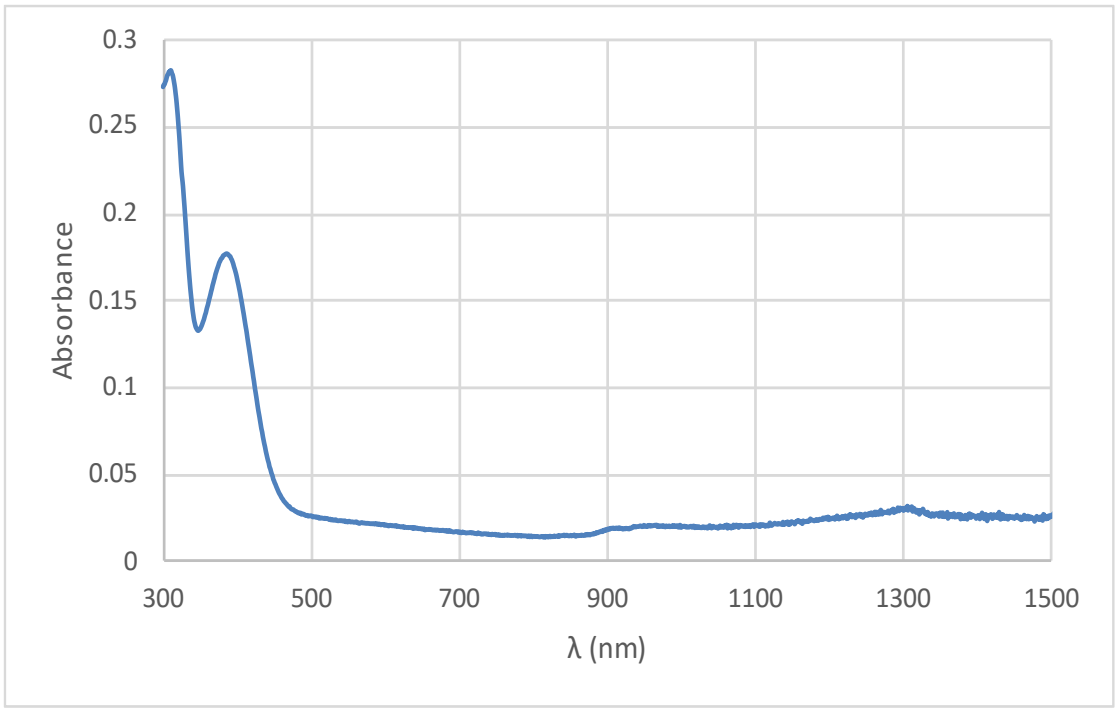

Figure 6.S17: UV-Vis spectrum of $\{Fe(OC_6H_3\text{-}2,6\text{-}Bu^t_2)_2\}_2$ (**2**) at 25 °C (77 μM in hexanes, 1 cm path length)

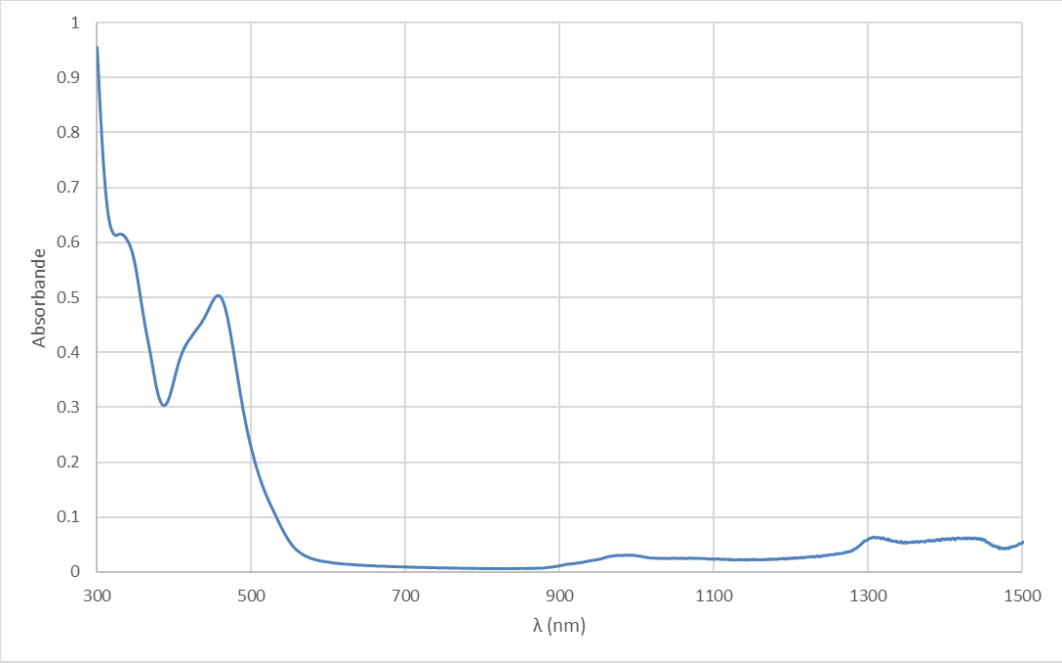

Figure 6.S18: UV-Vis spectrum of $Fe\{SC_6H_3\text{-}2,6\text{-}(C_6H_3\text{-}2,6\text{-}Pr^i_2)_2\}_2$ (**3**) at 25 °C (160 µM in hexanes, 1 cm path length)

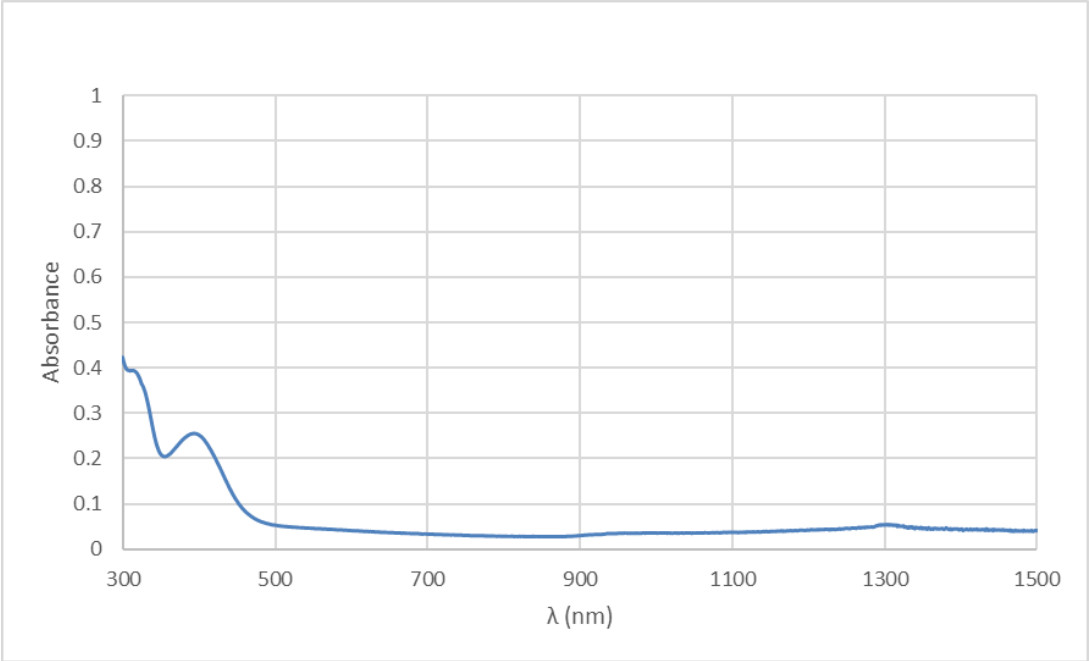

Figure 6.S19: UV-Vis spectrum of $Fe(OC_6H_3\text{-}2,6\text{-}Bu^t_2\text{-}4\text{-}Me)_2(OEt_2)$ (**4**) at 25 °C (130 µM in hexanes, 1 cm path length)

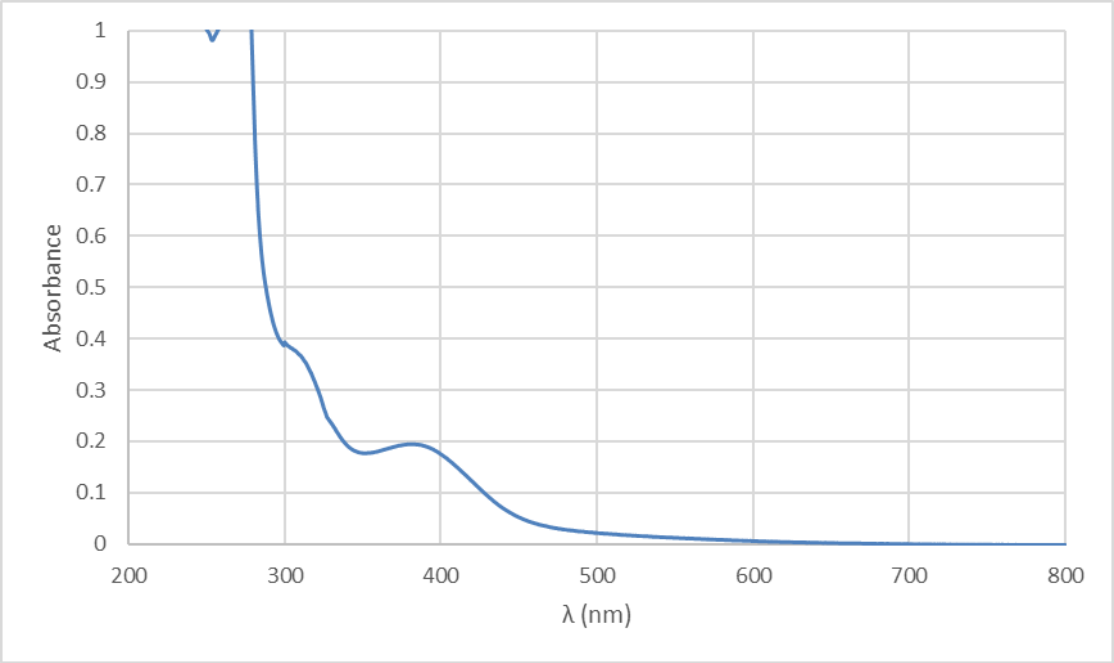

Figure 6.S20: UV-Vis spectrum of $Fe(OC_6H_3\text{-}2,6\text{-}Bu^t_2)_2(OEt_2)$ (**5**) at 25 °C (280 μM in hexanes, 1 cm path length)

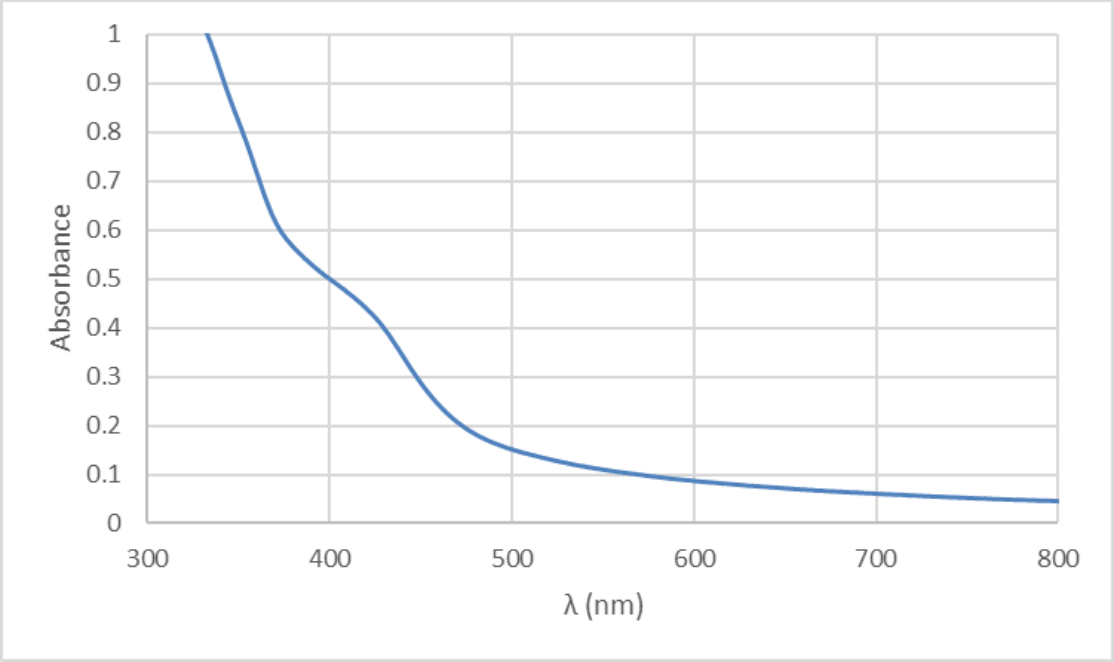

Figure 6.S21: UV-Vis spectrum of $Fe\{SC_6H_3\text{-}2,6\text{-}(C_6H_3\text{-}2,6\text{-}Pr^i_2)_2\}_2(NH_3)$ (**8**) at 25 °C (1.1 mM in hexanes, 1 cm path length)

Table 6.S1: Crystallographic and X-ray Data Collection Parameters of Complex **1**

Empirical formula	$C_{66}H_{105}Fe_2O_4$
Formula weight	1074.19
Temperature/K	90.15
Crystal system	triclinic
Space group	P-1
a/Å	13.8464(10)
b/Å	14.4507(11)
c/Å	16.8069(12)
α/°	80.1450(11)
β/°	84.3778(10)
γ/°	70.2509(10)
Volume/Å^3	3115.4(4)
Z	2
ρ_{calc}g/cm^3	1.145
μ/mm^{-1}	0.509
F(000)	1170.0
Crystal size/mm^3	0.391 × 0.357 × 0.336
Radiation	MoKα (λ = 0.71073)
2Θ range for data collection/°	3.128 to 54.962
Index ranges	$-17 \leq h \leq 17$, $-18 \leq k \leq 18$, $-21 \leq l \leq 21$
Reflections collected	27884
Independent reflections	14242 [R_{int} = 0.0156, R_{sigma} = 0.0222]
Data/restraints/parameters	14242/33/731
Goodness-of-fit on F^2	1.044
Final R indexes [I>=2σ (I)]	R_1 = 0.0329, wR_2 = 0.0878
Final R indexes [all data]	R_1 = 0.0375, wR_2 = 0.09095
Largest diff. peak/hole / e Å^{-3}	0.47/-0.40

Table 6.S2: Crystallographic and X-ray Data Collection Parameters of Complex **2**

Empirical formula	$C_{56}H_{84}Fe_2O_4$
Formula weight	932.93
Temperature/K	90.15
Crystal system	monoclinic
Space group	C2/c
a/Å	44.4824(19)
b/Å	13.8567(6)
c/Å	19.7745(9)
α/°	90
β/°	113.916(2)
γ/°	90
Volume/Å^3	11142.1(9)
Z	8
ρ_{calc}g/cm^3	1.112
μ/mm^{-1}	0.560
F(000)	4032.0
Crystal size/mm^3	0.31 × 0.225 × 0.188
Radiation	MoKα (λ = 0.71073)
2Θ range for data collection/°	4.068 to 59.442
Index ranges	$-61 \leq h \leq 61$, $-19 \leq k \leq 19$, $-27 \leq l \leq 26$
Reflections collected	123878
Independent reflections	15792 [R_{int} = 0.0423, R_{sigma} = 0.0267]
Data/restraints/parameters	15792/0/583
Goodness-of-fit on F^2	1.031
Final R indexes [I>=2σ (I)]	R_1 = 0.0504, wR_2 = 0.1419
Final R indexes [all data]	R_1 = 0.0710, wR_2 = 0.1566
Largest diff. peak/hole / e Å^{-3}	0.68/-0.46

Table 6.S3: Crystallographic and X-ray Data Collection Parameters of Complex **4**

Empirical formula	$C_{34}H_{56}FeO_3$
Formula weight	568.63
Temperature/K	90.15
Crystal system	orthorhombic
Space group	$Pna2_1$
a/Å	18.2039(5)
b/Å	12.6572(3)
c/Å	14.3079(4)
α/°	90
β/°	90
γ/°	90
Volume/Å^3	3296.69(15)
Z	4
ρ_{calc}g/cm^3	1.146
μ/mm^{-1}	0.487
F(000)	1240.0
Crystal size/mm^3	0.371 × 0.156 × 0.11
Radiation	MoKα (λ = 0.71073)
2Θ range for data collection/°	3.92 to 61.508
Index ranges	$-26 \leq h \leq 26$, $-18 \leq k \leq 18$, $-20 \leq l \leq 20$
Reflections collected	82435
Independent reflections	10167 [R_{int} = 0.0668, R_{sigma} = 0.0442]
Data/restraints/parameters	10167/1/359
Goodness-of-fit on F^2	1.061
Final R indexes [I>=2σ (I)]	R_1 = 0.0358, wR_2 = 0.0762
Final R indexes [all data]	R_1 = 0.0481, wR_2 = 0.0825
Largest diff. peak/hole / e Å^{-3}	0.44/-0.28
Flack parameter	-0.002(6)

Table 6.S4: Crystallographic and X-ray Data Collection Parameters of Complex **5**

Empirical formula	$C_{32}H_{52}FeO_3$
Formula weight	540.58
Temperature/K	90.15
Crystal system	orthorhombic
Space group	$P2_12_12$
a/Å	14.3983(16)
b/Å	18.603(2)
c/Å	11.6761(13)
α/°	90
β/°	90
γ/°	90
Volume/Å^3	3127.4(6)
Z	4
ρ_{calc}g/cm^3	1.148
μ/mm^{-1}	0.510
F(000)	1176.0
Crystal size/mm^3	1.264 × 0.518 × 0.493
Radiation	MoKα (λ = 0.71073)
2Θ range for data collection/°	3.488 to 65.026
Index ranges	$-21 \leq h \leq 21$, $-27 \leq k \leq 28$, $-17 \leq l \leq 17$
Reflections collected	51500
Independent reflections	10806 [R_{int} = 0.0244, R_{sigma} = 0.0273]
Data/restraints/parameters	10806/0/339
Goodness-of-fit on F^2	1.039
Final R indexes [I>=2σ (I)]	R_1 = 0.0251, wR_2 = 0.0645
Final R indexes [all data]	R_1 = 0.0278, wR_2 = 0.0658
Largest diff. peak/hole / e Å^{-3}	0.62/-0.17
Flack parameter	0.008(2)

Table 6.S5: Crystallographic and X-ray Data Collection Parameters of Complex **6**

Empirical formula	$C_{98}H_{176}Fe_3N_6O_8$
Formula weight	1733.99
Temperature/K	100.15
Crystal system	orthorhombic
Space group	Pccn
a/Å	32.1228(19)
b/Å	12.9251(7)
c/Å	25.0112(12)
α/°	90
β/°	90
γ/°	90
Volume/Å^3	10384.4(10)
Z	4
ρ_{calc}g/cm^3	1.109
μ/mm^{-1}	0.465
F(000)	3792.0
Crystal size/mm^3	0.483 × 0.268 × 0.106
Radiation	MoKα (λ = 0.71073)
2Θ range for data collection/°	4.94 to 55
Index ranges	$-41 \leq h \leq 41$, $-13 \leq k \leq 16$, $-32 \leq l \leq 32$
Reflections collected	53778
Independent reflections	11927 [R_{int} = 0.0392, R_{sigma} = 0.0253]
Data/restraints/parameters	11927/30/588
Goodness-of-fit on F^2	1.037
Final R indexes [I>=2σ (I)]	R_1 = 0.0384, wR_2 = 0.0916
Final R indexes [all data]	R_1 = 0.0499, wR_2 = 0.0979
Largest diff. peak/hole / e Å^{-3}	0.29/-0.32

Table 6.S6: Crystallographic and X-ray Data Collection Parameters of Complex **7**

Empirical formula	$C_{60}H_{80}FeN_2S_2$
Formula weight	949.23
Temperature/K	100.15
Crystal system	monoclinic
Space group	$P2_1/c$
a/Å	10.8276(12)
b/Å	19.563(2)
c/Å	26.586(3)
α/°	90
β/°	91.135(4)
γ/°	90
Volume/Å^3	5630.4(11)
Z	4
ρ_{calc}g/cm^3	1.120
μ/mm^{-1}	0.379
F(000)	2048.0
Crystal size/mm^3	0.434 × 0.229 × 0.227
Radiation	MoKα (λ = 0.71073)
2Θ range for data collection/°	4.438 to 61.122
Index ranges	$-15 \leq h \leq 15$, $-27 \leq k \leq 27$, $-38 \leq l \leq 37$
Reflections collected	112722
Independent reflections	17198 [R_{int} = 0.0326, R_{sigma} = 0.0242]
Data/restraints/parameters	17198/0/604
Goodness-of-fit on F^2	1.031
Final R indexes [I>=2σ (I)]	R_1 = 0.0368, wR_2 = 0.0933
Final R indexes [all data]	R_1 = 0.0478, wR_2 = 0.0995
Largest diff. peak/hole / e Å^{-3}	0.51/-0.43

Table 6.S7: Crystallographic and X-ray Data Collection Parameters of Complex **8**

Empirical formula	$C_{60}H_{77}FeNS_2$
Formula weight	932.19
Temperature/K	90.15
Crystal system	monoclinic
Space group	$P2_1/n$
a/Å	13.452(3)
b/Å	14.142(3)
c/Å	13.747(3)
α/°	90
β/°	94.616(3)
γ/°	90
Volume/Å^3	2606.7(9)
Z	2
ρ_{calc}g/cm^3	1.188
μ/mm^{-1}	0.408
F(000)	1004.0
Crystal size/mm^3	0.663 × 0.519 × 0.162
Radiation	MoKα (λ = 0.71073)
2Θ range for data collection/°	4.076 to 61.238
Index ranges	$-19 \leq h \leq 19$, $-20 \leq k \leq 20$, $-19 \leq l \leq 19$
Reflections collected	40807
Independent reflections	8006 [R_{int} = 0.0366, R_{sigma} = 0.0301]
Data/restraints/parameters	8006/0/316
Goodness-of-fit on F^2	1.052
Final R indexes [I>=2σ (I)]	R_1 = 0.0467, wR_2 = 0.1115
Final R indexes [all data]	R_1 = 0.0638, wR_2 = 0.1205
Largest diff. peak/hole / e Å^{-3}	0.43/-0.36

Figure 6.S22: Photograph of crystalline {Fe(OC_6H_2-2,6-Bu^t_2-4-Me)$_2$}$_2$ (**1**)

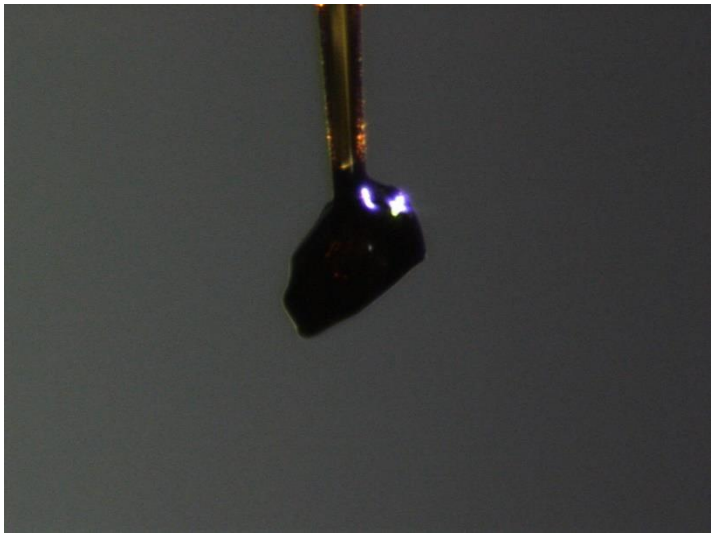

Figure S21: Photograph of crystalline {Fe(OC_6H_2-2,6-Bu^t_2)$_2$}$_2$ (**2**)

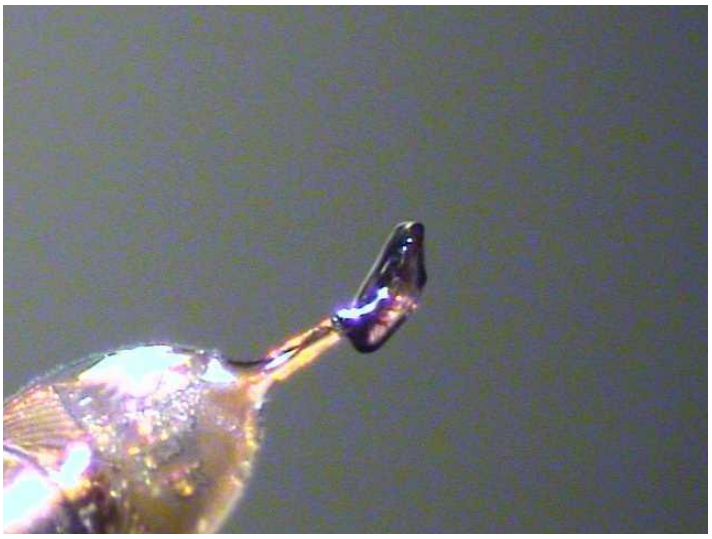

Figure 6.S24: Photograph of crystalline {Fe(OC_6H_2-2,6-Bu^t_2-4-Me)$_2$}$_2$(OEt_2) (**4**)

Figure 6.S25: Photograph of crystalline {Fe(OC_6H_2-2,6-Bu^t_2)$_2$}$_2$(OEt_2) (**5**)

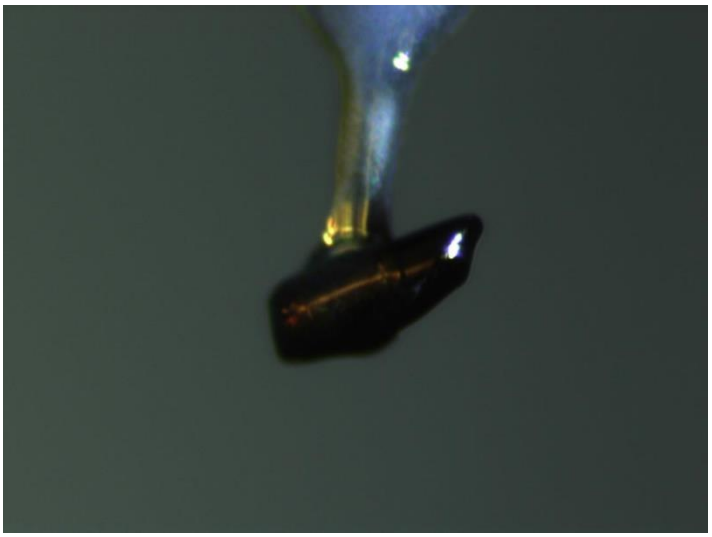

Figure 6.S26: Photograph of crystalline {Fe(OC_6H_2-2,6-Bu^t_2-4-Me)$_2$}$_2$(NH_3)$_2$ (**6**)

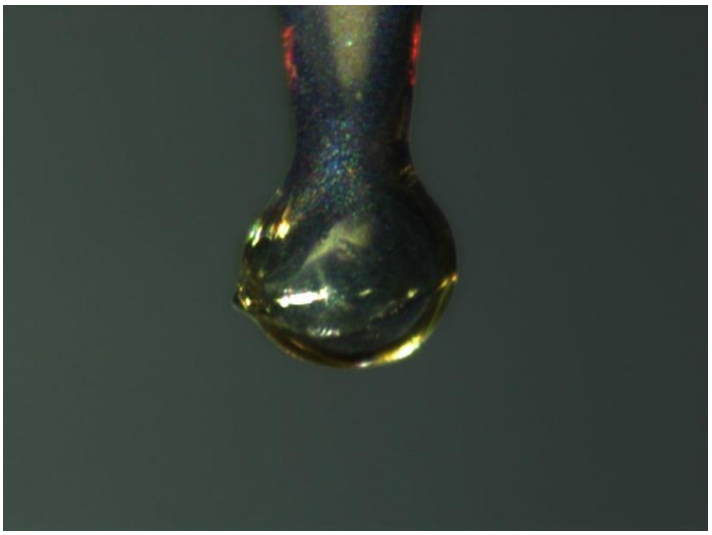

Figure 6.S27: Photograph of crystalline Fe{SC_6H_3-2,6-(C_6H_3-2,6-Pr^i_2)$_2$}$_2$(NH_3)$_2$ (**7**)

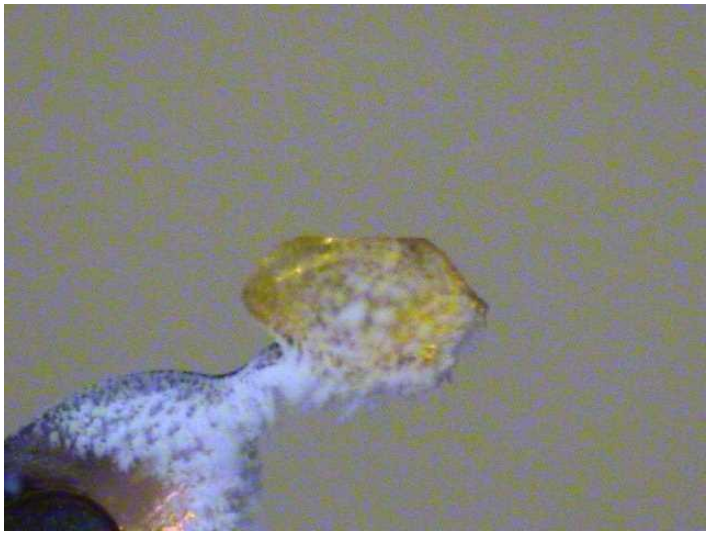

Figure 6.S28: Photograph of crystalline Fe{SC_6H_3-2,6-(C_6H_3-2,6-Pr^i_2)$_2$}$_2$(NH_3) (**8**)

Chapter 7. Designing a Solution-Stable Distannene: The Decisive Role of London Dispersion Effects on the Structure and Properties of {Sn(C_6H_2-2,4,6-Cy_3)$_2$}$_2$ (Cy = cyclohexyl).

Cary R. Stennett,[a] Markus Bursch,[b] James C. Fettinger,[a] Stefan Grimme,[b,*] and Philip P. Power[a,*]

a) Department of Chemistry, University of California, Davis, One Shields Avenue, Davis, California 95616, United States

b) Mulliken Center for Theoretical Chemistry, Institut für Physikalische und Theoretische Chemie, Rheinische Friedrich-Wilhelms-Universität Bonn, Beringstr. 4, 53115 Bonn, Germany

Abstract.

The reaction of 1 eq. of the lithium salt of a new London dispersion effect donor ligand {Li(C_6H_2-2,4,6-Cy_3)·OEt_2}$_2$ (Cy = cyclohexyl) with $SnCl_2$ afforded the distannene {Sn(C_6H_2-2,4,6-Cy_3)$_2$}$_2$ (**1**). Unusually, the distannene remains dimeric in solution, as indicated by its room temperature ^{119}Sn NMR signal (δ = 361.3 ppm) and its electronic spectrum, which is invariant over a temperature range of -10 to 100 °C. The formation of the distannene, which has a short Sn-Sn distance of 2.7005(7) Å, and much enhanced stability in solution compared to other distannenes, is due to increased interligand London dispersion (LD) attraction arising from multiple close approaches of ligand C-H moieties across the Sn-Sn bond. DFT-D4 calculations revealed a dispersion stabilization of the dimer **1** of 38 kcal mol^{-1} and a dimerization free energy of ΔG_{dimer} = -6 kcal mol^{-1}. In contrast, the reaction of 2 eq. of the similarly shaped but less bulky Li(C_6H_2-2,4,6-Ph_3)$_2$·(OEt_2)$_2$ with $SnCl_2$ yielded the monomeric stannylene Sn(C_6H_2-2,4,6-Ph_3)$_2$ (**2**), which is unstable in solution at ambient temperature.

Seminal work by Lappert and co-workers in the 1970s described the synthesis of the first sigma bonded stannylenes Sn{CH($SiMe_3$)$_2$}$_2$]$_2$[1,2] and Sn{N($SiMe_3$)$_2$}$_2$[3,4] (the latter species was also reported by Zuckerman and coworkers).[5,6] X-ray crystallography subsequently established that, whereas Sn{N($SiMe_3$)$_2$}$_2$ is monomeric, Sn{CH($SiMe_3$)$_2$}$_2$ exists in the solid state as the Sn-Sn bonded dimer [Sn{CH($SiMe_3$)$_2$}$_2$]$_2$ with pyramidal tin coordination.[2] Since then, much effort has been devoted to

understanding these heavier carbene analogues (ER_2, E = a group 14 element) and the multiple E-E bonding in their R_2EER_2 dimers.[7–9] The trans-pyramidalized coordination of the tin atoms in $[Sn\{CH(SiMe_3)_2\}_2]_2$ and other distannenes led to the description of the Sn-Sn bond as a non-classical double bond.[10] The distannenes R_2SnSnR_2 typically dissociate into stannylene ($:SnR_2$) monomers in the solution and gas phases.[11] Variations in the tin-tin bonding also exist. For example, Weidenbruch's $\{Sn(C_6H_2\text{-}2\text{-}^tBu\text{-}4,5,6\text{-}Me_3)_2\}_2$ features pyramidalized geometry at only one of its tin atoms, with nearly planar geometry at the other.[12] This results in a weaker Sn-Sn interaction and an exceptionally long Sn-Sn separation of 2.910(1) Å. In contrast, Sekiguchi's distannene $\{Sn(SiMe^tBu_2)_2\}_2$, displays essentially planar geometry at both tin atoms and an unusual, high torsion angle of ca. 45° between the SnR_2 planes.[13] Sekiguchi and Apeloig showed that this complex remains dimerized in solution at ambient temperature (the only known acyclic distannene to do so) and possesses the shortest known Sn-Sn bond length (2.6679(8) Å) among acyclic distannenes.[14]

Much of the discussion of the bonding in distannenes has concerned the direct orbital interactions between the tin atoms.[9] However, in a collaborative study by Nagase and this laboratory, a computational examination of the bonding in these heavier main group analogues revealed that the London dispersion (LD) interaction is mainly responsible for the stability of their dimeric structures.[15] The origin of this stability involves multiple close interligand contacts between C-H moieties across the Sn-Sn bond. This finding was later confirmed by Růžička and Hobza, who ultimately concluded that our initial calculations may have underestimated the importance of LD attraction in stabilizing heavier group 14 R_2EER_2 molecules.[16] Others have also addressed the effects of non-covalent interactions in organometallic molecules.[17,18] We have since reviewed LD effects in organometallic complexes and concluded that several counterintuitive phenomena are in fact hallmarks of intramolecular LD attraction.[19] Perhaps the most striking outcome of LD attraction is the often inverse relationship between steric congestion and structural features or reactivity. For example, we have previously shown that, due to LD attraction, increasing the steric demand of the ligands in $:ER_2$ complexes results in the closure of the R-E-R angle, although the angle

is expected to widen as the size of the R groups increases.[20,21] Schreiner has additionally shown that the hexaphenylethane 'dimer' is stabilized by interactions between bulky substituents on the phenyl groups.[22] Thus, we sought further information on ligands that would produce LD effects in the distannenes. Herein we demonstrate the dramatic effects of the LD stabilization effects arising from interligand H-C---H-C interactions of the hydrocarbon substituents. Thus, reaction of the new aryllithium reagent $\{Li(C_6H_2\text{-}2,4,6\text{-}Cy_3)\cdot(OEt_2)\}_2$ (Cy = cyclohexyl) with $SnCl_2$ affords the Sn-Sn bonded distannene $\{Sn(C_6H_2\text{-}2,4,6\text{-}Cy_3)_2\}_2$, which remains dimeric in solution even at elevated temperature. In contrast, reaction of the less bulky $Li(C_6H_2\text{-}2,4,6\text{-}Ph_3)_2\cdot(OEt_2)_2$ with $SnCl_2$ yields the monomeric stannylene, $Sn(C_6H_2\text{-}2,4,6\text{-}Ph_3)_2$. The LD attraction produced by the H--H contacts in the former is decisive in the stabilization of the distannene. The increased thermodynamic stability conferred by LD attraction is further underlined by the inherent instability of $Sn(C_6H_2\text{-}2,4,6\text{-}Ph_3)_2$, which decomposes into intractable products in solution.

Owing to their ease of modification, aryl ligands feature prominently among structurally characterized organometallic complexes. This also is true for tin(II) complexes of the form $(SnR_2)_n$.[23] However, only one structurally characterized metal complex of any kind is known for the 2,4,6-tricyclohexylphenyl ligand. This was formed by photolysis of $Ni(Br)_2(bipy)$ (bipy = 2,2'-bipyridine) in the presence of 2,4,6-tricyclohexylbromobenzene,[24] rather than by salt metathesis. Almost simultaneously with that report, Fürstner and coworkers showed that the exceptional iron(IV) tetraalkyl complex $FeCy_4$ is stabilized by attractive interligand LD interactions between the cyclohexyl substituents, despite the presence of multiple accessible β-hydrogens which would typically react further to result in its decomposition.[25] These results suggested an examination of what effects might ensue in metal complexes featuring the 2,4,6-tricyclohexylphenyl ligand. When preparing 2,4,6-tricyclohexylphenyllithium (see SI), we were encouraged by the fact that its diethyl ether complex has a dimeric structure with multiple close interligand H-H contacts in its crystal structure. In contrast, the less bulky 2,4,6-triphenylphenyllithium, which differs only in hydrogen content from the 2,4,6-tricyclohexylphenyl derivative, has a monomeric structure in which the lithium atom coordinates two diethyl ether molecules in the solid state.[26] Encouraged

by this apparent anomaly, we investigated the different properties conferred by these ligands to divalent tin complexes.

The reaction of $SnCl_2$ with 1 eq. of $\{Li(C_6H_2\text{-}2,4,6\text{-}Cy_3)\cdot OEt_2\}_2$ in diethyl ether results in the precipitation of a bright red powder. Extraction of the powder in toluene and recrystallization of the residue from a 1:2 mixture of hexanes/toluene at ca. -30 °C affords bright, cherry red crystals of $\{Sn(C_6H_2\text{-}2,4,6\text{-}Cy_3)_2\}_2$, the structure of which is shown in Figure 7.1. The distannene has the trans-pyramidalized geometry (sum of angles at tin = 343.71(15)°) and trans-bending angle (36.79(9)°) typical

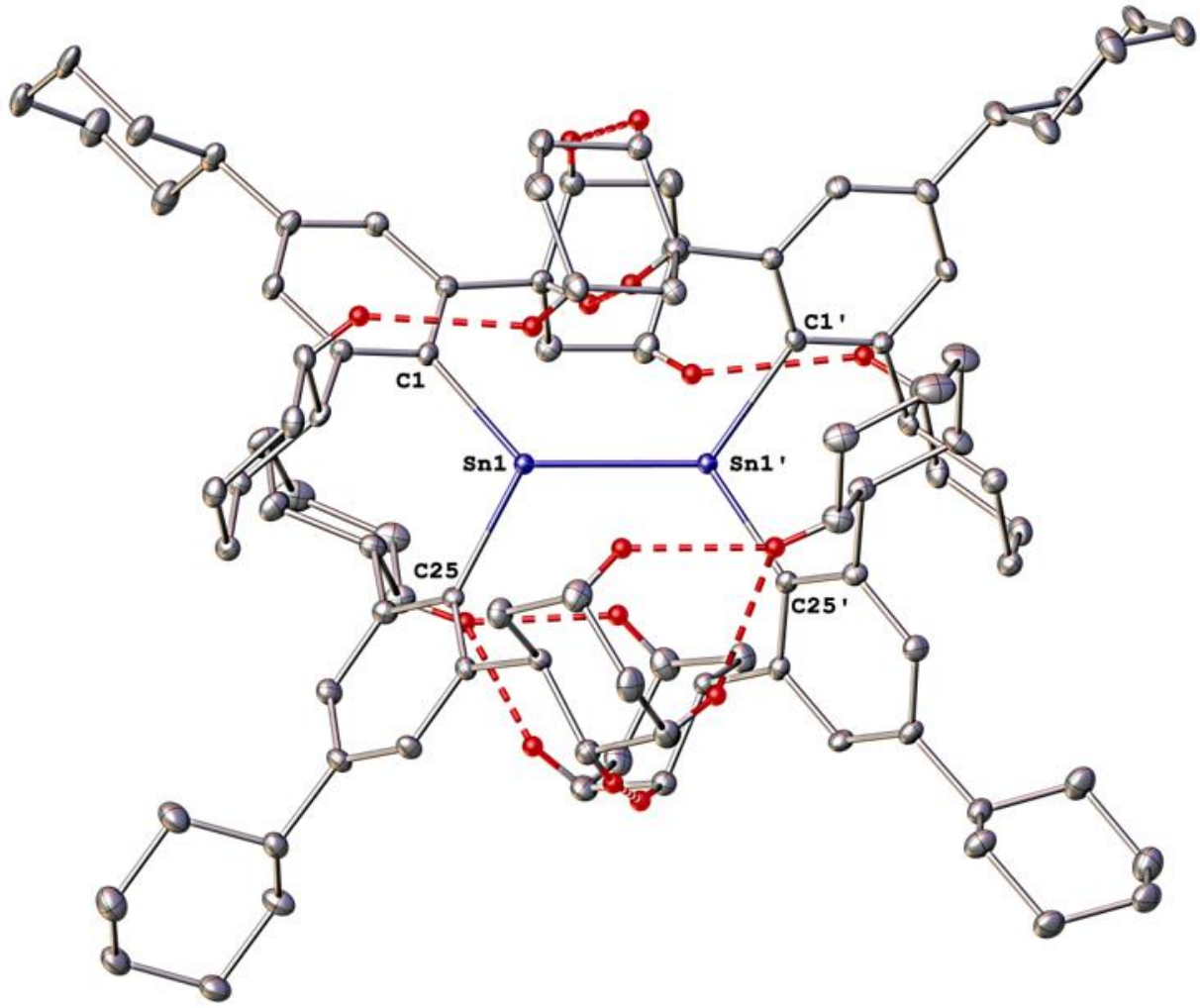

Figure 7.1. Molecular structure of $\{Sn(C_6H_2\text{-}2,4,6\text{-}Cy_3)_2\}_2$ (**1**) with thermal ellipsoids drawn at 30% probability. Interligand H-H contacts across the Sn-Sn bond below the sum of their van der Waals radii (ca. 2.4 Å) are indicated with dashed red lines. All other hydrogens are not shown. Selected bond distances (Å) and angles (°): Sn1-Sn1': 2.7005(7), Sn1-C1: 2.182(3), Sn1-C25: 2.185(3), C1-Sn1-C25: 106.84(11).

of distannenes,[9] with a slight twist angle of 8.21(10)° between the C-Sn-C planes. Thus, in agreement with the natural bonding orbital (NBO) analysis (cf. Figure 7.2b), the structural parameters of are consistent with a weak interaction between the tin atoms.[10] Despite the bulk of the ligands, **1** displays a short Sn-Sn separation of 2.7005(7) Å. In addition, there are several close interligand H-H contacts involving the cyclohexyl rings across the Sn-Sn bond, suggesting a high degree of LD attraction between SnR_2 units. Among structurally characterized $(SnR_2)_2$ complexes (excluding cyclic distannenes), only the distannene $\{Sn(Si^tBu_2Me)_2\}_2$ reported by Sekiguchi and coworkers in 2004 possesses a shorter Sn-Sn bond of 2.6679(8) Å.[13] That complex is the only distannene known to remain dimeric in solution at ambient (or higher) temperature as evidenced by its ^{119}Sn NMR chemical shift and its reactivity with CCl_4 and phenylacetylene to give $\{Sn(Cl)R_2\}_2$ or a four-membered [2+2] cycloaddition product. However, the tin atoms in that molecule are essentially planar coordinated, and the Si-Sn-Si planes have a torsion angle of ca. 45°. Thus, the shorter Sn-Sn bond and its high strength can be at least in part attributed to the presence of a covalent σ bond and a 'twisted' π bond between two triplet state tin units. In contrast, the trans-pyramidal structure of $\{Sn(C_6H_2\text{-}2,4,6\text{-}Cy_3)_2\}_2$ suggests weak Sn-Sn bonding, so that any unusually strong interaction between its SnR_2 units must originate from another source.

A computational study at the B3LYP-D4/def2-TZVP+COSMO-RS/r^{2}SCAN-3c(COSMO) level[27–31] (see SI) of {Sn(C_6H_2-2,4,6-Cy_3)$_2$}$_2$ indicated that, when dispersion effects are excluded, the monomeric stannylene of Sn(C_6H_2-2,4,6-Cy_3)$_2$ is favored (ΔG_{dimer} = +31.5 kcal mol^{-1}). In contrast, including LD effects in the calculations using the accurate D4 model shows that the dimer is clearly favored, with a ΔG_{dimer} of -

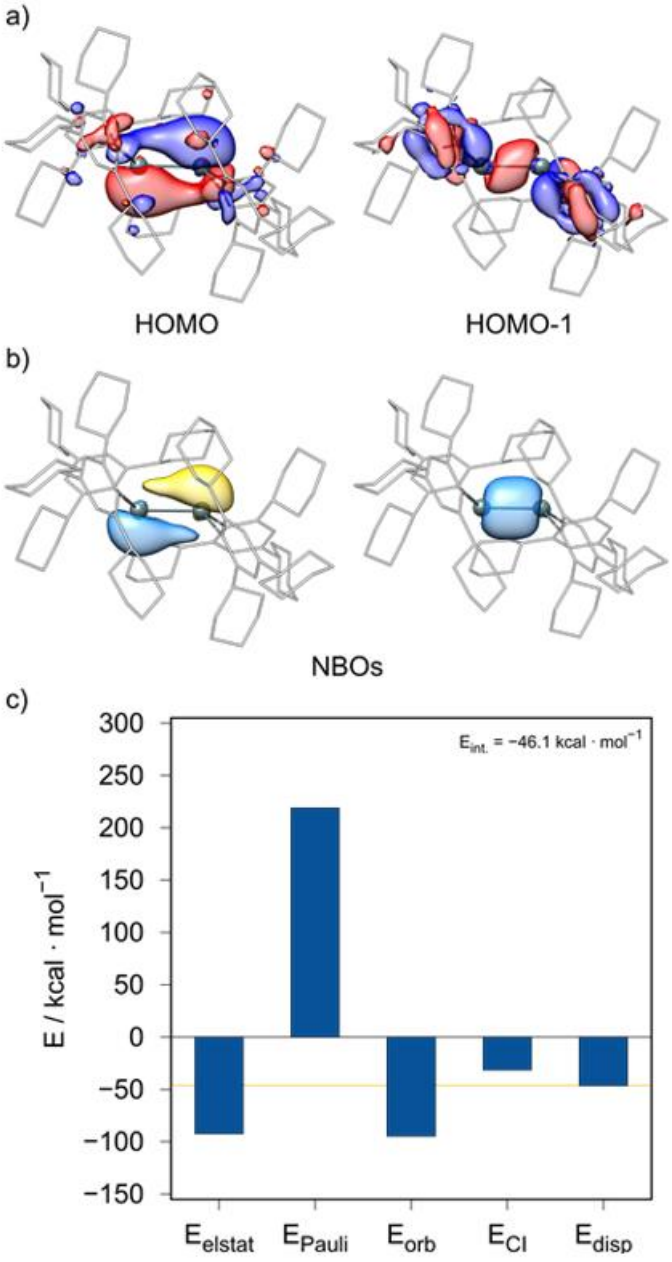

Figure 7.2. a) Selected Kohn-Sham orbitals, b) natural bonding orbitals (isosurface value = 0.05 a.u.), and c) EDA for **1** at the BLYP-D4/def2-TZVP//r2SCAN-3c level of theory. The yellow line represents the overall interaction energy of the stannylene fragments SnR_2. Isosurface value = 0.03 a.u.

6.4 kcal mol^{-1} (ΔH_{dimer} = -23.8 kcal mol^{-1}). According to the magnitude of this value, complex **1** should remain dimeric in solution even at elevated temperature (at 300 K, a ΔG value of ca. -6 kcal mol^{-1} indicates an equilibrium constant of ca. 10^4 favoring the dimer). The importance of LD contributions is further supported by an energy decomposition analysis of **1** (Figure 7.2b).

The predicted ^{119}Sn NMR chemical shift of δ = 388.2 ppm (SO-ZORA-revPBE(COSMO)/ZORA/TZP)[32–34] agrees well with the experimental spectrum of distannene **1** at room temperature, which displayed a single resonance at 361.3 ppm. This shift is in a region similar to the reported chemical shifts of SnR_2 complexes that possess a Sn-Sn bond in solution (cf. $\{Sn(SiBu^t{}_2Me)_2\}_2$, δ = 630.7 ppm, and $\{Sn(C_6H_2\text{-}2,4,6\text{-}^iPr_3)_2\}_2$, δ = 427 ppm (which remains dimeric in solution only at low temperatures of ca. -70 °C), and Wrackmeyer's reviews for a general overview on the topic).[14,35–37] At 350 K, this signal shifts slightly downfield to 369.3 ppm, but no signal for the monomer was detected in the range of 1250 to 3750 ppm (the chemical shift of the monomer was calculated to be 2569 ppm), indicating that complex **1** remains dimeric in solution even at elevated temperatures in agreement with the theoretical result. Additionally, a variable-temperature UV-visible spectroscopy study over the temperature range -10 °C to 100 °C showed only a single absorbance in the visible region at 505 nm. However, despite several attempts and a variety of conditions, no new products were isolated from its attempted reactions with excesses of either phenylacetylene or ethylene. The low reactivity $\{Sn(C_6H_2\text{-}2,4,6\text{-}Cy_3)_2\}_2$ toward these

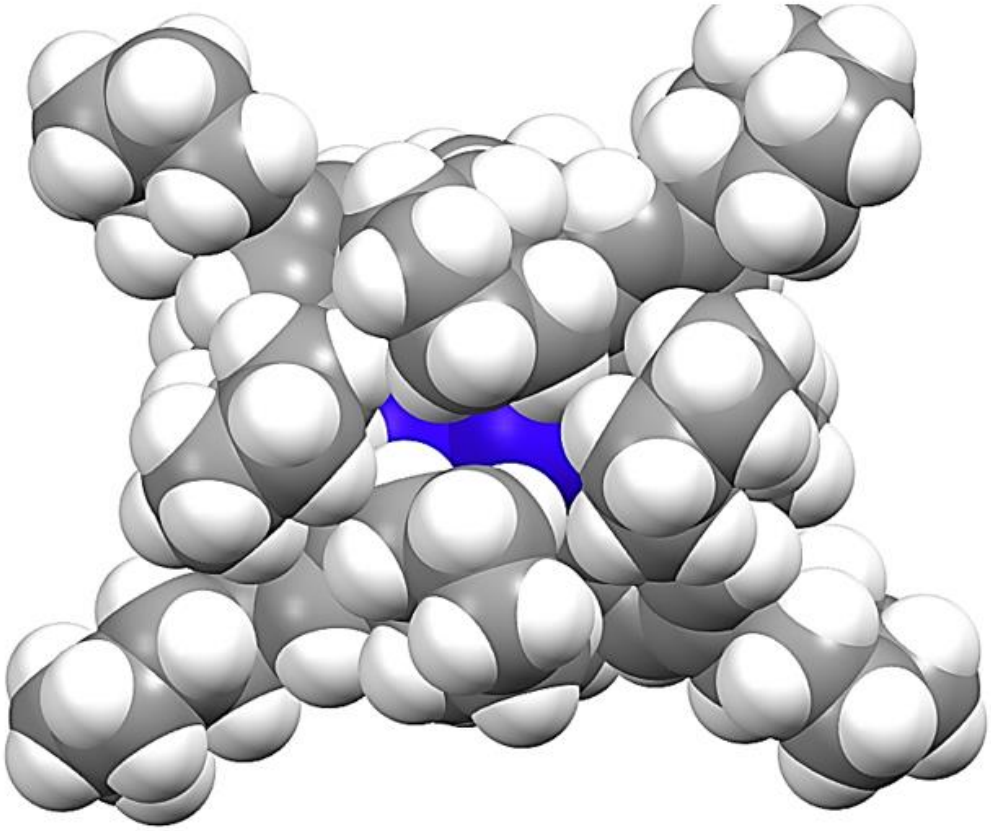

Figure 7.3. Space-filling model of **1** with tin atoms shown in dark blue. Spheres are shown at 100% of the van der Waals radius of the respective element.

reagents is consistent with high steric congestion around the tin atoms. A space-filling model of the structure (Figure 7.3) clearly shows that the tin atoms are almost wholly obscured in the dimer.

In contrast to the high stability of $\{Sn(C_6H_2\text{-}2,4,6\text{-}Cy_3)_2\}_2$, use of the 2,4,6-triphenylphenyl ligand, which is less bulky, but has a broadly similar configuration to the $\text{-}C_6H_2\text{-}2,4,6\text{-}Cy_3$ ligand used in **1,** gives very different results. In a preparation similar to that of $\{Sn(C_6H_2\text{-}2,4,6\text{-}Cy_3)_2\}_2$, $SnCl_2$ was treated with 2 eq. of $Li(C_6H_2\text{-}2,4,6\text{-}Ph_3)\cdot(OEt_2)_2$[26] in diethyl ether. After overnight stirring, a large amount of red powder precipitated from the reaction mixture. Extraction of the red material in toluene and recrystallization of a concentrated toluene solution layered with diethyl ether gave large, red crystals of $Sn(C_6H_2\text{-}2,4,6\text{-}Ph_3)_2$ (**2**) in moderate yield. Despite the reduced bulk of the ligand, a structural study showed that it is monomeric in the solid state (Figure 7.4). Its molecular structure is broadly similar to that of its lead analogue, which was

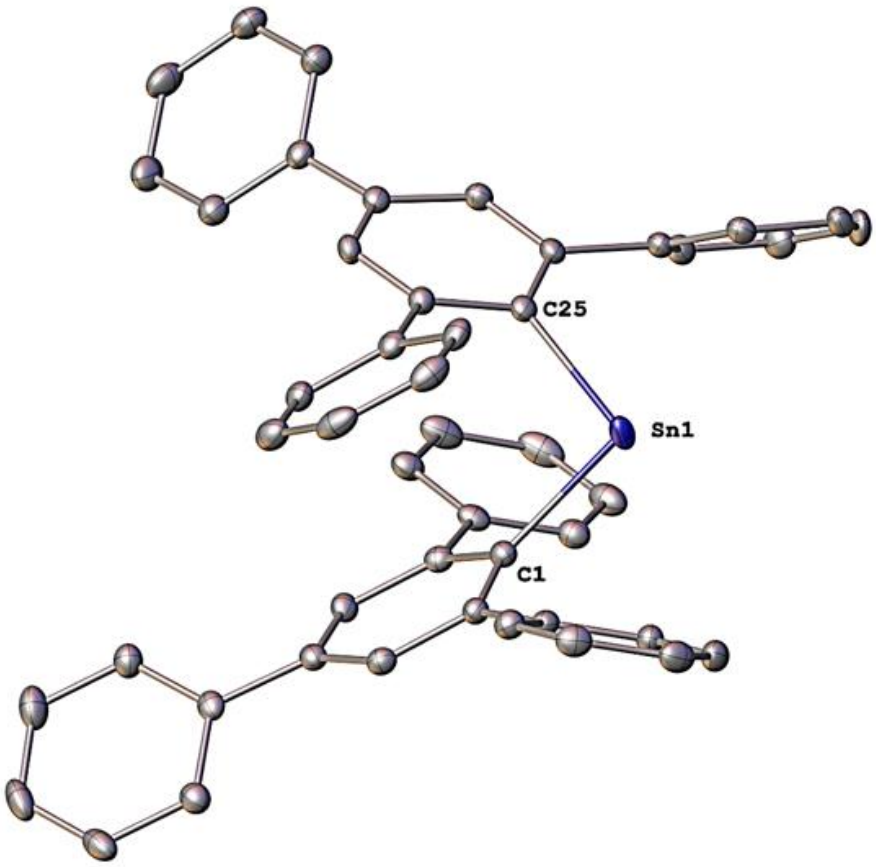

Figure 7.4. Molecular structure of **2** with thermal ellipsoids drawn at 30% probability. Hydrogen atoms are not shown. Selected bond distances (Å) and angles (°): Sn1-C1: 2.222(3), Sn2-C25: 2.233(3) C1-Sn1-C25: 96.36(9).

reported by Robinson in 2005.[38] Its C-Sn-C angle (96.36(9)°) is notably sharp, and is comparable to that of the stannylene Sn{C_6H_3-2,6-(C_6H_2-2,4,6-^{i}Pr$_3$)$_2$}(Ph) (C-Sn-C angle = 98.86°).[39] The shortest Sn-Sn distance in the crystal structure is 7.8870(9) Å. Sn(C_6H_2-2,4,6-Ph_3)$_2$ is unstable in solution, and attempts to redissolve it results in an immediate color change to brown and the deposition of an insoluble solid of currently unknown composition (likely polymeric,[40] see SI for spectra). Computational studies showed that the formation of the monomeric stannylene is favored over the distannene, even when LD effects are considered (ΔG_{dimer} = +8.8 kcal mol^{-1}). Although few further details are currently available due to its instability, its monomeric structure underlines the importance of the stabilizing effects of LD attraction in distannenes.

In conclusion, the trans-pyramidalized distannene $\{Sn(C_6H_2\text{-}2,4,6\text{-}Cy_3)_2\}_2$ (**1**) was shown to remain dimeric in solution over a wide range of temperatures. Its enhanced thermodynamic stability compared to other distannenes was determined computationally to be due to London dispersion (LD) attraction between SnR_2 units. Unlike the previously reported solution-stable distannene $\{Sn(SiBu^t_2Me)_2\}_2$, which possesses two comparably strong interactions between the tin atoms, the strong dimerization in **1** is dominated by the presence of these LD attractions, since its trans bent structure indicates only a weak non-classical double bond between the tin atoms in agreement with the NBO analysis. In contrast, using the less bulky 2,4,6-triphenylphenyl ligand afforded the monomeric stannylene $Sn(C_6H_2\text{-}2,4,6\text{-}Ph_3)_2$ (**2**), which was shown to be unstable in solution. The instability of monomeric **2** underscores the importance of LD attraction in stabilizing **1** via its dispersion effect donor ligand $\text{-}C_6H_2\text{-}2,4,6\text{-}Cy_3$.

Associated Content.

Supporting information.

The Supporting Information, including spectra (NMR, infrared, UV-Vis), crystallographic data, computational details, coordinates of the optimized structures, and photographs of material is available free of charge on the ACS Publications website at DOI: xxxxxxxxx. CCDC entries 2106457 (**1**), 2108933 (**1**, polymorph), 2098934 (**2**), and 2091040 ($\{Li(C_6H_2\text{-}2,4,6\text{-}Cy_3)\cdot(OEt_2)\}_2$), contain the supplementary crystallographic data of the complexes described here. These data can be obtained free of charge via www.ccdc.cam.ac.uk/data_request/cif, by emailing data_request@ccdc.cam.ac.uk, or by contacting The Cambridge Crystallographic Data Centre, 12 Union Road, Cambridge CB2 1EZ, UK; fax: + 44 1223 336033.

Author Information.

Corresponding author

*pppower@ucdavis.edu

*grimme@thch.uni-bonn.de

ORCID

Cary R. Stennett: 0000-0002-2727-5747

Markus Bursch: 0000-0001-6711-5804

James C. Fettinger: 0000-0002-6428-4909

Stefan Grimme: 0000-0002-5844-4371

Philip P. Power: 0000-0002-6262-3209

Notes

The authors declare no competing financial interest.

Acknowledgements

C.R.S, J.C.F, and P.P.P. wish to acknowledge the US National Science Foundation (CHE-1565501) for support of this work and for the purchase of a dual-source X-ray diffractometer (CHE-0840444). M.B. and S.G. acknowledge financial support from the DFG (SPP 1807). The authors acknowledge Dr. Ping Yu for key assistance with acquisition of ^{119}Sn NMR spectra.

References.

(1) Davidson, P. J.; Lappert, M. F. Stabilisation of Metals in a Low Co-Ordinative Environment Using the Bis(Trimethylsilyl)Methyl Ligand; Coloured Sn and Pb Alkyls, M[CH(SiMe$_3$)$_2$]$_2$. *J. Chem. Soc.*,

Chem. Commun. **1973**, No. 9, 317a-317a.

(2) Goldberg, D. E.; Harris, D. H.; Lappert, M. F.; Thomas, K. M. A New Synthesis of Divalent Group 4B Alkyls $M[CH(SiMe_3)_2]_2$(M = Ge or Sn), and the Crystal and Molecular and Molecular Strcuture of the Tin Compound. *J. Chem. Soc., Chem. Commun.* **1976**, No. 7, 261–262.

(3) Harris, D. H.; Lappert, M. F. Monomeric, Volatile Bivalent Amides of Group IV Elements, $M(NR^1{}_2)_2$ and $M(NR^1R^2)_2$(M = Ge, Sn, or Pb; $R^1 = Me_3Si$, $R^2 = Me_3C$). *J. Chem. Soc., Chem. Commun.* **1974**, No. 21, 895–896.

(4) Fjeldberg, T.; Hope, H.; Lappert, M. F.; Power, P. P.; Thorne, A. J. Molecular Structures of the Main Group 4 Metal(II) Bis(Trimethylsilyl)-Amides $M[N(SiMe_3)_2]_2$ in the Crystal (X-Ray) and Vapour (Gas-Phase Electron Diffraction). *J. Chem. Soc., Chem. Commun.* **1983**, No. 11, 639–641.

(5) Schaeffer, C. D.; Zuckerman, J. J. Tin(II) Organosilylamines. *J. Am. Chem. Soc.* **1974**, *96*, 7160–7162.

(6) Molloy, K. C.; Bigwood, M. P.; Herber, R. H.; Zuckerman, J. J. Variable-Temperature Tin-119m Moessbauer Study of Tin(II) and Tin(IV) Amines. *Inorg. Chem.* **1982**, *21*, 3709–3712.

(7) Mizuhata, Y.; Sasamori, T.; Tokitoh, N. Stable Heavier Carbene Analogues. *Chem. Rev.* **2009**, *109*, 3479–3511.

(8) Lee, V. Y.; Sekiguchi, A. 1.11 - Multiply Bonded Compounds of Group 14 Elements. In *Comprehensive Inorganic Chemistry II (Second Ed.)*; Reedijk, J., Poeppelmeier, K. B. T., Eds.; Elsevier: Amsterdam, 2013; pp 289–324.

(9) Fischer, R. C.; Power, P. P. π-Bonding and the Lone Pair Effect in Multiple Bonds Involving Heavier Main Group Elements: Developments in the New Millennium. *Chem. Rev.* **2010**, *110*, 3877–3923.

(10) Davidson, P. J.; Harris, D. H.; Lappert, M. F. Subvalent Group 4B Metal Alkyls and Amides. Part I. The Synthesis and Physical Properties of Kinetically Stable Bis[Bis(Trimethysilyl)Methyl]-

Germanium(II), -Tin(II), and -Lead(II). *J. Chem. Soc. Dalton Trans.* **1976**, No. 21, 2268–2274.

(11) Fjeldberg, T.; Haaland, A.; Schilling, B. E. R.; Lappert, M. F.; Thorne, A. J. Subvalent Group 4B Metal Alkyls and Amides. Part 8. Germanium and Tin Carbene Analogues MR_2[M = Ge or Sn, R = $CH(SiMe_3)_2$]: Syntheses and Structures in the Gas Phase (Electron Diffraction); Molecular-Orbital Calculations for MH_2 and $GeMe_2$. *J. Chem. Soc. Dalton Trans.* **1986**, No. 8, 1551–1556.

(12) Weidenbruch, M.; Kilian, H.; Peters, K.; Schnering, H. G. Von; Marsmann, H. Compounds of Germanium and Tin, 16. A Tetraaryldistannene with a Long Tin—Tin Multiple Bond and Differing Environments at the Tin Atoms. *Chem. Ber.* **1995**, *128*, 983–985.

(13) Fukawa, T.; Lee, V. Y.; Nakamoto, M.; Sekiguchi, A. Tetrakis(Di-Tert-Butylmethylsilyl)Distannene and Its Anion Radical. *J. Am. Chem. Soc.* **2004**, *126*, 11758–11759.

(14) Lee, V. Y.; Fukawa, T.; Nakamoto, M.; Sekiguchi, A.; Tumanskii, B. L.; Karni, M.; Apeloig, Y. $(^tBu_2MeSi)_2SnSn(SiMe^tBu_2)_2$: A Distannene with a >SnSn< Double Bond That Is Stable Both in the Solid State and in Solution. *J. Am. Chem. Soc.* **2006**, *128*, 11643–11651.

(15) Guo, J.-D.; Liptrot, D. J.; Nagase, S.; Power, P. P. The Multiple Bonding in Heavier Group 14 Element Alkene Analogues Is Stabilized Mainly by Dispersion Force Effects. *Chem. Sci.* **2015**, *6*, 6235–6244.

(16) Sedlak, R.; Stasyuk, O. A.; Fonseca Guerra, C.; Řezáč, J.; Růžička, A.; Hobza, P. New Insight into the Nature of Bonding in the Dimers of Lappert's Stannylene and Its Ge Analogs: A Quantum Mechanical Study. *J. Chem. Theory Comput.* **2016**, *12*, 1696–1704.

(17) Petrović, P.; Djukic, J.-P.; Hansen, A.; Bannwarth, C.; Grimme, S. Non-Covalent Stabilization in Transition Metal Coordination and Organometallic Complexes. *Non-covalent Interactions in the Synthesis and Design of New Compounds*. April 19, 2016, pp 115–143.

(18) Bursch, M.; Caldeweyher, E.; Hansen, A.; Neugebauer, H.; Ehlert, S.; Grimme, S. Understanding

and Quantifying London Dispersion Effects in Organometallic Complexes. *Acc. Chem. Res.* **2019**, *52*, 258–266.

(19) Liptrot, D. J.; Power, P. P. London Dispersion Forces in Sterically Crowded Inorganic and Organometallic Molecules. *Nat. Rev. Chem.* **2017**, *1*, 4.

(20) Rekken, B. D.; Brown, T. M.; Fettinger, J. C.; Lips, F.; Tuononen, H. M.; Herber, R. H.; Power, P. P. Dispersion Forces and Counterintuitive Steric Effects in Main Group Molecules: Heavier Group 14 (Si–Pb) Dichalcogenolate Carbene Analogues with Sub-90° Interligand Bond Angles. *J. Am. Chem. Soc.* **2013**, *135*, 10134–10148.

(21) McCrea-Hendrick, M. L.; Bursch, M.; Gullett, K. L.; Maurer, L. R.; Fettinger, J. C.; Grimme, S.; Power, P. P. Counterintuitive Interligand Angles in the Diaryls E{C_6H_3-2,6-(C_6H_2-2,4,6-$^{i}Pr_3$)$_2$}$_2$ (E = Ge, Sn, or Pb) and Related Species: The Role of London Dispersion Forces. *Organometallics* **2018**, *37*, 2075–2085.

(22) Rösel, S.; Balestrieri, C.; Schreiner, P. R. Sizing the Role of London Dispersion in the Dissociation of All-Meta Tert-Butyl Hexaphenylethane. *Chem. Sci.* **2017**, *8*, 405–410.

(23) Klinkhammer, K. W. Recent Advances in Structural Chemistry of Organic Germanium, Tin and Lead Compounds. *The Chemistry of Organic Germanium, Tin and Lead Compounds*. November 26, 2002, pp 283–357.

(24) Sakhapov, I. F.; Gafurov, Z. N.; Babaev, V. M.; Rizvanov, I. K.; Dobrynin, A. B.; Krivolapov, D. B.; Khayarov, K. R.; Sinyashin, O. G.; Yakhvarov, D. G. First Example of Organonickel Complex Bearing Three Cyclic Substituents in the σ-Bonded Aromatic Ring: Bromo[(2,2' -Bipyridine)-2,4,6-Tricyclohexylphenylnickel]. *Mendeleev Commun.* **2016**, *26*, 131–133.

(25) Casitas, A.; Rees, J. A.; Goddard, R.; Bill, E.; DeBeer, S.; Fürstner, A. Two Exceptional Homoleptic Iron(IV) Tetraalkyl Complexes. *Angew. Chem. Int. Ed.* **2017**, *56*, 10108–10113.

(26) Olmstead, M. M.; Power, P. P. Isolation and X-Ray Crystal Structure of a Monomeric, σ-Bonded Aryllithium Etherate Complex [Li(Et_2O)$_2$-2,4,6-$Ph_3C_6H_2$]. *J. Organomet. Chem.* **1991**, *408*, 1–6.

(27) Becke, A. D. Density-Functional Thermochemistry. III. The Role of Exact Exchange. *J. Chem. Phys.* **1993**, *98*, 5648–5652.

(28) Caldeweyher, E.; Ehlert, S.; Hansen, A.; Neugebauer, H.; Spicher, S.; Bannwarth, C.; Grimme, S. A Generally Applicable Atomic-Charge Dependent London Dispersion Correction. *J. Chem. Phys.* **2019**, *150*, 154122.

(29) Klamt, A. Conductor-like Screening Model for Real Solvents: A New Approach to the Quantitative Calculation of Solvation Phenomena. *J. Phys. Chem.* **1995**, *99*, 2224–2235.

(30) Moellmann, J.; Grimme, S. Importance of London Dispersion Effects for the Packing of Molecular Crystals: A Case Study for Intramolecular Stacking in a Bis-Thiophene Derivative. *Phys. Chem. Chem. Phys.* **2010**, *12*, 8500–8504.

(31) Furche, F.; Ahlrichs, R.; Hättig, C.; Klopper, W.; Sierka, M.; Weigend, F. Turbomole. *WIREs Comput Mol Sci* **2014**, *4*, 91–100.

(32) Zhang, Y.; Yang, W. Comment on "Generalized Gradient Approximation Made Simple". *Phys. Rev. Lett.* **1998**, *80*, 890.

(33) Schreckenbach, G.; Ziegler, T. Calculation of NMR Shielding Tensors Using Gauge-Including Atomic Orbitals and Modern Density Functional Theory. *J. Phys. Chem.* **1995**, *99*, 606–611.

(34) te Velde, G.; Bickelhaupt, F. M.; Baerends, E. J.; Fonseca Guerra, C.; van Gisbergen, S. J. A.; Snijders, J. G.; Ziegler, T. Chemistry with ADF. *J. Comput. Chem.* **2001**, *22*, 931–967.

(35) Masamune, S.; Sita, L. R. Hexakis(2,4,6-Triisopropylphenyl)Cyclotristannane (R2Sn)3 and Tetrakis(2,4,6-Triisopropylphenyl)Distannene ($R_2Sn)_2$, Their Unprecedented Thermal Interconversion, and the First Solution Spectral Characterization of a Distannene. *J. Am. Chem. Soc.*

1985, *107*, 6390–6391.

(36) Wrackmeyer, B. ^{119}Sn-NMR Parameters. In *Annual Reports on NMR Spectroscopy*; Webb, G., Ed.; Academic Press, 1985; Vol. 16, pp 73–186.

(37) Wrackmeyer, B. Application of ^{119}Sn NMR Parameters; Webb, G., Ed.; Academic Press, 1999; Vol. 38, pp 203–264.

(38) Yang, X.-J.; Wang, Y.; Wei, P.; Quillian, B.; Robinson, G. H. Syntheses and Structures of New Diaryl Lead(II) Compounds PbR_2 (1, R = 2,4,6-Triphenylphenyl; 2, R = 2,6-Bis(1′-Naphthyl)Phenyl). *Chem. Commun.* **2006**, No. 4, 403–405.

(39) Phillips, A. D.; Hino, S.; Power, P. P. A Reversible Valence Equilibrium in a Heavier Main Group Compound. *J. Am. Chem. Soc.* **2003**, *125*, 7520–7521.

(40) Olson, D. H.; Rundle, R. E. The Nature of R_2Sn Compounds. *Inorg. Chem.* **1963**, *2*, 1310–1311.

Supporting Information

Experimental Details.

General Considerations. All manipulations were performed under in an atmosphere of dry argon by using modified Schlenk techniques or in a Vacuum Atmospheres drybox. Solvents were dried and collected using an S2 Grubbs-type solvent purification system (Glass Contour) and degassed using the freeze, pump, thaw method. All physical measurements were obtained under strictly anaerobic and anhydrous conditions. IR spectra were recorded as Nujol mulls between CsI windows on a PerkinElmer 1430 spectrophotometer. UV–vis spectra were recorded as dilute toluene or hexane solutions in 3.5 mL quartz cuvettes using an OLIS modernized Cary 14 UV/vis/NIR spectrophotometer. ^{1}H and ^{13}C NMR spectra were internally referenced to residual solvent signals. The ^{119}Sn{^{1}H} NMR spectrum of **2** was referenced to an external standard of $SnMe_4$ ($\delta = 0$). Melting points were determined on a Meltemp II apparatus in flame-sealed glass capillaries equipped with a partial immersion thermometer. Complexes **1-4** melt (or decompose) over narrow temperature ranges (1-2 °C), indicative of their high purity. Elemental analyses were not attempted due to the high air and moisture sensitivity of these complexes. Cy_3PhBr and Ph_3PhBr were prepared according to literature methods.

{Li(C$_6$H$_2$-2,4,6-Cy$_3$)·(OEt$_2$)}$_2$. 2,4,6-tricyclohexyl-bromobenzene[1] (20 g, 49.5 mmol) was suspended in ca. 200 mL of a 1:1 (v/v) mixture of hexanes and diethyl ether and cooled to ca. 0 °C. 67 mL of a 1.6 M (107 mmol) of ^{t}BuLi in pentane was then dropwise added to the stirred suspension over ca. 30 minutes. The mixture was stirred at ca. 0 °C for two hours, then allowed to warm to ambient temperature and stirred for a further hour. The solvent was then completely removed under reduced pressure, and ca. 200 mL of hexanes was added to the residue. The mixture was then warmed to ca. 60 °C and filtered at this temperature. Overnight storage of the filtrate at ambient temperature yielded 4.5 g of crystalline 2,4,6-tricyclohexylphenyllithium ether complex, from which a crystal suitable for X-ray diffraction studies was obtained. Storage of the mother liquor at ca. -20 °C afforded an additional 9.5 g of the product (overall yield: 70%). M.p.: loses solvent from 139-141 °C, melts from 146-148 °C. IR (Nujol) $\tilde{\nu}$ [cm^{-1}] = 1585 (m,

sh), 1530 (m, sh), 1300 (m, sh), 1260 (m, sh), 1230 (w, sh), 1190 (m), 1160 (m), 1120 (m, shoulder), 1090 (s), 1070 (s) 1030 (m, shoulder), 985 (m, sh), 950 (m, sh), 930 (m, shoulder), 915 (m), 890 (m), 860 (s, sh), 845 (m, shoulder), 790 (w) 730 (w), 650 (m, sh), 620 (w, shoulder), 540 (m, sh), 500 (m, sh), 460 (m, shoulder), 440 (m, shoulder), 400 (s, br), 330 (m), 250 (m). ^{1}H NMR (600 MHz, C_6D_6, 298 K): δ = 7.19-7.08 (m, 2H, ArH), 2.95 (q, 4H, LiO($C\underline{H}_2CH_3)_2$), 2.75-2.56 (m, 2H, *o*-cyclohexyl, CH), 2.37-2.26 (m, 1H, *p*-cyclohexyl, CH), 2.20-1.17 (m, 30H, cyclohexyl CH_2), 0.75 (s, 6H, LiO($CH_2C\underline{H}_3)_2$). ^{13}C NMR (151 MHz, C_6D_6) δ = 160.75, 145.27, 119.95, 66.11, 51.34, 45.94, 36.87, 36.30, 35.60, 27.75, 27.39, 27.06, 26.94, 14.56.

{Sn(C_6H_2-2,4,6-$Cy_3)_2$}$_2$ (1). A solution of 2,4,6-tricyclohexylphenyllithium (2.0 g, 4.9 mmol) in ca. 50 mL of diethyl ether was added dropwise to a cooled (ca. -78 °C) slurry of $SnCl_2$ (0.46 g, 2.5 mmol) in ca. 10 mL of diethyl ether over ca. 10 minutes with stirring. The stirred orange/red mixture was then allowed to slowly warm to ambient temperature overnight. The mixture became dark red. The solvent was then completely removed under reduced pressure and the solid residue was extracted in ca. 40 mL toluene. The mixture was filtered, and the solvent was completely removed from the filtrate under reduced pressure. Diethyl ether (ca. 40 mL) was then added, and the mixture was briefly sonicated for ca. 1 minute to remove the solids from the walls of the flask. The mixture was then stirred for 30 minutes, and the ether was removed under reduced pressure until a volume of ca. 20 mL remained. The mixture was then cooled to ca. -40 °C for 30 minutes to effect precipitation of a dark red/violet microcrystalline solid. The solid was then isolated by cannula and washed twice with 5 mL portions of cold diethyl ether to give 1.0 g (50 %) of microcrystalline **2**. Storage of a concentrated solution of **2** in toluene for two weeks at -30 °C afforded crystals that were suitable for X-ray diffraction studies. M.p. >250 °C (dec.). UV/Vis: λ/nm (ε/$M^{-1}cm^{-1}$): 502 (7500). IR (Nujol) $\tilde{\nu}$ [cm^{-1}] = 1585 (m), 1490 (m), 1410 (m, shoulder), 1340 (m), 1100 (m), 1010 (m, br), 935 (w), 880 (w), 850, (s, sh), 835 (m, sh), 800 (m, br), 730 (m), 720 (m), 650 (w, sh), 540 (m), 490 (w), 390 (w, br), 350 (m), 310 (w, br). ^{1}H NMR (500 MHz, C_7D_8, 360 K): δ = 7.13 (s, ArH), 6.96 (s, ArH), 3.12 (s, broad, 3H, cyclohexyl CH), 2.50 (m, 3H, cyclohexyl CH), 2.06-1.04 (s, 60H, cyclohexyl CH_2)

$^{13}C\{^{1}H\}$ NMR (126 MHz, C_7D_8, 298 K): δ = Ar-C (155.3, 154.1, 153.6, 151.1, 149.8, 148.7, 148.5, 148.1, 147.8, 124.1, 123.5, 123.3, 122.9), cyclohexyl-C (65.9, 49.0, 48.8, 48.5, 47.9, 47.7, 45.8, 45.6, 45.4, 45.3, 38.9, 38.5, 38.0, 36.8, 36.6, 36.3, 35.9, 35.2, 35.1, 35.0, 34.9, 34.7, 34.4, 27.5, 27.5, 27.4, 27.3, 27.0, 26.9, 26.7, 26.6, 26.5 26.4, 26.2, 25.6, 25.2, 24.7, 15.6).

$Sn(C_6H_2$-2,4,6-$Ph_3)_2$ (2). 2,4,6-triphenylphenyllithium dietherate (1.0 g, 2.2 mmol) was dissolved in ca. 30 mL of diethyl ether and added dropwise over 10 minutes to a cooled (ca. 0 °C) slurry of $SnCl_2$ (0.2 g, 1.1 mmol) in ca. 10 mL of diethyl ether with stirring. After the addition was complete, the pink mixture was allowed to warm to ambient temperature. A large amount of red precipitate formed, and the mixture was allowed to stir overnight. The solvent was then completely removed under reduced pressure and the residue was extracted in ca. 40 mL toluene. The red mixture was then filtered, and the filtrate was concentrated under reduced concentration to a volume of ca. 10 mL. Diethyl ether (ca. 5 mL) was then carefully layered on top of this solution, and the flask was allowed to stand at ambient temperature overnight. The solvent was then decanted, affording a large crop of bright red crystals (0.4 g, 50 %) of **4** that were suitable for X-ray diffraction studies. M.p.: Color gradually changes from red to orange from 140-160 °C, melts at 165-167 °C. UV/Vis: λ/nm (ε/$M^{-1}cm^{-1}$): ca. 500 (250); decomposes in solution as indicated by color change and growth of absorbance at 451 nm after overnight storage. IR (Nujol) $\tilde{\nu}$ [cm^{-1}] = 1590 (m) 1580 (m, shoulder), 1570 (m, sh), 1530 (w) 1485 (s, sh), 1180 (w), 1150 (w), 1090 (w), 1070 (m), 1030 (m), 1010 (m), 920 (2), 900 (w), 890 (w), 870 (m, sh), 840 (w), 835 (w), 800 (w), 765 (s, shoulder), 750 (s, sh), 730 (m, sh), 700 (s, sh), 630 (m, sh), 610 (m, shoulder), 520 (m), 490 (m), 420 (m), 400 (w, shoulder), 330 (m). ^{1}H NMR (600 MHz, C_6D_6, 298 K): δ = 7.78, 7.60, 7.59, 7.58, 7.57, 7.54, 7.53, 7.30, 7.28, 7.27, 7.26, 7.25, 7.21, 7.20, 7.18, 7.13, 7.12, 7.07, 7.06, 7.05, 7.02, 7.01, 7.00. $^{13}C\{^{1}H\}$ NMR (151 MHz, C_6D_6, 298 K): δ = 150.01, 145.46, 142.95, 141.88, 141.69, 140.80, 129.30, 129.13, 129.11, 128.50, 127.78,127.74, 127.55, 127.52, 127.42, 125.67.

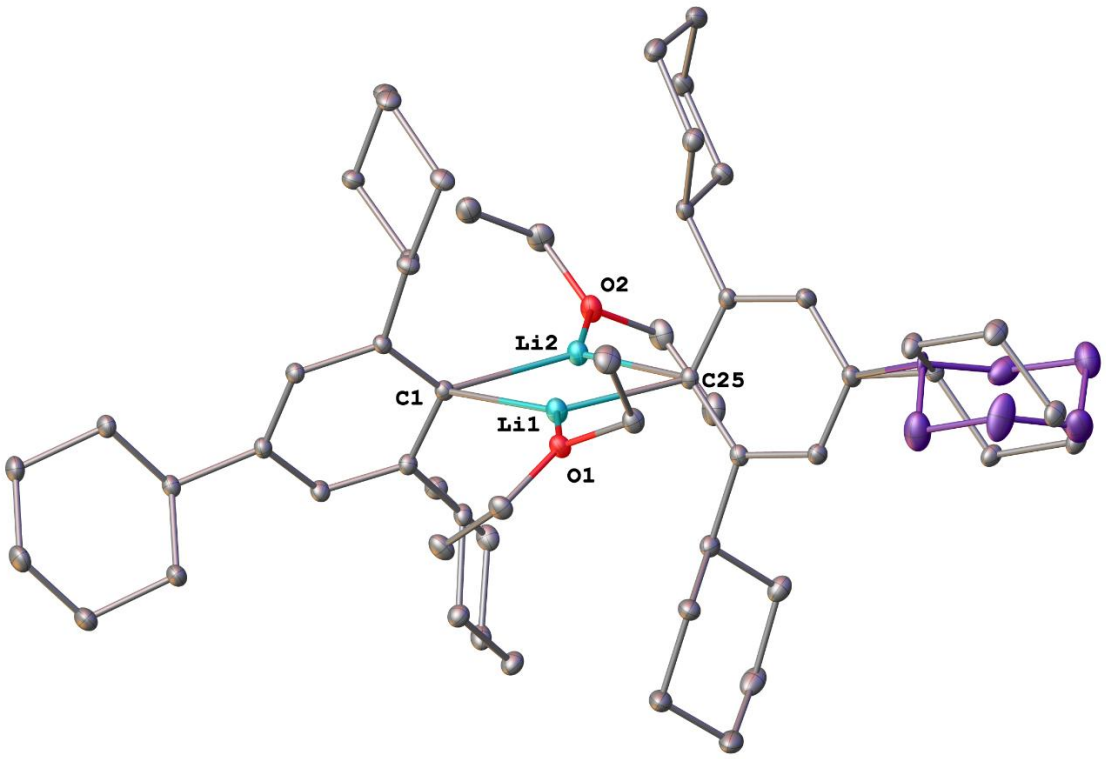

Figure 7.S1. Molecular structure of $\{Li(C_6H_2\text{-}2,4,6\text{-}Cy_3)\cdot(OEt_2)\}_2$ with thermal ellipsoids drawn at 30% probability. For clarity, hydrogens are not shown. Modeled disorder at right hand *p*-cyclohexyl is colored violet. Selected bond distances (Å) and angles (°): Li1-C1: 2.191(3), Li1-C25: 2.179(3) Li1-O1: 1.922(2), Li2-C1: 2.261(3) Li2-C25: 2.293(3), Li2-O2: 1.955(2), C1-Li1-C25: 119.33(11), C1-Li2-C25: 111.83(10), Li1-C1-Li2: 64.60(9), Li1-C25-Li2: 64.24(8).

Table 7.S1. X-ray Data Collection Parameters and Crystallographic Details of $\{Li(C_6H_2\text{-}2,4,6\text{-}Cy_3)\cdot(OEt_2)\}_2$

Empirical formula	$C_{56}H_{90}Li_2O_2$
Formula weight	809.15
Temperature/K	90.15
Crystal system	monoclinic
Space group	$P2_1/n$
a/Å	12.317(3)
b/Å	30.172(6)
c/Å	14.963(3)
α/°	90
β/°	113.956(3)
γ/°	90
Volume/Å^3	5081.6(18)
Z	4
ρ_{calc}g/cm^3	1.058
μ/mm^{-1}	0.061
F(000)	1792.0
Crystal size/mm^3	0.62 × 0.24 × 0.216
Radiation	MoKα (λ = 0.71073)
2Θ range for data collection/°	3.634 to 61.338
Index ranges	$-17 \leq h \leq 17$, $-43 \leq k \leq 43$, $-21 \leq l \leq 21$
Reflections collected	79184
Independent reflections	15651 [R_{int} = 0.0523, R_{sigma} = 0.0415]
Data/restraints/parameters	15651/24/599
Goodness-of-fit on F^2	1.026
Final R indexes [I>=2σ (I)]	R_1 = 0.0561, wR_2 = 0.1268
Final R indexes [all data]	R_1 = 0.0844, wR_2 = 0.1403
Largest diff. peak/hole / e Å^{-3}	0.35/-0.20

Table 7.S2. X-ray Data Collection Parameters and Crystallographic Details of $\{Sn(C_6H_2\text{-}2,4,6\text{-}Cy_3)_2\}_2$ (**1**) as it appears in the main text. The empirical formula does not include the disordered solvent of crystallization, which was excluded from the final model and refinements (SQUEEZE).

Empirical formula	$C_{96}H_{140}Sn_2$
Formula weight	1531.45
Temperature/K	90.15
Crystal system	monoclinic
Space group	C2/c
a/Å	19.9166(12)
b/Å	16.3978(10)
c/Å	33.566(2)
α/°	90
β/°	107.1800(10)
γ/°	90
Volume/Å^3	10473.1(12)
Z	4
ρ_{calc}g/cm^3	0.971
μ/mm^{-1}	0.512
F(000)	3264.0
Crystal size/mm^3	0.35 × 0.278 × 0.128
Radiation	MoKα (λ = 0.71073)
2Θ range for data collection/°	3.278 to 56.606
Index ranges	$-26 \leq h \leq 26$, $-21 \leq k \leq 21$, $-44 \leq l \leq 44$
Reflections collected	72095
Independent reflections	13006 [R_{int} = 0.0865, R_{sigma} = 0.0650]
Data/restraints/parameters	13006/0/442
Goodness-of-fit on F^2	1.020
Final R indexes [I>=2σ (I)]	R_1 = 0.0432, wR_2 = 0.1076
Final R indexes [all data]	R_1 = 0.0775, wR_2 = 0.1208
Largest diff. peak/hole / e Å^{-3}	1.63/-0.85

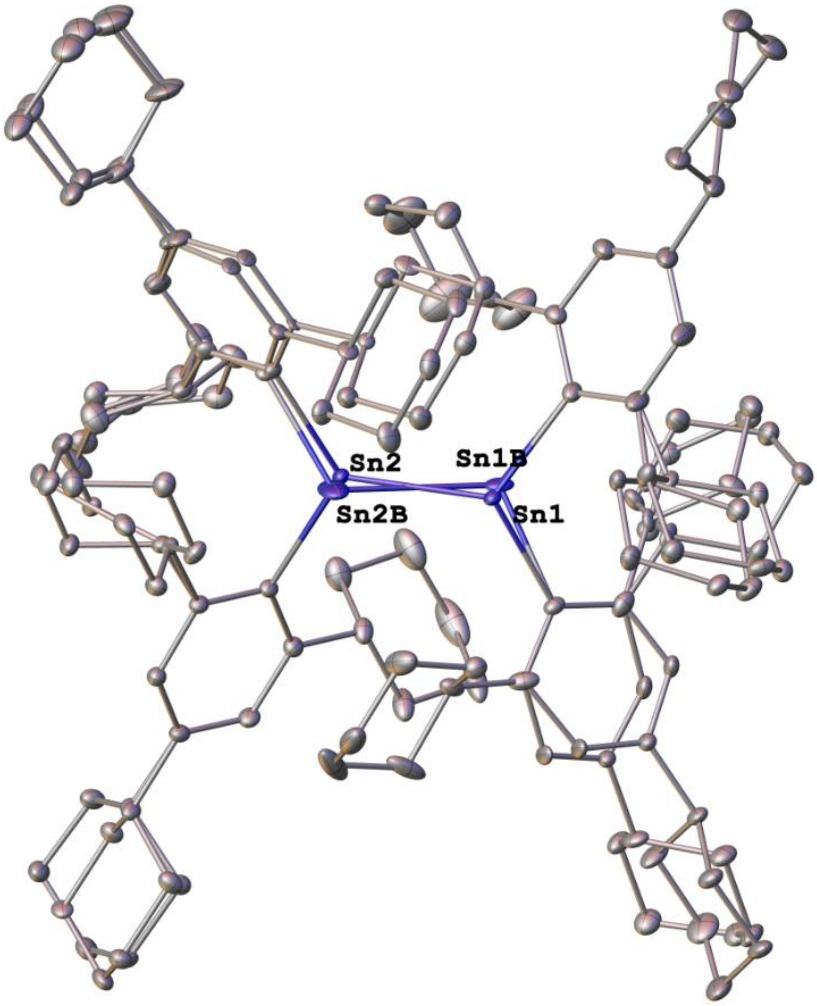

Figure 7.S2. Molecular structure of disordered polymorph of $\{Sn(C_6H_2\text{-}2,4,6\text{-}Cy_3)_2\}_2$ (**1a**) with thermal ellipsoids drawn at 30% probability. For clarity, hydrogens are not shown.

Table 7.S3. X-ray Data Collection Parameters and Crystallographic Details of $\{Sn(C_6H_2\text{-}2,4,6\text{-}Cy_3)_2\}_2$ (**1a**)

Empirical formula	$C_{96}H_{140}Sn_2$
Formula weight	1531.45
Temperature/K	90.15
Crystal system	triclinic
Space group	P-1
a/Å	11.973(2)
b/Å	17.542(3)
c/Å	21.782(4)
α/°	74.088(3)
β/°	74.546(3)
γ/°	72.524(3)
Volume/Å^3	4111.2(13)
Z	2
ρ_{calc}g/cm^3	1.237
μ/mm^{-1}	0.652
F(000)	1632.0
Crystal size/mm^3	0.282 × 0.139 × 0.121
Radiation	MoKα (λ = 0.71073)
2Θ range for data collection/°	3.78 to 60.952
Index ranges	$-17 \leq h \leq 17$, $-25 \leq k \leq 24$, $-31 \leq l \leq 31$
Reflections collected	48342
Independent reflections	24794 [R_{int} = 0.0483, R_{sigma} = 0.0735]
Data/restraints/parameters	24794/392/1384
Goodness-of-fit on F^2	1.050
Final R indexes [I>=2σ (I)]	R_1 = 0.0533, wR_2 = 0.1164
Final R indexes [all data]	R_1 = 0.0840, wR_2 = 0.1290
Largest diff. peak/hole / e Å^{-3}	1.32/-1.04

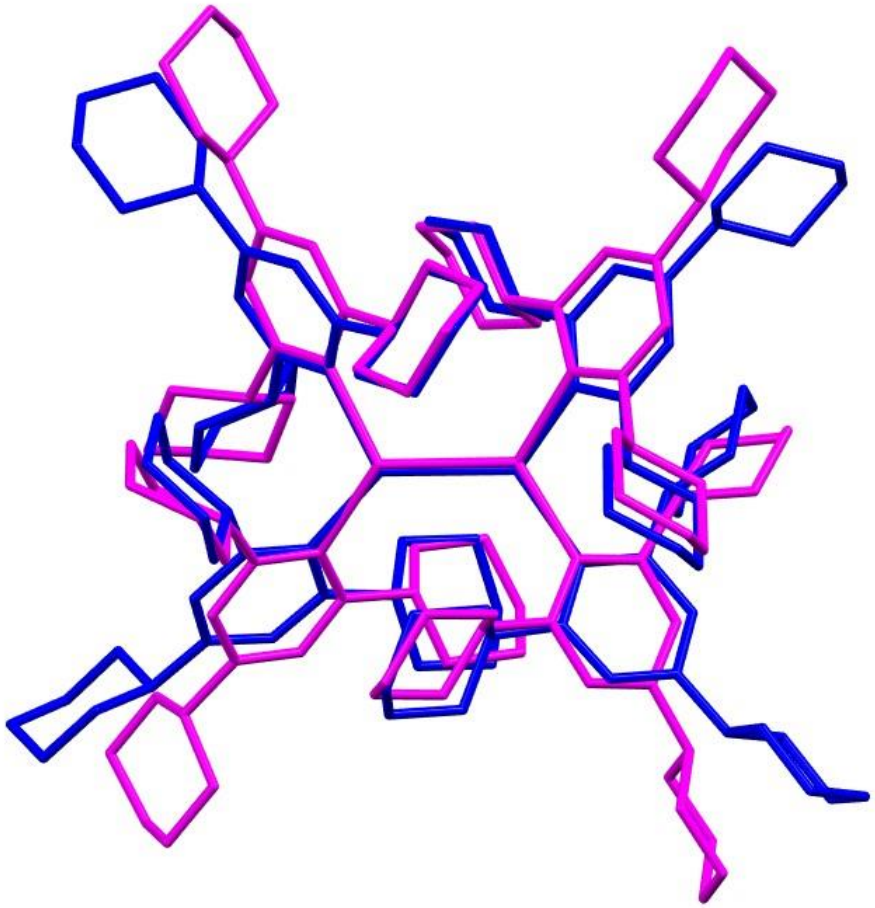

Figure 7.S3. Overlaid molecular drawings of **1** (blue) and the major component of its polymorph **1a** (magenta) showing the different orientation at each *p*-cyclohexyl in the ligand. This fluxionality was also observed in the VT ^{1}H NMR (vide infra).

Table 7.S4. X-ray Data Collection Parameters and Crystallographic Details of $Sn(C_6H_2$-2,4,6-$Ph_3)_2$ (**2**)

Empirical formula	$C_{48}H_{34}Sn$
Formula weight	729.44
Temperature/K	190
Crystal system	monoclinic
Space group	$P2_1/c$
a/Å	20.197(2)
b/Å	11.7335(13)
c/Å	14.5464(17)
α/°	90
β/°	91.1163(19)
γ/°	90
Volume/$Å^3$	3446.6(7)
Z	4
$\rho_{calc}g/cm^3$	1.406
μ/mm^{-1}	0.776
F(000)	1488.0
Crystal size/mm^3	0.561 × 0.157 × 0.056
Radiation	MoKα (λ = 0.71073)
2Θ range for data collection/°	4.014 to 55.046
Index ranges	$-26 \leq h \leq 26$, $-15 \leq k \leq 15$, $-18 \leq l \leq 18$
Reflections collected	15487
Independent reflections	7940 [R_{int} = 0.0353, R_{sigma} = 0.0496]
Data/restraints/parameters	7940/0/476
Goodness-of-fit on F^2	1.050
Final R indexes [I>=2σ (I)]	R_1 = 0.0368, wR_2 = 0.0813
Final R indexes [all data]	R_1 = 0.0557, wR_2 = 0.0893
Largest diff. peak/hole / e $Å^{-3}$	0.44/-0.91

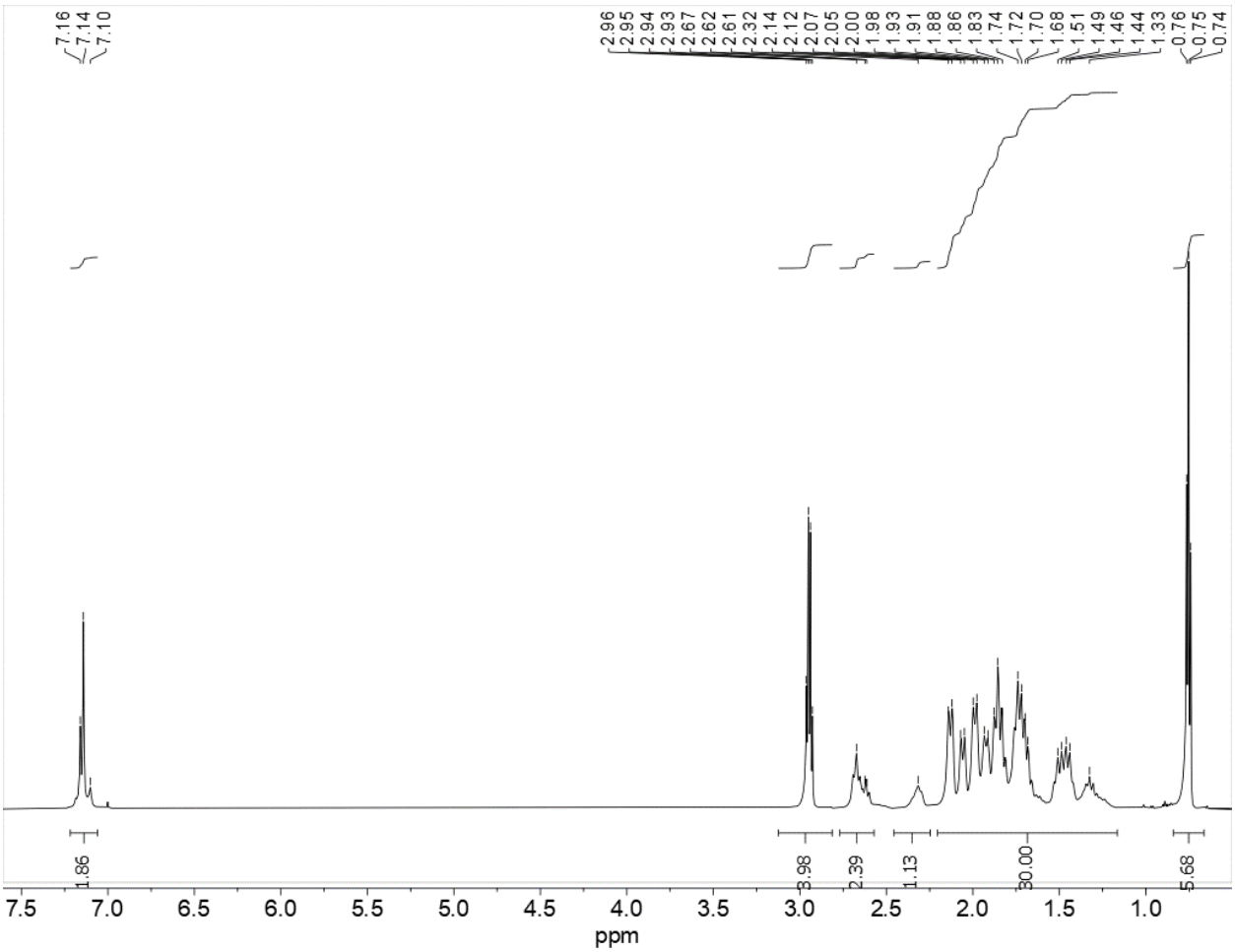

Figure 7.S4. ^{1}H-NMR spectrum of $\{Li(C_6H_2\text{-}2,4,6\text{-}Cy_3)\cdot OEt_2\}_2$ (benzene D_6, 300 K)

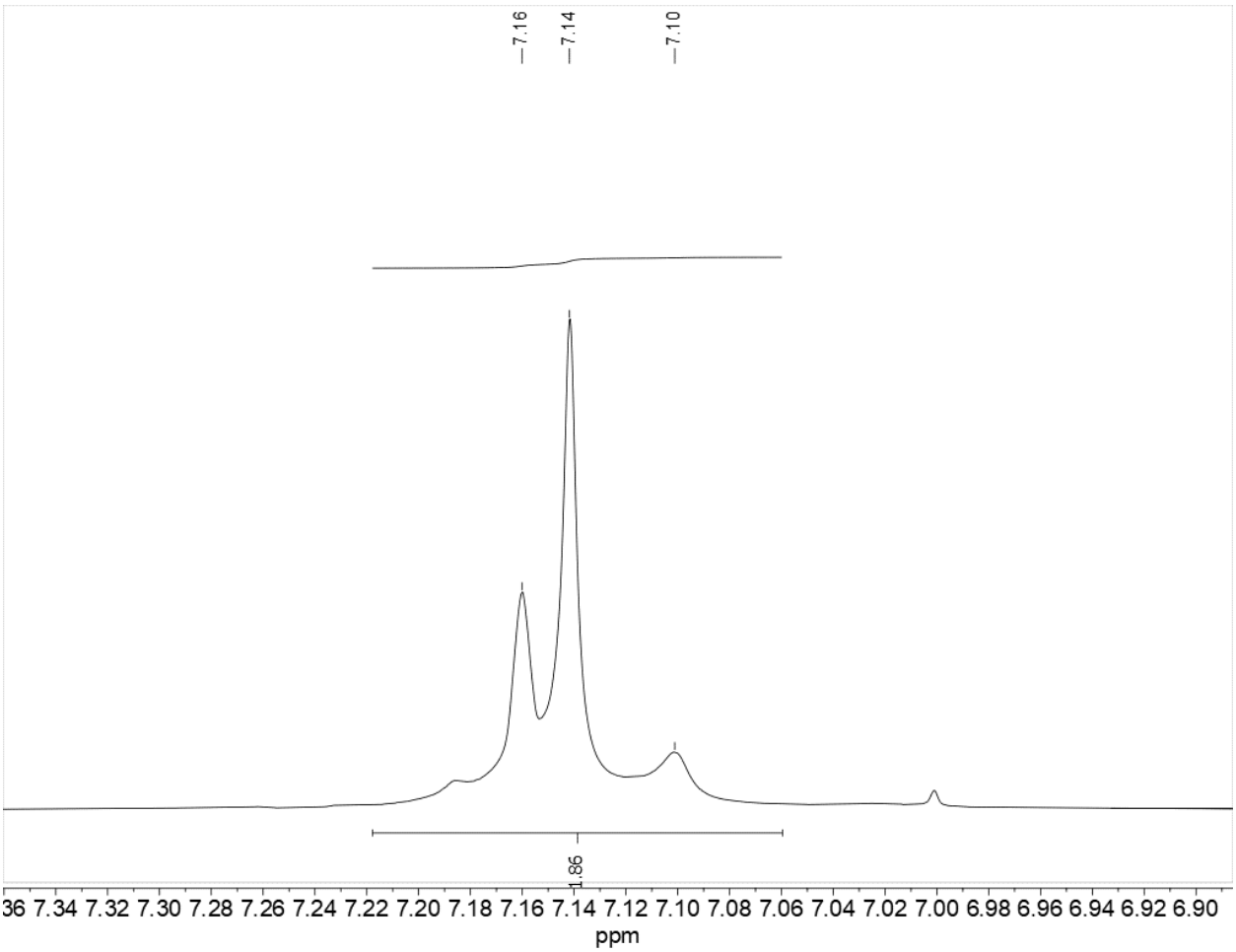

Figure 7.S5. Detail of ^{1}H-NMR spectrum of $\{Li(C_6H_2\text{-}2,4,6\text{-}Cy_3)\cdot OEt_2\}_2$ (benzene D_6, 300 K)

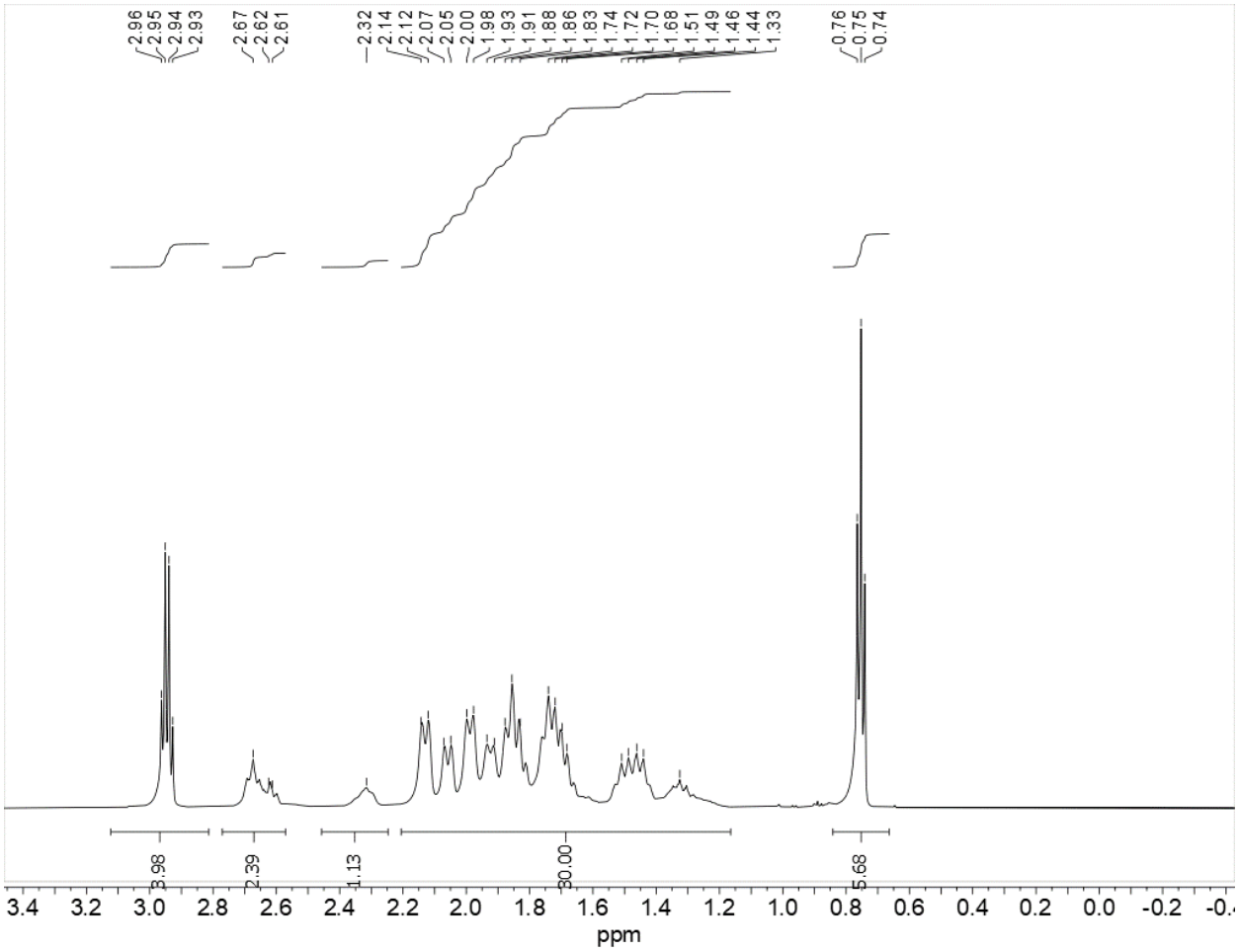

Figure 7.S6. Detail of ^{1}H-NMR spectrum of $\{Li(C_6H_2\text{-}2,4,6\text{-}Cy_3)\cdot OEt_2\}_2$ (benzene D_6, 300 K)

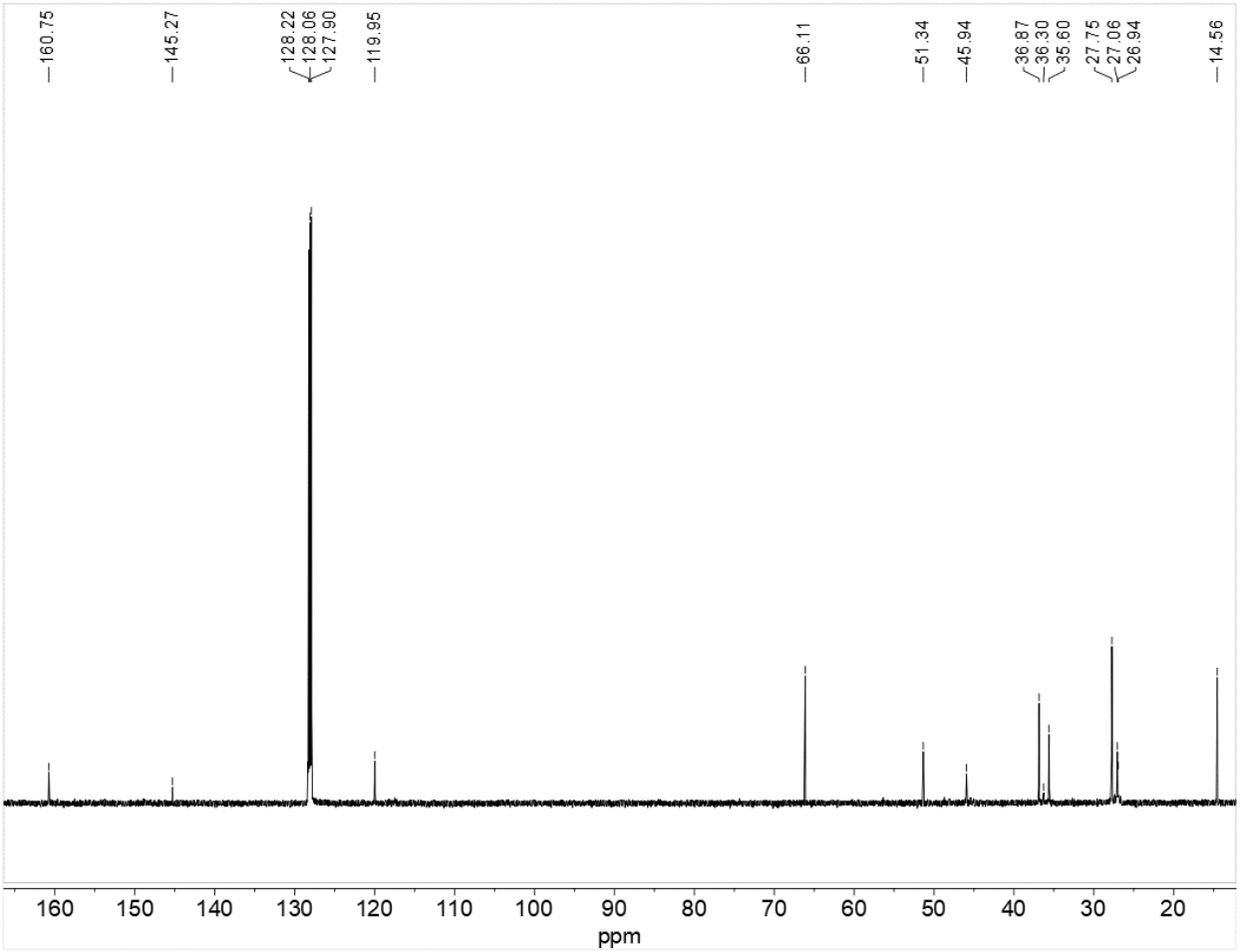

Figure 7.S7. ^{13}C-NMR spectrum of $\{Li(C_6H_2\text{-}2,4,6\text{-}Cy_3)\cdot OEt_2\}_2$ (benzene D_6, 300 K)

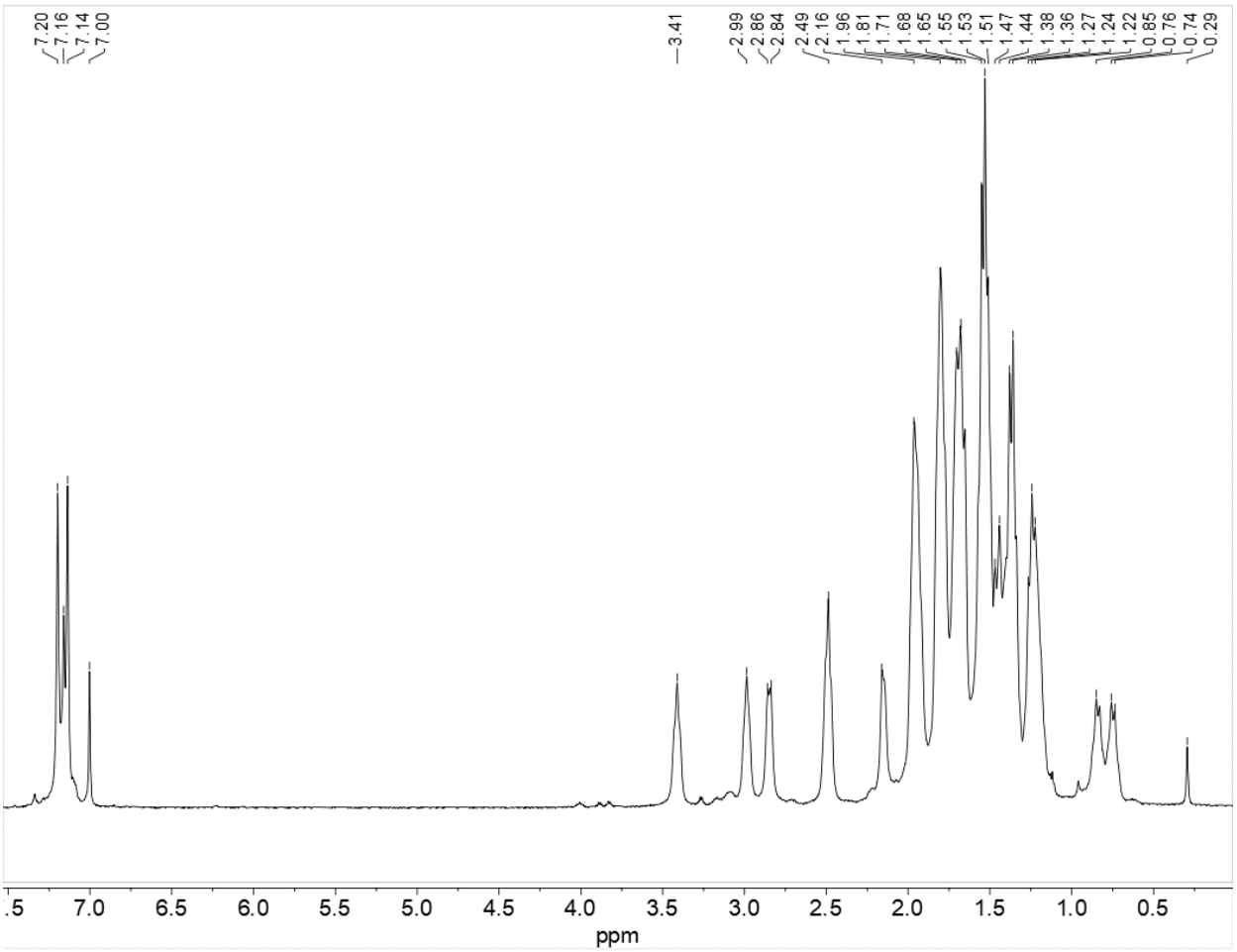

Figure 7.S8. ^{1}H-NMR spectrum of $\{Sn(C_6H_2\text{-}2,4,6\text{-}Cy_3)_2\}_2$ (**1**) (benzene D_6, 300 K)

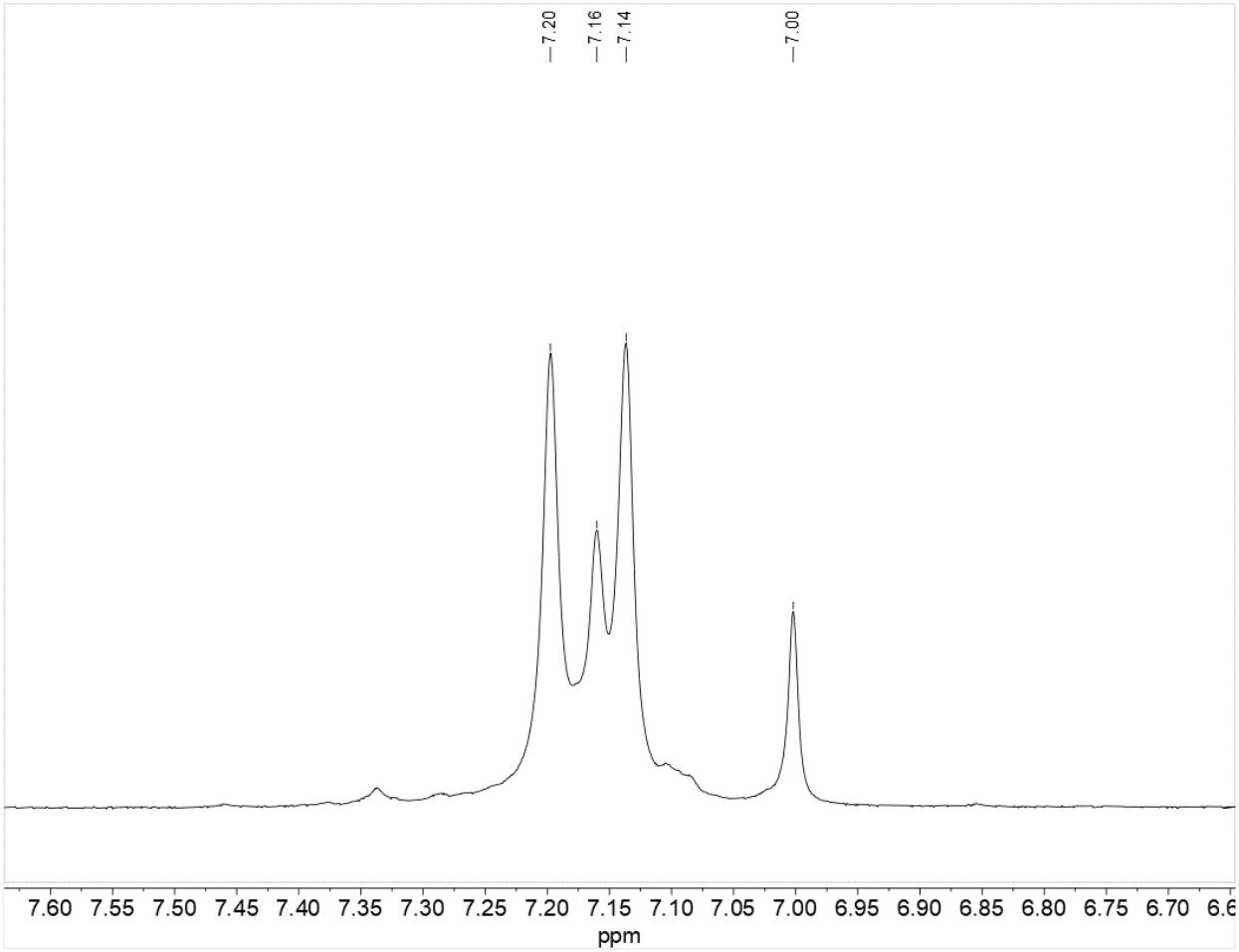

Figure 7.S9. Detail of ^{1}H-NMR spectrum of $\{Sn(C_6H_2\text{-}2,4,6\text{-}Cy_3)_2\}_2$ (**1**) (benzene D_6, 300 K)

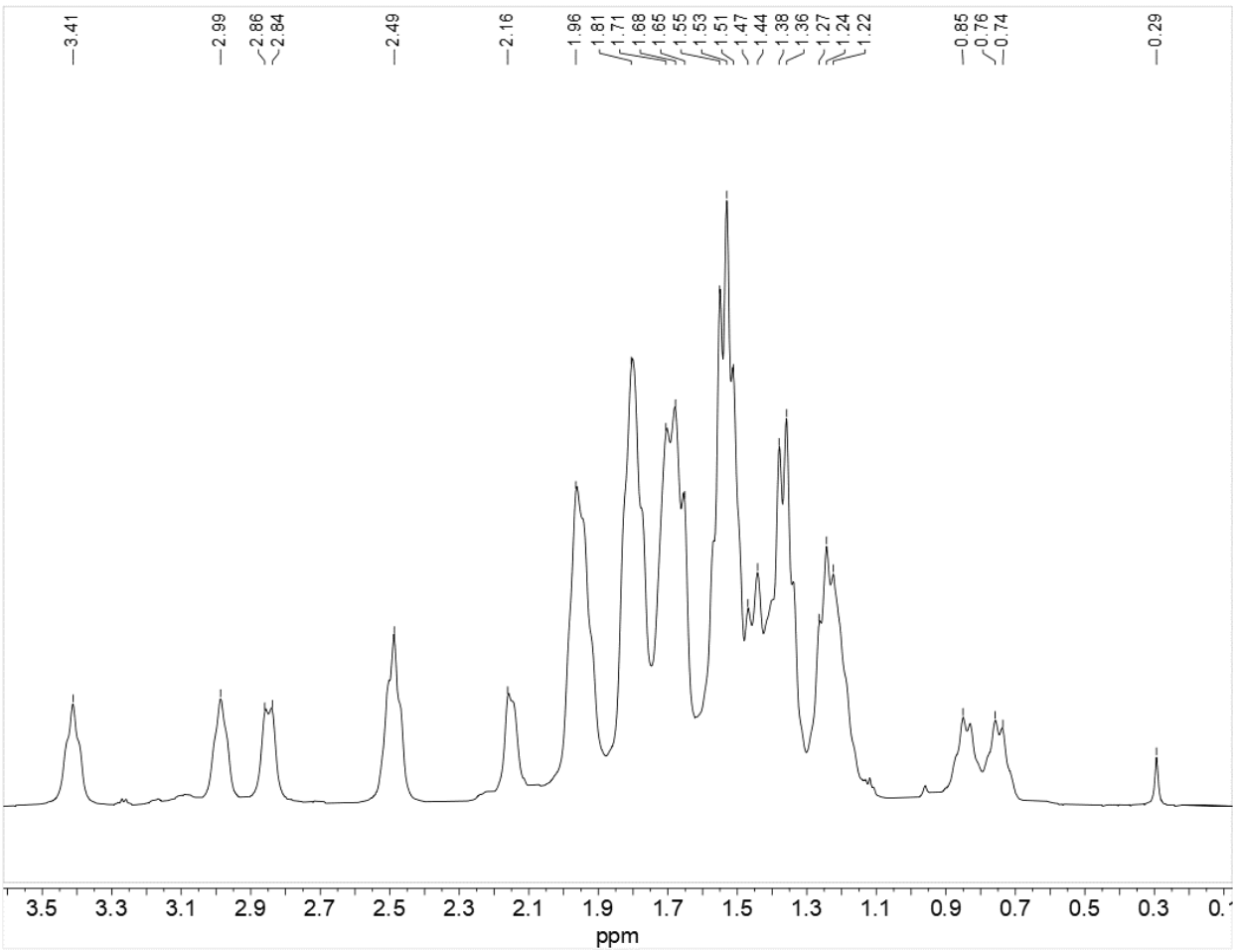

Figure 7.S10. Detail of ^{1}H-NMR spectrum of $\{Sn(C_6H_2\text{-}2,4,6\text{-}Cy_3)_2\}_2$ (**1**) (benzene D_6, 300 K)

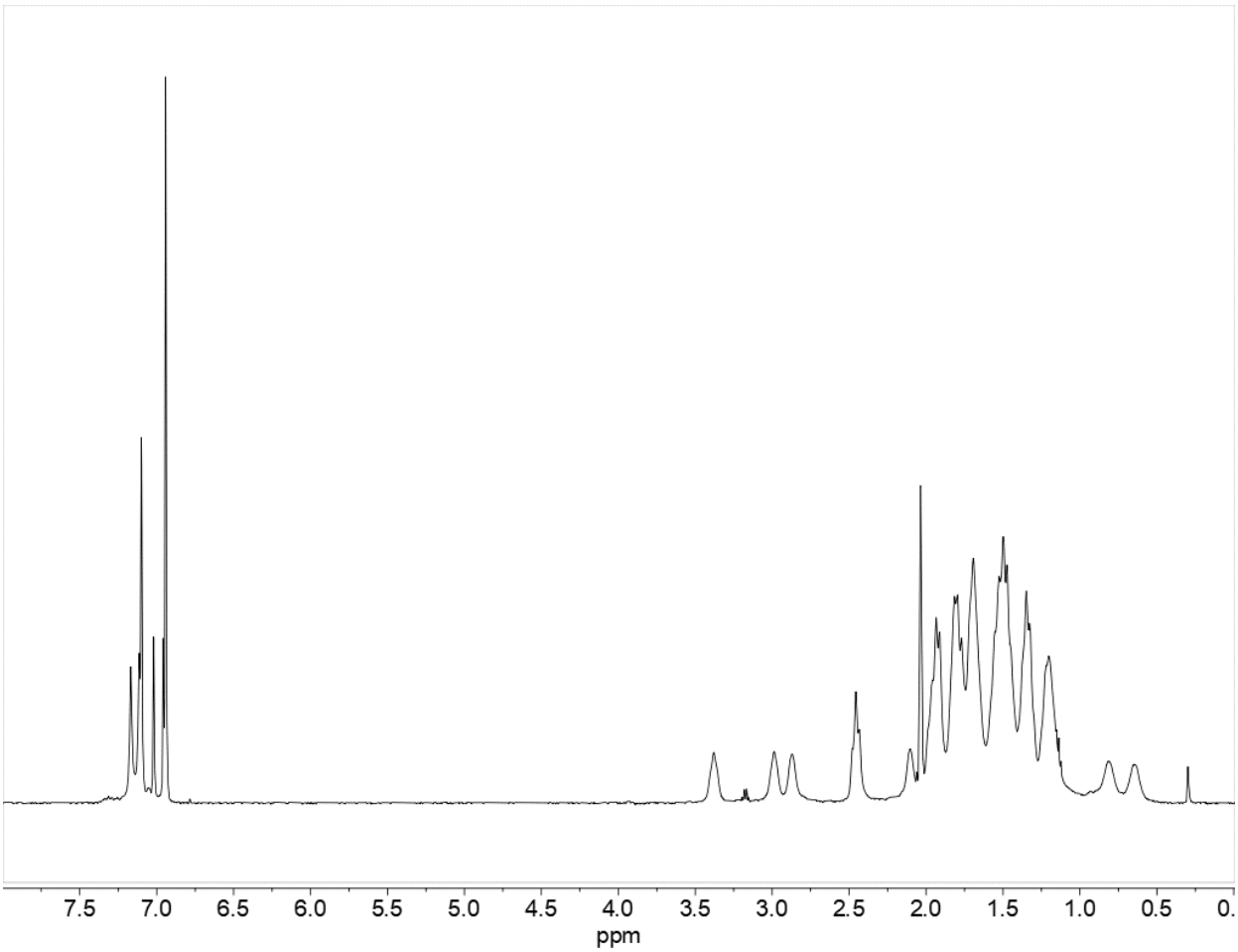

Figure 7.S11. ^{1}H-NMR spectrum of $\{Sn(C_6H_2\text{-}2,4,6\text{-}Cy_3)_2\}_2$ (**1**) (toluene D_8, 220 K)

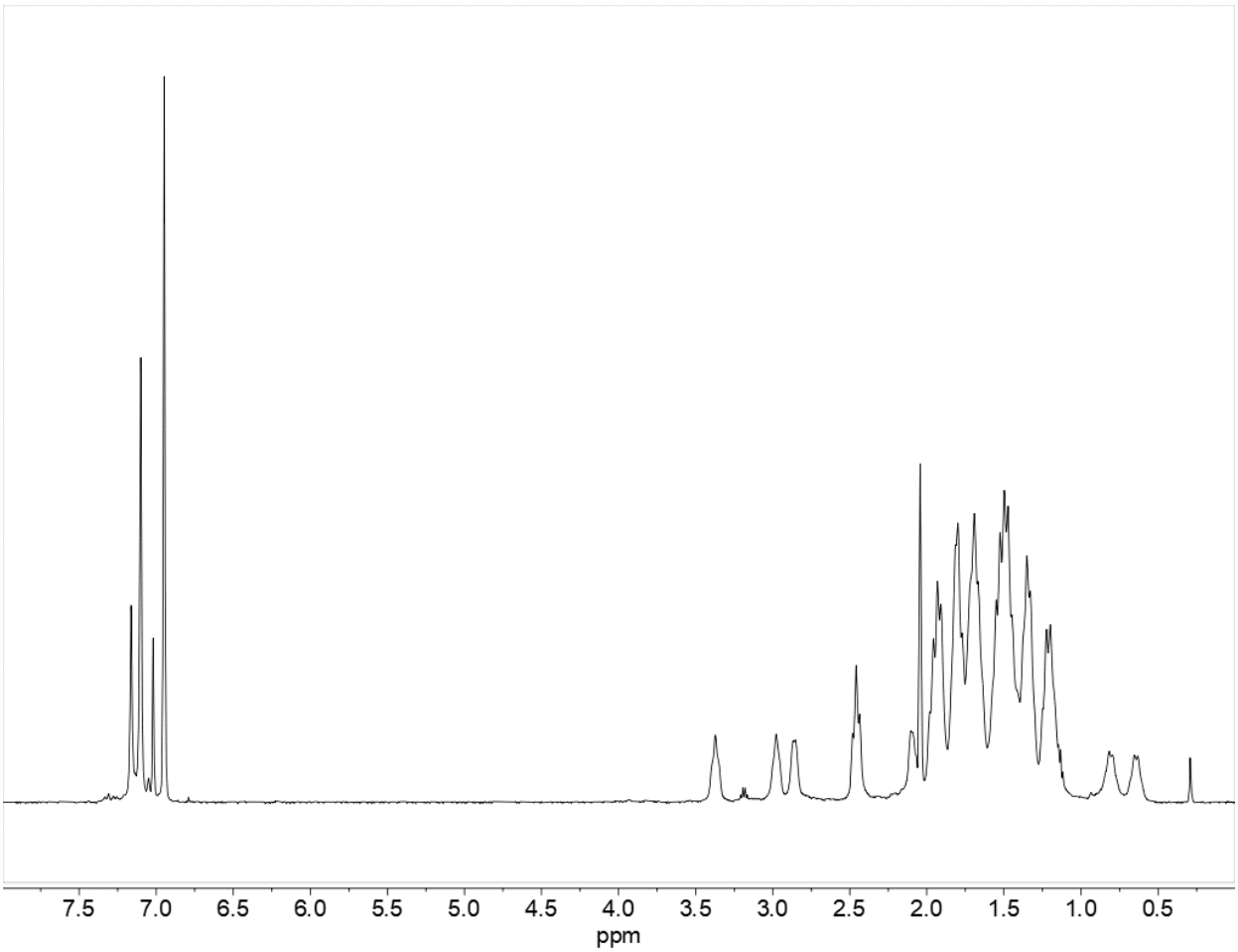

Figure 7.S12. ^{1}H-NMR spectrum of $\{Sn(C_6H_2\text{-}2,4,6\text{-}Cy_3)_2\}_2$ (**1**) (toluene D_8, 230 K)

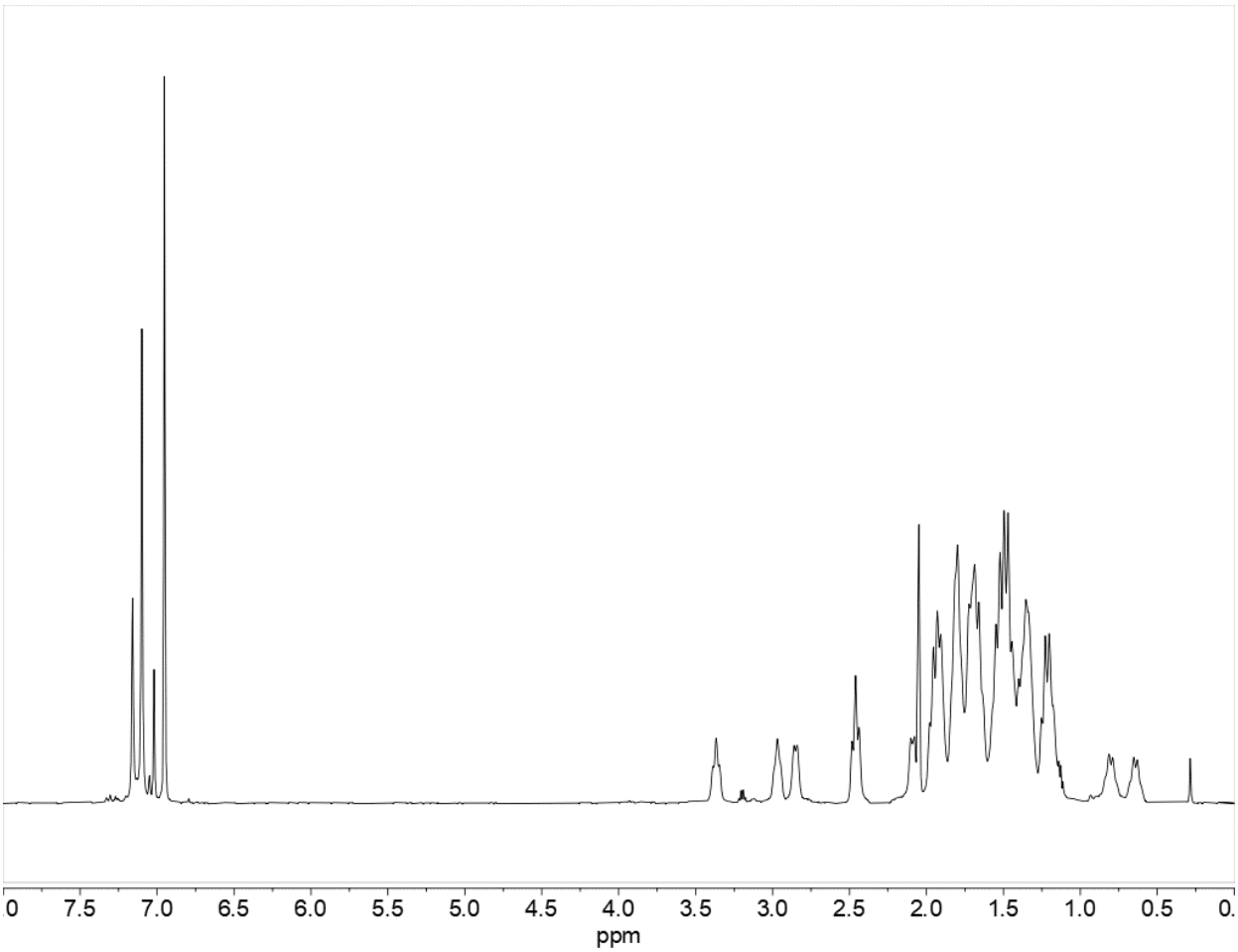

Figure 7.S13. ^{1}H-NMR spectrum of $\{Sn(C_6H_2\text{-}2,4,6\text{-}Cy_3)_2\}_2$ (**1**) (toluene D_8, 240 K)

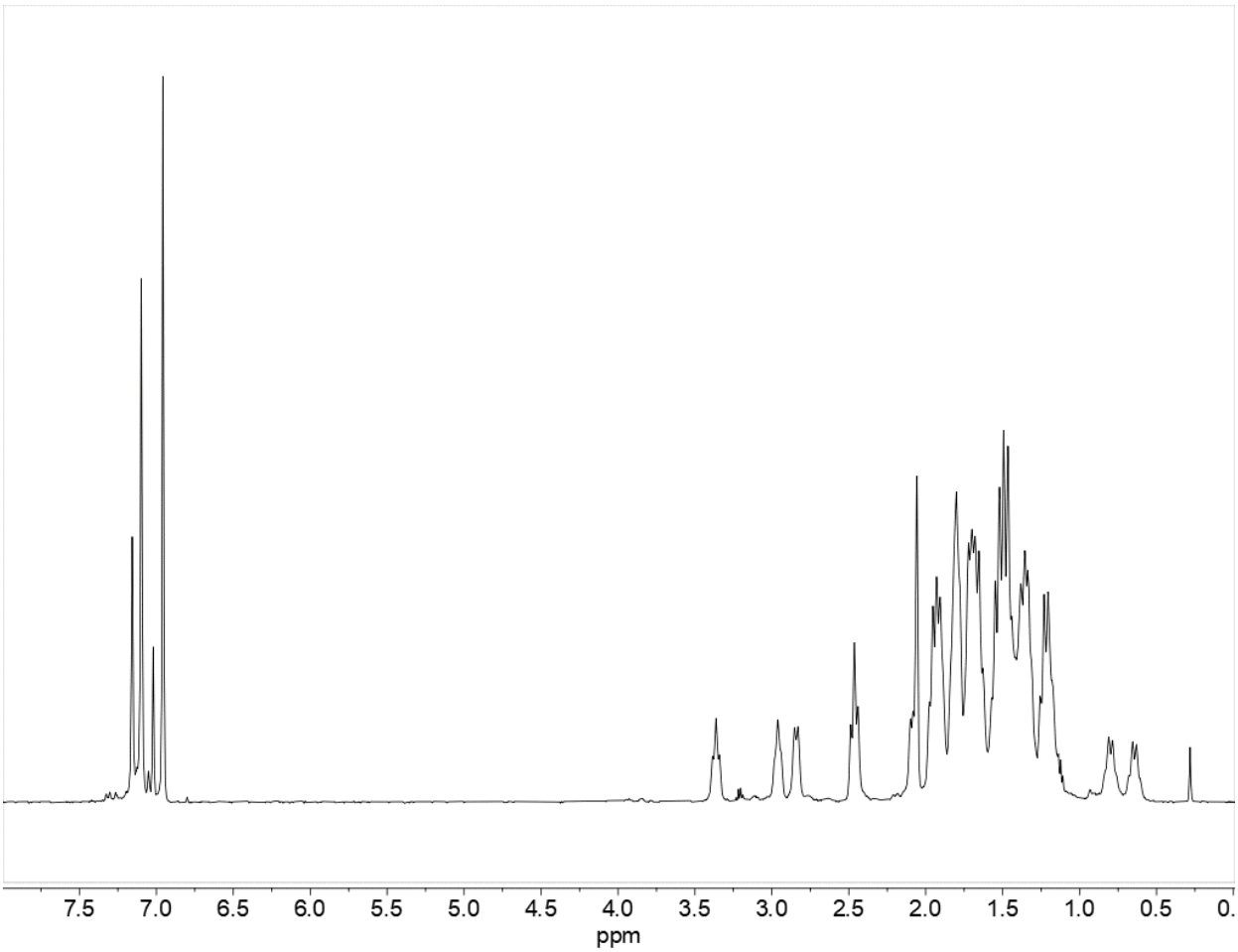

Figure 7.S14. ^{1}H-NMR spectrum of $\{Sn(C_6H_2\text{-}2,4,6\text{-}Cy_3)_2\}_2$ (**1**) (toluene D_8, 250 K)

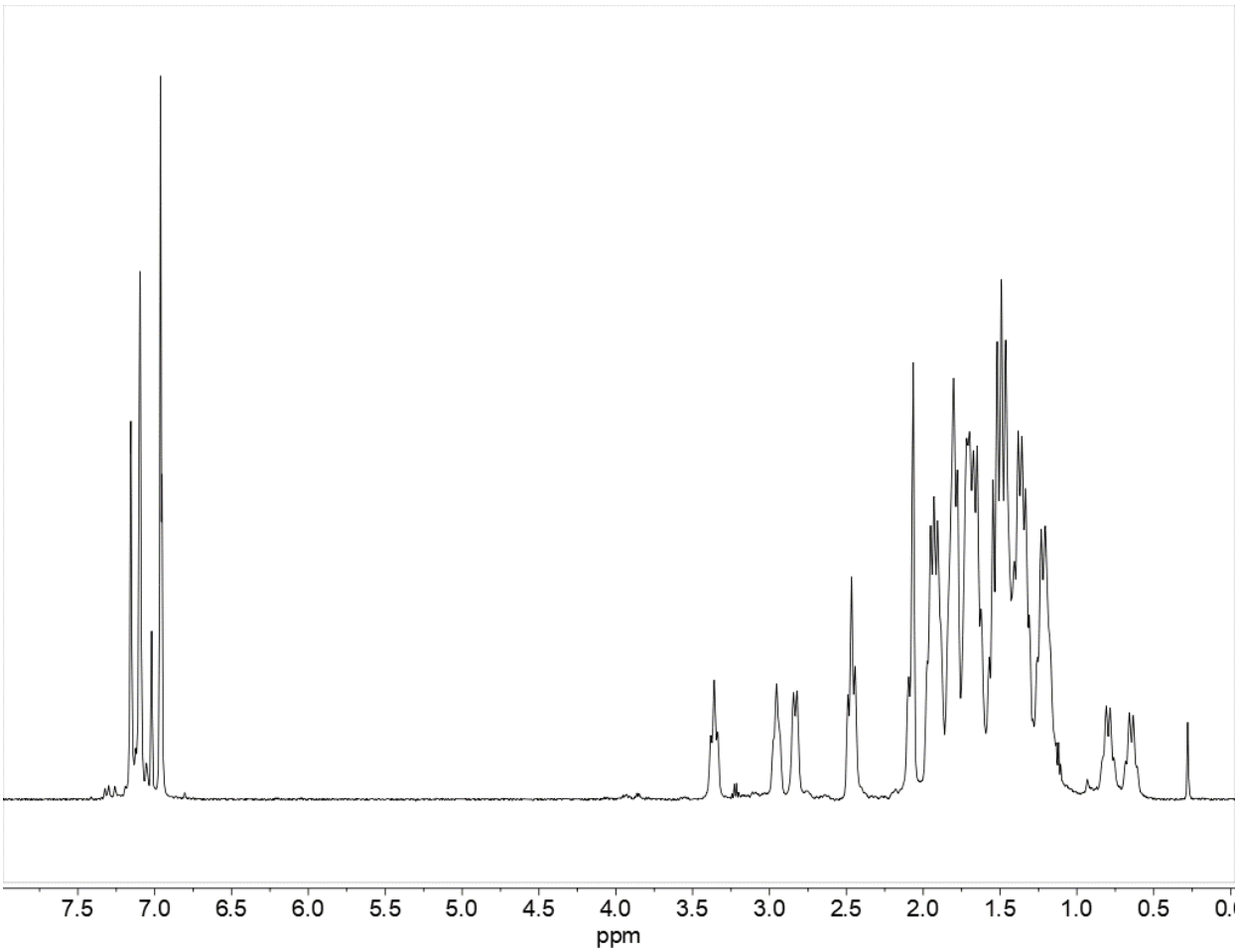

Figure 7.15. ^{1}H-NMR spectrum of $\{Sn(C_6H_2\text{-}2,4,6\text{-}Cy_3)_2\}_2$ (**1**) (toluene D_8, 260 K)

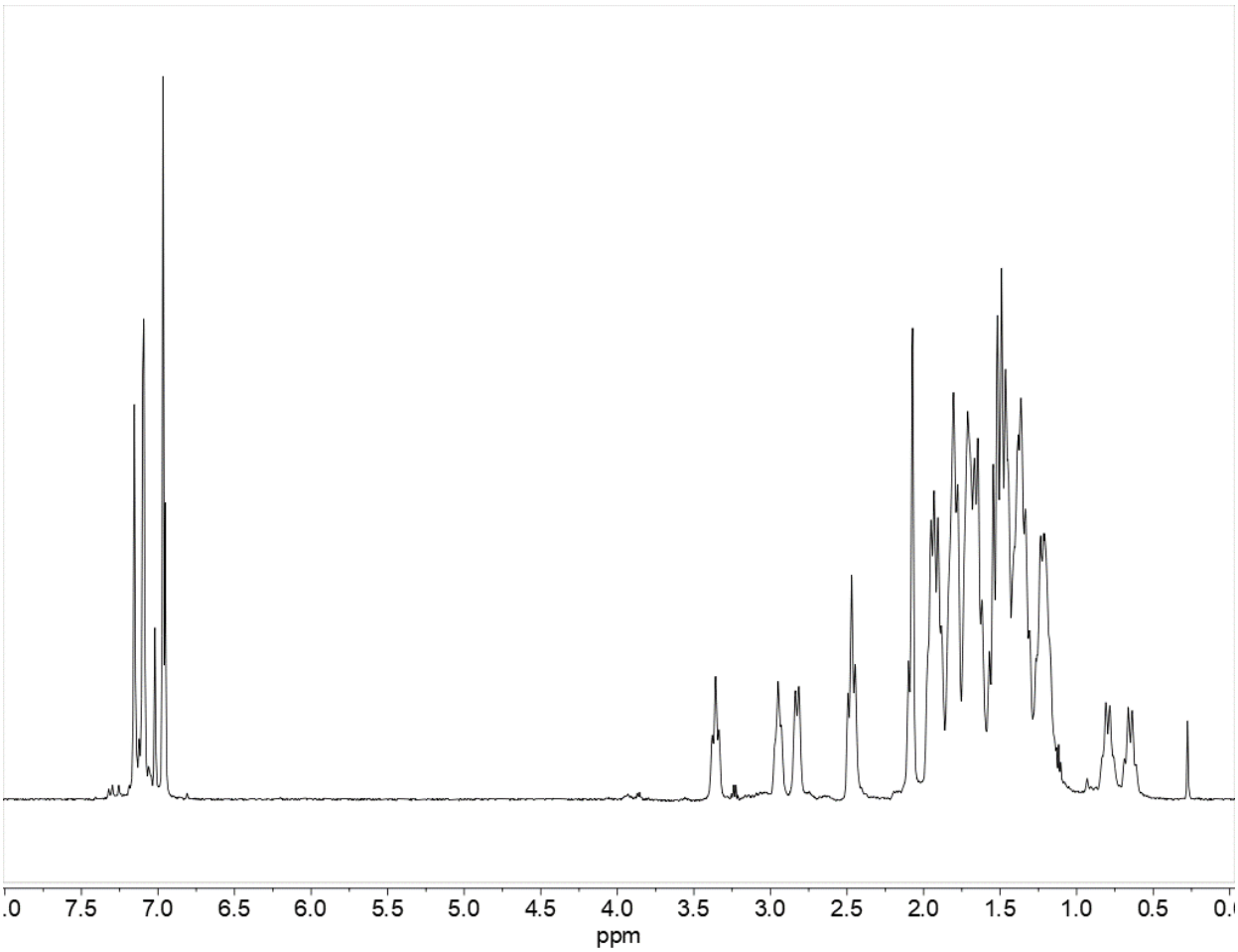

Figure 7.S16. ^{1}H-NMR spectrum of $\{Sn(C_6H_2\text{-}2,4,6\text{-}Cy_3)_2\}_2$ (**1**) (toluene D_8, 270 K)

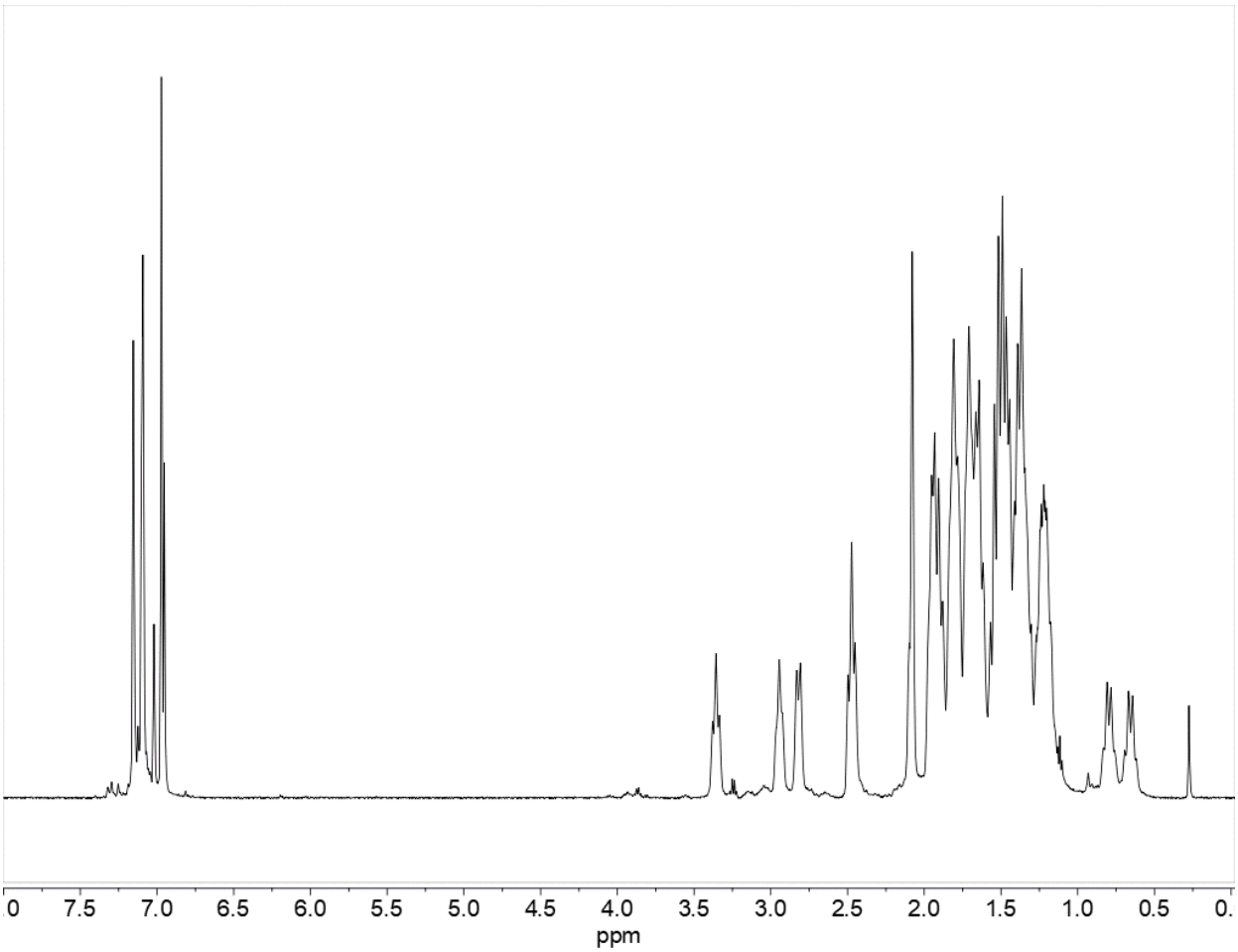

Figure 7.S17. ^{1}H-NMR spectrum of $\{Sn(C_6H_2\text{-}2,4,6\text{-}Cy_3)_2\}_2$ (**1**) (toluene D_8, 280 K)

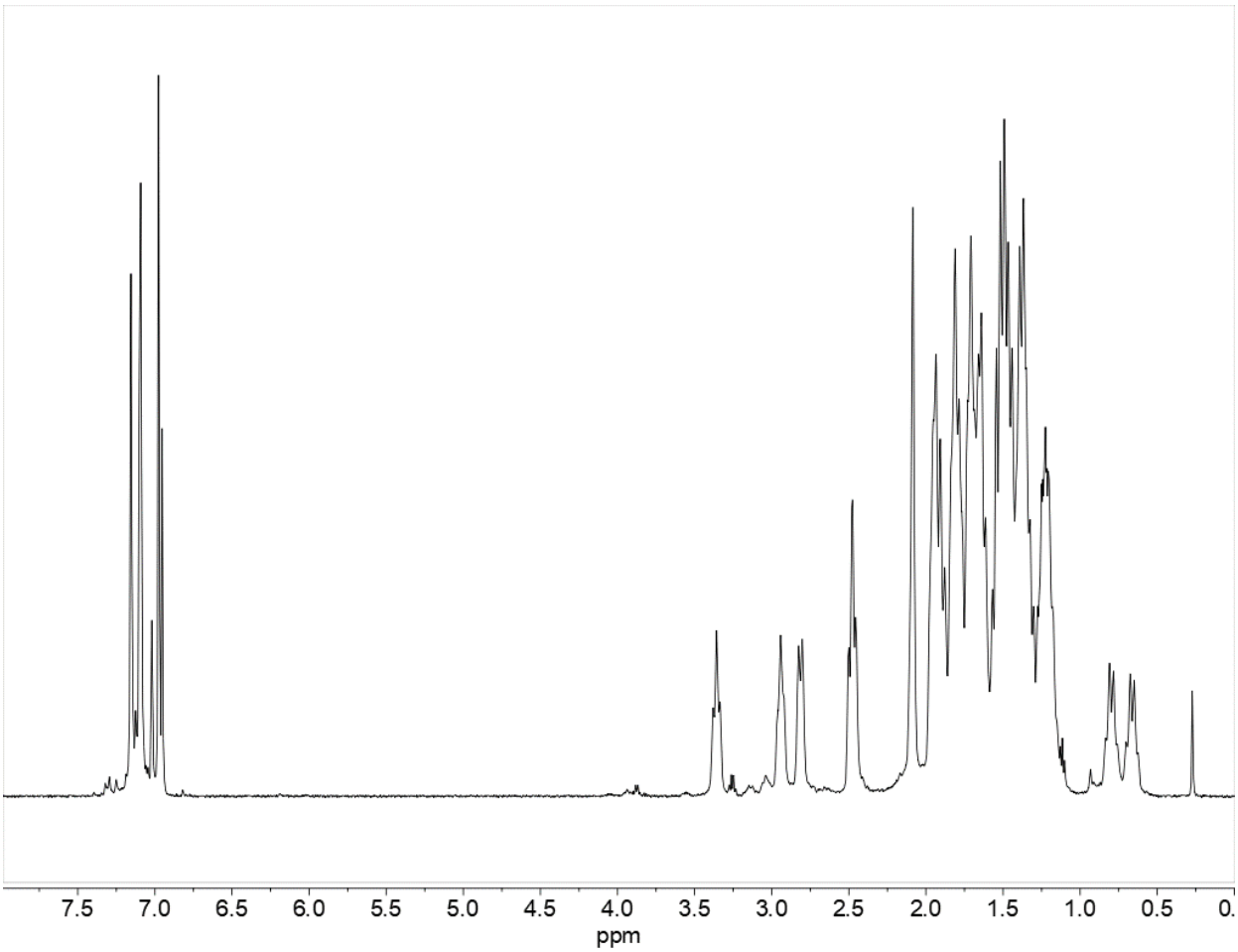

Figure 7.S18. ^{1}H-NMR spectrum of $\{Sn(C_6H_2\text{-}2,4,6\text{-}Cy_3)_2\}_2$ (**1**) (toluene D_8, 290 K)

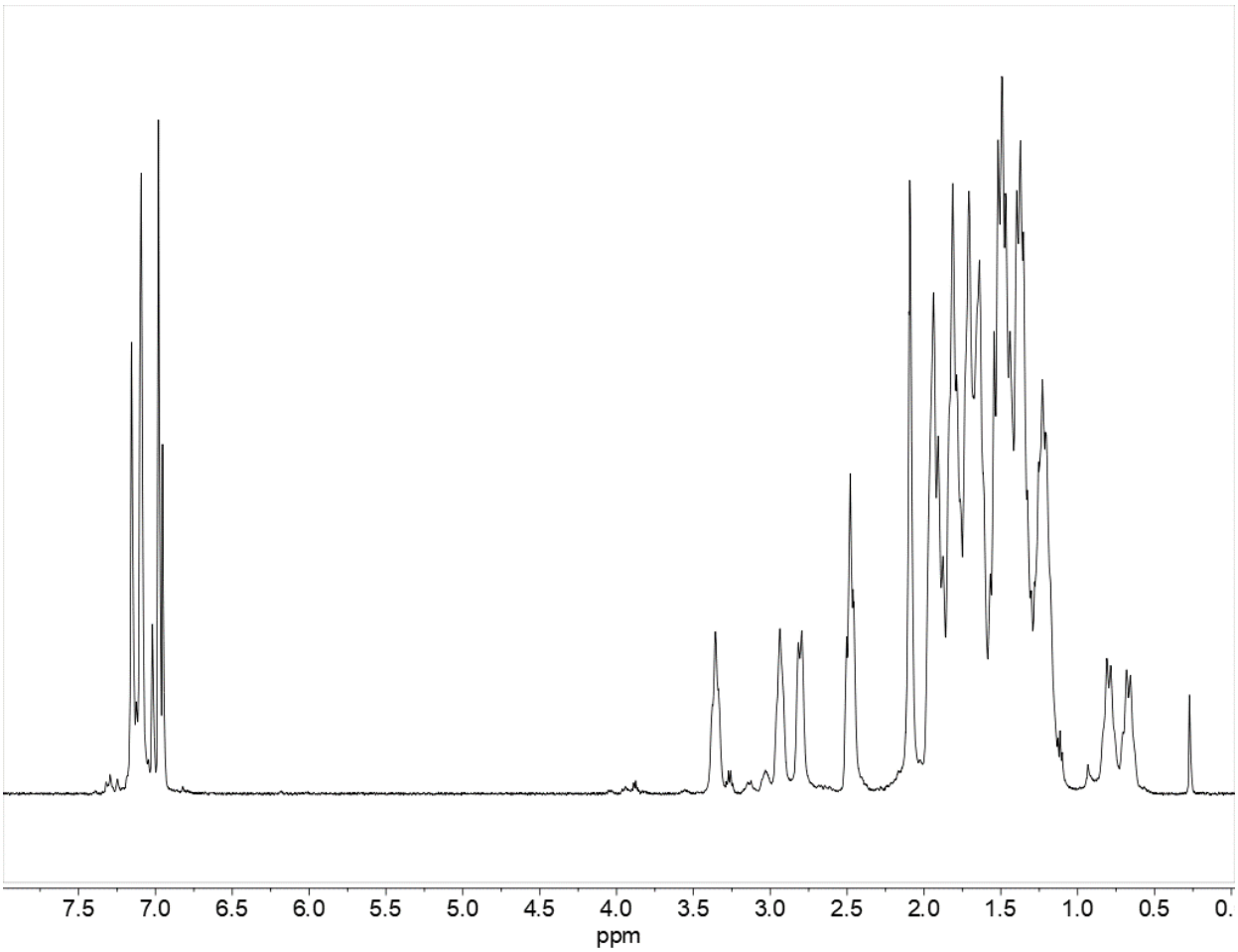

Figure 7.S19. ^{1}H-NMR spectrum of $\{Sn(C_6H_2\text{-}2,4,6\text{-}Cy_3)_2\}_2$ (**1**) (toluene D_8, 300 K)

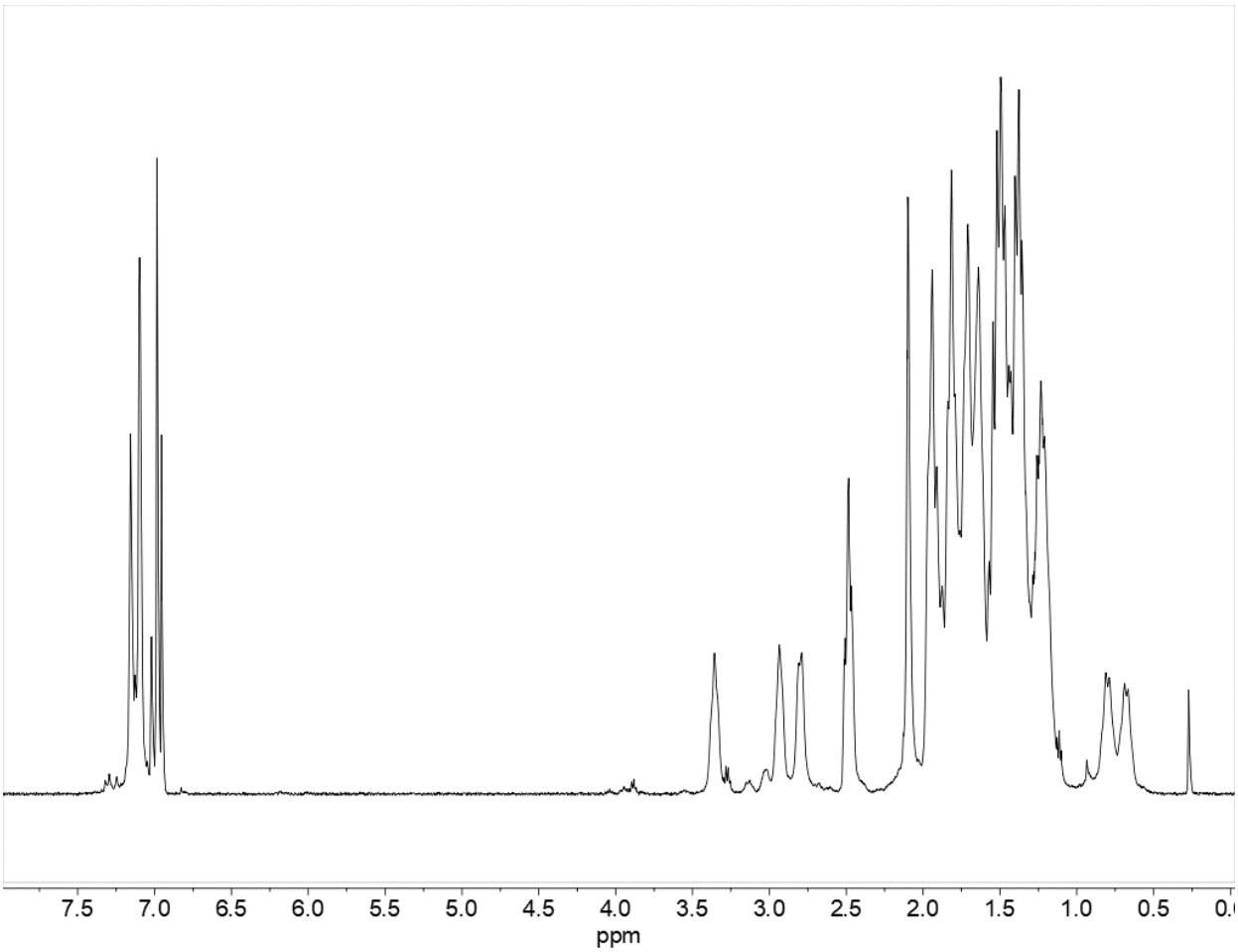

Figure 7.S20. ^{1}H-NMR spectrum of $\{Sn(C_6H_2\text{-}2,4,6\text{-}Cy_3)_2\}_2$ (**1**) (toluene D_8, 310 K)

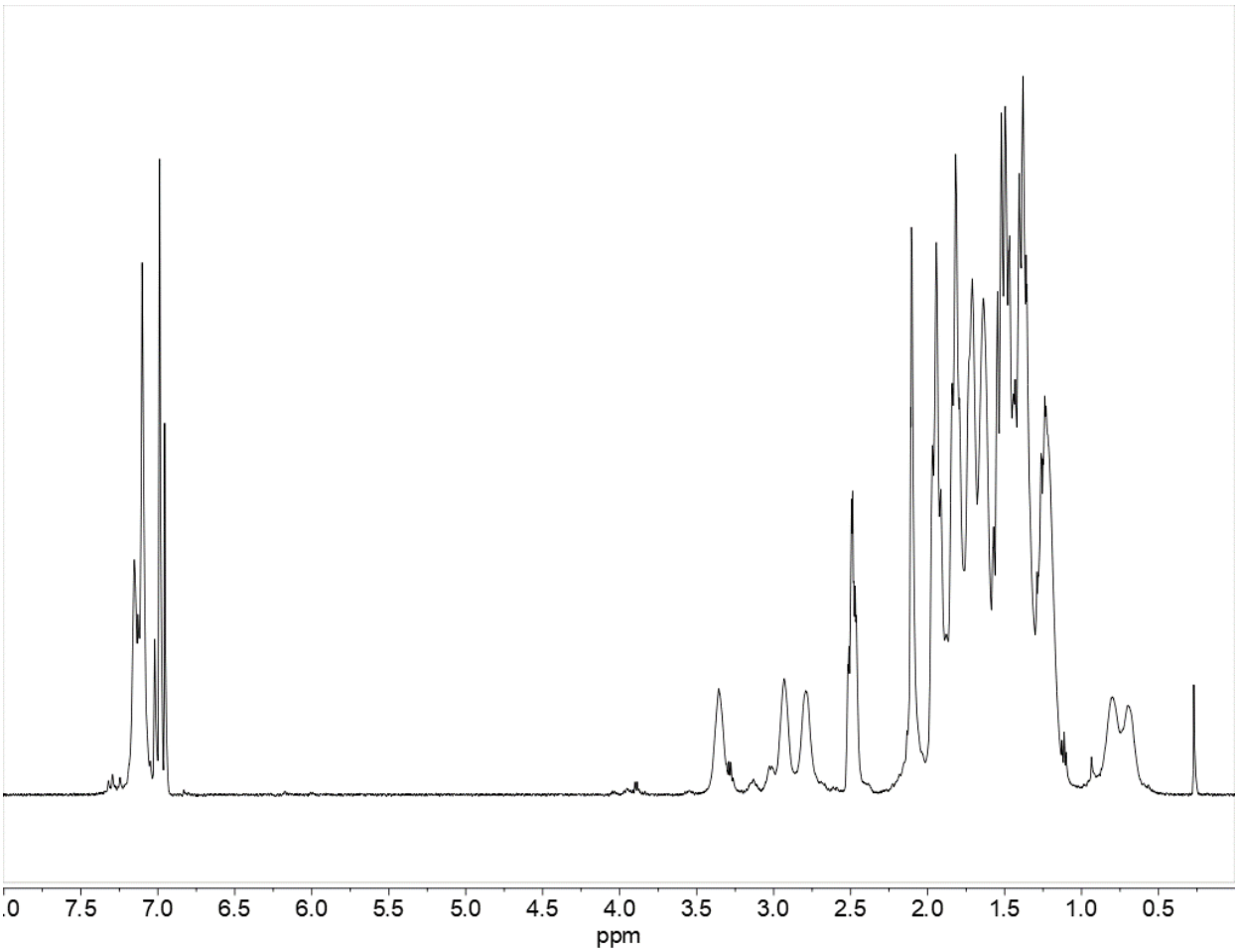

Figure 7.S21. ^{1}H-NMR spectrum of $\{Sn(C_6H_2\text{-}2,4,6\text{-}Cy_3)_2\}_2$ (**1**) (toluene D_8, 320 K)

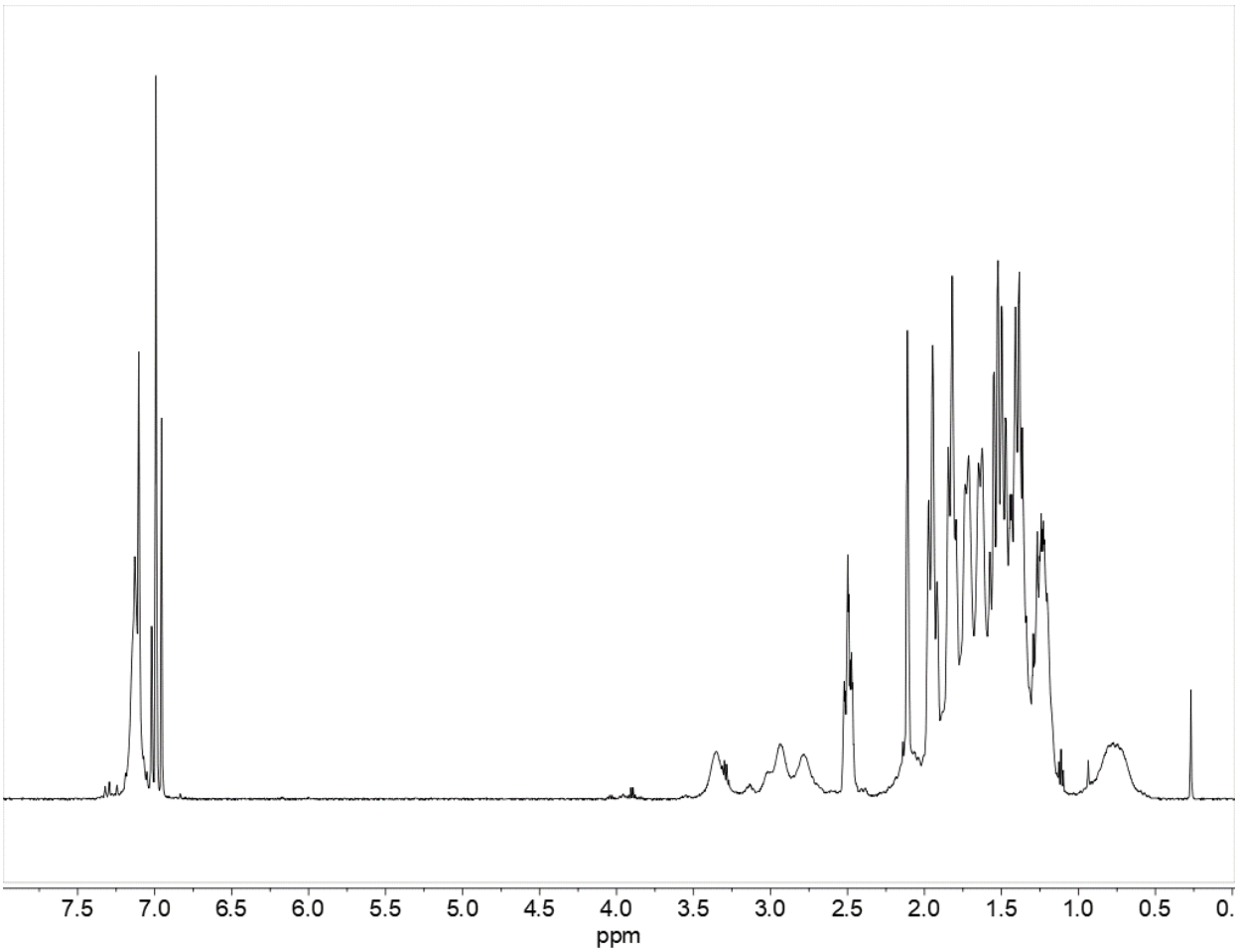

Figure 7.S22. ^{1}H-NMR spectrum of $\{Sn(C_6H_2\text{-}2,4,6\text{-}Cy_3)_2\}_2$ (**1**) (toluene D_8, 330 K)

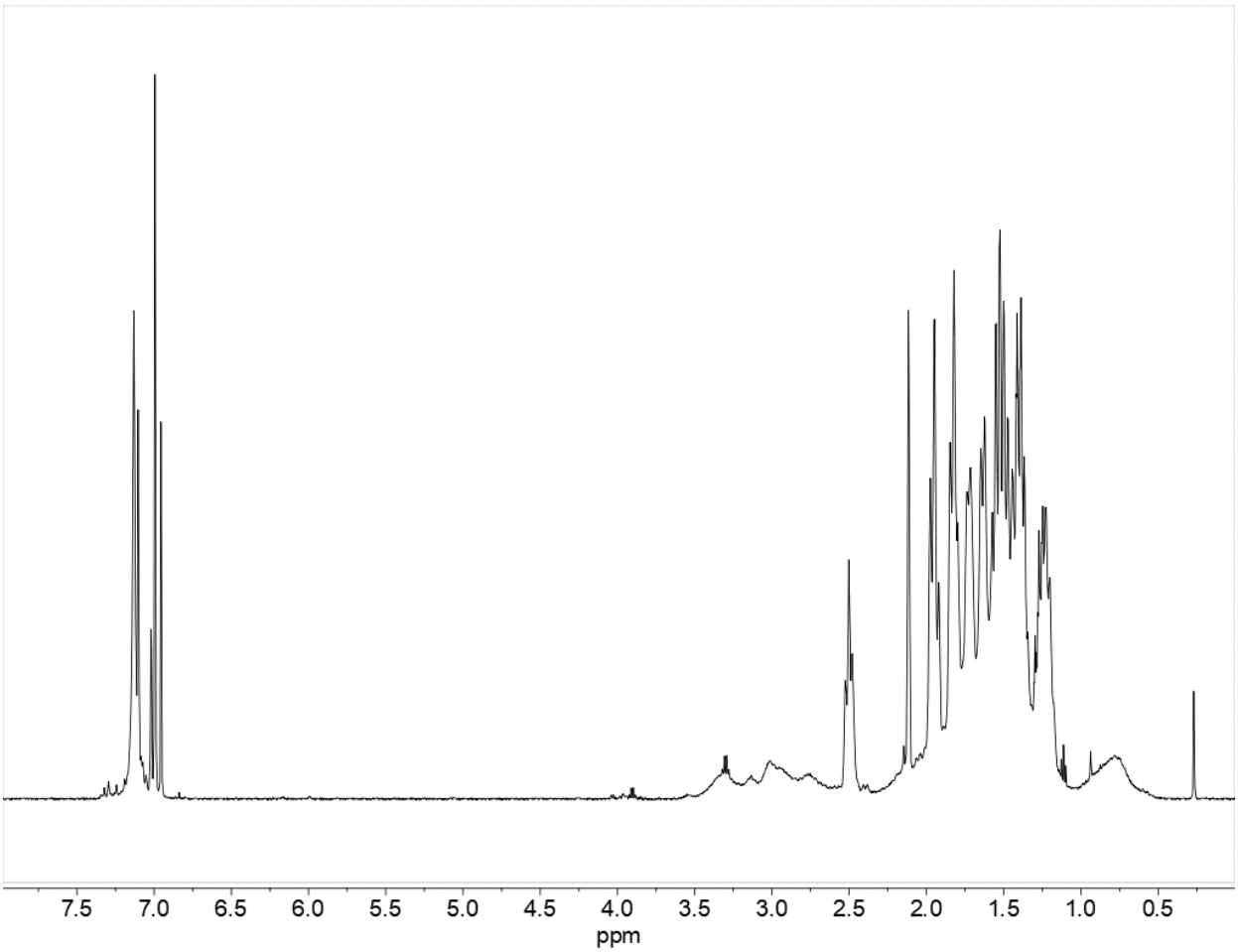

Figure 7.S23. ^{1}H-NMR spectrum of $\{Sn(C_6H_2\text{-}2,4,6\text{-}Cy_3)_2\}_2$ (**1**) (toluene D_8, 340 K)

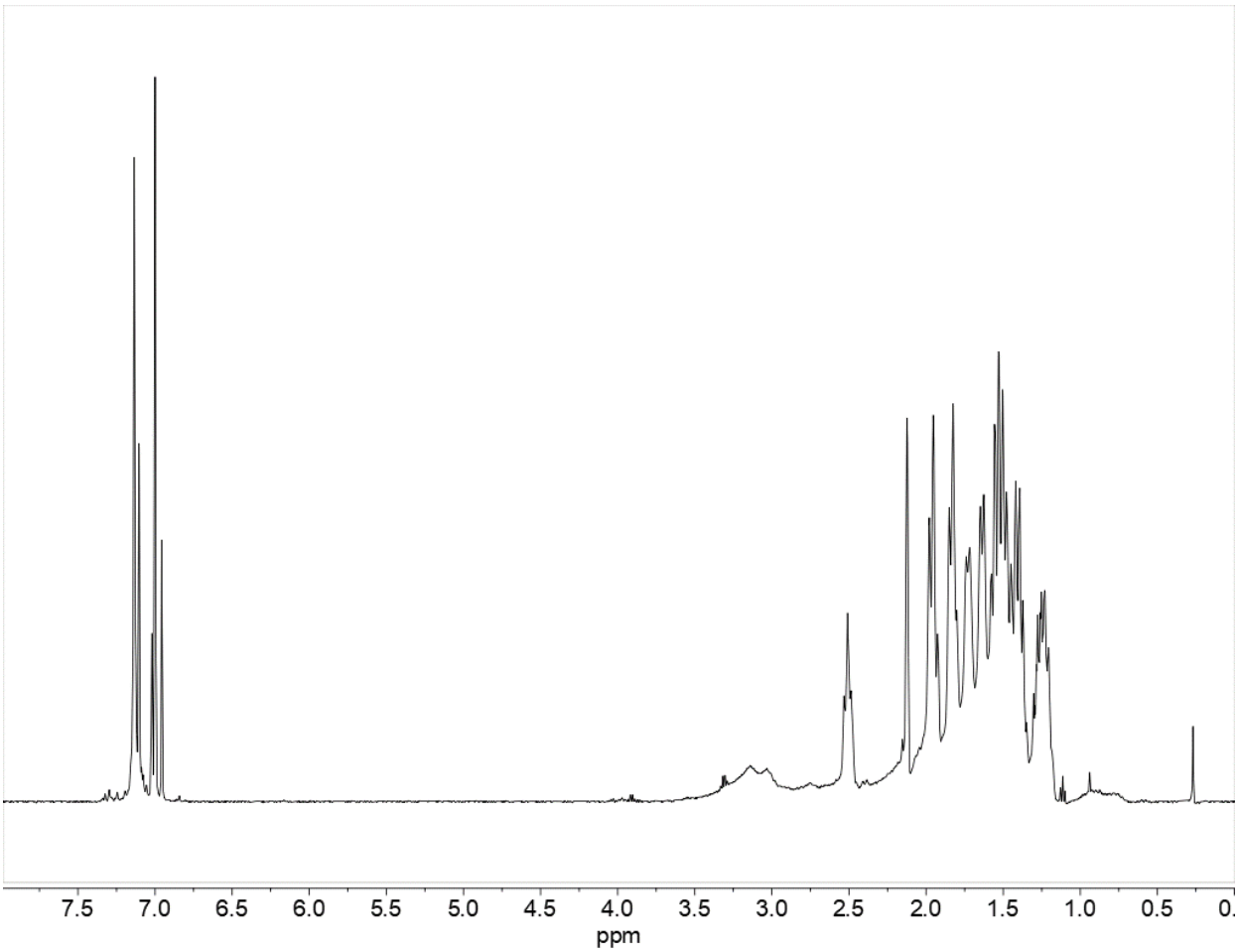

Figure 7.S24. ^{1}H-NMR spectrum of $\{Sn(C_6H_2\text{-}2,4,6\text{-}Cy_3)_2\}_2$ (**1**) (toluene D_8, 350 K)

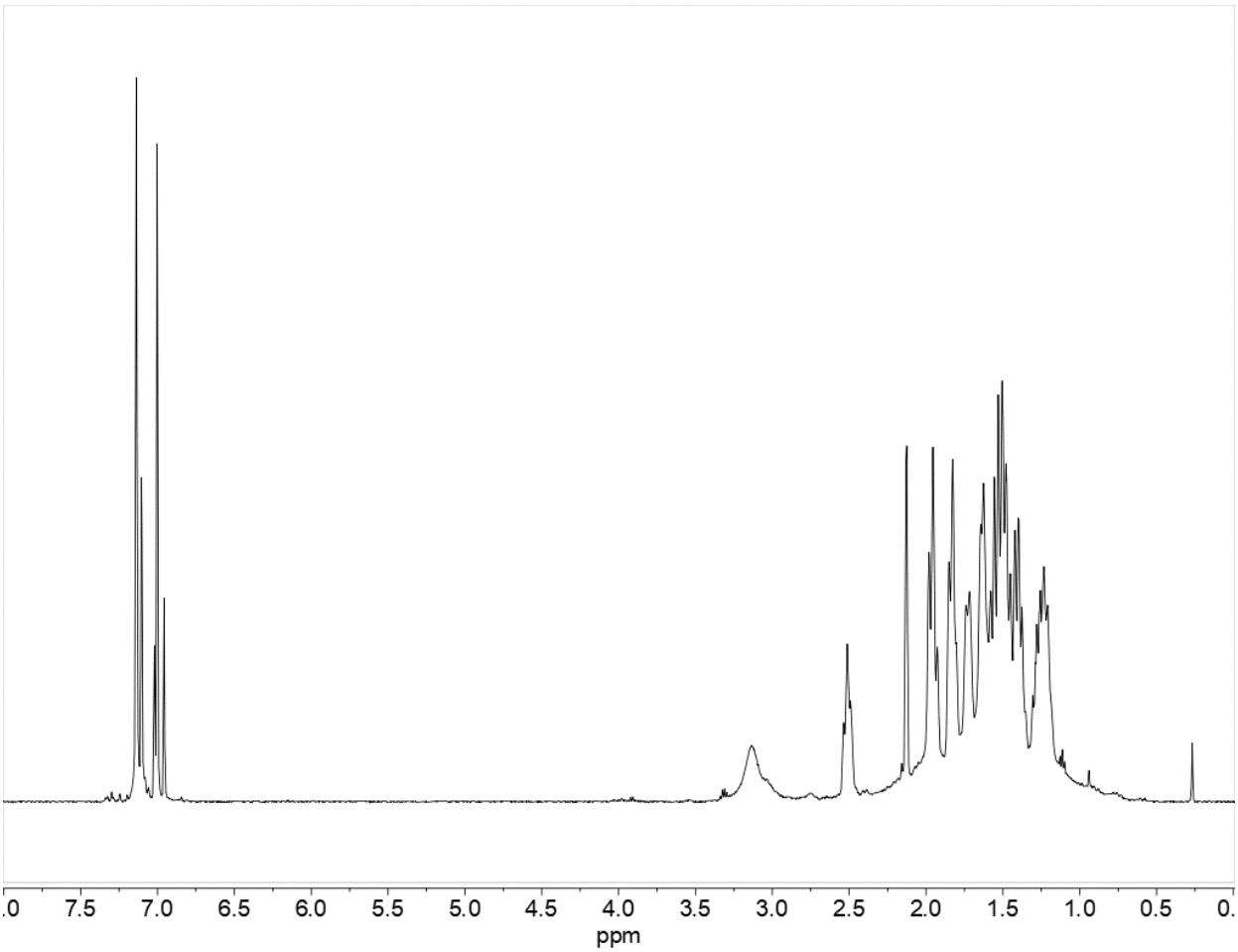

Figure 7.S25. ^{1}H-NMR spectrum of $\{Sn(C_6H_2\text{-}2,4,6\text{-}Cy_3)_2\}_2$ (**1**) (toluene D_8, 360 K)

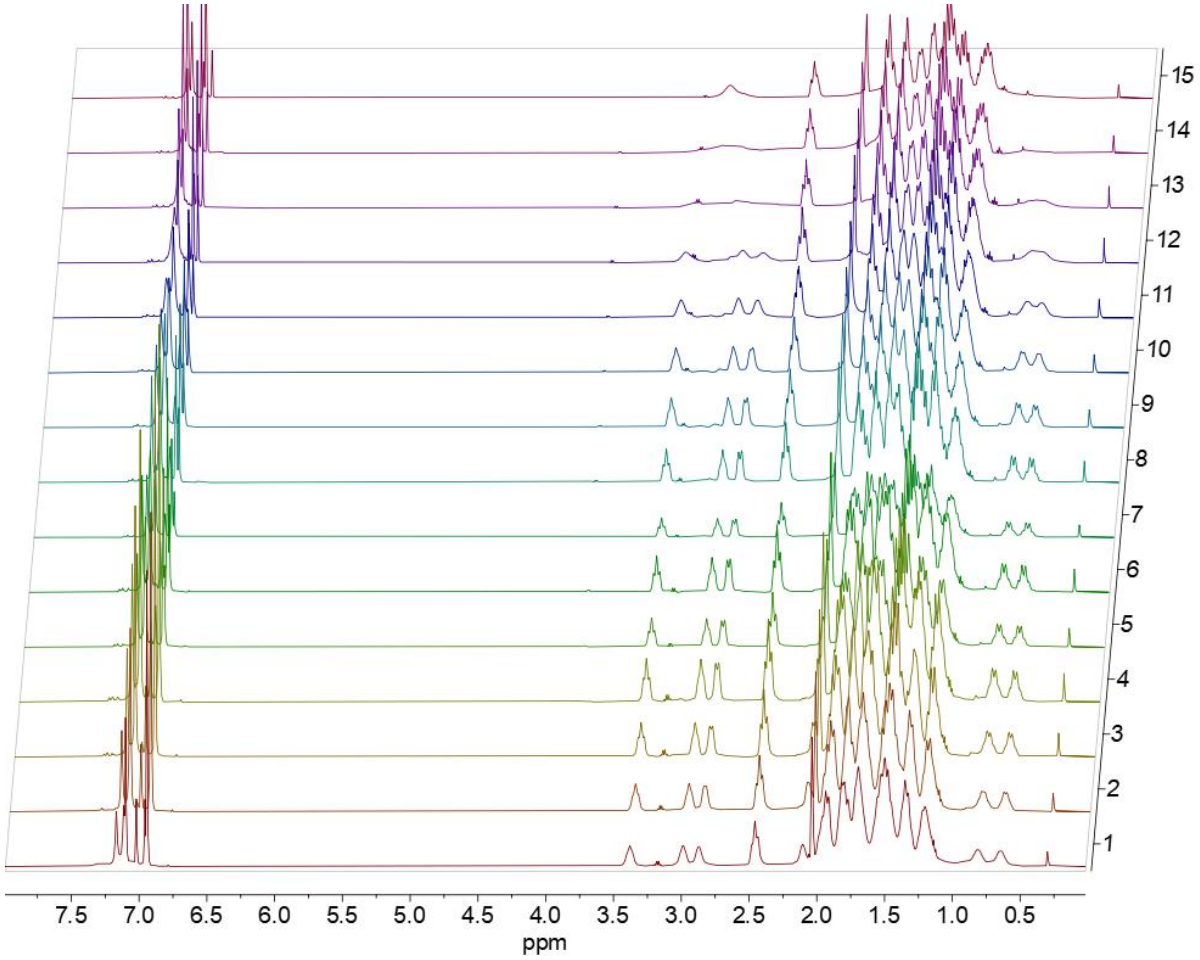

Figure 7.S26. Stacked plots of variable-temperature (from 220 K in the bottom plot to 360 K in the top plot, 10 K increments) ^{1}H-NMR spectra of $\{Sn(C_6H_2\text{-}2,4,6\text{-}Cy_3)_2\}_2$ (**1**) (toluene D_8)

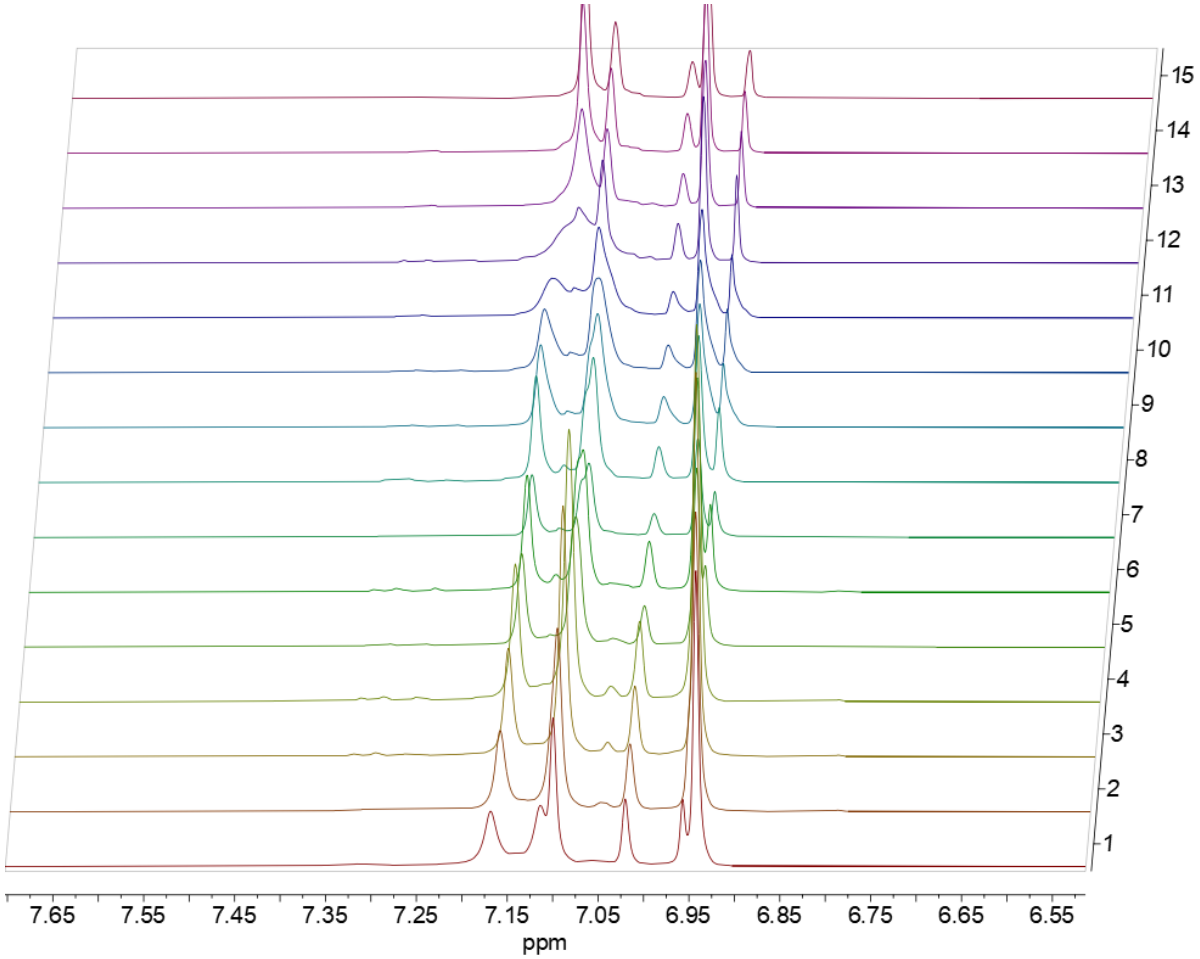

Figure 7.S27. Detail of stacked plots of variable-temperature (from 220 K in the bottom plot to 360 K in the top plot, 10 K increments) ^{1}H-NMR spectra of $\{Sn(C_6H_2\text{-}2,4,6\text{-}Cy_3)_2\}_2$ (**1**) (toluene D_8)

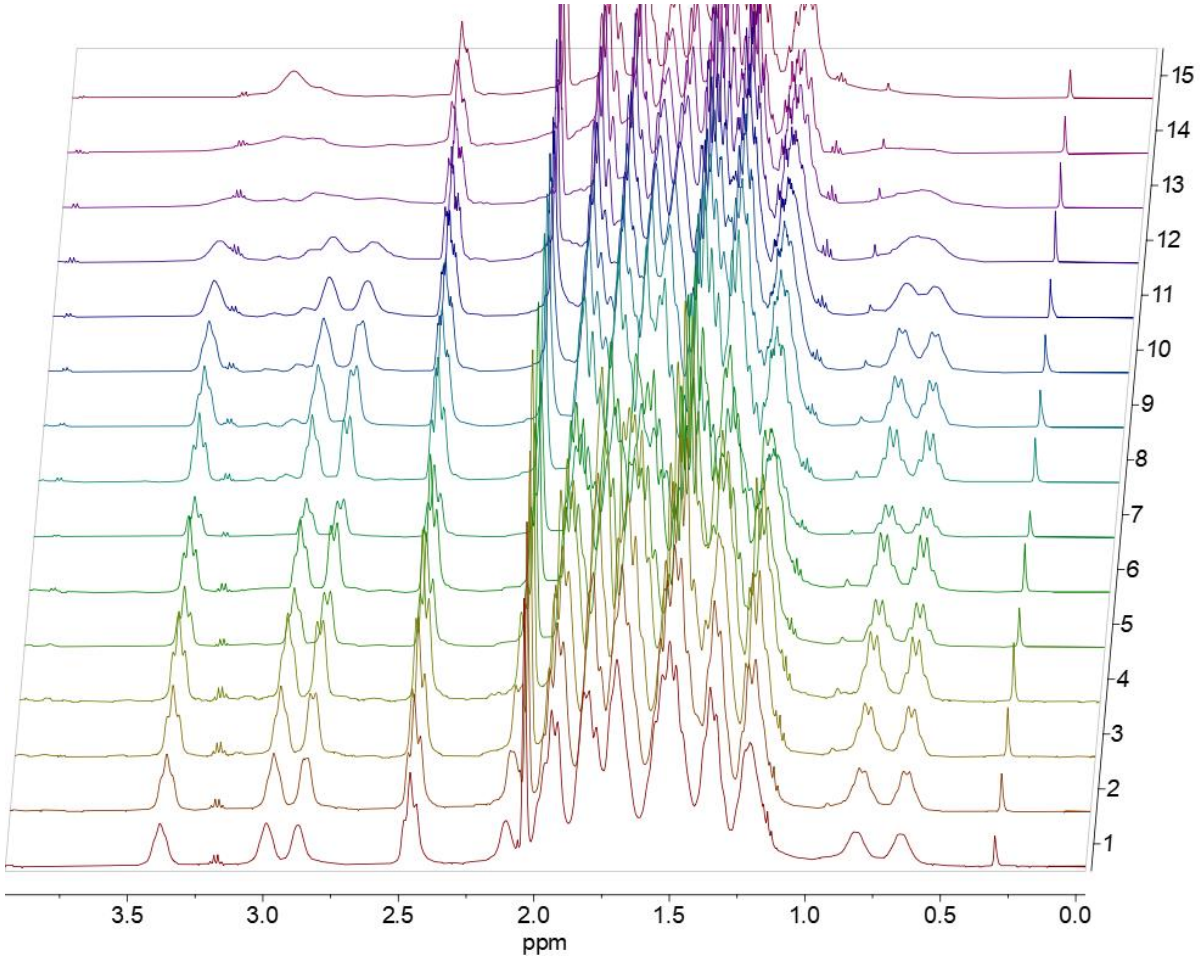

Figure 7.S28. Detail of stacked plots of variable-temperature (from 220 K in the bottom plot to 360 K in the top plot, 10 K increments) ^{1}H-NMR spectra of $\{Sn(C_6H_2\text{-}2,4,6\text{-}Cy_3)_2\}_2$ (**1**) (toluene D_8)

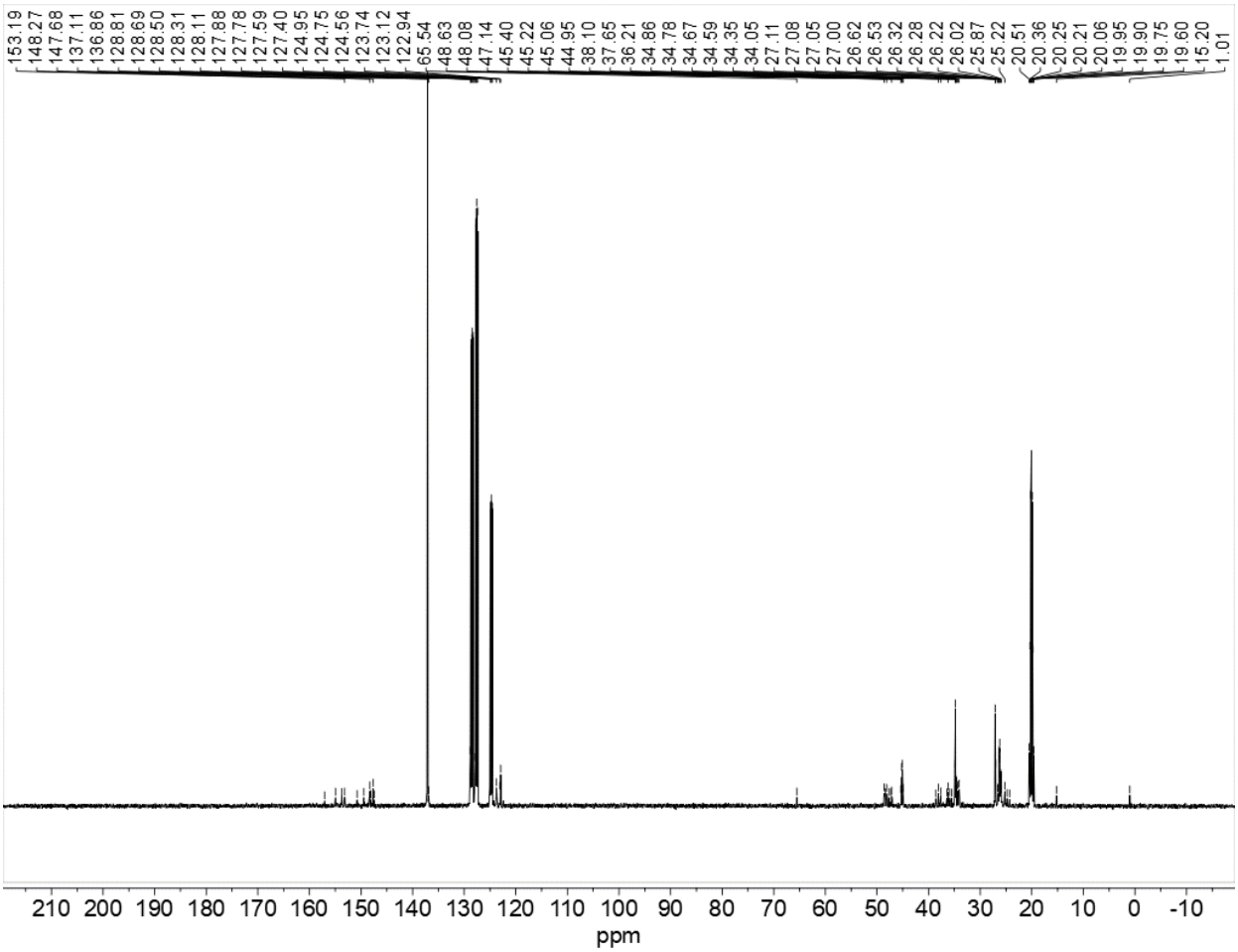

Figure 7.S29. ^{13}C NMR spectrum of $\{Sn(C_6H_2\text{-}2,4,6\text{-}Cy_3)_2\}_2$ (**1**) (toluene D_8, 300 K)

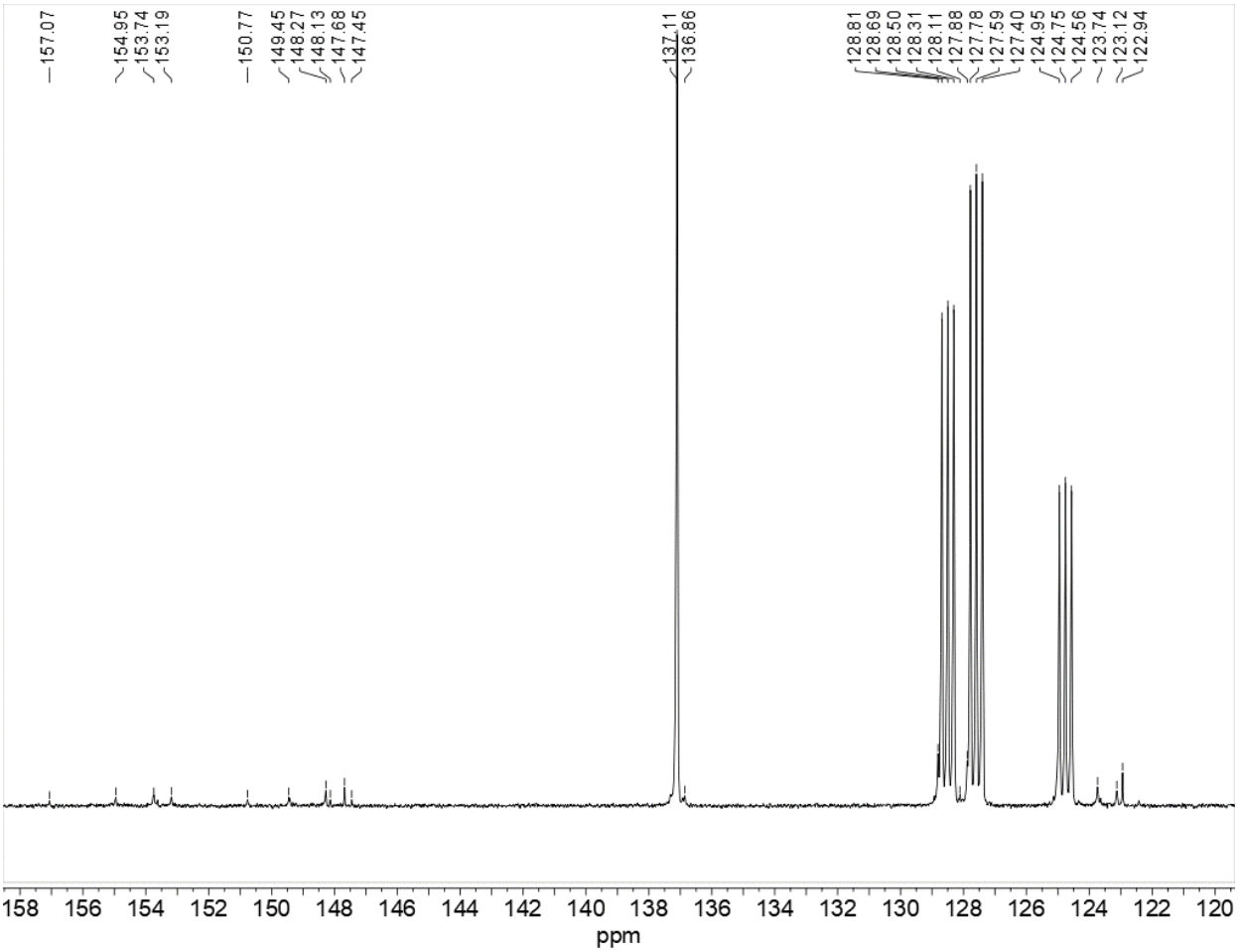

Figure 7.S30. Detail of ^{13}C NMR spectrum of $\{Sn(C_6H_2\text{-}2,4,6\text{-}Cy_3)_2\}_2$ (**1**) (toluene D_8, 300 K)

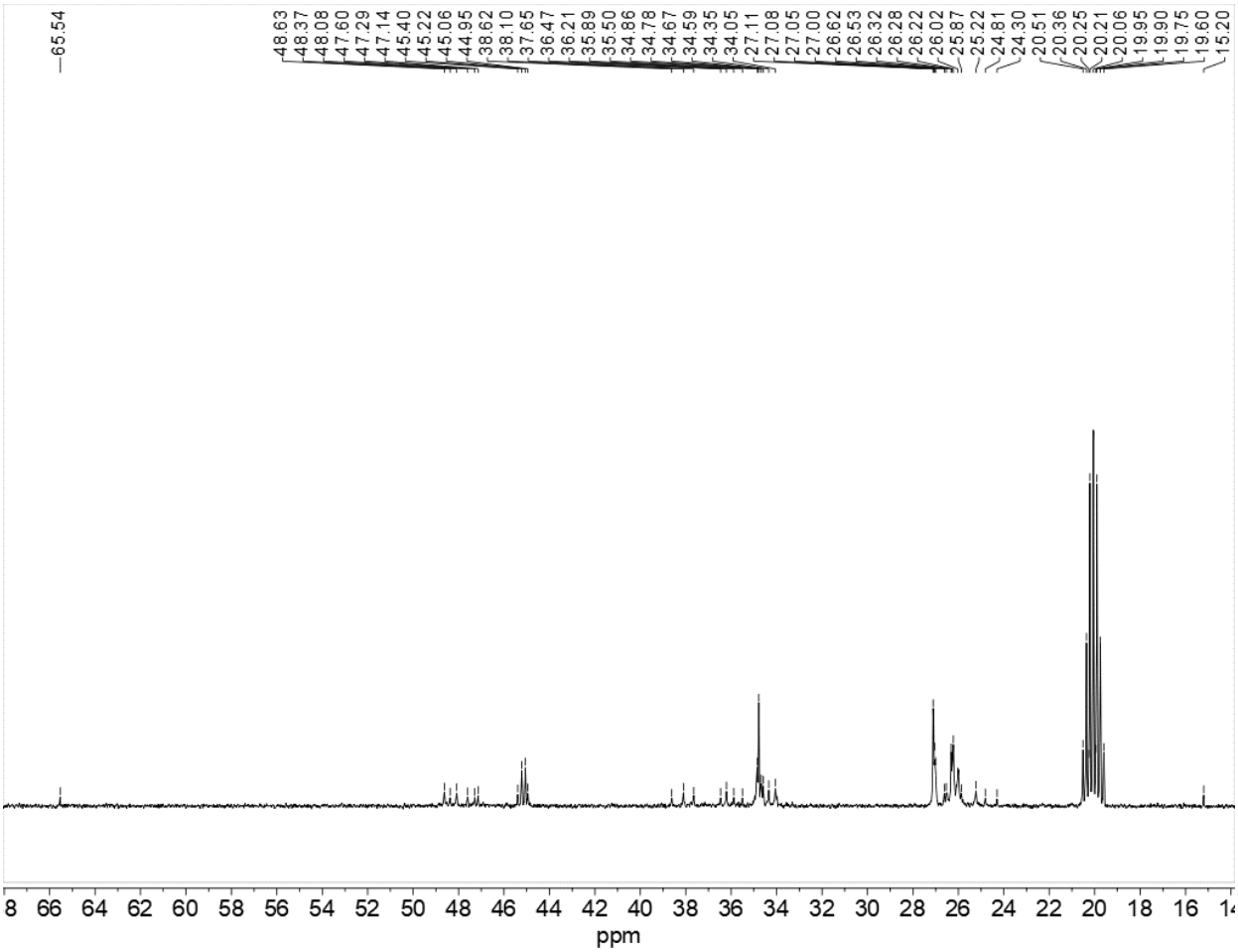

Figure 7.S31. Detail of ^{13}C NMR spectrum of $\{Sn(C_6H_2\text{-}2,4,6\text{-}Cy_3)_2\}_2$ (**1**) (toluene D_8, 300 K)

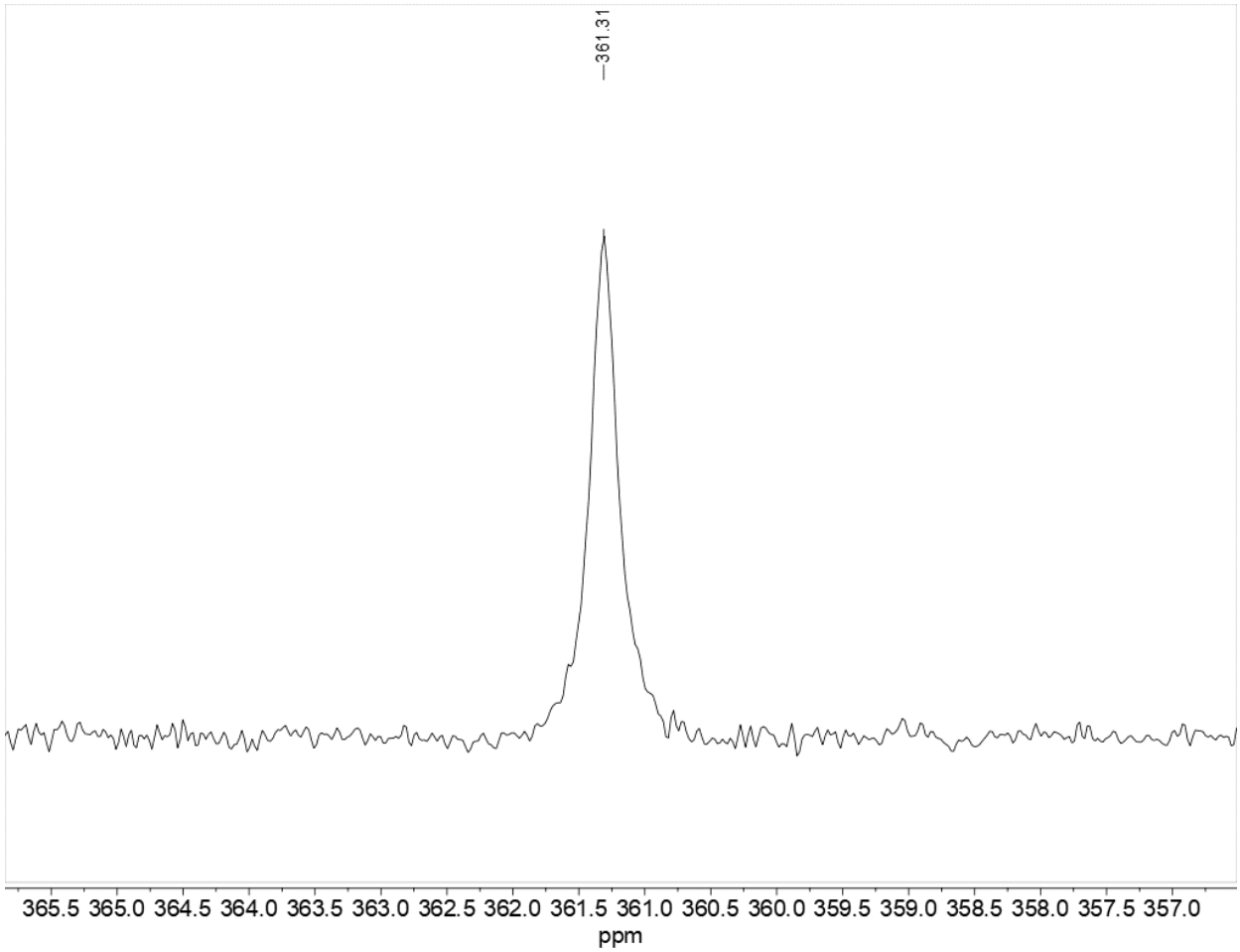

Figure 7.S32. ^{119}Sn NMR spectrum of $\{Sn(C_6H_2\text{-}2,4,6\text{-}Cy_3)_2\}_2$ (**1**) (toluene D_8, 300 K)

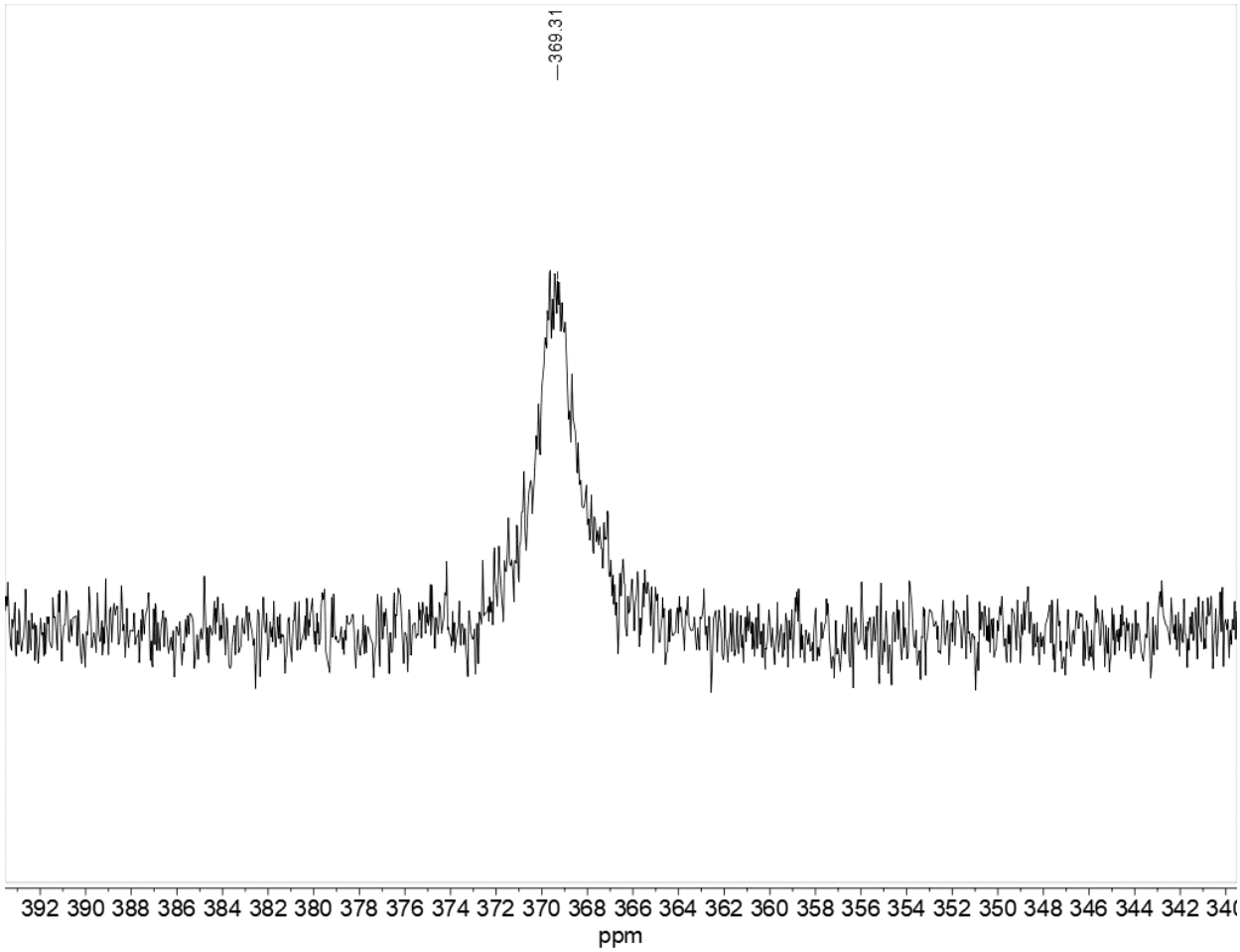

Figure 7.S33. ^{119}Sn NMR spectrum of $\{Sn(C_6H_2\text{-}2,4,6\text{-}Cy_3)_2\}_2$ (**1**) (toluene D_8, 350 K)

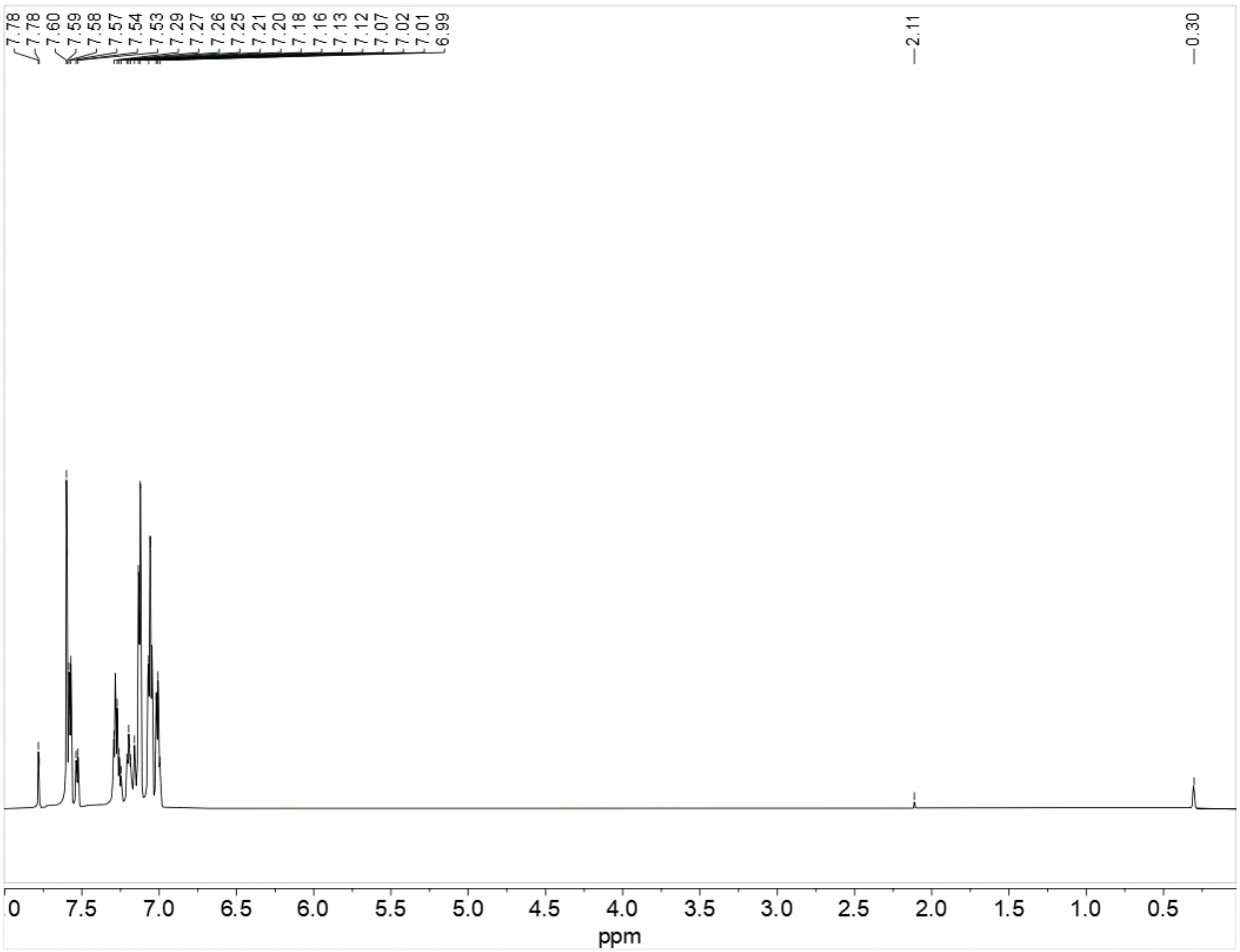

Figure 7.S34. ^{1}H-NMR spectrum of $Sn(C_6H_2\text{-}2,4,6\text{-}Ph_3)_2$ (**2**) immediately after sample preparation (benzene D_6, 300 K)

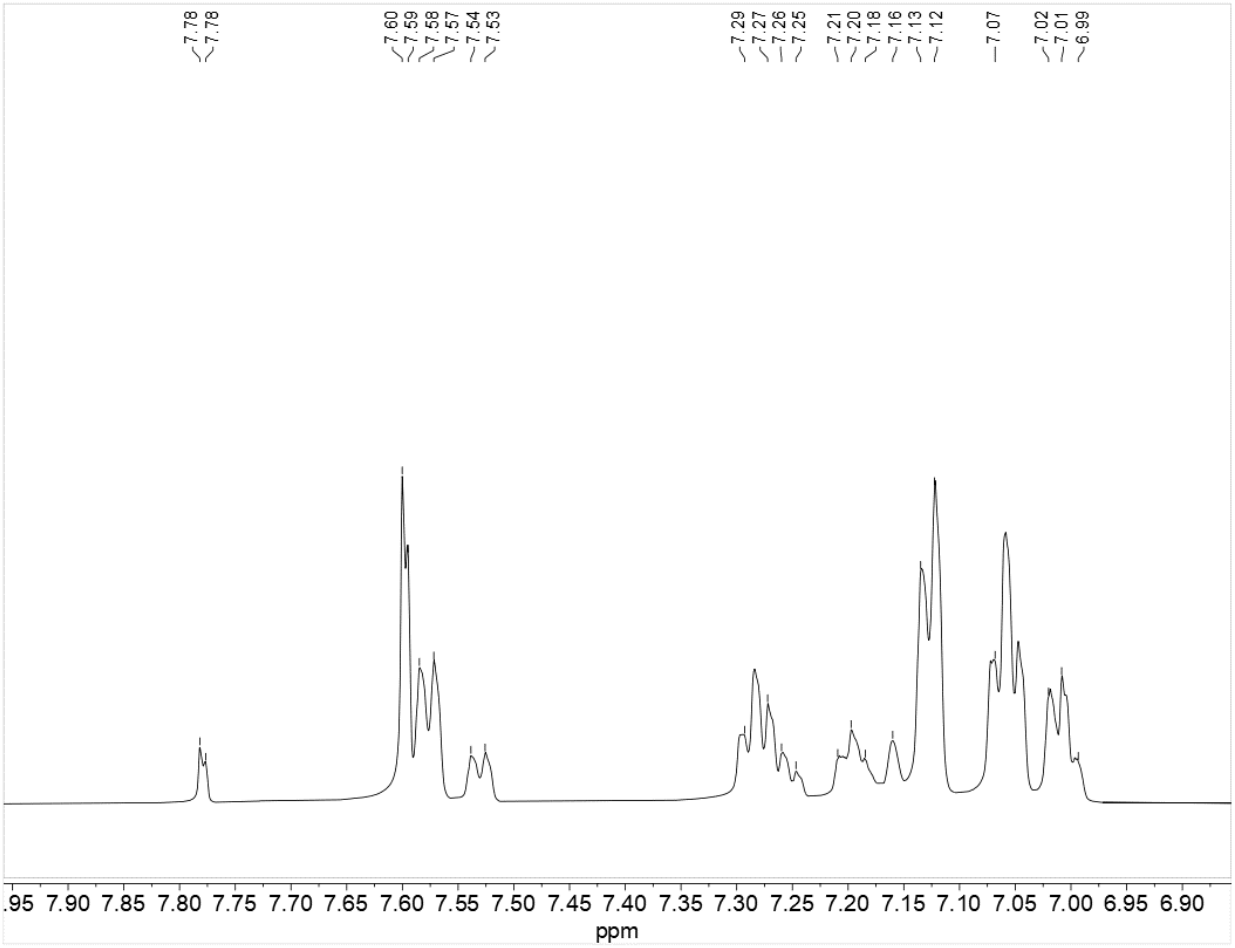

Figure 7.S35. Detail of ^{1}H-NMR spectrum of $Sn(C_6H_2\text{-}2,4,6\text{-}Ph_3)_2$ (**2**) immediately after sample preparation (benzene D_6, 300 K)

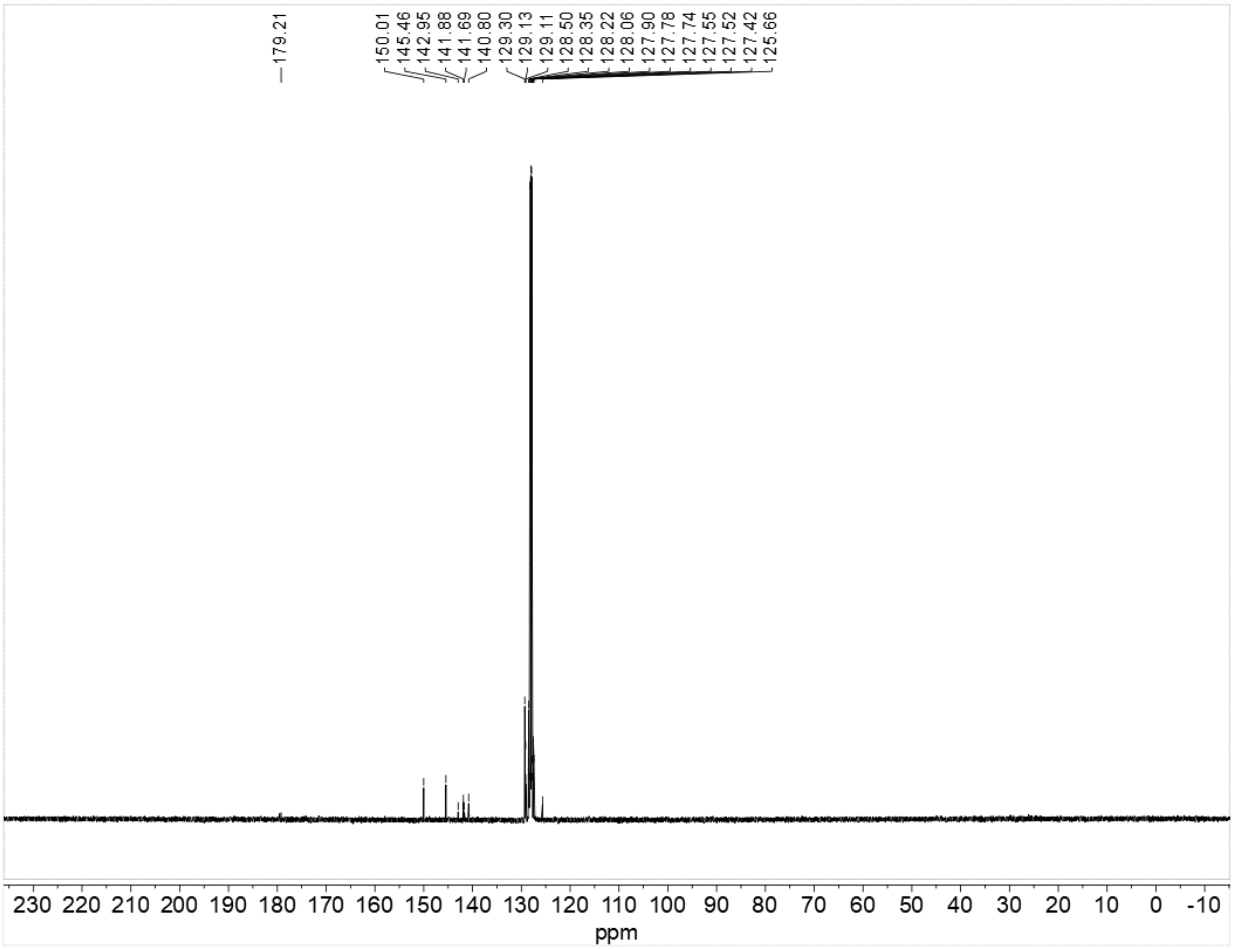

Figure 7.S36. ^{13}C-NMR spectrum of Sn(C_6H_2-2,4,6-Ph_3)$_2$ (**2**) immediately after sample preparation (benzene D_6, 300 K)

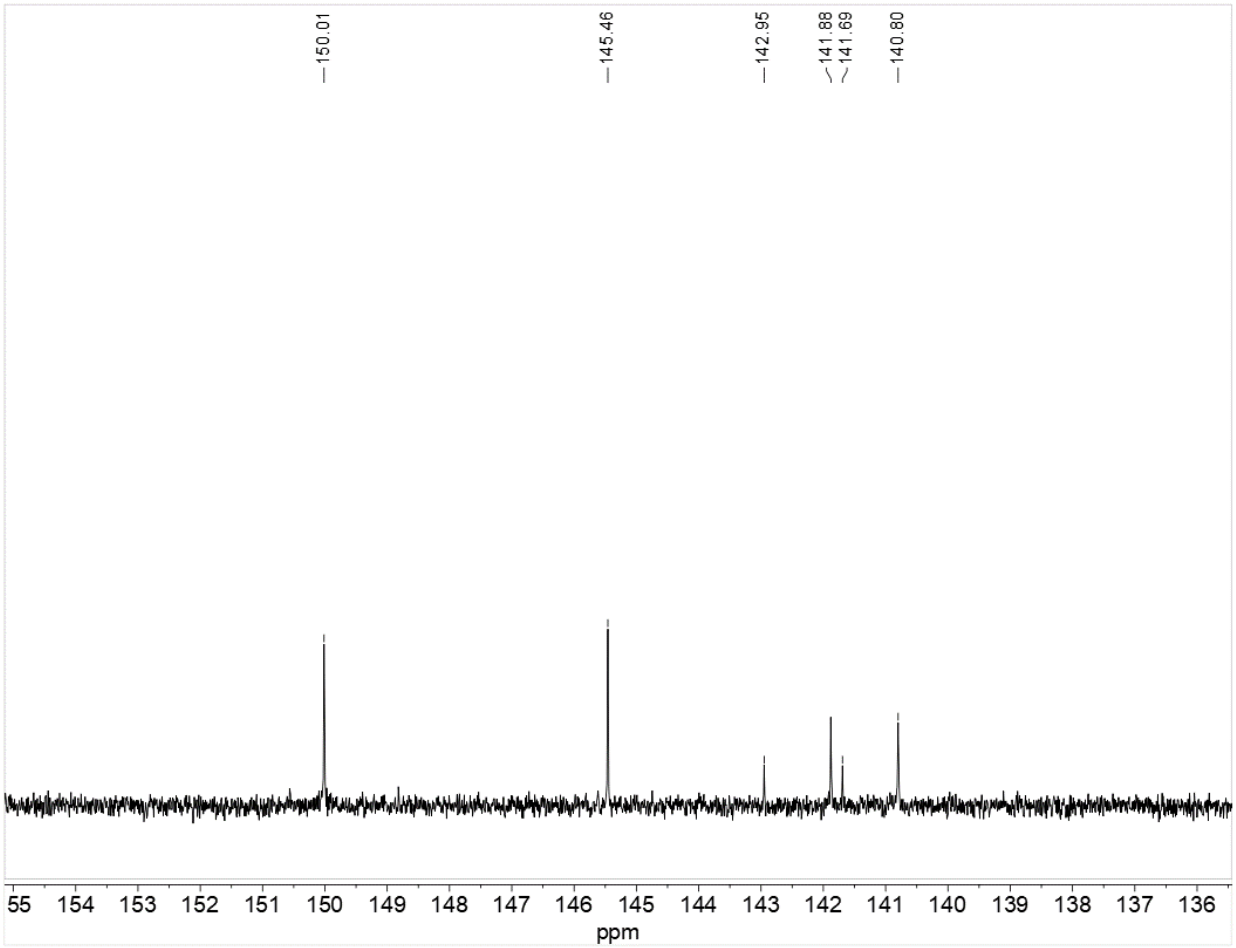

Figure 7.S37. Detail of ^{13}C-NMR spectrum of Sn(C_6H_2-2,4,6-Ph_3)$_2$ (**2**) immediately after sample preparation (benzene D_6, 300 K)

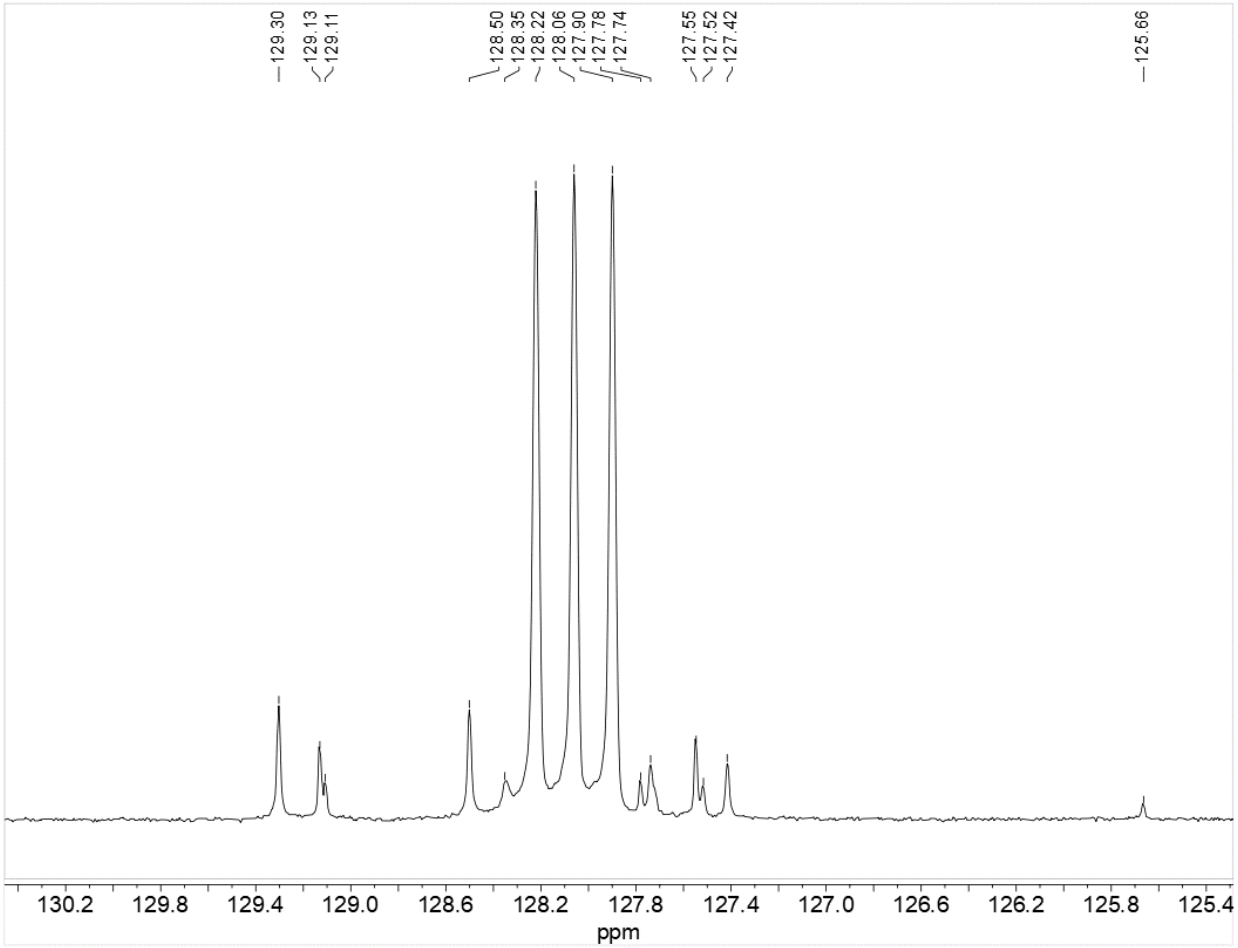

Figure 7.S38. Detail of ^{13}C-NMR spectrum of Sn(C_6H_2-2,4,6-Ph_3)$_2$ (**2**) immediately after sample preparation (benzene D_6, 300 K)

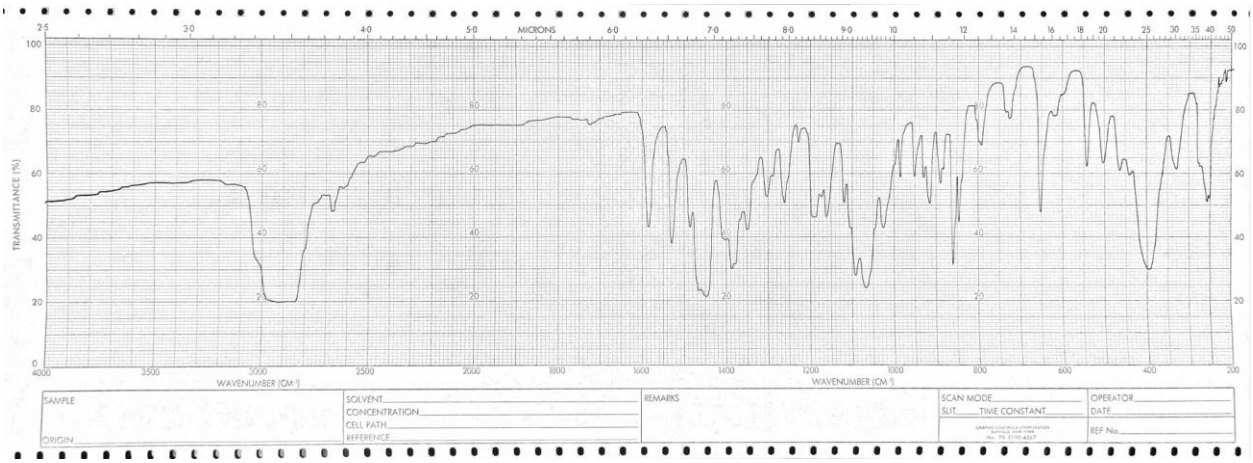

Figure 7.S39. Infrared spectrum of $LiPhCy_3 \cdot OEt_2$ (Nujol, CsI windows).

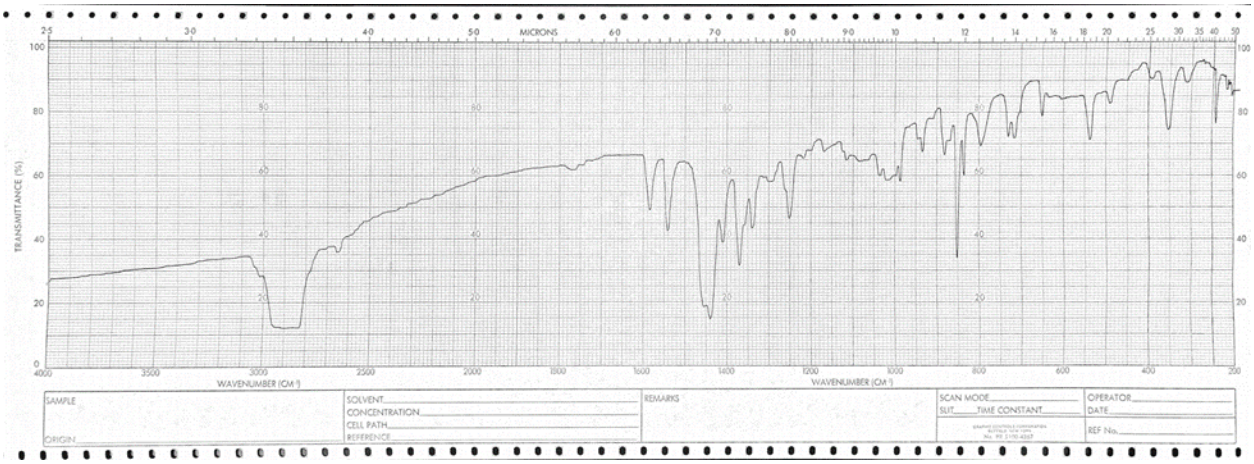

Figure 7.S40. Infrared spectrum of $\{Sn(C_6H_2\text{-}2,4,6\text{-}Cy_3)_2\}_2$ (**1**) (Nujol, CsI windows).

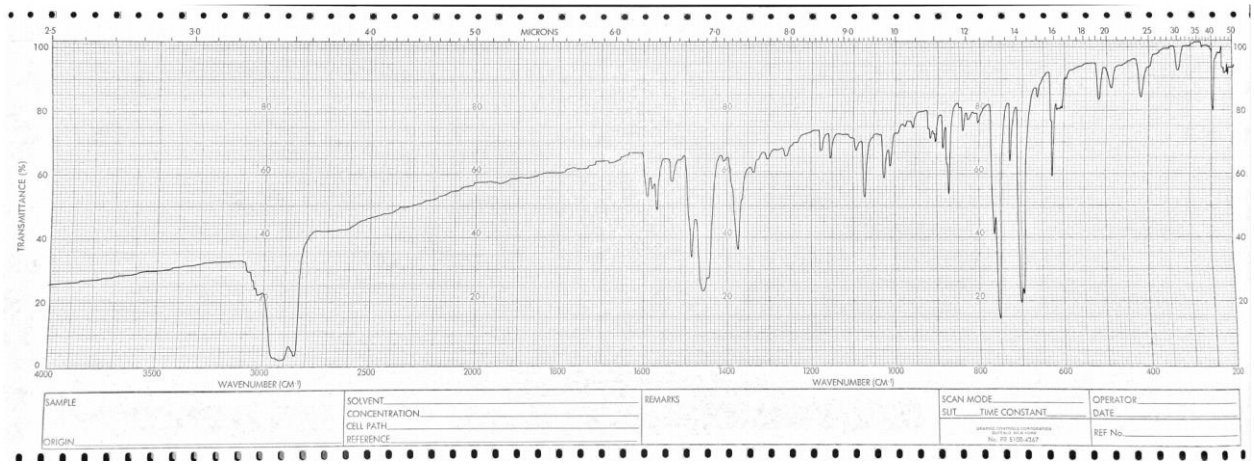

Figure 7.S41. Infrared spectrum of $Sn(C_6H_2\text{-}2,4,6\text{-}Ph_3)_2$ (**2**) (Nujol, CsI windows).

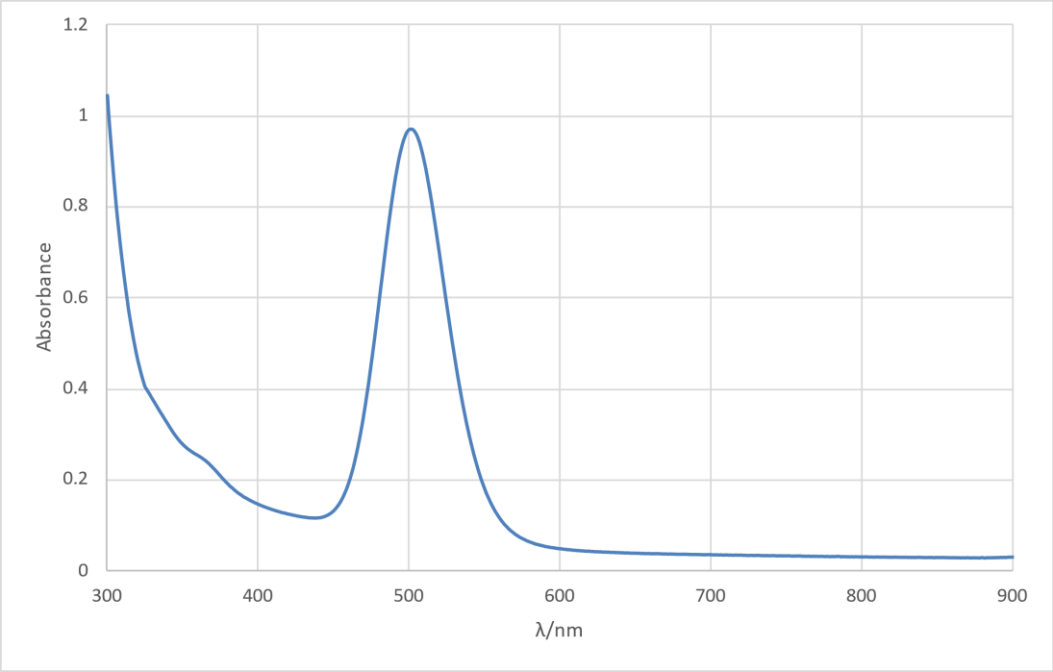

Figure 7.S42. UV-vis spectrum of {Sn(C_6H_2-2,4,6-Cy_3)$_2$}$_2$ (**1**) (130 μM, hexanes, 1 cm path length).

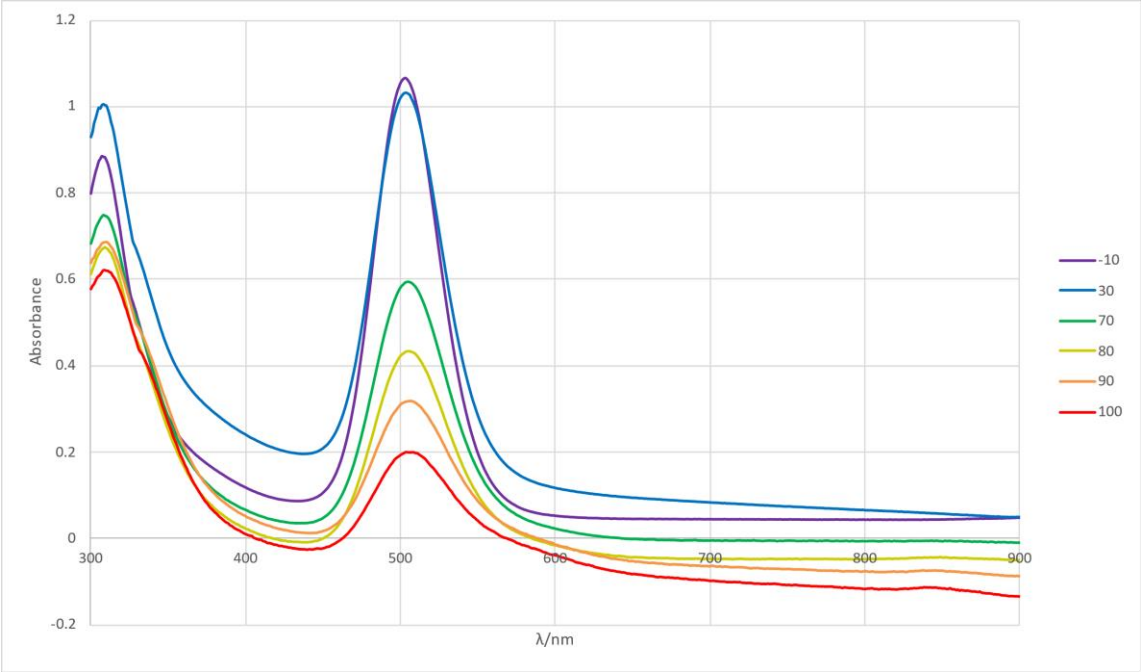

Figure 7.S43. Stacked variable-temperature UV-vis spectra of {Sn(C_6H_2-2,4,6-Cy_3)$_2$}$_2$ (**1**) from -10 °C to 100 °C (toluene, 1 cm path length)

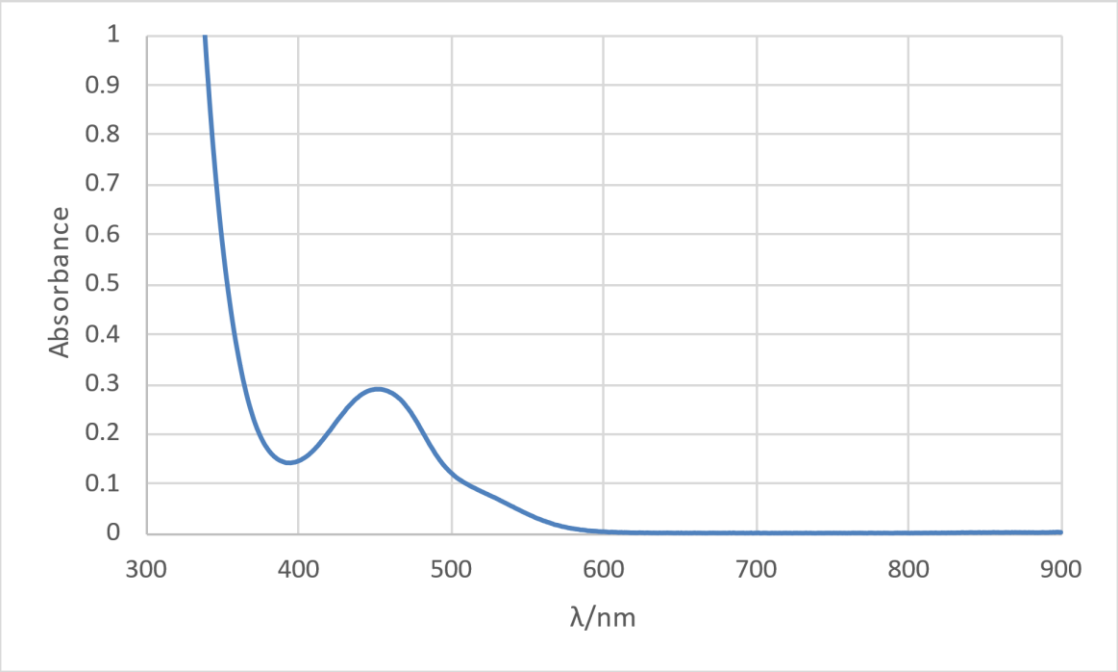

Figure 7.S44. UV-vis spectrum of $Sn(C_6H_2\text{-}2,4,6\text{-}Ph_3)_2$ (**2**) immediately after sample preparation (465 μM, toluene, 1cm path length)

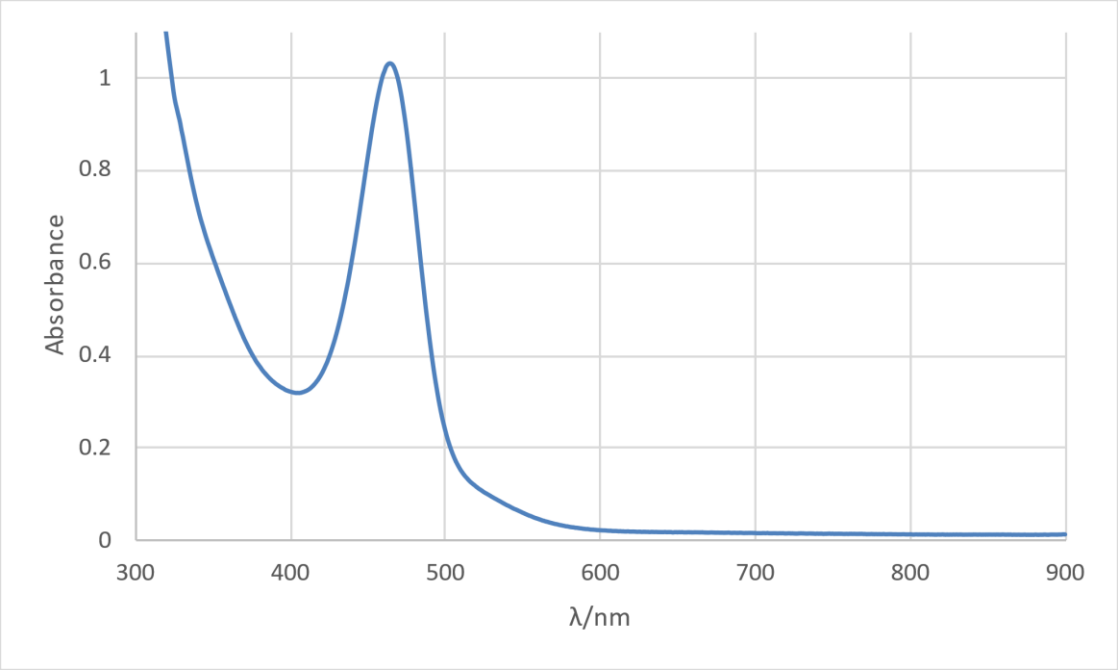

Figure 7.S45. UV-vis spectrum of $Sn(C_6H_2\text{-}2,4,6\text{-}Ph_3)_2$ (**2**), 14 hours after sample preparation (465 μM, toluene, 1cm path length)

Computational Details

General remarks, geometry optimizations and single point energies

Computed structures and orbitals were visualized with UCSF Chimera[2] 1.10.2. Quantum mechanical calculations were performed with the TURBOMOLE 7.5.1[3] and xtb 6.5[4,5] program packages. Geometries were pre-optimized with the GFN2-xTB[6] extended tight binding method applying the generalized born solvation with solvent accessible surface (GBSA)[7] model for toluene. For **2**, a semi-automated conformer sampling was conducted with the CREST and CENSO programs applying the GFN-FF(GBSA) method. For conformer re-ranking the composite DFT method r^{2}SCAN-3c[8] was applied. Final geometries were optimized applying r^{2}SCAN-3c with the COSMO[9] implicit continuum solvation model for toluene as implemented in TURBOMOLE. Minimum structures were verified as minima on the potential energy surface by the absence of imaginary frequencies ($i\omega$ > 35 cm^{-1}) in the harmonic vibrational frequency calculation conducted with the single-point hessian (SPH) approach[10] at the GFN2-xTB(GBSA) level of theory. All calculations were accelerated by applying the resolution-of-identity (RI) approximation for Coulomb integrals[11] with matching default auxiliary basis sets.[12]

Ro-vibrational corrections to obtain free energies were obtained from a modified rigid rotor harmonic oscillator statistical treatment[13] (T = 25.0 °C, 1 atm pressure) based on harmonic frequencies calculated with the SPH approach. To avoid errors in the harmonic approximation, frequencies with wave numbers below 100 cm^{-1} were treated partially as rigid rotors.[13]

Gas phase single point energies were calculated at the B3LYP-D4/def2-TZVP[14–17] level applying the *m5* numerical integration grid. Energy decomposition analysis (EDA)[18] was performed at the BLYP-D4/def2-TZVP level. The D4 correction to repulsive density functionals such as BLYP was found to reproduce the London dispersion contribution obtained from sophisticated, DLPNO-CCSD(T) based local energy decomposition schemes well.[16,19] Default def2 effective core potentials as implemented in TURBOMOLE were applied for Sn.

Solvation corrections and Gibbs free energies

Solvation effects were further considered by the COSMO-RS[20,21] model, used as implemented in COSMOtherm (Version C3.0, release 16.01)[22] with the 2016 fine parameterization for toluene (parameter file: BP_TZVPD_FINE_C30_1601.ctd; default G_{solv} option). Calculated solvation corrections were further corrected for the volume work of 1 bar to 1 M ideal gas.

Final Gibbs free energies were obtained by summing the gas phase single point energy *E*, the dispersion correction $E_{Disp.}$, the ro-vibrational correction G_{RRHO} and the solvation correction $\delta G_{solv., corr.}$ (Eq. S1).

$$G_{tot.} = E + E_{Disp.,} + G_{RRHO} + \delta G_{solv., corr.} \quad \text{(Equation S1)}$$

NMR parameter calculations

NMR chemical shifts δ for ^{119}Sn nuclei were calculated relative to tetramethylstannane following equation S2:

$$\delta(X) = \sigma(X_{ref}) - \sigma(X) \quad \text{(Equation S2)}$$

Isotropic chemical shielding (σ) and coupling constants were calculated applying the Amsterdam Modeling Suite AMS2020.102[23–25] program package. The revPBE[26] functional was applied with the all-electron ZORA/TZP[27] basis set and the zeroth-order regular approximation (ZORA)[28,29] including spin-orbit corrections (SO-ZORA)[30]. The COSMO[31] implicit solvation model was applied for toluene (*surf Esurf, solv Eps=2.38 Rad=3.48*; *div ndiv=5* settings). Otherwise, default settings including gauge-

including atomic orbital (GIAO) were applied as implemented in AMS. The chemical Shift was averaged for both tin atoms in the distannenes.

Table 7.S4. Calculated ^{119}Sn NMR chemical shifts.

#	$\delta_{calc}(^{119}Sn)$
$\mathbf{1}_{mono}$	2569.402
$\mathbf{1}_{dimer}$	388.182
$\mathbf{2}_{mono}$	1783.476
$\mathbf{2}_{dimer}$	418.884

Tabulated energy contributions

Table 7.S5. Tabulated contributions to G_{tot}.

#	E(r^{2}SCAN-3c) / a.u.	B3LYP/def2-TZVP / a.u.	E(D4) / kcal·mol^{-1}	G_{RRHO} (25 °C) / kcal·mol^{-1}	$\delta G_{solv., corr.}$ (25 °C) / kcal·mol^{-1}	G_{tot} / kcal·mol^{-1}
$\mathbf{1}_{mono}$	-2085.227	-2084.967	-179.919	619.793	-26.462	-1307923.035
$\mathbf{1}_{dimer}$	-4170.508	-4169.927	-397.787	1258.307	-44.546	-2615852.501
$\mathbf{2}_{mono}$	-2063.576	-2063.350	-161.564	358.334	-32.544	-1294607.537
$\mathbf{2}_{dimer}$	-4127.188	-4126.684	-356.791	734.771	-50.932	-2589206.307

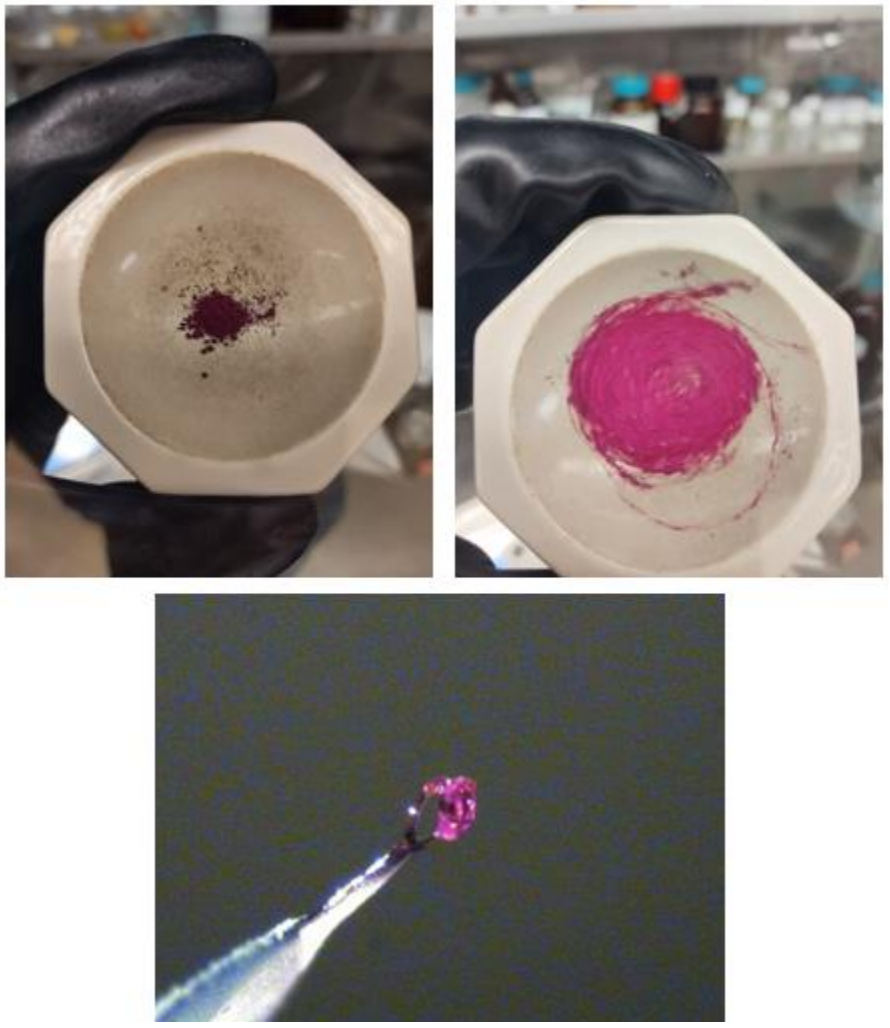

Figure 7.S46. Photographs of micrycrystalline (top left), powder (top right), and crystalline (bottom) $\{Sn(C_6H_2\text{-}2,4,6\text{-}Cy_3)_2\}_2$ (**1**).

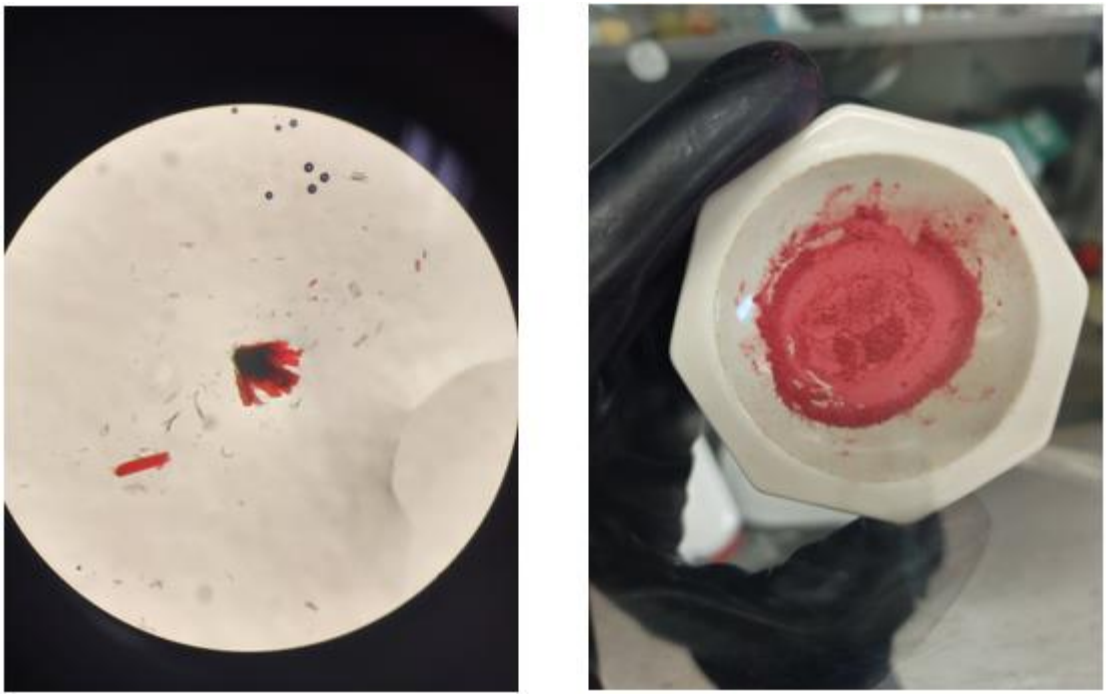

Figure 7.S47. Photographs of crystalline (left) and powdered (right) $Sn(C_6H_2\text{-}2,4,6\text{-}Ph_3)_2$ (**2**).

References.

(1) Salvi, L.; Davis, N. R.; Ali, S. Z.; Buchwald, S. L. A New Biarylphosphine Ligand for the Pd-Catalyzed Synthesis of Diaryl Ethers under Mild Conditions. *Org. Lett.* **2012**, *14*, 170–173.

(2) Pettersen, E. F.; Goddard, T. D.; Huang, C. C.; Couch, G. S.; Greenblatt, D. M.; Meng, E. C.; Ferrin, T. E. UCSF Chimera - A Visualization System for Exploratory Research and Analysis. *J. Comput. Chem.* **2004**, *25*, 1605–1612.

(3) Furche, F.; Ahlrichs, R.; Hättig, C.; Klopper, W.; Sierka, M.; Weigend, F. Turbomole. *WIREs Comput Mol Sci* **2014**, *4*, 91–100.

(4) *Semiempirical Extended Tight-Binding Program Package Xtb, Version 6.5, Https://Github.Com/Grimme-Lab/Xtb. Accessed: 2021-07-18*.

(5) Bannwarth, C.; Caldeweyher, E.; Ehlert, S.; Hansen, A.; Pracht, P.; Seibert, J.; Spicher, S.; Grimme, S. Extended Tight-Binding Quantum Chemistry Methods. *Wiley Interdiscip. Rev. Comput. Mol. Sci.* Blackwell Publishing Inc. March 2021, p e1493.

(6) Bannwarth, C.; Ehlert, S.; Grimme, S. GFN2-XTB - An Accurate and Broadly Parametrized Self-Consistent Tight-Binding Quantum Chemical Method with Multipole Electrostatics and Density-Dependent Dispersion Contributions. *J. Chem. Theory Comput.* **2019**, *15*, 1652–1671.

(7) Ehlert, S.; Stahn, M.; Spicher, S.; Grimme, S. Robust and Efficient Implicit Solvation Model for Fast Semiempirical Methods. *J. Chem. Theory Comput.* **2021**, *17*, 4250–4261.

(8) Grimme, S.; Hansen, A.; Ehlert, S.; Mewes, J.-M. R2SCAN-3c: A “Swiss Army Knife” Composite Electronic-Structure Method. *J. Chem. Phys.* **2021**, *154*, 064103.

(9) Klamt, A.; Schüürmann, G. COSMO: A New Approach to Dielectric Screening in Solvents with Explicit Expressions for the Screening Energy and Its Gradient. *J. Chem. Soc., Perkin Trans. 2* **1993**, *0*, 799–805.

(10) Spicher, S.; Grimme, S. Single-Point Hessian Calculations for Improved Vibrational Frequencies and Rigid-Rotor-Harmonic-Oscillator Thermodynamics. *J. Chem. Theory Comput.* **2021**, *17*, 1701–1714.

(11) Eichkorn, K.; Treutler, O.; Öhm, H.; Häser, M.; Ahlrichs, R. Auxiliary Basis Sets to Approximate Coulomb Potentials. *Chem. Phys. Lett.* **1995**, *240*, 283–289.

(12) Weigend, F. Accurate Coulomb-Fitting Basis Sets for H to Rn. *Phys. Chem. Chem. Phys.* **2006**, *8*, 1057–1065.

(13) Grimme, S. Supramolecular Binding Thermodynamics by Dispersion-Corrected Density Functional Theory. *Chem. - A Eur. J.* **2012**, *18*, 9955–9964.

(14) Becke, A. D. Density-Functional Thermochemistry. III. The Role of Exact Exchange. *J. Chem. Phys.* **1993**, *98*, 5648–5652.

(15) Caldeweyher, E.; Ehlert, S.; Hansen, A.; Neugebauer, H.; Spicher, S.; Bannwarth, C.; Grimme, S. A Generally Applicable Atomic-Charge Dependent London Dispersion Correction. *J. Chem. Phys.* **2019**, *150*, 154122.

(16) Bursch, M.; Caldeweyher, E.; Hansen, A.; Neugebauer, H.; Ehlert, S.; Grimme, S. Understanding and Quantifying London Dispersion Effects in Organometallic Complexes. *Acc. Chem. Res.* **2019**, *52*, 258–266.

(17) Weigend, F.; Ahlrichs, R. Balanced Basis Sets of Split Valence, Triple Zeta Valence and Quadruple Zeta Valence Quality for H to Rn: Design and Assessment of Accuracy. *Phys. Chem. Chem. Phys.* **2005**, *7*, 3297–3305.

(18) Hopffgarten, M. von; Frenking, G. Energy Decomposition Analysis. *Wiley Interdiscip. Rev. Comput. Mol. Sci.* **2012**, *2*, 43–62.

(19) Bursch, M.; Kunze, L.; Vibhute, A. M.; Hansen, A.; Sureshan, K. M.; Jones, P. G.; Grimme, S.;

Werz, D. B. Quantification of Noncovalent Interactions in Azide–Pnictogen, –Chalcogen, and –Halogen Contacts. *Chem. – A Eur. J.* **2021**, *27*, 4627–4639.

(20) Klamt, A. Conductor-like Screening Model for Real Solvents: A New Approach to the Quantitative Calculation of Solvation Phenomena. *J. Phys. Chem.* **1995**, *99*, 2224–2235.

(21) Eckert, F.; Klamt, A. Fast Solvent Screening via Quantum Chemistry: COSMO-RS Approach. *AIChE J.* **2002**, *48*, 369–385.

(22) Klamt, A.; Eckert, F.; Pohler, L. *COSMOtherm 2016, COSMOlogic GmbH & Co. KG, Leverkusen, Germany*; COSMOtherm 2016, COSMOlogic GmbH & Co. KG, Leverkusen, Germany, 2016.

(23) ADF 2019.3, SCM, Theoretical Chemistry, Vrije Universiteit, Amsterdam, The Netherlands, Http://Www.Scm.Com.

(24) Schreckenbach, G.; Ziegler, T. Calculation of NMR Shielding Tensors Using Gauge-Including Atomic Orbitals and Modern Density Functional Theory. *J. Phys. Chem.* **1995**, *99*, 606–611.

(25) Krykunov, M.; Ziegler, T.; Van Lenthe, E. Hybrid Density Functional Calculations of Nuclear Magnetic Shieldings Using Slater-Type Orbitals and the Zeroth- Order Regular Approximation. *Int. J. Quantum Chem.* **2009**, *109*, 1676–1683.

(26) Zhang, Y.; Yang, W. Comment on "Generalized Gradient Approximation Made Simple." *Phys. Rev. Lett.* **1998**, *80*, 890.

(27) Van Lenthe, E.; Baerends, E. J. Optimized Slater-Type Basis Sets for the Elements 1-118. *J. Comput. Chem.* **2003**, *24*, 1142–1156.

(28) Lenthe, E. van; Baerends, E. J.; Snijders, J. G. Relativistic Regular Two-component Hamiltonians. *J. Chem. Phys.* **1993**, *99*, 4597–4610.

(29) Van Lenthe, E.; Baerends, E. J.; Snijders, J. G. Relativistic Total Energy Using Regular

Approximations. *J. Chem. Phys* **1994**, *101*, 9783–9792.

(30) Van Lenthe, E.; Snijders, J. G.; Baerends, E. J. The Zero-Order Regular Approximation for Relativistic Effects: The Effect of Spin-Orbit Coupling in Closed Shell Molecules. *J. Chem. Phys.* **1996**, *105*, 6505–6516.

(31) Pye, C. C.; Ziegler, T. An Implementation of the Conductor-like Screening Model of Solvation within the Amsterdam Density Functional Package. *Theor. Chem. Acc.* **1999**, *101*, 396–408.